Characterisation of the Feline Leukaemia Virus Fusion Peptide: Implications for the Fusion Mechanism.

Sarah Margaret Anne Davies

Submitted in satisfaction of the requirements for the degree of Doctor of Philosophy

Department of Preclinical Veterinary Sciences,

Royal (Dick) School of Veterinary Studies,

The University of Edinburgh.

1998

Declaration

I declare that this thesis has been composed by myself, and that the work described herein is my own except where stated.

This thesis is dedicated to my parents and to my fiancé, Chris, for all their love, support and encouragement; and also to Buster, for his unerring capacity to make me laugh, even under the most dire of circumstances!!!

"To undertake research requires great patience; in science nothing happens quickly.
You must be persistent and not give up.
Every setback is a step forward, because you then know with certainty the things that don't work!"

Gertrude Elion,
Nobel Prize Winner in Medicine, 1988.

Acknowledgements

This thesis would not have been possible but for the following people:

Dr. Jeremy Bradshaw, my supervisor, and mentor for the past four years. A big thank you for all his unfailing help, support and encouragement.

Professor Richard Epand and Dr. Raquel Epand, of McMaster University, Hamilton, Canada; they were kind enough to allow me bench space in their lab, so that I could carry out the DSC and NMR experiments. Dr. Raquel Epand performed the actual fusion assays that are described in Chapter 7. Grateful thanks to them for all their practical help, their excellent advice and suggestions, and for their genuine interest in my project.

Professor Nick Price and Dr. Sharon Kelly of Stirling University, Stirling, U.K.; the CD experiments were performed using their CD facility. A special thanks to Sharon for making it fun as well as productive!

Mr. Steve Mitchell, R.(D).S.V.S., University of Edinburgh, U.K., and Dr. A. Holzenburg and Dr. S. Stoylova, Leeds University, Leeds, U.K., for their input to the electron microscopy work.

Dr. V. Gordeliy at the ILL, Grenoble, France and Dr. B.U. Komanschek at Daresbury Laboratory, Daresbury, U.K. for their expert technical assistance in the running of D16 and station 8.2 respectively.

Malcolm Darkes, my fellow PhD student in the lab. It wouldn't have been the same without you!

The Wellcome Trust for agreeing to give me a Veterinary Prize Research Training Scholarship!

Abstract

Membrane fusion, the merging of two initially distinct membranes to form one common lipid bilayer, is a fundamental mechanism of life. It occurs many times each day within every eukaryotic cell as part of essential daily homeostatic processes, as well as between individual cells, such as sperm and egg during fertilisation. The fusion mechanism is, however, also crucial to the development of many diseases. All enveloped viruses, and indeed many other obligate intracellular parasites, must fuse their own surrounding lipid bilayer with the membrane of their host's target cell in order to gain cell entry and thus the ability to replicate. These infections produce disease states, and possibly even death, in the host species.

Despite the clear importance of fusion, the precise molecular events that occur during this process are still not known. Fusion proteins of viruses have recently become popular tools for use in fusion studies. More specifically, several viruses have known fusion peptides, the sections of these proteins which confer their fusogenic activity. This thesis examines the structure and function of the putative fusion peptide of the retrovirus Feline leukaemia virus, (FeLV), using a variety of mainly biophysical techniques.

The structural effects of the FeLV fusion peptide on lipid polymorphism were studied. Using differential scanning calorimetry, ^{31}P nuclear magnetic resonance and time-resolved X-ray diffraction this peptide was found to induce changes in lipid conformation and motion similar to those of known fusogens: it favoured the formation of non-bilayer lipid conformations which have a relatively large negative curvature, namely the inverted hexagonal phase and isotropic lipid states. Moreover, using X-ray diffraction, a new lipid phase was observed in the presence of the FeLV peptide.

Neutron diffraction studies revealed a change in the packing of lipid molecules within a bilayer and also possible thinning of the bilayer, both of which were induced by interaction with the FeLV fusion peptide.

Fusogenic activity for this putative viral fusion peptide was demonstrated, using fusion assays, which measured the merging of lipid membranes in the presence of the FeLV fusion peptide.

These findings are discussed in the light of the current concepts of the fusion mechanism. They add support to two currently favoured theories of fusion: precession by a fusion peptide as a means of inducing the initial destabilisation of a bilayer, and the formation of highly bent, high energy lipid intermediates, such as the 'modified stalk', in the multistep fusion pathway.

Circular dichroism was employed to determine the secondary structure of the FeLV fusion peptide under a variety of experimental conditions. This peptide was observed to flip readily between α-helical and β sheet conformations. This suggests that structural plasticity may be an important dynamic property of fusion peptides. Possible relationships between peptide structure and function are discussed.

List of contents

List of exhibits

(titles comprehensively abridged)

Chapter 1.

Abbreviations

AA	arachidonic acid
ACN	acetonitrile
Ala	alanine
BHA	soluble HA trimer produced by bromelain cleavage of HA
BLV	Bovine leukaemia virus
CD	circular dichroism
CHEMS	cholesterol hemisuccinate
CMC	critical micellar concentration
CPP	critical packing parameter
DAG	diacylglycerol
DEPE	dielaidoylphosphatidylethanolamine
DiPoPE	dipalmitoleoylphosphatidylethanolamine
DMF	dimethylformamide
DMSO	dimethylsulphoxide
DNA	deoxyribonucleic acid
DOPE	dioleoylphosphatidylethanolamine
DOPG	dioleoylphosphatidylglycerol
DOPS	dioleoylphosphatidylserine
DPPC	dipalmitoylphosphatidylcholine
DSC	differential scanning calorimetry
DTA	differential thermal analysis
Env	retroviral fusion glycoprotein
FeLV	Feline leukaemia virus
FFEM	freeze-fracture electron microscopy
FTIR	Fourier transform infrared spectroscopy
FT-NMR	Fourier transform NMR spectroscopy
Gly	glycine
gp160	HIV fusion envelope glycoprotein
gp120	SU polypeptide subunit produced by proteolytic cleavage of gp160

gp41	TM polypeptide subunit produced by proteolytic cleavage of gp160
gp85	FeLV fusion envelope glycoprotein
gp70	SU polypeptide subunit produced by proteolytic cleavage of gp85
GPI	glycosylphosphatidylinositol
GPI-HA	glycosylphosphatidylinositol-anchored haemagglutinin
GTP	guanosine triphosphate
GTPγS	guanosine 5'-*O* -thiotriphosphate
H_I	phospholipid micellar phase
H_{II}	phospholipid inverted hexagonal phase
HA	Influenza virus haemagglutinin
HA0	fusion-incompetent HA precursor protein
HA1	globular surface polypeptide subunit produced by proteolytic cleavage of HA0
HA2	transmembrane polypeptide subunit produced by proteolytic cleavage of HA0
HFIP	hexa-fluoroisopropanol
HIV	Human immunodeficiency virus
HPLC	high performance liquid chromatography
ILA	interlamellar attachment
Ile	isoleucine
ILL	Institut Laue et Langevin, Grenoble, France
IMI	inverted micellar intermediate
L_α	phospholipid lamellar phase
Leu	leucine
LPC	lysophosphatidylcholine
LUV	large unilamellar vesicle
MeDOPE	N-monomethyldioleoylphosphatidylethanolamine
MoMLV	Molony murine leukaemia virus
NBD	L-α-*N*-(4-nitrobenzo-2-oxa-1,3-diazole)

OG	*n*-octyl glucopyranoside
^{31}P-NMR	^{31}Phosphorus nuclear magnetic resonance
PC	phosphatidylcholine
PE	phosphatidylethanolamine
PEG	poly-(ethylene glycol)
PI	phosphatidylinositol
POPG	palmitoyloleoylphosphatidylglycerol
Pro	proline
PS	phosphatidylserine
p15E	TM polypeptide subunit produced by proteolytic cleavage of gp85
Q	phospholipid cubic phase
Q_{II}	inverted phospholipid cubic phase
Q^{224}	bicontinuous cubic phase of spacegroup Pn3m
Q^{229}	bicontinuous cubic phase of spacegroup Im3m
Q^{227}	discontinuous cubic phase of spacegroup Fd3m
R_0	intrinsic radius of curvature of a lipid monolayer
RET	resonance energy transfer
Rh	L-α-*N*-(Lissamine-Rhodamine B Sulfonyl)
RNA	ribonucleic acid
RSV	Respiratory syncitial virus
SDS	sodium dodecylsulphate
SIV	Simian immunodeficiency virus
SFV	Semliki forest virus
SU	surface unit polypeptide subunit produced by proteolytic cleavage of a retroviral envelope fusion glycoprotein
SUV	small unilamellar vesicle
T_H	L_α-H_{II} phase transition temperature
T_I	temperature at which ^{31}P NMR isotropic resonances are first seen

T_r	temperature of reference material in differential thermal experiments
T_s	temperature of sample in differential thermal experiments
TBHA2	low pH BHA without the globular domain and fusion peptide
TEM	transmission electron microscopy
TFA	trifluoroacetic acid
TFE	trifluoroethanol
Thr	threonine
TM	transmembrane polypeptide subunit produced by proteolytic cleavage of a retroviral envelope fusion glycoprotein
TMC	transmonolayer contact
TMS	tetramethyl silane
TRC-TEM	time-resolved cryo transmission electron microscopy
TRXRD	time-resolved X-ray diffraction
UV	ultraviolet radiation
Val	valine
VSV	Vesicular stomatitis virus
wt-HA	wild type haemagglutinin

Chapter 1: Introduction to Fusion

1. Introduction

1.1 The Importance of Fusion

Membrane fusion is an essential, ubiquitous life process. It occurs many times each day within every animal cell, where it plays a vital role in endocytosis, organelle formation, interorganelle trafficking, and constitutive and regulated exocytosis. Fusion between individual cells is also important as, for example, between sperm and egg during fertilisation. However, fusion is also associated with many disease processes: the entry into host cells of all enveloped viruses and many other intracellular parasites utilises this mechanism.

It is now widely recognised that the essential structural element of a biological membrane is the lipid bilayer. This stable configuration, described in the 'fluid mosaic' model of Singer and Nicolson (1972), is formed spontaneously by the assembly of amphipathic membrane lipids. The resulting structure is normally largely impermeable, and so the cell membrane controls the entry and exit of substances into and out of the cell. Cell fusion, the merging of the lipid bilayers of two distinct cells to form one common bilayer, and the mixing of the two cells' contents (Figure 1.1), is a means of overcoming these imposed restrictions. Membrane fusion is thought to be the central process in cell fusion, with the mixing of cell contents following passively thereafter.

Despite the clear importance of fusion, the precise events which occur during this process are still not fully understood. Diverse fusion reactions are known to differ in their biochemical control, location and required speed. The essence of any biological reaction is controlled change. Thus different biological fusion systems are thought to be catalysed by their own specific 'fusion' proteins, which initiate the multistep fusion pathway. An understanding of the mechanism of fusion requires that key structural fusion intermediates be identified and characterised. Since fusion is a very rapid and localised event, and as the dimensions of individual lipid molecules are below the resolution of the electron microscope, this has proved to be very difficult. Consequently, many of the current ideas on fusion have developed from theoretical calculations of the energetics involved in this process. These models of fusion have then been used in attempts to explain past and present experimental findings. The

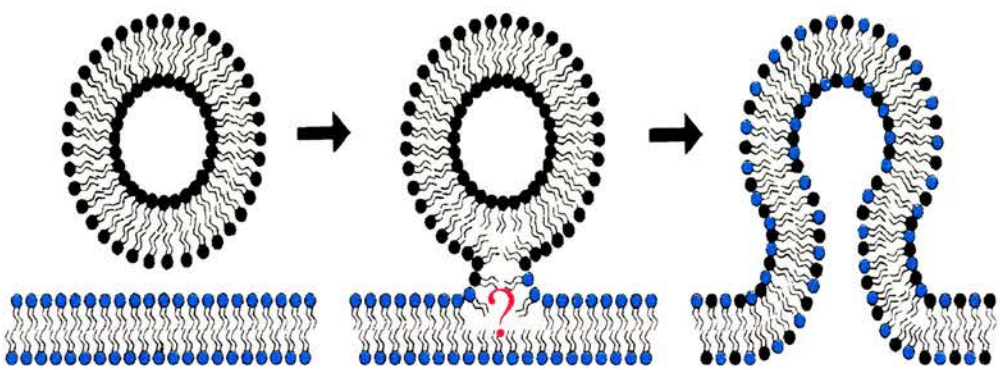

Figure 1.1. A general overview of the fusion process, as illustrated by fusion between a vesicle and a planar bilayer. Prior to fusion, the lipid molecules comprise two distinct bilayers. They then move through several unknown, intermediate conformations, to end as one common, stable bilayer conformation. Mixing of the aqueous contents of the two cells follows the initial steps in membrane fusion.

historical experimental and theoretical backgrounds are essential to an understanding of the current concepts of fusion.

1.2 The Role of Lipids in Fusion

1.2a. Non-bilayer Lipid Phases

Lipid-water systems are classed as lyotropic liquid crystals. 'Lyotropic' means that the systems have more than one component, for example lipid and water, while 'liquid crystalline' infers that they show crystalline periodicity in one, two or three dimensions, but that the lipid molecules are not locked in a rigid lattice and can diffuse freely. Thus these lipid arrangements are more ordered than a liquid but less ordered than a crystalline solid, hence their name. A phospholipid molecule has a polar headgroup, which prefers a polar water environment, and nonpolar hydrocarbon chains which, in contrast, aggregate to minimise contact with the polar solvent. This results in the spontaneous assembly of structures in which the lipid headgroups form a continuous interface between the hydrocarbon chains and the water. A lipid phase is such a macroscopically homogeneous arrangement at thermodynamic equilibrium. The bilayer, or lamellar, phase describes the stable and relatively planar configuration of biological membranes. A subdivision of the lamellar phase, L_α, represents lipid molecules at a temperature above that at which their chains 'melt' and the lipids gain an increase in mobility compared to that seen in the more rigid gel phase. *In vivo* biological membranes are in the L_α phase.

The ability of hydrated lipids to adopt a variety of different phases in addition to the bilayer phase is now well documented. It has long been known, since the pioneering work of Luzzati (Luzzati and Husson, 1962), that some phospholipids which are major components of biological membranes do not form lamellar phases in the purified form. Roughly 10-50% of membrane lipids will form non-bilayer phases in isolation (Cullis *et al,* 1985). These lipids assemble into a variety of different structures, or phases (see Figure 1.2).

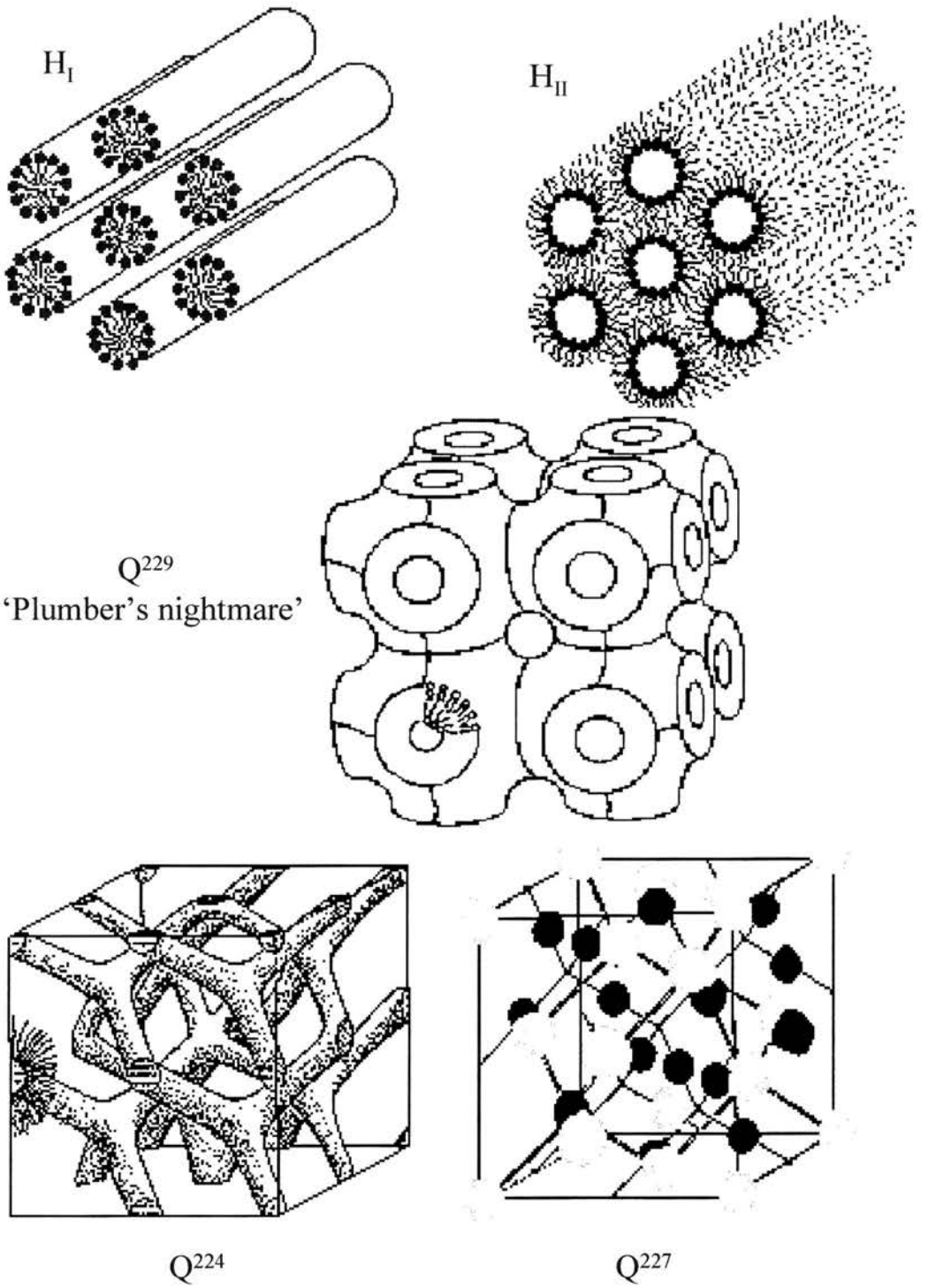

Figure 1.2. Important lipid phases: H_I, H_{II}, bicontinuous cubic phases Q^{229} and Q^{224}, and discontinuous cubic phase Q^{227}. In Q^{229} and Q^{224} two interpenetrating but unconnected water regions are separated by a single continuous lipid layer. In Q^{227} two discontinuous lipid micellar populations (shown as differently shaded micelles) are embedded in a matrix of water.

The inverted hexagonal phase

The inverted hexagonal (H_{II}) phase comprises lipid tubes which stack like pipes in storage (Turner and Gruner, 1992). In this arrangement, the lipid headgroups are directed towards the interior of the tubes and the hydrocarbon chains extend towards the outer surface. By convention, this lipid surface is defined as having a net negative radius of curvature (Tate *et al*, 1991) (see Figure 1.3). Positive curvature describes headgroup surfaces which curve towards the hydrocarbon region. In H_{II} the lipid headgroups are less exposed to the aqueous phase than in L_α: there is only a limited amount of water in the tubes. The L_α-H_{II} phase transition is thought to be important in fusion.

Cubic phases

Cubic (Q) phases are nonlamellar structures that some phospholipids form as a sidepath during the transition from L_α to H_{II} (Lindblom and Rilfors, 1989) (see Figure 1.4). This is consistent with the curvature sequence of phases, since the mean curvature of the headgroup surface in Q phase lies between those of the L_α and H_{II} phases (Gruner *et al*, 1988). Electron microscopic evidence suggests that some biological specimens contain extensive domains of cubic structures (Landh, 1995). In some lipid systems, cubic phases can be induced by repeated cycling of the system above and below the L_α-H_{II} phase transition temperature, T_H. Q phases represent three-dimensional structures, the exact symmetry of which depends upon the components present and the conditions of the system. Bicontinuous cubic phases contain a pair of three-dimensional labyrinths of the same polarity, apolar for type I and polar for type II, which are mutually intertwined and unconnected, being separated from each other by a continuous, fluid self-intersecting septum of the opposite polarity (Vargas *et al*, 1992). Thus, although named bicontinuous, these phases are really 'quadricontinuous', since the monolayers on each side of the minimal surface and the two labyrinths are distinct (Tate *et al*, 1991). In the inverted versions, Q_{II}, the labyrinth interiors are coated by the polar lipid headgroups, and the lipid surfaces are saddle-like in shape, having a negative interfacial curvature. These

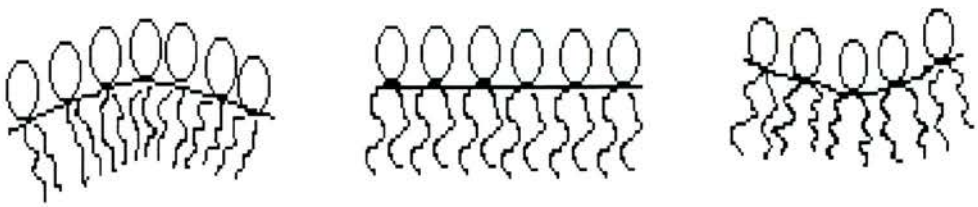

Figure 1.3 . Monolayer curvature. a: positive, b: zero and c: negative.

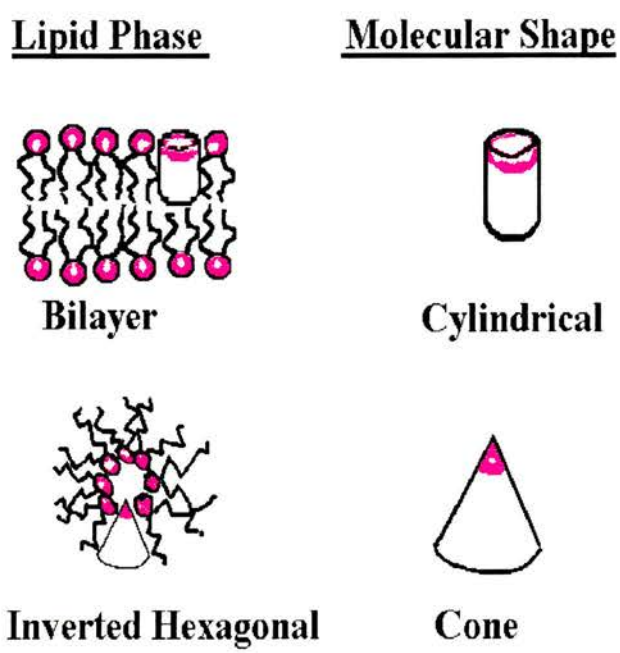

Figure 1.5. Model of preferential packing for lipids with different molecular shapes.

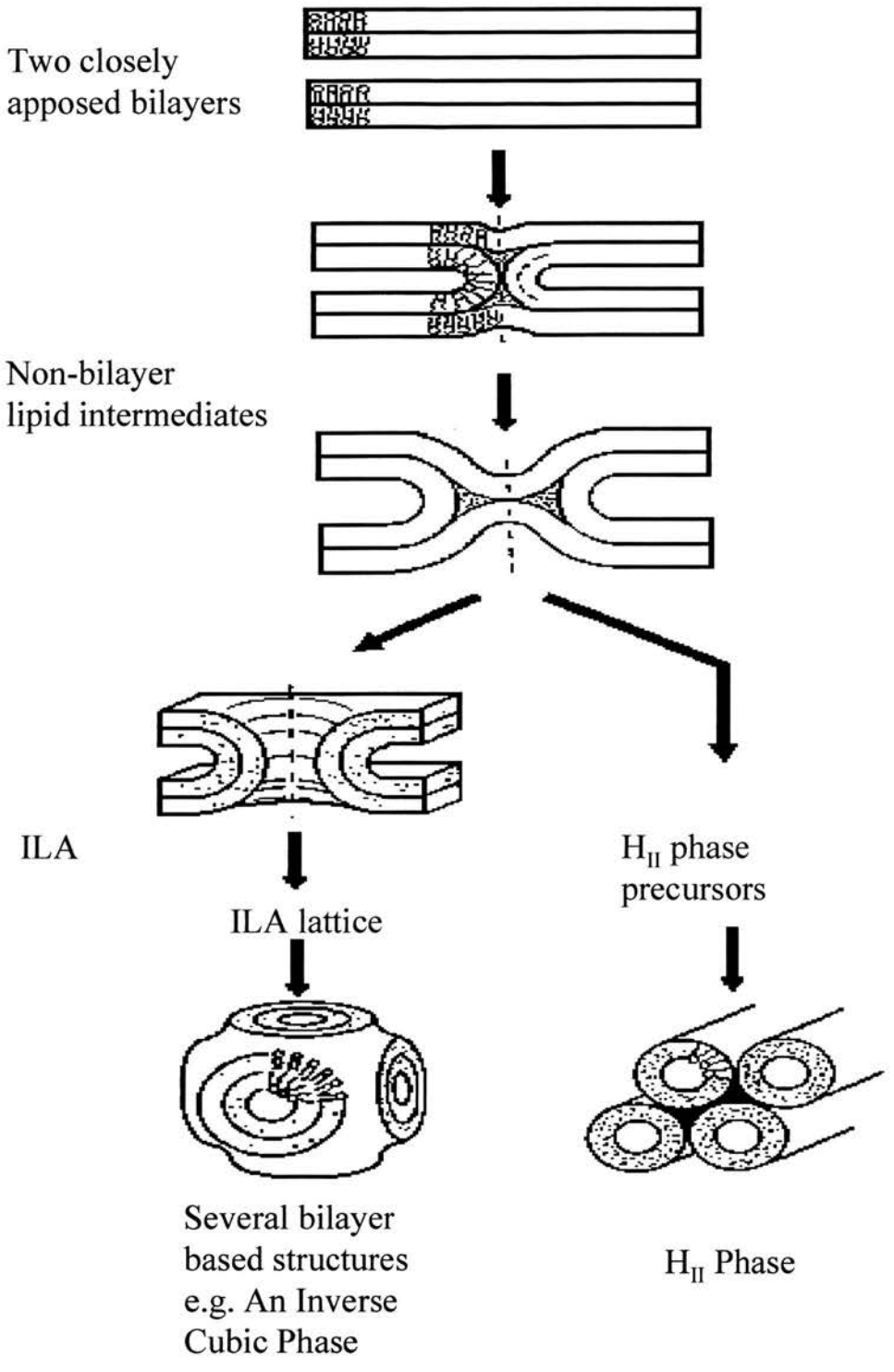

Figure 1.4. The relationship between cubic phases and the inverted hexagonal phase. Current theories suggest that the two pathways share common lipid intermediates early on in their formation. These early non-bilayer intermediates may also be involved in the fusion process (see text for details).

structures are like three-dimensional sponges, being highly permeable to both water- and hydrocarbon-soluble substances. Two important bicontinuous cubic phases are Q^{224} (spacegroup Pn3m), and Q^{229}, nicknamed 'Plumber's nightmare' (spacegroup Im3m). The other main group of cubic phases, discontinuous cubic phases, represents various complex packings of discrete micellar or inverse micellar aggregates, which are embedded in a continuous hydrocarbon matrix. These discontinuous phases are thus water impermeable. One such example is Q^{227} (spacegroup Fd3m).

Cubic phase structures were used by Luzzati *et al* (1993) to develop the 'patch the puncture' theory for repair of enzymatic attack on membranes. In this model, Q^{224} represents a lipid intermediate in the repair pathway, and Q^{227} a water-tight, end stage lipid conformation. Nieva *et al* (1995) have since successfully related this model to intermediate and end stages of membrane fusion.

Kinetically, cubic phases can be extremely stable, so that reversion to the L_α phase can be very slow. All cubic phases are seen to be highly viscous when compared to L_α or to H_{II}. This is probably due to the three-dimensional periodic structure: flow requires some elements to leave their energy troughs in the lattice.

Other lipid phases

Alternative lipid configurations include the H_I phase and rhombic phases. These are not currently implicated in the fusion process. The H_I phase consists of lipid molecules arranged in stacked rods like H_{II}, but in H_I the lipid headgroups face outwards and the acyl chains lie on the insides of the tubes. H_I is not normally observed for diacylphospholipids, but it is formed by lysolipids, which are known inhibitors of fusion.

1.2b. Factors Affecting Lipid Phase Formation

Force and energy calculations to fit Luzatti's data led to the realisation that Van der Waals forces were not sufficient to account for phase determination or lipid hydration (Parsegian and Ninham, 1971). Lipid phase formation is due to the balance of lateral forces that exist across a lipid bilayer. These consist of steric repulsions

between the lipid chains and the lipid headgroups, tension acting at the lipid-water interface, and additional attractive and repulsive headgroup-headgroup interactions from components such as hydration, charge and residual hydrogen-bonding (Seddon, 1992).

The molecular 'shape' concept

Israelachvili *et al* (1980) suggested that these various effects give rise to a preferred 'molecular shape' for a lipid molecule, which explains phase preference (see Figure 1.5). In greatly simplified terms, 'cylindrically shaped' lipids, such as diacyl phosphatidylcholines (PCs), whose headgroups and acyl chains are usually of approximately the same diameter, would prefer the bilayer phase, whilst 'cone-shaped' lipids such as diacyl phosphatidylethanolamines (PEs), which often have headgroups of smaller diameter than their acyl chains, would favour the H_{II} phase. Similarly, an increase in the unsaturation of the fatty acid chains, which increases the volume of the chain region, would promote H_{II} formation. It has been shown that PEs and unsaturated fatty acids do indeed promote the formation of H_{II} (Cullis *et al*, 1991; Epand *et al*, 1991).

This molecular 'shape' affects the lipid's critical packing parameter (CPP), which is described by the equation:

$$CPP = \frac{v}{al} \qquad 1.1$$

where v is the hydrocarbon volume, a is the optimal surface area at the hydrocarbon-water interface, and l is the critical chain length, or the maximum length a molecule can extend in a direction perpendicular to the plane of the bilayer. Under a given set of thermodynamic conditions (temperature, hydration etc.) a specific lipid molecule will generally have a preferred interfacial area per molecule, a preferred interfacial monolayer mean curvature, and a preferred interfacial Gaussian curvature. (The Gaussian curvature is the product of the two principle curvatures at a common point on a lipid surface). These effects compete with geometric packing constraints and

interactions transverse to the lipid bilayers (for example, hydration, electrostatic, van der Waals and fluctuation forces) to determine which phase is the thermodynamically stable one. Thus, for example, an increase in the water content (increased hydration force), or in the length of the acyl chains present (increased hydrophobic forces), or in the headgroup ionisation (increased electrostatic repulsion) will act to stabilise L_α. Conversely, an increase in the temperature of the system, and thus in lipid chain motion (increased monolayer negative curvature), will favour H_{II}. This is shown by the conversion of many phospholipid systems from L_α to H_{II} as the temperature of the system increases. A summary of these different effects is shown in Figure 1.6. The combination of all these individual factors produces characteristic phase transition temperatures for a given lipid system under a standard set of thermodynamic conditions.

Lipid monolayer intrinsic curvature

A more quantitative formulation of the 'shape' concept involves a determination of the free energy per molecule when it occupies a given molecular volume of a given shape.

Helfrich (1973) introduced the concept of intrinsic, or spontaneous, curvature of a lipid monolayer. This describes the monolayer's shape in a stress-free state, and thus relates the stress profiles of the monolayers to elastic moduli. Thus the free energy depends not only upon what shape the monolayer is in, but also upon the shape that represents its minimum energy state. For a lipid monolayer, this can be thought of as the shape it would assume if the headgroups were hydrated with water and the terminal methyl groups were surrounded by a nonpolar solvent (Epand *et al*, 1995). Deviations away from the preferred values of area or curvature will have associated elastic energy costs. Kirk *et al* (1984) successfully formulated the L_α-H_{II} transition by dividing the free energy into components arising from the elastic bending of the lipid monolayers and the hydrocarbon packing energies. Similarly, Gruner (1985) developed a more accurate and quantitative description of phase equilibrium, describing it as a competition between the elastic free energy of a lipid monolayer and the hydrocarbon packing constraints. This elastic free energy describes the tendency

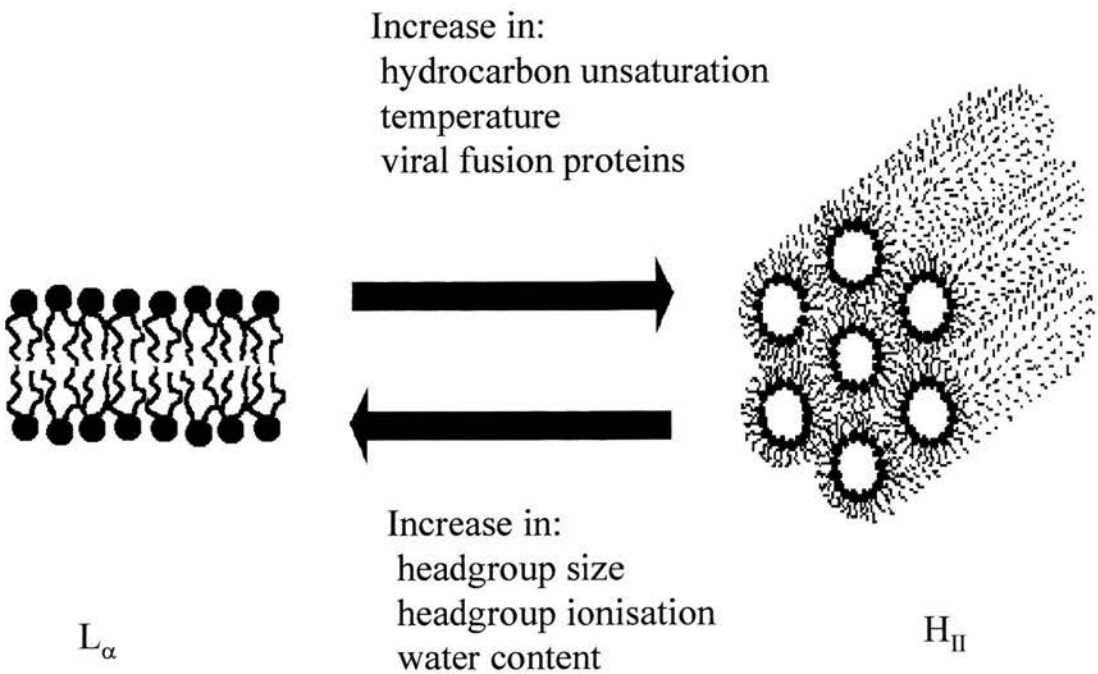

Figure 1.6. Factors that influence the L_α to H_{II} phase transition.

of the monolayer to bend to form a curved surface with an equilibrium radius of curvature, called the intrinsic radius of curvature, R_0. The smaller R_0 is, the greater is the instability of the bilayer structure, and also the tendency to form phases such as H_{II}. Generally the preferred phase adopted is a compromise, and some degree of physical 'frustration' remains (Anderson *et al*, 1988).

It is not possible to calculate R_0; it must be determined empirically. However, Marsh (1996) has recently suggested a new expression for the intrinsic curvature of a lipid monolayer in terms of a novel lipid packing parameter: V/Al, where V is the volume of the entire lipid molecule, l is its length and A is the area of the lipid headgroup at the lipid-water interface. It remains to be seen if this new parameter stands up to rigorous testing.

There is much experimental support for the overall concepts just described. As an example, Kozlov and co-workers (1994) used well-defined osmotic stresses to control the L_α-H_{II} phase transition, and to measure how much work this flat-to-negative curvature transition takes. They found that the required bending energy dramatically depended upon the type of lipids present in the monolayer, with increasing amounts of PE reducing this considerably.

1.2c. Non-bilayer Lipid Phases in Fusion

It was quickly realised that non-bilayer phases might have important biological structural and functional roles. Cells carefully control the ratio of 'bilayer' to 'non-bilayer' lipids present in their membranes. A number of prokaryotes alter the lipid compositions of their membranes depending upon their growth conditions. This alteration results in the membrane adjusting its properties so that it remains as a bilayer, but it lies close to the L_α to H_{II} phase boundary, suggesting that this composition is important. Wieslander (1996) proposed this for *Acholeplasma laidlawii* and it has also been found for other prokaryotes. Non-bilayer phases have now been implicated in a variety of biological processes.

Lucy (1970) first suggested that the fusion mechanism might involve a lipid phase change. Indeed, the structural analysis of fusion between liposomes began with

studies of lipid phase behaviour (Papahadjopoulos *et al*, 1977). Fusion of pure lipid bilayers is sensitive to the presence of non-bilayer lipids, and a variety of nonlamellar assemblies have been proposed as fusion intermediates. During fusion there must be a transient disruption in bilayer structure to permit lipid mixing, and to allow the fusing monolayers to bend.

Phases such as H_{II} are unlikely to participate directly in fusion. Early suggestions were made that the H_{II} phase might be involved (Cullis and Hope, 1978), but H_{II} is a thermodynamically stable and relatively long-lived phase, and fusion is an extremely rapid process, which may occur within a few microseconds (Almers and Tse, 1990). Potential candidates for intermediate structures in the fusion pathway must, therefore, be short-lived. Since the L_α and H_{II} phases are of very different topologies, the phase transition between the two must involve tearing and reorganisation within the lipid bilayer. Theoretically, the cost in free energy must be high, imposing a large kinetic barrier. The kinetics of the L_α-H_{II} phase transition are indeed very slow close to the phase boundary (Tate *et al*, 1992): time-resolved X-ray data that were collected for several PE-water systems showed the coexistence of L_α and H_{II} phases that exhibited well-ordered lattices throughout the transition period, under slow transition conditions. This indicated that the sample material could reorder itself in a shorter time than the transition time, and suggested that it is indeed a large kinetic activation energy barrier that limits the transition in this régime. Finally, there cannot be extensive formation of H_{II} in biological membranes, since this would result in a breakdown of the cell's permeability barrier.

It is probable that it is the tendency towards inverse phase formation that is the important factor in the fusion process, rather than the actual formation of these phases. Epand *et al* (1987) correlated the inhibition of membrane fusion by some compounds with their ability to increase T_H. Similarly, several known fusogens have been shown to lower T_H (Epand and Epand, 1994; van Gorkom *et al*, 1992; Siegel *et al*, 1989a). The tendency towards H_{II} phase formation will result in a less stable bilayer structure with a more hydrophobic surface, which can more readily attach to another hydrophobic membrane surface.

Work on fusion of large unilamellar vesicles (LUVs) composed of N-monomethyldioleoylphosphatidylethanolamine (MeDOPE) and PE/PC mixtures directly correlated the appearance of nonlamellar structures with initial fusion rates (Ellens *et al*, 1989). This suggested that the nonlamellar structures might be intermediates in the fusion pathway, or that they might be formed from an intermediate shared with the fusion pathway. Since the detected nonlamellar structures were not transient, and the kinetics of formation of the nonlamellar structure in MeDOPE have been shown to be slow relative to the initial rates of fusion (van Gorkom *et al*, 1992), it is more likely that these observed structures utilised a common intermediate with the fusion pathway.

As mentioned earlier, cubic phases can form as a sidepath in the L_α-H_{II} phase transition. It has been suggested that cubic phases, or cubic-like structures, are intermediates in membrane fusion. Thus diacylglycerol (DAG) promotes both fusion between LUVs and also the formation of cubic phases (Basáñez *et al*, 1996). The cubic phase is an extremely stable thermodynamic phase, so its direct participation as a fusion intermediate seems very unlikely. However, the fusion pore, the end stage of fusion, bears a remarkable similarity to the local structure of the inverse Im3m bicontinuous cubic phase Q^{229} (Ellens *et al*, 1989).

If these ideas are correct, it should be possible to inhibit fusion with agents which spontaneously partition into a membrane and which contain polar groups that will make the membrane surface more hydrophilic, and thus stabilise the bilayer phase. Thus cholesterol sulphate inhibits model membrane fusion, fusion of Sendai virus to ganglioside-containing liposomes, and Sendai-induced haemolysis (Cheetham *et al*, 1990). Moreover, sperm have high concentrations of cholesterol sulphate, and its hydrolysis is thought to play an important role in the capacitation reaction that is required for mammalian sperm-egg fusion (Langlais *et al*, 1981).

Further support comes from the observation that lysophosphatidylcholine (LPC), whose headgroup has a very large diameter in comparison to that of its single lipid tail, is a bilayer-stabilising lipid. Addition of exogenous LPC to a wide variety of fusion systems causes fast, dose-dependent and potent inhibition of fusion, which is reversible upon withdrawal of the lipid. Fusion reactions affected include:

1. syncitium formation caused by low pH and either Influenza haemagglutinin (HA) or baculovirus gp64 (Zimmerberg *et al*, 1995) ;

2. fusion between Sendai virus and liposomes (Yeagle *et al*, 1994) ;

3. myoblast fusion (Schudt and Pette, 1976) ;

4. calcium-triggered exocytosis of either sea urchin egg cortical granules or digitonin-permealised bovine chromaffin cells (Zimmerberg *et al*, 1995);

5. mast cell degranulation triggered by GTPγS (Zimmerberg *et al*, 1995);

6. protein trafficking between successive cisternae of the Golgi stack (Glick and Rothman, 1987);

7. rat endoplasmic reticulum fusion mediated by GTP (Zimmerberg *et al*, 1995);

LPC also inhibits the redistribution of fluorescent membrane dye between fusing membranes. This inhibition of fusion cannot be ascribed to any specific chemical group; zwitterionic LPC, lysoPE, negatively charged lysophosphatidylserine and lysophosphatidylinositol and a set of LPCs of varying length of chain and degree of unsaturation all had similar effects on fusion (Chernomordik *et al*, 1993). However, caution should be used in ascribing all of the effects of LPC to membrane changes; recent work by Günther-Ausborn and co-workers (1995) suggests that LPC inhibits the binding of Influenza virus to liposomal membranes, and that this effect is due to non-membrane-bound LPC. Thus free LPC must be washed away before starting experiments, and this factor must be considered when looking at results obtained in some of the previous LPC studies.

Obversely, *cis*-unsaturated fatty acids, such as arachidonic acid or oleic acid, which have previously been shown to act as H_{II} promoters, do enhance fusion. This effect has been found in a number of situations, for example low pH syncitia formation by baculovirus (Chernomordik *et al,* 1995a), fusion between endosomes (Mayorga *et al,* 1993), Ca^{2+}-triggered fusion of chromaffin granules (Creutz, 1981) and GTP-dependent fusion of microsomes (Paiement *et al*, 1994). Furthermore, Bailey and Cullis (1997) have correlated liposome fusion rates with an increase in the unsaturation of the PE acyl chain, and thus the tendency towards inverted phase formation. The replacement of PC, a bilayer stabiliser, with PE, an H_{II} promoter, also promotes virus-liposome fusion (Hoekstra and Kok, 1989). Although the precise

monolayer composition of myoblast membranes is not known, lipid changes do occur just before fusion (Santini *et al*, 1990; Santini *et al*, 1991). The amounts of PC and phosphatidylinositol (PI) decrease, whereas PE, cholesterol and phosphatidic acid levels all increase. Agents that delay fusion delay these changes in lipid composition. Finally, DAG promotes both H_{II} phase formation and fusion (Siegel *et al*, 1989a, 1989b; Basáñez *et al*, 1996).

These findings suggest that the tendency to form non-bilayer lipid phases is important in a very diverse range of fusion reactions. Phase transitions between L_{α}, Q and H_{II} appear to occur by the formation of discrete intermediate structures. Verkleij *et al* (1979) first observed such intermediates near the L_{α}-H_{II} boundary using freeze-fracture electron microscopy (FFEM). These were called 'lipidic particles', and thereafter have been observed frequently (eg. Hui *et al*, 1981; Hui *et al* 1983; Gagné *et al*, 1985). Several different structures have been suggested for lipidic particles, but, to date, their structure has not been established unequivocally. Cryo-electron microscopy also revealed the interlamellar attachment (ILA) (Siegel *et al,* 1989c), which is a semi-toroidal (tyre rim-shaped) attachment between flat bilayer sheets. Thus ILAs have been directly imaged, but once again, the precise molecular structure is unknown. The first step of the L_{α}-Q phase transition may be the formation of an ordered array of ILAs: Siegel (1989c) found, using time-resolved cryo transmission electron microscopy (TRC-TEM), that ILAs appear to mediate both fusion and the L_{α}-Q phase transition. This supports Ellens and co-workers findings that membrane fusion and inverted cubic (Q_{II}) phase formation occur via the same structure (Ellens *et al,* 1986; Ellens *et al*, 1989). Their results also show that, for MeDOPE, lipidic particles are ILAs, and suggest that, in the temperature range where ILAs are formed, fusion is an obligatory step in the L_{α}-Q_{II} phase transition for this lipid system. It has also been suggested that ILAs may correspond to the 'stalks' mentioned below.

Siegel and Epand (1997) have very recently studied the L_{α}-H_{II} transition. They found evidence that this transition occurs in at least three steps:

1. Many small connections form between apposed membranes.
2. The connections aggregate within the planes of the bilayers to form arrays with hexagonal order in some projections.

3. These quasi-hexagonal structures elongate into small domains of H_{II}, acquiring molecules by diffusion from contiguous bilayers.

The non-lamellar morphology they observed by cryo-TEM was transient, with a lifetime of minutes or less.

Theoretical models (e.g. Siegel, 1993) also show successive formation of transient and local non-bilayer intermediates along the fusion pathway, the energetics of these intermediates depending upon the bending elastic energy of the lipid monolayers. Siegel and Epand (1997) suggest that the lipid intermediates observed in the L_{α}-H_{II} transition agree well with the putative fusion intermediates of Siegel (1993).

Liposome fusion kinetics have also been correlated with lateral phase segregation of the different lipid constituents present (Bentz *et al*, 1987). This allows for the possibility of production of local domains of inverted-phase promoting, and thus fusion enhancing, lipid molecules.

A putative model of the overall relationship between fusion and lipid phase changes is shown in Figure 1.7. Certainly experimental work on lamellar/inverted phase transitions has greatly improved our understanding of the relative stability of lipid structures of different geometrical structure.

1.2d. Lipid Fusion Mechanisms

It will not be possible to determine logically the mode of action of fusion proteins until we understand the energetic and conformational changes of the lipid molecules present in the two apposed and fusing bilayers. If we appreciate the fusion mechanisms of pure lipid systems we may then identify methods by which proteins can catalyse similar processes under different conditions, and also what type of protein structures would be the most effective catalysts.

Biological fusion is driven mainly by proteins, but there is a fundamental stage of actual membrane merging which may be regulated by the properties of the lipid bilayers. Thus, exogenously added lipids do not need to be present during the triggering stage for fusion to be affected: lysolipids and *cis*-unsaturated fatty acids

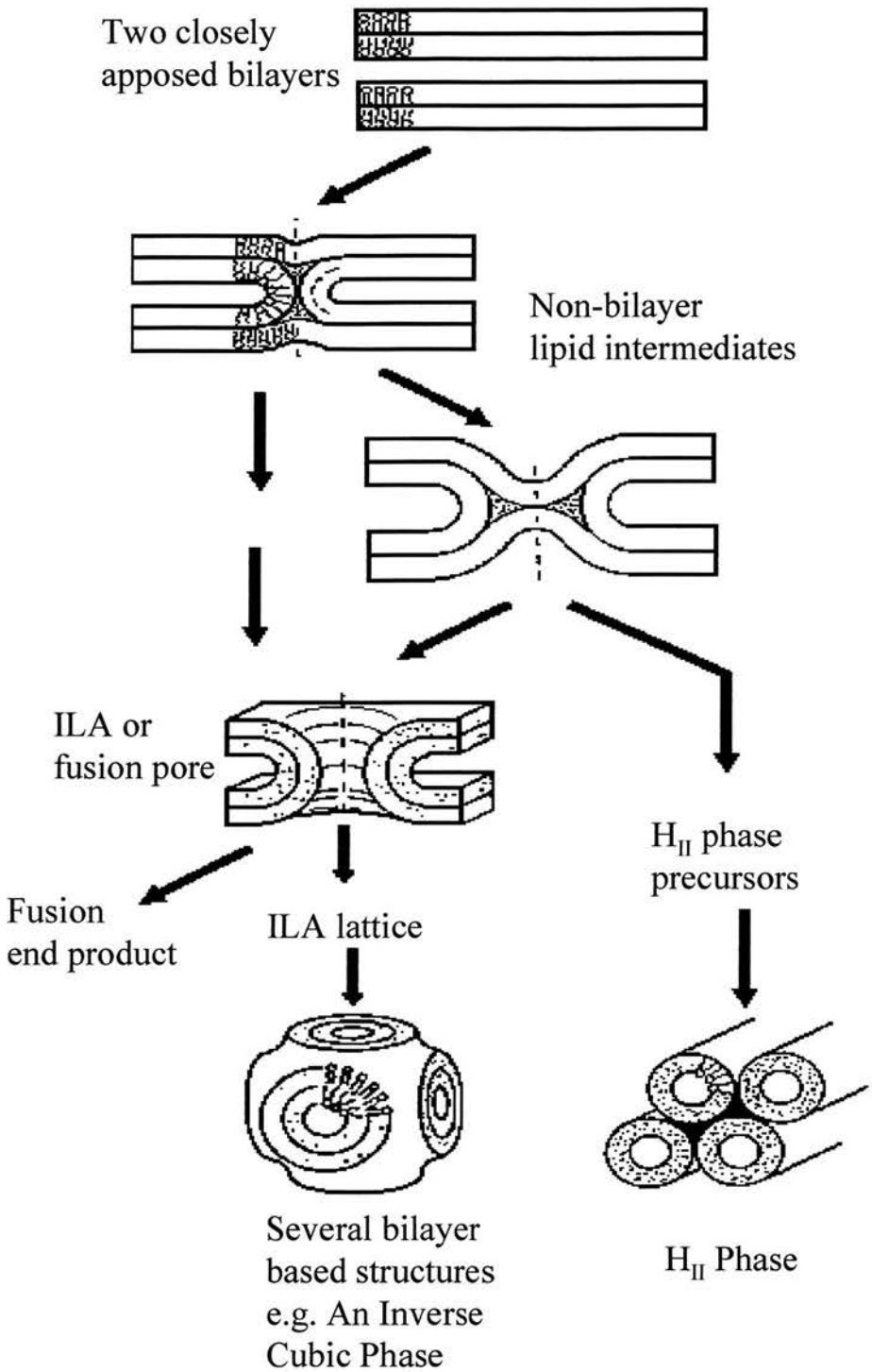

Figure 1.7. The relationship between fusion and non-bilayer phases. Fusion and cubic phase formation are thought to share common early lipid intermediate structures. The precise pathway followed will depend upon the constituents and the thermodynamic conditions present.

respectively inhibit and promote baculovirus-mediated fusion even when added immediately after application of a low pH pulse (Chernomordik, 1996). Lipids therefore appear to affect fusion downstream of the triggering process, which explains why, at this particular stage, different biological and model fusion reactions may converge to common lipid structural intermediates, driven by similar forces. Lipid composition can thus determine whether or not an activated complex proceeds to complete fusion. Fusion of pure lipid bilayers can model biological fusion in lipid sensitivity and, hopefully, in the intermediates involved. The use of such model systems allows control of the total lipid composition of the component membranes, and also independent alteration of this in the different monolayers of the fusing membranes. Thus many theoretical calculations and much experimental proof for the various fusion hypotheses have come from the use of such systems, which may be based on fusing planar lipid bilayers and/or liposomes. Liposomes are lipid bilayers enclosing an aqueous compartment, so they are good models of simple cells. They allow manipulation not only of the lipids present, but also of the aqueous contents. Thus by labelling membrane lipids with fluorescent dye, and by enclosing aqueous fluorescent dyes, or polymers such as dextran, or ions such as H^+, within the liposome, it is possible to follow the mixing of lipids and the mixing of contents as separate processes, any leakage that occurs, and also the formation of intercellular pores. This helps to reveal the sequence of individual steps in the fusion process. The kinetic analysis of fusion, based mainly on the use of these fluorescent markers, is now well developed (Nir *et al*, 1980; Bentz *et al*, 1983, 1985, 1988; Ellens *et al*, 1984). The findings from these experiments can then be compared with results obtained by electron microscopy and with biophysical data for the same lipid systems, in an attempt to relate observed lipid structures and changes in lipid conformation and motion to individual, kinetically-discernible steps in the fusion process.

Many fusion mechanisms have been proposed. Bentz and Ellens (1988) suggested that the overall process of membrane fusion required at least three steps:

1. The close approach of the fusing membranes.
2. The formation, at least transiently, of higher energy, highly bent lipid structures that involve non-bilayer assemblies.

3. The mixing of membrane components to fuse into one common membrane.

Close membrane approach

Close approach requires membrane dehydration (Rand, 1981). Phosphatidylserine (PS) bilayers are known to form dehydrated contacts in the presence of Ca^{2+} ions, which are proven fusogenic agents for liposomes composed of this lipid (Bentz *et al*, 1985). Thus it seems that, for some systems at least, the first step in fusion is governed by hydration forces (Rand and Parsegian, 1989), more specifically by the need to remove tightly bound water molecules from the lipid headgroups. An estimation of the work required to bring two 300Å unilamellar vesicles to within a separation of 13Å yields a figure of the order of $10kT$, which corresponds to a statistical weighting of 10^{-4} against this mutual approach (Lis *et al*, 1982; Parsegian *et al*, 1979). This will be affected by the lipids present. Cholesterol can facilitate, or may even be essential, for liposome/viral fusion processes (Asano and Asano, 1988; Gollins and Porterfield, 1986; Hoekstra and Kok, 1989; White and Helenius, 1980). Cholesterol also promotes fusion of secretory granules with liposomes (Vogel *et al*, 1992). Furthermore, the lipid envelopes of viruses, which one might expect to be specialised for fusion, are known to be rich in cholesterol (Klenk, 1973). Cholesterol may modify repulsions between adjacent membranes by interfering with the organisation of interfacial water, since it decreases the depth to which water penetrates into a lipid bilayer (Simon *et al*, 1982). It may also reduce steric repulsions between membranes due to its ability to spread the lipid headgroups further apart in the bilayer (McIntosh *et al*, 1989).

PE can hydrogen bond to adjacent lipids through its amino and phosphoryl groups, whilst the PC headgroup lacks a group that can act as a hydrogen bond donor, and so it is expected to interact more strongly with water than does PE. Thus bilayers that are rich in PE can dehydrate and aggregate more readily than can bilayers rich in PC (Seddon *et al*, 1983; Chang and Epand, 1983). Partial phase separation, with the accumulation of more weakly hydrated lipids, like PE, in the fusion region might reduce the hydration barrier. A large body of evidence indicates that biological membranes are indeed laterally structured. Recently, Lehtonin (1996) found domain

formation in certain lipid mixtures. He suggested that hydrophobic mismatch is the cause of this microdomain formation for lipids in fluid, liquid crystalline bilayers. Thus, in membranes containing lipids with large variations in hydrophobic thickness (such as biological membranes), the minimum energy state of the system is represented by enrichment of its short chain and long chain constituents into microdomains, to avoid exposure of hydrocarbons to water, and to minimise the length of domain boundaries. Close approach may also require local defects in lipid packing, which will result in some exposure of hydrophobic surfaces in the membrane (Bentz and Ellens, 1988; Rand, 1981).

Clearly the large hydration barrier will prevent mutual close approach of membranes in any significantly large area, since the energy necessary to overcome repulsion is proportional to the area of close contact. Local bending of the membranes will decrease this mutual repulsion. It has been suggested that membrane bending may be produced by out-of-plane thermal fluctuations of the apposed bilayers (Leikin *et al*, 1987). Certainly, the diameter of the membrane contact region prior to fusion has been shown to be small: approximately 10nm (Chandler, 1984; Siegel and Epand, 1997).

The definitive answer to the question of the mechanism by which the hydration barrier is overcome is still elusive. It seems likely that it will vary amongst different fusion systems, depending upon the specific components present in each individual process.

Formation of lipid fusion intermediates

It is unlikely that a fusion pore, the end stage of membrane fusion, would be formed by a single catastrophic rearrangement, involving energy-intensive rearrangements of a large number of molecules, since the activation energy required would be prohibitively large. Much more likely is the concept of fusion occurring through the formation of one or more discrete intermediate structures, which would have continuous lipid-water interfaces with no free monolayer or bilayer edges. Thus each intermediate could preserve some of the equilibrium structure of the original bilayers, and hence reduce the number of molecules that need to be perturbed in order

to be converted to the next step in the fusion pathway. Fusion could then occur at an overall faster rate by means of successive stages that required lower activation energies. Intermediate formation is likely to be co-operative, since large perturbations made to one lipid molecule will substantially change the energy required to perturb its neighbour. It is logical to assume that the structures which require the least activation energy would be the most likely to occur.

The difficulties involved in the direct visualisation, in any great detail, of the tiny, localised and extremely transient fusion intermediates has led to the proposal of a variety of possible structures. Two main fusion pathways have been proposed as a result of these ideas, one involving micellar intermediates, and the other utilising a stalk-like structure. Lucy (1970) envisaged the formation of normal micelles at fusion sites. Siegel (Siegel, 1984) then modelled the fusion pathway using inverted micellar intermediates (IMIs) (see Figure 1.8). IMIs had, theoretically, the required short lifetimes and the structural ability to mix the lipid components of the two opposing bilayers. However, IMI formation seems to be very unlikely for a wide range of membrane compositions. Siegel (1993) subsequently showed, using calculations of free energy, that IMIs are unlikely to take part in most fusion mechanisms, even in the vicinity of the L_{α}-H_{II} phase transition, where IMI formation would be easiest.

Hemifusion, the merging of the two outer membrane leaflets only, has long been suggested as an intermediate in the fusion pathway (Palade, 1975; Pinto da Silva and Nogueira, 1977). Theoretical calculations led to the proposal of 'stalks' as achievable fusion intermediates (Markin *et al*, 1984; Chernomordik *et al*, 1987) (see Figure 1.9). Very little activation energy was thought to be required to achieve this state, and the IMI free energy was shown to be higher than that of the stalk, for all values of marginal radius (Siegel, 1993). Also the stalk's lifetime could be sufficiently short for it to act as a candidate for a fusion intermediate. Stalks could form a subsequent fusion intermediate much faster than IMIs (Siegel, 1994).

A stalk is a neck-like, or semi-toroidal, local connection between the outer, contacting monolayers of two fusing membranes, which thus become continuous. The best analogy for its shape is the waist of an hourglass, and its radius is comparable to the length of a component lipid molecule. Stalk formation is thought to occur

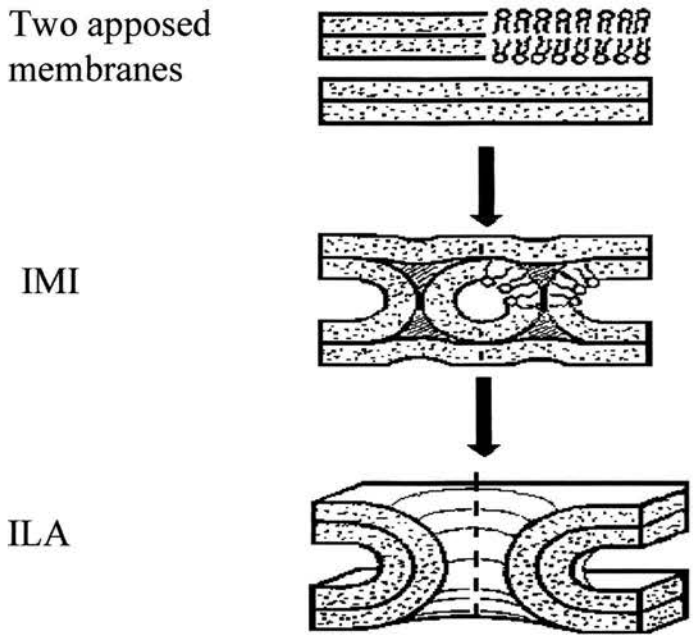

Figure 1.8. Inverted micellar intermediate (IMI) formation as a fusion mechanism. IMIs are cylindrically symmetrical about the vertical midline axis, and are composed of cylindrical micelles inside a semitoroidal outer monolayer. For certain values of R_0, IMIs can transform into interlamellar attachments (ILAs), or fusion pores, thus fusing the two monolayers.

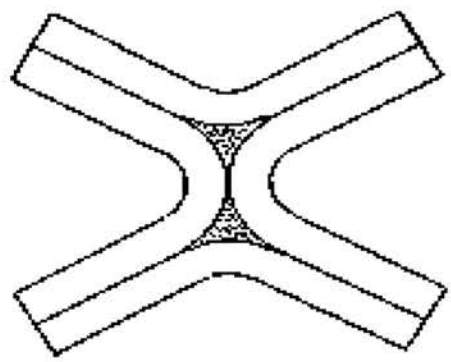

Figure 1.9. The basic stalk model for a fusion intermediate. The upper and lower stalk surfaces are formed from the original inner monolayer leaflets of the two apposing membranes, whilst the stalk sides comprise the original outer or contacting monolayers. The stalk is cylindrically symmetrical about the midline vertical axis.

following transient point contact between the two apposed membranes. Monolayer rupture is related to the competition between the hydration forces and the hydrophobic energy of contact between the monolayer interior and water. At small distances between membranes the energy of hydration repulsion becomes so large that it is energetically more favourable to replace it by the hydrophobic energy required to rupture the contacting monolayers. Thus stalk formation leads to a hemifusion stage, in which fusion of contacting monolayers occurs without merger of inner, or distal, monolayers.

Stalks are hard to visualise due to their low image contrast; they are calculated to have a diameter of only ~4nm at their narrowest point, which is the minimum possible diameter, being the thickness of a bilayer. Most of the total free energy of the stalk is associated with this waist. In general terms, the larger the spatial extent of a structural change the more slowly it occurs. We know that fusion is a very rapid process, so the rate-limiting step(s) should logically involve as small a structure as possible.

The original stalk theory calculated its free energy by assuming that the main contribution came from the elastic bending of the contacting monolayers of the two membranes. Stalks have a net negative curvature, and the spontaneous curvature of the contacting monolayers should determine the energy of the stalk, its formation and expansion. Certainly, the effects of membrane composition on lipid bilayer fusion are consistent with the hypothesis that the rate-limiting intermediates of membrane fusion have net negative curvature. The stalk hypothesis was based on morphological studies (e.g. Hui *et al*, 1981; Markin *et al*, 1984) and theoretical analysis (e.g. Kozlov and Markin, 1983; Chernomordik *et al*, 1987).

The original stalk model has recently been modified by Siegel (1993). This modification includes the possible contributions of hydrophobic void spaces within the intermediate (Figure 1.10). Formation of any intermediate structure between two membranes has to be accompanied by the peeling apart of the hydrophobic sides of lipid monolayers, thus creating hydrophobic voids within the intermediate. This creation of voids is similar to the packing problem seen for H_{II}, in which voids are created between the individual lipid cylinders. These must be filled by the intercalation

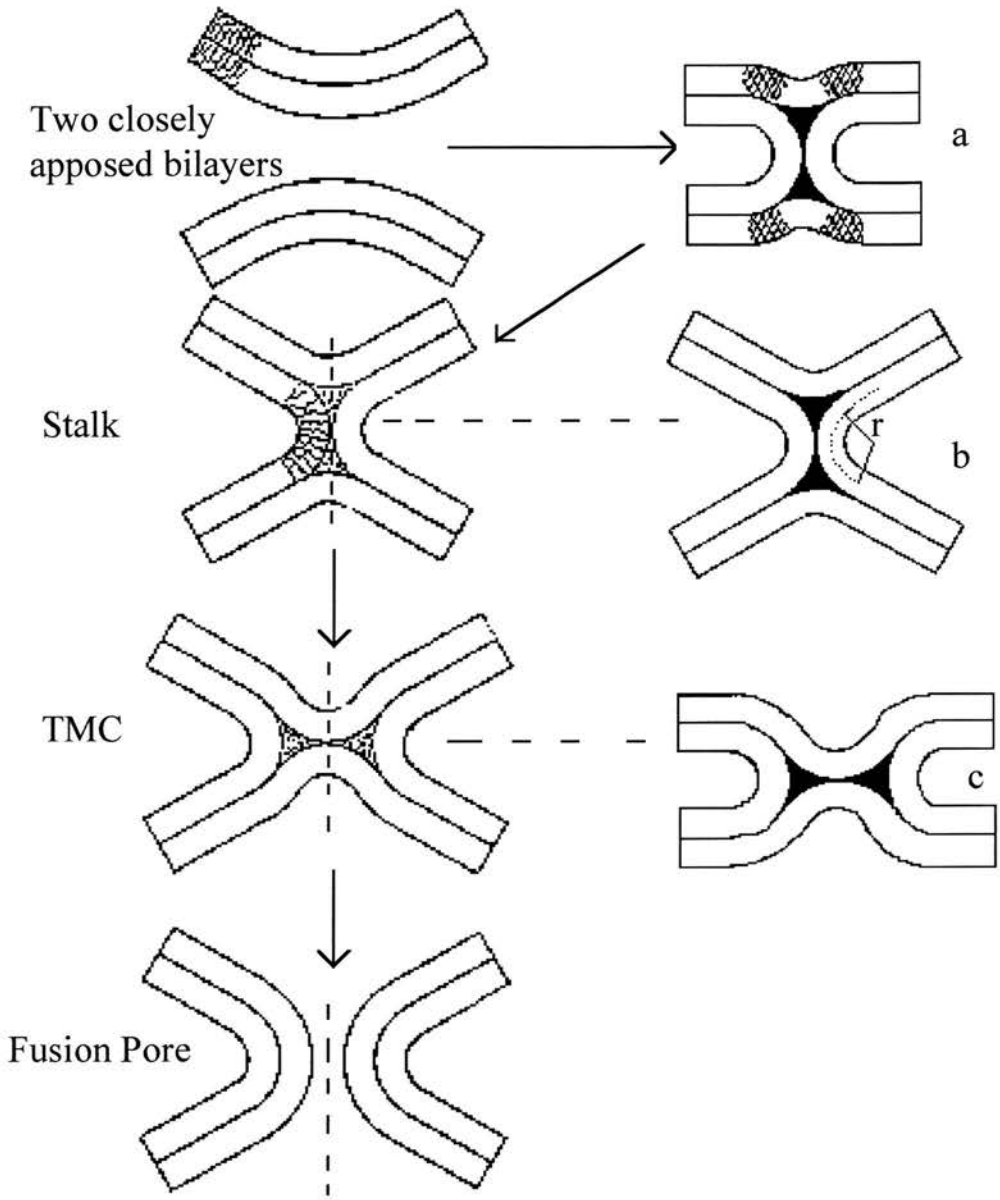

Figure 1.10. Modified stalk mechanism of fusion. This takes into account the energy contributions caused by the formation of hydrophobic voids, shown as filled black areas in a, stalk b and TMC c. The effect of dimpling of the inner, or distal, monolayers during stalk formation, as shown in a, is also considered in this model. a is an early, stalk-like conformation. The marginal radius, r, of the stalk is shown in b.

of the lipid acyl chains. The larger the H_{II} tube diameter, the larger are the voids that must be filled. Seddon (1990) and Tate *et al* (1991) successfully rationalised the relative stabilities of the L_α, Q and H_{II} phases in excess water by purely considering R_0 of the constituent monolayers and the free energy associated with the hydrophobic packing voids present. Moreover, the void energy contributions may explain the observed effects of traces of hexadecane on fusion rates of anionic lipid systems (Walter and Siegel, 1993): hexadecane is a fusion promoter, and it can partition to fill, and thus reduce in size, these voids. These findings led Siegel (1993) to suggest that a similar approach would be valid for continuous-monolayer intermediates in general, and thus for fusion intermediates.

Void energy may dramatically increase stalk energy, both directly and indirectly, by requiring the inner, or distal, monolayers to bend and dimple in order to reduce the void volume. Void energy may be very large if all of the lipid molecules in the bilayer are identical, but it will significantly decrease for model bilayers formed from lipid mixtures, and also in the presence of small amounts of impurities, such as neutral lipids or any lipids with longer hydrocarbon chains, which may fill the voids. Biological membranes surpass simple lipid membranes in their complexity. Thus the energy balance for a stalk connecting two biological membranes should differ from that of a stalk intermediate of lipid bilayer fusion. The energy of hydrophobic voids ought to be much less significant for biological membranes known to consist of complex mixtures of lipids, including apolar ones.

Another important modification of the original stalk model is the consideration of the effects of the geometry of the fusion site: as two membranes pucker towards each other, the contribution of the negative meridional curvature will decrease and the contribution of the positive parallel curvature will increase. Thus, deformation of the original membranes at the contact site not only affects the elastic energy of a stalk but may even change the sign of its net curvature from negative to positive.

Helm *et al* (1989) have developed a different model which suggests that the energy for lipid bilayer hemifusion comes solely from the long range attractive forces of the hydrophobic interiors of the membranes. However, they used supported planar

lipid bilayers which cannot undergo elastic deformation as easily as, for example, free liposomal lipids. No further evidence to support this theory has so far come to light.

The 'stalk-pore' model is based on minimising the free energy of the two highest-energy, non-bilayer intermediates, the stalk and the pore. Two mechanisms have been suggested to describe the conversion of the hemifusion intermediate into the complete fusion product. In the first, a slight radial expansion of the stalk results in the formation of a transmonolayer contact (TMC), so named because as the stalk radius increases, the distal, or trans, monolayers, which form the upper and lower stalk surfaces, dimple inwards and meet in the centre of the structure. Siegel (1993) showed that the amount of free energy required for this stalk-TMC conversion depends upon the marginal radius of the stalk, and R_0 of the system. For a certain range of values for these, the TMC will have a lower energy than the stalk, and TMC formation will be spontaneous. TMC formation is produced by continuous, slight deformations of continuous monolayers, so no great energy barriers exist between the stalk and the TMC. Once formed, the expansion of this TMC is constrained by the lipid comprising the outer membrane leaflets, which must have somewhere to go (Chernomordik *et al*, 1987). Since monolayers in the same membrane cannot lose contact with each other, stalk expansion results in the compression of the original contacting monolayers and the extension of the distal ones. This brings the contact bilayer under mechanical tension which in some cases may superimpose with pre-existing membrane tension. An additional constraint that may limit TMC expansion is the energy contribution of the hydrophobic void spaces within the intermediate (Siegel, 1993). If the void energy of the hydrophobic spaces in the TMC intermediate is very high, then it is quickly released by the spontaneous and direct formation of a fusion pore. Rupture of the dimpled monolayers to form a pore releases some of the curvature energy and all of the interstice energy. Alternatively, for certain values of R_0, and if the void energy is lower, the TMC will expand radially to produce an extended bilayer diaphragm (e.g. Chernomordik *et al*, 1995d). This then ruptures to form a fusion pore. In both lipid models, the walls of the pore are formed by the merger of the original distal monolayers of the membranes.

These postulated intermediates are consistent with models for the relative chemical potentials of the inverted phases (Kirk *et al*, 1984; Gruner, 1985; Gruner *et al*, 1986), and also with X-ray diffraction results (Tate and Gruner, 1987; Gruner *et al*, 1988), and they can explain most of the ^{31}P nuclear magnetic resonance (^{31}P-NMR), differential scanning calorimetry (DSC) and morphological data concerning these transitions (Siegel, 1993; Siegel and Epand, 1997).

Two successive bending deformations of membrane monolayers in opposite directions are required by this model: stalk energy will decrease with an increase in the negative spontaneous curvature of the outer membrane monolayer, whilst pore edge energy will decrease with a positive increase in spontaneous curvature for the inner membrane monolayer. Chernomordik *et al* (1985) studied hemifusion and pore formation in parallel for planar lipid bilayers of PE in the presence of different concentrations of LPC. The exponential increase in the waiting time of hemifusion, and the linear decrease in the linear tension of pores with LPC concentration, and even the actual ratio between the slopes of these dependencies were in quantitative agreement with the theoretical stalk model. Siegel (1993) has rationalised the mechanism of fusion catalysed by the Influenza virus fusion protein using the modified stalk model.

Biological membranes are dynamic structures with a lipid composition known to be very asymmetric and heterogeneous. If the 'stalk-pore' model is true, then to be ideally suited for fusion, membranes should be asymmetrical, with the contacting monolayers containing H_{II} phase-promoting lipids and distal monolayers containing micelle-forming lipids. PE is located predominantly in the outer monolayer of the secretory chromaffin granules (Zachowski *et al*, 1989), whilst the inner monolayer of these granules has a very significant amount of lysolipids in it; up to 17% of the total phospholipid (Voyta *et al*, 1978). The Golgi apparatus membranes contain 10% of lysolipids in their inner monolayers (Mutz and Helfrich, 1990). Thus the lipid asymmetry in these membranes, which are presumably specialised for fusion, is consistent with the predictions of the 'stalk-pore' model for 'ideally fusible' membranes.

In the final stage of membrane fusion the initially narrow pore subsequently widens to achieve complete fusion, when an aqueous pathway develops between the two initially distinct aqueous volumes. The pore tends to grow slowly, followed by a final fast expansion. The most sensitive assays for pore formation, electrophysiological recordings, allow the detection of a pore as soon as ions can pass through.

In the 'stalk-pore' theory the fusion pore is lined by lipid molecules. An alternative hypothesis for biological fusion is that the pore is lined by fusion protein molecules, which line up around the pore and present hydrophilic surfaces to the aqueous pore channel and hydrophobic surfaces to the nearby lipid molecules in the pore vicinity. Electrophysiological recordings performed simultaneously with measurements of the mixing of lipids and aqueous contents, and of the surface area of one of a pair of fusing cells showed that HA-mediated fusion was first detected by the formation of the fusion pore, which occured prior to lipid dye or aqueous dye spreading (Zimmerberg *et al*, 1995). This HA-mediated fusion pore is reversible and small, and its growth is characterised by semi-stable stages (Spruce *et al*, 1991), as is the growth of the exocytotic fusion pore (Curran *et al*, 1993). Thus there is still some controversy over the structure of this fusion end product. It is most probable that the structure of the fusion pore varies between individual fusion systems.

Recent experimental evidence to support the 'stalk-pore' fusion mechanism

There is now good evidence that an altered form of the fusogen Influenza virus haemagglutinin (HA) leads to hemifusion in unfixed, unglycerinated samples of cells (Kemble *et al*, 1994; Melikyan *et al*, 1995). Kemble *et al* engineered HA to be anchored in the outer leaflet of cell membranes by a glycosylphosphatidylinositol (GPI) tail, rather than by its normal transmembrane domain. For low pH-triggered fusion of the HA-expressing cells with erythrocytes, GPI-HA, like wild type HA (wt-HA), promoted rapid mixing of lipids. In contrast to wt-HA, GPI-HA did not promote mixing of any water-soluble probes. These results strongly suggest that GPI-HA mediates hemifusion. Melikyan *et al*, using video fluorescence microscopy and time-resolved electrical admittance measurements, demonstrated that the

establishment of lipid continuity during fusion of GPI-HA expressing cells to planar lipid bilayers is not accompanied by fusion pore formation. They suggest that hemifusion may also be an intermediate in the wild-type viral fusion reactions. If this is so, merging of contacting monolayers should precede fusion pore formation. Hemifusion is also documented in phospholipid model membrane fusion (Chernomordik *et al*, 1995b, 1995c).

For polymer-mediated fusion, very recent work by Lee and Lentz (1997) has identified distinct kinetic steps in poly(ethylene glycol)(PEG)-mediated fusion of small unilamellar vesicles (SUVs), which support the 'stalk-pore' hypothesis. (PEG is a dehydrating agent). Their results separate fusion into several distinct kinetic stages:

1. outer leaflet mixing accompanied by
2. transient pore formation, both occurring on a time scale of approximately 10 seconds, and leading to an initial reversible intermediate. This was measured by H^+ transfer and appears to be a flickering pore. (It is possible that the first intermediate formed is a dynamic mixture of a stalk structure and a transient pore).
3. a 1-3 minute delay leading to formation of a fusion-committed second intermediate.
4. inner leaflet mixing on a time scale of about 150 seconds.
5. contents mixing on a time scale of 150-300 seconds.

Inner leaflet mixing, which had never before been shown to be distinct from outer leaflet mixing, began simultaneously with, but was completed before, contents mixing. The fusion intermediates were shown to have merged outer leaflets and distinct inner leaflets prior to pore formation. Removal of PEG allowed the first intermediate to revert to SUVs, but the second intermediate irreversibly continued to form a fusion pore. Pore dilation appeared to be slow, as noted by the slower mixing of large molecular contents compared to H^+ transfer and inner leaflet lipid mixing. This sequence shows remarkable homology to protein-mediated fusion events.

Very recent work by Siegel and Epand (1997) suggests that the first step in the fusion of pure DiPoPE LUVs is the formation of stalks, which in this system almost immediately expand slightly to form TMCs.

The formation of fusion pores from either TMCs or extended hemifusion diaphragms will depend upon the lipid system involved. Thus it is also likely that the

intermediates formed may vary between different biological fusion systems, and it is also very possible that each step that we have discussed in the fusion process may well have several different structural components.

The modified stalk mechanism of Siegel (1993) predicts that formation of both stalks and TMCs requires least energy when the spontaneous curvature of the system has values corresponding to proximity to L_α-H_{II} phase transitions. This has led to the study of fusion intermediates near the L_α-H_{II} or L_α-Q phase boundaries.

1.2e. Other Possible Effects of Lipids on Fusion

Lipids influence some important biological reactions by direct interactions with proteins. It is possible that they may regulate some fusion processes by acting as specific receptors, or even as cofactors, to produce a change in the conformation and activity of the proteins involved. Specific requirements for small amounts of particular lipids might be expected for this type of effect. This is seen for Semliki Forest virus-mediated fusion, which depends upon the presence of cholesterol (White and Helenius, 1980) and sphingolipids (Nieva *et al*, 1994a) in the target membrane.

Lipids could also affect the lateral association of fusion proteins into multimolecular complexes. Alternatively they could alter the mode of insertion of the fusogenic peptide into the target membrane.

1.3 The Role of Fusion Proteins

1.3a. General overview

Initially proteins were considered to be a barrier to fusion. Early electron microscopy studies showed the production of areas devoid of protein, called 'bare lipid patches', during the fusion process. The subsequent realisation that proteins could indeed act as fusogens followed the discovery by virologists and cell biologists that animal viruses could induce fusion between cells, and moreover, that this process depended upon the presence of certain virus-specific proteins (Poste and Pasternak,

1978; White *et al*, 1983). The ensuing use of ultrafast freezing techniques combined with electron microscopy also showed that proteins were not in fact cleared from the fusion site, as had been previously thought (Schmidt *et al*, 1983; Plattner *et al*, 1988). Since enveloped viruses employ specific proteins to fuse with host cells, it was thought likely that cellular fusion reactions were also protein mediated. Currently there is a large number of known and putative fusion proteins, of which the viral ones, which tend to be the simplest, are by far the best characterised. Many processes, such as intra-Golgi fusion, require a 'fusion machine', a complex of integral and peripheral proteins that is necessary and sufficient to promote fusion (White, 1992). Thus the simpler viral fusion proteins are useful tools with which to study the fusion process. It must be realised, however, that they serve only as a limited prototype for cellular fusion, particularly for fusion events that initiate between cytoplasmic leaflets.

A fusion protein is an integral membrane protein which, upon triggering, changes conformation to expose a hydrophobic domain that promotes the mixing of the lipid components of the two apposed bilayers (White, 1992). Proof of fusion activity can be obtained either by reconstitution of the purified candidate fusion protein *in vitro,* often in lipid vesicles, followed by demonstration of fusogenic capacity for this system (e.g. Stegmann *et al*, 1987), or by expression of fusion activity following transfection of the cloned gene that encodes the candidate fusion protein (e.g. White *et al*, 1983). The abolition of fusion activity by site-directed mutagenesis of a fusion protein also provides strong evidence for its role in fusion (e.g. Gething *et al*, 1986), and suggestive evidence has come from the application of antibodies that inhibit fusion without inhibiting viral binding (e.g Fuller and Spear, 1987).

We still do not understand the energetic driving force for the molecular mechanisms by which fusion proteins cause separate bilayers to merge. 'Even a thorough knowledge of each player's personality does not yield an understanding of the rules of the game.' (Chernomordik *et al*, 1995)! Is fusion driven by conformational changes of fusion proteins, with lipids acting as a passive matrix, or do lipids fuse directly, without guidance from proteins, when it is energetically favourable for them to do so? Individual fusion proteins may merge lipid bilayers

differently, with fusion depending upon specific protein-lipid interactions. Proteins may aid in overcoming the repulsive hydration forces that discourage fusion, or in promoting the hydrophobic attractive forces that favour the process. Fusion proteins may determine the geometry of the fusion site, and act to lower the free energy of a lipid intermediate so that lipids spontaneously rearrange. Proteins would substantially lower the curvature energy of catenoidal or semitoroidal structures if they locally deformed the two original bilayers towards each other at the fusion site. This type of deformation has been observed in a prefusion step in Influenza virus-mediated fusion (Ruigrok *et al,* 1992). It has been suggested for Influenza virus-mediated fusion that a hemifusion intermediate might resemble the 'stalk', but the precise nature of such intermediates has not yet been definitively established for any protein-mediated reaction. Recent experiments indicate that viral proteins are perfectly capable of mediating fusion of lipid bilayers that do not contain H_{II} phase-competent lipids (Alford *et al*, 1994; Stegmann, 1993). Thus, at least for viral protein-mediated fusion, it seems probable that the critical decrease in the energy of the bent intermediates is caused by the effects of these proteins on the spontaneous curvature of membrane monolayers and the geometry of the fusion sites. Fusion proteins might also serve to limit potentially catastrophic side reactions, such as the lysis of one or more interacting membranes.

1.3b. Viral Fusion Proteins

Fusion proteins have now been identified for most enveloped viruses of animals. They can be broadly divided into two classes, according to the dependence of their fusogenic activity on pH. There are two distinct pathways by which enveloped viruses enter cells (see Figure 1.11). They may bind to receptors on the target cell's plasma membrane and then fuse their lipid envelope with this lipid bilayer at pH 7.4. Alternatively, receptor binding by a virus may cause viral internalisation by endocytosis, and thus exposure to acidic pH within the endosome. At a pH that is specific for each individual viral strain, triggering will occur, and thus fusion between the viral envelope and the endosomal membrane. Both entry mechanisms result in the

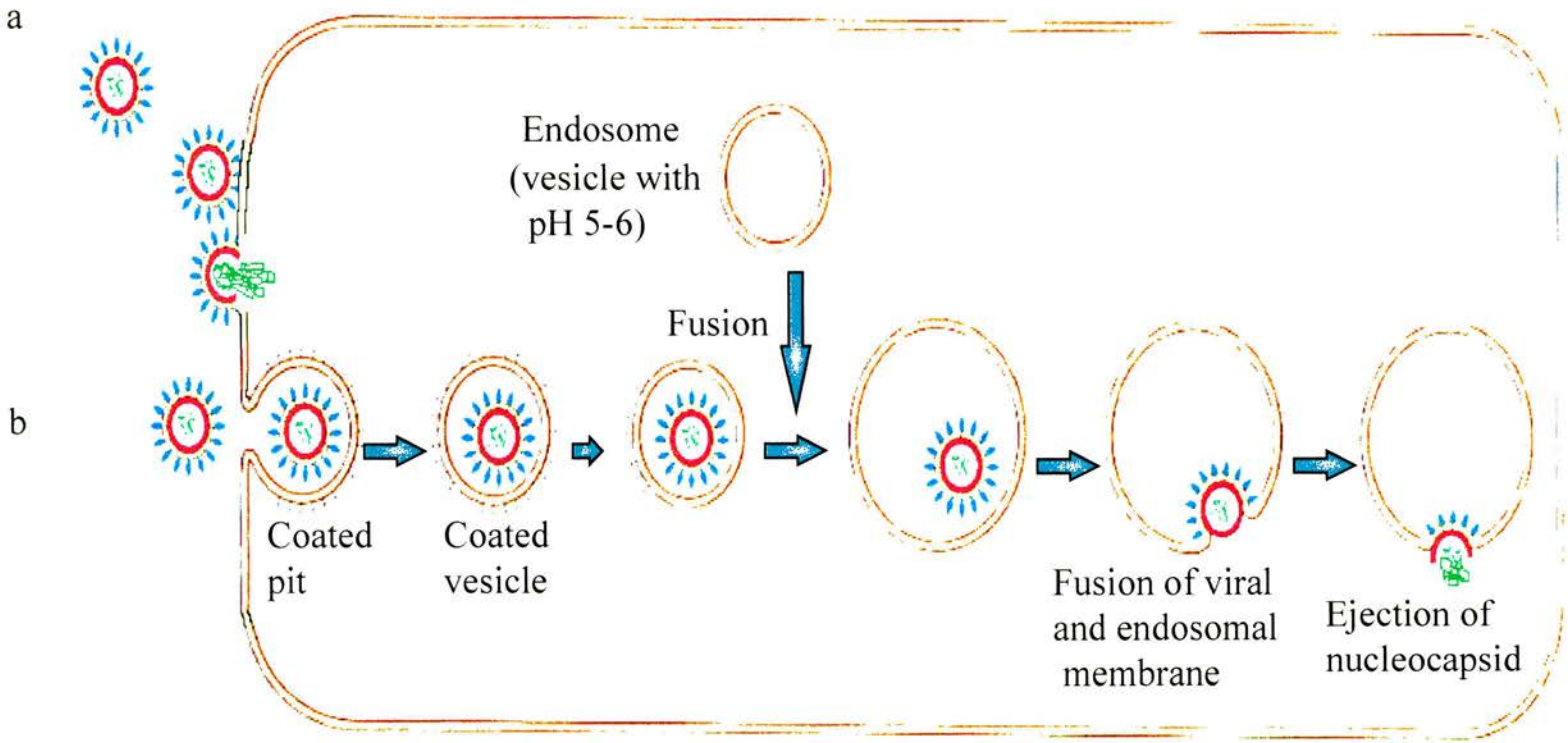

Figure 1.11. Viral entry mechanisms into animal cells.
a: by fusion of the enveloped virus with the plasma membrane.
b:by endocytosis, followed by a decrease in pH of the vesicle, leading to the release of the genome.

release of the viral nucleocapsid into the cell cytoplasm. pH dependence tends to be a property of the virus family: as examples, all orthomyxoviruses and rhabdoviruses require low pH to fuse (Marsh and Helenius, 1989; Ohnishi, 1988), whilst all coronaviruses and herpesviruses are pH-independent (Sturman *et al*, 1985; Spear *et al*, 1989). The retroviruses, however, appear to be an exception: Mouse mammary tumour virus requires a low pH to fuse (Redmond *et al*, 1984), whilst Human immunodeficiency virus (HIV) can fuse at pH 7.4 (McClure *et al*, 1988; Stein *et al*, 1987). This pH dependence is a property of the viral fusion protein. Viruses which fuse with the plasma membrane have a pH-independent fusion protein (these can also fuse with acidic endosomes), whilst those which require endocytosis to gain cell entry have low-pH dependent fusion proteins. Experimental proof for this has come from cellular expression of viral fusion proteins: thus cells expressing these proteins from Influenza virus, Vesicular stomatitis virus (VSV) or Semliki forest virus (SFV) only fuse if exposed to low pH, whilst expression of Simian virus 5, Respiratory syncitial virus (RSV) or HIV fusion proteins allow cell fusion at neutral pH (Kowalski *et al*, 1987; Lifson *et al*, 1986; Paterson *et al*, 1985; Stegmann *et al*, 1989; White *et al*, 1983). Low pH-dependent fusion proteins require acidic conditions to achieve their fusion-active molecular conformations, whilst those which are pH-independent are thought to be directly triggered to change conformation by receptor binding, although this is less clear. Other host cell factors are often required for optimal fusion, particularly for pH-independent viruses.

Different viral fusion proteins possess distinct native structures and the dynamics of their fusion-inducing conformational changes differ markedly. Nonetheless, most share many common properties. They are all class 1 integral membrane proteins, with at least 85% of their mass lying external to the viral membrane, and they are present at high surface density (there are about 500 fusion protein molecules on the surface of an Influenza virion). They have characteristic shapes, which consist of a long fibrous stem topped by a globular domain, and are commonly referred to as 'spike' proteins (see Figure 1.12). Most contain N-linked oligosaccharides, and many are fatty acylated. They all form higher order oligomers. These are often trimeric, as is the case for haemagglutinin (HA) of Influenza virus

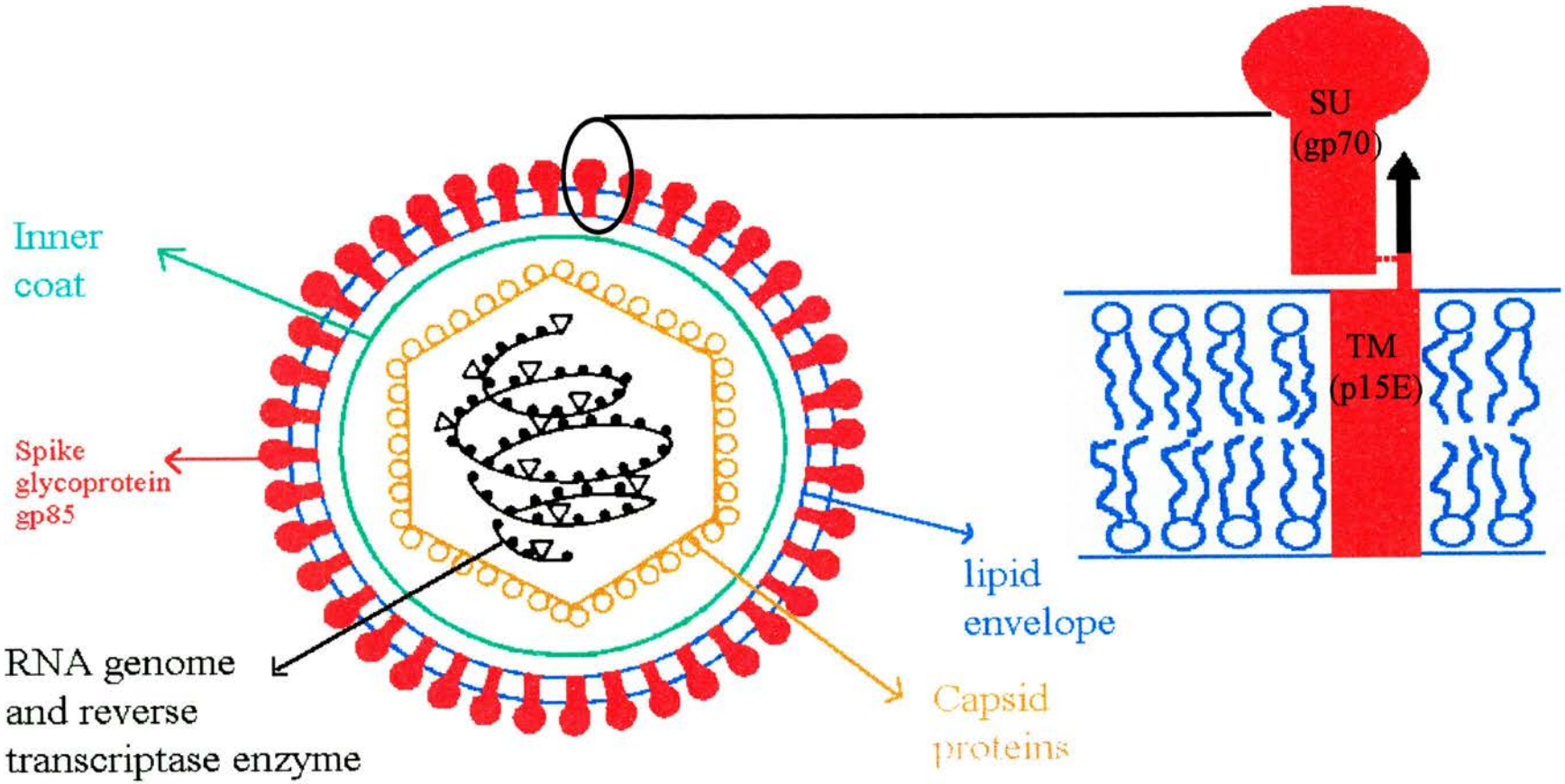

Figure 1.12. Main picture: the structure of a typical retrovirus (FeLV). Inset: a slightly more detailed schematic model of the viral fusion protein spike. The fusion peptide is shown in black.

(Wiley and Skehel, 1987), in which all three subunits are involved in fusion (Boulay *et al*, 1988). The fusion protein usually forms a single active oligomeric spike; Herpesvirus is unusual in requiring the cooperation of several distinct spike proteins to form a fusion-active complex.

Many fusion proteins are synthesised as large, inactive precursors. Proteolytic cleavage of a single peptide bond produces two polypeptide chains, which remain associated through disulphide bonds or through noncovalent interactions (see Figure 1.12 inset). The C-terminal polypeptide product anchors the protein to the viral membrane, and normally contains three distinct regions: extracellular, membrane spanning and cytoplasmic. The extracellular region contains a short, apolar sequence called the fusion peptide. The N-terminal product contains the receptor binding site and most of the antigenic determinants. This proteolytic processing is required to activate the fusion ability of the protein.

Fusion peptides are highly conserved within viral families. The fusion peptides of various Retroviridae are shown in Table 1.1, where they can be seen to display extreme similarity. It was this homology of the amino acid sequences of the amino (N)-termini of viral fusion proteins that led to the proposal that this region was intimately involved in the fusion process (Gething *et al*, 1978). Viral fusion peptides lie either at the proteolytically generated new N-terminus of the membrane anchored polypeptide fragment or internally within this fragment. HA and the Env glycoproteins of HIV, Simian immunodeficiency virus (SIV) and probably also Feline leukaemia virus (FeLV) have amino terminal fusion peptides (McCune *et al*, 1988; Ohnishi, 1988; Stegmann *et al*, 1989; White *et al*, 1983). There is no relationship between the pH dependence of fusion and the fusion peptide's location. Hydrophobic affinity labelling experiments (Harter *et al*, 1989) and site-directed mutagenesis studies (Gething *et al*, 1986; Bosch *et al*, 1989) have established the active participation of the fusion peptides of Influenza HA and SIV Env in mediating fusion. Work with synthetic peptides corresponding to these two fusion peptide sequences has also demonstrated their active roles in fusion, and mutations of these synthetic peptides have been shown to alter, reduce or abolish fusion (e.g. Lear and Degrado, 1986; Rafalski *et* al, 1990; Düzgünes and Shavnin, 1992; Nieva *et al*, 1994b; Delahunty *et*

Retrovirus	*Sequence of Fusion peptide*
Feline leukaemia virus FeLV (strain Garner-Arnstein)	EPISLTVALMLGGLTVGGIAAGVGTGT
FeLV (strain Snyder-Theilen)	EPISLTVALMLGGLTVGGIAAGVGTGT
Moloney murine leukaemia virus (MoMLV)	EPVSLTLALLLGGLTMGGIAAGIGTGT
Kirsten murine leukaemia virus	EPVSLTLALLLGGLTMGGIAAGVGTGT
AKV murine leukaemia virus	EPVSLTLALLLGGLTMGGIAAGVGTGT
Simian immunodeficiency virus (SIV)	GVFVLGF LGFLATAGSIA GAA
Bovine leukaemia virus (BLV)	SPVAALT LGLALSVGLT GINVAV

Table1.1 Sequences of the fusion peptides of two strains of FeLV and of several other *Retroviridae*. Homologous residues are shown in red.

al, 1996; Gray *et al*, 1996). Furthermore, site-directed mutations in the fusion peptide of Influenza virus that abolish fusion activity do not compromise haemagglutinin biosynthesis, surface expression, post-translational cleavage or the low-pH induced conformational change (Gething *et al*, 1986). All viral fusion peptides tend to be rich in glycine and alanine residues, and are either exclusively apolar, as are most retroviruses, or contain a few negatively charged residues, as in Influenza HA. Thus it has been postulated that the presence of two relatively apolar sequences (the fusion peptide and the transmembrane region) within a single polypeptide chain may allow the fusion protein to interact simultaneously and hydrophobically with both the viral and target membranes, and hence to promote rapid and efficient fusion (e.g. Stegmann *et al*, 1989). Further support for this comes from the finding that non-membrane anchored HA can affect fusion between SUVs, but the rate of fusion is much less than that seen with intact HA (Wharton *et al*, 1986).

Individual viruses tend to require specific conditions to be activated for fusion. Thus SFV requires the presence of cholesterol (e.g. Phalen and Kielian, 1991) and sphingolipids (e.g. Corver *et* al, 1995) in the target membrane for fusion to occur. More specifically, the results of Corver and co-workers suggest that sphingolipids may act as a cofactor in SFV fusion. HIV has a very strong affinity for cardiolipin such that its absence in LUV membranes decreases the fusion rate by at least two orders of magnitude (Larsen *et al*, 1993). HIV fusion is also promoted by physiological levels of calcium, and the presence of CD4 receptors also enhances the overall rate of fusion. PS is thought to be the cellular receptor for VSV (Marsh and Helenius, 1989). Influenza virus (Stegmann *et al*, 1985), SIV (Larsen *et al*, 1990) and Sendai virus (Nir *et al*, 1986) all fuse preferentially with negatively charged liposomes. These are but a few specific examples of important factors for individual fusion processes cited in the literature to date. Other common features include temperature dependence of viral fusion reactions (the rate of Sendai-induced fusion is zero at 22°C and increases about 25 times between 25°C and 37°C; White, 1990), and a lack of requirement for ionic gradients or osmotic pressure.

Efforts to understand how viral fusion proteins work have been aided in recent years by the crystallographic determination of the structures of several fusion proteins.

The current understanding of the Influenza virus fusion process is described in detail, as HA is, at present, the best characterised fusion protein. HIV-mediated fusion is also then discussed, since HIV has the best characterised retroviral fusion protein. Influenza virus undergoes low pH-induced fusion, whilst HIV shows pH independence. Thus these serve as specific examples of the two classes of viral fusion protein.

Influenza virus HA-mediated fusion

The biosynthesis, folding, oligomerisation and native structure of HA have all been described in detail (Wiley and Skehel, 1987; Doms *et al*, 1993). HA0, the initial fusion-incompetent precursor protein, is cleaved proteolytically to form two disulphide-bonded units. These are HA1, a 328 amino acid residue globular unit which houses the sialic acid receptor-binding domain in its uppermost region (Weis *et al*, 1988), and HA2, a 221 residue fibrous stem-like subunit, which forms the centre of the molecule and which has an amino-terminal fusion peptide and a transmembrane segment. Between the globular domain and the fibrous stem there is a hinge region. These dipeptide monomers associate to form trimers that project about 135 Å from the viral membrane. This would seem likely to prevent the virus from closely approaching the target membrane.

The neutral pH structure of BHA has been determined by X-ray crystallography to a 3 Å resolution (Wilson *et al*, 1981) (see Figure 1.13). BHA represents a fragment of HA, in which each HA2 chain has been cleaved once, after residue 175, by the protease bromelain (Brand and Skehel, 1972). Bromelain thus produces a soluble trimer without the membrane anchoring segment of HA2. In the neutral pH conformation, the three fusion peptides, one from each monomer, are located about 100 Å from the target membrane, and are tucked into the trimer interface by a network of hydrogen bonds, lying roughly parallel to the plane of the viral membrane. They are thus not readily accessible for participation in any membrane interactions.

It is known that low pH, between pH 4.9 and pH 5.2 for different strains of Influenza virus, is required to elicit a fusion-inducing conformational change in HA.

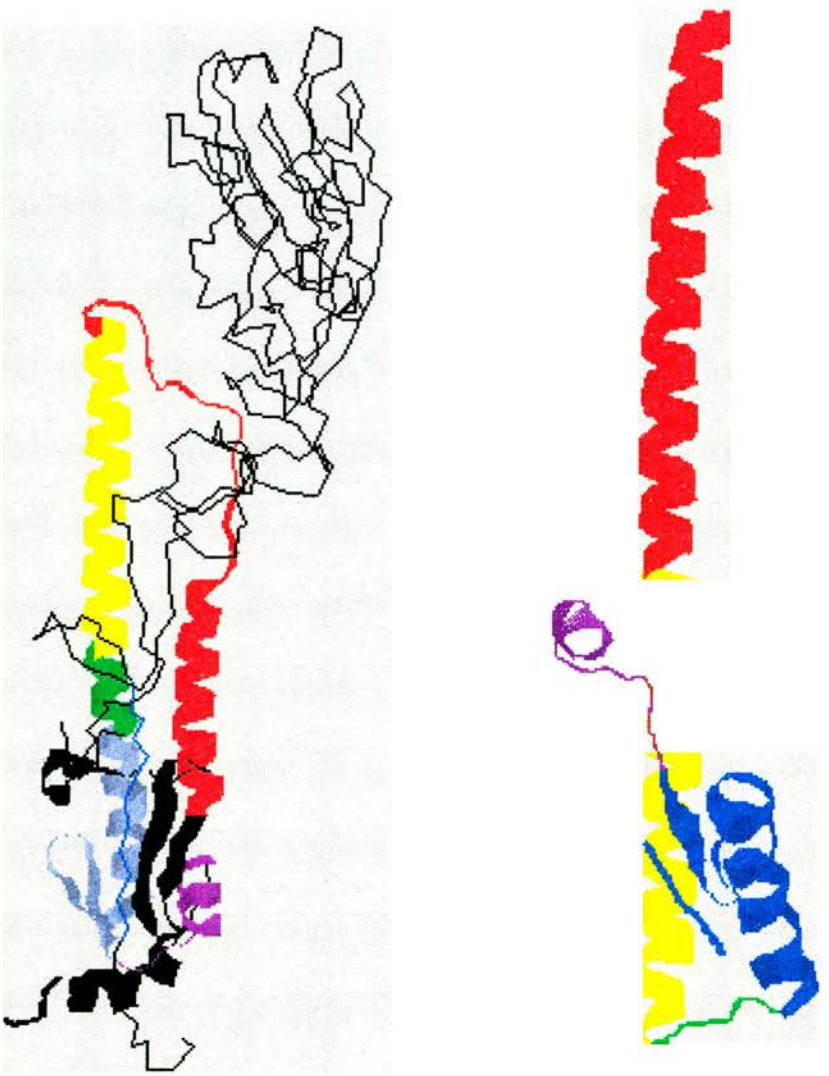

BHA TBHA2

Figure 1.13. Comparison of the structure of an intact BHA monomer (left) to that of a TBHA2 monomer (right). Corresponding regions are coloured identically. BHA regions which are proteolytically cleaved to form TBHA2 or which are apparently disordered in TBHA2 are shown in black. The HA1 β strand, which is disulphide linked to HA2, is blue (reproduced from Bullough *et al*, 1994).

This has been most convincingly demonstrated by the use of monoclonal antibodies that are specific for either the acid or neutral HA conformation (Daniels *et al*, 1983; Webster *et al*, 1983; Copeland *et al*, 1986; Kielian *et al*, 1990). This low-pH induced conformational change is a regulated process: it is not denaturation since the acidic form maintains a definite structure (Wharton *et al*, 1988), whilst denaturation has been shown to abolish recognition of the acidic form (Kielian *et al*, 1990).

The release of the fusion peptide from the molecular interior of HA is a key feature of the low-pH conformational change. HA simultaneously acquires hydrophobic properties (e.g. Stegmann *et al*, 1989), and can thus bind to target membranes (e.g. Stegmann *et al*, 1991), which is an obvious requirement for fusogenic activity. It would thus appear likely that the fusion peptide is responsible for most of the concomitantly observed increase in hydrophobicity. This is supported by several studies. Firstly, Gething and co-workers (1986) found that a mutant HA, which had the fusion peptide's Glycine at position 1 replaced by Glutamate, had a greatly reduced ability to interact with membranes. Secondly, HA0 does not acquire amphipathic properties on exposure to low pH (Doms and Helenius, 1988). Thirdly, the fusion peptide is the only sequence to be labelled with hydrophobic photoaffinity labels when BHA is added to preformed liposomes at low pH (Harter *et al*, 1989). Fourthly, BHA is seen to aggregate at low pH, but thermolysin, which digests the fusion peptide, can resolubilise these aggregates (Ruigrok *et al*, 1988), and finally, drugs that prevent the the extrusion of the fusion peptide from its pH 7.4 location inhibit fusion (Bodian *et al*, 1993).

Exposure of the fusion peptides was described by Doms *et al* (1993) and also dissociation of the globular head domains of HA, such that the heads bend outwards radially (similar to a tulip opening). Carr and Kim (1993) used circular dichroism (CD) and modelling studies to propose a model for the low-pH induced conformational change in the HA stem domain. HA2 contains a long region of heptad repeats, that is hydrophobic amino acids that are spaced every four and then every three residues. Hydrophobic amino acids that recur with this periodicity often stabilise the cores of α-helical coiled coils. There are 88 residues in this heptad repeat region, yet only 34 were seen to form a coiled coil in BHA (Wilson *et al*, 1981). The first 54

residues form a buttressing helix and an extended loop. Thus Carr and Kim suggested that these flanking regions might be recruited into the central coiled coil at low pH. This would be made possible by the fusion peptide's release from its buried location, where it appears to serve as a linchpin and stabilise the initial, hairpin-like stem arrangement.

HA is the only fusion protein for which atomic resolution structures are available for both its pH forms. The strain X:31 has been studied in the main, and it should be remembered that there are important differences in the conformational changes of HA for different viral strains (Tsurudome *et al*, 1992). It is thought that the distinctions in pH threshold which occur for different strains and subtypes are due to the relative displacement of structural domains (e.g. the elimination of electrostatic and hydrophobic interactions) that occur during the conformational change (Wharton *et al*, 1988).

Influenza virus enters the cell by receptor-mediated endocytosis. Both attachment of the viral envelope to cell surface receptors and fusion with the endosomal membrane after acidification of the endosomal lumen are mediated by HA (Gething and Sambrook, 1981). Influenza virus fusion exhibits a lag phase between binding and the onset of detectable fusion (this lag phase is seen even if the virus is pre-bound to the target membranes). Thus it is likely that fusion is a multistep process. Exposure of the HA fusion peptide and its insertion into LUVs occurs early during the lag phase, preceding the onset of fusion (Stegmann *et al*, 1990). This indicates that the fusion peptide exposure is not a rate-limiting step. Moreover, the duration of the lag phase varies non-linearly with HA surface density suggesting that more than one HA trimer participates in the initiation of fusion (Danieli *et al*, 1996). A Hill plot of these data suggested that a minimum of three or four HA trimers is required to intitiate fusion. Thus cooperativity at the level of the HA trimers appears to required.

Ideally, one would like to reconstruct the three dimensional structure of intact HA in its low pH form, since it is possible that proteolytic cleavage leads to stabilisation of a different structure, or generation of additional degrees of freedom that are unavailable in the resulting fragments. However, even whole BHA aggregates

at low pH through exposure of its fusion peptides, which makes it unsuitable for crystallographic studies. One fragment, comprising most of HA1, showed no significant change on lowering of the pH (Bizebard *et al*, 1995). Bullough *et al* (1994) determined the crystal structure of TBHA2, which has been a major step forward in our knowledge of the HA low pH conformation. TBHA2 is formed by exposing BHA to a pH of 5, and then treating it with trypsin to cleave off the globular domain, and finally with thermolysin to digest the exposed fusion peptide (see Figure 1.13). Thus each monomer includes residues 38-175 of HA2 disulphide bonded to residues 1-27 of HA1. Their results show that several changes have occurred in the HA2 stem at acidic pH.

Three major changes take place on lowering the pH, as shown in Figure 1.14. Firstly, a prominent loop, B in Figure 1.14, transforms into an α helix, as had been previously proposed by Carr and Kim, and thus connects the existing helical regions A and C. This elongation of the helical region would propel the fusion peptide upwards towards a target membrane. Secondly, residues 106-112 convert from a helix to a loop. In the neutral structure the fusion peptide and a loop comprising HA1 residues 14-52 cross this region of the native long α helix. Thus the fusion peptide becomes exposed in the pH change. This would also flip the rest of helix D through 180° so that it runs antiparallel to the C helix, and is stabilised by an extensive hydrophobic interface between these two helices. This docking of helix D against helix C would be blocked by the fusion peptide and adjacent sequences in their original positions, and thus it seems likely that the two changes described occur sequentially. Thirdly, about 20 C-terminal amino acids become undetectable by X-ray techniques, suggesting that they are in a disordered, and possibly even extended, conformation, which could be as long as 100 Å. Thus only 30 residues of each HA2 subunit, which comprise the invariant triple-stranded coiled coil at the stem centre, retain their neutral pH conformation. Regions of disorder are also seen in HA1 at low pH, suggesting that the head domains may be attached to the stems by a flexible tether, which could extend as far as 100 Å.

Support for these crystallographic results comes from work by Daniels *et al* (1987,1985). The fusion protein mutants that were studied changed their

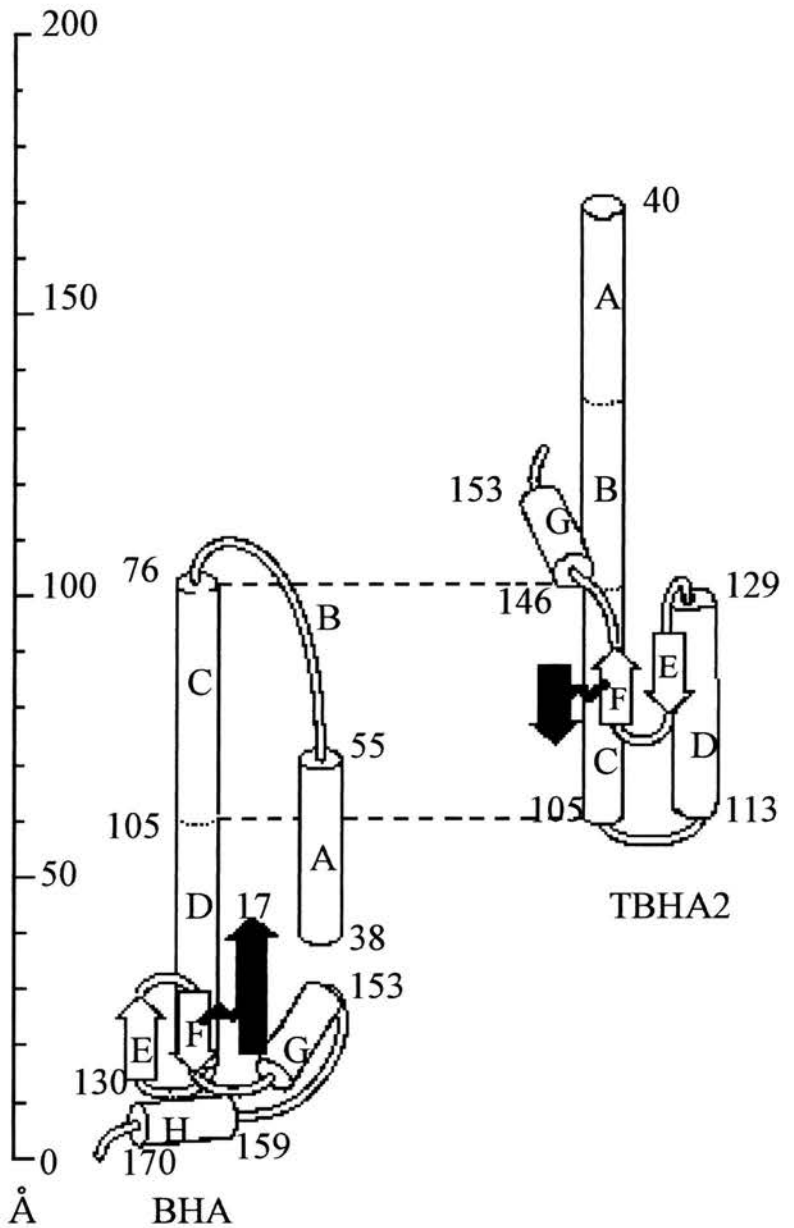

Figure 1.14. Model comparing the structures of TBHA2 (right) with the corresponding regions of BHA (left). One monomer is shown for clarity. The black arrow represents the HA1 chain which is disulphide bonded to HA2. Regions of HA2 are labelled A to H (see text for details). Helix H is not seen in TBHA2, and may be disordered (reproduced from Hughson, 1995).

conformation, and hence mediated fusion, at elevated pH. Thus interactions which are modified in the transition to the fusion-active structure were identified by the distribution of these mutations. One mutation group stabilised the buried location of the fusion peptide. Another stabilised the short helix A and the loop B against the long CD helix, whilst a third group stabilised contacts between HA1 and B and CD of HA2. A fourth group of mutations altered the interface between the HA1 subunits which suggested that the globular domains do dissociate at fusogenic pH. Their dissociation is probably accompanied by the refolding of loop B since HA1 is docked against this loop in BHA. The dimensions and shape of TBHA2 revealed by X-ray structure also agree well with electron micrographs of the molecule.

These structural data of Bullough and co-workers (1994), combined with results from other experimental techniques, have led to the proposal of a model of HA mediated fusion (White, 1995). The basic principle is that conformational changes in HA drive the transitions that are required to fuse two membranes, that is to bring them close together and to induce the bending required to produce hemifusion and the opening and subsequent dilation of a fusion pore. Thus several different HA conformational states participate in fusion at different stages in the process. Figure 1.15 shows the different putative HA conformations for each step of the fusion model. It is likely that there are more HA conformations between these different forms.

In this model, step 1 of fusion involves the 'spring-loaded' conformational change of the B loop to produce an extended coiled coil which drives the initial interaction of the fusion peptides with the target membrane. This corresponds to 'low-pH 1' HA in Figure 1.15. Separation of the globular heads is essential for this step: proof for this comes from the non-fusogenic phenotype of a mutant HA in which Kemble *et al* (1992) linked these domains by chemically manufactured disulphide bonds. The neutral pH structure presumably keeps the viral and target membranes too far apart to be capable of mediating further steps in fusion.

Step 2 includes the observed lag phase and is suggested to involve clustering, orientation and binding to the target membrane of at least 3 or 4 HA trimers. The higher order assembly of trimers may be facilitated by the increased flexibility of HA due to the apparent disorder in the 20 C-terminal residues. Further conformational

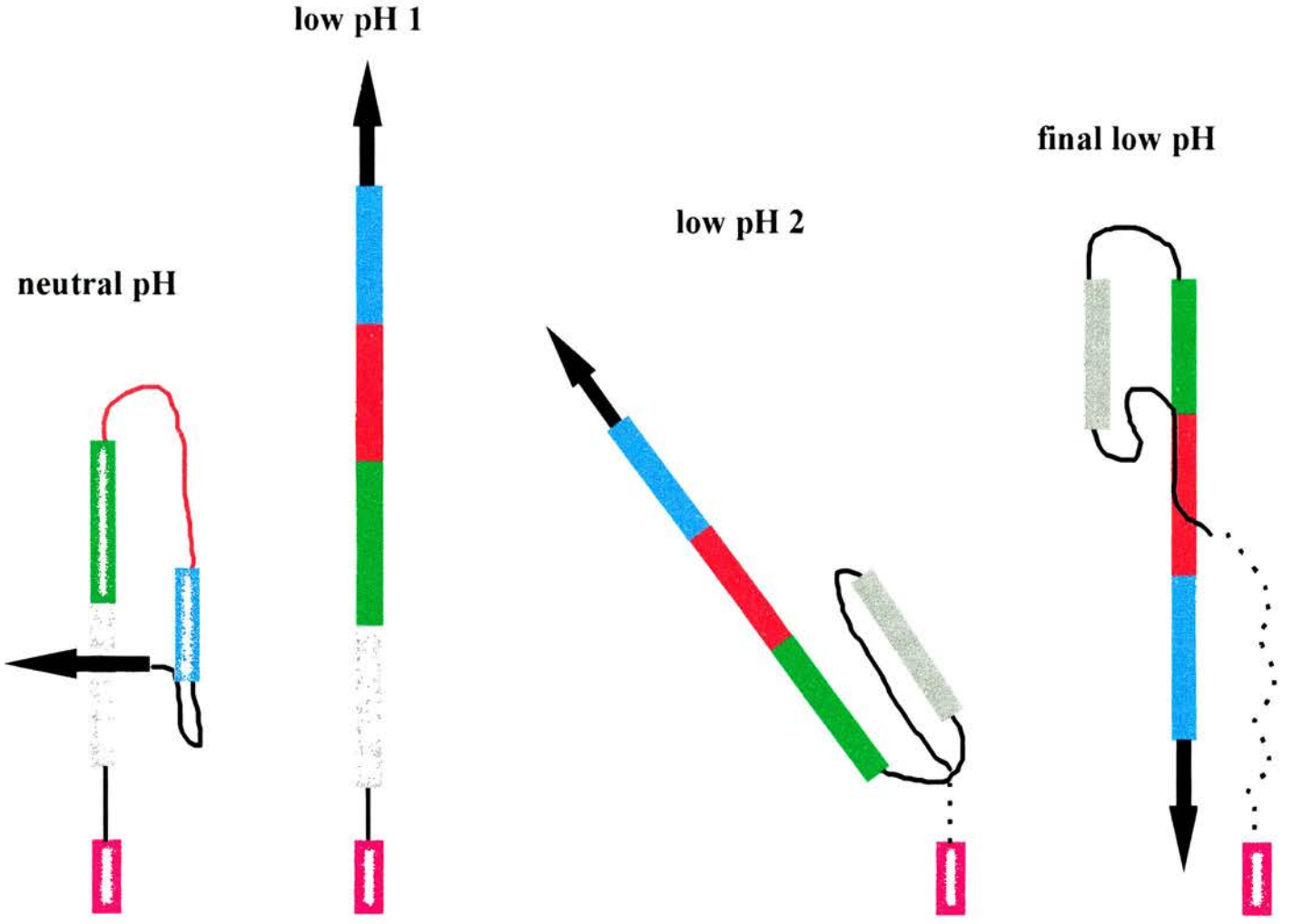

Figure 1.15. Model of the low pH-induced conformational changes in HA2 (adapted from White, 1995). The fusion peptide is shown as an arrow. Helix A is blue, region B is red, helix C is green, helix D is and the transmembrane domain is pink. In 'low pH 2' and 'final low pH' residues 154-185 are shown as dashed lines, since they cannot be visualised in TBHA2. It is likely that HA undergoes several conformational changes before attaining 'low pH 1'. Exactly when the globular heads dissociate in this early section of the pathway is also uncertain.

changes (Stegmann *et al*, 1990) as well as rotational and lateral mobility (Junankar and Cherry, 1986) for HA may be required to establish a fusion site.

In step 3 the HA trimers encircling the nascent fusion site bend, thus forming the 'low-pH 2' structure (Figure 1.15). This may require the helix-to-loop transition of HA2 residues 106-112. If the HA trimers remain firmly anchored to the target membrane via the fusion peptides, and also firmly tethered to the viral membrane by their transmembrane domains, then if several trimers simultaneously bend radially outwards from the fusion site, they will force the interacting bilayers to bend with them, thus producing a hemifusion intermediate. This bending of the trimers may be facilitated by the increased flexibility of the 20 carboxy-terminal residues, which lie nearest to the transmembrane anchor. Wharton *et al* (1995) performed electron microscopy studies which showed that the HA trimer can bend asymmetrically. The results of Tatulian *et al* (1995) suggest that HA trimers do indeed tilt at the fusion site: at fusogenic pH HA trimers tilted 55-70° from the membrane normal. However, a recent study of HA-induced fusion using quick freezing electron microscopy did not observe any tilting of HA trimers (Kanaseki *et* al, 1997). At this stage the fusion peptides could also insert into the target membranes at an oblique angle, as has been suggested by Brasseur *et al* (1990), to produce destabilisation of these lipid membranes.

Step 4 involves HA imposing tension on the hemifusion diaphragm so that it eventually breaks. This rupture may require a transmembrane anchor that spans the viral membrane, as suggested by the results of Kemble *et al* (1994) and Melikyan *et al* (1995) (see earlier). In this elastic coupling model, bending of the HA ectodomain pulls on the transmembrane domain and cytoplasmic regions of HA, thus forcing the transmembrane domain to orientate more parallel to the membrane plane. This would generate stresses on the diaphragm and disturb the configuration of the component lipids.

Step 4 is probably reversible, since the early HA fusion pores 'flicker', that is they repeatedly open and close (Spruce *et al*, 1991). The dimensions of the initial aqueous connection inferred from electrophysiological studies (1-2 nm) are consistent with a structure involving a small number of trimers (Spruce *et al*, 1989). Lipid flow

is known to be restricted in the initial fusion pore (Zimmerberg *et al*, 1994; Blumenthal *et al*, 1995). This may be due to the formation of a barrier by the clusters of HA transmembrane domains in the early and narrow fusion pore (Kemble *et al*, 1994; Zimmerberg *et al*, 1994). If this is so, the HA trimers would have to move apart to allow unimpeded lipid flow. It is known that small aqueous contents can move through the fusion pore before larger ones (Zimmerberg *et al*, 1994). This could be due to progressive widening of one pore, or alternatively to the coalescence of several smaller pores. There is still controversy over the precise molecular nature of the HA-mediated fusion pore.

Finally, in step 5, the fusion pore opens irreversibly and dilates. For fusion between HA-expressing fibroblasts and red blood cells, this occurs over tens of milliseconds (Spruce *et al*, 1989). This may be driven by the conversion of HA into its final low pH form, as seen for TBHA2. If so, the proposed extension of the 20 C-terminal residues might allow HA to continue to bend, and thus to sweep through the toroid of the membrane comprising the initial fusion pore. This would relax the tension and the high bilayer curvature of the lipid-protein fusion intermediate conformations. In this step, the fusion peptides would finally embed in an antiparallel orientation in the same membrane as their transmembrane domains. This represents the 'final low-pH' HA form (Figure 1.15 and Figure 1.16c).

Various experimental results add support to this theory. Possible orientations of the low pH form of HA are shown in Figure 1.16. It is known that most Influenza strains undergo irreversible inactivation in the absence of a target membrane (Skehel *et al*, 1982; White and Wilson, 1987). This appears to correlate with gross morphological changes in the viral coat, as seen using electron microscopy (e.g. Doms *et al*, 1985): Influenza virions display distinct, closely packed HA spikes at neutral pH, but after brief incubation at low pH, the viral coat seems much more disorganised, with the individual HA trimers no longer being distinguishable. Moreover, electron microscopy of inactivated virus digested by trypsin allows visualisation of individual trimers. These studies suggest that the trimer stems are indeed inverted with respect to the viral membrane (see Figure 1.16b). Hydrophobic affinity labelling of inactivated virus also suggests that the fusion peptides insert into

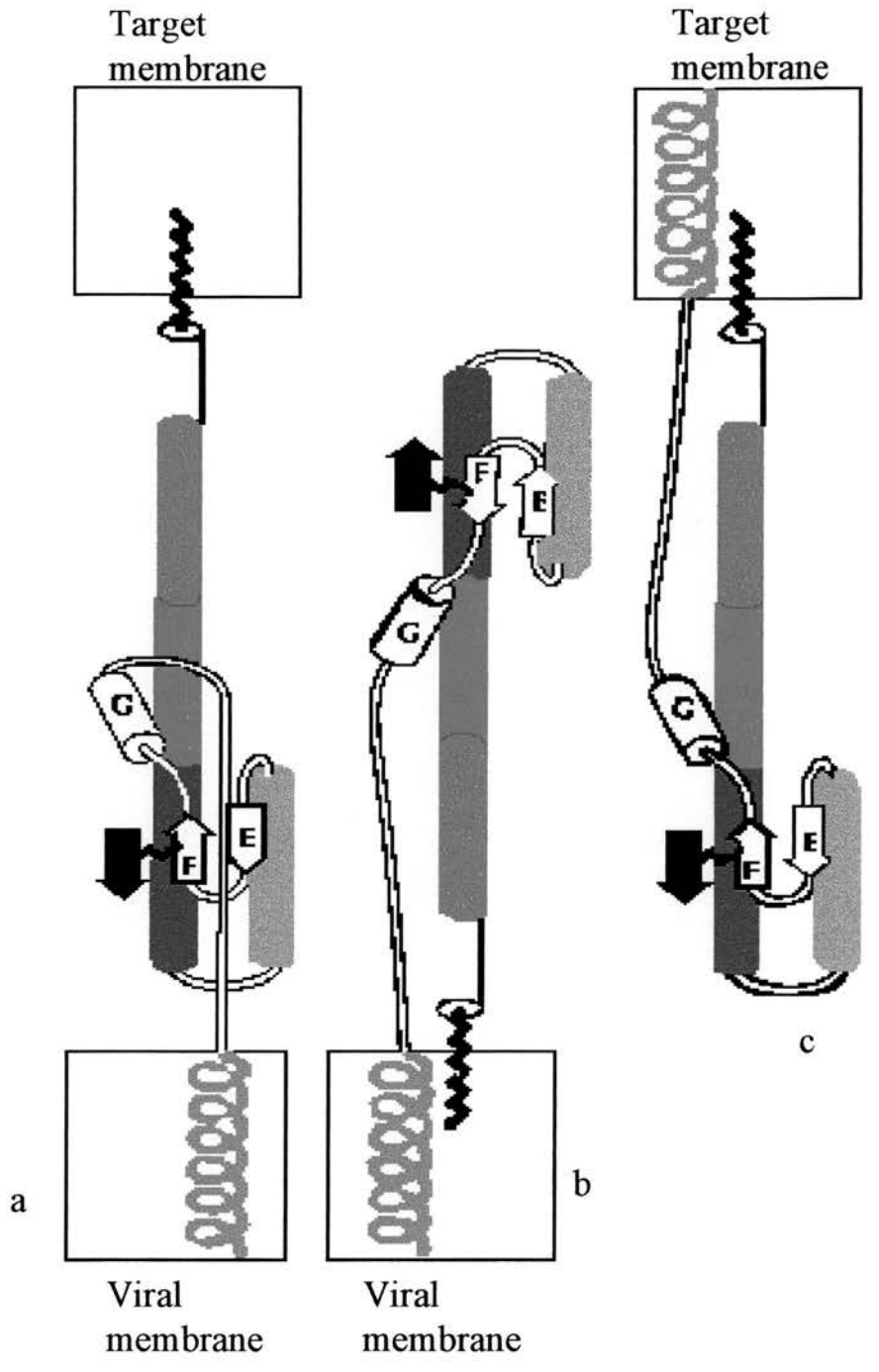

Figure 1.16. Possible orientations of low-pH treated HA relative to viral and cellular membranes (adapted from Hughson, 1995). The TM unit is pink. The fusion peptide is black. Regions A to D are colour coded as in the previous diagram. Only one monomer is shown. TBHA2 a: in a putative initial stage of membrane fusion. b: in inactivated virus, in the absence of a target membrane c:in 'final low pH' form The fusion peptide and TM unit are inserted into the same, fused membrane.

the viral membrane (Weber *et al*, 1994), but not the coiled coil region (Durrer *et al*, 1996), as had been previously suggested (Yu *et al*, 1994). Yu and co-workers had proposed that the inserted coiled coil might drag the two fusing membranes closer together, with HA maintaining its upright position. Further support for the inversion of HA comes from Wharton *et al* (1995), who found that an antibody, which recognises the HA region that undergoes the helix-to-loop transition, is bound to the membrane-distal region of inactivated HA, 110Å from the viral membrane. Interestingly, a role for the fusion peptide in pore dilation has also been suggested. Schoch and Blumenthal (1993) found that non-lethal mutations in the fusion peptide affected the transfer of large molecules between fusing partners. They suggested that the fusion peptide may be important in holding together the HA trimers to form a fusion pore.

If, at the end of fusion HA is in an inactive form, then we know the structure and orientation of segments of HA in its pre- and post-fusogenic forms. This model is highly speculative, but it does allow for the logical coordination of the dynamic rearrangements of both lipids and HA that must occur during membrane fusion.

Other hydrophobic sequences of the HA ectodomain also become accessible to a fluorophore at low pH (Korte and Herrmann, 1994). A Scatchard plot of their results for the binding to HA of a fluorescent probe indicated that the ectodomain had at least two types of binding site, which differed in their affinity for this probe. Modelling studies have shown the existence of several hydrophobic sequences in the ectodomain at pH 5.0, which are comparable in length and hydrophobicity to the fusion peptide (Korte *et al*, 1992). It is therefore possible that interactions between regions of the globular domains of HA1 and HA2 or the target membrane may also play a role in fusion.

There is still much controversy over the precise events in HA-mediated fusion. Kanaseki *et al* (1997) have recently published a study of Influenza virus fusion with LUVs, using quick freezing electron microscopy. They observed 10-20 nm diameter outward bendings of the LUV bilayer, where the LUV and viral membranes had made contact. These protrusions were arranged polygonally to reflect the array of HA spikes on the virus, and sometimes had a tiny hole, of diameter about 4 nm in their

centre. The pits had particles in them, which they suggested were the fusion peptides, but no bending of HA trimers was observed. Thus they surmised that penetration of the fusion peptide may occur in upright HA, and that these straight spikes of HA tug and deform the apposing membranes into closer contact.

The current, widely held hypothesis is that viral-mediated fusion utilises common lipid intermediates with pure lipid fusion systems. However, Shangguan *et al* (1996) studied fusion between Influenza virus and LUV of varying lipid composition. They found that LPC and arachidonic acid (AA) at physiologically relevant concentrations, and also hexadecane, had no effect on the fusion kinetics. Thus they concluded that monolayer curvature and void stabilisation do not seem to affect the rate-limiting step in HA-mediated fusion, and thus it may not proceed through common intermediates with liposome-liposome fusion.

Kim *et al* (1996) studied various mutants of the peripheral part of the HA2, in particular the region that is proposed to undergo the loop-to-helical coiled coil. They found good flexibility for this region, and thus concluded that it was unlikely to form a well defined coiled coil as suggested by Bullough and co-workers. Finally, a very recent paper by Shangguan and co-workers (1998), which correlated the kinetics of low pH-induced fusion of Influenza virus with liposomes and the conformational changes that occurred in HA, suggests that the crystallographically determined low-pH form of HA is not a precursor of viral fusion, but an end product of this process.

Influenza virus-mediated fusion is seen as the general prototype for fusion processes, since it by far the most thoroughly studied mechanism. The amount of conflicting experimental evidence indicates how much is still unknown about fusion in general.

HIV-mediated fusion

Less is known about the activation of fusion proteins that function at neutral pH. Their requirement for host cell receptors led to the belief that it was the interaction between the viral fusion protein and its host cell receptor which triggered the fusion-activating conformational change. The mechanism of retrovirus-mediated

membrane fusion has, until very recently, remained elusive due to the lack of detailed structural information about Env proteins. The low virus titre in natural systems, the large size of the envelope complexes, and the labile association between SU and TM have all hindered structural studies. However, a recent study by Hernandez *et al* (1997) on an avian retroviral fusion protein has demonstrated that receptor binding does indeed appear to activate this fusion protein in much the same manner as low pH activates the low pH-dependent viral fusion proteins. HIV is currently the best studied of the neutral pH viruses, due to its extreme medical importance.

The Env proteins of retroviruses bind to cell receptors and promote fusion (Hunter and Swanstrom, 1990). Env proteins are synthesised as polyprotein precursors and, like Influenza HA, they require proteolytic cleavage into a large surface (SU) and a smaller transmembrane (TM) subunit to become fusogenic. SU contains the receptor binding site, whereas TM houses the transmembrane anchoring domain and the fusion peptide. In HIV this cleavage has also been shown to be important for efficient incorporation into virus particles (Dubay *et al*, 1995). Unlike Influenza HA1 and HA2, SU (gp120) and TM (gp41) of HIV remain associated only through noncovalent bonds on the external surface of the virus. gp120 binds to CD4, the primary HIV receptor (Weiss, 1992), and subsequently to a 7-span transmembrane chemokine receptor (D'Souza and Harden, 1997). gp41 is responsible for fusion activity, with both the amino terminal fusion peptide and the transmembrane domain playing important roles (Freed *et al*, 1990; Owens *et al*, 1994). The HIV Env is almost certainly a tetramer (Pinter *et al*, 1989; Weiss *et* al, 1990; Schawaller *et al*, 1989; Thomas *et al*, 1991).

The binding of HIV Env to CD4 induces a number of conformational changes. These have been detected by antibody and protease probes (Moore *et al*, 1990; Clements *et al*, 1991; Hart *et al*, 1991). Some of these are temperature dependent, as indeed is HIV fusion (Frey *et al,* 1995). Dissociation of gp120 is instigated by CD4 binding (Moore *et al*, 1990). This shedding of gp120 may parallel the displacement of HA1 which occurs during the low-pH conformational change.

The presence of CD4 alone was discovered to be insufficient to allow HIV entry into primate cells. Thus cofactors must exist to support fusion. Fusin, a new

member of the G-protein-coupled transmembrane receptors, has been shown to fulfil this role for T lymphocytes (Feng *et al*, 1996). HIV isolates that differ in their cellular tropism use different subsets of chemokine receptors as entry cofactors. Thus macrophage-tropic HIV strains primarily use CCR5, whereas T-cell tropic and dual-tropic isolates use CXCR4 receptors (D'Souza and Harden, 1997). HIV (and SIV) forms a complex between the Env protein and the two appropriate cell-surface membrane receptors. Very recent work by Weissman *et al* (1997) has shown that macrophagotropic strains of HIV (and SIV) induce a signal through CCR5 on $CD4^+$ T cells, which induces chemotaxis of T cells. Whilst this signal is not required for efficient fusion and viral entry (Oravecz *et al*, 1996), it may contribute to the pathogenesis of HIV by attracting $CD4^+$ cells to sites of viral replication, by promoting viral replication by increasing the activation of target cells, and/or by altering viral-associated cytopathicity or apoptosis (Weissman *et al*, 1997).

HIV is also able to infect human cells that have no detectable CD4, which suggests that there must be another HIV receptor. A glycosphingolipid, galactosylceramide, will bind gp120 (Long *et al*, 1994). The level of expression of this lipid on colonic epithelium is associated with permissiveness to HIV-1 infection (Fantini *et al*, 1993). Several other putative HIV receptors have also been reported.

Two sequences containing heptad hydrophobic repeats follow the fusion peptide in gp41. These are predicted to form a coiled coil (Delwart *et al*, 1990). This coiled coil is critical for fusion, but it not known at which stage it is required. Lu *et al* (1995) studied a bacterially-expressed gp41, which they suggested formed a stable α-helical trimer of heterodimers. In this model, the first predicted coiled coil region forms an interior and parallel homotrimer, and the second coiled coil packs around the exterior in an antiparallel manner. This is very like the C and D helices of TBHA2. A recent study of the predicted coiled coil region of the retrovirus Molony murine leukaemia virus (MoMLV) also suggests that this region does indeed form a stable and trimeric coiled coil, adjacent to the fusion peptide, in the absence of the SU subunit (Fass and Kim, 1995) (see Figure 1.17b). Other evidence of the importance this region comes from proline substitutions in the heptad repeat region which lies nearest to the fusion peptide. These abolished fusion (Dubay *et al*, 1992; Chen *et al*,

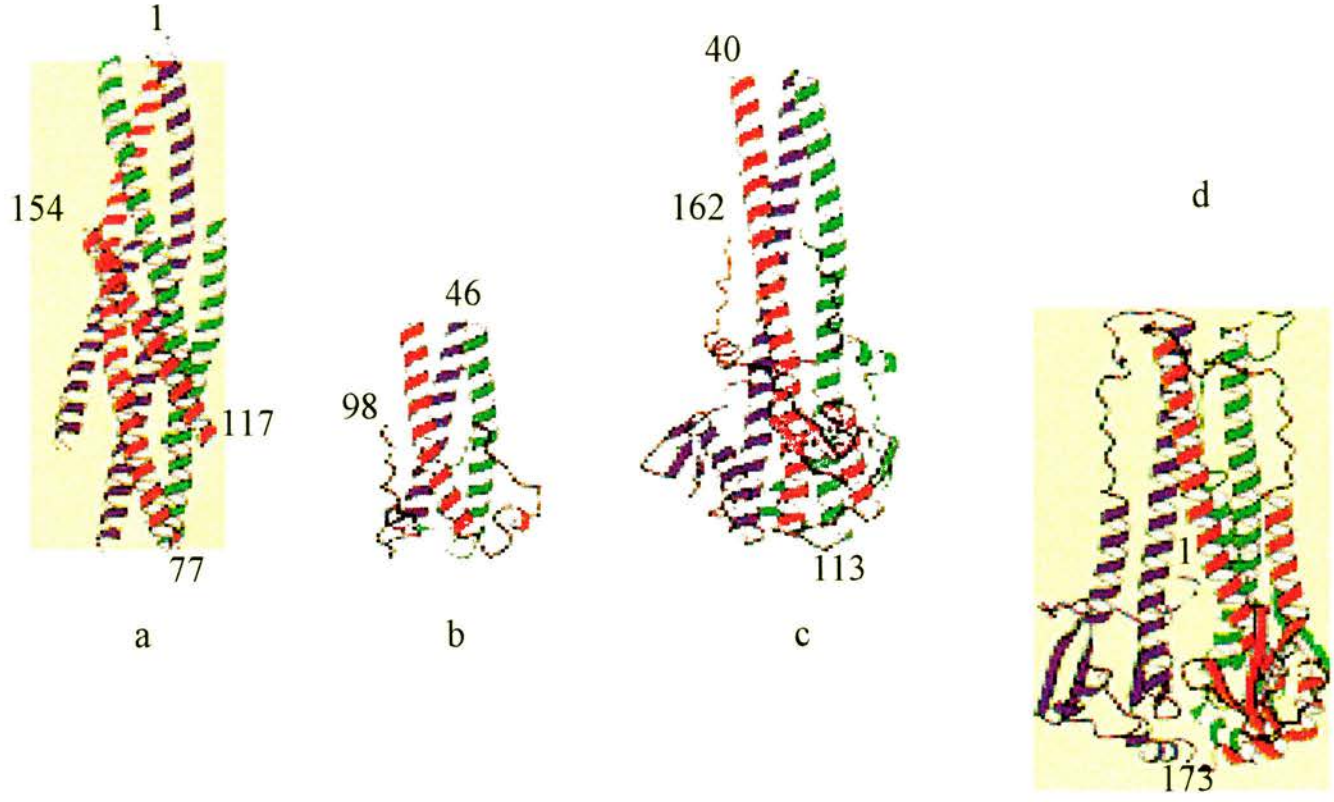

Figure 1.17. Comparison of trimeric viral fusion proteins (reproduced from Weissenhorn *et al*, 1997). The individual subunits are coloured red, green, and blue.
a. HIV-1 gp41, as shown in Weissenhorn *et al*, 1997.
b. Moloney murine leukameia virus TM subunit, as shown in Fass *et al*, 1996.
c. Low pH- induced structure of influenza virus HA2 subunit, as shown in Bullough *et al*, 1994.
d. Neutral pH structure of influenza virus HA2 subunit, as shown in Wilson *et al*, 1981.

1993). Synthetic peptides corresponding to the coiled coil region also inhibited fusion (Wild *et al*, 1994). However, the most recent evidence for structural similarity of this predicted coiled coil region of gp41 to TBHA2 comes from crystallographic studies by Weissenhorn *et al* (1997) (see Figure 1.17a). They replaced the HIV fusion peptide with a trimeric GCN4 coiled coil, and performed X-ray crystallography on the resulting solubilised, protease-resistant fragment of the gp41 ectodomain, which represents about 10% of the original gp120/gp41 complex. The core of this molecule was found to be an extended, triple stranded α helical coiled coil with the amino terminus at its tip. Furthermore, a carboxy-terminal α helix packed against the outside of the coiled coil in an antiparallel fashion, thus placing the amino and carboxy termini near each other at one end of the long rod. This study was performed in the absence of gp120, and since the dissociation of gp120 is required for fusion activity, the assumption is that the gp41 structure formed in the absence of gp120 may well be the final fusogenic form, as was assumed for HA2. The extreme thermostability of the observed structure adds support to this view: triggering of viral fusion proteins would be expected to produce a stable conformation, probably from an initially trapped, metastable form. Chan and co-workers (1997) have also very recently determined the crystal structure of a smaller fragment of gp41, and their results agree very closely with those of Weissenhorn *et al*, as described here.

All lentiviruses have long cytoplasmic tails: 150 to 200 amino acids in length. Mutations in the tail region can affect both the Env ectodomain conformation (Mulligan *et al*, 1992) and the kinetics of HIV infection (LaBranche *et al*, 1994). Rein *et al* (1994) generated a mutant of MoMLV in which the cytoplasmic tail was absent. Cells which expressed this truncated p15E form induced rapid cell-cell fusion. Similar findings have also occurred for SIV (Zingler and Littman, 1993).

It is clear that, despite the lack of any obvious evolutionary relationship between the orthomyxovirus and retrovirus families, there are many similarities between HA and gp160, and indeed TM of MoMLV (see Figure17.a to c). Thus, although individual viral fusion proteins differ in their native structures and triggers required for fusion, the end results of their conformational changes may be the same. Firstly, all three viruses shown here expose and reposition their fusion peptides to

achieve closer approach to their target membranes. Secondly, their polypeptide chains reverse their direction at the far end of the coiled coil from the fusion peptide and proceed back towards the N-terminal tip. This turn occurs at the same place in HIV-1 and MoMLV, residue 78, and the following 15 amino acid residues are also very similar. Thirdly, like the B loop in HA2, which undergoes a loop-to-helix transition at the pH of fusion, gp41 is particularly rich in polar and charged side chains between residues 39 and 53. Thus this region may not be α helical in the native gp120/gp41. Fourthly, the C-terminal link which connects to the transmembrane anchor is probably flexible in all three viruses. The structure of GCN4/gp41 adds more support to the hypothesis that the fusion peptide and transmembrane anchor are indeed likely to be juxtaposed at one end of the coiled coil once the outer layer of helices have assembled onto the core, or in other words, once the protein has turned back on itself. It is not, however, known whether the central coiled coil of gp41 is extended by the conformational change, or whether it exists in this elongated configuration throughout the lifetime of the molecule, with the gp120 subunit protecting it from premature exposure. If the folding of buttressing helices to form a six-helix bundle is indeed a common feature of viral fusion protein activation, then it may provide a new target for the development of antiviral drugs.

More generally, subsequent steps may also involve similar principles: lateral association of oligomers to form fusion active complexes, possible induction of hemifusion, and finally reversible opening of narrow fusion pores, which subsequently and irreversibly dilate (see Figure 1.18). The exact extents to which the same basic mechanisms apply to cellular fusion events remain to be seen.

1.3c Viral Fusion Peptides

The destabilisation of the target cell and viral membranes within the virus-cell adhesion area is a critical step in membrane fusion. The observation that conformational changes of viral fusion proteins led to the uncovering of their fusion peptides suggested that the exposed hydrophobic peptide would initiate fusion,

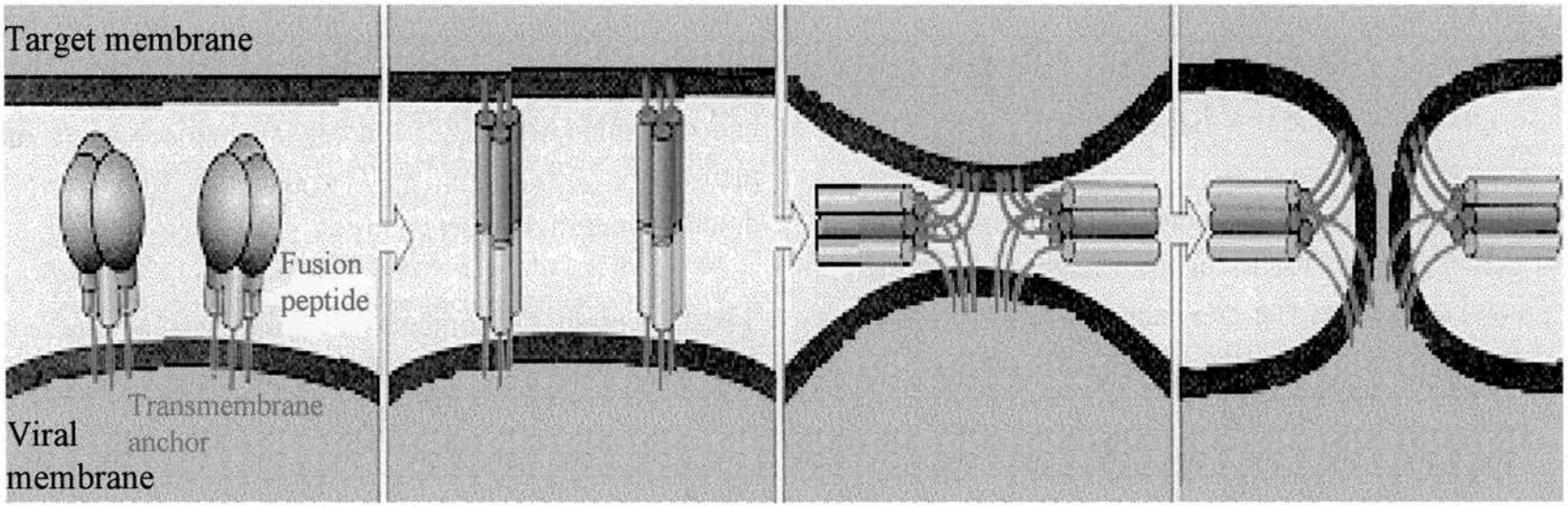

Figure 1.18. Model for the membrane fusion mechanism of viral envelope proteins (adapted from Hughson, 1997). The fusion peptides are exposed following conformational changes in the proteins, and they then embed in the target membrane. The close approach of viral and target membranes are accompanied by further structural changes in the fusion proteins. This brings the transmembrane anchors and the fusion peptides into relative proximity, where they remain after fusion is completed. Cellular receptors are omitted for clarity.

probably by inserting into the target membrane. Thus the ability of synthetic peptides corresponding to these sequences to penetrate into membranes and cause their destabilisation can reveal some of the molecular mechanisms of viral-mediated membrane fusion. The discovery of specific requirements for particular amino acid sequences and peptide structures for fusogenic activity can also aid our understanding of the fusion process. By studying synthetic fusion peptides, it is therefore possible to determine the minimum molecular requirements for protein-mediated fusion. These are usually studied in model membrane systems, which allow complete control of the lipid composition present in the fusing bilayers.

It is clear that many of the features of the intact virus are not present in the simple system of a peptide segment of a viral fusion protein. Receptor binding does not occur, and insertion of a fusion peptide does not cross link two membranes. The viral and target cell membranes are likely to have different physical properties from those of two identical liposomes present in a model system. Oligomerisation is less likely to occur in simple peptide systems, and the conformation adopted by an isolated fusion peptide may be different from that present in the whole fusion protein. On the other hand, the molecular nature of the early steps in fusion may be much harder to unravel in the more complex system of an intact virus. Other parts of the fusion protein, and indeed other members of the oligomeric protein structure, are also involved in fusion. Thus studies on the membrane-destabilising effects of fusion peptides, and the molecular and structural requirements for this process, appear to be more relevant than investigations of the induction of membrane fusion by these peptides.

A number of viruses now have fusion peptides with proven fusogenic capacity, for example Influenza virus, HIV and SIV (e.g. Influenza virus: Lear and Degrado, 1987; HIV: Freed *et al*, 1990; SIV: Bosch *et al*, 1989). Moreover, the specific requirement for the precise amino acid sequence of certain fusion peptides has been demonstrated by mutagenesis. Work by Martin and colleagues (1994) showed that synthetic peptides, which had the same hydrophobicity as the fusion peptide from SIV but an altered amino acid composition, were non-fusogenic. Similarly, Düzgünes and Shavnin (1992) found that the fusion peptides of VSV and the 17 residue fusion

peptide fragment from Influenza virus have the same hydrophobicities per unit but they have different effects upon membranes of the same composition. Thus, whilst the hydrophobicity of these peptides is clearly important if they are to interact with hydrophobic lipid membranes, it alone is not sufficient to provide the ability to promote fusion.

There are still many viruses for whom the fusion peptide is inferred from homology with other known fusion peptides, and for whom the precise length of this fusogenic region is uncertain. This includes the fusion peptide of FeLV.

The mode of action of viral fusion peptides is still not clear. There is, however, much evidence that fusion peptides do not merely act as aggregation agents for neighbouring bilayers. A number of studies have been performed on the effects of specific viral fusion peptides on lipid polymorphism and bilayer stability (e.g. Epand *et al*, 1994; Epand and Epand, 1994; Colotto *et al*, 1996). These have attempted to correlate fusion activity with the induction of bilayer destabilisation, and with the promotion of the formation of non-bilayer phases of negative curvature. The studies involve a very small sample of viral fusion peptides, but they do appear to demonstrate a relationship between these two processes. Fusion peptides may act, at least in part, by increasing the negative curvature of lipid systems. It is unlikely that fusion peptides would significantly reduce the hydrophobic packing voids that are present in inverted phases, since these peptides are not sufficiently hydrophobic to pack into these defects.

Siegel and Epand (1997) have very recently suggested that fusion peptides might also act by lowering the tension required for rupture of the TMC lipid intermediate, thus resulting in more rapid ILA, or fusion pore, formation. If TMCs are common intermediates in two competing pathways, namely the L_{α}-H_{II} and L_{α}-Q_{II} transitions, then the stability of the TMC may be central to the differential rate of formation of these two lipid phases. The longer-lived are TMCs, the more likely they are to aggregate and form quasihexagonal arrays of H_{II} precursors. However, if the TMCs are less stable, they are more likely to rupture and form ILAs, or fusion pores. The lowering of the rupture tension of the TMC diaphragm may occur through an effect of the fusion peptide on the cohesion of the lipid membrane, for example,

through a local change in bilayer thickness around the adsorbed peptide (He *et al*, 1996).

It was suggested by White (1992) that fusion peptides do not actually embed in either the target membrane or the viral membrane, but that they provide a hydrophobic surface along which the lipid molecules could flow between fusing membranes. However, a large body of experimental evidence now exists to suggest that fusion peptides do indeed insert into the target membrane, and, as previously mentioned for HA, possibly also into the viral membrane in the final stages of fusion. Brasseur *et al* (1990) used modelling studies to examine a range of viral fusion peptides. It was assumed that the peptides adopted a purely α-helical conformation, and this study concluded that the oblique insertion of these peptides into the target membrane disrupted lipid packing and thus produced bilayer destabilisation. Epand *et al* (1992) then suggested that longitudinal precession of the obliquely oriented peptide would lead to greater disruption of the bilayer centre than of its surface, thereby increasing the negative curvature pressure, and hence favouring both the formation of inverted lipid phases and fusion.

The secondary structures of individual fusion peptides have been studied (e.g. Düzgünes and Shavnin, 1992; Nieva *et al*, 1994b; Gray *et al*, 1996; Ishiguro *et al*, 1996). This has led to conflicting evidence on their active conformations, with different experiments supporting either the α helix or a β structure for this role.

Attempts have been made to elucidate the angles and depths of membrane insertion of viral fusion peptides (e.g. Martin *et al*, 1993; Martin *et al*, 1994; Macosko *et al*, 1997), once more endeavouring to correlate these factors with fusogenic activity.

The different experimental protocols of previous relevant work on fusion peptides will be considered in each of the related chapters of this thesis, since this prior knowledge provided the foundation from which this project was derived. Thus Chapters 2, 3, 4 and 5 of this thesis are concerned with the structural effects of the fusion peptide of FeLV on lipid polymorphism. Chapter 6 examines the different secondary structures adopted by this peptide under various experimental conditions, and Chapter 7 provides experimental evidence for the fusogenic capacity of this

putative viral fusion peptide. The results obtained from the experiments in this thesis will also be discussed in detail in the light of the previous findings of other research groups.

1.4 Feline Leukaemia Virus (FeLV)

The cat has the widest spectrum of naturally occurring retrovirus-induced diseases of any nonlaboratory animal (Rojko and Hardy, 1994). Of these feline retroviruses, FeLV is the best characterised. FeLV is now recognised as the most common single, non-traumatic cause of death in adult cats worldwide (Rojko and Hardy, 1994). Due to its extremely immunosuppressive nature, it is also responsible for more feline diseases than any other single agent. Clinical symptoms and disease conditions caused by FeLV include lymphosarcomas, leukaemias and anaemias, marrow aplasia, membranous glomerulonephritis, fibrosarcoma, gastroenteritis, polyarthritis, infertility and many more! At present, there is no truly effective vaccine for FeLV; there are 11 different vaccines available in the USA, and the claims by their manufacturers of the efficacies of the individual vaccines may be extremely overinflated. Novel alternative treatments or preventive measures would, therefore, be of great benefit.

FeLV and its related diseases have now been studied for a more than a quarter of a century, partly because of their importance to the cat population, but also as a retroviral animal model (Cotter and Essex, 1977) for human immunosuppressive and neoplastic disorders, such as HIV. The early observations on feline retroviruses were crucial to our current understanding and management of retroviral diseases, both in veterinary and human medicine. Even now, FeLV is still used as a valuable model for the mechanisms of human diseases such as cancer and immunodeficiency. This is partly due to the fact that FeLV is a natural pathogen, which is endemic in an outbred mammalian population, and thus it may parallel human retroviral diseases more closely than than those produced by retroviruses that occur almost exclusively in inbred laboratory animals. As a recent example, Rohn and co-workers (1996) have used experimental infection with molecularly cloned FeLV strains to isolate and

characterise different novel FeLV variants that evolve *in vivo*. They have found that different variants are associated with different pathogenic aspects of the development of thymic lymphoma.

On the public health front, the possible zoonotic potential of FeLV is still unresolved. Oncogenic retroviruses have jumped species barriers in the past to cause lymphomas (Rojko and Hardy, 1994). These have been identified, in the main, by molecular hybridisation techniques or observations of shared DNA sequences. Experimental innoculation of neonatal puppies with FeLV has been shown to cause lymphomas (Rickard *et al*, 1969). Since domestic cats and humans live in close proximity there is great potential for FeLV transmission to humans via cat saliva. *In vitro* experiments have shown that FeLV subgroups B and C can readily replicate in human cells (Jarrett *et al*, 1969; Jarrett, 1971). An American study established that the risk of leukaemia in children was doubled by exposure to sick cats (Bross and Gibson, 1970), whilst a British study found that this increased the risk of childhood lymphoid cancer, but not of other forms of cancer (Penrose, 1970). In the case of adults, no link has been found for the general public, but veterinarians were found to have an almost twofold increase in lymphomas compared to the general adult population (Gutensohn *et al*, 1980). The investigators could neither prove nor disprove FeLV as a possible aetiological factor. Human serum complement does destroy FeLV rapidly and completely, but since this defence system is not fully developed in children, possibly until the age of 6 years, and as it may be impaired in immunosuppressed adults, there exists a possibility of zoonotic infection in these individuals. Thus FeLV possibly has direct importance as a human pathogen. It should be noted, however, that human retroviruses are considered to be very different from all known feline retroviruses.

Jarrett *et al* (1964) first discovered FeLV in 1964. It is a pathogenic, exogenous retrovirus of cats, originally of rodent origin: its nucleic acids are closely related to chromosomal DNA of the modern rat (Benveniste *et al*, 1975). The belief is that, one to ten million years ago, in a northern African desert, an ancestral cat ate an ancestral rat, which had harboured and replicated its own endogenous retrovirus. Thus the cat became infected with the rat virus! In 1973 it was shown that FeLV is transmitted contagiously (Jarrett *et al*, 1973; Hardy *et al*, 1973), thus dispelling the

belief that cancer-causing retroviruses were laboratory artefacts. This also led to the eventual realisation that contagious transmission is far more frequent than genetic transmission for most retroviruses. The commonest route of FeLV horizontal transmission is by excretion in infected cat saliva.

FeLV belongs to the Family Retroviridae, Subfamily Oncovirinae, and has three subtypes A, B and C, each of which has several different strains. It is an enveloped RNA virus, of diameter 110nm. Its structure is shown in Figure 1.12. Surrounding the genome is a hexagonal core protein coat, containing the p27 protein, then an acidic coat of protein p12, and finally an envelope containing viral gp85 glycoprotein spikes. gp85 is the fusion protein of FeLV, and comprises two polypeptide subunits, generated by proteolytic cleavage. The SU subunit is called gp70 and is linked by disulphide bridges to the TM subunit, p15E (Schäfer and Bolognesi, 1977; Bolognesi *et al*, 1978). gp70 contains the receptor binding site (Laird *et al*, 1973) and has an FeLV subgroup-specific antigenic domain (Jarrett and Russell, 1978). FeLV-B infects many non-feline cell lines *in vitro* and recognises the human Pit1 receptor, a sodium-dependent phosphate symporter, although certain strains of FeLV-B can also use the human Pit2 receptor (Boomer *et al*, 1997). FeLV-A primarily infects feline cells; the receptor for FeLV-A is not as yet known. p15E houses the transmembrane-anchoring region, an extremely immunosuppressive amino acid sequence, and the putative amino-terminal fusion peptide. This extremely hydrophobic putative fusion peptide is 27 amino acids in length and shows a large degree of homology to other known retroviral fusion peptides (see Table 1.1). It is also completely conserved between all known strains of FeLV. FeLV fuses directly with the target cell's plasma membrane (Laird *et al*, 1973), and thus shows pH-independent fusion.

1.5 The Aims of This Project

The main objective of this research project was to characterise the fusion peptide of FeLV, using a variety of complementary biophysical and biochemical techniques. The FeLV fusion peptide sequence is listed in the Swiss Protein Data

Base, and has also been quoted in several scientific papers. However, to my knowledge, there is currently no published experimental work on the molecular mechanisms of FeLV-induced fusion that follow receptor binding, and more especially, on the fusion peptide of FeLV. Thus, on commencing this research, the aims were to ascertain the membrane-destabilising effect of this peptide sequence, and to identify the secondary structures of the peptide in its active and inactive forms. A variety of complementary biophysical techniques have been employed to obtain this information. Biochemical fluorescent fusion assays were also performed, in an attempt to induce fusion by this peptide, and to determine the conditions required for this to occur.

By studying one specific fusion peptide in detail, it is hoped that one may gain a wider understanding of the principles of viral fusion in general, and possibly even some insights into certain aspects of cellular fusion processes. It is only by fully understanding basic life processes such as fusion that we can logically design therapeutic agents to alter these processes when required. Even at present it is possible to use the correlations between observations in model systems and in biological membranes to predict the effect of membrane additives, and to design new therapeutic agents on this basis. Thus several antiviral drugs are bilayer stabilisers, for example carbobenzoxy-D-Phe-L-Phe-Gly (Epand, 1986), and tromantidine (Cheetham and Epand, 1987). Cyclosporin also stabilises bilayers, and it inhibits membrane fusion in model systems at low concentration (Epand *et al*, 1987). Furthermore, this agent specifically inhibits herpes simplex virus induced cell-cell fusion (McKenzie *et al*, 1987). Tromantidine, an inhibitor of herpes penetration, inhibits the increased cell membrane protein diffusion caused by this virus (Epand, 1990). In view of the extremely limited range of clinically useful antiviral agents available at the current time, and the particular difficulties associated with the treatment, and indeed prophylaxis, of retroviral infections, an increase in our understanding of the infective mechanisms of these obligate intracellular parasites, and the design of novel antiviral therapeutic agents can only be advantageous.

Chapter 2: The use of Differential Scanning Calorimetry to determine the effects of the Feline Leukaemia Virus Fusion Peptide on a Lipid Bilayer to Inverted Hexagonal Phase Transition Temperature

2. Differential Scanning Calorimetry

2.1. Theoretical Background to Thermal Analysis

Thermal analysis can be used to measure certain aspects of phase transitions of lipids. A substance, such as a lipid, that is heated will maintain a constant temperature during a phase transition despite continued heat input, since energy is required to separate the component lipid molecules. The heat energy supplied during a phase transition thus enables the molecules to overcome the forces between them, causing their regular molecular packing to break down and giving them a greater degree of freedom and disorder, or entropy. This heat energy, which the sample absorbs in an endothermic transition and releases in an exothermic transition, is called the latent, or hidden, heat, since it does not produce a change of temperature in the sample. Thus a plot of sample temperature against time as a lipid is heated will show an inflection which gives an indication of the lipid's phase transition temperature. 'Thermal analysis' originally referred to such simple heating experiments, which date from the middle of the 18th century. Thermal analysis methods use calorimeters, which are measuring devices in which a precisely determined amount of heat is supplied to a sample, or abstracted from a sample, and the resultant temperature change in the sample is measured.

In 1899 Roberts-Austen found that a more accurate measure of transition temperatures could be obtained by plotting the difference in temperature between the sample and its surroundings. This then led to the development of Differential Thermal Analysis (DTA), notably by Le Chatelier. Present day DTA compares the sample with an inert reference under carefully controlled conditions of heating or cooling. Thus the sample and a similar mass of reference material are placed in separate holders and inserted into a heating block. The reference material is a substance which does not undergo a phase transition in the temperature range of interest, for example a quantity of the pure solvent that was used in the sample preparation. The temperatures of both sample and reference are measured electrically using thermocouples or platinum resistance thermometers. The same heat flow is supplied to the two materials, and thus their temperatures rise at approximately the same rate until a phase change

occurs. The sample will then maintain a constant temperature until it has changed phase, whilst the temperature of the reference material will continue to rise. When the phase transition is complete, the sample then increases in temperature once more until it equilibrates with the heating block, and the temperatures of the sample and reference will thus reconverge. A plot of the sample temperature (Ts) minus the reference temperature (Tr) will show a negative asymmetric peak, the position of which gives an accurate measure of the phase transition temperature (see Figure 2.1). Moreover, the area under the peak is related to the amount of heat absorbed during the transition. However, quantitative measurements are obtained more accurately using the related technique of Differential Scanning Calorimetry (DSC).

In DSC experiments the sample and reference materials are heated individually so that a constant temperature difference is maintained between them, even during phase transitions. This is accomplished by a feedback mechanism which alters the rate of heat flow to the sample. Thus when the sample reaches its phase transition temperature, the required constant temperature difference between sample and reference can only be achieved by a large increase in the rate of heat flow to the sample. The measured signal in DSC is proportional to the rate of heat flow to the sample, and a plot of this quantity against the sample temperature will show a positive peak during endothermic transitions (see Figure 2.2). (Endothermic processes have positive peaks by definition in thermodynamics). The total area under a DSC peak can also be measured, and, providing that the sample is totally enclosed within the heating block, this area is directly related to the heat of transition with an accuracy of about 2% (Warren, 1987).

DSC has several advantages over DTA: disturbances such as temperature variations in the environment of the measuring system affect the sample and reference materials similarly in DSC studies and, moreover, compensation is made for these disturbances when the difference between the two individual systems is determined.

There are still some problems and limitations associated with DSC of which one should be aware. Firstly, there is no theoretically well-founded, complete understanding of DSC, nor is there, as yet, an international agreement on procedures for the temperature calibration and caloric calibration of DSCs which have been

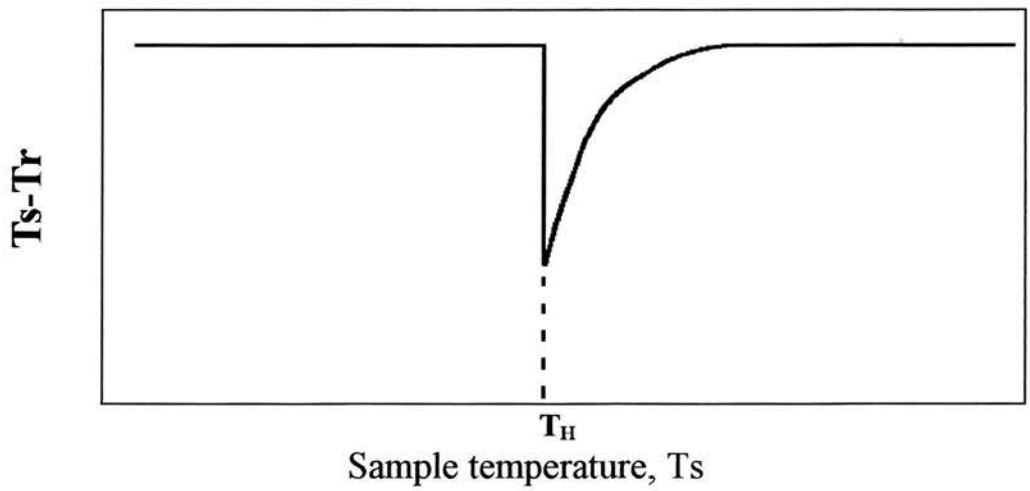

Figure 2.1. Ideal DTA heating curve of a pure substance undergoing a phase transition at a temperature T_H. The sample is heated at a constant rate, and the difference between the sample temperature, Ts and the reference temperature, Tr, is plotted against the sample temperature.

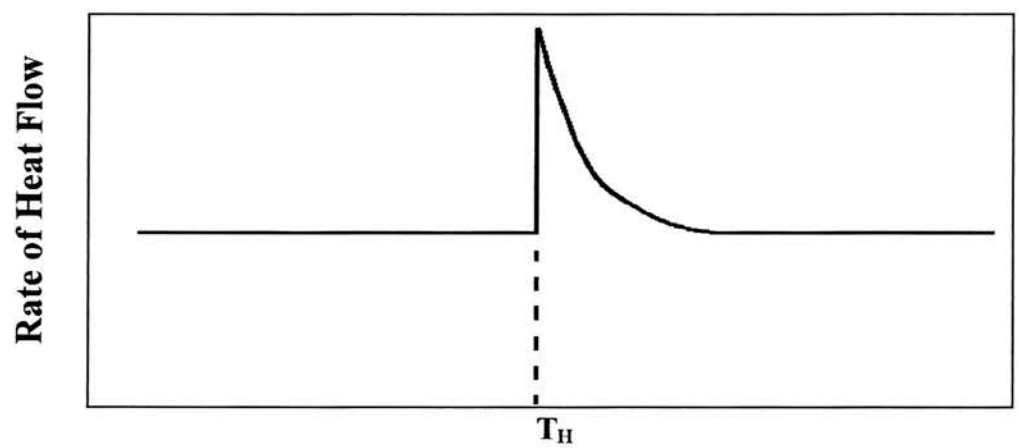

Figure 2.2. Ideal DSC heating curve of a pure substance undergoing a phase transition at temperature T_H. The required rate of heat flow to sustain a constant temperature difference between the sample and reference is plotted against the sample temperature.

definitely backed up both theoretically and experimentally. Secondly, the basic information regarding the behaviour of two substances when they are mixed together is contained in the binary phase diagram for the system. This phase diagram relates to the behaviour under equilibrium conditions, and the validity of phase boundaries determined by DSC will depend upon the rate at which equilibrium conditions are obtained. Thus differential thermal methods are most suitable for the study of systems in which equilibrium conditions are attained rapidly. Nonetheless, DSC is a recognised technique for the study of the effect of fusogens on T_H of lipid systems, since it is perfectly accurate for relative measurements, even if it may be slightly inaccurate for some absolute measurements. Thus whilst the recorded values of T_H for these systems may not be precisely the same as the true thermodynamic values, the effect of an added impurity, such as a fusion peptide, on T_H will be valid.

2.2 Practical considerations for DSC

The development of highly sensitive calorimeters, which require only milligram quantities of sample, has increased the resolution of DSC, and has also extended its application to materials that are only available in small amounts. The best results are obtained using the minimum size of sample, and also the minimum heating rate which will provide a satisfactory signal. It is essential for DSC measurements that the measuring system is composed of solid parts, and has defined heat conduction paths. This allows the sample reaction to be regarded as a small disturbance of the steady-state temperature field that is produced by the heating protocol. The noise of the system must be low to enable sensitive measurement of heat flow rates. Good thermal contact between the sample capsule and holder, and an even distribution of sample within the capsule, are essential to allow satisfactory interpretation of the baseline. This can be difficult with multi-component systems, since it may be hard to obtain a small sample that is homogeneous, and thus truly representative. The shape of the DSC peak is also affected by these factors, as well as the thermal resistance between the sample and its holder, and the thermal conductivity within the sample. Thus a granular sample may produce an irregular peak, and sample purity is of utmost

importance. A minimum of deadspace within the sample capsule is also essential in order to prevent separation of a free water layer by evaporation and recondensation of water within the capsule.

2.2a Power Compensation DSC

The DSC calorimeter consists of two identical microfurnaces of the same type (usually made of a platinum-iridium alloy), each of which contains a temperature sensor (platinum resisitance thermometer) and a heating resistor (platinum wire). The microfurnaces, which are thermally decoupled, are positioned in an aluminium block of constant temperature. A purge gas of nitrogen or helium flows through the chambers continuously. (Helium is preferred to nitrogen due to its higher thermal conductivity). During heating scans, the same heating power is supplied to both microfurnaces, using a control circuit to change their mean temperatures at a preset scanning rate. If there is ideal symmetry, the temperature of both microfurnaces will be identical. However, when an asymmetry occurs, a temperature difference between the two microfurnaces results, which generates an input signal, in the form of a voltage, to a second control circuit. This control circuit then tries to compensate for the temperature difference by changing an additional heating power. The compensating power is proportional to the temperature difference, and the total compensating energy, the integral of power against time, is equal to the reaction heat, or the heat of the phase transition. A heat flow rate is internally assigned to the real measured signal using factory-installed calibration. The output signal is also given as a heat flow rate signal, and is related to the true heat flow rate by a constant value, which must be determined by caloric calibration. Calibration at several different temperatures is required, since the response of the system is non-linear. This is achieved using substances of known melting point.

There is no ideal power compensation DSC. In real machines the sample is always put into a container which is then placed into a heater, so that at least one heat conduction path and thus at least one time constant exists between the heating control and the sample location. Moreover, the proportional controller can never completely

compensate for the measured temperature difference, so that a slight temperature difference remains between the sample and the reference. Thus the calibration factors depend upon the temperature and thermal conductivity of the sample, the heating rate and on the magnitude of the heat of the phase transition. The temperature difference between the two microfurnaces is also not totally compensated for in commercial DSC machines. During a phase transition peak there is still, therefore, a temperature difference between sample and reference, which is proportional to the reaction heat flow rate. Hence the measured signal is 'smeared' in comparison with the processes inside the sample, and the measured curve put out by the DSC machine is only a 'smeared' representation of the function searched for. In many cases however, this measured curve is sufficiently accurate for the desired evaluations to be made. This is true for the determination of the temperatures of lipid phase changes.

2.3 Application of DSC to Fusion Studies: Aims of these DSC Experiments

Correlations have been found between the promotion of membrane fusion by certain compounds and their ability to lower the lipid bilayer to inverted hexagonal phase transition temperature, T_H, as measured by high sensitivity DSC (e.g. Siegel *et al*, 1989b; Epand *et al*, 1994; Epand and Epand, 1994). Similarly, fusion inhibitors have been shown to raise T_H (Epand, 1986). Whilst kinetically-stable lipid phases, such as the H_{II} phase, may not be involved in biological fusion, the first steps in their transition pathways from the lamellar phase may be very important, in particular the bilayer destabilisation thus produced. Fusion catalysts are thought to affect the kinetics of the phase transitions, and not the thermodynamic stability of the individual lipid phases themselves. Moreover, a favouring of the conversion of the lipid bilayer to non-lamellar phases, such as the H_{II} phase, should enhance the rate of formation of fusion intermediates, such as the 'modified stalk' (Siegel and Epand, 1997).

In the light of these previous experimental findings for known fusogens, a DSC study of the FeLV fusion peptide was performed. The aims were to ascertain the effect of a range of peptide concentrations on T_H, and thus determine any effects of the FeLV fusion peptide on the conversion of the lipid bilayer to the H_{II} phase. This,

in turn, might identify certain membrane destabilising properties of the FeLV fusion peptide, and might also provide some support for the link between the bilayer-inverted hexagonal phase transition and membrane fusion.

2.4 Materials and Methods

2.4a FeLV Fusion Peptide

The 27 amino acid sequence of the amino-terminal fusion peptide, which is common to all documented strains of FeLV, was ascertained to be EPISLTVALML-GGLTVGGIAAGVGTGT (Swiss Protein Data Bank, 1996; release number 34.0). This peptide has proved to be extremely difficult to work with, due to its high hydrophobicity, and its total lack of solubility in almost all common solvent systems. Initially, two batches of peptide were synthesised, using the Merrifield solid-phase principle, by two different commercial companies. Neither of these companies could purify the resulting crude peptides due to the aforementioned lack of peptide solubility. Consequently, several attempts were made to purify these crude peptides, using reverse-phase high performance liquid chromatography (HPLC). A Phenomenex C8 Primesphere column (250 × 4.6mm) was used, which is a preparative column, with a C8 guard column in place. The peptides were partially dissolved in dimethylformamide (DMF) with prolonged sonication, and aliquots of this solution were applied to the column, and eluted using the solvent gradient method of:

Time (mins)	%B	Flow Rate
0	0	0.75ml/min
5	0	throughout
45	100	elution
50	100	process
51	0	
70	0	

where solvent A was water/0.1% trifluoroacetic acid (TFA) and solvent B was acetonitrile (ACN)/0.1% TFA. Both solutions were filtered before use.

A Pharmacia LKB HPLC machine with low pressure mixing system was employed. Identical aliquots of the peptide did not elute from the column at a constant time, nor were the peptide peaks of constant size and shape. This was most probably due to the difficulties in obtaining a true solution of the peptide in DMF. However, the peptide also appeared to stick on the column during some runs, so that no peaks other than those of the solvents were obtained. The peptide chemical research group, which is headed by Professor Ramage in the Chemistry Department at Edinburgh University were then contacted, and asked for advice on purifying these crude peptides. Initial Mass Spectrometry runs confirmed speculation that there was indeed very little of the desired peptide present in these samples, and that it would be uneconomical and extremely difficult to attempt any purification processes. However, Professor Ramage's group, which now works commercially under the name of Albachem Ltd, 26 Craigleith View, Edinburgh, EH4 3JZ, Scotland, UK, are very experienced in the handling of highly hydrophobic peptides and they offered to attempt the synthesis and purification of this peptide, partly in the interests of their research on this topic. A lysine (which is the next naturally occurring carboxy terminal residue in the fusion protein) was included on the carboxy terminus to increase peptide solubility. The peptide was synthesised on an Applied Biosystems 430A instrument, using Fmoc chemistry with the side chain protecting groups selected as tBu (Ser, Thr) and OtBu (Glu). The completed peptide was cleaved with a solution of TFA/H_2O (95%:5%) plus scavengers (ethanedithiol/thioanisole/triisopropanesilicane) and the solvent was evaporated under vacuum. The crude peptide was then dissolved in 50% TFA/H_2O and successfully purified by reverse-phase HPLC, using a RPC4 (10 x 100mm) column, eluting with a linear gradient from 10% acetonitrile in water (0.1% TFA) to 60% acetonitrile in water (0.1% TFA) over 30 minutes. The peptide was characterised by mass spectroscopy (MALDI, PerSeptive Biosystem laserTec) (see Figure 2.3), amino acid analysis (LKB 4150 alpha amino acid analyser) (see Table 2.1) and analytical HPLC using PRC4 (4.6 x 100mm), RPC8 (4.6 x 220mm) and Vydac C8 (4.6 x 250mm) columns, running a linear gradient of 10% acetonitrile in water (0.1% TFA) to 90% acetonitrile in water (0.1% TFA) over 30 minutes (see Figure 2.4). The assembly of the peptide was reasonably efficient, but the purification

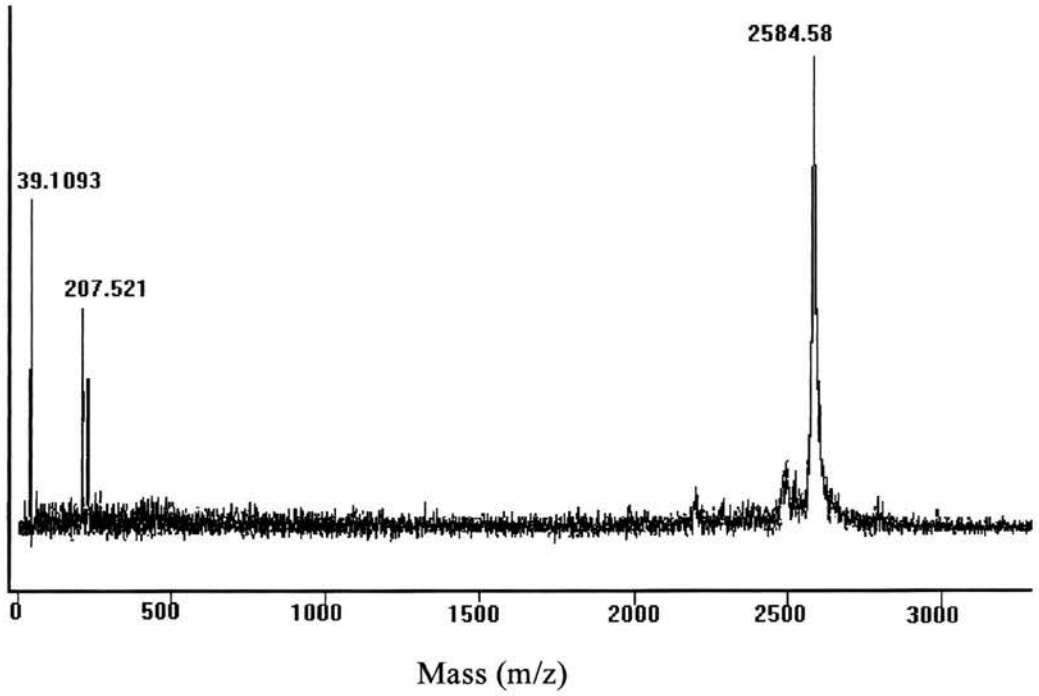

Figure 2.3. Mass spectrometry analysis of the purified FeLV fusion peptide. The low molecular weight peaks represent components of the matrix used to support the sample. The main peak of high molecular weight represents the purified FeLV peptide. The predicted mass is 2583.57.

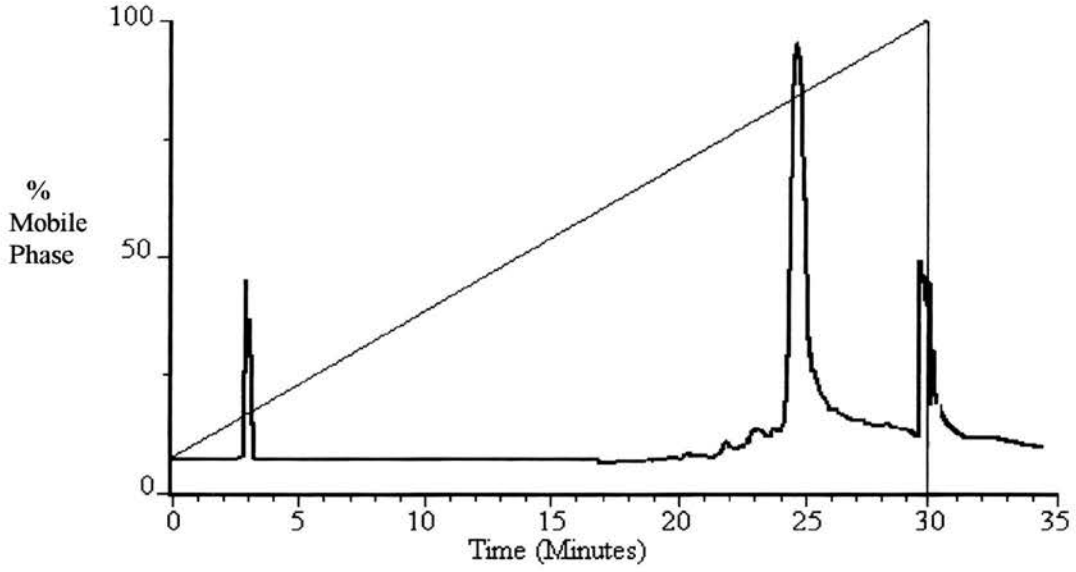

Figure 2.4. Analytical HPLC trace for the purified FeLV peptide. The peaks at 3 mins and at 31 mins are solvent peaks. The diagonal line represents the percentage mobile phase present at any specific time.

Amino Acid	FeLV Peptide:	
	Composition of synthesised peptide	**Stoichiometric %s expected from amino acid sequence**
ASX	0.1	0.0
GLU/GLX	4.8	5.0
SER	3.2	3.5
GLY	15.3	15.5
HIS	0	0.0
ARG	0	0.0
THR	17.1	15.8
ALA	8.7	8.3
PRO	3.3	3.8
TYR	0	0.0
VAL	11.9	11.6
MET	4.8	5.1
PE-CYS	0	0.0
ILE	8.5	8.8
LEU	16.9	17.6
PHE	0	0.0
TRP	0	0.0
LYS	5.4	5.0

Table 2.1. Comparison of the stoichiometric percentages of individual amino acids present in the synthesised FeLV fusion peptide, as determined by amino acid analysis, with the expected stoichiometric percentages for each individual amino acid, calculated from the peptide sequence.

process was found to be very difficult. The peptide was found to be very insoluble; accordingly, 50% TFA was added to take it into solution. However, a very broad peak without any resolution was obtained under normal eluting conditions, unless a very dilute solution was applied. Thus the purification could only be carried out batchwise on a small, analytical-sized scale (0.5 to 1.0 mg per run). Even so, some runs yielded no peaks due to the peptide remaining stuck on the column.

2.4b Preparation of Lipid and Lipid/Peptide films

Pure PE is readily able to adopt the H_{II} phase structure. The transition from the lamellar to the H_{II} phase is induced by an increase in temperature. PEs have several advantages for use in DSC studies on fusion peptides. They do not form well sealed vesicles, which increases the likelihood of the peptide having access to all of the lipid present in the sample. Also, PEs are lipids which enhance the rate of virus-induced fusion (White *et al*, 1982; Stegmann *et al*, 1985). Dipalmitoleoylphos-phatidylethanolamine (DiPoPE) was chosen for this study as it had been used previously for DSC studies on other known viral fusion peptides, and as it was known to have a relatively low T_H of 43.2°C (Epand, 1990). Thus studies of this lipid can be performed at temperatures that are at, or close to, biologically relevant temperatures, which are unlikely to cause significant thermal denaturation of any folded form of the fusion peptide and which are sufficiently close to the ambient temperature that heat losses due to exchanges with the environment are small. (DSC experiments performed at high temperatures have the added problem that the heat flows exchanged with the surroundings, by conduction, convection and radiation, will be relatively large compared to the quantity of heat to be measured.) The disadvantage of PEs is that they do not form well-dispersed aqueous suspensions, and thus great care is required to produce homogeneous samples.

DiPoPE was purchased from Avanti Polar Lipids (Alabaster, AL, USA). Purity was confirmed by Thin Layer Chromatography, which showed a single spot for this lipid.

Weighed amounts of the lipid, or lipid plus peptide, were vortexed thoroughly in chloroform. The peptide-containing samples were then sonicated until the peptide dissolved. The chloroform was evaporated using a stream of dry nitrogen gas, depositing each lipid or lipid/peptide sample as a film on the walls of a 13 × 100mm Pyrex test tube. The surface area of the film should be as large as possible so that the lipid film produced is very thin (New, 1990), and nitrogen is used in order to try to prevent peroxidation and oxidation of the lipids. These samples were then placed under vacuum for four hours, followed by lyophilisation overnight to remove any residual solvent molecules. The resulting films were then suspended in buffer, and vortexed vigorously at room temperature for 10 minutes. The buffers used were 20mM PIPES, 1mM EDTA, 150mM NaCl and 0.002% sodium azide for the experiments conducted at pH 7.4, and 10mM citrate, 0.15M NaCl for the pH 5.0 samples. All samples were made to a final DiPoPE concentration of 10mg/ml, including varying peptide concentrations as required, and they and the reference buffers were degassed under vacuum just prior to use. Thorough mixing was applied to ensure as uniform a sample suspension as possible for injection into the sample chamber.

2.4c Differential Scanning Calorimetry

An MC-2 high sensitivity scanning calorimeter (Microcal Co., Amherst, MA, USA) was employed, which is a power compensation DSC machine. This is calibrated by an electrical pulse which travels through a heating element of known resistance in the reference cell. This calibration was also verified by measuring the enthalpy of well established phospholipid phase transitions, such as that of Dipalmitoylphosphatidyl-choline (DPPC). The sample chamber held 1.4ml, and nitrogen gas purged the system. A scan rate of 45K/h was used. Continous heating scans were run from 25°C through to 60°C.

Using the MC2, the raw data curve is the difference in power supplied to the two cells to maintain their temperatures identical to within 0.0001°C. Thus raw data are in units of mCalories(mCal)/min. The computer software was then used to divide

these figures by the scan rate, so that the data were now in units of mCal/°C. Next the data were divided by the number of millimoles of lipid present in the sample, having taken into account the cell volume. Thus the results were now in units of Cal/°C/Mole lipid. A baseline was then drawn to connect the parts of the curve before and after the phase transition. At least two points before and after the peak were selected. This yielded a curve which showed the excess enthalpy of the phase transition compared to the baseline values. A 'Deconvolute' programme was then used to determine the enthalpy and phase transition temperature for this curve. This recorded bilayer to hexagonal phase transition was fitted to one ideal two state process, as described by a single van't Hoff component, using the DA2 software pakage from Microcal, and the reported transition temperature is that for the fitted curve.

The van't Hoff equation relates the decrease in the phase transition temperature of the lipid/peptide mixture to the amount of peptide present. This is based on the simplest theory, which treats the sample as a eutectic mixture (a eutectic mixture has the lowest freezing point of any possible proportions of its constituents). In principle, any phase transition of a eutectic mixture starts at the eutectic temperature and ends at a temperature T, which is related to the composition of the mixture by:

$$x_{imp}(T) = \Delta H \frac{T_{trs} - T}{RT^2_{trs}} \qquad 2.1$$

where x_{imp} is the mole fraction of the eutectic impurity, in this case peptide; T_{trs} is the phase transition temperature of the completely pure component, which is DiPoPE here; ΔH is the phase transition enthalpy of the pure component, or lipid, at the resulting temperature, and R is the gas constant, 8.31441 J mol^{-1} K^{-1}. Thus if the amount of impurity, or peptide, present is known, the transition temperature can be calculated more accurately than that which is measured directly.

2.5 DSC Results and Discussion

Figure 2.5 shows three representative thermograms, at pH 7.4, from which values for T_H were obtained. The curves are displaced vertically from one another for convenience of display. It can be seen that T_H is lowered in the presence of both of the concentrations of FeLV fusion peptide shown. At very high peptide concentrations, such as are seen in Figure 2.5(c), the baselines were in some instances slightly irregular. This reflects the difficulties that were encountered in maintaining samples with large amounts of the FeLV peptide present in a completely homogeneous state for the entire duration of experiment. Plots of the change in T_H with increasing peptide mole fraction, at pH 7.4 and pH 5.0, are shown in Figures 2.6a and 2.6b respectively. The resultant curves show an initial decrease in T_H, followed by an increase in T_H with consecutive rises in the peptide:lipid molar ratio. At peptide mole fractions of $>1.5 \times 10^{-3}$, a broadening of the enthalpy peaks was observed, which indicates a decrease in cooperativity for this transition. A broadening of endotherms has been seen previously in the presence of the fusogen DAG (Siegel *et al*, 1989b). The two pH curves are at least biphasic: obviously the possibility exists that these curves are described by more complex functions.

T_H is the temperature at which the free energies of the L_α and H_{II} lipid phases are equal. Thus T_H is a measure of the relative stability of the L_α and H_{II} lipid phases, and the effect of a peptide on T_H is a measure of how the peptide affects the relative stability of these two phases. The reduction in T_H that was observed initially with increasing peptide concentration suggests that, at peptide mole fractions less than or equal to 1.5×10^{-3}, the FeLV fusion peptide favours the formation of the H_{II} phase over the L_α phase at both pH 5.0 and pH 7.4. The FeLV virus fuses with biological cells at pH 7.4 (Laird *et al*, 1973), so a decrease in T_H at both pH values is to be expected with this fusion peptide. DSC experiments performed at pH 7.4 using a synthetic dodecapeptide corresponding to the amino-terminal SIV fusion peptide also showed a decrease in T_H with the wild type fusion peptide, while little change in T_H was seen with a non-fusogenic mutant (Epand *et al*, 1994). Experiments which studied the effect of the Influenza virus fusion peptide on T_H found a difference with

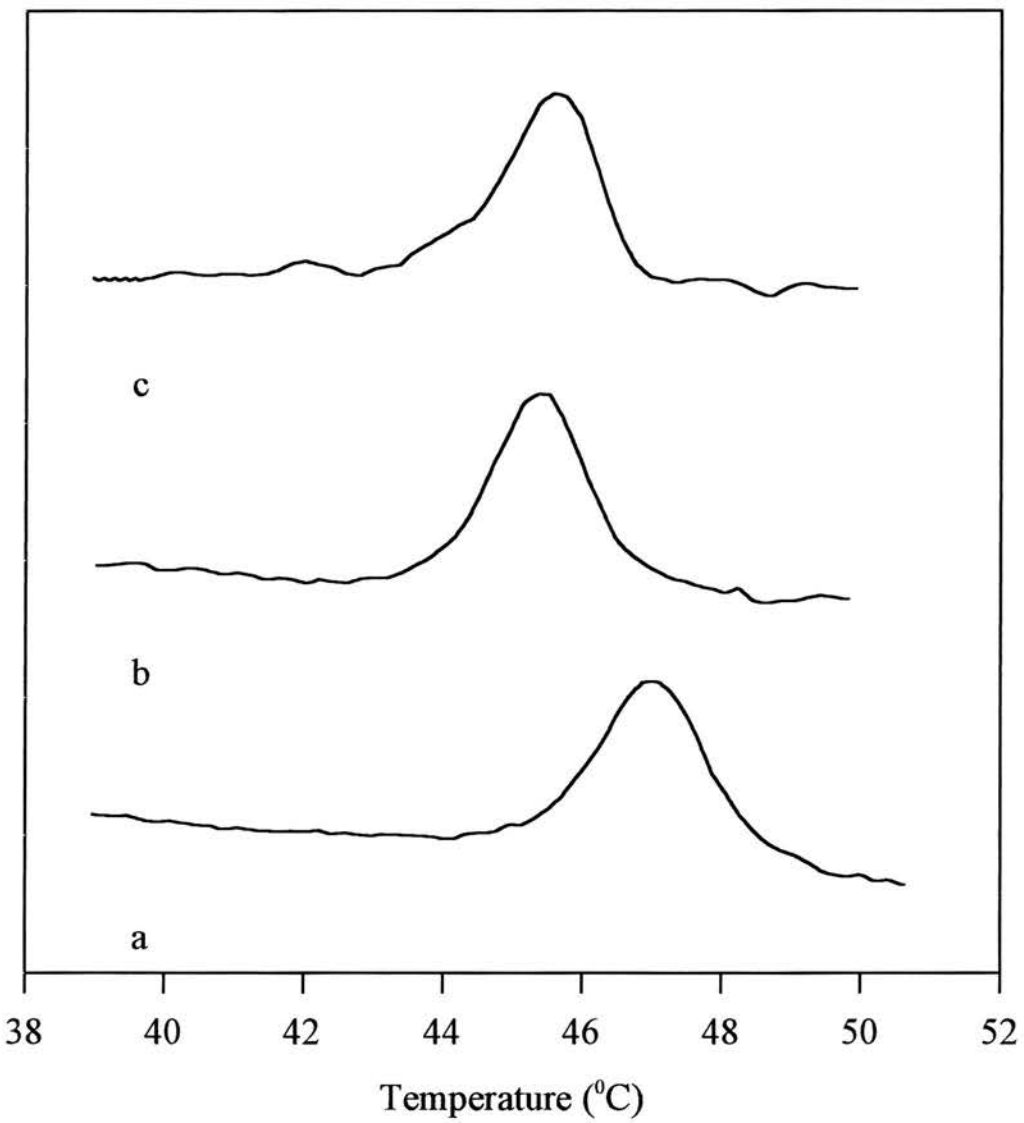

Figure 2.5. Some representative thermograms, obtained at pH 7.4. Pure DiPoPE (a); DiPoPE with FeLV peptide, at a peptide mole fraction of 0.5×10^{-3} (b) and 0.65×10^{-3} (c). T_H is lowered in the presence of the FeLV peptide. DSC heating scan rate 45K/hr.

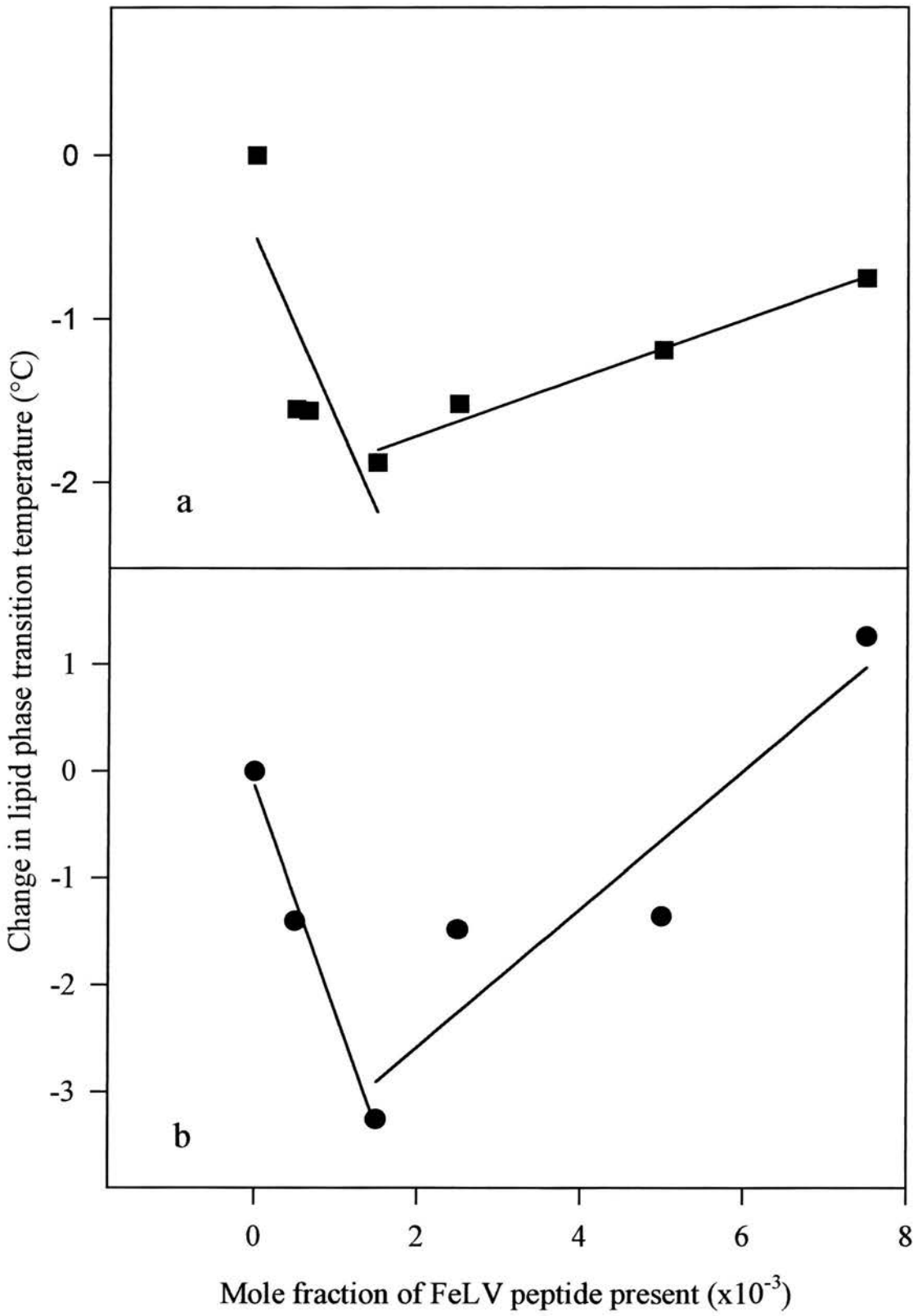

Figure 2.6. Change in the lamellar to inverted hexagonal phase transition temperature as a function of the mole fraction of Feline leukaemia virus fusion peptide present at pH 7.4 (■) (a) and pH 5.0 (●) (b).

pH (Epand & Epand, 1994): this fusion peptide lowered T_H at pH 5.0, but increased T_H at pH 7.4. These findings correlate with the Influenza virus peptide's pH-dependent fusogenic ability. In the same study two non-fusogenic Influenza virus mutants, which had a glutamate substituted for the glycine at position 1 or 4 of the fusion peptide, were found to raise T_H, at both pH 5.0 and pH 7.4. This suggests that, at low peptide concentrations, a lowering of T_H is a fundamental property of viral fusion peptides. Table 2.2 shows the values of the slopes for the dependence of T_H on the mole fraction of fusion peptide for these three peptides, which provide a measure of the effect of the peptides on bilayer stability. It should be noted that the range of peptide concentrations included here is not the same for FeLV as for the other two peptides studied, since only the FeLV data which show a reduction in T_H are considered, that is the first half of the plotted results. This may explain, in part, why the FeLV gradients are so much steeper. However, some of the quantitative differences between these values may be due to the difference in the structures of the fusion peptides. The FeLV peptide has an acidic residue on its amino terminus, the Influenza peptide has several acidic residues along its length, and the SIV peptide has no polar residues. These factors will affect the depth and angle of peptide penetration into the lipid bilayer: alteration of the amino acid sequences of fusion peptides changes the membrane orientation of these peptides (Brasseur *et al*, 1990).

Other known fusogens have also been shown to stabilise the H_{II} phase relative to L_α. Thus 2 mol% DAG, which is produced *in vivo* by the phosphotidylinositol cycle, can lower T_H (Siegel *et al*, 1989a) for some lipid systems by as much as 20°C. Moreover, T_H decreases in an approximately linear fashion with increasing DAG in the concentration range of 0-3mol% (Siegel *et al*, 1989b). CHEMS (cholesterol hemisuccinate) promotes H_{II} phase formation at acidic pH, and significantly enhances the rate of Sendai virus fusion at pH 5.0 (Cheetham and Epand, 1987).

The reduction in T_H is less at FeLV peptide mole fractions above 1.5×10^{-3}, at both pH 5.0 and pH 7.4. This may be due to increased self-aggregation of the extremely hydrophobic FeLV peptide molecules at these higher concentrations, thus preventing them, in part, from inserting into the lipid bilayers. Grossly, the peptide does appear to self-aggregate in these concentration ranges, as seen by the

Viral Fusion Peptide	Slope of line (°C/molar fraction peptide) at pH 5.0.	Slope of line (°C/molar fraction peptide) at pH 7.4.
Influenza HA2	-453 ± 112 [a]	301 ± 49 [a]
SIV	not studied	-360 ±100 [b]
FeLV	-2128 ± 233	-1116 ± 444

[a]: from Epand,R.M., & Epand, R.F. (1994).

[b]: from Epand, R.F. *et al* (1994).

Table 2.2. Comparison of the effect of viral fusion peptides on T_H of DiPoPE.

formation of gel-like masses in these samples by the end of the heating scans. It has been observed previously that fusion peptide analogues aggregate in solution (e.g. Wharton *et al*, 1988; Takahashi, 1990). A similar phenomenon has also been observed with Amphotericin B, which is extremely hydrophobic in nature (Epand, R.M., personal communication). A synthetic 19 amino acid peptide corresponding to the amino terminus of the F1 subunit of the Measles virus fusion protein lowered T_H of Dielaidoylphosphatidylethanolamine (DEPE), but only by a maximum of 1.5°C (Epand *et al*, 1992). However, this peptide is also extremely difficult to solvate, and thus it is probable that it is not uniformly distributed in the samples, which may reduce its effect on lipid phase behaviour.

The FeLV pH 5.0 results show a more marked decrease in the lowering of T_H compared to the pH 7.4 data. Presumably there is more self-aggregation of the peptide at this pH, possibly due to a decrease in negative charge of the glutamate residues at acidic pH. The portion of the FeLV peptide which is aggregated may lie along the bilayer surface, rather than insert into the membrane, and actually stabilise the L_α phase, possibly by reducing its negative curvature strain.

Further support for the link between bilayer destabilisation and the enhancement of fusion comes from the effects of fusion inhibitors on the L_α-H_{II} phase transition. Some examples are cholesterol sulphate (Cheetham *et al*, 1990) and cholesterol phosphorylcholine (Cheetham *et al*, 1994), which are potent inhibitors of Sendai virus fusion with both human red blood cells and liposomal membranes, and which raise the T_H of DEPE. Similarly, LPC inhibits a number of membrane fusion processes (Chernomordik *et al*, 1993), and it also can raise T_H (Epand, 1985). Finally, Tromantidine, which is a therapeutic agent used against Influenza and Herpes virus infections, raises the T_H of a variety of synthetic PEs.

Enhancement of H_{II} formation may be due to disruption of lipid packing and/or effects on lipid hydration, producing an increase in monolayer negative curvature strain (Gruner, 1985). X-ray studies of the H_{II} phase lattice constant at constant temperature can determine whether alteration of the spontaneous radius of curvature of the lipid/water interface, R_0, occurs, and thus a change in monolayer negative

curvature strain. This is indeed seen for DiPoPE samples containing the FeLV peptide (see Chapter 4).

An increase in the negative curvature strain of bilayers is believed to result in increased rates of viral fusion (Siegel, 1993). The first structures to form in the L_α-H_{II} phase transition may be similar to those that mediate membrane fusion in many lipid systems. This may explain the relationship between an increase in membrane fusion rates and the effect of a fusion promoter on lipid polymorphism. Central to the currently favoured theory on this link is the formation of the 'modified stalk' intermediate, which has overall negative curvature (Siegel, 1993). Thus the formation of this intermediate would be accelerated by agents or conditions which favour the formation of inverted phases. Very recent work by Siegel and Epand (1997) suggests that both the L_α-H_{II} phase transition and membrane fusion do indeed proceed via the formation of modified stalks. These then almost immediately expand to form transmonolayer contacts (TMCs), which were seen using TRC-TEM in this study as small connections between apposed membranes. The TMCs were then observed to aggregate side-to-side, forming arrays with hexagonal order in some directions. Aggregation would reduce some of the free energy of the system. Thus at temperatures below T_H, although the lipid in each individual TMC still has a higher free energy than bilayer lipid, the activation energy required to revert this process is higher in a TMC aggregate than for isolated TMCs. Hence kinetically metastable TMC arrays are formed, which can then elongate directly into H_{II} domains. These findings support previous theoretical predictions that local defects in membranes are likely to arise or accumulate near phase boundaries. The subsequent formation of fusion pores from the TMCs will depend upon the individual lipid system involved.

Although H_{II} itself is not seen in biological membranes, related non-bilayer structures such as H_{II} precursors could well form and could be involved in membrane fusion processes. In support of this, Zellmer and co-workers (1994) found that vesicle fusion could be catalysed by lipid chain melting alone, provided that the temperature of the system was not far below T_H. Thus the whole lipid system does not have to go through a non-bilayer phase transition to promote fusion.

In this present work it is demonstrated using DSC that the putative fusion peptide of FeLV can lower T_H of DiPoPE, particularly at low mole fractions of peptide. Thus this peptide appears to be a bilayer destabiliser. This agrees with previous findings for known fusogens, and hence adds support to the link between the bilayer-inverted hexagonal phase transition and membrane fusion.

Since the 1960s thermal analysis methods have frequently been used in studies of membranes. However, to understand fully the phase transitions of lipids in biological membranes it is not sufficient to consider the behaviour of pure isolated lipid species alone, since biological membranes are highly heterogeneous in their phospholipid content and since they also contain a variety of non-phospholipid components, which can interact with the phospholipids and influence their behaviour. Nonetheless, studies of the effects of viral fusion peptides on the thermotropic properties of pure lipid species aim to provide a basic insight into the mode of action of these fusogens, in particular their modulation of lipid polymorphism. Moreover, whilst biological membranes are indeed heterogeneous, the existence of microdomains of individual lipid species may be important for fusion. Webb and co-workers (1993) studied mixtures of DOPC and dioleoylphosphatidylethanolamine (DOPE), and found that, by decreasing the water content, these lipids demixed prior to undergoing a phase change to H_{II}. Thus they concluded that the differential hydration characteristics of various membrane components may induce lateral fluid lipid demixing during dehydration. Since dehydration has been identified as an early step in fusion, the study of one individual lipid species may thus be quite relevant to biological fusion events.

Chapter 3: ^{31}Phosphorus Nuclear Magnetic Resonance Spectroscopy studies on the effect of the Feline Leukaemia Virus Fusion Peptide on Lipid Polymorphism

"What an enormous revolution would be made in biology, if physics or chemistry could supply the physiologist with a means of making out the molecular structure of living tissues comparable to that which spectroscopy affords to the inquirer into the nature of heavenly bodies."

Thomas Huxley, 1800's.

3. ^{31}Phosphorus Nuclear Magnetic Resonance Spectroscopy

3.1 General Introduction

Spectroscopy measures the absorption of electromagnetic radiation by substances, and can be used to determine the structure of organic compounds.

Nuclear Magnetic Resonance Spectroscopy (NMR) measures the change of the spin state of a nuclear magnetic moment when the nucleus absorbs electromagnetic radiation in a strong magnetic field. ^{31}Phosphorus NMR (^{31}P NMR) can be used to study the structure and dynamics of model and biological membranes. Since the ^{31}P nucleus is the only isotope of phosphorus that is found in natural biological structures, and since each phospholipid molecule within a membrane contains at least one phosphate radical in its headgroup, ^{31}P NMR studies can be performed without the addition of any probes to the membrane under study. ^{31}P NMR is thus a non-invasive technique, and it is also extremely sensitive.

^{31}P NMR primarily senses the behaviour and the environment of the phosphorus atom in the phospholipid headgroup, and so this technique measures the properties of the membrane surface; other properties are sensed indirectly. ^{31}P NMR is also 'blind' to any materials in the sample that do not contain phosphorus.

3.2 Theoretical Background to NMR Spectroscopy

When a compound absorbs energy, it undergoes transitions to different energy states. Since these energy states are 'quantised', a particular atomic nucleus will only absorb the precise amount of energy required to change state. Thus one can correlate the frequency of electromagnetic radiation absorbed by a compound with its structure. The frequency of absorbed radiation is measured by a spectrometer.

Certain elements have isotopes the nuclei of which are intrinsically magnetic. These include the ^{31}P nucleus, but not those of the common natural isotopes of carbon, nitrogen or oxygen. An intrinsically magnetic nucleus spins about an axis, in a similar manner to that in which the Earth spins around the sun. This intrinsic spin is called the spin angular momentum of the nucleus, and it is quantised. The spin

quantum number of a nucleus is largely determined by the number of unpaired protons and neutrons. Protons and neutrons each have a spin quantum number of ½. Thus a ^{31}P nucleus, which has one unpaired neutron, also has a spin quantum number of ½. It is the spinning of the ^{31}P nucleus, which acts like a single charged particle, that creates the small intrinsic magnetic field. The magnitude and direction of this field are described by a vector called the magnetic moment.

When a compound containing ^{31}P is placed in a strong magnetic field, the magnetic moments of the spinning ^{31}P nuclei can align in only two directions: with the direction of the applied field (parallel), or opposed to the direction of the applied field (antiparallel) (see Figure 3.1a). The nuclei which have magnetic moments that adopt a parallel alignment have slightly lower energy than those with magnetic moments showing antiparallel alignment. Thus slightly more than half of the nuclei will have their magnetic moments in the parallel state. It is only the magnetic moments of the nuclei, and not the molecule as a whole, that become aligned with the field. The two states are separated by an amount of energy ΔE, as shown in Figure 3.1b, which depends upon the strength of the magnetic field and the size of the nuclear magnetic moment.

The spin properties of the nucleus, however, slightly complicate this situation. Thus, instead of aligning directly with or against the direction of the field, the magnetic moment vector precesses, that is it rotates about the external field direction whilst tracing out the shape of the surface of a cone (see Figure 3.2). The frequency of this precessional rotation of the magnetic moment is called the Larmor frequency, and the magnetic moment vector can adopt either a low energy, 'spin-up' state, or a high energy, 'spin-down' state.

The magnetic moment of a particle, μ, is related to its angular momentum, J, by a fixed constant called the gyromagnetic ratio, γ:

$$\mu = \gamma J \qquad 3.1$$

where γ is a fixed property of each particle.

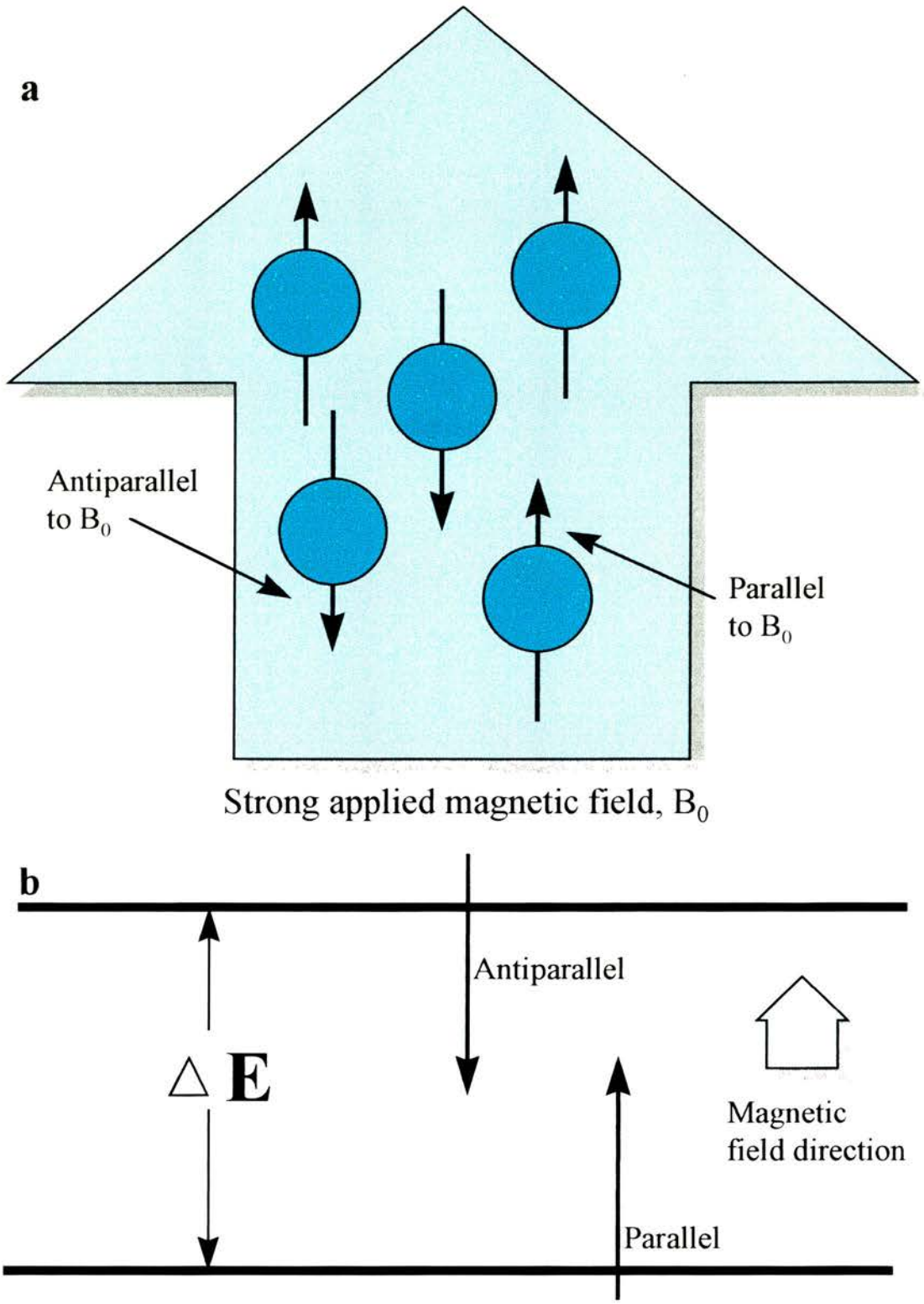

Figure 3.1. a: The two permitted alignments for spin states of spin 1/2 nuclei within a strong applied magnetic field. **b**: Energy levels of a spin 1/2 nucleus in a magnetic field. The two permitted orientations of the nuclear magnetic moment differ in energy by ΔE.

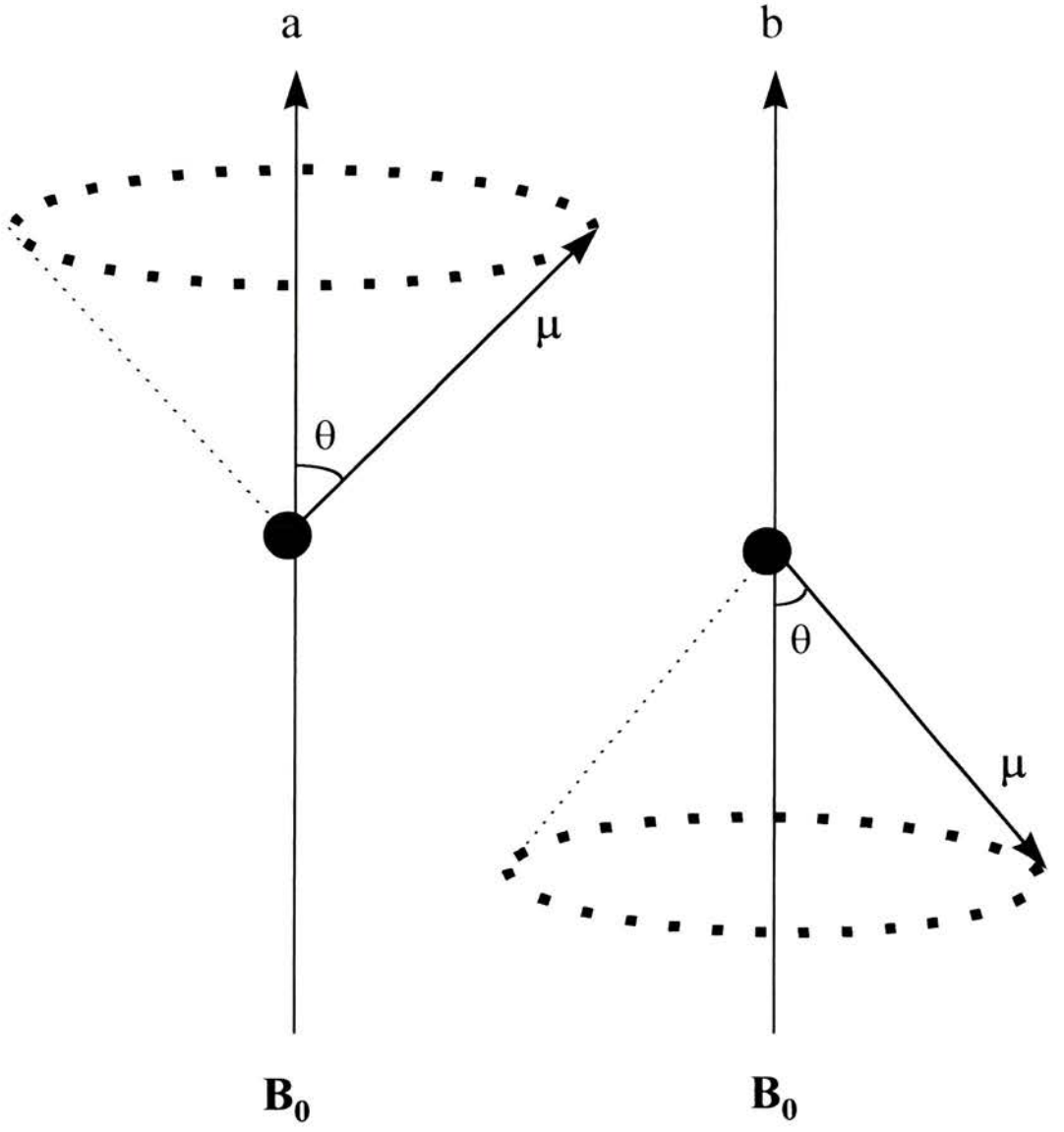

Figure 3.2. Precession of the magnetic moment vector, μ, of a particle or nucleus with spin quantum number 1/2 about a magnetic field, B_0. μ traces out the surface of a cone, with a half-angle, θ, of 55°. (a) Low-energy configuration, the 'spin-up' state; (b) High-energy configuration, the 'spin-down' state.

When a particle is placed in a magnetic field, the Larmor precessional frequency of the magnetic moment vector, ν_0, varies with the external field strength, B_0, according to the following equation:

$$\nu_0 = \frac{\gamma B_0}{2\pi} \qquad 3.2$$

An electromagnetic wave may be regarded as a varying electric field coupled with a varying magnetic field that are at right angles to each other and to the direction of travel (see Figure 3.3). If electromagnetic radiation is directed towards a particle that is in a strong magnetic field, the magnetic component of this radiation will affect the motion of the particle. Thus the magnetic moment of the particle will now attempt to precess about both external magnetic fields, and the second magnetic vector will induce a wobbling in the original direction of precession. Moreover, if the magnetic vector of the electromagnetic radiation is linearly polarised and is perpendicular in direction to the original magnetic field, and if its frequency is equal to the Larmor frequency of the particle's magnetic moment, then the magnetic moment of the particle will attempt to rotate in phase with a circular component of this wave (see Figure 3.4). (Linearly polarised electromagnetic waves may be perceived as being composed of two circularly polarised components, which are described by a helical wave which rotates clockwise and an identical wave rotating anticlockwise). Quantum mechanics, however, will allow only two orientations of the particle's magnetic moment with respect to either magnetic field. Thus the particle's magnetic moment cannot precess about either magnetic field; instead, when the frequency of the electromagnetic radiation equals the Larmor frequency, a few of the lower-energy, parallel 'spin-up' nuclei absorb energy and switch their spin states from the lower-energy, parallel state to the higher-energy, antiparallel 'spin-down' state (see Figure 3.2). This conversion is called a 'flip'. The higher-energy, antiparallel nuclei can also lose energy to their surroundings and return to the parallel state. At the frequency that causes 'flips', the nuclei are said to be in resonance with the radiation, hence the origin of the term 'Nuclear Magnetic Resonance'.

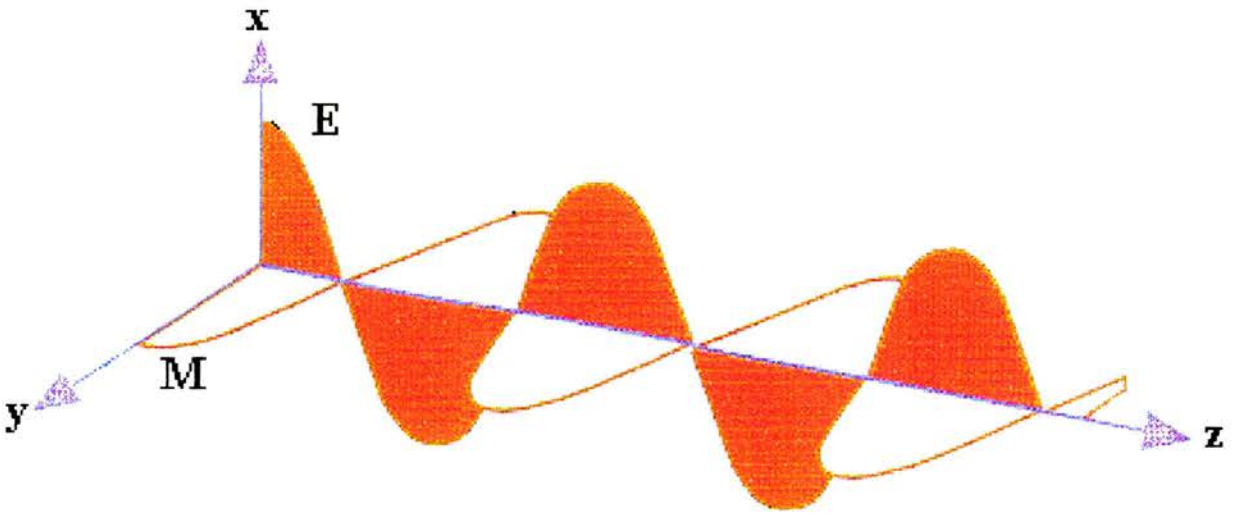

Figure 3.3. A linearly polarised electromagnetic wave with direction of propagation z. M represents the magnetic component, and oscillates in the zy plane; E represents the electric component, and oscillates in the zx plane. M and E are at right angles to each other, and the energies associated with M and E are equal.

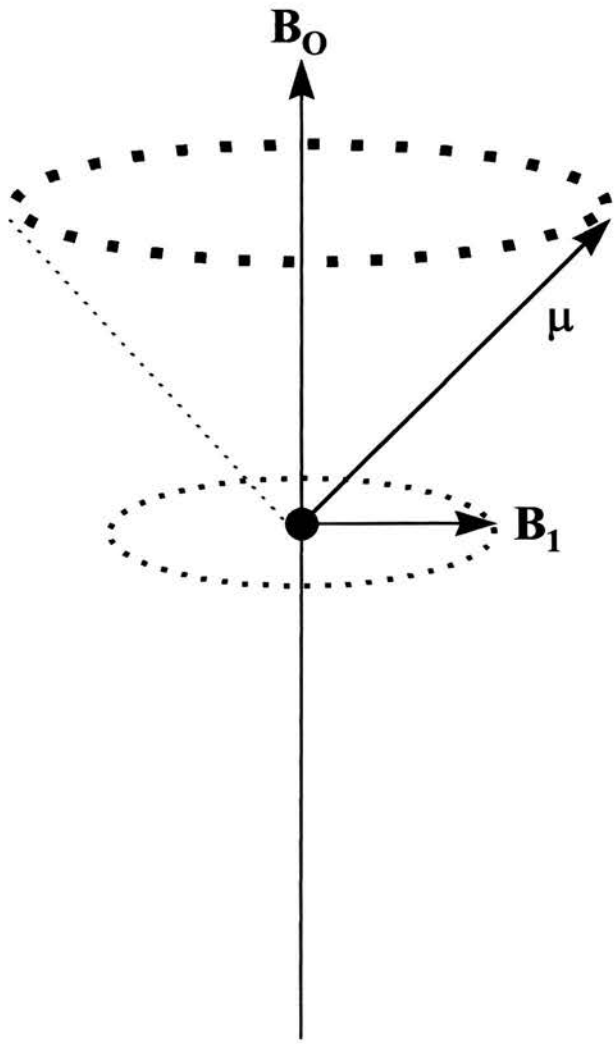

Figure 3.4. Relationship between the magnetic moment vector, μ, of a particle and the magnetic vector of a linearly polarised electromagnetic wave, B_1. At the Larmor frequency, μ and a circular component of B_1 rotate in phase.

The exact frequency of electromagnetic energy that is required to produce resonance depends mainly upon the strength of the applied field and the isotope being studied (see Equation 3.2). For a given field strength, the resonance frequency is determined principally by the type of nuclide under observation, since every nucleus has a characteristic magnetic moment. In addition, the resonance frequency also depends to a slight extent upon the chemical environment of a nucleus in a molecule.

^{31}P nuclei in an organic molecule are surrounded by electrons. Under the influence of a strong external magnetic field these electrons circulate within their orbitals, leading to the creation of tiny magnetic fields, called molecular fields. The molecular fields oppose the externally applied field. This means that the actual magnetic field strength at the location of a ^{31}P nucleus in a compound will be slightly less than the applied field strength. The ^{31}P nucleus is thus said to be 'chemically shielded' from the applied field by the local molecular field of the molecule, and the resultant change in the resonance frequency of the nucleus is called the 'chemical shift'.

The molecular magnetic field of a compound will vary within its structure, since the electron density varies from one part of the molecule to another, depending upon the chemical bonding present. The molecular axis which has the lowest electron density will, for example, produce the least chemical shielding, and will result in the smallest chemical shift.

Other factors affect the amount of shielding that a ^{31}P nucleus experiences. The electron density of the bonds near a ^{31}P nucleus can be altered by the presence of other atoms within the molecular structure. Thus a nearby electronegative atom will withdraw electrons from the vicinity of the ^{31}P, which will cause a decrease in the size of the induced molecular magnetic field. Consequently the size of the applied magnetic field that is required to induce flip in the spin state of that ^{31}P nucleus is reduced, and that ^{31}P nucleus is 'deshielded' to some extent. This will cause a 'chemical shift' in the opposite direction to that produced by chemical shielding.

The particular arrangement of bonds and other atoms around a ^{31}P nucleus will thus produce an overall combined effect upon the resonance frequency of this nucleus. Different ^{31}P nuclei will therefore experience slightly different magnetic fields

depending upon their location within the molecule, and will come into resonance at slightly different combinations of applied magnetic field strength and radio frequency. The resulting signals are plotted to produce a spectrum. Since, in practice, it is impossible to obtain a spectrum from an isolated nucleus, the resulting chemical shifts are expressed in fractional units (parts per million, ppm) relative to a standard compound, which is normally the methyl resonance of tetramethylsilane (since proton NMR was the first type of NMR performed, most spectrometers are calibrated for ^{1}H).

A phosphorus atom that exists as part of a phosphate diester, for example the phosphorus within a phospholipid molecule, has an anisotropic electron distribution (see Figure 3.5). This will lead to anisotropic chemical shielding, and thus an anisotropic chemical shift. By defining three principle axes, σ_{11},σ_{22} and σ_{33}, it is possible to calculate the chemical shift for any orientation of a phosphate diester within a magnetic field (see Figure 3.5a). However, in order to perform this calculation, a knowledge of the chemical shift values for all three reference axes would be required. This three-dimensional character of the chemical shift is called the 'chemical shift tensor'. The recorded lineshape, or 'powder pattern', for a rigid solid represents the superposition of all possible orientations for a phosphate diester within a sample, with $\sigma_{11}$and σ_{33} defining the extreme edges of the spectrum, and σ_{22} a single intermediate peak. Measurements of these principle elements of the chemical shift tensor have been made for phospholipids in dry powders. Such a powder pattern is shown in Figure 3.6a. Moreover, the relationship between the three principle elements of the chemical shift tensor and the molecular coordinates of the phosphate has been determined in crystals of organic phosphodiesters (Kohler and Klein, 1977).

The first ^{31}P NMR studies of membranes were performed in 1972 (e.g. Barker *et al*, 1972; Horwitz and Klein, 1972). As in the rigid phosphate diester, there is anisotropic shielding of the phosphorus nuclei from the applied magnetic field due to the anisotropy in the local electron distribution around the phosphorus nucleus. This results in chemical shift anisotropy. Thus the resonance frequency of a phosphorus atom will depend upon the angle between the phosphate region of the lipid headgroup and the magnetic field. However, biological membranes are not rigid structures: they

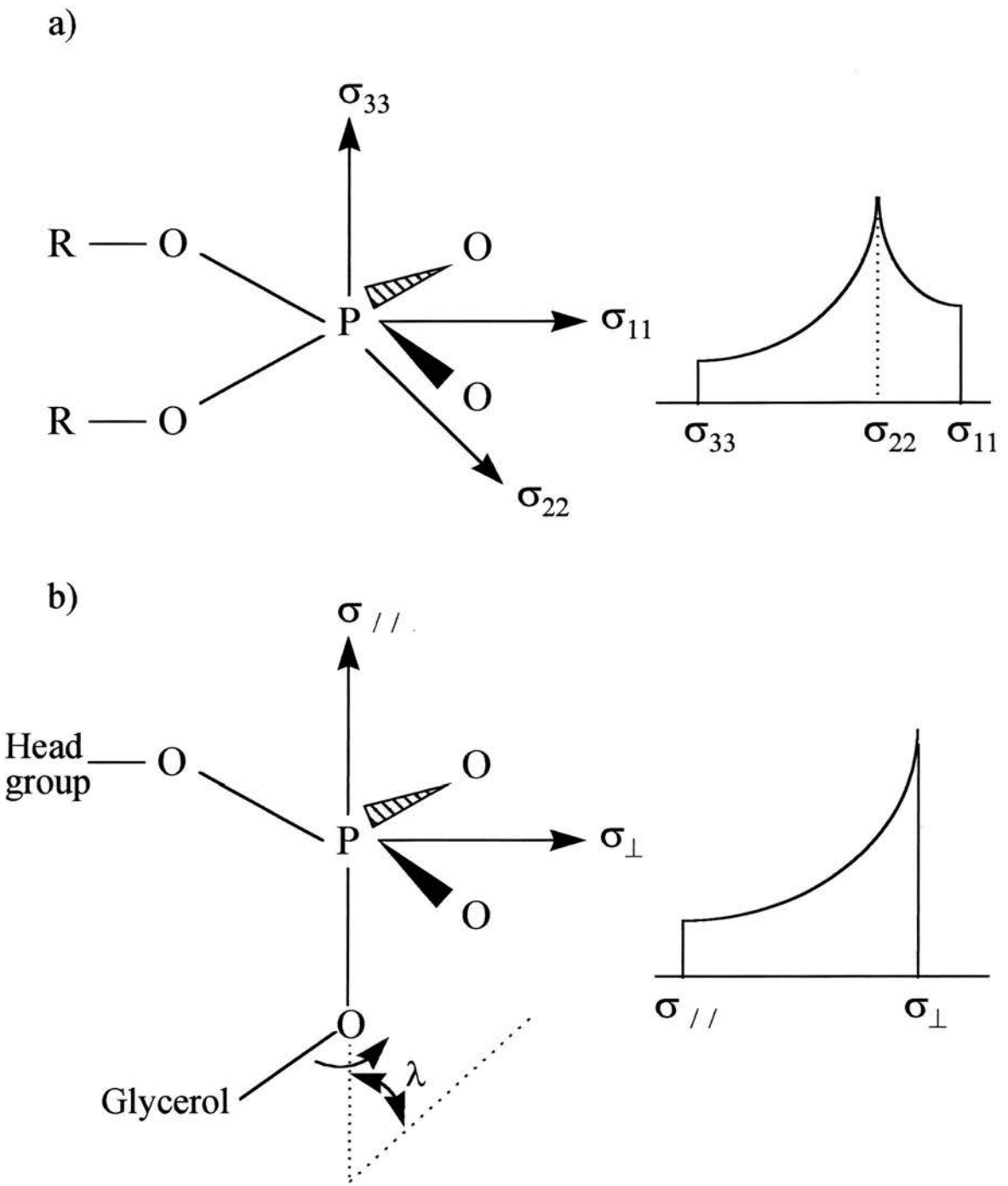

Figure 3.5. The principle axis system for phosphate diesters, as found in lipid systems. a) a rigid phosphate diester and b) a phosphate diester, such as is found in a phospholipid, undergoing rapid rotation about the long axis of the molecule, whilst the rotational axis simultaneously wobbles with restricted amplitude. The expected corresponding ^{31}P NMR spectra are shown.

are sufficiently fluid to allow considerable translational, rotational and flexing movements of the constituent phospholipid molecules. This will alter the chemical shielding in comparison to the shielding under static conditions, and hence the chemical shift. Rapid motion will average some of the chemical shift tensors. As an example, if rotation occurred about the σ_{33} axis, then the σ_{11} and σ_{22} axes would be averaged; this would produce the lineshape shown in Figure 3.5b. The resulting powder spectrum will display a maximum intensity for the axis of rotation that is perpendicular to the magnetic field ($\sigma_{\perp}$) whilst the least intense end of the spectrum, or shoulder, represents the chemical shift when the axis of rotation is parallel to the magnetic field ($\sigma_{//}$) (Tilcock *et al*, 1986). A reduction in the chemical shift anisotropy occurs when the rotational axis itself undergoes a wobbling motion, resulting in partial averaging of $\sigma_{\perp}$ and $\sigma_{//}$ (Seelig *et al*, 1977). The extent of the reduction is a direct measure of the amplitude of motion. Thus it can be seen that the resultant ^{31}P NMR lineshapes are determined by the extent of motional averaging, on the ^{31}P NMR time scale, of the chemical shift anisotropy of the ^{31}P atom present in the phospholipid headgroup. This, in turn, is directly influenced by the amount of motion possible within the phospholipid dispersions: the greater the motion, the narrower will be the NMR lines. Moreover, the characteristic lineshapes which are observed for the different lipid phases can be readily predicted from the motional averaging that exists in that particular structure (Yeagle, 1989).

Within a given lipid phase, the phospholipid molecules diffuse about rapidly, subject to the constraint that the headgroups move within the lipid-water interface. Thus in a lamellar phase, the constituent phospholipids can diffuse laterally within the plane of the membrane. If the lamellar systems are large enough, the lateral diffusion will not produce significant motional averaging. However, the molecules can also rotate and flex, and these movements are characterised, on average, by cylindrical symmetry, with the bilayer normal as the axis of motional averaging. This rapid rotational motion along the long axis of the phospholipid molecule averages two of the chemical shift tensors. This motion is believed to originate from motion around the P/ODAG bond (see Figure 3.5b). Translational diffusion perpendicular to the membrane surface is severely restricted by the hydrophobic effect. The hindered

movements of the phospholipid molecules are therefore 'anisotropic': correlations exist between the initial and final orientations of the phospholipid molecules over the 10^{-5}s time scale of an NMR measurement. This anisotropy of movement is reflected in the resultant chemical shielding anisotropy, such that the static chemical shielding anisotropy is partially averaged out. Thus the observed maximum resonance for the L_α phase in a spectrum is asymmetric (see Figure 3.6), and occurs about 12-15ppm from zero. The width of the recorded powder pattern, which is the spectrum obtained for a random dispersion of membranes, and which represents the weighted sum of many spectra for all possible molecular orientations, represents the degree of chemical shielding anisotropy present. Thus an increase in the width of a powder pattern represents an increased restriction of motion of the phospholipid headgroups. Often there is a gradual decrease in the chemical shift anisotropy with temperature. Thus the axis of rotation wobbles more at higher temperatures, as expected.

The H_{II} phase has cylindrical symmetry, and these cylinders tend to be small in diameter. As an example, if the diameter of the H_{II} aqueous pores is about 2nm, and the diffusion coefficient for lateral diffusion is assumed to be about $10^{-8}cm^2s^{-1}$, then a phospholipid molecule can circumnavigate an H_{II} cylinder in about 10^{-6} seconds (Yeagle, 1989). This is rapid when compared to the width in Hz of the ^{31}P powder pattern in the lamellar phase. Thus an additional motional averaging occurs for the chemical shift tensor compared to that of the lamellar phase, and if all other factors remain constant, the transition from L_α to H_{II} reduces the width of the powder pattern by half (see Figure 3.6). The shape of the powder pattern is also reversed. Thus the maximum resonance for H_{II} occurs about 6ppm from zero on the spectrum. ^{31}P NMR lineshapes for hexagonal phases do not distinguish between the H_I and the H_{II} phases. However, since the H_I phase occurs only when lysolipids are present at high lipid concentrations, this does not present a real problem.

Finally, if phospholipid motion through all orientations with a short correlation time (~10^{-5} sec; Gruner *et al*, 1985) is possible, in other words in a structure where the molecules can tumble rapidly through all angles of space, then an isotropic narrow ^{31}P NMR resonance is obtained, which is centred on zero in the spectrum, (see Figure 3.6), and no powder pattern is seen. Structures giving rise to isotropic ^{31}P NMR

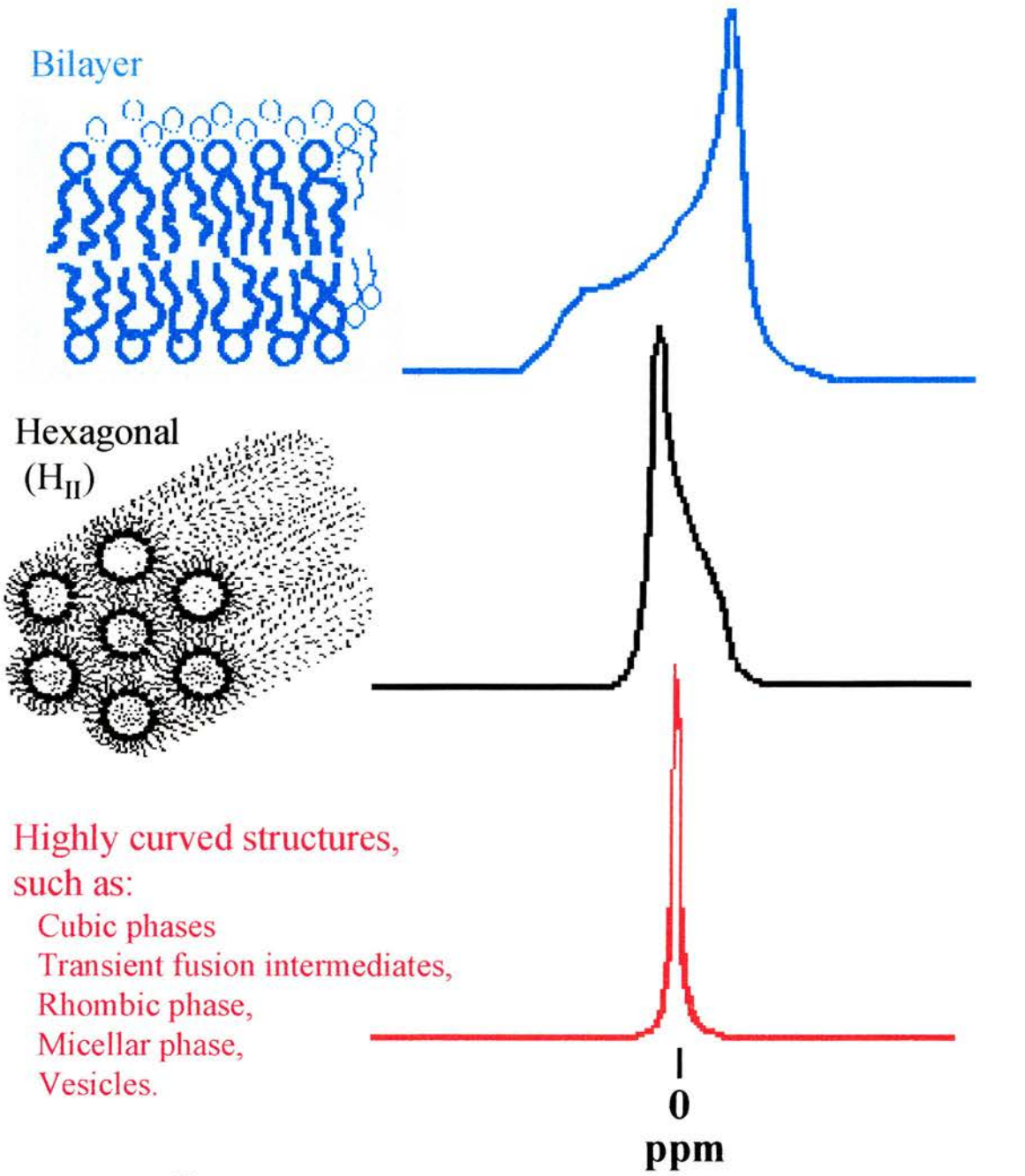

Figure 3.6. ^{31}P NMR spectra for various aqueous dispersions of phospholipids: bilayer, hexagonal and isotropic.

resonances are themselves termed 'isotropic', but this term encompasses several different structures. There are at least five different possibilities:

1. a solution phase, with the phospholipid dissolved in organic solvent.
2. a micellar phase; micelles are small enough to have a rotational correlation time that is shorter than 10^{-6} sec (Yeagle,1989).
3. SUV; their rotation is fast enough to satisfy the requirement.
4. a cubic phase; cubic phases consist of a series of short rods connected at right angles which resemble the H_{II} phase. Thus phospholipids diffusing from one segment to another will experience 90° of rotational freedom. Moreover, since the lengths of the segments are similar to their diameters, normal lateral diffusion rates of phospholipids are adequate to provide sufficiently rapid movement through the 90° of rotational freedom to produce isotropic resonance.
5. An inverted micellar phase; this was postulated to coexist within the phospholipid bilayer, and has been described as an IMI in fusion (e.g. Siegel, 1984). The structure offers rapid rotational freedom through lateral diffusion around the inverted micelle. The details of this structure have still not been adequately demonstrated experimentally.

It can be seen, from the explanations above, that the averaged lineshape for the ^{31}P resonance is indirectly related to the phospholipid phase present; it is dependent upon the local environments of the phosphorus atoms within the lipid, and the motion available to them in a given lipid phase. Thus the observed ^{31}P lineshapes do not have unique relationships with particular phase structures. For example, the inability of ^{31}P NMR to distinguish between the various possible sources of isotropic resonances does represent a weakness. Low angle X-ray and neutron diffraction studies are the definitive techniques for identification of lipid phase structure. However, these techniques require a regular lattice that exhibits long-range order if one is to obtain the higher order reflections that are required for unambiguous phase assignment. One advantage of ^{31}P NMR is that it does not require a regular lattice exhibiting long-range order. The question of the 'phase' of nonperiodic structures has been addressed by applying ^{31}P NMR to periodic structures for which X-ray diffraction has been performed and the identity of the physical phase present is thus

clear. Extrapolation is then carried out, by asserting that, since ^{31}P NMR is sensitive to the microscopic constraints of the structures, and not to the lattice on which these structures are placed, these characteristic ^{31}P NMR lineshapes may be used to indicate the presence of the microscopic structures even when no lattice is present. This procedure is valid, as long as tests for self-consistency are continually applied.

An extensive study performed by Tilcock and co-workers (1986) to determine the extent of the correlation between determinations of lipid phase by ^{31}P NMR and small-angle X-ray diffraction techniques showed that this correlation is in fact excellent. Thus their results strongly support the use of ^{31}P NMR as a convenient diagnostic technique for detecting phospholipid phase structures in model and biological membranes.

3.3 Practical Considerations for ^{31}P NMR

There are three essential requirements for an NMR experiment: a strong static magnetic field, a source of radiofrequency radiation to excite the nuclei in the sample and a method for detecting the NMR signal.

The magnetic field used should be as strong as possible. This will optimise sensitivity, maximise the separation of chemical shift differences and minimise strong coupling effects. A superconducting solenoid, which is a coil of resistance-free alloy that supports a persistent current, is often used, since it can produce a strong, homogeneous and stable magnetic field. Spinning the sample, at rates of up to 50Hz, helps to average any non-uniformities in the magnetic field and yields sharper resonances.

The electromagnetic radiation is usually generated by passing a sinusoidally oscillating current through a coil arranged around the sample, which sits inside the magnet. The electrons circulating in the coil generate an oscillating electromagnetic field whose magnetic component excites the sample, provided its frequency equals the Larmor frequency of the ^{31}P atoms present in the sample. Radio frequency waves are used for ^{31}P NMR, since they are the correct frequency to induce ^{31}P nuclear magnetic resonance. During resonance the ^{31}P nuclei flip to the spin-down state. Thermal

fluctuations within the sample and random magnetic interactions result in the continual return to the spin-up state. Thus the sample continually absorbs and re-emits radiofrequency radiation, and the re-emitted radiation induces an alternating current in a suitably placed receiver coil. This current is then amplified to produce the NMR signal.

The most common type of ^{31}P NMR performed nowadays is the pulse NMR technique, or Fourier transform NMR spectroscopy (FT-NMR). In this method, a short, intense burst of radiofrequency radiation is applied to the sample to induce resonance. The resulting oscillating magnetisation is detected as a function of time after the end of the pulse, and is processed in a computer to produce the final spectrum. The NMR probe holds and spins the sample, couples the radiofrequency field to the spins, and picks up the ensuing NMR signal. After amplification, the NMR signal from the probe is mixed with a reference voltage, which is of the same radio frequency as the pulse that was used to excite the spins. This results in subtraction of the reference frequency from the NMR signal to produce an audiofrequency voltage which is further amplified, digitised and processed in the computer. Fourier transform is used to analyse the signal, or free induction decay. The signal is the sum of the individual oscillating voltages from the various nuclei in the sample. Thus the individual components that make up the spectrum are determined. FT-NMR is much more rapid and sensitive than the older, continuous sweep NMR methods, and the signal-to-noise ratio is greatly improved.

One problem that exists for ^{31}P NMR experiments on lipid membranes is that ^{1}H, which is intrinsically magnetic, accounts for 99.98% of naturally occurring hydrogen atoms (Fessenden and Fessenden, 1990). This nucleus can affect the response of the ^{31}P nucleus to the external magnetic field, and thus result in spectral distortion. One way of overcoming this problem is to employ spin decoupling. Spin decoupling uses the technique of simultaneously transmitting an intense beam of radio frequency radiation which has a frequency equal to the Larmor frequency of the unwanted ^{1}H nuclei. These nuclei then flip at too fast a rate for the ^{31}P nuclei to detect their orientation, and thus the resulting spectrum will not be distorted by the presence of the ^{1}H nuclei. This means that the signals for each group of magnetically-equivalent

phosphorus nuclei will appear as singlets, unsplit by any protons that are directly bonded to these nuclei.

A spectrum is a graph of the intensity of the absorption (in practice usually re-emission) of radio waves versus the delta values, where 1 delta value is one part per million of the instrument's radio frequency. Thus for an instrument operating at 60MHz, 1delta is equal to 60Hz. A standard sample is used to set delta to zero: this is usually tetramethylsilane (TMS). This allows the comparison of NMR spectra, which have been obtained using different instruments. The difference in delta values from zero to each signal represents the chemical shift.

Since it is the shape of the powder pattern which is sensitive to the morphology of the phospholipid molecules within the sample, it is very important to obtain undistorted spectra in order to interpret results correctly. The commonest problem in ^{31}P NMR studies of membranes is indeed spectral distortion, which makes lineshape interpretation both difficult and uncertain. The study of phospholipids in the liquid crystalline state and the use of high magnetic fields mean that obtaining conditions for adequate ^{1}H decoupling is generally not too difficult. However, lipid membranes produce broad powder patterns: as wide as 200ppm for an amorphous phospholipid sample, which means that the decay of the signal in the time domain is rapid. Single-pulse acquisition experiments can lead to a loss and/or distortion in the first portion of the time domain, which is where the majority of the information on the lineshape usually resides. As a rule these distortions cannot be removed by further processing of the data. However it has been shown that, by using a simple Hahn echo pulse sequence, along with extensive phase cycling, spectral artefacts can be avoided (Rance and Byrd, 1983).

The initial part of the spectrum is usually missed; this is because of receiver dead time. A two pulse system can be used to overcome this problem. The second pulse causes a complete refocusing of the nuclear magnetisation (providing that there are no irreversible effects from application of the first pulse). Thus the signal starting at the peak of the echo is identical to the signal following a single pulse, and by having the echo form beyond the receiver dead time following the second pulse, it is possible to avoid distortions due to finite recovery time. This principle is used to generate a

'Hahn echo', and Fourier transforming the signal starting at the peak of the echo will provide an undistorted spectrum (see Figure 3.7). The echo time must be short relative to the spin lattice relaxation times of the resonances being measured. The pulse widths should also be adequate to excite the full extent of the expected powder pattern. In practice, data acquisition should start prior to the echo maximum, and then after signal averaging is complete, a point is chosen which should represent the start of the Fourier transform. Usually the software performs this task.

3.4 Application of ^{31}P NMR to Fusion Studies: Aims of these ^{31}P NMR Experiments

Many lipid systems that exhibit the classical thermodynamic L_α and H_{II} phases also exhibit other distinct morphological states between these two phases. These have been correlated with cubic phase X-ray diffraction patterns, isotropic ^{31}P NMR signals, and/or lipidic particles/interbilayer attachment sites using FFEM (e.g. Luzzati and Reiss-Husson,1966; Cullis and de Kruijff, 1978; Verkleijj *et al*, 1979; Larsson *et al*, 1980; Tilcock *et al*, 1982; Verkleijj, 1984; Gagné *et al*, 1985). Since biomembrane lipid compositions are not far from the L_α/inverted cubic(Q_{II})/H_{II} phase boundaries under physiological conditions, intermediates that form in these phase transitions may be relevant to biological membrane fusion.

In view of these findings, experimental evidence was sought to link the fusion pathway to the production of isotropic lipid states. Gagné *et al* (1985) showed that the phospholipid N-Monomethyldioleoylphosphatidylethanolamine (MeDOPE) existed in the L_α phase below 20°C, in the H_{II} phase above 70°C, and showed isotropic NMR resonances at intermediate temperatures. Ellens *et al* (1986) correlated the initial kinetics of fusion between pure MeDOPE lipid vesicles with the development of isotropic states by this lipid. They found that, at temperatures where MeDOPE produces isotropic ^{31}P NMR resonances, the initial rates of fusion between MeDOPE LUVs increase. Thus at 20°C the initial rate of fusion between MeDOPE vesicles was very slow: ~1%/min, whereas at 60°C, the temperature at which first isotropic structures were first observed, the initial fusion rate abruptly increased to a

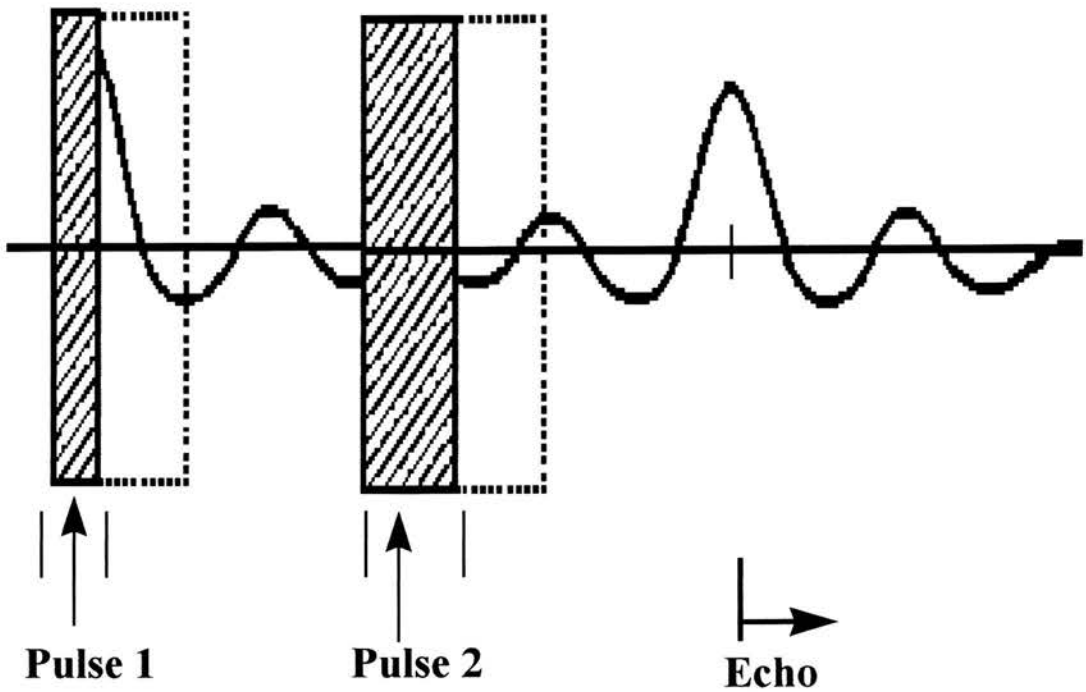

Figure 3.7. Schematic diagram to show the principle behind the two-pulse Hahn echo sequence. The dashed lines following the pulses represent receiver dead time. The start of the echo is marked, and can be seen to be identical to the original signal produced by the first pulse.

much higher value: ~5%/sec. Furthermore, the amount of isotropic ^{31}P NMR resonance present in the ^{31}P NMR spectrum has been directly correlated with the rate of membrane fusion between MeDOPE vesicles (Yeagle *et al*, 1992). Other experimental work with pure lipid systems has also suggested that isotropic structures may be intermediates in lipid membrane fusion (e.g. Ellens *et al*, 1984; Ellens *et al*, 1989; Siegel *et al*, 1989a).

As regards viral fusion mechanisms, Kelsey *et al* (1990) found that Sendai virus could fuse with pure MeDOPE vesicles, but not with pure egg PC LUVs (in the absence of receptors for HN, the Sendai virus fusion protein); egg PC is not capable of forming isotropic lipid structures. Work with the fusion peptides from SIV (Epand *et al*, 1994) and Influenza virus (Epand and Epand, 1994) has showed a large increase in the amount of isotropic resonance of MeDOPE in their presence.

^{31}P NMR is particularly useful for the detection of non-bilayer structures that might be important to the fusion event. Because of the narrowness of the ^{31}P NMR resonances, it is possible to observe such components when they arise from as little as a few percent of the total phospholipid. ^{31}P NMR does not depend upon ordered arrays of lipid molecules, so it can detect some isotropic structures which are not readily apparent by X-ray diffraction. This is important, as a complete model of fusion requires as much knowledge of transient fluctuations as of the equilibrium configurations of the constituent phospholipid molecules. It also does not depend upon representative sampling, as does electron microscopy for example, since it is sensitive to all the phospholipids in the sample. Since DSC rarely shows evidence of cubic phases, because of the long incubation periods necessary for the appearance of macroscopic amounts of this phase and the small enthalpies involved, ^{31}P NMR is much more suitable for examination of the cubic phase pathway. This is illustrated by the results of van Gorkom *et al* (1992), who showed that DSC studies with MeDOPE and the fusion promotor DAG, which together produce ^{31}P NMR isotropic resonances, could not detect the formation of isotropic lipid states unless a very slow scan rate was used.

The aims of the experiments described in this chapter were, first, to determine the effects of the FeLV fusion peptide on lipid polymorphism, as observed by ^{31}P

NMR, in particular any changes in the formation of the isotropic state, and therefore, second, to provide support for a link between the pathways for the formation of cubic phases and the fusion mechanism.

3.5 Materials and Methods

3.5a Sample Preparation

MeDOPE and DiPoPE were purchased from Avanti Polar Lipids (Alabaster, AL, USA). Purity was confirmed by Thin Layer Chromatography, which showed a single spot for each. MeDOPE forms irregular, nonlamellar structures, which produce an isotropic resonance over a wide range of temperatures using ^{31}P NMR (e.g. Gagné *et al*, 1985; Ellens *et al*, 1986), so it is a good choice for ^{31}P NMR studies of the effects of fusion peptides on lipid polymorphism. Previous X-ray studies have shown that DiPoPE does not form detectable amounts of inverted cubic phases when heated through T_H (Colotto *et al*, 1996; Colotto and Epand, 1997), and thus the pure lipid is not as well suited to NMR studies of isotropic signals as MeDOPE (see Discussion section on cubic phase formation). However, the effect of the FeLV fusion peptide on the polymorphism of DiPoPE is of interest, particularly for comparison with the results obtained in the DSC and X-ray diffraction experiments, in which DiPoPE was studied (see Chapters 2 and 4).

Preparation of lipid and lipid/peptide films was as described in Chapter 2, except that the lipid concentration was 50mg/ml. One disadvantage of ^{31}P NMR is that it does require quite large amounts of lipid: the sample must be large enough to provide an adequate signal-to-noise ratio in the time allotted for acquisition of data. Dispersions of MLVs were thus formed, as described in Chapter 2. These are much more suited to NMR experiments than biological membranes, since the multimolecular structures can pack much more closely. The high lipid concentration also aids the formation of non-bilayer phases. The lipid/peptide molar ratios were 100:1 or 200:1 for the peptide-containing samples.

Care must be taken as the lamellar to H_{II} phase transition exhibits considerable thermal hysteresis. The starting point for a thermal study must, therefore, be carefully established. This necessitates several freeze-thaw cycles of the lipid sample, in order to produce a reproducible starting lamellar phase structure, before commencing the study at the temperature of interest. Thus, prior to commencing the measurements, the samples were subjected to three freeze-thaw cycles. This was achieved by immersing them in liquid nitrogen for two minutes, and then holding them under a running cold water tap until they thawed. This also ensured that that full hydration of the dry MeDOPE and DiPoPE had occurred.

Finally, the suspensions were vortexed vigorously to produce a thick lipid paste, and loaded into 5mm diameter thin-walled NMR tubes.

3.5b ^{31}P Nuclear Magnetic Resonance Spectroscopy

A Bruker drx500 spectrometer, operating at a frequency of 202.45 MHz with broad band proton decoupling, was used to obtain the spectra. Gated proton decoupling was employed during data acquisition only, to eliminate sample heating. Other spectral parameters were: sweep width (the range of frequency values over which the spectra are measured), 48.5 KHz; time domain, 32,768 data points, and acquisition time (the measuring time of the signal), 0.34s.

Samples were heated in 5°C steps in the temperature regions near to T_H, and in 10°C steps elsewhere. After raising the sample temperature an equilibration time of approximately 15 minutes was used before starting measurements. Fast temperature equilibration was obtained by using small volumes. The temperature was then maintained to within ± 0.1°C by a Bruker B-VT 1000 variable temperature unit, which uses liquid nitrogen for lower temperatures and nitrogen gas flow for temperatures above 45°C. It is very important when conducting heating experiments that samples are kept below each temperature of interest prior to measurement. If the lipids are heated above the required temperature and then recooled lipid can become trapped in a cubic phase, and this phase may persist even after lowering the temperature to well below that at which cubic phase appears on sample heating.

100 scans were collected for each measurement. A relaxation delay of 3 seconds was used between scans. This is long enough to ensure that there is no attenuation of some of the resonances present. The spin lattice relaxation time for phospholipids is fairly similar, regardless of the headgroup structure or the lipid morphology present, so a constant delay time can be used throughout the experiment. Prior to Fourier transformation of the signal, exponential line-broadening of 100Hz was applied. The standard substance used to calibrate the spectrometer was phosphoric acid, and thus the resonance from this compound represented 0ppm on the spectra obtained for the samples.

3.6 ^{31}P NMR Results and Discussion

Figure 3.8 shows the ^{31}P NMR powder patterns obtained for pure MeDOPE, and MeDOPE plus FeLV fusion peptide over a range of increasing temperatures. The lipid dispersion of pure MeDOPE at 40°C shows a ^{31}P NMR powder pattern that is indicative of a liquid-crystalline bilayer arrangement with axially symmetric motions. In the pure lipid, the formation of an isotropic signal was not observed until 50°C. (The lamellar, isotropic and hexagonal spectral components overlap if they appear concurrently). The amount of isotropic phase increases with increasing temperatures. At 55°C and above, a powder pattern indicative of a hexagonal phase is also seen.

The temperature at which isotropic resonances are first seen, T_I, depends upon the history and age of the sample and the purity of the synthetic lipid. Hydrophobic impurities, lipid degradation products and incomplete hydration lower T_I significantly. Data reported here were obtained with fresh lipid suspensions which were fully hydrated by freeze-thaw cycling and by an equilibration period after each temperature increment. In the literature, there is a large discrepancy with regard to T_I. However, the ^{31}P NMR spectra obtained depend upon the experimental conditions present, and especially upon the temperature equilibration around the L_α-H_{II} phase transition. Thus some of the differences in the reported results are likely to arise from systematic differences in the protocols used. A standard protocol was used throughout the

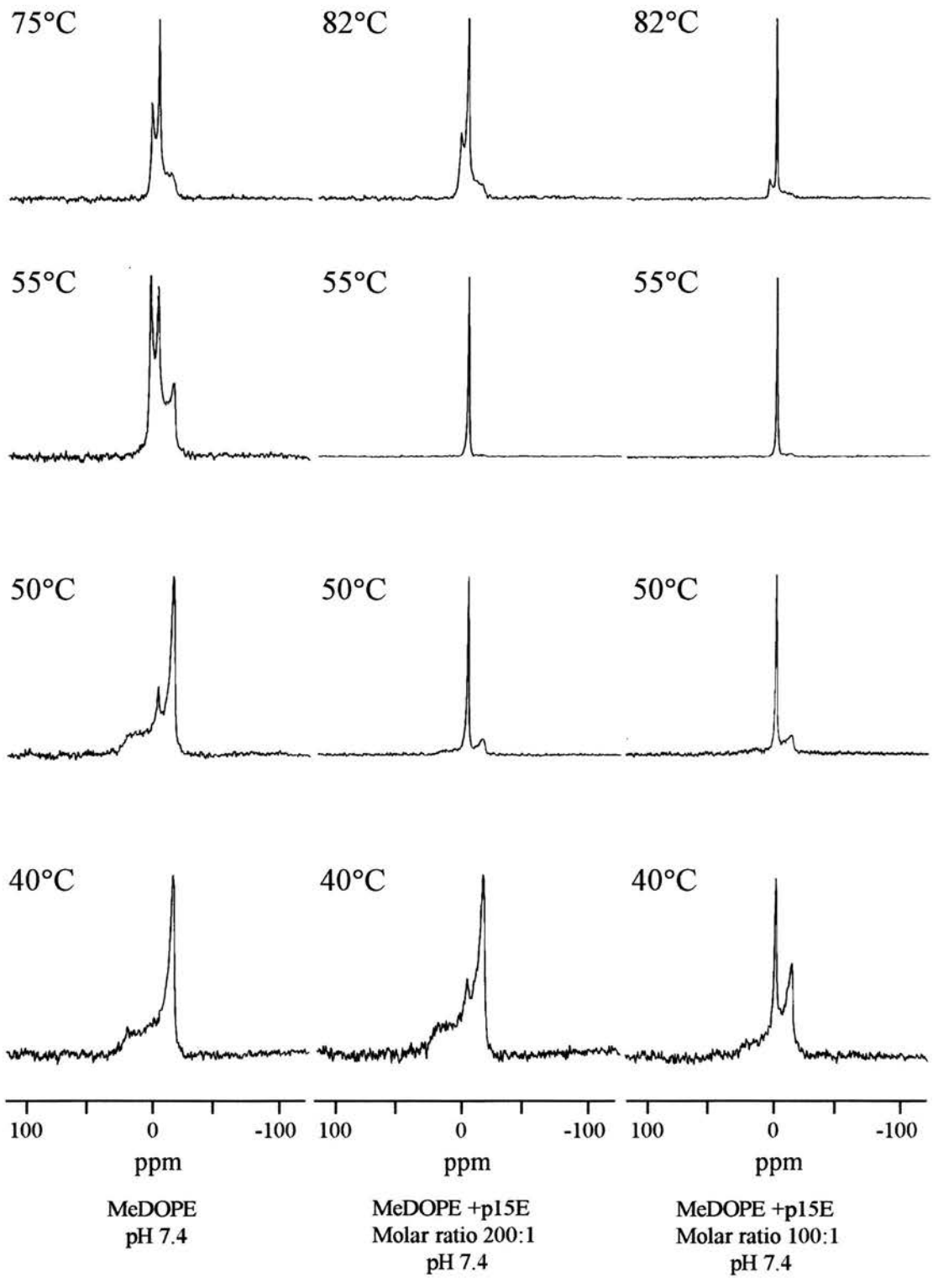

Figure 3.8. ^{31}P NMR spectra of pure MeDOPE, and samples containing different molar fractions of the FeLV fusion peptide, as a function of temperature. Only the pH 7.4 data are shown, but the pH 5.0 results were qualitatively similar.

experiments described here, and thus any differences in lipid polymorphism should be attributable to the effect of the fusion peptide.

In the presence of the FeLV fusion peptide, T_I is lowered. There is also a direct correlation between the molar fraction of peptide present and the amount of isotropic signal seen at 40°C. It can also be seen that, with FeLV fusion peptide present, a larger percentage of the lipid remains in the isotropic state over the full range of recorded temperatures. At 82°C, a small amount of MeDOPE with FeLV peptide has converted to the H_{II} phase, whereas by 75°C, the pure lipid already has a larger H_{II} signal. No significant differences were found between the pH 7.4 and the pH 5.0 data.

Figure 3.9 shows the ^{31}P NMR powder patterns obtained for pure DiPoPE, and DiPoPE plus FeLV fusion peptide as a function of temperature. The pure DiPoPE samples show a direct transition from the lamellar to the hexagonal phase; there is no significant isotropic peak at any of the recorded temperatures. In the presence of the FeLV peptide, however, a substantial isotropic component is seen throughout the entire recorded temperature range. Only pH 5.0 data are shown, but the pH 7.4 results were qualitatively similar.

These results clearly demonstrate the promotion of the formation of lipid isotropic states by the FeLV fusion peptide, in two different lipid systems and at pH 5.0 and pH 7.4. These findings agree with previous work using known viral fusion peptides. Epand and co-workers (1994) showed that the wild type fusion peptide from SIV enhanced the production of isotropic signals by MeDOPE, whereas these structures were formed much less readily in the presence of a non-fusogenic peptide mutant, SIVmutV. Similar work with the Influenza virus fusion peptide (Epand and Epand, 1994) showed that the wild type fusion peptide promoted the formation of isotropic lipid structures by MeDOPE at pH 5.0, the fusogenic pH for this virus. Two mutant fusion peptides, with Glu for Gly substitutions in position 1 or position 4 of the peptide, induced much less isotropic signal in MeDOPE at pH 5.0 than that obtained in the presence of the wild type fusion peptide. Moreover, the E1 mutant, which is known to induce the least membrane destabilisation of the two mutants, as measured by DSC experiments (Epand and Epand, 1994) and by leakage of vesicle

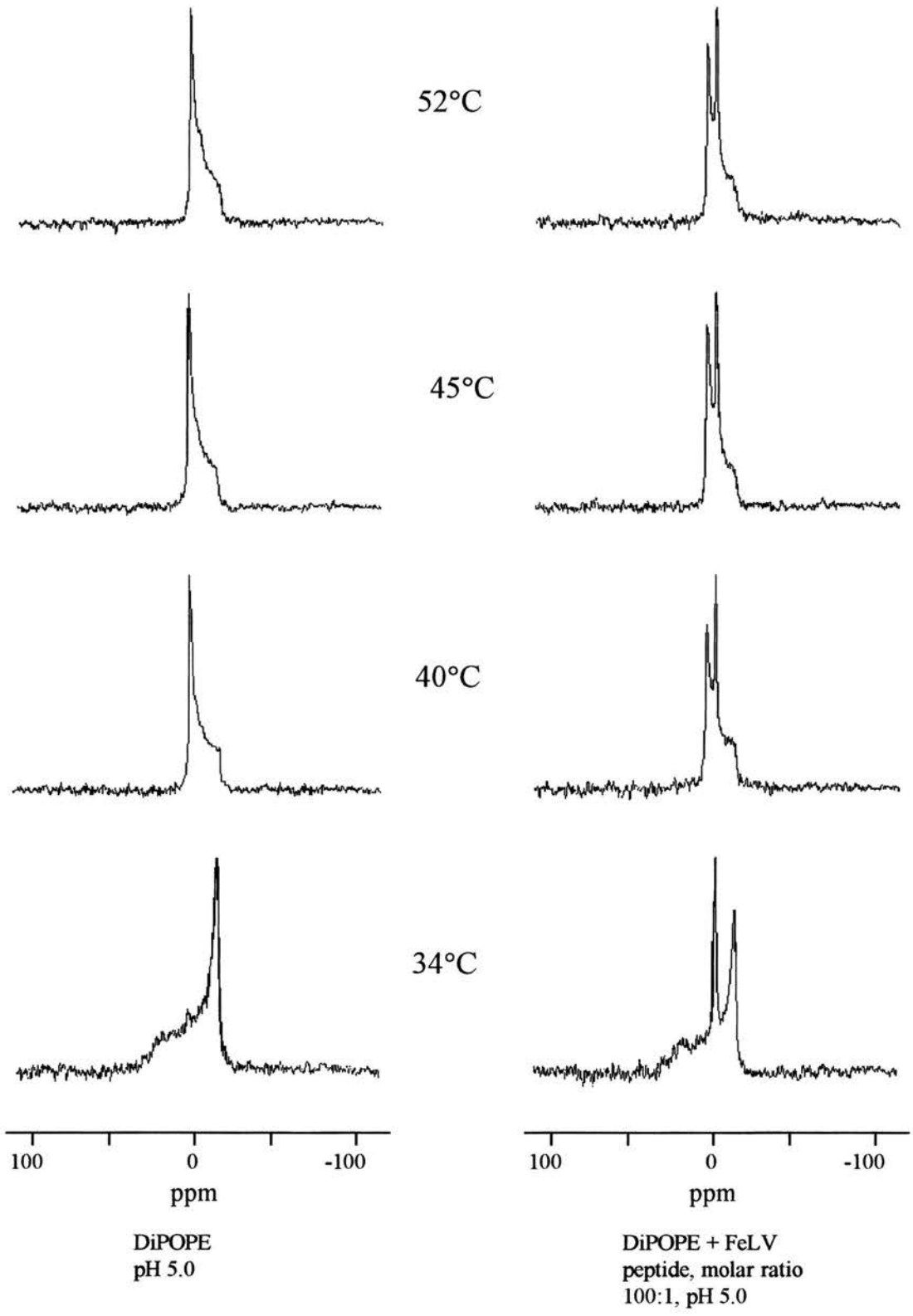

Figure 3.9. ^{31}P NMR spectra of DiPoPE alone, and in the presence of a 100:1 molar ratio of lipid:FeLV peptide. Only pH 5.0 data are shown but the pH 7.4 results were qualitatively similar.

contents (Rafalski *et al*, 1991), was also found to induce the smallest amount of isotropic resonance at pH 5.0. Yeagle *et al* (1991) showed that the presence of the Measles virus fusion peptide at a lipid:peptide molar ratio of 200:1, or 0.5mol% peptide, significantly facilitated the formation of isotropic ^{31}P resonances by MeDOPE. Furthermore, at a lipid:peptide molar ratio of 100:1, the effect was even greater: T_I dropped by about 30°C. In this same study, the Measles virus fusion peptide was also shown to enhance the initial rates of fusion between Sendai virus and MeDOPE LUVs by about 30%, at the lower peptide concentration of 0.5mol%.

Comparable findings have occurred for studies of other known fusogens. Thus the addition of DAG to PC bilayers (Dawson *et al*, 1984) or to PC:PE: cholesterol mixtures (Basáñez *et al*, 1996) was seen to induce isotropic ^{31}P NMR signals. Siegel *et al* (1989a) studied the effect of DAG on MeDOPE polymorphism and fusion between MeDOPE LUVs, and found that 2mol% DAG could lower both T_I and the temperature for the onset of fast membrane fusion by 15-20°C. Similar results were obtained by van Gorkom *et al* (1992). Epand and co-workers (1993) studied the peptide fFGOBz, which promotes fusion between MeDOPE vesicles. This peptide was, in addition, found to promote the formation of isotropic states in MeDOPE, both by lowering T_I and by increasing the relative intensity of the isotropic signal at temperatures of 45°C and higher.

The relationship between the fusion pathway and the formation of isotropic lipid states has been further endorsed by work with known fusion inhibitors. Thus a ^{31}P NMR study of LPC, which inhibits fusion between MeDOPE LUVs and between Sendai virus and MeDOPE LUVs, showed that it also stabilised the lamellar lipid phase and reduced the formation of non-lamellar structures throughout the entire studied temperature range (Yeagle *et al*, 1994). Furthermore, LPC was seen to suppress the increased formation of isotropic resonances induced in MeDOPE by the SIVwt fusion peptide (Epand *et al*, 1994), and to counteract the promotion of the isotropic state in PC:PE:cholesterol by DAG (Basáñez *et al*, 1996). As another example, the peptide ZfFG is a potent anti-Measles agent (Richardson *et al*, 1980), which inhibits fusion between MeDOPE vesicles, and also Sendai virus fusion with human red blood cells (Kelsey *et al*, 1991). Kelsey and co-workers (1990, 1991)

correlated this inhibition of fusion with the inhibition of non-bilayer phase formation: ZfFG was seen to decrease the relative intensity of the isotropic ^{31}P NMR resonances of MeDOPE by broadening the resonance, over a wide range of temperatures.

It is, therefore, clear that some connection exists between the formation of isotropic lipid states and the fusion pathway, at least in certain lipid systems. The studies described above use lipids that have a nearby H_{II} boundary, and the connection between fusion and isotropic structure formation is also only valid for systems which show ^{31}P isotropic resonances on the first heating scan.

Factors that determine the relative stability of bilayer and non-bilayer phases are the intrinsic radius of curvature of each monolayer of a bilayer, and the hydrocarbon packing constraints (Gruner, 1985; Siegel *et al*, 1989a) and energy contributions of the hydrophobic void spaces (Siegel, 1993) for the different structures present. An increase in the isotropic resonance of a lipid may represent a decrease in the effective radius of curvature of the existing lipid structures, since a reduction in ^{31}P NMR linewidth is due to an increase in the motional averaging of the chemical shift anisotropy. Support for this change in monolayer curvature comes from work by Kelsey *et al* (1991), who found that the fusion inhibitor ZfFG hindered the formation of SUV, which are structures of small radius of curvature. Similarly, Yeagle and co-workers (1992) also found that ZfFG appeared to destabilise lipids in structures with a negative radius of curvature. Yeagle *et al* (1994) also showed that LPC, which inhibited Sendai virus fusion, also stabilised the bilayer phase and reduced the formation of all non-lamellar structures. Thus they, too, concluded that at least some of the intermediates in Sendai virus fusion must contain lipid surfaces with a small radius of curvature. Finally, DAG, which promotes membrane fusion and isotropic state formation, is thought to increase the relative volume of the hydrocarbon region of phospholipid molecules, since unsubstituted glycerol headgroups are known to partition preferentially into the hydrocarbon region (Gulik *et al*, 1988), with their hydroxyl groups positioned at the membrane surface (Hamilton *et al*, 1991a, 1991b). Thus DAG should increase the monolayer negative curvature, as discussed in Chapter 1. It should be noted that it is theoretically possible that the decrease in the observed NMR linewidth could result from either a decreased

diffusion rate between the isotropic structures and the bilayer, or an increased diffusion rate within the isotropic structures. It is hard, however, to envisage how such dynamic alterations would cause a decrease in the observed rate of membrane fusion.

The isotropic state may represent a kinetically hindered transition to the H_{II} phase (Ellens *et al*, 1986). It is also thought to represent the first step in the formation of inverted cubic phases (Ellens *et al*, 1989). Lipids with 'intermediate' values of spontaneous radius of curvature, such as MeDOPE, can form cubic phases, which have space groups of Im3m and Pn3m, as seen by X-ray diffraction (Gruner *et al*, 1988; Siegel and Banschbach, 1990). It is unlikely that ordered cubic phases are intermediates in the fusion pathway, since fusion intermediates are isolated structures, not phases (Yeagle, 1994), and cubic phases have extreme kinetic stability (Gruner *et al*, 1988). It has, however, been suggested that fusion intermediates may resemble intermediates formed on the pathway to cubic phase formation (Siegel & Epand, 1997). Thus the observed ^{31}P NMR isotropic states may represent disordered bilayer intermediates or regions of cubic phases that lack long range order, and the metastability of these molecular intermediates may cause fusion.

Theoretical predictions suggest that all lipid intermediates form between apposed bilayers in the L_α phase. It has been suggested that the formation of cubic phases may occur via high-curvature intermediates such as ILAs (Siegel 1986a; 1986b), which are catenoidal bilayer connections between apposed L_α lamellae (see Figure 3.10). ILAs should yield isotropic ^{31}P NMR resonances and 'lipidic particle' morphology in FFEM micrographs. Inverted cubic phase formation can occur then once a large number of ILAs are present within a bilayer. As the ILAs increase in number they automatically form a lattice with the same periodicity as one of the infinite periodic surface-based Q_{II} phases. Formation of Im3m symmetry from the ILA lattice is easy, as it involves no further change of connectivity between the bilayers. The other observed Q_{II} geometries are nearly isoenergetic, and have the same genus, so interconversion between these phases should be relatively easy.

ILA formation should also result in membrane fusion, since an ILA resembles a fusion pore in appearance. Thus for the pure lipid systems described above, fusion

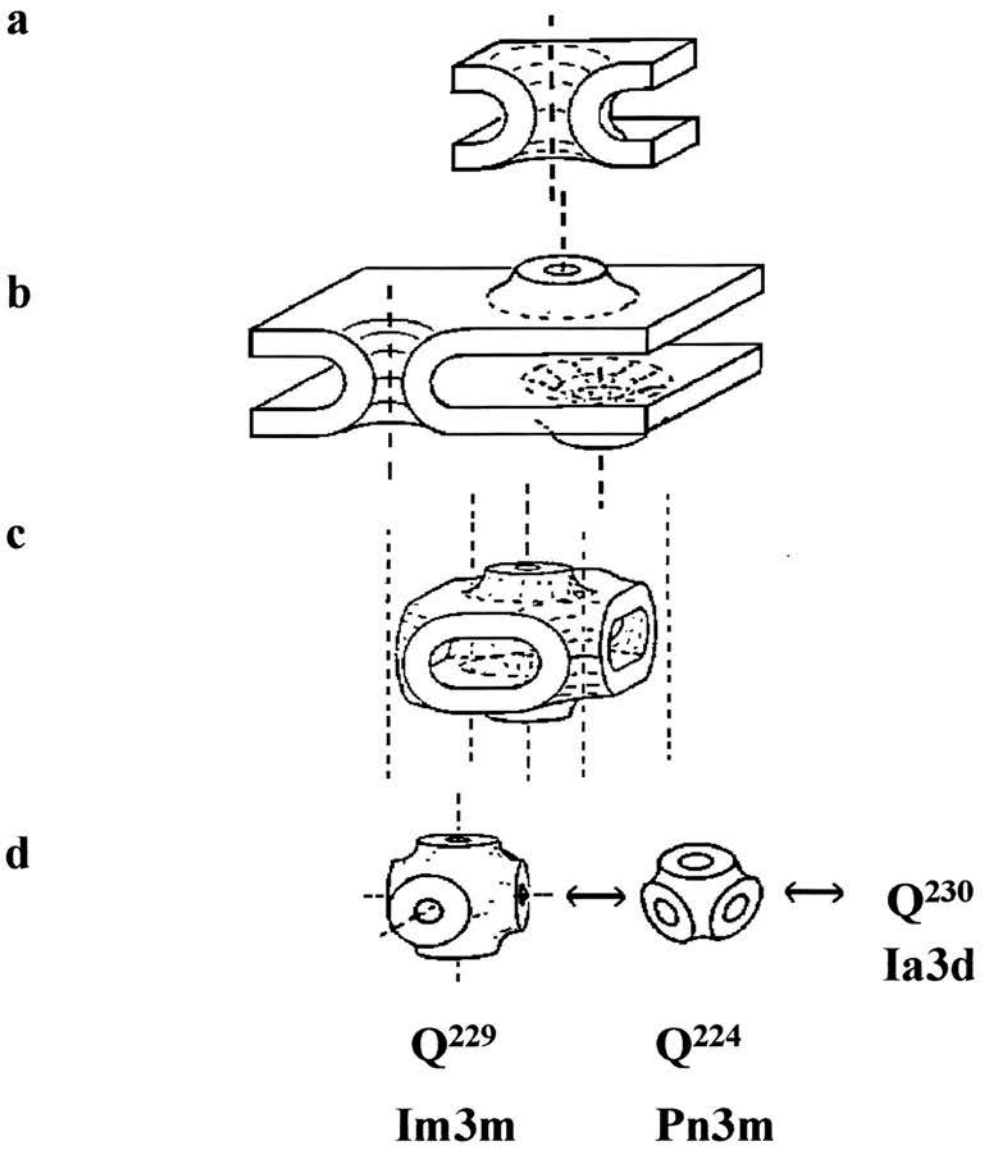

Figure 3.10. Proposed mechanism for the L_α/Q_{II} phase transition. a) ILAs form between apposed L_α bilayers. ILAs resemble fusion pores. b) many ILAs form, so the L_α lattice disorders. c) Eventually an ILA array forms with a primitve tetragonal unit cell. This has the same connectivity as Q^{229}, which is shown in d). Conversion into Q^{229} requires only bilayer bending, as does the inter-conversion between the different inverted, bicontinuous cubic phases shown in d). The driving forces for the conversion between c) and d), and within d) are the different thermodynamic stabilities of the Q_{II} phases (Anderson *et al*, 1988) and constraints imposed by the water content of the sample (Siegel, 1986c).

may be an obligatory step in the transition to the cubic phase. Fusion may result from the gradual accumulation of isolated intermembrane intermediates, which can then transform into fusion structures. Siegel *et al* (1989c) used TRC-TEM to image the intermediates in bilayer to non-bilayer transitions. They visualised ILAs, and showed that ILAs did assemble into a lattice. Moreover, ILAs appeared to mediate both membrane fusion and the L_α/Q_{II} phase transition. Siegel (1986b, 1986c) also explained the hysteresis seen for the L_α/Q_{II} phase transition on the basis of the formation of numerous ILAs, which rearrange into isotropic states that are metastable over a broad temperature range. The type of phase transition that occurs in a lipid system will thus be determined by the tendency of the system to form ILAs.

Fusion promoters, such as viral fusion peptides, could increase the formation of isotropic lipid states, and thus favour the fusion process in several possible ways. Firstly, they could act by reducing the intrinsic radius of curvature of the lipid monolayers present, thus destabilising the bilayer phase relative to more negatively curved, non-bilayer structures. Evidence to support this mechanism is seen in the experiments using the FeLV fusion peptide, namely its effect on the H_{II} phase lattice constant of DiPoPE (see Chapter 4). Secondly, fusion promoters might either relieve the packing constraints or reduce the void energies present in these curved lipid arrangements. This may also be relevant to the mode of action of the FeLV fusion peptide, as shown by its effect on lipid packing arrangements in the stacked bilayers which were used for neutron diffraction experiments (see Chapter 5). According to the 'modified stalk' theory of membrane fusion, ILAs are formed from TMCs (transmonolayer contacts) (see Chapter 1). Thus a third possible mode of action for fusion peptides is that they might lower the rupture tension of the TMC diaphragm, thus increasing the formation of ILAs and fusion pores. Siegel and Epand (1997) suggest that TMC diaphragm rupture tension may be a crucial factor in determining how much Q_{II} forms, and therefore also the fusogenic capacity of lipid and lipid-protein systems where the lipid present is a PE. Thinning of the lipid bilayer will reduce this rupture tension, and this is seen in the presence of the FeLV fusion peptide, using neutron diffraction (see Chapter 5).

In conclusion, my results presented here for the putative fusion peptide from FeLV suggest that it is indeed favouring the production of lipid structures, which are likely to be involved both in the formation of cubic phases, and in the rate-limiting intermediate stages of the fusion pathway.

Chapter 4: The use of Time-Resolved X-ray Diffraction to observe the effects on Lipid Phase Transitions and Lipid Structural Parameters produced by the FeLV Fusion Peptide.

X-ray Diffraction

4.1 General Introduction

X-ray diffraction is the most important and least ambiguous method of structural determination of lipid phases (Luzzati, 1968). It is directly sensitive to the relative positions of the component atoms that are present in a lipid sample, and so it can identify the structural rearrangements that distinguish different lipid phases. The relatively recent development of powerful synchotron X-ray sources has greatly reduced the sample exposure times that are required to obtain good diffraction data. This has led to the evolution of time-resolved X-ray diffraction (TRXRD). Direct and quantitative measurements can be made of phase transitions in bulk lipid samples using TRXRD. This approach allows a more dynamic examination of lipid phase changes compared to traditional X-ray diffraction methods. TRXRD enables both the kinetics of the transitions and the formation of intermediate structures to be studied, which, in turn, hopefully provide some understanding of the mechanisms of the lipid phase transitions.

4.2 Theoretical Background

Diffraction is defined as the deviation of a wave from its natural direction of propagation when it encounters an object or a medium with spatially varying transmittance (Warren, 1987). Diffraction at single or multiple slits is due to the superposition of secondary wavelets that are produced by different parts of the same wavefront. The diffraction pattern produced by a single bilayer is similar to that seen for Young's double slits, since the bilayer contains two parallel polar headgroup regions, which diffract X-rays strongly. Thus diffraction from a single lipid bilayer results in the production of alternating regions of constructive and destructive interference. A pattern similar to Young's fringes is produced by this interference, which is called the diffraction pattern, or diffractogram.

If a multiple slit arrangement, such as a diffraction grating, which has identical, equally spaced diffracting elements, is used to produce diffraction, each narrow slit in

the grating will act as a source of secondary wavelets (see Figure 4.1). These wavelets superpose beyond the slits, resulting in constructive interference in certain directions and destructive interference in others. Furthermore, different secondary wavelets from the same slit also interfere with each other. This combined effect results in the production of a diffraction pattern, with maxima corresponding to the regions of constructive interference, and minima to those of destructive interference. Moreover, a grating which has a large number of slits produces completely destructive interference in all directions other than those which are described by the equation:

$$\sin\theta = \frac{n\lambda}{d} \qquad 4.1$$

where θ is the diffraction angle relative to the normal, λ is the wavelength of the incident radiation, d is the distance between adjacent lines of the grating, and n is an integer, or order of diffraction (see Figure 4.2).

It is not practical to record the diffraction pattern from one molecule as its interaction with radiation is very weak, and hence it would take an extremely long time to obtain a sufficiently strong diffraction pattern. In order to study the structure of lipid bilayers, a regular stack or a random dispersion of bilayers are thus normally used. Regular stacks of biological membranes or artificial lipid bilayers form a similar type of structure to a diffraction grating. This stacked bilayer arrangement produces a relatively large distance between adjacent slits, and thus it gives rise to a small angle, or 'low angle', diffraction pattern. (It can be seen from Equation 4.1 that there is an inverse relationship between the distance between the individual slits and the resultant angle of diffraction. The reciprocal of d is also known as the 'spatial frequency' of the diffraction grating).

The analogy with a diffraction grating only describes the two-dimensional effects of diffraction by lipid bilayers. The situation is further complicated by the three-dimensional arrangement of atoms and molecules within the bilayer structure. If one regards the arrangement of these bilayer constituents, and also of the individual bilayers, as comprising layers or planes (see Figure 4.3), then, in addition, each individual plane will reflect radiation. Constructive interference will only occur

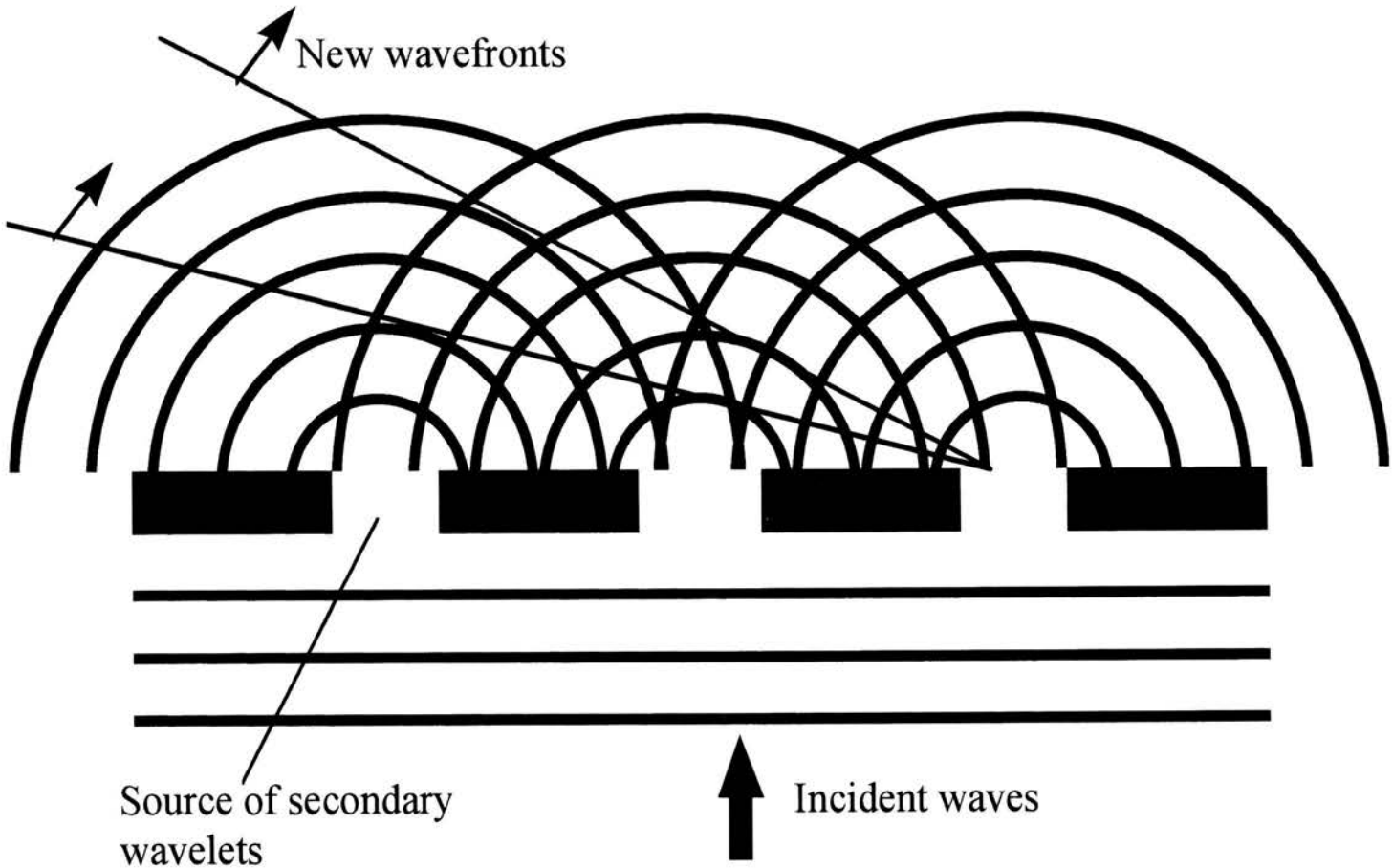

Figure 4.1. Diffraction at a grating. Each slit acts as a source of secondary wavelets, which superpose beyond the slits. The wavelets interfere constructively in certain directions, in which they are in phase, and form new, straight wavefronts. Interference also occurs between secondary wavelets from different points in the same slit. The diffraction pattern from one slit is thus superimposed upon the interference pattern and determines the variations of intensity of the observed orders of diffraction.

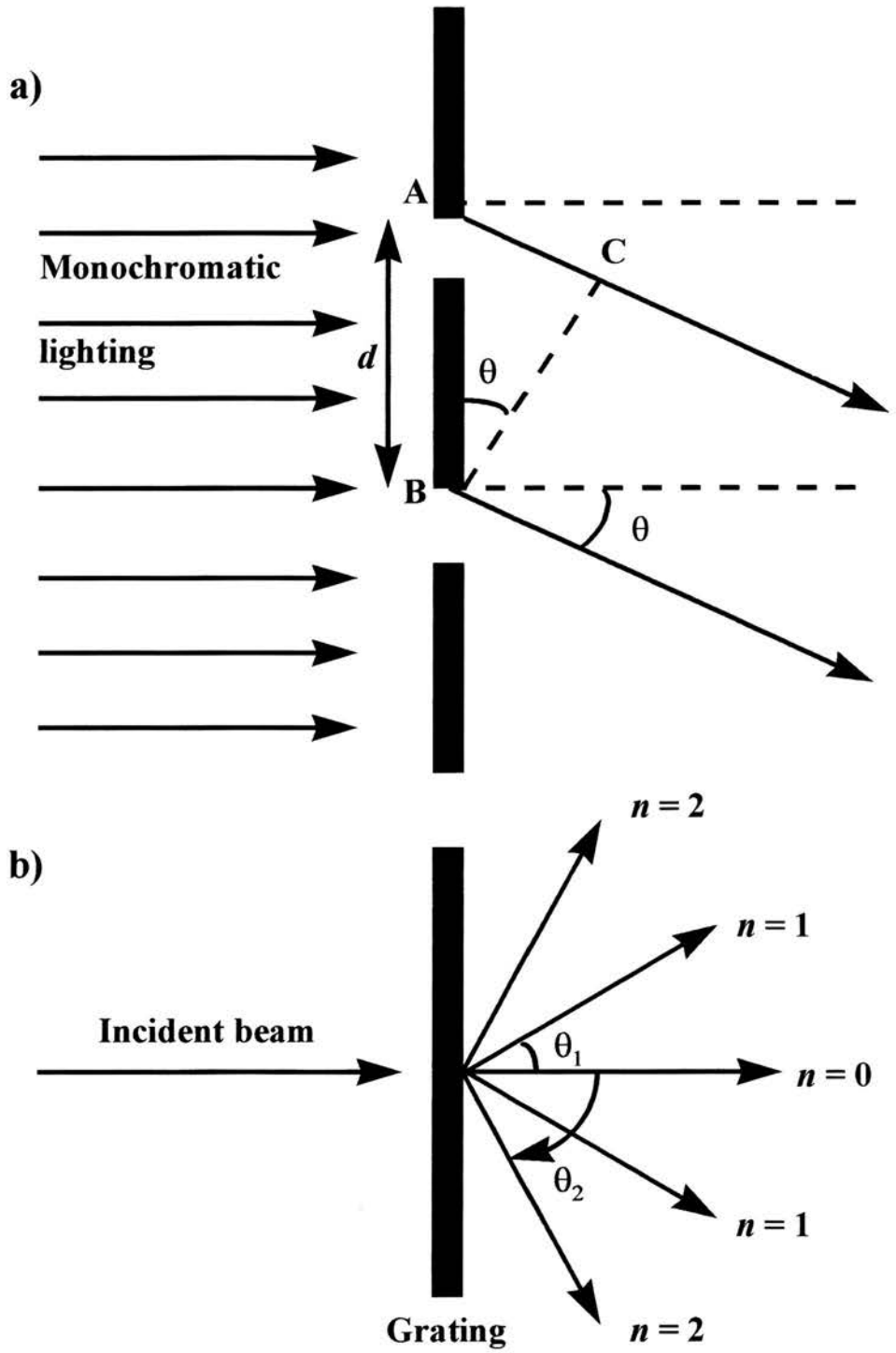

Figure 4.2. a) Diffraction at a multiple slit grating. Wavelets can arise from points A and B on two successive slits and travel at an angle θ to the direction of the incident wave. The path difference AC between the wavelets is $d\sin\theta$. If $d\sin\theta = n\lambda$, then reinforcement of the diffracted wavelets will occur. b) Diffraction orders produced by such diffracted wavelets.

between waves reflected from parallel planes when the angle of reflection is given by the Bragg equation, namely:

$$\sin\theta = \frac{n\lambda}{2d} \qquad 4.2$$

where d is the perpendicular spacing between the molecular planes, and θ is the angle between the incident beam and the molecular planes, λ is the wavelength of the incident radiation and n is an integer, or order of diffraction. W.L. Bragg (1913) was the first person to realise that diffraction from a regularly repeating structure could be described in terms of 'reflections' from planes of equal scattering density. This greatly simplified the analysis of three-dimensional X-ray data, since now diffraction in only one plane needs to be considered.

There are only certain angles for the incident radiation beam which fulfill the Bragg equation when considering the three-dimensional diffraction produced by planes of molecules. This is because, in order for constructive interference to occur between radiation reflected from points in adjacent planes, the difference in the path length travelled by these waves must be an integral number of wavelengths, which will cause these waves to be in phase. At all other angles, there is destructive interference and so no observable diffraction. Thus the sample must either contain a totally random dispersion of lipid bilayers, which will clearly satisfy every possible angular requirement, or else the sample must be moved around a static beam direction until the required Bragg angle is achieved. From Equation 4.2 it can be seen that:

$$2\sin\theta = \frac{n\lambda}{d} \qquad 4.3$$

The angle of the diffracted beam is called the 'scattering angle' and is the angle between the main beam and the diffracted beam. Its size is twice that of the incident beam (see Figure 4.3). Moreover, at small angles, such as are used for low orders of low angle diffraction experiments, $\sin\theta \approx \theta$. Thus the scattering angle, θ_s, can be approximated by the equation:

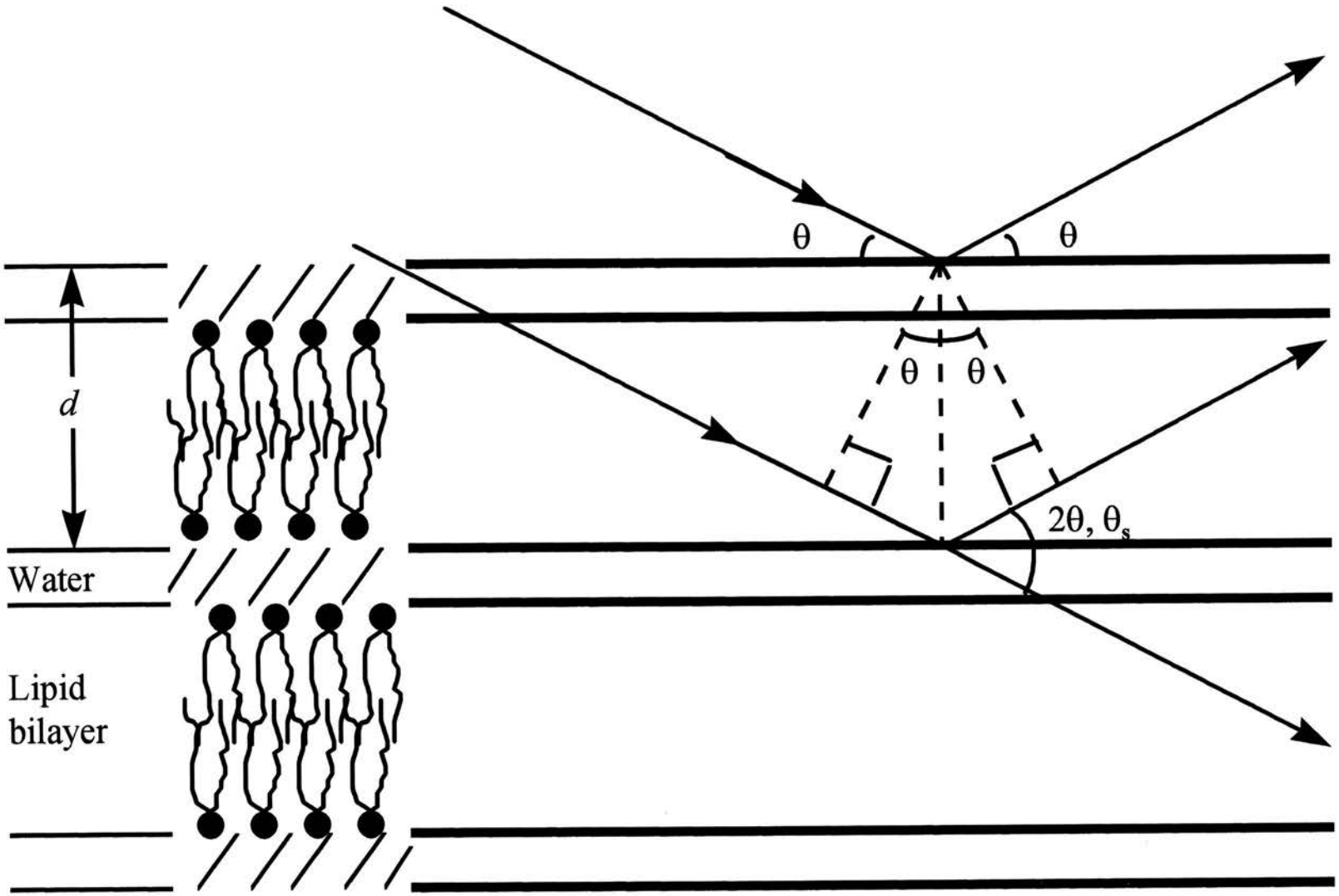

Figure 4.3. Diffraction from planes of molecules, or stacked bilayers, as described by Bragg's Law- see text for details.

$$\theta_s = \frac{n\lambda}{d} \qquad 4.4$$

In 1923 de Broglie suggested that matter might exhibit wave-particle duality and thus have wave properties, an idea that had already been accepted for electromagnetic radiation. This is now an accepted concept for matter, and beams of X-rays or electrons or neutrons are currently used for diffraction experiments on biological membranes. These are particularly suited for use in these experiments because of the size of lipid bilayers: a typical membrane is less than 10nm in diammeter, and therefore radiation of 1nm or less is required in order to produce a useful, detailed diffraction pattern.

X-rays are scattered by the electrons present in the sample; this occurs as a result of the interaction of the incident electromagnetic radiation with the charged electron clouds. Both coherent and incoherent scattered radiation are produced. The diffraction pattern is due to the interference of the coherent scattered radiation, whilst the incoherent scattering is responsible for the background radiation that is produced during a diffraction experiment. Subtraction of this background component is a prerequisite step in the determination of the intensity values for the diffraction peaks.

In a typical X-ray diffraction experiment, a narrow, well-defined beam of X-rays is directed through the specimen, and the distribution and intensity of the X-rays that are scattered are recorded as a function of angle. Most of the X-ray beam will pass straight through the sample, and this radiation is not recorded. Since X-ray diffraction is directly sensitive to geometrical structure, it is an excellent technique with which to study lipid phase transitions; indeed, different lipid phases are often determined by the symmetry of the small angle X-ray diffraction produced by a lipid sample. Thus the L_α phase consists of a one-dimensional periodic lattice that is composed of locally planar and parallel bilayers, which are separated by layers of water of uniform thickness. The inverted hexagonal phase, on the other hand, constitutes a two-dimensional phase, in which rod-like structures are laterally placed on a two-dimensional lattice. Finally, cubic phases demonstrate three-dimensional periodicity. Thus, by using X-ray diffraction, a phase diagram of a lipid system can be

obtained. This is usually accomplished by observing the sequence of equilibrium phases that the system adopts as the thermodynamic variables of the sample are altered. In practice, the inherent disorder of the liquid crystalline state can often restrict the number of observable diffraction orders significantly.

If lipid phase changes are physiologically relevant, they must take place on a time scale which is comparable to that of changes occurring *in vivo* (Caffrey, 1989). Traditional X-ray diffraction requires long exposure times, and any lipid phase changes that occur during the fusion mechanism must occur very rapidly (on a millisecond time scale). TRXRD is therefore the best option for the investigation of the effects of a viral fusion peptide on lipid phase changes.

The first TRXRD study of lipid phase transitions in membranes and membrane lipid extracts was described in 1972 (Dupont *et al*, 1972). TRXRD requires an intense, monochromatic X-ray beam with a very high repetition rate, and a live-time X-ray imaging device, which constantly monitors the diffracted X-rays that are produced by the lipid sample. Thus a set of consecutive X-ray diffraction scans, which have a set time interval between each scan, is obtained. By examining the positions of the diffraction orders that are observed on each of the consecutive scans, it is possible to determine the lattice types or packing symmetries of the lipid molecules in the sample, and thus the lipid phases present. As an example, if the lipid in the specimen is all present in the lamellar phase, the diffraction pattern will consist of a lamellar series of Bragg peaks, but if more than one phase is present then the diffraction pattern will consist of more than one series of Bragg reflections. The lattice parameters, or *d*-spacings, can be calculated from the distance of the individual peaks from the centre of the diffraction pattern. Absolute lattice spacing can be obtained by comparison with that obtained for a known standard under the same experimental conditions. The nature of any phase transitions, that is whether they are ordered, the time-span of any co-existence of domains of the converting lipid phases, and the temperature ranges over which any transitions occur can also be determined very easily. Any correlations between the variable parameter, for example the temperature of the sample, and the phase changes that occur within the sample can be determined. Furthermore, if the areas under the individual diffraction peaks are measured, which is normally done by

the fitting of Gaussians using the least squares method, then the relative amounts of the different lipid phases can be ascertained throughout the lipid phase transitions.

4.3 Application of Time-Resolved X-ray Diffraction to Fusion Studies: Aims of these Experiments

TRXRD data were obtained to confirm the identity of the phase transitions that were measured by DSC (see Chapter 2). The same type of lipid and similar peptide mole fractions were therefore used for the DSC and the TRXRD experiments. There have been very few previous investigations using TRXRD of the effects of fusogens on lipid phase transitions, and even conventional X-ray diffraction studies are limited. The fusion peptides of SIV (Colotto *et al*, 1996) and Influenza virus (Colotto and Epand, 1997) have been examined using X-ray diffraction methods. Both of these fusion peptides were shown to have a bilayer destabilising effect. The SIV peptide also increased the spontaneous curvature of the hexagonal phase lipid, whilst the Influenza virus fusion peptide, which is activated at low pH, induced cubic phase formation at pH 5.0. DAGs, which are fusion promotors, have been found, by X-ray diffraction, to increase the spontaneous negative curvature of MeDOPE (Ellens *et al*, 1989). A second aim was, therefore, to determine any effects of the FeLV fusion peptide on lipid structural parameters. In particular, any changes in the lattice spacings, and thus in the spontaneous radius of curvature of the monolayers present, were of great interest.

4.4 Materials and Methods

4.4a Sample Preparation

DiPoPE was purchased from Avanti Polar Lipids (Alabaster, AL, USA). Preparation of lipid and lipid/peptide films was as described in Chapter 2. The buffer used for the subsequent preparation of the lipid suspensions was 20mM PIPES, 1mM EDTA, 150mM NaCl and 0.002% NaN_3, at pH 7.4. After addition of the required amount of buffer, the suspensions were vortexed thoroughly several times and were

then subjected to 3 freeze-thaw cycles, as described in Chapter 3, in order to obtain as homogeneous a sample as possible. In practice this must potentially be one of the main errors in the experimental proceedure, as it is extremely difficult to obtain good homogeneity of PE lipids in aqueous suspension. Samples were stored in the fridge at 4°C and re-vortexed just before use. All samples were used within 24 hours of preparation. Ideally a check should be made for possible radiation damage and/or oxidation of lipids at the end of the experiments using TLC. In practice, careful preparation of the samples should minimise oxidative deterioration. Studies by several groups have failed to reveal any radiation damage to samples, providing that the beam is running as expected (K.R. Jeffrey, personal communication).

4.4b X-ray Diffraction

The X-ray diffraction experiments were performed at station 8.2 of the synchotron radiation source at the Daresbury Laboratory, Daresbury, UK. By using a subsidiary accelerator a synchotron increases the speed of the electrons so that it is close to that of light. Accelerators work on the principle of synchronous acceleration. The electrons then follow a circular path under the action of a magnetic field, and their energy is increased by applying synchronous electrical pulses from a high-frequency alternating potential difference that is connected to several cylindrical electrodes arranged around the track. Whenever the electrons pass through the bending magnets they lose energy in the form of electromagnetic radiation. The electrons that reside in the storage ring do not form a continuous stream, but occur in groups that are separated in time by 10^{-8} to 10^{-9} seconds. Thus the emitted radiation is also pulsed at a similar frequency, which allows time-resolved experiments to be performed on nanosecond timescales. Devices called wigglers are used to alter the wavelength of the radiation produced, while undulators produce interference effects and thus produce a spectrum of radiation that is a series of narrow harmonics. By changing the settings within the undulators the wavelength that is produced can be tuned, and thus the useful flux can be greatly increased. A monochromator is then used to select the appropriate wavelength required; this is fixed at 1.54Å for Station 8.2. The beam of electrons was collimated so that only the sample was irradiated.

Beam instability and decay during any diffraction measurement are potential sources of error, and so the intensity of the incident beam must be monitored continually during the experiment in order to allow subsequent normalisation of the data. This is achieved by the use of a separate small detector which intercepts a small part of the incident beam.

A teflon-lined brass chamber with mica windows was used as the sample holder. Since the samples were composed of lipid bilayers that were completely disordered with respect to the direction of the incident beam, they could be held stationary in the beam and still fulfill the required geometry of diffraction. An external circulating water bath was used to control the sample temperature, which was monitored continuously by a thermocouple. A major source of error in TRXRD experiments is often a lack of rapid and uniform changes in the temperature of the sample. Thus a liquid of high coefficient of heat transfer, namely ethylene glycol, was used in place of water in the water bath, at a high circulation rate. Furthermore, the sample size was the minimum that would produce good diffraction data. The temperature of the sample cell was linearly increased from 30°C to 70°C, at a heating rate of 90°C/hour. Each temperature scan consisted of 120 frames of diffraction data. An INEL position-sensitive, curved detector, was used to detect the diffracted radiation, which ionises argon gas within the detector, and an 'avalanche' phenomenom is created. An inducted charge is produced at the impact point of the avalanche on the cathode readout strips, and this position is determined by the delay-line method, which depends upon the difference in the arrival times of this charge at each end of the delay line. An electronic position-sensitive processor then processes the data. Most of the incident radiation is transmitted without interacting with the specimen and so a beam stop is placed just in front of the detector to intercept the directly transmitted beam and thus help to reduce fogging of the entire detector.

The XOTOKO programme was used to correct the raw data. Corrections for sample thickness, and variation in detector response were applied, and background counts were subtracted. Detector response was determined by measuring a fixed source, ^{59}Fe, for several hours, at the start and the end of data collection. The detector was calibrated for small angle scattering using rat tail collagen, mounted in a

cell and lightly stretched, as a standard. Under these conditions, collagen has a unit cell size of 676.08 Å (Fraser and MacRae, 1981). The corrected data were then plotted using this calibrated x-axis, in order to obtain absolute values for lattice spacings. The areas under the diffraction peaks were determined using the commercial programme Sigmaplot, version 2.01.

4.5 X-ray Diffraction Results and Discussion

The diffraction patterns that were obtained verify that the transitions which occurred in the DSC experiments were from L_α to H_{II}; no other phases were observed in the X-ray data. Figure 4.4 shows a three-dimensional plot of the series of diffraction patterns obtained over the entire measured temperature range for DiPoPE plus FeLV peptide, present at a peptide mole fraction of 3.1×10^{-3}. Figure 4.5 shows a typical diffractogram for the T_H region of the scan: this was taken from the data for DiPoPE with FeLV peptide, present at a peptide mole fraction of 1.6×10^{-3}, and at 42°C. In the lamellar phase, the Bragg spacings, or *d*-spacings, of all of the orders of diffraction are the integrals of one fundamental spacing. In the hexagonal phase, the ratio of Bragg spacings of the reflections is $1:\sqrt{3}:\sqrt{4}:\sqrt{7}$. Thus samples were assigned the H_{II} phase if a minimum of three diffraction peaks were observed which indicated spacings in the ratios $1:\sqrt{3}:\sqrt{4}:\sqrt{7}$. The *d*-spacings for all samples were calculated from the distance of peaks from the origin. The *d*-spacings for the L_α and H_{II} phases for pure DiPoPE and the peptide-containing samples are plotted in Figure 4.6. The *d*-spacings found in the present work are in good agreement with those previously reported (Colotto *et al*, 1996; Colotto and Epand, 1997). It should be noted that in the values presented in the references the definition used for the repeat spacing was that adopted by Gruner (1991) and others in which the *d*-space corresponds to the distance from the centre of one H_{II} cylinder to the next. This distance is related to the lattice spacing reported in the present work by multiplying the lattice spacing by $2/\sqrt{3}$. The small differences between this data and the two previous sets of data may be the result of different heating protocols, different batches of DiPoPE and different calibrations. The transition from the L_α to the H_{II} phase is ordered, that is both

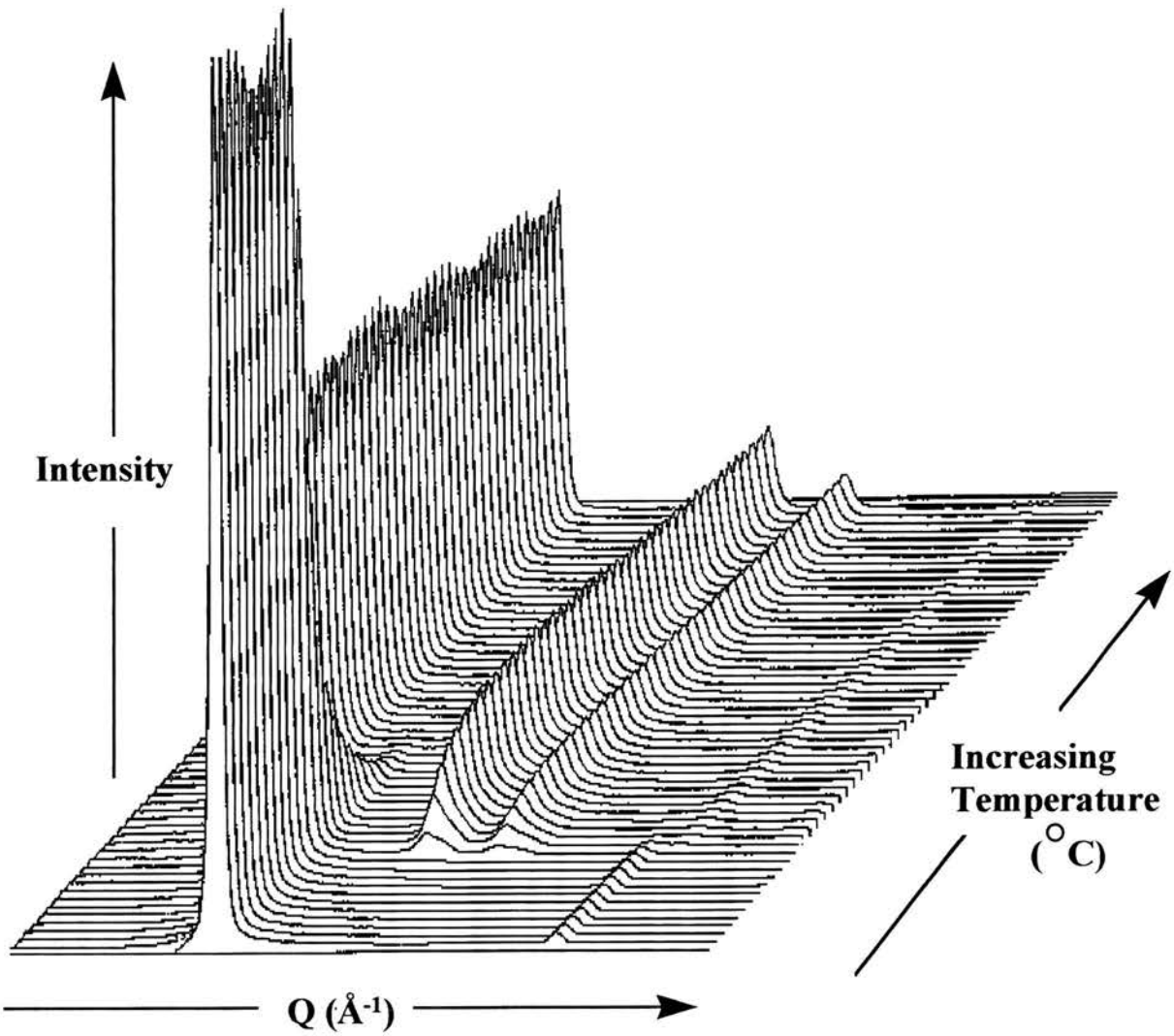

Figure 4.4. Three-dimensional plot of the series of consecutive diffraction patterns obtained on heating from 30°C to 70°C for DiPoPE plus FeLV fusion peptide, peptide mole fraction 3.1 x 10^{-3}. The heating scan rate was 90°C/hour.The origin is on the left, and the right hand limit represents channel 270 of the 512 recorded. Thus each trace is a plot of diffracted intensity vs detector position, the scattering angle increasing from left to right. The first two lamellar and first three hexagonal diffraction orders are visible as well defined peaks. The transition from the lamellar to the hexagonal phase can be seen. The presence of a third, peptide-induced phase can be seen as a shoulder on the second and third hexagonal phase peaks.

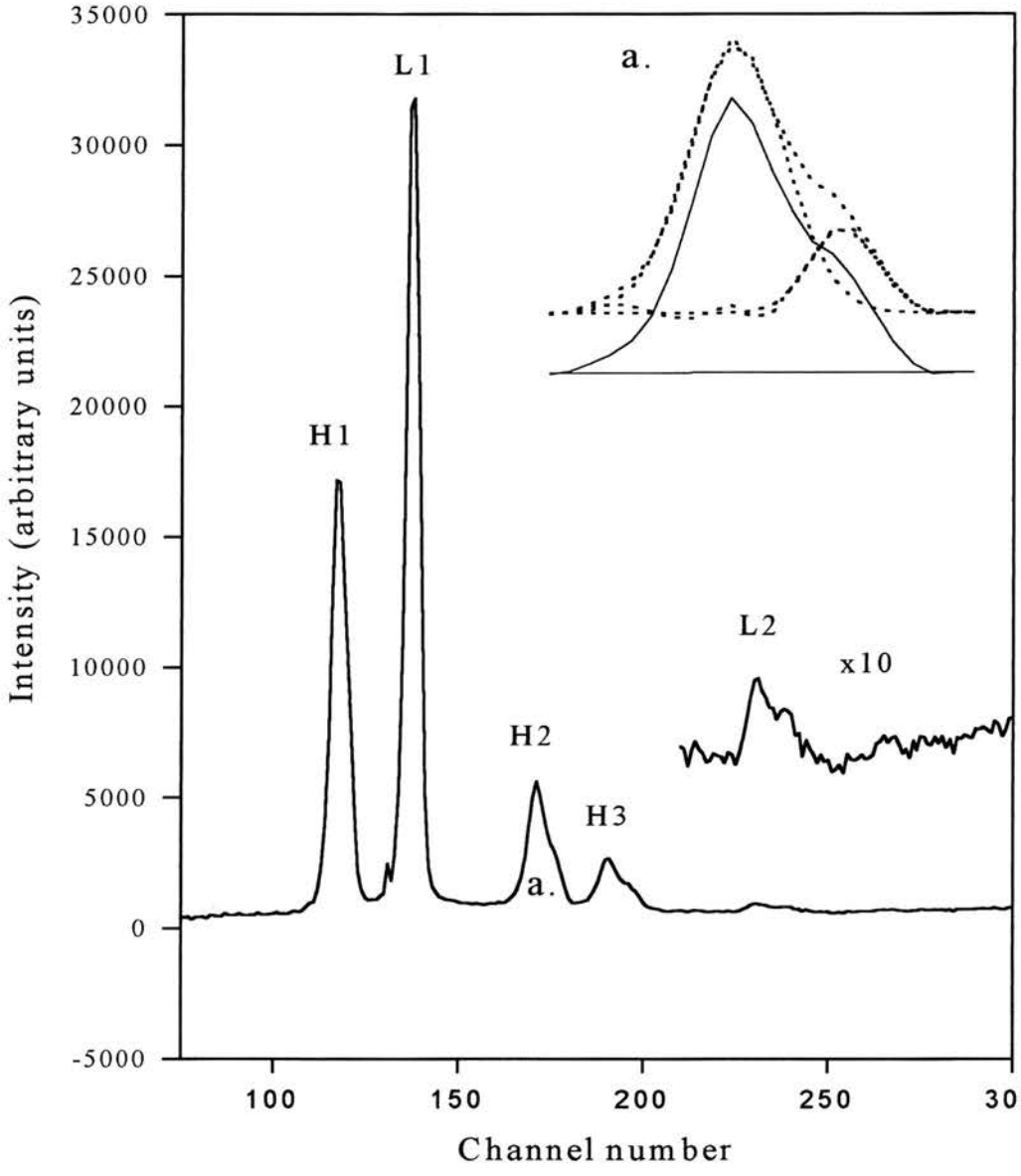

Figure 4.5. Typical small angle X-ray diffraction profile in the T_H region of the scan series for DiPoPE plus FeLV fusion peptide, peptide mole fraction 1.6 x 10^{-3}, at 42°C. Channel numbers 50-300 of the 512 recorded are shown. Part of the data has been amplified by a factor of 10 (x10) for the sake of clarity. The inset, a, shows an enlargement of the Bragg peak for the third diffraction order of the H_{II} phase, and the presence of a smaller peak, of smaller *d*-spacing than the main H_{II} peak (solid lines). Gaussian analysis of the two peaks is shown above (dotted lines).

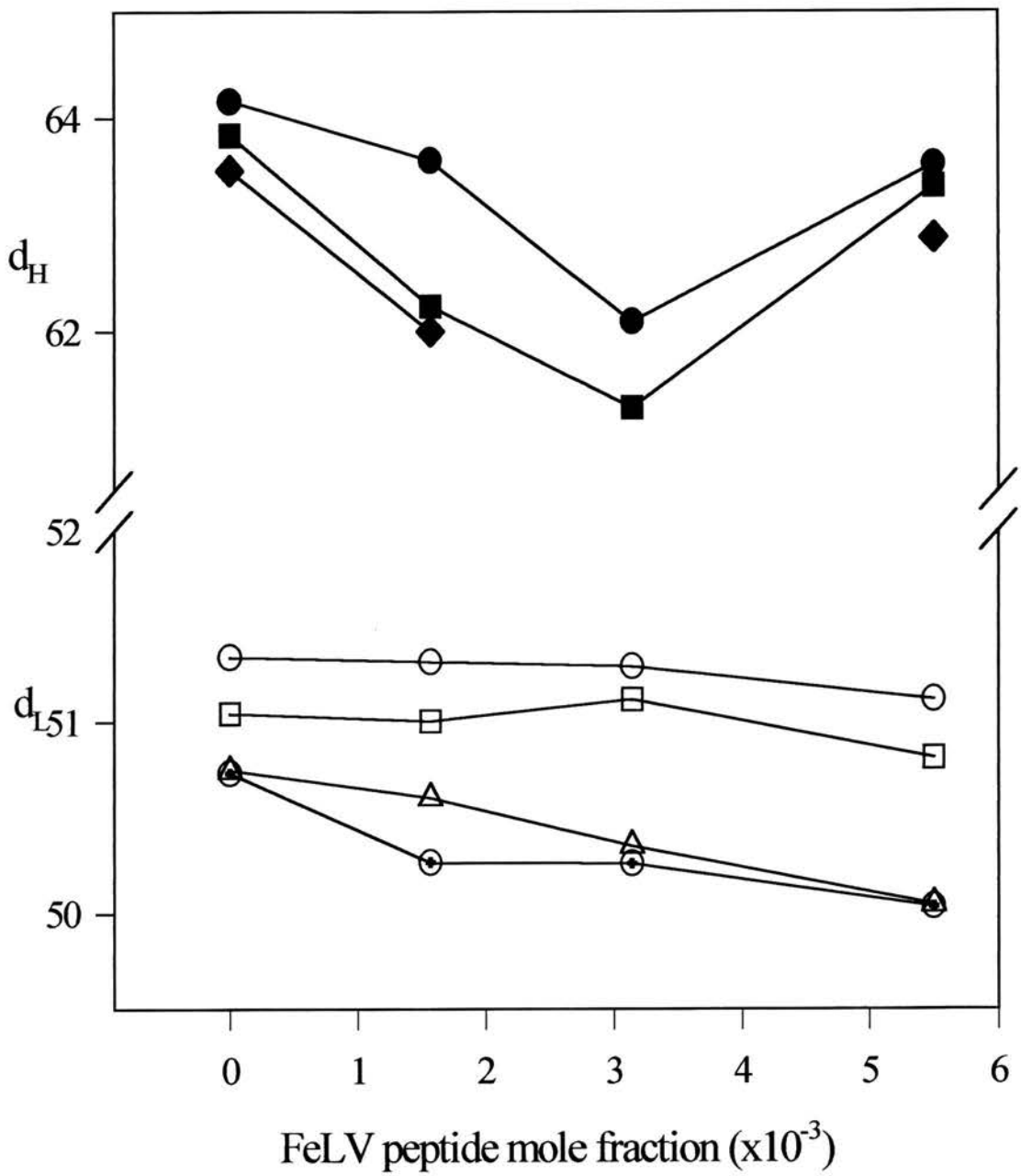

Figure 4.6. Variation in *d*-spacings (Å) for the L_α and H_{II} phases of DiPoPE with increasing FeLV peptide concentration. d_H measured (●) at 49°C, (■) at 50°C, and (◆) at 52°C. d_L measured (O) at 33°C, (□) at 40°C, (Δ) at 44°C, and (⊕) at 45°C.

lamellar and hexagonal phase domains coexist in the transition temperature region. This was seen for the pure lipid and the peptide-containing samples. The preservation of long range order throughout a lipid phase transition suggests that the transition may be co-operative, with long range order being established in the nascent phase (Caffrey, 1989). The slow rate of water penetration into the nascent H_{II} phase seen with multilamellar vesicle (MLV) samples may prolong the detection of co-existence of L_{α} and H_{II} domains.

No cubic intermediates are seen. It is possible, however, that very transient phases are not detected due to the high scan rate employed (disordered structures would not be seen either). In simple kinetic models of a phase transition, the free energy difference between the two phases drives the transition but the intermediate structures are at a higher free energy and thus they present a rate-limiting activation energy barrier (Tate *et al*, 1992). Many lipids have very low monomer solubilities in water and so kinetic relaxation of a lipid assembly into a state of lower free energy may be so severely hindered that the system may be unable to attain true equilibrium in the time available to it during an experiment. Moreover, the absence of lattice structure in the observed diffraction pattern simply means that there is no lattice with long range order present within the sample. Furthermore, over 12 orders of diffraction are required before a cubic phase can be definitively assigned (Franks and Lieb, 1979). Thus some of the previous studies have detected putative, as opposed to definite, cubic phases.

Figure 4.5a (inset) shows the Gaussian analysis of the Bragg peak of the third order of diffraction of the hexagonal phase. It can be seen that, in the presence of the FeLV peptide, a second and different lattice was observed, of slightly narrower *d*-spacing than that of the main H_{II} phase. As one cannot assign a lamellar or hexagonal phase on less than three diffraction orders, it is not possible to state definitively what this novel, peptide-induced phase is: there are only two observable diffraction peaks for this phase, which represent the second and third diffraction orders. The diffraction amplitudes of higher orders were too small to detect, and the first orders of the two hexagonal phases probably overlap due to the decrease in spatial resolution that was seen at smaller diffraction angles. This may account for the observed slight increase in

the mosaic spread of the first order of diffraction of the hexagonal phase in the presence of peptide. However, the two observed novel peaks fitted to a *d*-spacing of 1: $\sqrt{3}$, and they occurred as a shoulder on the definitely identified main H_{II} phase. Thus this may represent a novel H_{II} phase, which was most noticeable in the samples containing 1.6×10^{-3} mole fraction of FeLV peptide. A measure of the maximum percentage of DiPoPE present in this phase as a proportion of the total amount of hexagonal phase lipid yielded the following data:

Table 4.1. The amount of DiPoPE present in the novel, peptide-induced lipid phase as a function of the concentration of FeLV fusion peptide present in the sample.

Mole Fraction of FeLV fusion peptide present	**Amount of DiPoPE in novel 'hexagonal' phase as a percentage of total hexagonal phase lipid present**
0	0
1.6×10^{-3}	32
3.1×10^{-3}	20
5.5×10^{-3}	21

Evidence of the peptide-induced lattice disappeared completely as heating continued well above T_H, indicating that this phase was transient. No extra peaks were seen in the pure lipid samples, and thus it is clear that this novel phase was due to the presence of peptide. This novel phase may be due to the formation of extremely peptide-rich domains within the sample, which have a higher intrinsic negative curvature than that of the pure lipid. Not all of the peptide was incorporated into these domains, since the *d*-spacing of the main H_{II} phase (d_H) was also decreased in the presence of the FeLV peptide (see Figure 4.6): this also suggests that the FeLV peptide is decreasing the spontaneous radius of curvature, R_0, of the system in this range of peptide concentration.

A reduction in R_0 will destabilise bilayer structures relative to inverted non-bilayer phases. DAGs have been found to decrease R_0, that is to increase the

spontaneous negative curvature, of MeDOPE (Ellens *et al*, 1989). Physiological levels of DAGs are known to promote fusion. (Siegel *et al*, 1989a), and have also been found to enhance a L_α to Q_{II} transition (Basáñez *et al*, 1996), to bicontinuous Q^{224} (Luzzati *et al*, 1993). This cubic phase is related to the putative fusion intermediate, in the 'patch-the-puncture' fusion model (Nieva *et al*, 1995).

An interesting observation of these experiments is that of marked broadening of the L_α diffraction peaks on heating in the presence of the FeLV peptide, and in a manner that depends upon the peptide concentration. (The width of the peaks was determined by fitting Gaussians and measuring the width at half height). This represents disordering of the L_α phase, and may be consistent with the start of a transition to an inverted cubic phase (Gruner *et al*, 1988). X-ray studies of DiPoPE with an SIV mutant fusion peptide at pH 7.4 (Colotto *et al*, 1996), and from Influenza virus at pH 5.0 (Colotto and Epand, 1997) have indeed detected the formation of a cubic phase. The heating scan rates used in these studies were considerably slower than that used here, which may explain why no ordered cubic phase was detected in our study. When rapid heating was used with the Influenza fusion peptide, no cubic phase was observed (Colotto and Epand, 1997). It has also been observed that, even with pure MeDOPE, the extent of cubic phase formation is very dependent upon scan rate (Siegel and Banschbach, 1990; van Gorkom *et al*, 1992).

The FeLV peptide also produced broadening of the H_{II} peaks. Part of the peak broadening may be due to vesiculation of the MLVs present in the samples, as suggested for the SIV fusion peptide/MeDOPE system: the conversion of MLVs to smaller vesicles with fewer lamellae is thermodynamically favourable, but the fusion peptide may greatly accelerate this process (Colotto *et al*, 1996).

The effect of the FeLV peptide on d_H is seen to exhibit a biphasic trend with peptide concentration, reminiscent of that seen for T_H in our DSC measurements. The fusion peptide had little effect on d_L at temperatures well below T_H, (see Figure 4.7), but as T_H is approached, d_L decreases with increasing peptide concentration. It can be seen from Figure 4.7 that the temperature-dependance of d_H and d_L is very similar for both pure lipid and the peptide-containing samples. Bragg spacings for a particular

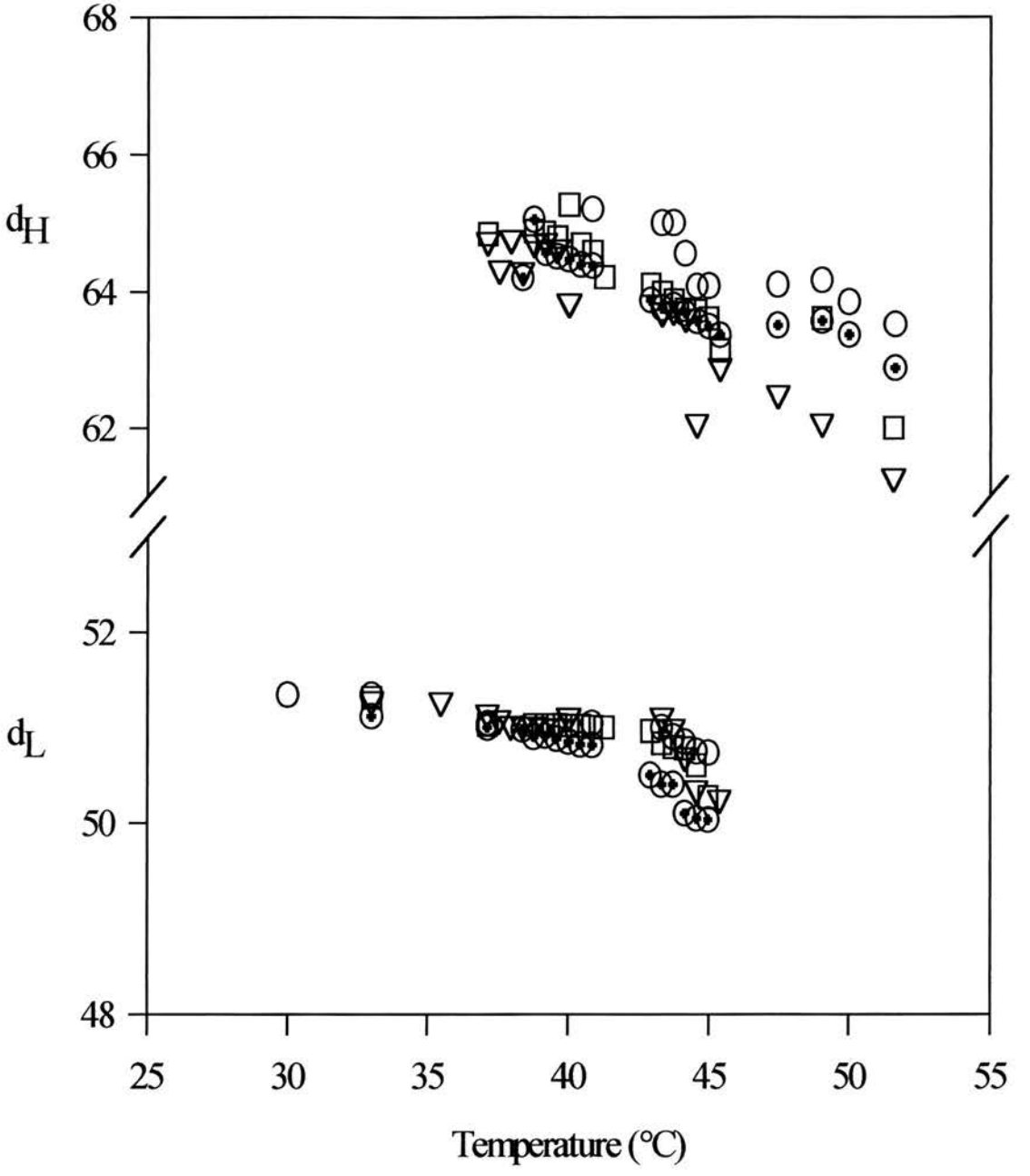

Figure 4.7. Change in *d*-spacings (Å) of the L_α and H_Π phases with temperature as calculated from the X-ray diffraction patterns. DiPoPE alone (O); DiPoPE plus FeLV peptide, at peptide mole fractions: of 1.6×10^{-3} (□), 3.1×10^{-3} (▽) and 5.5×10^{-3} (⊕).

lipid phase tend to decrease as the temperature rises, due to increased disorder of the hydrocarbon chains at higher temperatures (Luzzati and Husson, 1962).

There are two aspects of membrane fusion mechanisms that can explain the relationship between a peptide-induced increase in membrane fusion rates and the effect of the peptide on lipid polymorphism. The first aspect is the formation of a stalk or interlamellar attachment (ILA) intermediate which has overall negative curvature (Siegel, 1993). Thus the formation of this first intermediate would be accelerated by agents or conditions which favour the formation of inverted phases. The monolayers involved in the formation of this stalk intermediate are the *trans* or contacting monolayers (Chernomordik, 1996). The X-ray diffraction data shown here demonstrate that the putative fusion peptide of FeLV causes d_H to decrease (Figure 4.6), indicating that the peptide does indeed promote negative monolayer curvature.

Another mechanism by which peptides can promote the rate of fusion is by favouring the partitioning of the TMC intermediate toward the fusion pore/cubic phase pathway (Siegel and Epand, 1997). This mechanism has been suggested for the Influenza fusion peptide (Colotto and Epand, 1997). The relationship between conditions leading to cubic phase formation and to increased rates of membrane fusion has also been noted for fusion induced by DAG (Basáñez *et al*, 1996; Basáñez *et al*, 1997). The possibility of such a phenomenon occurring with the FeLV peptide is suggested by the fact that low concentrations of peptide promote the formation of isotropic resonances in ^{31}P NMR of MeDOPE and DiPoPE (see Chapter 3, Figures 3.8 and 3.9). Although no cubic phases were observed for DiPoPE by X-ray diffraction, this lipid forms cubic phases less readily. As a pure lipid, the cubic phase has never been observed with DiPoPE and, in the presence of the Influenza peptide, the cubic phase is only found with DiPoPE mixed with other phases and with a low degree of order, presenting limited evidence for the formation of a cubic phase. Moreover, disordering of the L_α phase in the presence of the FeLV peptide was seen, which, as noted, may be consistent with the start of a transition to an inverted cubic phase (Gruner *et al*, 1988). Thus this mechanism certainly cannot be ruled out for the FeLV fusion peptide, and a further TRXRD study of the effects of the FeLV peptide

on phase transitions of lipids using a lipid such as MeDOPE, which forms cubic phases much more readily than DiPoPE, would be extremely beneficial.

The experiments that have been described in this chapter and the two chapters preceeding this one have used pure lipid species. Biological membranes are much more complex than this, consisting of a heterogeneous mixture of lipid types. It is, however, quite possible that the interaction of peptides occurs with (a) particular lipid species rather than with the membrane as a whole (see Chapter 7). Moreover, in lipid mixtures where the possibility of lateral phase separation occurs, there might exist a difference between the global and local monolayer curvature (Polozov *et al*, 1997). As mentioned in Chapter 1, a large body of evidence indicates that biological membranes are indeed laterally structured. Thus studies of the effects of a fusion peptide on lipid phase parameters using single lipid species, which show a higher degree of intrinsic negative curvature than that of a whole biological membrane, have relevance to the effects that this peptide may produce *in vivo*.

Chapter 5: Investigation of the effects of the FeLV Fusion Peptide on the Molecular Organisation of Lipid Bilayers using Neutron Diffraction

Neutron Diffraction

5.1 General Introduction

The existence of the neutron was first predicted by Ernest Rutherford in 1920, and it was first identified by Sir James Chadwick in 1932. In 1939, following some work by Fermi in Italy and Hahn and Strassman in Germany, it was found that the bombardment of uranium by neutrons could split the uranium nucleus into two large nuclei, for example barium and krypton, and that fission neutrons were emitted during this process. This discovery formed the basis for the production of chain reactions using uranium 235 in nuclear reactors, and hence a source of high energy neutrons.

It is only relatively recently, since the early 1970's, that neutron beams have been used to study biological membranes and their constituent molecules. The theoretical background and practical applications of neutron diffraction are very similar to those of X-ray diffraction. Similarly, the main aim of this technique also is to identify the conformations of the molecules that are being studied.

5.2 Theoretical Background to Neutron Diffraction

The basic theory of diffraction has been discussed, in part, in Chapter 4. As mentioned previously, neutrons can be considered to possess wave properties, and thus the diffraction of a beam of neutrons obeys the same laws as those seen for X-ray diffraction. However, neutrons being uncharged are not scattered by electron clouds, but by the atomic nuclei present within a sample. One advantage of neutron diffraction, therefore, is that it is sensitive to the isotopes that exist in a sample, in particular to the presence of deuterium. Substitution of deuterium for hydrogen in a sample will thus alter the neutron scattering properties of that sample. This can be used to locate individual atoms and to determine the phases of the diffracted amplitudes (Hvoslef, 1958) (see below).

In the work reported in Chapter 4 a large amount of information was obtained about the structure of the lipid phases that were present in samples, by the relatively simple measurement of the positions of the observed diffraction peaks. The

measurement of the existing lattice symmetry does not, however, describe the structure fully, since many molecular arrangements are possible within a given unit cell. Quantitative analysis of the relative intensities of the orders of diffraction produced by a sample reveals much more detailed information about the structure of the lipid bilayer. This is because the diffracted intensities describe the distribution of the scattering matter within the lipid bilayer (Franks and Lieb, 1981); in other words, the intensity of the radiation that is diffracted through a given angle depends both upon the angle of diffraction and also upon the substructure of the diffracting object. Thus by measuring the distribution of the intensity of radiation diffracted by a lipid bilayer, the neutron scattering density profile, and hence the structure, of this bilayer can be determined.

The strength of the scattering from an atom that is measured in diffraction is called its coherent scattering amplitude. In X-ray diffraction the X-ray scattering amplitudes of atoms are directly proportional to their electron densities, and thus to their atomic numbers. There is, however, no logical sequence to the coherent neutron scattering amplitudes of biological molecules, as seen by examination of the atomic numbers of atoms. Moreover, there is a phase change of 180° for the diffracted beam relative to the incident beam upon interaction with all biological molecules except for neutrons that are scattered by hydrogen atoms (Bacon, 1975); these do not exhibit a phase change, and thus, by convention, hydrogen is given a negative scattering amplitude.

The scattering amplitude density of a molecule can be described by the sum of the coherent scattering amplitudes of its constituent atoms divided by the volume of the molecule. Figure 5.1 shows the scattering amplitude densities for water and for various regions of a phospholipid molecule, as shown in Franks and Lieb (1981). Hydrogen and deuterium have vastly different neutron coherent scattering amplitude densities: -3.7 and +6.7 Fermi units respectively (Zaccai *et al*, 1975), and so, therefore, have water and 'heavy' water, or ^2H_2O. Thus the introduction of ^2H_2O into the sample will change the scattering density of that region enormously. For an H_2O-hydrated lipid bilayer, the main peaks of neutron diffraction occur at the fatty acid ester region, because there is relatively little hydrogen present, and because carbon

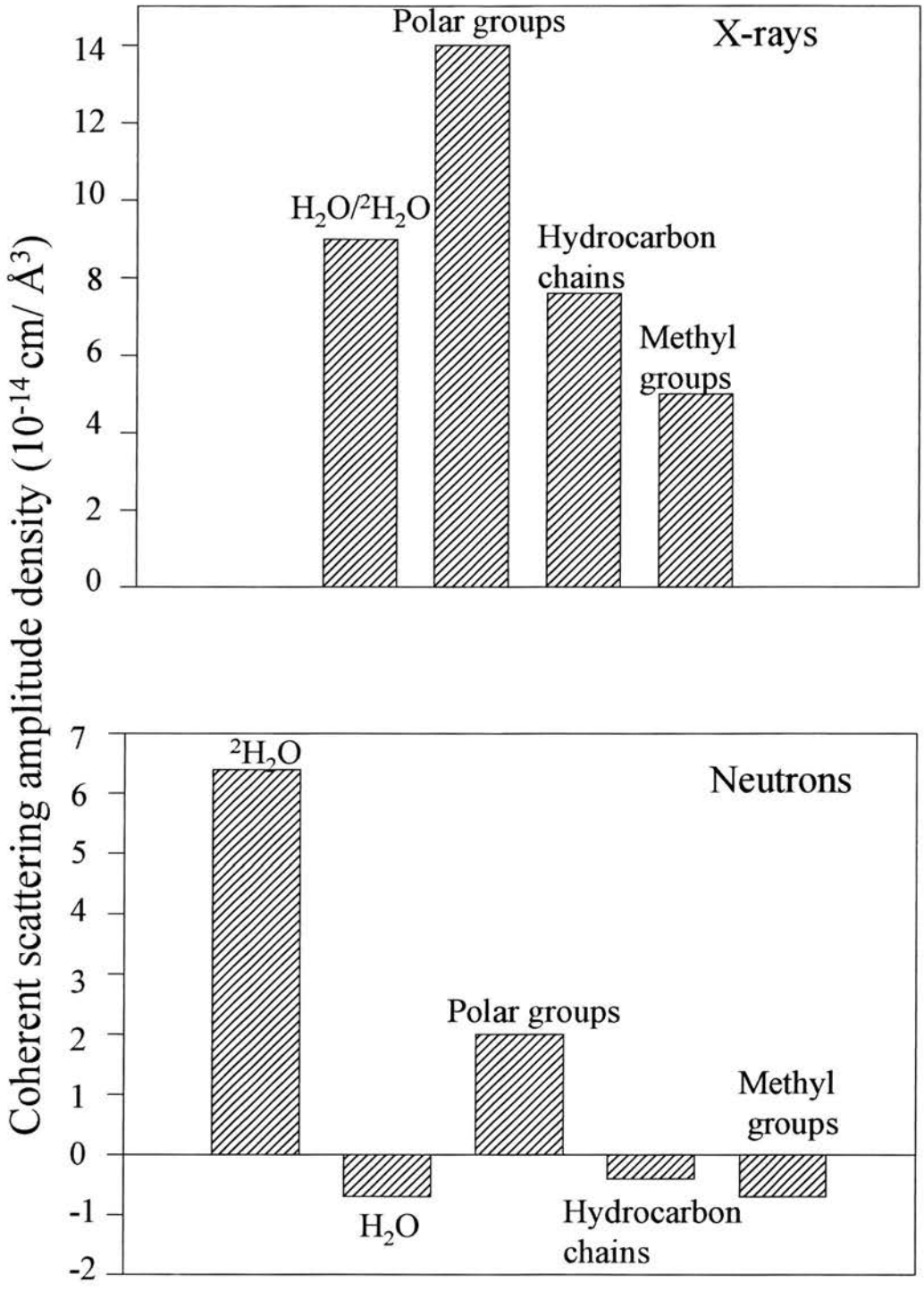

Figure 5.1. X-ray and neutron coherent scattering amplitude densities for water and different regions of a typical phospholipid molecule (Franks and Lieb, 1981). The same absolute scale is used for both graphs.

and oxygen atoms scatter neutrons strongly. The polar phosphates of the lipid headgroup region also have a large neutron scattering amplitude, while the hydrocarbon chains and the terminal methyl groups show poor neutron scattering. The relative X-ray scattering densities for the different regions of a bilayer are somewhat different, and thus these two techniques can be used in a complementary fashion.

The diffraction pattern, which is composed of the observed orders of diffraction, can be thought of as an analogue form of a spatial frequency analysis, or Fourier analysis. Fourier's theorem states that any mathematical function can be considered as the sum of a series of sinusoidal frequency components (Warren, 1987). Thus a mathematical function can be used to describe the intensity of neutrons that are diffracted by a grating, or indeed by stacked lipid bilayers. By adding together all of the component cosine waveforms, which have different amplitudes and spatial frequencies, a wavefront is produced which provides an exact waveform description of the distribution of the diffracted neutrons, and thus the neutron density profile of the lipid bilayer. The spatially varying cosine wave components are a mathematical model; they do not describe real objects. The spatial frequencies will all be multiples of the fundamental frequency, rather like the harmonics of a musical note. Thus the part of the beam which is undiffracted and passes straight through the sample is not measured, but each order of diffraction is measured in turn, with the sample positioned at the appropriate Bragg angle relative to the incident beam. The first order of diffraction is equivalent to the first musical harmonic, the second order to the second harmonic and so on. The fine details of the unit cell are described by the high-frequency cosine wave components, or the higher orders of diffraction.Thus if the high spatial frequency components are unobtainable, an imperfect wavefront will result, which thus gives a 'low-resolution' structure for the lipid bilayer. In practice, the higher orders of diffraction can be very difficult to measure and to phase unambiguously. This is particularly true of neutron, as opposed to X-ray, diffraction studies of hydrated bilayers, as the hydrogen nucleus produces a large amount of incoherent neutron scattering, due to the different spin orientations of the hydrogen nuclei in the sample, which significantly lowers the signal-to-noise ratio.

The distribution of the neutron scattering density in the unit cell, or hydrated bilayer, can thus be calculated in practice from a Fourier series by using the measured amplitudes of the observed diffraction peaks as the Fourier components. The amplitudes are often referred to as the structure factors, which are the amplitudes after they have been correctly 'phased' relative to one another (see below). The structure factors of the diffraction pattern are transformed into wave functions, and these cosine waves are then added together to produce the final neutron scattering profile for the sample. This process is called a Fourier transform, or Fourier synthesis if the sample is non-randomly distributed, and the scattering density distribution thus produced can then be used to determine the structure of the bilayer. By comparing the scattering density profiles of different samples, any changes in the structure of the bilayer that may have occurred on addition of substances, such as fusion peptides, can be determined.

The underlying diffraction from a stack of N bilayers is similar to that for a single bilayer, only it is N times larger and it is subject to the restrictions imposed by the lattice. Thus the neutron density profile of a stack of membranes represents the neutron density profile of a single bilayer that is repeated at regular intervals, and at the Bragg angles of the lattice, the diffracted waves will interfere constructively. The sum of the scattered amplitudes at each Bragg angle of a regular stack of bilayers is proportional to the Fourier transform of the scattered density distribution for a single bilayer. Thus the measurement of the scattered amplitude at these distinct points is equivalent to the sampling of the Fourier transform or synthesis of a single bilayer unit at the particular points in reciprocal space where :

$$R = \frac{n}{d} \qquad 5.1$$

R being the reciprocal space coordinate, n the order of diffraction and d the bilayer repeat distance.

It is vital that the amplitudes of the cosine wave components are correct if the Fourier function is to represent the bilayer structure accurately. In practice, various corrections have to be applied to the observed values of the diffraction amplitudes in

order to allow for errors that arise from the basic experimental proceedure of diffraction and also from the particular conditions of each individual experiment (see Results and Discussion section).

In addition to determining the moduli of the individual cosine wave components, the signs of the different amplitudes must also be determined. This is because the different component cosine waves must be 'phased' with respect to each other; in other words, their positions along the x-axis relative to one another must be calculated. The phasing of diffraction data represents the most difficult part of the entire analytical proceedure. By using oriented multilayers the analysis required to deduce the distribution of the scattering density across a bilayer is reduced, as the bilayers are centrosymmetric and hence only one dimensional analysis is necessary. This is because symmetrical structures produce diffracted beams which are always either in phase or 180° out of phase. Artificial lipid bilayers are usually symmetrical, and even if the membrane itself is asymmetric, for example by the insertion of a fusion peptide, a pair of membranes will form a symmetric unit. Even so, the amplitudes of the different components could have either a positive or a negative value, depending upon where the maxima reside on the component cosine wave of interest.

It is the intensity of the diffracted wave that is recorded by an order of diffraction. Since the intensity equals the square of the amplitude, the information on the sign of the amplitude is unavailable. Moreover, there are no direct methods by which this can be obtained, and so a variety of different techniques are used for the determination of the signs of amplitudes. One method is based on model building. This is only applicable to membranes for which there have been comprehensive structural studies using other techniques, which enable the construction of a model that describes the predicted structure of that membrane accurately. The Fourier transform of this model may then be calculated and used as a reference for the different combinations of the possible phases of the measured amplitudes of the experimental diffraction data. The Fourier transform that agrees most closely with that of the model may then be assumed to be the correct one, providing that the agreement is acceptably high.

As mentioned earlier, the neutron scattering amplitudes of hydrogen and deuterium are very different. This is utilised in the isomorphous replacement of hydrogen by deuterium, another method used for the phasing of diffraction data. Isomorphous replacement infers that the exchange of one atom for another does not alter the structure of the component under study. This allows the subtraction of the phased amplitudes of the same sample in the presence of precise and different relative percentages of H_2O and ^2H_2O to produce the difference scattering profile for the ^2H_2O region between the bilayers. Franks and Lieb (1981) demonstrated that the scattering density of the region between the lipid bilayers progressively increases with increasing ^2H_2O concentration. Weiner and co-workers (1991) showed that this ^2H_2O distribution can be represented with good accuracy by a pair of Gaussian curves. Thus the location and distribution of the heavy atoms are known, and the phases of the structure factors that produce the correct Fourier transform of these Gaussians can then be used to phase the original experimental data. Other methods, such as the use of a swelling series, can also be used to phase neutron data; these are not described as they were not used in the current study.

Once the signs and values for the amplitudes have been obtained, computer based programmes are usually used to calculate, using a Fourier synthesis, the component frequencies of the bilayer structure present in the sample, and thus the structure of the bilayer unit that is present in that sample.

5.3 Application of Neutron Diffraction to Fusion studies: Aims of these Neutron Diffraction Experiments

The results reported in the previous three chapters demonstrate that the fusion peptide of FeLV appears to increase the negative curvature of the lipid monolayers present in certain lipid-water systems. Neutron diffraction studies were, therefore, performed on stacked, hydrated phospholipid bilayers in order to determine the effects of the FeLV fusion peptide on membrane structure. Of particular interest was the determination of any changes in the molecular organisation of the lipid bilayers, and also in the distribution of the water molecules present in the samples, particularly those closely associated with the bilayers.

5.4 Materials and Methods

5.4a Sample Preparation

Lipid bilayers were composed of pure DOPC, or DOPC with 50% (mol) DOPG. Both lipids were purchased from Avanti Polar Lipids (Alabaster, AL, USA). The deuterium oxide (^2H_2O) was purchased from Sigma Chemical Company Ltd. (Fancy Road, Poole, U.K.). 20mg of total lipid, or lipid plus 1% (mol) peptide, were vortexed thoroughly in chloroform. The peptide-containing samples were then sonicated until the peptide dissolved. Samples were applied to flat quartz microscope slides using an airbrush spraying technique. A minimum of 12 hours was allowed for sample drying time in vacuo, to remove any residual solvent molecules. The same time period was also allowed for rehydration with H_2O, 50% ^2H_2O or 100% ^2H_2O, which were present as an atmosphere of 98% relative humidity, so that the lipid lattices could swell to their limits of hydration under these conditions. This method results in a regularly stacked and virtually fully-hydrated conformation of alternating layers of lipid and water (see Figure 4.3, Chapter 4). Incoherent neutron scattering by the hydrogen atoms present in a sample produces a strong background count, and so it is very important that the samples are well-oriented in order to detect the weaker, higher orders of diffraction. A highly-reproducible technique for sample preparation is also required, in order to permit comparisons to be drawn between individual samples. Three different ^2H_2O concentrations were used for each sample, since this is the minimum number that is required to determine whether or not the structure factors change their signs; in other words, whether the linear plot of neutron scattering amplitude against ^2H_2O concentration passes through zero. When altering the relative amount of ^2H_2O present for a sample, the sample was dried out in a normal atmosphere for about 30 minutes before it was placed in the newly required ^2H_2O concentration. The use of four ^2H_2O concentrations per sample is preferable, but the amount of time required for this proceedure precluded its use in the beam time that was available.

5.4b Neutron Diffraction

Neutron diffraction measurements were performed on the D16 instrument at the Institut Laue et Langevin (ILL) (Grenoble, France). Neutrons are produced in a nuclear reactor by fission of uranium 235. The fission energy appears mostly as kinetic energy of the fission products, including the fission neutrons. These neutrons can start a chain reaction by causing the splitting of further uranium 235 nuclei. This is controlled by the moderator, which comprises rods of boron steel that absorb neutrons. The neutrons so produced have a continuous spectrum of wavelengths, which are usually mainly less than 0.1nm. A longer wavelength is required for diffraction studies; this is achieved by causing collisions between the neutrons, and thus the partial loss of energy, until the neutrons attain thermal equilibrium with their surroundings. By employing diffraction from a crystal, the 'cold' neutron beam is then collimated and monochromatised: neutrons diffracted from a single angle will have the same wavelength. As mentioned above, neutron beams are much weaker than X-ray beams, and so both the neutron beam and specimens must have a much larger cross-sectional area than those used in X-ray studies.

A schematic diagram of the experimental set up for D16 is shown in Figure 5.2. A graphite monochromator is used to deflect the incident beam out of the guide. A cooled berylium filter enables wavelengths of greater than 4Å to be obtained. The neutron wavelength that was used in these experiments was 4.516Å. Variable slits allow adjustment of the width of the incident neutron beam. The neutron diffractometer holds the sample and detector. Diffraction will only be observed when a sample is located at the Bragg angles around an axis that is perpendicular to the incoming beam of radiation (see Figure 4.3, Chapter 4). For an unoriented dispersion of membranes, such as that used in Chapter 4, this condition will be fulfilled, because all angles of bilayer orientation are equally probable. If, however, the sample is composed of oriented multilayers, for example stacked, hydrated bilayers on a flat glass support, then the sample must be rotated through the Bragg angles in order to collect the different orders of diffraction. The neutron diffractometer is used to achieve this; it rotates both the specimen and the detector about a common axis. If the

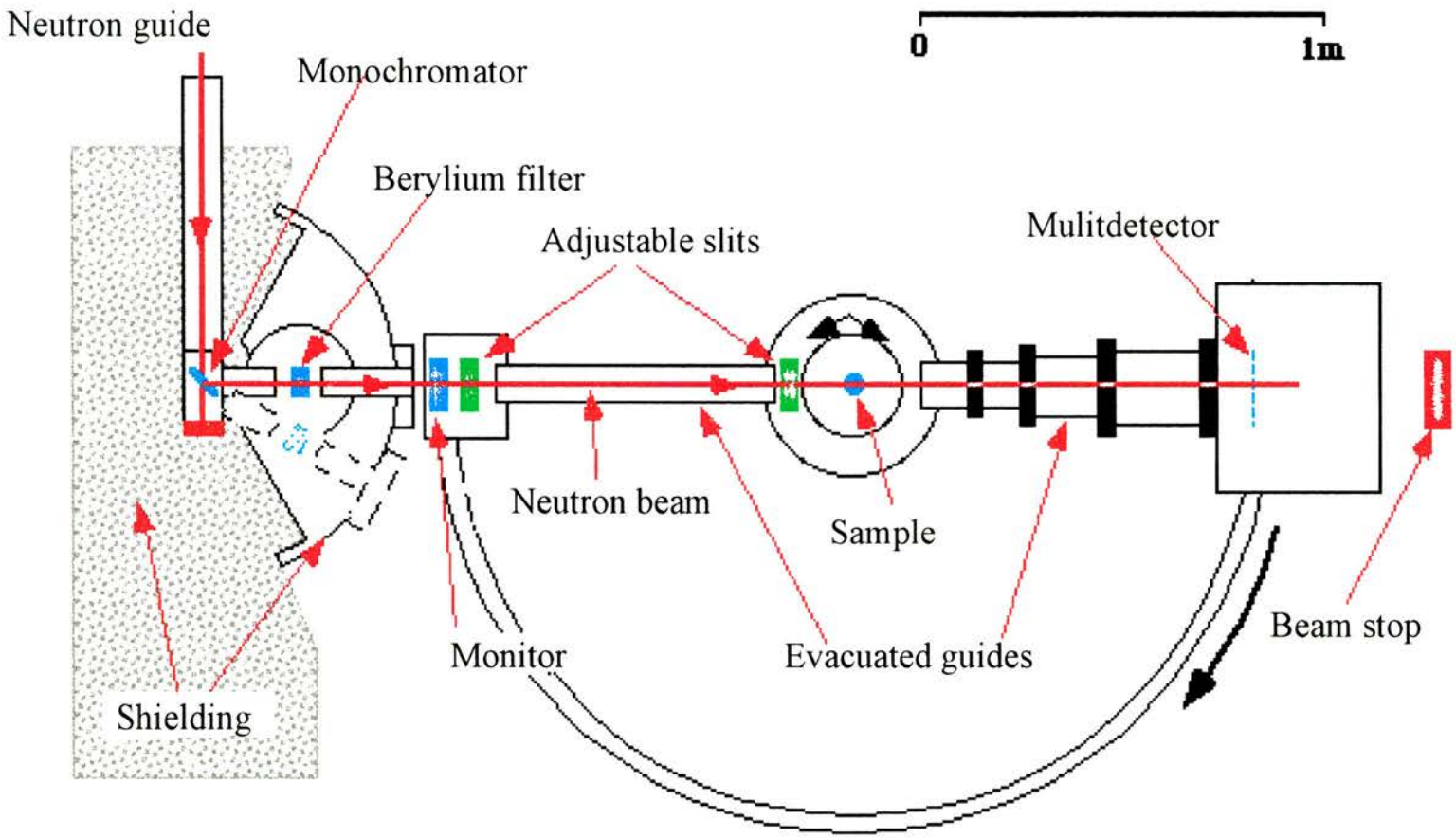

Figure 5.2. Diagram of the experimental set up of the neutron diffractometer D16 at the ILL. See text for details.

specimen is rotated through an angle of θ radians, then the detector must be rotated through 2θ radians, since the scattering angle is twice that of the incident angle (see Figure 4.3, Chapter 4). This is called a θ:2θ scan, and has the advantage that the scattering angle is determined directly. Thus when the sample is at angle θ, the first order of diffraction is collected, at 2θ the second diffraction order and so on. It can be seen that the diffraction orders are thus collected sequentially, and not simultaneously. A low efficiency detector (the monitor) monitored the incident neutron beam. The duration of each scan was set at a certain number of counts of this monitor, rather than a fixed time interval; this eliminates potential errors due to changes in the beam flux during the experimental proceedure. The acquisition time for the higher, weaker orders was increased compared to that for the lower orders in order to obtain diffracted intensies that were of sufficient strength to permit subsequent analysis.

All samples were run at 25°C. Each sample slide was mounted on a goniometer, and thus held vertically inside an aluminium sample can. Water from a thermostatically-controlled water bath was used to control the temperature of the sample environment, by circulating in the wall of the can. Two water baths containing either H_2O or the required percentage of ^2H_2O were placed in the bottom of the can. The sample was then left for 12 hours before measurements commenced, so that it had time to re-equilibrate fully after exposure to the atmosphere during transfer. The size of the interior of each sample can was quite considerable; one potential error lies in the lack of production of a fully humidified, homogeneous atmosphere within the can itself. Even with two water baths present, the dead space in the cans was large. This might cause the sample to shift during the course of each experiment. For each sample, the diffraction experiment comprised a series of repeat θ:2θ scans in which the detector scanned the sample through a narrow range of angles centered on the appropriate Bragg angle. The individual scans from each series were then added together to give a final total for each order of diffraction. Virtually no change in the positions or intensities of the individual diffraction orders was observed during the course of the scan series. Thus it appears that the 12 hour period was sufficient to allow full equilibration within the sample can, and also between the sample and the atmosphere within the can.

Neutrons do not cause ionising damage to specimens, which allows samples to be exposed to neutron beams for long time periods of up to several days. This is essential, as the flux of neutron beams is low: several orders of magnitude less than the photon fluxes that are produced by common X-ray sources. The average exposure time used for a sample was 8 hours at each ^2H_2O concentration. Further, since neutrons are non-ionising, their detection requires reaction with certain nuclei, which convert them into ionising radiation; a gas-filled (^3He) area detector was used for this purpose. A beam stop was used to block the direct beam. The sample-to-detector distance was measured, which was 1 metre. This was used to calibrate the detector, according to the relationship:

$$\theta s = \tan^{-1}\left(\frac{y}{Y}\right) \qquad 5.2$$

where θs is the scattering angle, y is the distance of the diffraction order from the centre of the diffraction pattern, and Y is the specimen-to-detector distance. Figure 5.3 illustrates this relationship diagramtically. Thus if the specimen-to-detector distance and the scattering angle are known, then the absolute positions of the diffraction peaks on the detector, and hence on the observed diffraction pattern can be calculated.

Six orders of diffraction were recorded that were of sufficient strength to permit their analysis. The raw data were initially analysed using the D16 software. This software joined together the individual frames of data for the individual orders such that the six Bragg peaks for each scan were contained in one continuous plot. Corrections to allow for any variation in the response of the different regions of the detector were also applied at this stage. The detector response was calibrated using the scattering of H_2O in a 1mm thick quartz cell, which is constant throughout the range of angles that were measured in this experiment. The diffracted intensities were also corrected for background radiation at this point.

Sigmaplot, version 2.01, was used to fit Gaussian distributions to the diffraction peaks. Each Gaussian curve was allocated a position, width and amplitude. A computer programme, lattice fit, was then used to calculate the *d*-repeat of each

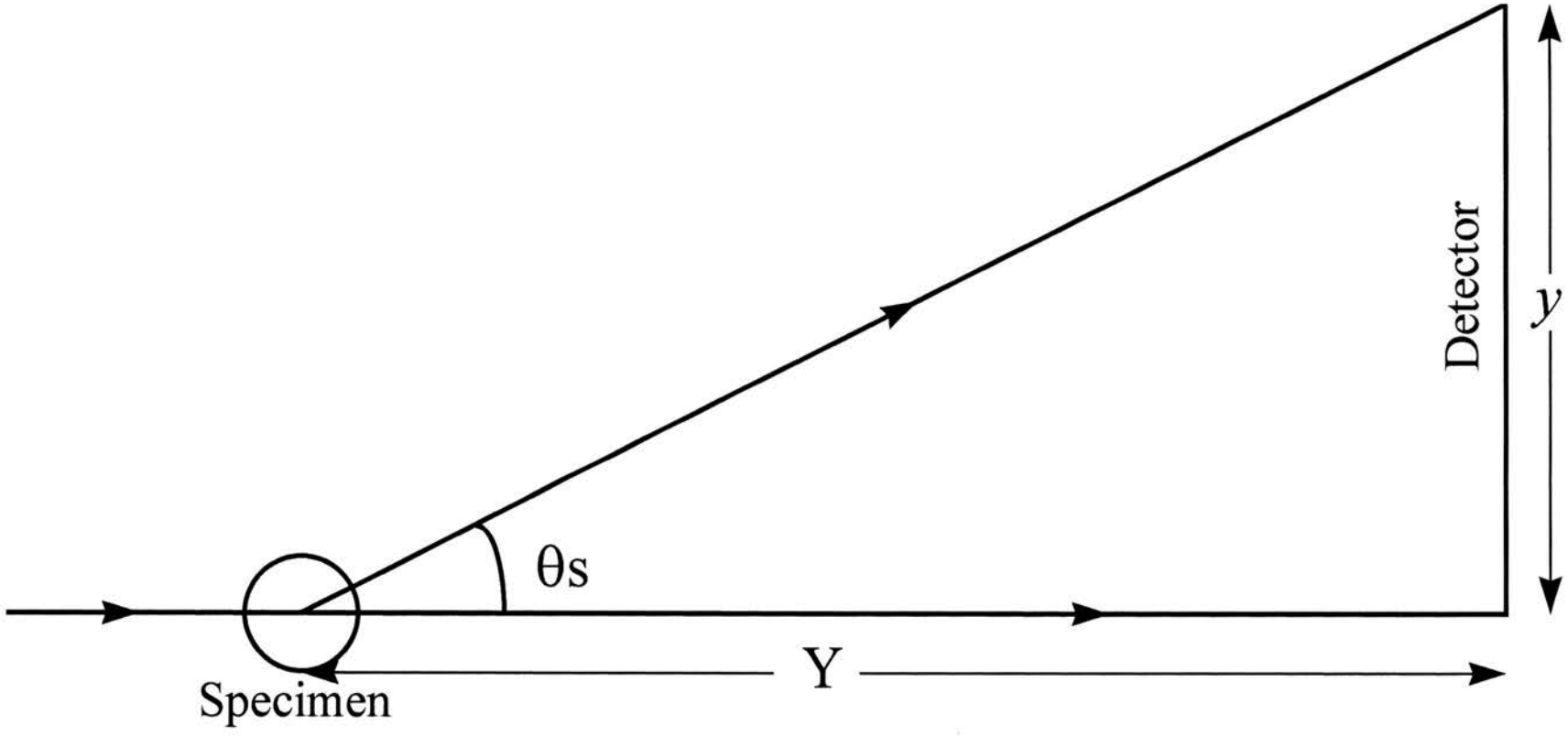

Figure 5.3. Diagram showing the relationship between the scattering angle of a diffraction order, θs, the specimen-to-detector distance, Y, and the distance, *y*, of a diffraction order from the centre of the diffraction pattern.

scan. These values for all of the scans of the same sample were within 1Å; these were then averaged to give the final *d*-repeat value for each sample. The calculated *d*-repeats were 55.25Å ± 0.58Å for DOPC/DOPG and 55.60Å ± 0.51Å for DOPC/DOPG plus FeLV peptide.

The intensity of each order of diffraction was given by the area under the fitted Gaussian peak. Various further corrections were then applied to the values for these intensities, using a programme called datstore, which uses both the calculated *d*-repeat value and the individual intensities for each scan.

Absorption in the specimen, which leads to the removal of neutrons from the diffracted beams, must be considered. This is largely due to the substantial incoherent scattering of the hydrogen atoms in the sample. The amount of absorption depends upon the path lengths of the incident and the diffracted beams within the sample. If a radiation beam enters a sample tangentially, the radiation that gives rise to the lowest angle of diffraction will be more heavily absorbed than the higher orders. This is because the path length of the beam in a sample that is,for example, at an angle θ to the incident beam is longer than that for a beam with the same sample located at angle 2θ. Moreover, the amount of radiation that is absorbed by a sample is also affected by the relative percentages of H_2O and ^2H_2O that are present in the sample, and this must also be allowed for.

The Lorentz factor correction was applied to the data. Ewald (1921) produced the Ewald construction, which allows the geometry of diffraction to be predicted, and the Lorentz factor to be determined. This factor corrects for the spreading out of each diffracted intensity in reciprocal space, and the fact that the detector only samples a certain amount of reciprocal space and hence it does not record all of the diffracted intensities. In particular, the higher order intensities tend to be less thoroughly sampled.

The mosaic spread of each sample was also measured, by performing a rocking curve; here the sample is rotated around the position of a Bragg peak and the detector is fixed at the position required to detect the Bragg reflection. The mosaic spread is a measure of the amount of disorder within the sample, or the angular distribution of the planes of the bilayers with respect to the glass slide. If the bilayer

stacking is irregular, it will result in the intensity of the diffraction describing an arc, which has the same degree of angular extent as the mosaic spread of the sample, instead of a spot that is centred on the detector (Worcester, 1976). If this arc of diffraction is greater than the size of the detector, part of the diffracted intensity will be lost, and this loss must be reversed. The mosaic spread was then calculated for each sample by measuring the full width at half-height of the Gaussian curve that describes the distribution of the diffracted intensity around the third Bragg angle.

The samples used in this study had low mosaic spreads: 0.65° for DOPC/DOPG and 0.6° for DOPC/DOPG plus FeLV fusion peptide. No correction was thus required for the potential lack of recording by the detector of part of the widths of the diffraction peaks, as the mosaic spreads of the samples were less than a few degrees (Worcester, 1976). Unsaturated phospholipids characteristically show low values for mosaic spreads, and the values obtained here correlate well with preceding measurements on comparable systems (e.g. Duff *et al*, 1993; Bradshaw *et al*, 1994). It can be seen that the presence of the FeLV fusion peptide had little effect upon the mosaic spread of the lipid bilayers.

Extinction of the first order of diffraction for samples that contain 100% ^2H_2O can be a problem. It results in a false reduction of the size of the first order of diffraction relative to the weaker orders. In practice it is hard to correct for extinction; the use of lower ^2H_2O concentrations can reduce this effect. Extinction did not produce any obvious errors in this data, as the straight line plot for the first order amplitudes against ^2H_2O concentration did not show any underestimation of the value for the structure factor for this ^2H_2O concentration (see below).

The result of this stage of the datstore programme was thus the production of a corrected value for each intensity of diffraction. These were then converted into amplitude values, which are the square root values of each observed diffraction intensity.

The data sets that were obtained for an individual sample at the three different ^2H_2O concentrations were then scaled to each other by a programme called New_3D_2O. This programme scales the different amplitudes of each order of diffraction at the different ^2H_2O concentrations to each other using a least squares

fitting to determine the appropriate scale factors. Thus, for example, the amplitudes of the first orders of diffraction at the three ^2H_2O concentrations are scaled to each other to give the best fit. These should fit to a straight line. This is because, when considering a unit cell that is centro-symmetric with scattering densities at each point that are either constant or else change linearly with the isotopic composition of the water vapour, it also holds that the structure factors change linearly (e.g. Perutz, 1954; Worcester and Franks, 1976), since the difference in the structure factors at the different ^2H_2O concentrations should represent the ^2H_2O distribution. It follows that simultaneous scaling of several of the observed orders of diffraction for the different ^2H_2O concentrations should be possible, as they should all be affected identically by any differences in the samples at the different ^2H_2O concentrations. The use of the straight line relationship for scaling only really holds for the first four orders of diffraction, as the water distribution is a relatively broad function and it contains little information about the high resolution orders. Figures 5.4 and 5.5 show the graphs produced by the straight line fitting proceedure for the DOPC/DOPG data alone and in the presence of 1mol% FeLV fusion peptide.

Information on the phasing of the data may also be obtained by this technique, which is routinely used for this purpose (e.g. Worcester and Franks, 1976; Büldt *et al*, 1979; Franks and Lieb, 1979; Jacobs and White, 1989). Any change in sign which is required to produce a straight line fit for the values of the amplitudes of an order of diffraction can be determined. Thus, if, for example, the numerical values for the amplitudes of the first order at 0, 50 and 100% ^2H_2O are 15, 15, 45, then, assuming that the first order becomes more negative, the values at 50 and 100% ^2H_2O must be negative in order to produce a straight line fit for these three points. Moreover, by choosing the centre of the bilayer as the origin of the unit cell, the distribution of the water present resembles a Gaussian distribution with its maximum at the centres of symmetry, $x = \pm d/2$ (Worcester and Franks, 1976). The phasing of the orders is then fairly straightforward (Franks *et al*, 1978), as the general rule applies that states that the phasing of a Gaussian curve, which describes the ^2H_2O distribution, causes the amplitudes of the even-numbered orders of diffraction to increase algebraically with increasing ^2H_2O concentration, while those of the odd-numbered orders decrease

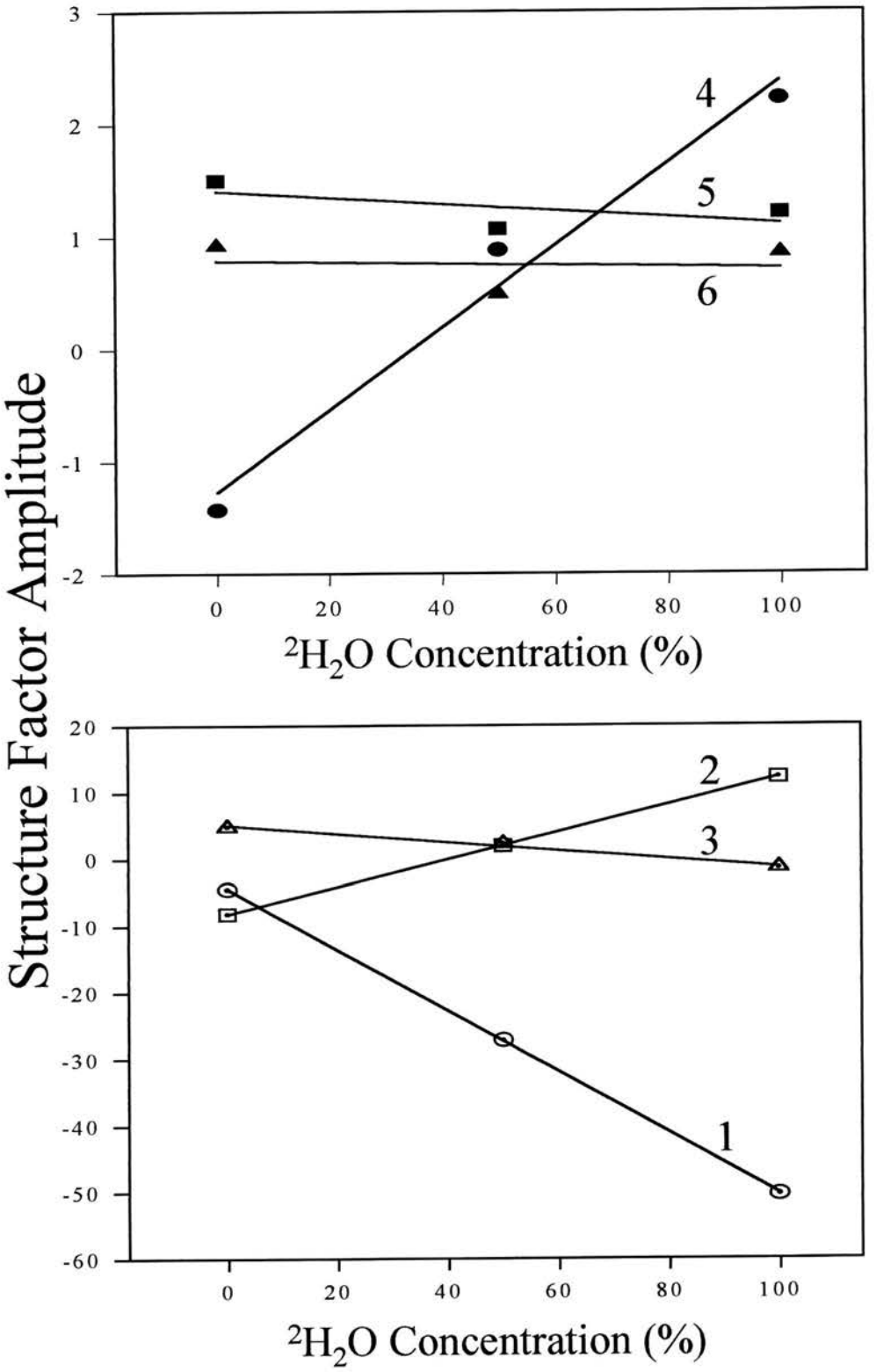

Figure 5.4. The ^2H_2O phasing method, as shown for the pure DOPC/DOPG lipid data. The order numbers are noted. The structure factor amplitudes change linearly with the percentage of ^2H_2O present. The symbols represent the experimentally-determined structure factors for each diffraction order.

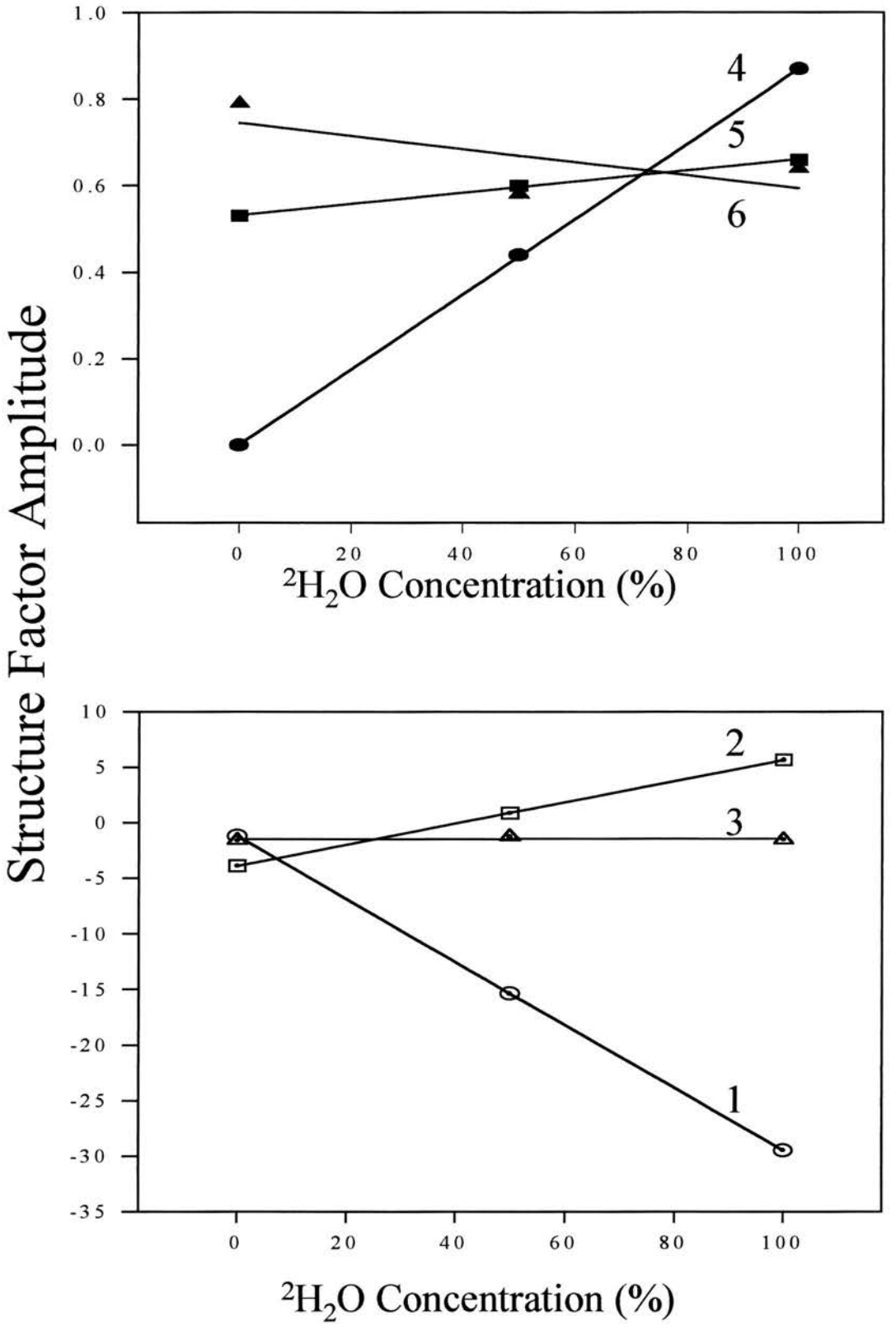

Figure 5.5. The ^2H_2O phasing method, as shown for the DOPC/DOPG plus 1mol% FeLV fusion peptide. Details as described for Figure 5.4.

algebraically. This also is only accurate for the determination of the first four orders of diffraction.

Once the appropriate scale factors have been determined, the amplitude values that were calculated by the datstore programme were then multiplied by the scale factor for that data set. These were then plotted in Sigmaplot, and a straight line fit was applied to these scaled amplitude values. The plots for pure DOPC/DOPG and DOPC/DOPG plus 1mol% FeLV fusion peptide are shown in Figures 5.4 and 5.5. It can be seen that, whilst the values for the first three orders fall on good straight lines, the fourth, fifth and sixth order points show some deviation from the predicted straight line fit. This is partly due to the difficulties in obtaining very accurate values for weaker orders of diffraction. The amplitude values that were produced by the fitted straight line were then used as the correct individual structure factors for each $^{2}H_2O$ concentration.

Next the data were phased in a complementary manner, using a combination of the modelling technique and the information from $H_2O/^{2}H_2O$ exchange. A computer programme was utilised that created bilayer profiles from the scaled, corrected structure factors, by adding together these known structure factors and thus calculating a Fourier synthesis. Various combinations of signs for the different diffraction orders, in particular the fifth and sixth orders, were tested until a sensible, best fit to a bilayer profile was obtained. The distribution of the heavy water in the samples was thus also calculated by subtracting the Fourier profile for a sample when it was hydrated with H_2O from that for the same sample hydrated with $^{2}H_2O$. If both sets of data are correctly phased, this should describe two Gaussian distributions.

In order to compare bilayer profiles produced by different samples, these must first be scaled relative to each other with respect to amplitude. The sizes of the Gaussian distributions were then used to scale the data sets to each other. This places the data on the 'relative absolute scale' of Weiner *et al* (1991). This scale allows the detailed examination and modelling of diffraction data without precise knowledge of the lipid cross-sectional area. It scales the data absolutely with respect to the contents of the unit cell; in other words, it utilises the known differences in mean scattering density that are induced by the selective replacement of hydrogen by deuterium to

scale the data sets with respect to the unit cell contents. Thus the relative scaling of each pair of data sets was altered until the total area under their difference transform was equal to the difference in their total scattering lengths per unit cell, whilst ensuring that the area under the transform for each individual data set was equal to the total scattering length for its unit cell contents.

Different samples may well have different amounts of water present in their unit cells, which will affect the scaling of the samples to each other. Thus it was necessary to determine the water content of the samples. This was achieved by the use of ^{14}C-DOPC and ^{3}H-water (both isotopes from Amersham International, Amersham, U.K.) as constituents in the individual samples, which were made up exactly as before, under identical experimental conditions, except for the isomorphous replacements that were present. Thus ^{14}C-labelled lipid was spread evenly over the 5mm surface of a halved coverslip and the solvent was evaporated to produce a dry lipid film. The samples were placed under vacuum overnight, in order to remove any residual solvent molecules, and they were then placed in a chamber, which was at approximately 98% relative humidity and which contained tritiated water. The samples were left in this atmosphere, at 25°C, which was the temperature used for the experiments, for at least 12 hours. Each sample was then very rapidly transferred to a tube containing scintillant fluid, and the amount of radiation, and thus of each isotope, present within each sample was measured using a scintillation counter. For both of the isotopes of interest, three standard samples were run that contained a known amount of that isotope. This enabled any variation in sensitivity between the different 'lanes' in the counter to be determined, and also allowed for any 'cross channel' interference. Blank coverslips were counted too to give as accurate a background reading as possible. Four identical labelled samples were measured for each type of sample used in the diffraction studies, and the values for the four samples were averaged to give a final ratio of the number of water molecules present per lipid molecule. Once this ratio had been determined for each different type of diffraction sample, the size of the water distribution peaks could then be used to scale the different samples to each other.

The scattering density of the FeLV fusion peptide was calculated by adding together the different values for the scattering amplitude densities of this peptide's

component amino acids, using the values quoted in Jacrot (1976). This total was then subtracted from the scattering density profiles for the peptide-containing samples, so that any changes in neutron scattering for these samples were due to changes in the water and/or lipid molecular arrangements present. Finally, the neutron scattering density profiles were calculated for 8.07% ^2H_2O, which is the concentration of ^2H_2O that has zero scattering density. Thus, at this ^2H_2O concentration, the scattering density distribution is due to the phospholipid molecules alone, and hence any changes in their molecular packing on addition of the FeLV fusion peptide can be determined.

5.5 Neutron Diffraction Results and Discussion

Table 5.1 lists the experimentally determined, corrected and scaled structure factors that were used in the Fourier syntheses and subtractions for pure 50% (mol) DOPC/DOPG and for 50% (mol) DOPC/DOPG with 1mol% FeLV fusion peptide present. The errors quoted were calculated using the straight line fits for each diffraction order at the three different measured ^2H_2O concentrations. The difference in amplitude between each individual data point and the corresponding value that lay on the straight line fit were calculated, and these differences for the three ^2H_2O concentrations were averaged to produce a value for each individual order of diffraction. The phasing of the fifth and sixth orders was performed, in the main, by selecting the combination of signs for these two phases, from every possible permutation, that, after performing Fourier syntheses, produced the most plausible neutron scattering density profiles at the three different ^2H_2O concentrations, and also the most plausible ^2H_2O distributions, whilst still fitting the straight line plots. It is very difficult to ensure that these are corrrect in the absence of additional information, such as the introduction of a localised label into the bilayer scattering profile. Happily, these weaker orders of diffraction do not provide a vast amount of information on the bilayer scattering profile. The structure factors for the samples of DOPC/DOPG and of DOPC/DOPG plus FeLV fusion peptide were also calculated in the presence of 8.07% ^2H_2O. These were obtained from the linear relationship between the final, corrected and scaled structure factor amplitudes and ^2H_2O concentration for each

Order of Diffraction	Structure factors for DOPC/DOPG at varying percentages of ^2H_2O:		
	0% ^2H_2O	50% ^2H_2O	100% ^2H_2O
1	-15.61 ± 0.09	-96.29 ± 0.09	-176.98 ± 0.09
2	-29.00 ± 0.02	6.98 ± 0.02	42.96 ± 0.02
3	17.65 ± 0.27	6.56 ± 0.27	-4.53 ± 0.27
4	-4.46 ± 0.22	1.96 ± 0.22	8.38 ± 0.22
5	4.95 ± 0.13	4.44 ± 0.13	3.93 ± 0.13
6	2.78 ± 0.18	2.65 ± 0.18	2.53 ± 0.18

Order of Diffraction	Structure factors for DOPC/DOPG plus 1mol% FeLV fusion peptide at varying percentages of ^2H_2O:		
	0% ^2H_2O	50% ^2H_2O	100%^2H_2O
1	-6.79 ± 0.02	-88.16 ± 0.02	-169.52 ± 0.02
2	-22.25 ± 0.01	5.19 ± 0.01	32.64 ± 0.01
3	-8.44 ± 0.14	-8.24 ± 0.14	-8.04 ± 0.14
4	0.01 ± 0.01	2.51 ± 0.01	5.01 ± 0.01
5	3.06 ± 0.01	3.43 ± 0.01	3.80 ± 0.01
6	-4.25 ± 0.06	-0.41 ± 0.06	3.45 ± 0.06

Table 5.1. Experimentally determined, corrected and scaled structure factors, obtained at 25°C and 98% relative humidity, used in Fourier transforms and subtractions for : 50 mol% DOPC/DOPG (top table) and 50 mol% DOPC/DOPG plus 1mol% FeLV fusion peptide (lower table).

order of diffraction. 8.07% ^2H_2O has a scattering density of zero, and thus examination of a bilayer profile at this ^2H_2O concentration allows the exclusive observation of the scattering density of the other components that are present in the sample, namely the lipid, or lipid plus peptide. Figure 5.6 shows the neutron scattering density profiles at 8.07% ^2H_2O of bilayers of DOPC/DOPG alone and in the presence of 1% (mol) FeLV fusion peptide. The difference profile, calculated by subtracting the scattering density due to lipid alone from the profile for lipid with peptide present, is also shown. Phospholipid molecules are shown above the profile to orientate the relative densities seen. The origin of the profile is thus the centre of the lipid bilayer. The neutron scattering density profile for the pure DOPC/DOPG bilayer contains two outer troughs corresponding to the water regions, and two high peaks that are located about ± 19Å from the centre of the bilayer. These peaks correspond to a region of strong scattering within the bilayer that contains the fatty acid ester groups and the phosphorus molecules of the headgroups. A trough of low scattering density is seen in the centre of the bilayer, due to the terminal methyl groups. These three features are classic of a neutron scattering density profile of a lipid bilayer (e.g. Worcester and Franks, 1976; Büldt *et al*, 1979; King and White, 1986). The introduction of DOPG to a DOPC bilayer has been shown to increase the neutron scattering of the headgroup region (Bradshaw, 1997); this is thought to be due to the presence of counterions that associate with the anionic DOPG.

The difference profile for the bilayer neutron scattering density (dotted line, Figure 5.6) shows that the addition of FeLV peptide to the bilayers causes an increase in scattering density close to the bilayer centre, a reduction at the surface and an increase in the water region. The scale of these perturbations is much too high for them to represent simply the scattering density of the peptide: the amount of peptide present is tiny, only 1% (mol). They must, therefore, be caused by alterations in the phospholipid packing (changes in water distribution have been eliminated from the figure by showing the 8.07% ^2H_2O profiles). The difference profile must, therefore, be an increase in the packing density of the phospholipid fatty acids, and a decrease in the packing density of their headgroups.

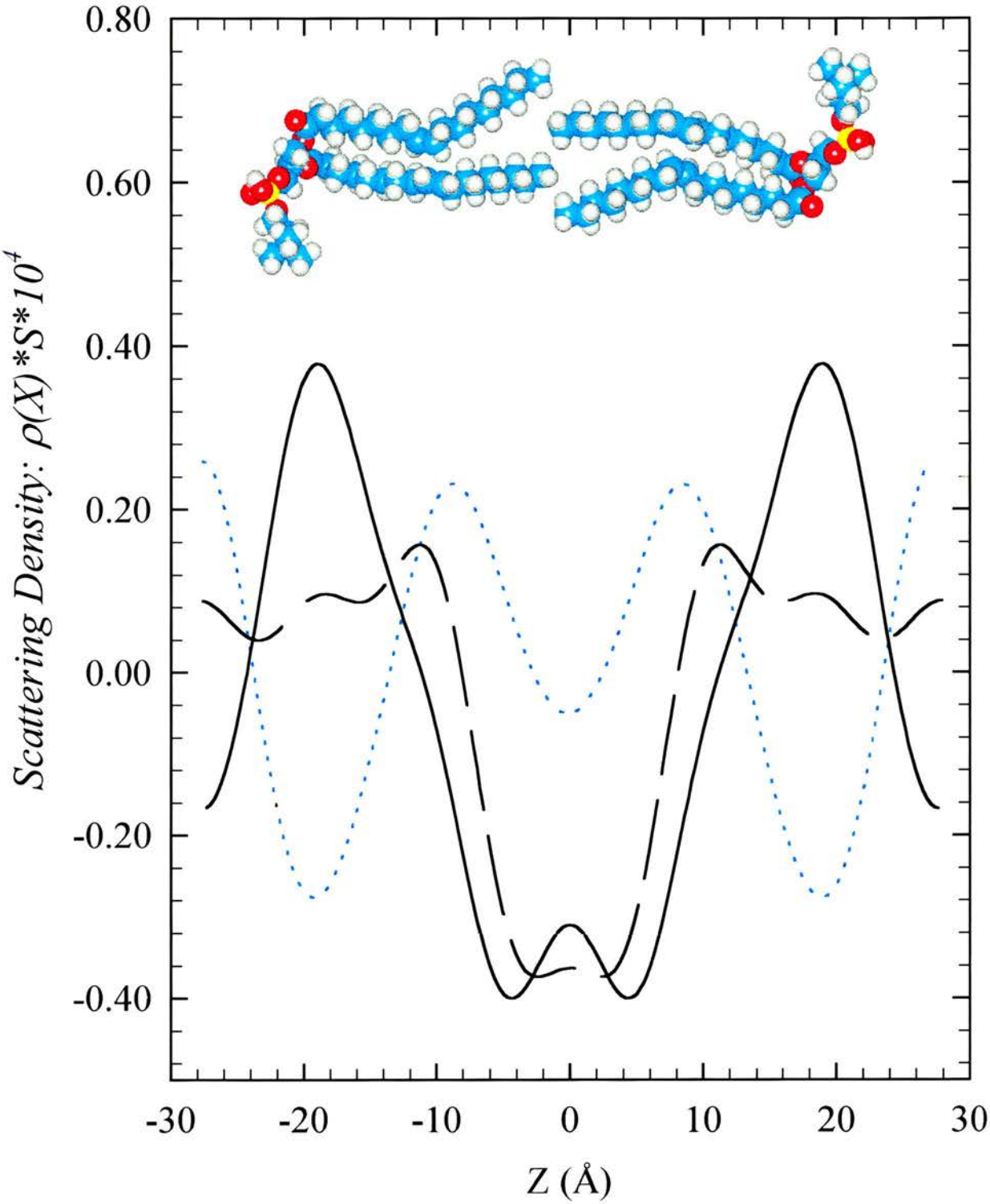

Figure 5.6. Neutron scattering density profiles at 8.0 % ^2H_2O of pure DOPC/DOPG bilayers (solid line) and DOPC/DOPG plus 1% (mol) FeLV fusion peptide (broken line). The difference profile calculated by subtracting structure factors for the lipid alone from those of lipid plus 1 mol% FeLV peptide is also shown (blue, dotted line). Two phospholipid molecules are shown for orientation. The headgroups contain the red oxygen atoms.

This interpretation is totally consistent with the emerging models for the mode of action of a fusion peptide. It has been demonstrated that fusion peptides become embedded in the target cell membrane before fusion occurs (e.g. Stegmann *et al*, 1991). Previous modelling work has suggested that viral fusion peptides insert obliquely into lipid bilayers and thus cause some of the bilayer acyl chains that are in close contact to the peptides to become tilted (Brasseur *et al*, 1988; 1990; 1997). This oblique orientation of viral fusion peptides with respect to the bilayer plane has been correlated with fusogenic activity (e.g. Martin *et al*, 1991, 1993, 1994, 1995; Lüneberg *et al*, 1995; Ishiguro *et al*, 1996). The tilting of the acyl chains could precede a more dramatic change in lipid ordering, producing new lipid phases that are thought to be associated with the initial events of membrane fusion. Martin and co-workers (1993) have also related the oblique insertion of a viral fusion peptide to the promotion of the formation of inverted lipid phases. Furthermore, it has been suggested that a possible mechanism by which obliquely inserted peptides may perturb bilayer structures is by expanding the centre of the bilayer more than the bilayer surface (Colotto *et al*, 1996). A suggested mode of action for this is precession by the fusion peptide, that is the tracing out of an inverted cone-shape by its motion (Epand *et al*, 1992). Figure 5.7 shows a model of this concept. This would greatly increase the negative curvature of the target membrane's outer lipid monolayer. The increase in negative curvature could cause the outer monolayer to bend towards the apposing bilayer, and hence it would allow the closer approach of the two fusing membranes at the stage when they are still initially distinct and also an increased area of contact between the two membranes (Colotto *et al*, 1996). Further, it would facilitate the formation of transient, highly bent lipid intermediates in the fusion pathway, such as are described in the 'stalk hypothesis'. The concentration of FeLV fusion peptide that was used in these neutron studies (1 mol%) has been shown to promote the formation of non-bilayer lipid phases significantly and to increase the negative curvature of lipid monolayers (see Chapter 3). Since the lipid molecules in these neutron diffraction samples were confined to a planar bilayer configuration, any changes in elastic monolayer curvature forces would be expressed as effects on molecular packing. Thus an increase in scattering density close to the bilayer centre and a

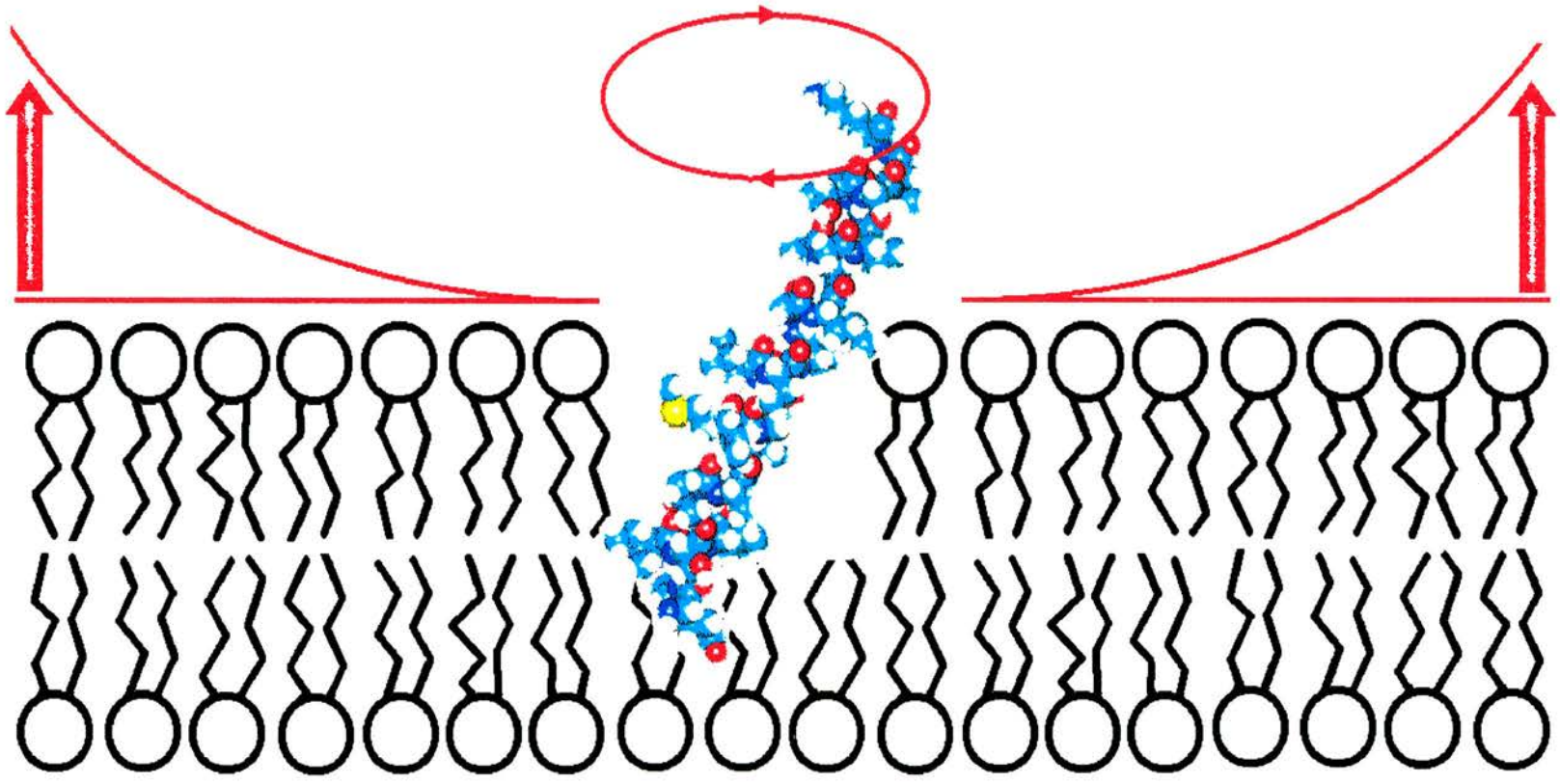

Figure 5.7. Model of precession of the FeLV fusion peptide in a lipid bilayer. Precession is thought to increase the negative curvature of the bilayer (see arrows).

reduction at the bilayer surface were observed. The results described here add support to these hypotheses for the fusion mechanism. It must, however, be remembered that the results produced by conventional diffraction techniques such as this one do not distinguish between static and dynamic disorder: the observed effects of the fusion peptide on lipid packing are the time-averaged effects. For the future, more detailed information on the effects of this fusion peptide on lipid packing and molecular configuration could be obtained by specific deuterium labelling of different regions of the phospholipid molecules. This would map the lipid structure along the normal to the bilayer plane, as the deuterated portion of the lipid would produce an intense peak in the neutron density profile and hence it would be readily located in the membrane (e.g. Zaccai *et al*, 1975; Worcester and Franks, 1976; Büldt *et al*, 1978), with a potential accuracy of greater than ± 1Å (Büldt *et al*, 1978).

Figure 5.8 shows the distributions of 'heavy' water within and between bilayers of pure DOPC/DOPG and DOPC/DOPG plus peptide. These were obtained by subtracting the neutron scattering density profile for each sample in 0% ^2H_2O from the scattering density profile for the same sample in 100% ^2H_2O. The difference profile for the ^2H_2O distribution due to the presence of the FeLV peptide is also shown; this is calculated by subtraction of the 'heavy' water distribution for the pure lipid sample from that for the lipid plus FeLV peptide. For clarity, the origin has been shifted from the centre of the bilayer to the centre of the water distribution between two adjacent bilayers. The ^2H_2O distributions should describe pairs of Gaussian curves, with the maxima close to the centre of the region between adjacent lipid bilayers This is indeed observed for both the pure lipid and the lipid plus peptide samples. It can be seen, from a comparison of the pure lipid profile in Figure 5.6 and the ^2H_2O distribution for the DOPC/DOPG profile in Figure 5.8, that water penetrates some distance between the lipid polar headgroups, but that it is totally excluded from the hydrophobic region of the lipid bilayer. This is consistent with previous findings for pure lipid bilayers (e.g. Zaccai *et al*, 1975; Duff *et al*, 1993; Bradshaw *et al*, 1994).

The profiles in Figure 5.8 also show that the ^2H_2O distribution changes in the presence of the FeLV fusion peptide: there is a slight increase in the width of the

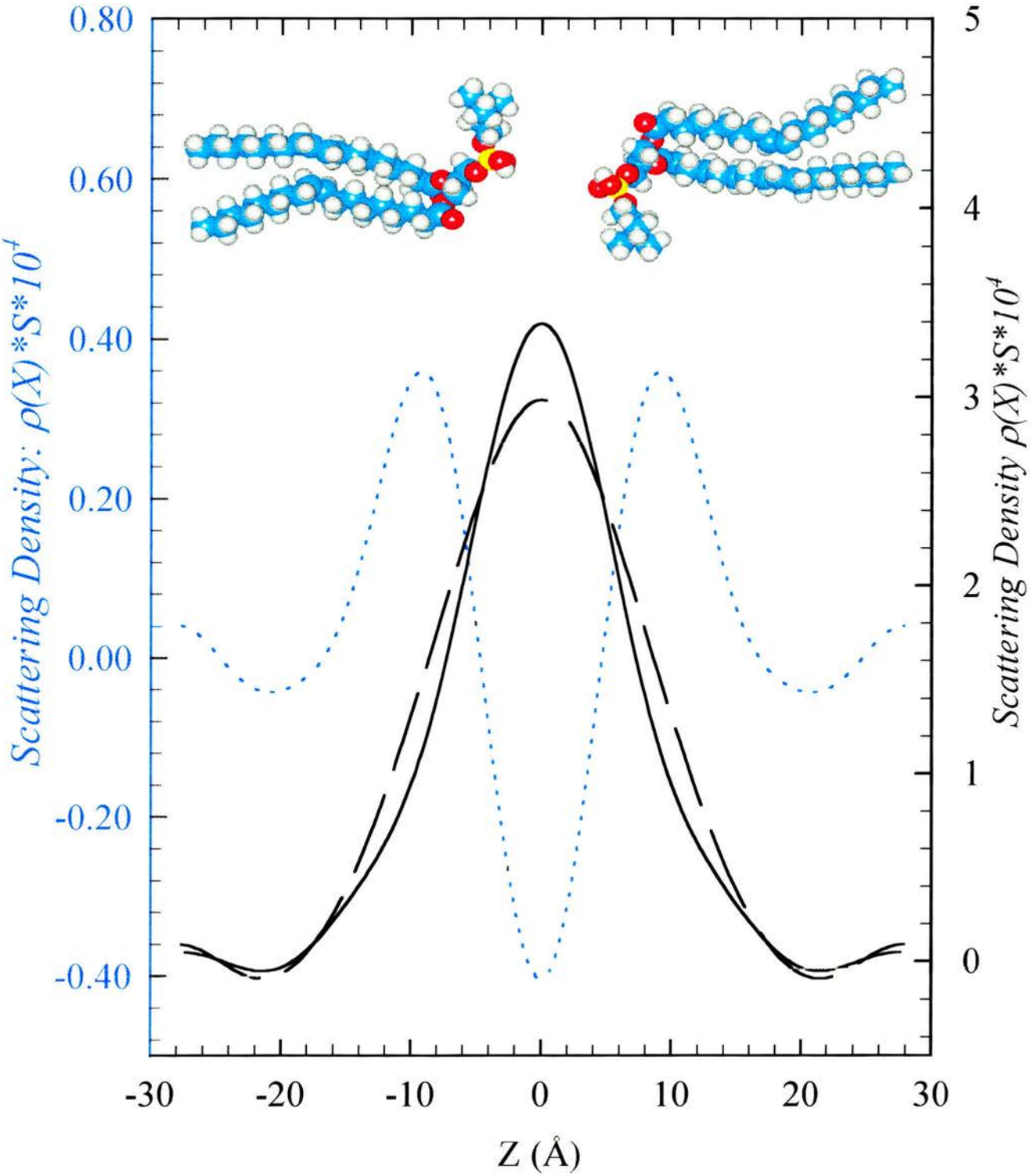

Figure 5.8. $^{2}H_{2}O$ distribution within and between bilayers of DOPC/DOPG (solid line), and DOPC/DOPG with 1 mol% FeLV peptide (broken line). The difference profile due to the presence of the FeLV peptide is also shown (blue, dotted line). Two phospholipid molecules are shown for orientation (the head groups contain the red oxygen atoms).

water distribution. This could be as a result of the occurrence of bilayer thinning, since adsorption of amphiphilic peptides to the headgroup region of a lipid bilayer can cause membrane thinning (Heller *et al*, 1997). Adsorption of the peptides magainin 2 (Ludtke *et al*, 1995, 1996) and alamethicin (Wu *et al*, 1995) were shown to cause lateral expansion of the headgroup region of a bilayer. The degree of bilayer thinning is thought to depend upon the amount of lateral expansion that is caused by the absorption of the peptide. The lipid chains are thought to adjust to this by *trans-gauche* excitations. The lipid chain volume remains constant and thus the hydrocarbon region of the bilayer thins.

Longo and co-workers (1997) have, very recently, developed a micropipette aspiration assay by which they can measure the effects of the addition of peptides to lipid vesicles. Their study, using the fusion peptide from Influenza virus, showed that exposure of lipid vesicles to this fusion peptide resulted in a rapid expansion of the area of the vesicles' lipid membranes. Furthermore, the rate of expansion of the area of the lipid membranes by the Influenza virus fusion peptide was greater as the pH was lowered to that at which Influenza-mediated fusion is optimal. This, therefore, adds support to the concept of fusion peptides producing bilayer thinning.

A local thinning of the bilayer around an adsorbed fusion peptide might lower the tension that is required for rupture of the TMC lipid intermediate in the fusion pathway (Siegel and Epand, 1997). This would result in a more rapid formation of fusion pores. TMCs are thought to be common lipid intermediates in two competing pathways, namely the L_α-H_{II} and L_α-Q_{II} transitions. The stability of the TMC may, therefore, be central to the differential rate of formation of these two lipid phases. The longer that TMCs exist, the more likely they are to aggregate and to form quasihexagonal arrays of H_{II} precursors. On the other hand, if the TMCs are less stable, they are more likely to rupture and form ILAs, or fusion pores. Bilayer thinning by a fusion peptide might decrease the stability of the TMC by reducing the cohesion of the lipid molecules locally.

In-plane neutron scattering work on magainin 2 has also suggested that the lateral expansion of the headgroup region of a bilayer that is produced by this peptide causes a bending of the lipid molecules, and the formation of a pore-like arrangement

(Ludtke *et al*, 1996). This pore is very similar in structure to that of a fusion pore. Thus some of the effects of the FeLV fusion peptide on bilayer packing could also be explained by thinning of the bilayer. There is, however, no evidence for the formation of an aqueous channel or pore in DOPC/DOPG bilayers by the FeLV fusion peptide at the molar concentration of peptide used in these experiments. A channel or pore is represented by a continuous band of water that spans the entire width of the lipid bilayer, as seen, for example, with melittin (Bradshaw *et al*, 1994), Influenza virus M2 peptide (Duff *et al*, 1994) and salmon calcitonin (Bradshaw, 1997).

It is possible that pore formation might be seen at higher concentrations of fusion peptide: work with other membrane-associating peptides, for example the 20 amino acid peptide alamethicin (He *et al*, 1995, 1996), has shown that the type of membrane association adopted by the peptide depends upon the peptide concentration. Thus, at low concentrations this peptide adsorbs to the surface of the membrane, whilst at high concentrations the peptide inserts across the membrane and hence forms pores. The proposed driving force for this transition is the energy cost of membrane thinning (Huang, 1995). Similar findings have occurred for magainin (Ludtke *et al*, 1995), and the authors suggest that the dependency of peptide-bilayer interactions on the energetics of bilayer thinning should hold for a wide variety of peptide/lipid systems. The length of peptide chain that is required to span a typical lamellar bilayer, which has a thickness 30Å, is ~20 amino acids, and so the 28-residue FeLV fusion peptide is certainly of sufficient length to form pores in a bilayer. In view of the possible involvement of this fusion peptide in the formation of biological fusion pores, and the fact that oligomerisation of fusion proteins/peptides is thought to be crucial to the formation of a stable fusion pore, it would be interesting to repeat this study, using a range of lipid:peptide molar ratios, in order to determine if the FeLV fusion peptide does indeed exhibit a biphasic type of membrane interaction. However, the great tendency of this peptide to self-aggregate at high peptide concentrations might well provide serious practical problems for this study. Further, self-aggregation is likely to result in the formation of a population of peptide, which might not associate with the membranes at all. The use of in-plane neutron scattering would also

be very beneficial to determine whether membrane thinning and pore formation are indeed effects of the FeLV fusion peptide.

Results obtained for samples of pure DOPC with and without FeLV peptide showed negligible effect for the fusion peptide on bilayer structure (data not shown). All diffraction data are incomplete, due to the limitations of the instrumentation used. Thus profiles that are calculated by Fourier transformation of this data show termination errors which may show as a Fourier ripple (Duff *et al*, 1994). The DOPC data did indeed show such ripples.

It is interesting to note that the fusion peptide had a significant effect upon lipid packing in the DOPC/DOPG bilayers but not in pure DOPC bilayers. Circular dichroism (CD) studies of the secondary structure of the FeLV fusion peptide showed that it formed a very small amount of α helix in the presence of DOPC/DOPG bilayers, and that its overall CD spectrum was of a more charcteristically β type. No helical structure was seen for this peptide in the presence of pure DOPC bilayers, and the overall CD spectrum was also less classically β in shape qualitatively (see Chapter 6). Whilst this difference is indeed very small, it might be significant in view of the lack of reliability of CD as a method of determination of peptide secondary structure, other than that which is helix.

It would be of great interest to deuterate different amino acid residues of the FeLV fusion peptide specifically and use these deuterated peptides for neutron studies. It would thus be possible to locate the atomic coordinates of the deuterated residues to a fairly high degree of accuracy, and hence to determine the depth of penetration of the peptide into the lipid bilayer. The possible existence of more than one population of peptide molecules within a sample, for example one population that inserts into the lipid bilayer and another that lies along the bilayer surface, could also be resolved.

Chapter 6: Circular Dichroism studies to investigate the Possible Secondary Structures and Structural Plasticity of the Feline Leukaemia Virus Fusion Peptide

Circular Dichroism

6.1 General Introduction

Proteins fold up into a remarkable variety of well-defined, three-dimensional forms. The 'conformation' of a protein molecule is the specific three-dimensional arrangement of atoms in such a structure, and it is this precise conformation which bestows corresponding function. Thus, in the study of proteins, a major aim is to define their structure, and so discover how they work.

For most proteins, all of the information needed to define the conformation of a protein molecule is contained within its amino acid sequence. It is possible, therefore, to study the structure of an isolated, synthetic peptide that corresponds to a peptide fragment within a protein molecule and, to a large extent, extrapolate from these results to the structure of the native peptide fragment.

A peptide chain will fold in such a way as to minimise the free energy of the system. The local spatial arrangement of the amino acid residues within a peptide is known as its 'secondary structure', which involves recognised structural motifs. Stability of secondary structure tends to arise from the simultaneous formation of many intramolecular hydrogen bonds. The properties of the particular amino acid side chains present and of the peptide bond also impose some restrictions upon the folding of a peptide. Due to the sharing of electrons between its constituent carbon, nitrogen and oxygen atoms, the peptide bond has tortional inflexibility. Thus it resists rotation about its axis, and the peptide chain can only fold through rotations of the alpha-carbon bonds (see Figure 6.1).

These factors lead to the potential for the formation of certain periodic secondary structures by peptide chains. These are broadly classed as either α-helical or β structures, the most extensive form of the latter being the β sheet (see Figure 6.2). The term 'random' structure is often used to describe non-regular peptide structure.

As in the case of proteins, the determination of a peptide's secondary structure is necessary in order to understand fully its biological mode of action. The use of Circular Dichroism (CD) allows rapid, quantitative estimates of the relative amounts

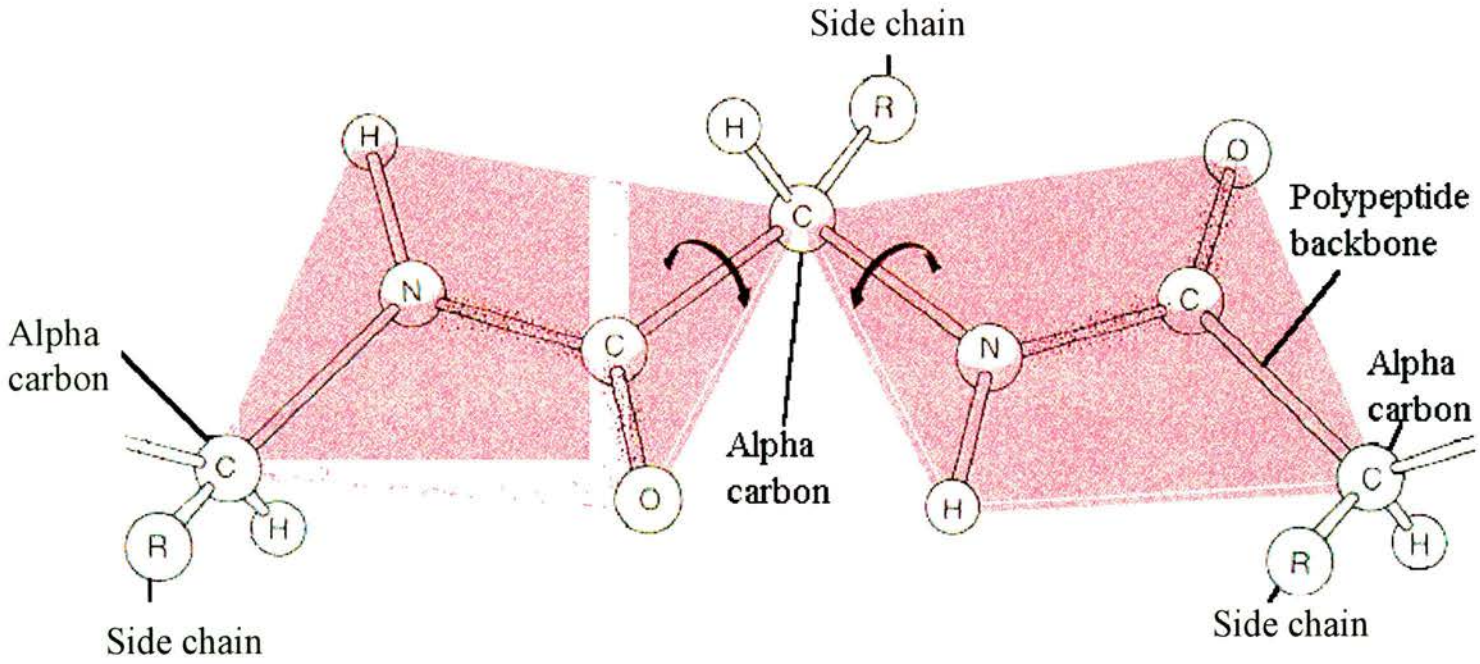

Figure 6.1. The peptide bond. The sharing of electrons between the nitrogen, carbon and oxygen atoms makes the bond resistant to twisting. Thus each amino acid is like a rigid plane, and the peptide can only fold by rotations about the bonds to the alpha carbons. Modified from Doolittle, 1985.

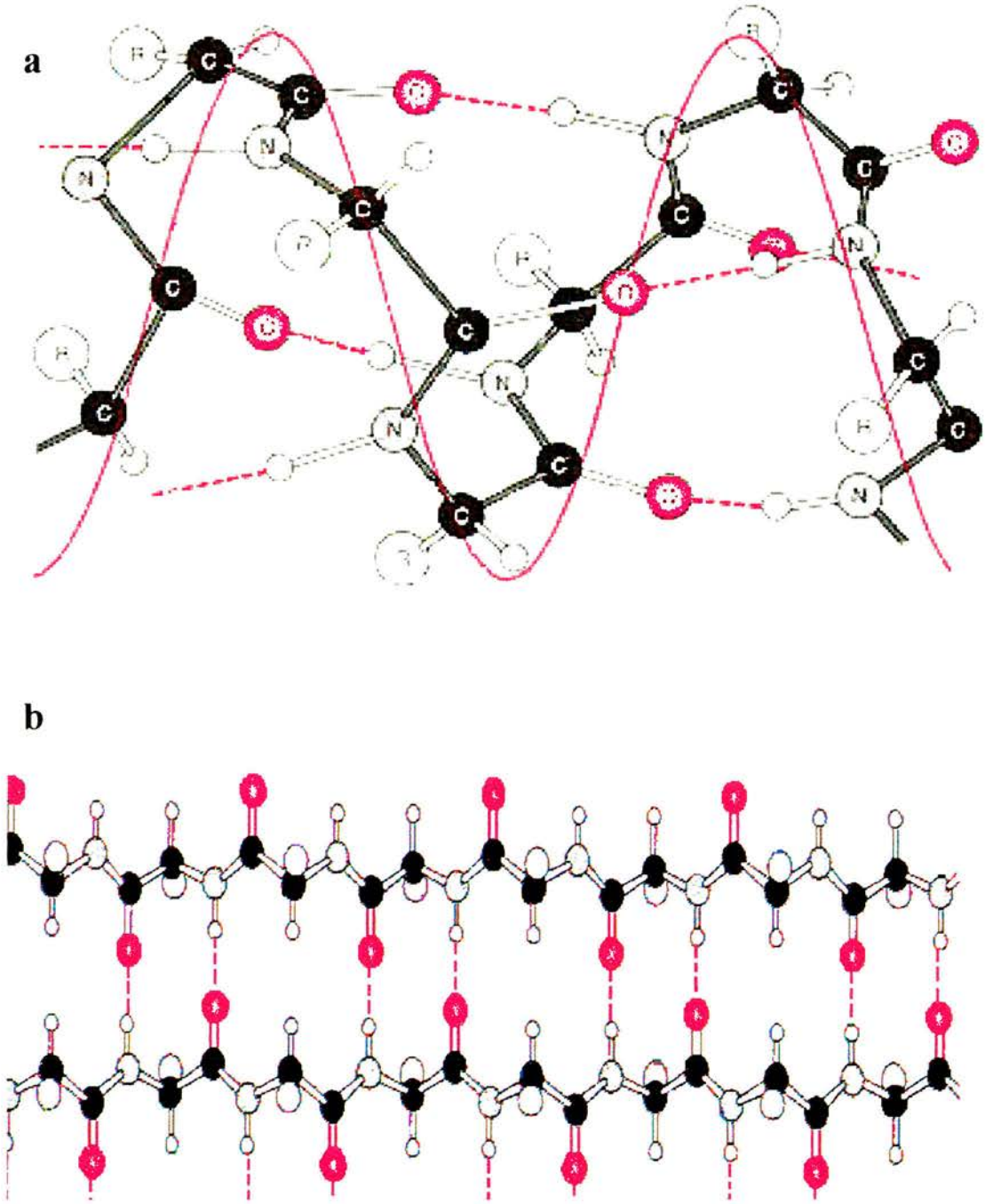

Figure 6.2. Diagram of an alpha helix (a), and an antiparallel beta sheet (b). Both of these secondary structures are stabilised by hydrogen bonds, shown as dashed lines, in which a hydrogen serves as a bridge between oxygen and nitrogen atoms. Adapted from Doolittle, 1985.

of the different secondary structures adopted by a peptide in solution, and requires only a small sample. For these reasons, it is an excellent technique for investigating changes in the behaviour of a peptide in different solvents.

6.2 Theoretical Background

"Let not your left hand know what your right hand is doing"

Matthew 6:3

CD refers to the differential absorption of the left and right circularly polarised components of plane, or linearly, polarised radiation, in the absence of a magnetic field (Price, 1996).

As mentioned in Chapter 3, electromagnetic waves may be considered to possess two wave motions that are at right angles to each other, namely an electric component and a magnetic component (see Figure 3.3). In contrast to NMR, CD is concerned, in the main, with the electrical properties of electromagnetic radiation.

The electric vector of electromagnetic radiation rotates about the direction of propagation, executing one full revolution in one wavelength of the light wave. Plane, or linearly, polarised radiation has an electric vector which is confined to a plane perpendicular to the direction of propagation. Plane polarised radiation can also be considered to be composed of a right and a left circularly polarised beam, which have equal amplitude and are in phase. Conversely, a circularly polarised beam consists of two perpendicular, plane polarised beams of equal amplitude that are 90° out of phase (see Figure 6.3). Thus the electric vector of a right circularly polarised beam (see Figure 6.4a) will trace out a right handed helix along the direction of propagation (see Figure 6.4b), and to an observer looking towards the light source, the electric vector will rotate in a clockwise direction (see Figure 6.4c). Left circularly polarised light has the opposite characteristics.

Dichroism of circularly polarised light results when the absorbance of a medium varies with the direction of rotation of a circularly polarised beam (Warren, 1987). If plane polarised light is transmitted through such a material, then after the

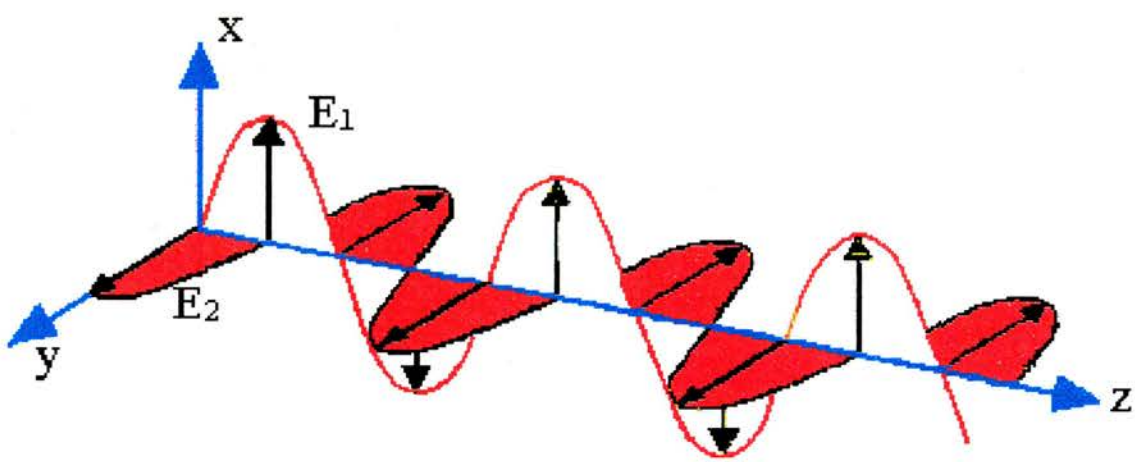

Figure 6.3. Circularly polarised radiation, produced by the electric vectors of two beams, which are at right angles to each other and 90° out of phase.

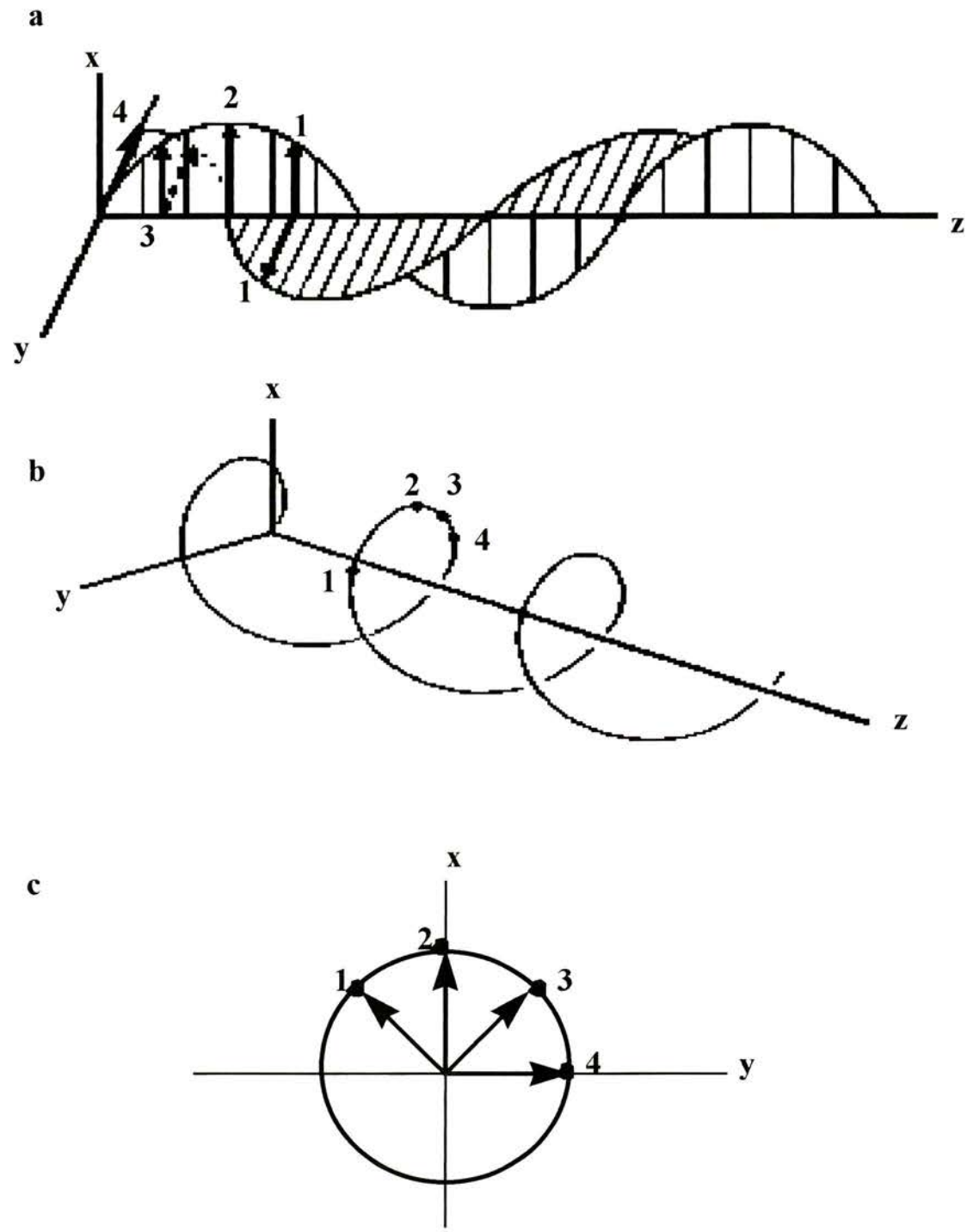

Figure 6.4. Right circularly polarised light. a) two electrical perpendicular vectors 90° out of phase. b) the position of the resultant sum of the electrical vectors along the direction of propagation. c) the sum of the electrical vectors traces out a circular path when viewed along the axis of propagation towards the light source.

left and right beams have passed through the sample, their sum is no longer a plane polarised beam but is elliptically polarised (see Figure 6.5). The difference in absorption, ΔA, which is the parameter that is measured experimentally, is defined as:

$$\Delta A = A_L - A_R \qquad 6.1$$

where A_L and A_R are the absorbances of the left and right beams. CD results are expressed either as the difference in molar absorbance, $\Delta\varepsilon = \varepsilon_L - \varepsilon_R$, (i.e. $cm^{-1}.M^{-1}$), or as the mean residue ellipticity $[\theta]_{mrw,\lambda}$. This latter parameter is defined by the following:

$$[\theta]_{mrw,\lambda} = \frac{MRW\theta}{10\,dc} \qquad 6.2$$

where MRW is the mean residue weight, that is the molecular weight divided by the number of peptide bonds present (the peptide bond is the repeating unit of interest, see later), θ is the observed ellipticity, d is the path length in cm, and c is the concentration (g/ml). Thus the units are $deg.cm^2.dmol^{-1}$.

To exhibit differences in absorption of left and right circularly polarised light, a molecule must be chiral, that is its mirror image cannot be superimposed upon it, and thus it must lack any elements of reflection symmetry. Since left and right circularly polarised light beams have helical symmetry themselves, an asymmetric molecule will present a different polarisable medium to the two beams. These chiral groups are termed intrinsic chromophores, an example being the peptide bond (see Figure 6.1).

The peptide bond absorbs light in the far ultraviolet (UV) region, in the range of 180-240nm. The spectral properties of a peptide in the far UV mainly depend upon the molecular environment and the mobility of the peptide bonds. Thus the different principal types of secondary structure adopted by peptides give rise to characteristic CD spectra in the far UV. CD can thus be used to determine the presence of these different secondary structures within a peptide.

The origin of the CD absorption bands is explained as follows. In the far UV region of the electromagnetic spectrum, the interaction of radiation with electrons of a

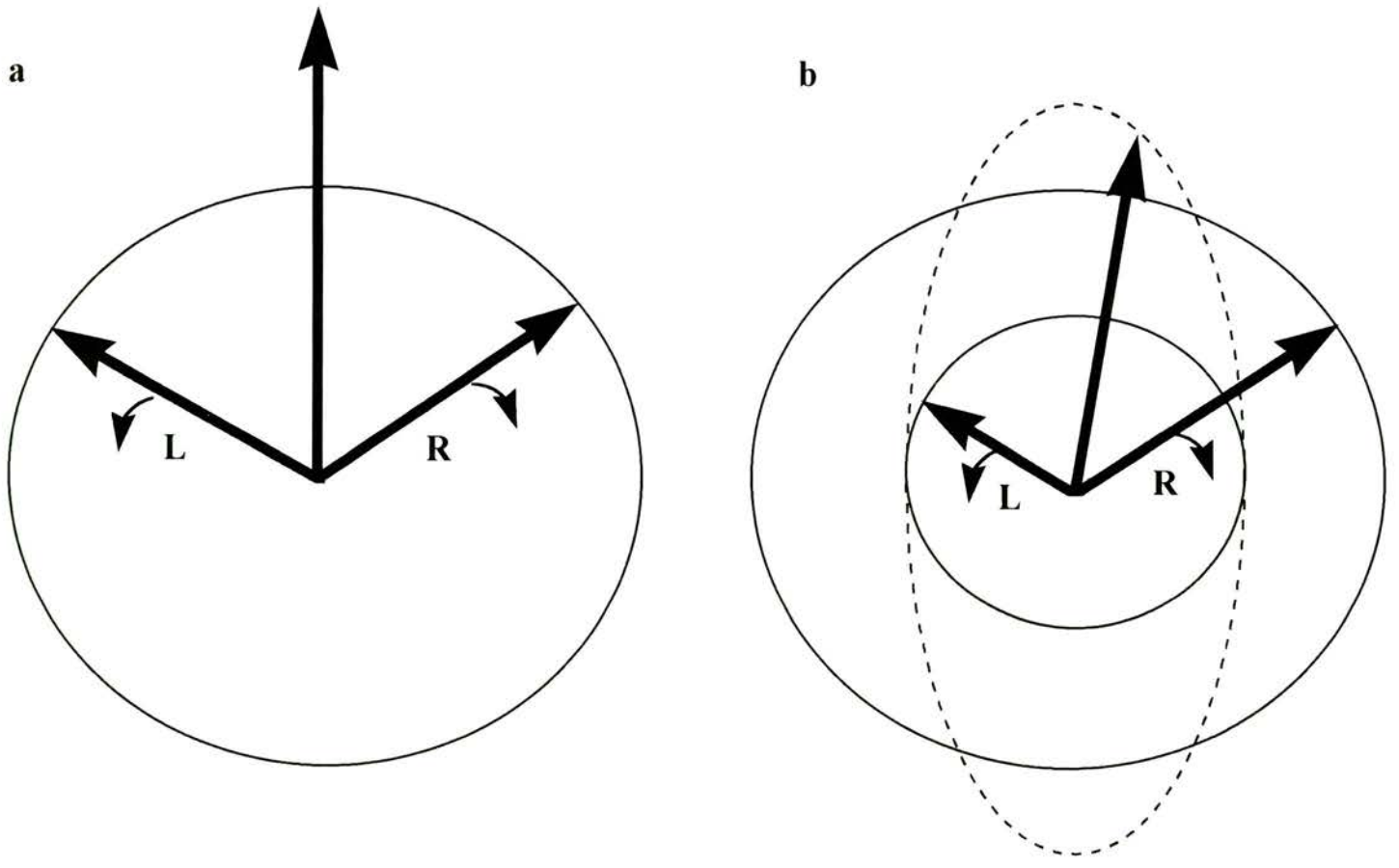

Figure 6.5. a) Plane polarised light can be considered to be composed of a left and a right circularly polarised component, of equal amplitude. b) if plane polarised light is passed through a dichroic medium, the left and right components are absorbed to different extents. The resultant light beam will be elliptical. The major and minor axes of the resultant ellipse are, respectively, the sum of and difference between the amplitudes of the emergent circular components. The ellipticity is defined as the angle whose tangent is the ratio of the major and minor axes.

peptide causes a redistribution of electron density and a reduction in the velocity of the radiation. At certain frequencies ν, the photon energy of the incident radiation will satisfy the condition $\Delta E = h\nu$, where ΔE is the energy difference between the ground state and the electronic excited state, and the electron will undergo a transition into the excited state. This transition is characterised by the frequency or wavelength at which it occurs, and the magnitude of the electronic displacement involved. Thus the electronic absorption spectra approximate to a collection of discrete lines, corresponding to such transitions. In solution the CD spectra are broadened by interaction of the chromophore with the solvent, and smooth curves are obtained with defined band shape. Each CD band is characterised by its wavelength or frequency at which maximum light absorption occurs, by its intensity, which is the peak value for the band and which may be positive or negative, and by its shape. CD spectra of peptides in solution usually contain bands that represent sets of overlapping electronic transitions.

Electronic transitions from the ground state to the excited state involve a linear displacement of charge. To produce CD, a transition must involve both a linear and a circular displacement of charge, with the two motions having a common vector component. The circular displacement of charge generates a magnetic field and is thus the magnetic component. This combination of linear motion along an axis with circular motion about the same axis produces a helical charge displacement (see Figure 6.6). The direction of rotation of the helix will be determined by the relative signs of the electric and magnetic components. Thus, when this criterion is met, left and right circularly polarised beams will interact differently with peptide molecules in solution, and this will manifest as a difference in absorption. This helical charge displacement only occurs for asymmetrical molecules.

The amide group has three π orbitals, as shown in Figure 6.7. With four π electrons there will be two $\pi\pi^*$ transitions. The transition into the lowest π^* orbital is represented by the 190nm peptide band. Electronically this transition is mainly accounted for by the displacement of π electron density from the region of the nitrogen atom into the π^* orbital, where it is located mainly on the carbon and oxygen atoms (Schellman and Nielsen, 1967). There are also two lone pairs on the carbonyl

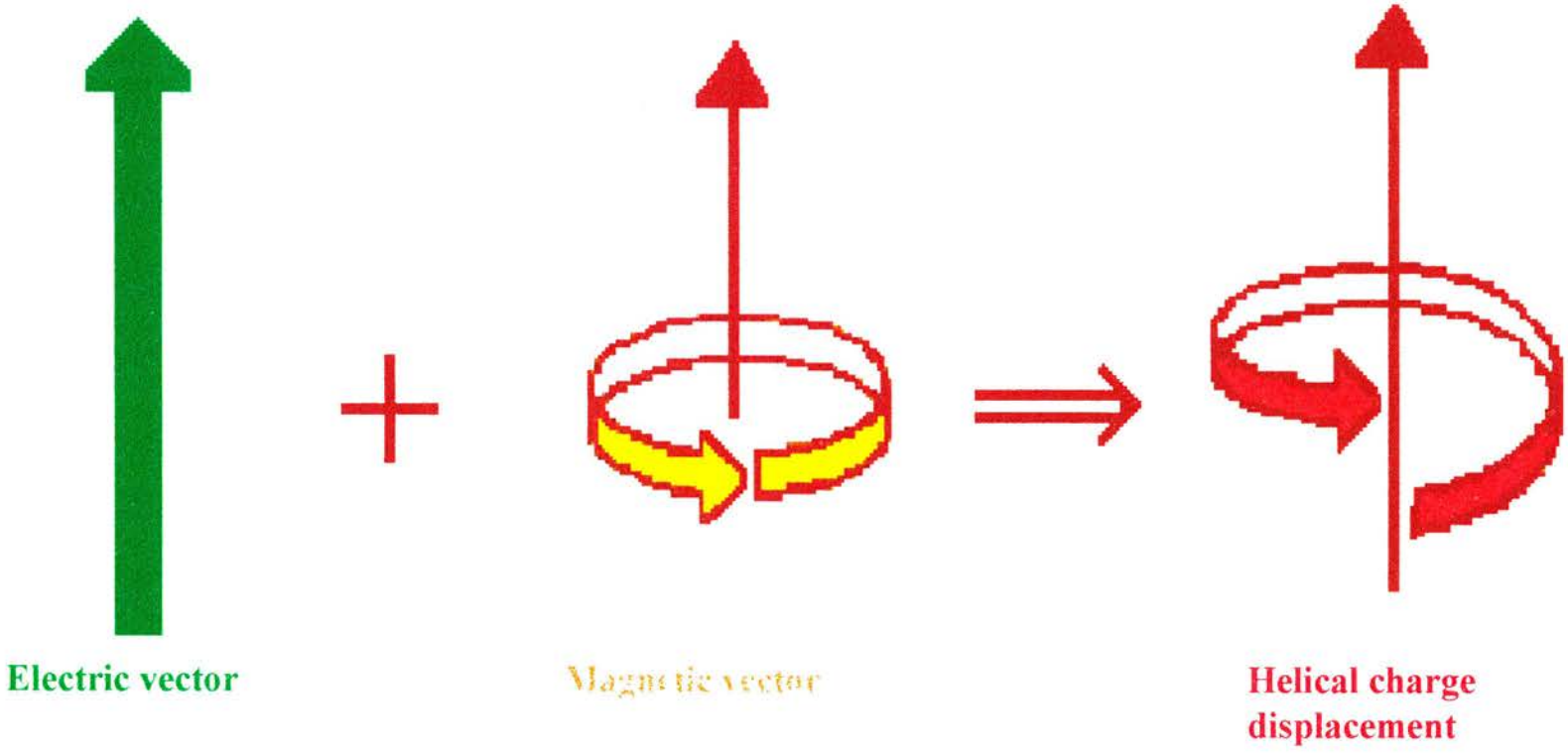

Figure 6.6. Production of an optically active transition. A linear electric vector combined with a circular magnetic vector generate a helical charge displacement, and thus an optically active transition.

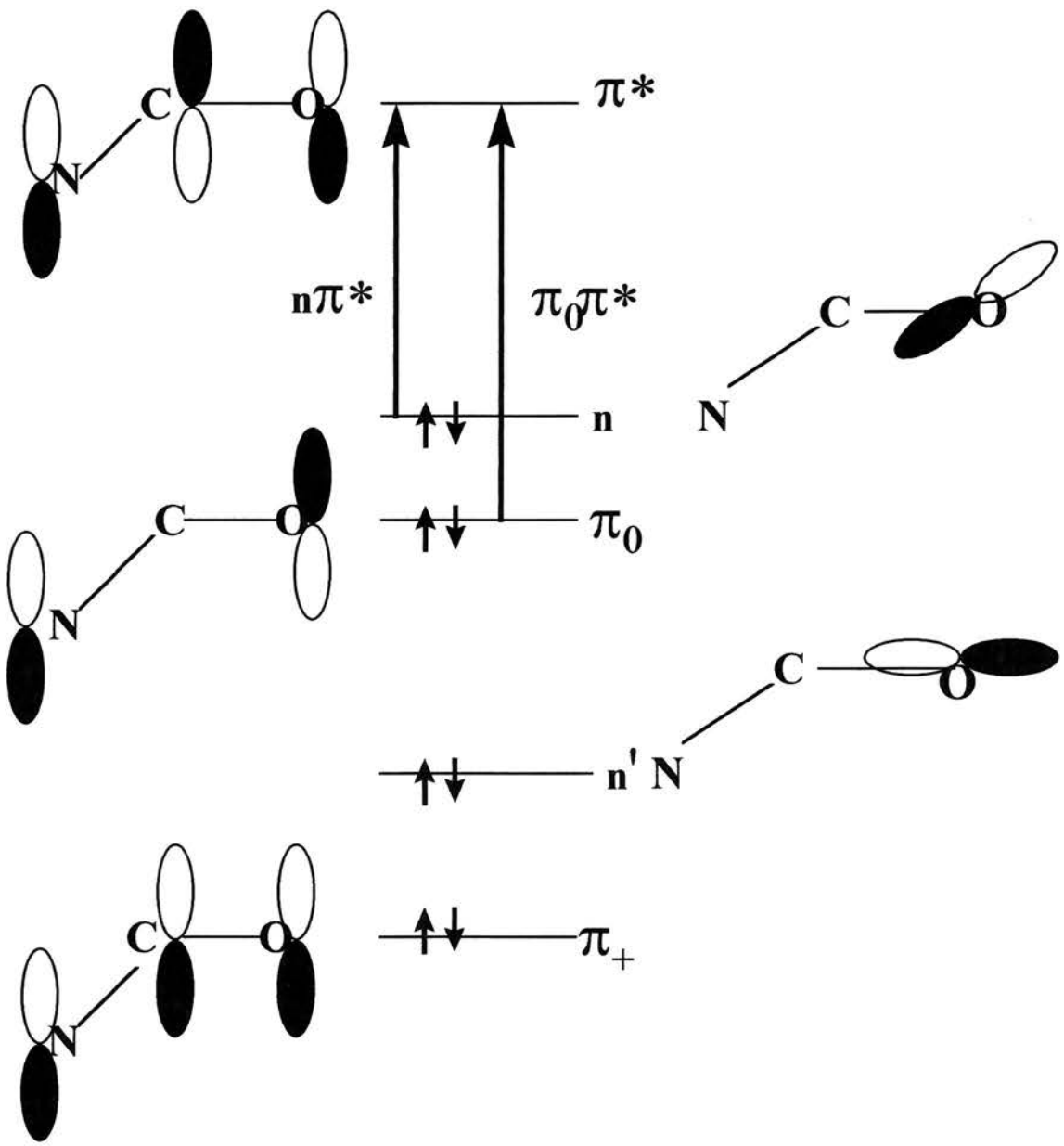

Figure 6.7. The molecular orbitals of the amide group comprise 3π orbitals and two lone pairs. The $\pi_0\pi^*$ transition occurs near 190nm, and the $n\pi^*$ transition near 220nm. The other possible transitions have yet to be definitively identified.

oxygen. The highest energy lone pair (n orbital) is largely localised on the carbonyl oxygen. The $n\pi^*$ peptide transition involves the transition of an n electron into an orbital of π^* symmetry. Of the two non-bonding orbitals associated with C=O, it is the axial n_σ orbital which acts as hydrogen-acceptor, and the $n_{p\gamma}$ which contains the optical electron (Bayley, 1973). The transition from P_y symmetry to P_z symmetry constitutes a rotation of charge about the C=O bond (Bayley, 1973). The lack of linear displacement means that this band is very weak in absorption. In peptides this is seen as a CD band lying near 220nm.

A peptide bond is always optically active, regardless of the surrounding chemical groups. The latter can, however, modify the optical properties of the peptide bond. Thus, if peptide bonds are near each other in space, the transition dipole moments can interact, which causes a splitting of the absorption bands (Campbell and Divek, 1984). Any changes in the angle between adjacent groups will alter the transition probability, the position of the absorption bands and also the rotational strengths (Campbell and Divek, 1984). Thus for a given configuration, the optical properties of two interacting peptide bonds will show marked dependence upon conformation for both the $n\pi^*$ and $\pi\pi^*$ transitions. Hence it can be seen that the CD spectrum is very sensitive to peptide secondary structure.

A major class of peptide secondary structure is the α helix (see Figure 6.2a). The CD spectra for all α helices show negative bands at 222nm and 209nm, and a positive band at 190nm (see Figure 6.8). These have been attributed to three major effects: the $n\pi^*$ transition (222nm) (Schellman and Oriel, 1962; Woody and Tinoco, 1967) and two of the $\pi\pi^*$ transitions (209nm and 190nm) (Rosenheck and Doty, 1961).

The β sheet has a different and characteristic spectrum (see Figure 6.8). The negative band near 215nm is attributed to the $n\pi^*$ transition, whereas the $\pi\pi^*$ transitions are thought to be responsible for the positive band near 198nm and the negative band near 175nm. The CD spectra of β structures are, however, less well defined than that of the α helix. They are weaker and, moreover, the β structure shows strong reliance upon environmental conditions for its optical properties. In hydrogen-bonded parallel and anti-parallel β sheets, the chromophores in adjacent

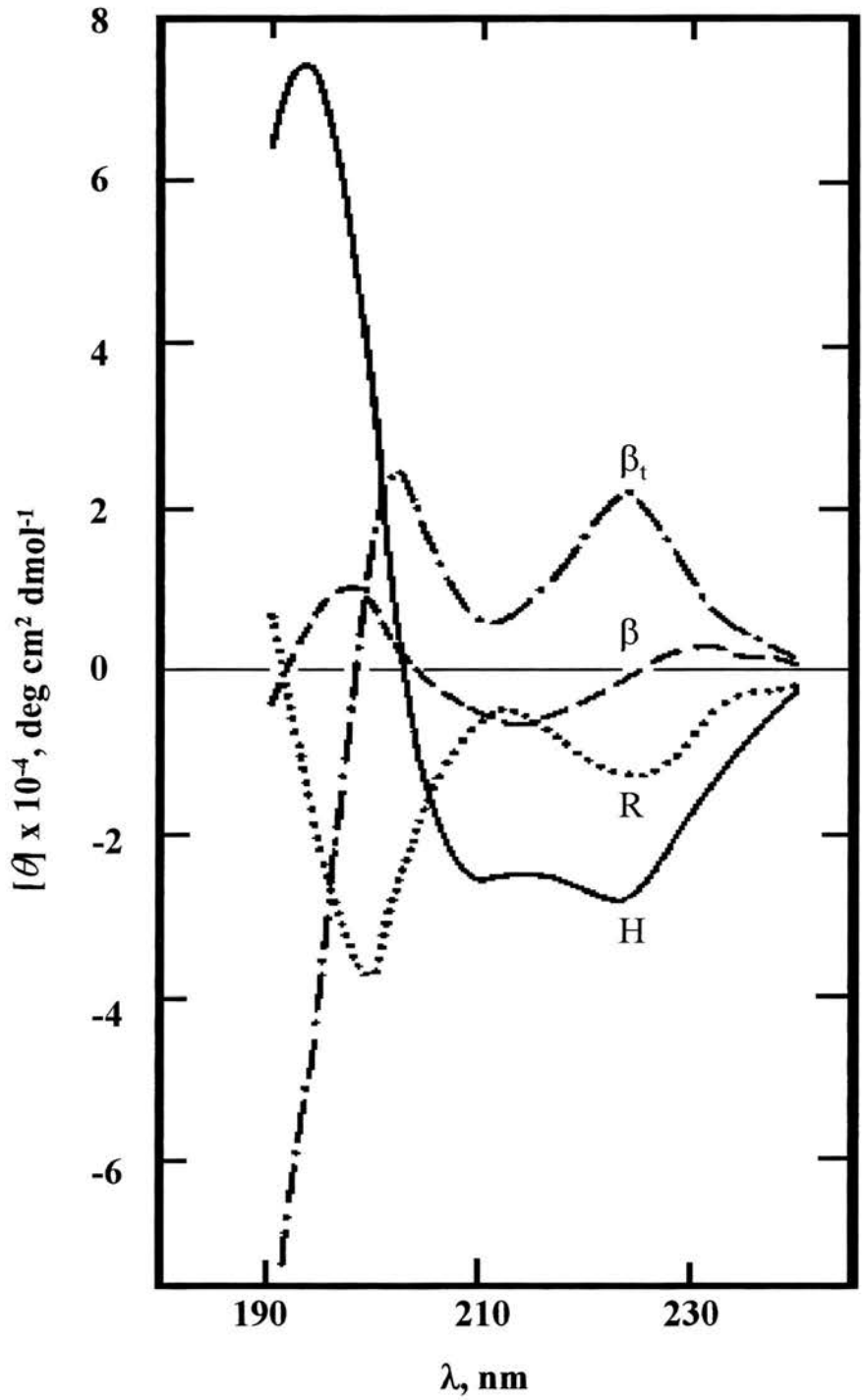

Figure 6.8. Characteristic CD spectra of the helix (H), β–form (β), β-turn (β_t) and unordered form (R). Reproduced from Chang *et al*, 1978.

sheets are near enough to interact, and distinguishing properties are predicted for the two structures (Woody, 1969). Thus, since both arrangements exist in biological proteins, there is more variability in the optical properties of this secondary structure group, and hence quantitative estimates are less reliable than for α helices. This is also true for β turns.

The random coil peptide conformation displays, not surprisingly, optical properties that are strongly non-conservative. There is still much debate as to the precise origin of the CD bands seen for random coils, but the pronounced negative band at 190nm (see Figure 6.8) is thought to represent the $\pi\pi^*$ transition, and the weak positive band at 217nm is considered to represent the $n\pi^*$ transition (Bayley, 1973).

The CD spectrum of a peptide or protein molecule in the far UV region can be represented as a linear combination of the different elements of secondary structure, according to the equation:

$$[\theta(\lambda)] = f_\alpha[\theta_\alpha(\lambda)] + f_\beta[\theta_\beta(\lambda)] + f_t[\theta_t(\lambda)] + f_n[\theta_n(\lambda)] \qquad 6.3$$

where $[\theta_\alpha(\lambda)]$, $[\theta_\beta(\lambda)]$,$[\theta_t(\lambda)]$ and $[\theta_n(\lambda)]$ are the basis spectra for α helix, β sheet, turn and non-regular structures, and the f_i are the respective fractions of these structural elements (Schmid, 1989). The coefficients f_i are obtained by solving this equation simultaneously at a set of selected wavelengths. The major errors of this procedure lie in the choice of standard reference spectra. In the late 1960's, model polypeptides were used to represent the different classes of secondary structure. The structures of these model polypeptides were known from X-ray crystallography data, and it was also assumed that each polypeptide only adopted a single conformation in solution. The three forms of poly-*L*-lysine were used, which show α helix, β sheet and random coil conformations. Multicomponent analysis was then performed, in order to calculate the secondary structure of the protein of interest. This analysis method involved simulation of the sample protein's CD spectrum by suitable graphical addition of the three standard curves. Thus:

$$S = a[\alpha] + b[\beta] + r[R] \qquad 6.4$$

where α is the α helix, β the β sheet and R the random coil components. The variation of α, β and R with wavelength is taken from suitable standards, and then *a,b* and *r* varied so as to obtain a fit to the experimental curve over the entire wavelength region.

The problem associated with this method is that real proteins and peptides may not possess the exact geometrical configurations of those in the standard models. CD properties depend upon the length of the secondary structural elements. The CD spectrum of the peptide bond may also be influenced by the presence of aromatic side chains, disulphide bridges and prosthetic groups in the sample protein or peptide. Furthermore, the peptide bond may exist in conformations other than the three forms that are examined in the reference polypeptides.

More recent approaches are based on sophisticated fitting procedures that use data sets comprising spectra of well-characterised proteins, whose secondary structures are known. In order to improve accuracy, Chen and co-workers (Chen *et al,* 1974) introduced an empirical factor that was dependent upon chain length for the helix spectrum, and Chang *et al* (1978) added the β turn class. The CONTIN method of Provencher and Glöckner (1981) avoids the problem of trying to define single reference CD spectra that are supposed to characterise such broad and variable classes as helix, sheet, turn and remainder, and thus permits a more flexible and accurate analysis. Instead, it uses a linear combination of the CD spectra of 16 reference proteins for a direct analysis of the CD spectrum of a protein. (The secondary structures of the 16 reference proteins have been determined to a high resolution by X-ray crystallography.) Standard proteins range from highly α-helical proteins, such as myoglobin (79% α helix, 0% β sheet by X-ray) to those such as concanavilin A, which contain large amounts of β sheet (2% α helix, 51% β sheet by X-ray). A thorough analysis of the CONTIN procedure showed that the α helix and β sheet contents could be estimated fairly reliably when considering data over the range of 190nm to 240nm; the percentages of β turns and remainder (random structure), however, were much less well calculated. As a general rule, the accuracy of the results

obtained is better for proteins which consist of mainly α helix or mainly β sheet conformations than for those which contain similar proportions of these two types of structure. Also, the most reliable results are likely to be obtained when a related, well characterised protein can be employed as a reference.

6.3 Practical considerations for CD

A diagram of a typical CD machine is shown in Figure 6.9. The light source is usually a xenon arc lamp. The light is plane polarised by passage through prisms. The phenomenon of CD could be detected by a double beam instrument containing two independent beams of left and right circularly polarised light. It is possible, however, to split plane polarised radiation into its components using a crystal that can be made to pass either right or left polarised light, depending upon the applied voltage of an electric field. This electro-optic crystal, usually composed of ammonium dihydrogen phosphate (Pockel's cell), comprises the high frequency modulator, which alternately transmits each of the two circularly polarised light beams. A modulator was used in the experiments described in this thesis. A double monochromator arrangement reduces stray light. Nitrogen gas is used to flush the instrument both before switching on the lamp and during measurements. This minimises the damage to the optical system, and also removes as much oxygen as possible from the sample compartment, which is important as oxygen absorbs strongly below 200nm.

Once the beam has passed through the sample, it is enhanced by a photomultiplier. If a sample displays CD, the periodic variation in the polarisation of the beam produced will lead to a periodic change in the extent of absorption and hence in the light level reaching the photomultiplier. This leads to a small alternating current in the photomultiplier output, which can be further amplified. This ac component is proportional to the difference in absorption of the left- and right-circularly polarised light. The detected signal can then be processed to give a CD spectrum, which is a plot of ΔA or θ as a function of wavelength. Corrections for any signals due to cuvettes and buffers are made by running the appropriate blanks, and subtracting these signals from the sample signal.

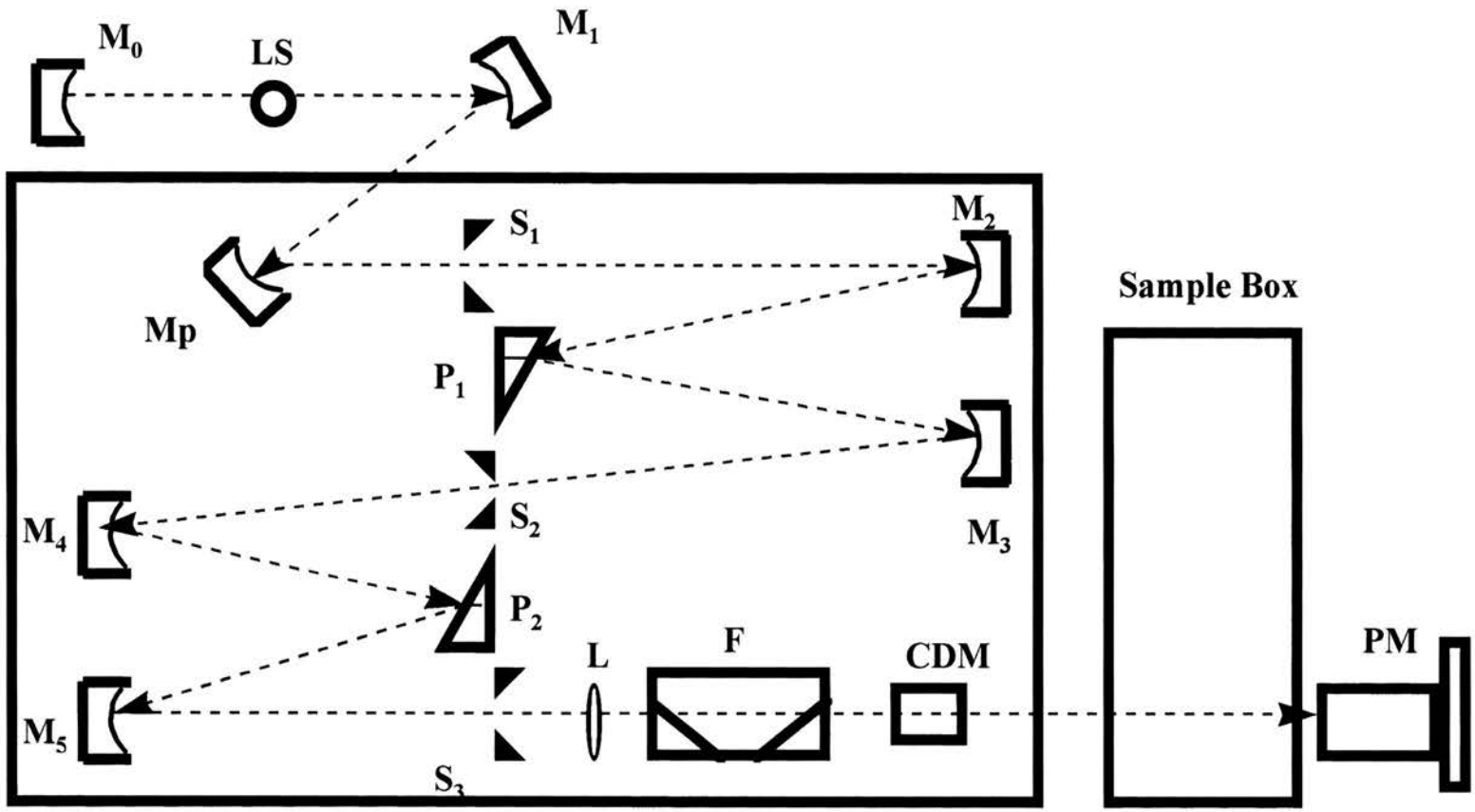

Figure 6.9. Schematic diagram of the basic optical system of a CD machine. LS: light source; M_0, M_1 etc: mirrors; S_1, S_2 etc: slits; P_1 and P_2: prisms; L: lens; F: filter; CDM: modulator and PM: photomultiplier. Plane polarised light is produced by passage through the two prisms. This is focussed and streamlined by the slits and mirrors. The modulator then resolves this radiation into its circularly polarised components.

Proteins produce very small differences in absorption: usually around 10^{-4} to 10^{-6} absorbance units for a sample with a total absorbance of 1 unit (Schmid, 1989), which means that less than 0.1% of the total absorbance signal must be measured with a high degree of accuracy and reproducibility. Thus great care is needed in both the control of experimental conditions and sample preparation.

The size of the CD signal depends upon the amount of protein or peptide present, and therefore to optimise the signal-to-noise ratio, the protein or peptide should provide as large a contribution as possible to the total optical density of the sample. Thus the absorbance by the solvent should be as small as possible. The choice of solvent is crucial, as some common buffers absorb strongly in the UV region. A solvent blank should always be run first, to check that this is not a problem. Solutions must be clarified by centrifugation or by passage through a ~0.2μm filter. Fused quartz cuvettes are used to hold the sample; these are highly transparent below 200nm.

The total sample absorbance must be maintained at less than 1 absorbance unit. This is usually achieved by using small sample cell lengths, often around 0.01 - 0.02cm. Numerous scans, usually 2 to 4, of a sample are performed, which improves the signal-to-noise ratio. Scan rates must be kept fairly slow, at around 10nm/min, to allow the use of a high time constant, and thus the accumulation of many measurements. Finally, the spectral bandwidth used should be narrow, to allow good resolution of wavelength.

6.4 Application of CD to Fusion Studies: Aims of these CD Experiments

A viral fusion peptide, which comprises a span of relatively hydrophobic amino acids, is thought to insert into the target membrane of its host cell and disrupt bilayer stability, so initiating the fusion process (Brasseur *et al*, 1990). In the preceding chapters, experimental work using the FeLV fusion peptide has provided support for this membrane destabilising effect. Translocation from an aqueous environment, such as extracellular fluid, to a lipid environment, such as a biological membrane, is likely to involve substantial structural alterations of a peptide. Many

proteins and peptides insert into membranes, and concomitantly alter their own secondary structure, but they do not trigger extensive changes in the arrangements of the lipid molecules in their target membranes. This poses a question; namely, what features of the structure of a fusion peptide confer upon it these specific functional properties?

There is much conflicting evidence on the active secondary structure of fusion peptides. A modelling study of several viral fusion peptides assumed that they completely formed α helices upon insertion into a membrane (Brasseur *et al*, 1990). The resulting theoretical calculations suggested a favourable free energy for the oblique insertion of 'sided' helices at a shallow angle into the bilayer. Such 'sided' helices have the majority of their more bulky, hydrophobic residues distributed on one side of the α helix. Gallaher and co-workers (1992), however, have cautioned against the earlier assumption that all fusion peptides are 'sided' helices in their active form. Indeed, the Measles virus fusion peptide was found to adopt a conformation of 73% β sheet in one study (Epand *et al*, 1992) and, under different experimental conditions, fusion peptides from different strains of HIV have been shown to be mainly α-helical (Rafalski *et al*, 1990), or conversely mainly β sheet (Nieva *et al*, 1994b), in their active forms. Hepatitis B virus fusion peptide favours a β sheet conformation in the presence of lipid vesicles (Rodríguez-Crespo *et al*, 1996), as does PH-30, a sperm fusion peptide involved in sperm-egg fusion (Muga *et al*, 1994). It thus appears possible that viral fusion peptides may not all share a common active secondary structure. One aim of the CD studies in this chapter, therefore, was to determine the active secondary structure of the FeLV fusion peptide.

The conclusion drawn from the studies described above is that fusion peptides change from one defined, inactive secondary structure to another different, and equally well-defined, active secondary structure. None of these studies examined the same viral fusion peptide in a whole range of different solvent systems. Since membrane fusion is a dynamic process, involving large changes in the component molecules, it is also possible that structural plasticity may be an essential property of these initiators of fusion. The FeLV peptide contains significant numbers of amino acids that characteristically favour three different secondary structures, namely the α

helix, the β sheet and a coiled conformation. It could be postulated that this would lead to a large amount of dynamic structural flexibility for the FeLV fusion peptide. Indeed, computer modelling work has suggested that this might be an important factor for fusion peptides in general (Callebaut *et al*, 1994). Thus another aim of the CD work reported in this thesis was to examine the secondary structure of the FeLV fusion peptide in a variety of environments of differing hydrophobicity, and hence to determine any changes in peptide secondary structure asscoiated with changes in environment. The ultimate goal was to link peptide structure to function.

6.5 Materials and Methods

6.5a Sample Preparation

Samples for liposome studies

The far UV CD spectra of proteins and peptides are much stronger than those of lipid molecules. It is possible, therefore, to study the secondary structure of peptides that have been reconstituted into membranes or LUVs.

Previous fusion studies have suggested that the type of lipid present in the target membrane can affect the fusogenic capacity of certain viruses (e.g. Larsen *et al*, 1993; Novick and Hoekstra, 1988), and, more specifically, of certain viral fusion peptides (Martin *et al*, 1991, 1993). Thus, in order to determine any effects of the type of lipid on the secondary structure of the FeLV fusion peptide, several different lipids were used to prepare the LUVs:

1) pure DOPC (a zwitterionic and thus neutral lipid, and the single most physiologically representative lipid species).

2) DOPC present at a 50:50 molar ratio with one of the following:-

a) DOPE (PEs are fusion promoting lipids, and have been used for most of the biophysical studies in this thesis; PE is necessary for HIV-induced fusion between LUVs (Martin *et al*, 1993).

b) DOPG (PGs are negatively charged lipids; a variety of PGs have been used in previous CD studies of fusion peptides and DOPC:DOPG bilayers were used in the neutron studies described in Chapter 5 of this thesis).
c) dioleoylphosphatidylserine (DOPS) (PSs are also negatively charged and are common constituents of mammalian cell membranes).

Proteoliposomes containing the FeLV fusion peptide and a variety of different pure lipid species were prepared in the following manner. Initially, a lipid:peptide molar ratio of 50:1 was chosen, as this ratio is commonly used in fusion assays. The 50:1 ratio did not, however, yield a sufficiently strong signal-to-noise ratio, and so the lipid molar fraction was progressively reduced until a good peptide signal was produced. The final lipid:peptide molar ratio was thus 12:1, with a peptide concentration of 1mg/ml.

Dried lipid films were prepared using the required amounts of peptide and chosen lipids, as described in Chapter 2. Detergent dialysis was then used to prepare the proteoliposomes (New, 1990; Nordmeier *et al*, 1992). This method has the disadvantage that it is virtually impossible to remove every detergent molecule from the final preparation, and these may influence the interactions between the peptide and the lipids. However, it was found to be impossible to use the 'cleaner' method of high pressure extrusion through stacked polycarbonate filters (Hope *et al*, 1985) to produce proteoliposomes containing the FeLV fusion peptide. This was because large, uncertain quantities of the peptide became trapped in the filters, which led to very poor peptide signals for samples of unknown peptide concentration. The detergent *n*-octyl glucopyranoside (OG) was chosen to use for the dialysis regime as it does not show strong light absorbance in the UV region. A solution of OG at a final molar concentration of four times that of the lipid (Sizer *et al*, 1987) was prepared in Tris-HCl buffer (10mM Tris-HCl, 0.1mM EDTA, 0.001% sodium azide, pH 7.4). Low molarity Tris-HCl buffer (≤20mM) also has a relatively low absorbance above 190nm in cells of path length 0.1cm or less.

The dried lipid films were dissolved in the detergent solution and sonicated briefly to ensure thorough mixing and micelle formation. Next the samples were dialysed at length against Tris-HCl buffer. Four consecutive 5l flasks of pH 7.4 Tris

buffer were used and were changed after 6, 12, 24 and 48 hours. After 24 hours of dialysis, the dialysate was seen to become cloudy: this occurrence has been used to ascertain the formation of liposomes using spectrophotometry (Huang, 1971). Finally, after 90 hours of dialysis, the dialysate was transferred to centrifuge tubes and centrifuged to remove any MLVs present. The resulting supernatant was used for the CD measurements.

Samples for solvent studies

All chemicals were supplied by Sigma Chemical Co., UK. FeLV fusion peptide was added to produce a concentration of 1mg/ml to (a) 2M guanidine/50% ethanol, a solvent often used in order to dissolve a fusion peptide for addition to fusion assays, (b) trifluoroethanol (TFE), and (c) hexa-fluoroisopropanol (HFIP). TFE and HFIP promote intramolecular hydrogen bonding at the expense of hydrogen bonds with water, and thus they promote formation of secondary structures in peptides. These samples were then diluted 1:1 with distilled water, giving a final peptide concentration of 0.5 mg/ml. Peptide was also added to sodium dodecylsulphate (SDS) at concentrations of (c) 3mM and (d) 6mM in distilled water, to give a final peptide concentration of 0.5mg/ml. SDS is a detergent, and thus forms micelles at concentrations approaching and above its critical micellar concentration (CMC). Lastly, the resulting suspensions were sonicated in a bath sonicator until the peptide dissolved. TFE, HFIP and SDS all show little absorption in the UV region. Guanidine, however, absorbs strongly below 205nm, and so the spectrum for this sample was set at zero below this wavelength.

Negative staining transmission electron microscopy was used to examine the peptide samples used in the solvent study to confirm the presence of β structure. The peptide solutions were dried onto plastic-coated carbon grids, and then negatively stained using 4% sodium phosphotungstate at pII 7.2. These stages of the sample preparation for EM were performed by Mr. S. Mitchell, R.(D).S.V.S, University of Edinburgh, EH9 1QH. A Philips 400 TEM was used to examine the samples, at 80kV, and x 60,000 magnification. Negative controls were performed by staining an empty plastic-coated carbon grid, and also by staining the corresponding pure solvent.

6.5b Circular Dichroism

CD spectra were recorded using a JASCO J-600 spectropolarimeter, over the wavelength range 195-260nm, in a cell of path length 0.02cm, at 25°C. At least 4 spectra were averaged for each sample. A similar number of blank spectra were also recorded for each sample in order to allow the subtraction of solvent and liposomal contributions to the corresponding sample spectra. The blank samples contained the same type and amount of solvent and, when appropriate, of liposomes, as were present in the corresponding peptide sample. This produced difference spectra, which were due purely to the FeLV peptide. Data points were recorded and plotted at 0.2nm intervals. The raw data curves were smoothed and the data converted into molar ellipticity units for analysis of secondary structural content. This analysis utilised the CONTIN procedure of Provencher and Glöckner (1981) to determine the amounts of α helix and β sheet present. The method of Chang *et al* (1978) was used to verify the overall trend in α helix contents. All CD measurements were performed at the CD facility at Stirling University, Stirling, FK9 4LA, U.K. with expert technical assistance from Dr. S.M. Kelly.

6.6 CD Results and Discussion

The far ultraviolet CD spectra of the FeLV fusion peptide in the various liposomal preparations are shown in Figure 6.10. Satisfactory data could only be obtained down to 195nm; below this wavelength the noise levels produced by vesicle-induced light scattering prevented accurate determination of ellipticity. This significantly reduces the reliability of estimates of secondary structures other than the α helix.

Table 6.1 lists the percentages of α helix, as determined by the two independent analysis methods of Provencher and Glöckner, (1981) and Chang and co-workers (1978). The amount of β sheet is also quoted, as obtained by the analysis of Provencher and Glöckner, but, as mentioned above, the exact figures quoted for this secondary structure should be viewed with caution. A further error may lie in the fact

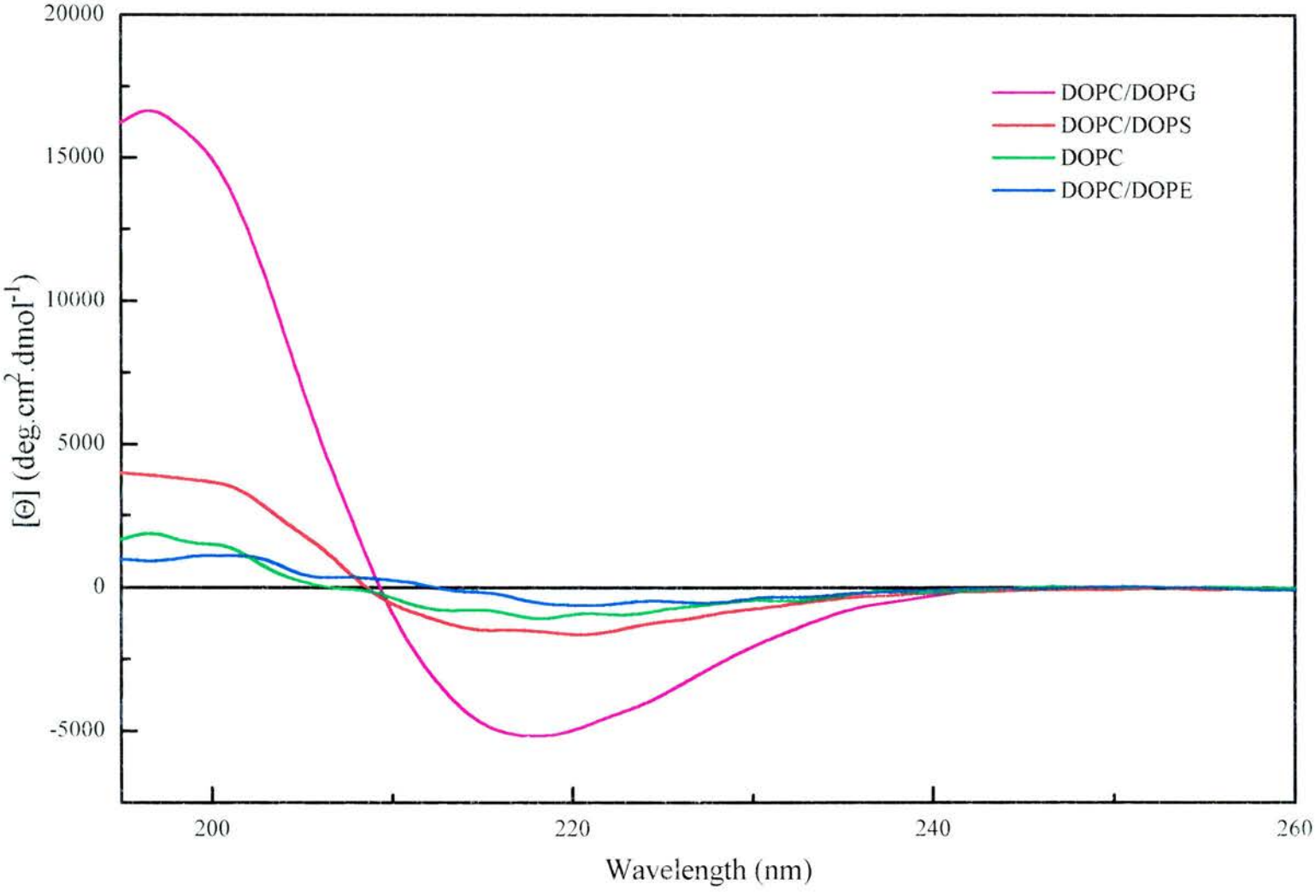

Figure 6.10. CD spectra of the FeLV fusion peptide in liposomes of various lipid compositions.

Table 6.1. Percentages of FeLV peptide secondary structure in liposomal suspensions of different phospholipids, as calculated by the methods of Provencher and Glöckner, (1981) and Chang *et al*, (1978).

Sample FeLV peptide (1mg/ml) in LUVs composed of:	% secondary structure as calculated by the methods of: Provencher & Glöckner (helix, sheet)	Chang et al (helix)
pure DOPC	0, 71	0
DOPC:DOPE	0, 79	0
DOPC:DOPS	1, 66	3.1
DOPC:DOPG	1, 73	22

Table 6.2. Percentages of FeLV peptide secondary structure in a range of solvent systems, as calculated by the methods of Provencher and Glöckner, (1981) and Chang *et al*, (1978).

Sample FeLV peptide (0.5mg/ml) in :	% secondary structure as calculated by the methods of: Provencher & Glöckner (helix,sheet)	Chang *et al* (helix)
1M guanidine in 25% ethanol	0, nd*	0
50% TFE	20, 36	16
50% HFIP	30, 35	22
3mM SDS	2, 57	11
6mM SDS	12, 47	14

*The value for the sheet content of this sample could not be determined using the method of Provencher and Glöckner without an unacceptably large error.

that it may be inappropriate to apply to peptides methods of analysis that have been derived for proteins. It is also possible that the amounts of helix present may be underestimated, as up to two-fold reductions in ellipticity have been found in membrane-bound proteins (Glaeser and Jap, 1985). Thus the amounts of helix quoted here should be viewed as the minimum amounts of helix present in the various samples.

It appears, from the results obtained in these experiments, that the FeLV fusion peptide adopts a mainly β sheet structure in the presence of liposomes that are composed of a range of different lipid species. No detectable α helix is formed in the presence of uncharged vesicles, even those containing 50 molar% PE. Very small amounts of helical peptide are detectable in both types of negatively charged proteoliposomes. Selection of distinct conformations, which depend upon the lipidic environment, is characteristic of many membrane peptides and proteins (Surewicz *et al*, 1992). It is well known that the surface pH in negatively charged vesicles is lower than in bulk solution. This can affect the binding affinity of peptides and proteins to lipid bilayers, and also the conformation adopted by the bound peptide or protein (e.g. Spuhler *et al*, 1994; Leenhouts *et al*, 1995; Dunne *et al*, 1996; Pinheiro *et al*, 1997). These four studies found that peptides, which contained negatively charged residues at their interfacial regions, showed a marked prefence for binding to anionic vesicles. This surprising discovery was explained by the creation of an increased proton concentration at the anionic surface, which would result in protonation and charge neutralisation of the negatively charged residues of the peptide, thus increasing the hydrophobicity of the peptide. The differences noted here for the FeLV fusion peptide are extremely small, however, and further studies are required to determine whether this difference is significant. The estimate of helix content for the FeLV peptide in the DOPC:DOPG sample as calculated by the method of Chang *et al* is at wide variance with that of Provencher and Glöckner, and qualitatively seems unlikely on inspection of the plotted spectrum for this sample. The DOPC:DOPG spectrum shows many features that are classicallly β in character.

Previous studies of the HIV fusion peptide have suggested that the β conformation may be the active secondary structure for fusogenic activity. Thus Nieva

et al (1994b) studied the fusion peptide of HIV type-1, LAV_{1a} strain. They found that the secondary structure of this peptide was an extended, antiparallel β structure under the same experimental conditions that enabled it to promote fusion between negatively charged LUVs. Moreover, when the HIV peptide induced leakage from vesicles rather than fusion, an α-helical structure was observed. The α helix conformation has been previously suggested to be associated with pore formation by peptides in vesicle membranes (e.g. Lear *et al*, 1988; Degrado and Lear, 1990). Nieva and co-workers thus proposed that it was the extended β structure that rendered the vesicles susceptible to fusion, and that this peptide structure was likely to reside primarily at the lipid-water interface, since in membrane proteins, transmembrane β structures tend to be the exception rather than the rule (Unwin, 1993).

Rafalski and co-workers (1990) also studied the fusion peptide of the same HIV strain. Using POPG vesicles, which do fuse in the presence of this peptide, and fairly low lipid:peptide ratios (30:1), their results demonstrated a β peptide conformation for this peptide, but at higher lipid:peptide ratios of about 200:1, the peptide adopted an α-helical structure. Furthermore, in the presence of POPC vesicles, which are not induced to undergo fusion by this peptide, the peptide adopted a β conformation, regardless of the lipid:peptide ratio.

Pereira and colleagues (1997) studied the interaction of the HIV LAV_{1a} strain fusion peptide with neutral LUVs composed of a mixture of DOPC, DOPE and cholesterol. For this vesicle system, the fusion peptide adopted an extended β structure under different experimental conditions that supported either peptide-induced vesicle fusion or vesicle leakage. Moreover, the secondary structure of the peptide was not affected by the peptide concentration, which is at variance with the results of Rafalski *et al* (1990). One important difference in the experimental protocols used by the two groups is that Rafalski and co-workers prepared proteoliposomes, whereas Pereira *et al* added their peptide to prepared pure lipid vesicles. The latter group suggest that it may be better to study the structure of a peptide after partitioning of the peptide from the aqueous phase, in order to account for any possible effects of the bilayer interface on the adopted peptide conformation. However, when peptide is added to a LUV suspension, peptide-peptide interactions

are favoured with respect to peptide-lipid interactions, and this may affect the fusogenic activity of the peptide (Martin *et al*, 1993), particularly that of very hydrophobic fusion peptides, which have a very strong tendency to self-aggregate in aqueous solutions. Self-aggregation has been noted previously by Slepushkin *et al* (1992) and by Nieva *et al* (1994a). It appears that this self-aggregation is irreversible. It has also been a serious problem when working with the FeLV fusion peptide. Another important difference in the experimental protocols used is that Pereira *et al* used a very low lipid:peptide ratio of 10:1, which further increases peptide-peptide interactions.

Work on other fusion peptides has also demonstrated a possible role for the β structure in fusion. Epand *et al* (1992) ascertained that the fusion peptide from Measles virus displayed 73% β structure, but this was at a low lipid:peptide ratio (6:1). As another example, the structure of the fusion peptide of Hepatitis B virus was examined by Rodríguez-Crespo *et al* (1996) and found to be a highly stable β sheet in the presence of negatively charged vesicles. Finally, the fusion peptide from PH-30, which is the putative fusion protein of mammalian sperm, adopted a β conformation on binding to both neutral and negatively charged lipid vesicles (Muga *et al,* 1994).

Signal sequence peptides, like fusion peptides, must insert into membranes in order to function. Reddy and Nagaraj (1989) studied certain of these sequences in a variety of solvent systems. They found that increasing amounts of β structure were seen on increasing the hydrophobicity of the peptide's environment. Moreover, a non-functional mutant peptide did not show β structure in a hydrophobic environment. Further, relatively recent support for the ability of peptides that are in a β-type conformation to destabilise membranes comes from work by White *et al* (1995) on the interaction with vesicles of the antimicrobial peptides defensins. It thus appears possible that peptides can function in a hydrophobic environment when present in a β conformation.

Conversely, a correlation between α-helical secondary structure and fusion activity has also been shown for several fusion peptides. Thus Lear and Degrado (1987) studied a 16 and a 20 amino acid peptide which corresponded to regions of the Influenza virus fusion peptide. The 20 amino acid peptide was fusogenic at low pH,

and adopted an α-helical structure when bound to POPC vesicles. Furthermore, the amount of helix formed increased at low pH. The 16 amino acid peptide neither adopted a helical structure nor promoted vesicle fusion.

Takahashi (1990) studied various synthetic peptides which were closely related to the Influenza virus fusion peptide. Each of the peptides that could promote vesicle fusion adopted an α-helical conformation when bound to lipid membranes.

Lüneberg *et al* (1995) also demonstrated that the Influenza virus fusion peptide adopted an α-helical conformation upon insertion into lipid bilayers, as did Gray and co-workers (1996). The latter group studied several fusogenic and non-fusogenic mutants of this peptide as well. They found that the non-fusogenic mutants had larger β/α ratios, with the non-fusogenic mutants having about 50-60% β structure.

Rafalski *et al* (1991) investigated the secondary structure of the Influenza virus fusion peptide and also the 2 mutant peptides, E1 and E4, which were studied in whole virus work by Gething and co-workers (1986) (see Chapter 1). They correlated the adoption of an α-helical structure with the promotion of fusion between LUVs by these peptides.

Martin *et al* (1993, 1996) studied the fusion peptide of HIV. In contrast to the results of Nieva and co-workers (1994b) described above, an α-helical structure was seen after interaction of the fusion peptide with LUV: the HIV peptide adopted 99% β sheet and 0% α helix in dimethylsulphoxide (DMSO), but 25% α helix in the presence of LUVs. Similarly, Martin and co-workers demonstrated that the fusion peptide of SIV also adopts an α-helical structure under experimental conditions which enable it to promote fusion of both SUVs (1991) and LUVs (1994).

Clearly there is conflicting evidence as to the active secondary structure of viral fusion peptides. Whilst it is quite possible that distinct viral fusion peptides adopt different fusogenic conformations, due to differences in their primary structures, the results of certain studies that were performed on the same fusion peptide by different research groups provide opposing ideas on the active secondary structure of that particular peptide. This may be due to a lack of a systematic approach. Thus individual research groups use different experimental protocols: the types of lipids and

vesicles, the lipid:peptide ratio, the presence or absence of cations and the lengths of peptide fragments can all alter the dominant secondary structure of a fusion peptide. Moreover, filtration, or density flotation and centrifugation, to remove the non-lipid bound peptide is essential if the recorded spectrum is to be assigned purely to the membrane-associated peptide.

The proteoliposomes that were used in this study of the FeLV peptide's conformation were prepared by extensive dialysis. This should have removed any free peptide molecules, unless they had aggregated into very large masses. In view of the fact that proteoliposomes were prepared, and thus the peptide and lipid were dried down together to form a film, it seems unlikely that large peptide aggregates would be present. However, the lipid:peptide ratio was low, which does tend to increase peptide-peptide interactions. In the absence of electron microcopy studies of the samples, or re-examination of the same samples after filtration or centrifugation, it is not possible to exclude fully the possibility that some of the peptide present was in the form of peptide aggregates that were closely associated with the membrane surface. Further studies are required in order to determine the active secondary structure for this fusion peptide more definitively. Specifically, variation of the lipid:peptide ratio would be useful, since an increase in this ratio will tend to favour partitioning of the peptide into the membrane. This may alter the proportions of the different secondary structures present in the peptide population. Examination of samples before and after filtration, or density flotation and centrifugation, to determine any changes in the relative amounts of the different secondary structures present would also be necessary, and the use of Fourier transform infrared spectroscopy (FTIR) would be very helpful, as this technique is much more accurate than CD at estimating the β content of a sample, and, unlike CD, it is not affected by light scattering by vesicles.

The amino acid sequences of many fusion peptides suggest that these peptides may show particular diversity in their range of possible secondary structures (Callebaut *et al*, 1994). In order to examine this hypothesis, the secondary structure of the FeLV fusion peptide was determined in a variety of solvent systems of varying hydrophobicity.

The far ultraviolet CD spectra of the FeLV fusion peptide in the various solvents are shown in Figure 6.11. Once again, satisfactory data could only be obtained down to 195nm. The CD spectra exhibit an increase in α-helical character on changing from 1M guanidine/25% ethanol, through a selection of increasingly hydrophobic solvents, to 50% HFIP. In the guanidine/ethanol sample, the peptide produced a CD spectrum that was characteristic of random coil secondary structure. This is to be expected for a hydrophobic peptide in a polar solvent that contains a chaotropic agent. Short peptides are usually unordered in aqueous solution because of strong water-peptide backbone interactions. To minimise these interactions, and to mimic the environment within a lipid membrane, surfactants or organic solvents are used.

SDS micelles provide a similar anisotropic environment to lipid vesicles (Tanford and Reynolds, 1976). Wu and Yang (1978) studied the structure of a number of peptide hormones in solutions of SDS micelles. Whilst this detergent promoted secondary structure formation, it did not do so indiscriminately: the secondary structure that was adopted by a peptide closely agreed with that predicted from its amino acid sequence. SDS micelles are a system now widely used to study peptide-lipid interactions (e.g. Hoyt and Gierasch, 1991; Li and Deber, 1994). The critical micellar concentration (CMC) of SDS is 8mM at 20°C. In 3mM SDS, the peptide's CD spectrum is typical of a β sheet, but as the SDS concentration increases towards the CMC, the spectrum indicates that some α-helical structure is present.

It is generally accepted that TFE does not induce helical structure; rather it stabilises helices in regions with an existing α-helical propensity (Segawa *et al*, 1991). TFE also stabilises β structures (e.g. Lu *et al*, 1984). 50% TFE is quoted as the concentration of TFE at which complete helicity of a peptide is obtained (Jasanoff and Fersht, 1994). The CD spectrum of the FeLV fusion peptide in 50% TFE shows considerably more α-helical character (~20% α helix) than that seen in SDS. Slepushkin *et al* (1992) found that the HIV fusion peptide adopted approximately 32% α helix in pure TFE. The proportion of helix formed by the FeLV peptide is even more pronounced in 50% HFIP, the most hydrophobic solvent system used in this study. Analysis of the spectra gives the percentages of α helix and β sheet in each

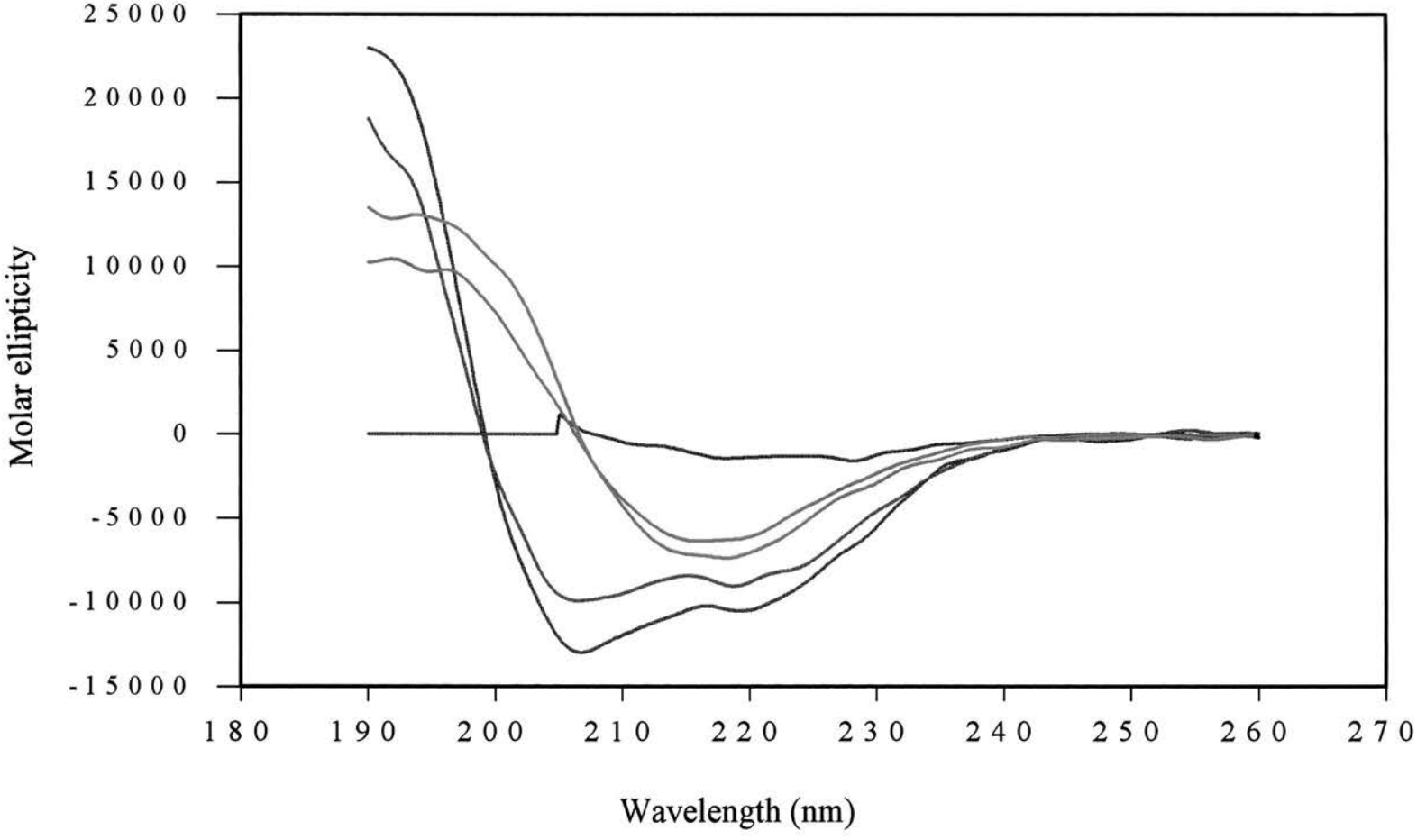

Figure 6.11. CD spectra of the FeLV fusion peptide in a variety of solvents. a) in 1M guanidine/25% ethanol (green line); this data has been zeroed below 205nm; b) in 50% TFE (red line); c) in 50% HFIP (blue line); d) in 3 mM SDS (pink line), and e) in 6 mM SDS (cyan line).

sample listed in Table 6.2. As mentioned for the liposomal samples, the exact values of these estimates should be viewed with caution, particularly those of the β sheet. However, an overall trend from random coil, through predominantly β sheet, to significant amounts of α helix can clearly be seen.

Figure 6.12 shows electron micrographs of (a) FeLV peptide in 3mM SDS (b) FeLV peptide in 50% HFIP and (c) a negative control, namely a stained empty grid. β fibrils are visible in the 3mM SDS sample, and these were only seen when there was little evidence of α-helical content by CD spectroscopy (other data not shown). These β fibrils appeared long and unbranched and were arranged in a meshwork.

FTIR has been used to study the secondary structures of the fusion peptides of two other retroviruses: SIV (Martin *et al*, 1991, 1994) and HIV (Martin *et al*, 1993). These peptides were found to show a partial conversion from a β sheet conformation in an aqueous solvent to an α helix in a lipid environment. Moreover, the amount of α helix present was found to be proportional to the lipid:peptide ratio. In view of this finding, and since the conversion from sheet to helix is incomplete, they suggested that there might be two populations of peptide, one of which penetrated the lipid bilayer, whilst the other remained in the aqueous phase. (One serious drawback to CD and FTIR is that they are incapable of distinguishing between a single population of peptide, in which each individual peptide molecule has a varied secondary structure along its length, and the presence of two distinct peptide populations, each with its own distinct structure, the average of these yielding the same overall percentages for the different secondary structure components as the single mixed population.) Martin and co-workers (1991) argued that it was hard to believe that two well-defined secondary structures could co-exist within the same short sequence. Consequently the assumption from their SIV and HIV studies was that the α-helical form is the single, fusion-active conformation. This view has, however, been questioned recently (Gray *et al*, 1996; Chang *et al*, 1997).

Gray and co-workers found that the wild type fusion peptide of Influenza virus contained about 40% α helix and about 30% β structure when bound to POPC SUV at pH 5.0. They suggested that, whilst a minimum number of residues in an α-helical conformation did appear to be important for the fusion activity of the Influenza virus

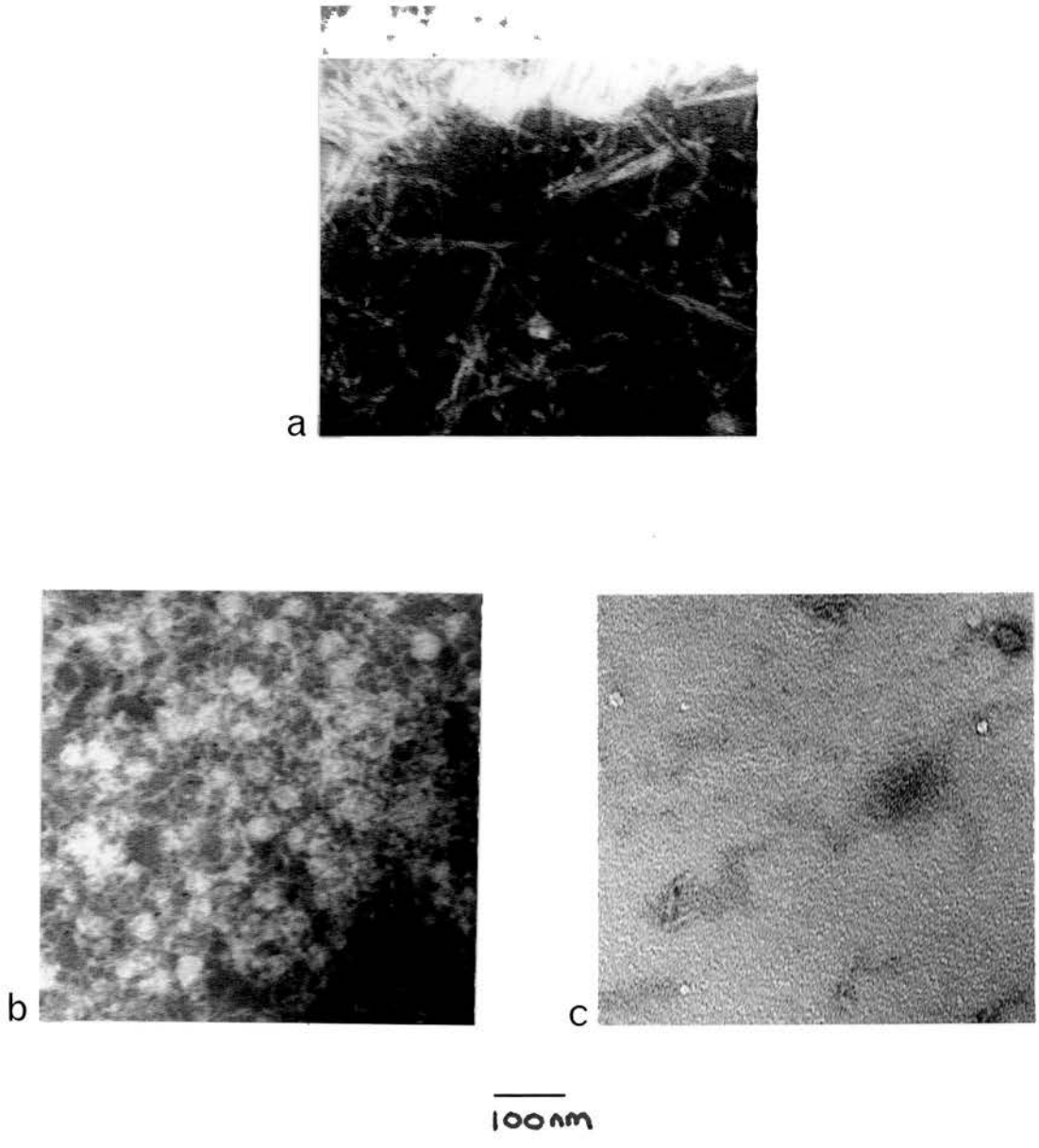

Figure 6.12. Electron micrographs of a) FeLV peptide in 3 mM SDS, showing β fibres, b) FeLV peptide in 50% HFIP and c) stained grid control.

fusion peptide (e.g. Lear and Degrado, 1987), a certain amount of β structure may also be required. Chang *et al* (1997) found that the HIV-1 fusion peptide inserted into SDS micelles primarily as a helix (59%), but with substantial β structure present concurrently (27%). They also used spin-label-attenuated ^{1}H NMR to study peptide insertion and structure, and showed that the N-terminal portion of the fusion peptide formed a helix, whilst a flexible hinge region was present at positions 15 and 16. This hinge region was located at the micelle surface. Furthermore, the amino acids present at positions 15 and 16 (Ala and Gly) are absolutely conserved between all strains of HIV-1 and HIV-2 (Myers *et al*, 1994). Possibly the peptide sequence following the hinge region, which is on the micelle surface, may adopt a β conformation.

It is clear that a balance between α and β structure exists for many fusion peptides, including the FeLV peptide, and this might allow these peptides to adopt both α and β structures in different segments of the sequence. It also enables the peptides to change their conformation in response to environmental changes.A previous study has indeed demonstrated conformational flexibility for a synthetic, 21 amino acid peptide when it was inserted in a lipid bilayer (Vogel *et al*, 1988). However, this flexibility was between a variety of different substructures, while the conformation of the peptide as a whole remained predominantly helical.

Fusion is an extremely rapid, multi-step process, and so structural measurements are obtained mainly from fusion end products. Thus only the final, equilibrium conformations of the peptide are observed; none of the intermediate structures and changes in conformation, which occur during the different stages of fusion, are seen. It is possible that structural flexibility, rather than the rigid adoption of a particular secondary structure, is a key property of fusion peptides. In other words, since membrane fusion is a dynamic process which involves large structural changes in the participating molecules, a critical feature of these catalytic peptides may be their ability to 'flip' between different secondary structures extremely rapidly, rather than, or as well as, the adoption of any single, well-defined secondary structure. The energy barriers between these different secondary conformations must be low: the peptide must be able to adopt, at least transiently, these various structures, which presumably represent local energy minima. Logically this leads to an examination of

the amino acid sequence of a fusion peptide, in order to attempt to predict the most likely secondary structure of that peptide.

Waterhous and Johnson (1994) suggested in 1994 that the current *a priori* predictions of secondary structure from amino acid sequence were about 70% accurate. Little has changed since then. Problems arise because it is still not possible to identify and estimate definitively all of the different energetic factors in a system that lead to the adoption of a particular secondary structure by a peptide or protein molecule.

Wu and co-workers (1982) first suggested that peptides in lipid solutions could adopt either an α or a β conformation, depending upon the secondary structure forming potential of the peptide in aqueous solution. Thus Val and Ile, which are β branched residues, strongly favour β sheet formation in soluble proteins (Chou and Fassman, 1987). Similarly Gly and Pro are helix-breaking residues in globular proteins. Ala has a certain 'plasticity', so it can be easily fitted into various structural contexts. Using the Chou-Fassman method of analysis, the FeLV fusion peptide is predicted to form mainly β sheet (data not shown).

Many membrane-active peptides gain secondary structure on partitioning into membrane interfaces. The membrane interface is about 15Å thick, and comprises a thermally disordered mixture of water and headgroups and methylenes from the edges of the hydrocarbon core (Wiener and White, 1992). Work by Li and Deber (1994) demonstrated that the factors affecting the propensity of a particular amino acid residue to form an α helix may be different within a hydrophobic environment compared to that seen under aqueous conditions. They identified that there was a definite bias towards the residues Gly, Val, Ile and Thr in membrane-spanning regions. Thus, for example, the bacteriophage M13 contains 3 Gly and 9 β-branched residues (Ile, Val, Thr) in its 19 residue effective transmembrane segment (Deber *et al*, 1993). Certainly many viral fusion peptides, including that of FeLV, have an abundance of these 3 types of amino acid residue. Experiments described by Li and Deber (1994) suggested that the flexibility of Gly may be greatly constrained within a bilayer, and the amino acid sequence surrounding a Gly has a great influence on its helix-forming potential. This may explain how fusion peptides such as the FeLV

fusion peptide manage to have a large number of Gly residues and still form helical structures. Richardson and Richardson (1989) noted that a Pro residue is preferred at the N-cap + 1 position of an α helix, where it presumably acts as a helix initiator. Despite the original supposition that Pro acts as a helix-breaking residue, Rodríguez-Crespo and co-workers (1996) found that the fusion peptide of Hepatitis B virus formed a significant amount of α helix in TFE, and this peptide has a Pro residue situated about two thirds of the way along the peptide. The FeLV fusion peptide also has a Pro residue, at position 2. Charged groups may play a critical role in stabilising the formation of helices by isolated peptides (Shoemaker *et al*, 1997). In particular, interactions between the charged groups and the helix macrodipole influence the stability of the helix. Acidic residues occur preferentially near the amino terminus but not near the carboxy terminus. The FeLV fusion peptide has an acidic glutamate residue at its N-terminal, and the first residue following its C-terminal is a basic lysine. It seems that these various factors may well be important for the FeLV fusion peptide, on examination of its sequence, and possibly the Chou-Fassman method is not the most suitable one to use, although it is still quoted in many publications on viral fusion peptides. Accordingly, a different and more recent computer programme, PHDsec, was used to attempt to predict the secondary structure-forming potential of the FeLV fusion peptide. The method of PHDsec is described in Rost and Sander (1993). This programme also predicted a mainly β structure for this peptide. Whilst both of these programmes that have been used may not be ideal, it does seem as if the FeLV fusion peptide has a certain propensity to form β structure, which agrees with the experimental findings for this peptide in liposomal systems.

Figures 6.13 and 6.14 show the FeLV fusion peptide modelled as an α helix, whilst Figure 6.14 also shows it adopting a β strand structure. It is clear, on examination of the depicted α helices, that the FeLV fusion peptide does not adopt the 'sided', amphipathic helical structure that has been suggested as being the crucial peptide structure which confers fusogenic activity (e.g. Harter *et al*, 1989; Blobel *et al*, 1992). [An amphipathic helix has opposing polar and non-polar faces along the long axis of the helix (Segrest *et al*,1974)]. Gallaher and co-workers (1992) noted previously that several putative retroviral fusion peptides only presented a completely

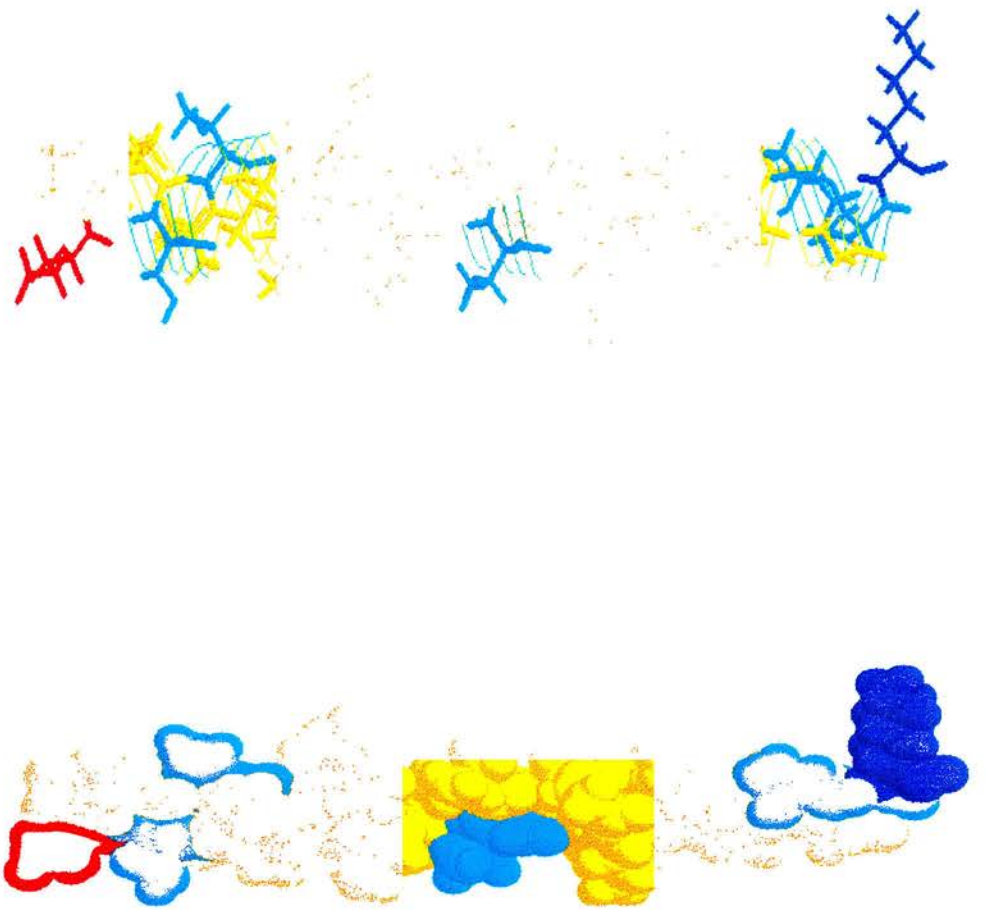

Figure 6.13. FeLV fusion peptide modelled as an alpha helix. Hydrophobic residues are shown in , polar residues in cyan, acidic in red and basic residues in blue. The top model shows the backbone structure, whilst the lower diagram is a space-filling model of the peptide. Peptides modelled using Raswin.

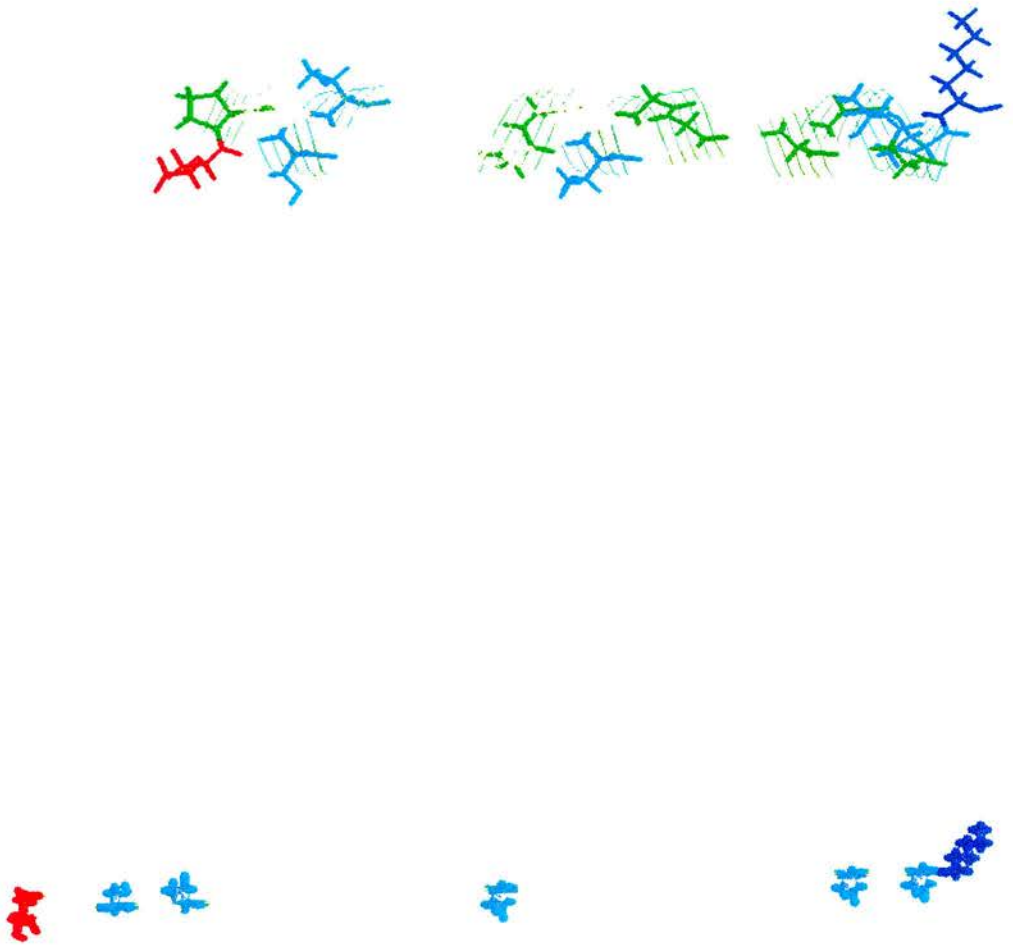

Figure 6.14. FeLV peptide modelled as an alpha helix, with Pro and Gly, the helix-breaking residues in the Chou-Fassman analysis, coloured green in the top diagram. Using this scale of helix-forming potential for amino acid residues, it can be seen that there is little scope for helix formation for the FeLV fusion peptide. The lower diagram shows the FeLV fusion peptide modelled as a beta strand. Modelling performed using Raswin.

hydrophobic face over three turns of a helix. Murata *et al* (1993) have suggested that the uneven distribution of side-chain bulkiness around the helix may be crucial to its functional capacity, but Gallaher and co-workers pointed out that, for the same retroviral fusion peptides, bulky, hydrophobic residues were located on the less hydrophobic side of the helix. It is certainly unlikely that the acidic Glu residue of the FeLV fusion peptide, which is negatively charged at pH 7.4, is inserted near to the hydrophobic region of the target membrane. According to the interfacial hydrophobicity scale of Wimley and White (1996), Glu shows a very low tendency to partition into the bilayer. Much still remains to be elucidated as regards this peptide's structure on interaction with a lipid membrane.

It is also important to remember that it is possible that the structures adopted by any isolated peptide are not the same as those adopted by it when it is present in the entire glycoprotein molecule. As an example, hydrophobic interactions between the fusion peptide and other neighbouring domains of the fusion protein may be important in stabilising a particular secondary structure of the fusion peptide after it is activated and before it interacts with the target membrane. Oligomerisation of viral fusion proteins is also believed to play an essential role in their mode of action. Such specific cooperation is unlikely in a simple peptide model. A major practical problem is the tendency for massive self-aggregation of these isolated hydrophobic peptides, which would be restricted naturally when they formed part of a whole glycoprotein molecule. Finally, other factors may also be equally as important as the secondary structure of the peptide for the promotion of fusion. As mentioned in Chapter 5, the orientations of fusion peptides with respect to the lipid bilayer have been studied (e.g. Martin *et al*, 1991, 1993, 1994; Lüneberg *et al*, 1995; Ishiguro *et al*, 1996) and these results suggest a role for this factor in the fusion process, although, like the secondary structural work, there are several conflicting results.

There is no doubt that the secondary structure is crucial to the functioning of fusion peptides. As an example of this, Lear and Degrado (1987) observed that, whilst the fusion peptide region of Influenza virus HA2 shows about 65% homology between different Influenza strains, the nature of each residue, that is whether it is hydrophobic, acidic or small, is absolutely conserved and occupies an invariant

position in the aligned peptide sequences. Similarly, Bosch *et al* (1989) studied various mutant fusion peptides from SIV, and found that mutations which increase the overall hydrophobicity of the peptide enhance virus-induced cell fusion reactions, whereas polar substitutions reduce or abolish the fusogenic activity of this peptide. The importance of a specific sequence is well illustrated in the FeLV fusion peptide, as this sequence is totally conserved for all known FeLV strains (see Chapter 1). Nonetheless, despite an appreciation of the fundamental importance of secondary structure, the precise conformational features of a fusion peptide that are required for its fusion activity are still only partially understood.

In conclusion, the results of the CD studies described in this chapter provide direct experimental proof of structural flexibility for the FeLV fusion peptide, which had been previously suggested by a computer modelling study (Callebaut *et al*, 1994). No definitive conclusion can be drawn as to the active secondary structure of this fusion peptide, however; more experiments are required before this can be decided with reasonable certainty.

Chapter 7: Investigation of the ability of the Putative Fusion Peptide of Feline Leukaemia Virus to promote Fusion

Fusion Studies

7.1 Theoretical Background to Lipid Mixing as a Fusion Assay

Complete fusion between two cells or vesicles involves the merging of their lipid membranes, followed by the mixing of their aqueous contents (see Chapter 1, Figure 1.1). As mentioned in Chapter 1, liposomes are a useful model cell system, and they are used extensively in fusion assays.

The fusion between lipid membranes can be followed using the principle of resonance energy transfer (RET) (see Figure 7.1). RET depends upon the transfer of fluorescent energy from a donor lipid molecule to a different acceptor lipid molecule. A fluorescent molecule is excited by absorbing a photon of energy from electromagnetic radiation of a precise wavelength, which is characteristic for that fluorophore. A very short time later it then re-emits this energy, at a characteristic but different wavelength. Thus if there are two chemically distinct fluorescent molecules present in a lipid bilayer, and if the emission wavelength of the first fluorophore is the same as the excitation wavelength of the second, then the first can act as a donor of fluorescent energy to the second, acceptor molecule (Forster, 1949). It is then possible to excite the donor with radiation of the appropriate wavelength and to measure the transfer of fluorescent energy to the acceptor by monitoring the emission of the latter, always provided that sufficient acceptor molecules are nearby in the bilayer. The efficiency of energy transfer between two given fluorophores depends upon their spatial separation (Fung and Stryer, 1978). If both donor and acceptor molecules lie close together within a membrane, resonance energy transfer can be almost 100%.

The incorporation of known percentages of both fluorophores into the same lipid bilayers of a liposome population enables measurement of fusion with a population of unlabelled liposomes. In the event of cell fusion occurring, the surface density of the fluorescent lipids will be reduced, as a labelled bilayer merges with an unlabelled bilayer. This method is called 'probe dilution'. The donor and acceptor fluorophores will then be less close to each other, and less RET will occur, with a resultant decrease in emission by the acceptor. Concurrently, emission by the donor

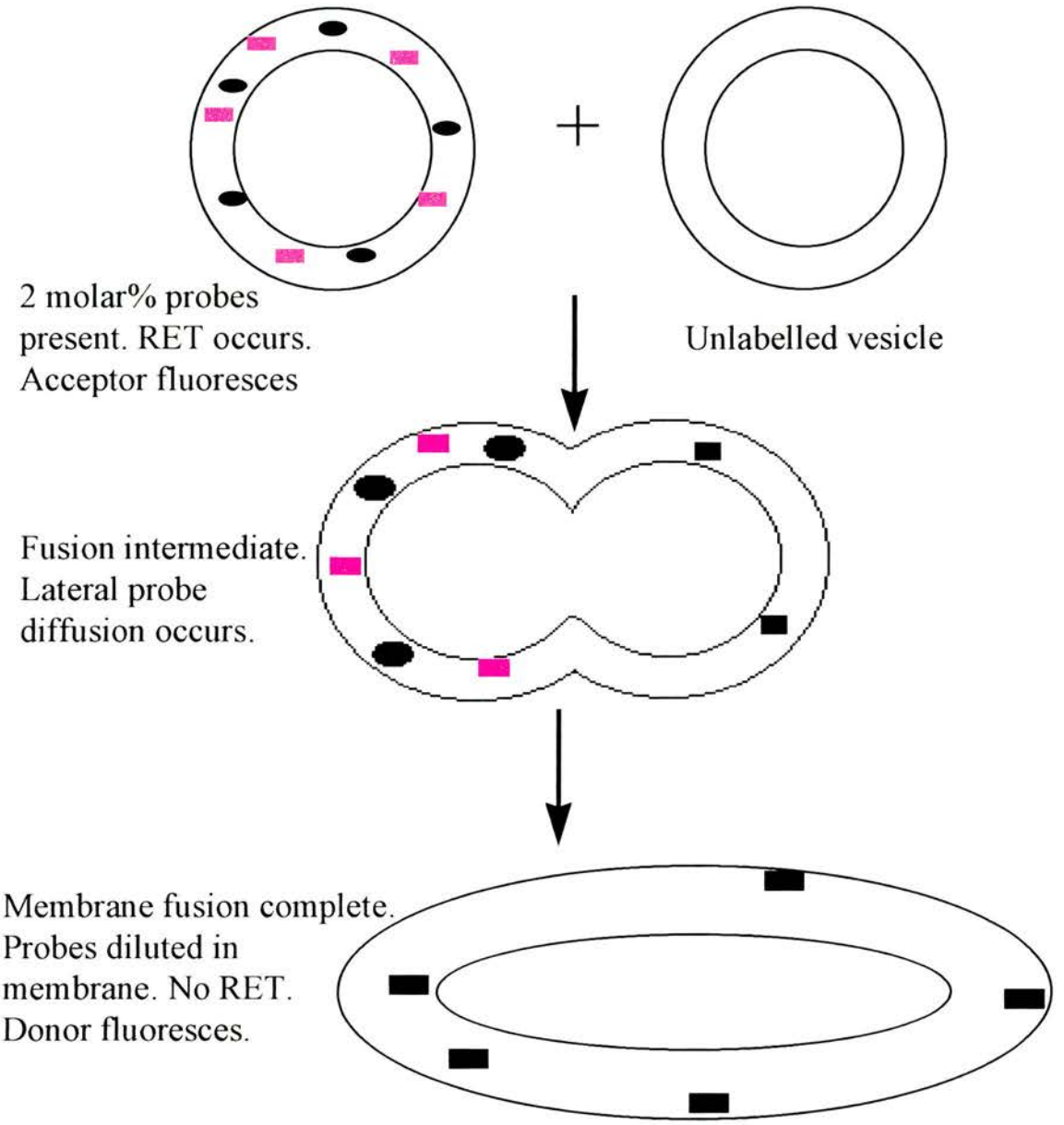

Figure 7.1. The principle of resonance energy transfer (RET), which is the transfer of fluorescent energy from a donor lipid molecule (shown in pink) to an acceptor lipid molecule (shown in). If both donor and acceptor lipids lie close together within a membrane, RET can be almost 100%. If both are incorporated into one set of liposomes, and if fusion occurs with unlabelled liposomes, the fluorescent lipids will be diluted. The donor and acceptor will then be less close together, so less RET will occur, and thus the emission by the acceptor lipid will decrease. Concurrently, emission by the donor lipid will increase.

molecules will increase, as less energy transfer has occurred. Usually the increase in donor fluorescence is used as the measure of fusion of the lipid membranes. Control experiments have shown that it is fusion which causes the observed changes in RET and not non-specific processes, such as lipid exchange between bilayers (e.g. Roseman and Thompson, 1980; Nichols and Pagano, 1981).

Struck *et al* (1981) developed an RET assay for liposome-liposome fusion, using the fluorophores L-α-*N*-(4-nitrobenzo-2-oxa-1,3-diazole) (NBD) as the fluorescent energy donor and L-α-*N*-(Lissamine-Rhodamine B Sulfonyl) (Rh) as the acceptor. These were attached to the free amino group of separate PE molecules to produce fluorescent lipid analogues, which were then easily incorporated into lipid bilayers of vesicles. The efficiency of RET, E, was then shown to be calculated from the emission of NBD-PE at 530nm, using the equation:

$$E = 1 - \frac{F}{F_0} \qquad 7.1$$

where F is the fluorescence at 530nm in the presence of Rh-PE and F_0 is the fluorescence in the absence of Rh-PE and in the presence of 1% Triton-X, a detergent which lyses the vesicles. It is vital to correct the value for the quantum yield for any effect of Triton-X on this parameter, and also for sample dilution. The effect of Triton X-100 on the quantum yield of NBD-PE can be determined by incorporating NBD-PE into vesicles at a concentration where essentially no self-quenching occurs, in the absence of Rh-PE, and measuring fluorescence before and after the addition of Triton X-100. Rates of fusion between vesicles can thus be followed by measuring the change in fluorescence at 530nm as a function of time.

This assay enables membrane mixing to be measured with high kinetic resolution. There is a significant overlap between the emission band of NBD-PE and the excitation band of Rh-PE, so RET is relatively efficient, even when the probes are present at low surface densities. Moreover, Rh-PE has a minimum in its excitation spectrum at 450nm, which is close to the maximum excitation wavelength of NBD-PE. Thus there is very little direct excitation of the energy acceptor, Rh-PE. At low

surface densities of Rh-PE, the efficiency of energy transfer was found to be nearly proportional to the ratio of Rh-PE to total lipid in the vesicle bilayer. In this concentration range, therefore, any decrease in the surface density of the energy acceptor will result in a proportional decrease in measured transfer efficiency. The efficiency of energy transfer was found to be independent of the surface density of the energy donor, a situation which is similar to that found for other donor-acceptor pairs (e.g. Vanderwerf and Ullman, 1980).

The RET assay of Struck and co-workers (1981) is widely used for monitoring liposomal fusion. In addition to the points mentioned above, RET is a fairly simple, very sensitive method, as it requires only low concentrations of lipid probes. It enables lipid mixing to be monitored continuously, which allows kinetic studies to be performed. Whilst some fluorescent probes perturb the packing properties of the lipid bilayer, NBD-PE and Rh-PE do not *per se* cause perturbation of the bilayer, since they protrude into the interface. Furthermore, head-group labelled lipid analogues such as these are essentially non-exchangeable by spontaneous or collision-mediated transfer between vesicles. Their quantum yields are also relatively insensitive to their micro-environment. By performing a probe dilution type of lipid mixing assay, any error due to RET occurring during vesicle aggregation, as opposed to fusion, is avoided. Finally, lipid mixing assays in general are unaffected by leakage, which usually does occur during vesicle fusion and which often interferes with assays that are based on contents mixing.

Ideally, fusion should be studied by the measurement of both the lipid mixing and the mixing of contents, which occur in complete fusion. This provides a more detailed description of the molecular events that are occurring and also helps to reduce possible artefacts. As an example, hemifusion, that is the fusion of only the outer monolayers of LUVs, will produce a decrease in RET. On the other hand, fusion of liposomes is often leaky, and then contents mixing cannot be studied. Often, therefore, lipid mixing alone has to be relied upon to monitor the fusion process, and certainly lipid mixing assays are usually the initial types of fusion experiments to be performed when studying a potential fusogen.

Fusion activity can be confirmed either by demonstration of the fusion activity *in vitro* from the purified candidate protein or peptide, or by expression of fusion activity following transfection of the cloned gene(s) encoding the candidate fusion protein or peptide (White, 1990).

Synthetic peptides corresponding to the N-terminal segment of the Influenza virus HA2 were shown to interact with lipid bilayers and to promote fusion of lipid vesicles (e.g. Lear and Degrado, 1987; Murata *et al*, 1987; Wharton *et al*, 1988; Rafalski *et al*, 1991). Similar observations have since been made with the fusion peptides from the retroviruses SIV, HIV-1, MuMLV and BLV (e.g. Rafalski *et al*, 1990, HIV-1; Martin *et al*, 1991, SIV; Defrise-Quertain *et al*, 1992, BLV; Nieva *et al*, 1994b, HIV-1; Pereira *et al*, 1995, HIV-1; Martin *et al*, 1996, HIV-1; Pereira *et al*, 1997, HIV-1; Zhu *et al*, 1998, MuMLV). Several mutational studies have also implicated the amino terminus of retroviral TM proteins as being important in catalysing the fusion of viral and cellular membranes (e.g. Bosch *et al*, 1989, SIV; Schaal *et al*, 1995, HIV type-1; Delahunty *et al*, 1996, HIV type-1). Furthermore, studies of the wild type and certain mutant fusion peptides from Influenza virus by Gething and co-workers (1986), Düzgünes and Gambale (1988) and Wharton *et al* (1988) and Rafalski and co-workers (1991), and from certain HIV strains by Martin *et al* (1991) and Freed *et al* (1990) have correlated the fusogenic activity of the synthetic fusion peptides *in vitro* with that of their corresponding parent glycoproteins *in vivo*. Similarly, Düzgünes and Shavnin (1992) found an increase in membrane destabilisation produced by the fusion peptide of Sendai virus at low pH, which correlated with the enhanced fusion at low pH of whole Sendai virus with various liposomes (e.g. Nir *et al*, 1986) and of one Sendai virus isolate with cultured cells (Pedroso de Lima *et al*, 1991).

It can, therefore, be seen that synthetic fusion peptides are widely employed to study the basic molecular mechanisms of virally-induced fusion, and that the results obtained from these studies often show good correlation with the corresponding biological fusion process. Synthetic peptides are particularly useful for the determination of the minimum and precise molecular requirements of fusion. In particular, the demonstration of fusion activity by the amino-terminal region of a TM

protein from a virus requires that this be studied in isolation from the rest of the protein molecule, as other regions of certain viral fusion proteins have been shown to enhance fusion (e.g. Lear and Degrado, 1987, HA2).

7.2 Aim of the Fusion Assays

The sequence of the FeLV fusion peptide is recorded in the Swiss Protein Data Bank (1996; release number 34.0). This sequence is, however, the putative fusion peptide of FeLV, since there is no experimental evidence for fusogenic activity of this peptide. It does show marked homology to other known fusion peptides of viruses, and it is an N-terminal segment that is released by proteolytic activation of the fusion protein, which is also a feature shared with several other viral fusion peptides. The aim of the fusion assay was thus to provide direct experimental evidence for the fusogenic capacity of this peptide.

7.3 Materials and Methods

7.3a Materials

Previous fusion studies using synthetic peptides corresponding to the fusion peptides from the retroviruses HIV (Martin *et al*, 1993), Bovine leukaemia virus (BLV) (Defrise-Quertain *et al*, 1992) and SIV (Martin *et al*, 1994) have shown that these peptides can induce lipid mixing between LUVs when the vesicles contain PE. The lipid MeDOPE was chosen for the fusion assays of the FeLV peptide, since its use in such assays has been well-documented (e.g. Ellens *et al*, 1984; Ellens *et al*, 1986). Furthermore, its use in the ^{31}P NMR experiments described in Chapter 3 might enable some comparisons to be drawn between certain membrane destabilising effects and the fusion activity of the FeLV fusion peptide. Ideally, the use of similar types of vesicles when comparing structural characteristics with fusion processes is preferred. It is, however, often very difficult to obtain sufficiently large signals from LUV preparations in a reasonable timespan to allow their use in structural studies. Thus it

must always be borne in mind that there will be inherent differences in the lipid preparations, which may influence the results obtained during these experiments.

MeDOPE was purchased from Avanti Polar Lipids (Alabaster, AL, USA). Thin Layer Chromatography showed a single spot. The fluorescent lipids L-α-*N*-(4-nitrobenzo-2-oxa-1,3-diazole)PE from egg (NBD-PE) and L-α-*N*-(Lissamine-Rhodamine B Sulfonyl)PE from egg (Rh-PE) were also purchased from Avanti. DMSO was obtained from BDH Chemicals (Toronto, ON). The FeLV 28 amino acid and SIV 12 amino acid peptides were synthesised by Albachem Ltd. (26 Craigleith View, Edinburgh, EH4 3JZ, Scotland, UK) using solid phase synthesis. Their purities were >95%, as determined by analytical HPLC, Maldi-Tof Mass spectrometry and amino acid analysis. The FeLV fusion peptide sequence was as shown in Chapter 2 (section 2.4a). The SIV fusion peptide was chosen as a positive control since it is the most homologous retroviral fusion peptide for which there is definite experimental proof of fusogenic activity.The SIV peptide sequence used in these experiments was GVFVLGFLGFLA. This has been shown previously to promote lipid mixing, and thus membrane fusion (Martin *et al*, 1994). The buffers used for the RET assays were 10mM Glycine, 0.1mM NaCl, 0.1mM EDTA for the pH 9.5 buffer and 10mM Hepes, 0.15M NaCl, 1mM EDTA for the pH 7.0 buffer.

7.3b Liposome Preparation

Lipid films were prepared as described in Chapter 2, using pure MeDOPE for the unlabelled LUVs, and with 2 mol% of both NBD-PE and Rh-PE present for the labelled LUVs. The dried lipid films were suspended initially in an iso-osmotic Glycine buffer at pH 9.5, at a lipid concentration of 20mg/ml. Liposomes were then prepared from these suspensions.

It is difficult to prepare stable liposomes of PE at the physiological pH of 7.4 in isotonic buffers (Papahadjopoulos and Miller, 1967). Pure PE liposomes can only be made above pH 9.0, where the PE is negatively charged (Stollery and Vail, 1977). The pK_a of the amine group of PE has been estimated to be about 9.5 (Tsui *et al*, 1986). Thus, injection of PE liposomes into buffers of pH 6, where the PE is protonated, leads to liposomal aggregation, leakage and lipid mixing (Kolber and

Haynes, 1979; Pryor *et al*, 1983). By raising the pH, the amine group becomes deprotonated and so the stability of the liposomal suspension is greatly improved. Aggregation, and thus possible fusion or collapse, of the liposomes is prevented by the liposomes carrying a sufficiently large net negative charge, which causes charge repulsion between liposomes.

True 'model membrane' systems require that the vesicles present be closed, unilamellar and reasonably large to avoid problems associated with small, highly curved systems (Hope *et al*, 1985). The high degree of curvature of SUV and their intrinsic instability seem to facilitate peptide penetration and they may also provide a driving force for fusion processes. Small vesicles may have phospholipid packing defects that render them more susceptible to fusion (e.g. Wilschut *et al*, 1981; Düzgünes, 1985; Parente *et al*, 1988; Stegmann *et al*, 1989). Thus, although fusion reactions that are catalysed by viral fusion peptides in SUV systems do reveal peptide-induced bilayer destabilisation, they do not necessarily reflect the intrinsic fusogenicity of the particular peptide. It is generally thought to be essential to investigate the fusion activity of fusion peptides using large, unilamellar vesicles.

On the other hand, Ott and Wunderli-Allenspach (1994) studied fusion between Influenza virus and liposomes of varying size. They concluded that the kinetics of fusion between virus and SUVs and between virus and LUVs were identical. This agrees with data obtained by Van Meer *et al* (1985) on Influenza virus and by Sarkar and Blumenthal (1987) on Sendai virus fusion. It is possible, therefore, that the choice of LUVs for fusion assays is less important than is currently widely believed, but it is certainly less physiological to study fusion between SUVs. LUVs were thus used in the assays described in this chapter, since the curvature of these vesicles more closely resembles that of the plasma membrane.

After vigorous vortexing in the pH 9.5 glycine buffer on an orbital incubator, the resulting lipid suspensions were subjected to five freeze-thaw cycles, in each of which immersion in liquid nitrogen for two minutes was followed by plunging into a water bath, at a temperature of 40°C to 60°C, until the samples thawed. Repeated freeze-thaw cycles rupture and re-fuse any MLVs present, which results in the production of some LUVs (New, 1990). A certain amount of fusion between

individual liposomes also occurs, so that the average size of the vesicles increases as well as the proportion of unilamellar vesicles (Hope *et al*, 1985; New, 1990). Next the samples were filtered under high pressures of ~ 400 lb/in^2 through two stacked polycarbonate membrane filters, of pore size 0.1μm, (Nucleopore Corp., Pleasanton, CA, USA), using a high pressure extruder (Lipex Biomembranes Inc., Vancouver, Canada) to yield LUVs. The samples were injected into the central chamber of the extruder, above the stacked polycarbonate membranes, and nitrogen pressure was applied from a standard gas cylinder that was fitted with a high pressure regulator. The vesicles were collected and reinjected for extrusion for a total of 10 passes through the filters. Once prepared, the liposomes were stored under refrigeration, in air-tight glass containers, preferably under nitrogen. Deterioration of the preparation, most commonly lipid oxidation and peroxidation, does occur with time, so that it is recommended that liposomes be used within 2 days (Ellens *et al*, 1989; Allen and Cleland, 1980). All of the LUVs were thus used within 48 hours of their preparation.

The extrusion method of Hope *et al* (1985) for the preparation of LUVs has many advantages. Extrusion does not require the presence of organic solvent or detergent, whereas the dialysis method of LUV production cannot completely remove these contaminants. Dialysis is lengthy; for example, the detergent dialysis procedure using octylglucoside that was discussed in Chapter 6 required days of dialysis, whilst extrusion is a very rapid procedure. Extrusion also produces a population of LUVs that are of a fairly homogeneous size.

In order to ascertain the lamellarity of the extruded LUVs, negative staining transmission EM and cryo-transmission EM were performed. The two-step drop method was used for the negative staining proceedure (New, 1990). A drop of bacitracin was placed on a coated EM grid, and removed 1 minute later using a piece of filter paper, which was held just touching the edge of the grid and at 90° to its plane. The grid was then covered with a drop of the liposome sample and left for 2 minutes to allow the vesicles to stick to the grid. Thereafter the remainder of the drop was drawn off with filter paper, as described previously for the removal of the bacitracin and a drop of negative stain quickly placed on the grid, before the film had time to dry. 1% ammonium molybdate at pH 7.0 in distilled water was used as the

stain. One minute later, the drop of stain was drawn off and the grid was allowed to dry completely. The samples were then examined, using a Philips 400 TEM that was operated at an acceleration voltage of 80kV, and x 160,000 magnification.

Negative staining EM is much more readily available, but it is prone to staining artefacts, so a range of samples were taken to Leeds University, where they were subjected to cryo-EM. The cryo-EM was performed with initial help from Dr. S Stoylova. The samples were observed in their frozen-hydrated state. 5μl of the sample suspension was deposited on a bare 1000-mesh copper grid, blotted with filter paper and rapidly plunged into liquid nitrogen-cooled ethane, which was just above its freezing point. The grids were next transferred into liquid nitrogen and then, by a cryo-transfer workstation, they were inserted into a cryo-holder (Oxford Instruments, Oxford, U.K.). The samples were thus kept in liquid nitrogen throughout the entire transfer procedure. The samples were examined using a Philips CM10 EM, which was operated at an acceleration voltage of 100kV at temperatures that were below -160°C. Images were recorded on Agfa Scientia 23 D 56 electron image sheet film and also directly in digital format using a TVIPS (Tietz Video and Image Processing Systems, Gauting, Germany) on-line image acquisition and analysis system, which is based on a Photometrics AT 200 Peltier-cooled slow-scan 512 × 512 CCD camera controlled by Photometrics PMIS software (Photometrics, Tuscon, AZ, USA).

The size distribution of the LUVs was determined using photon correlation spectroscopy (PCS). This technique is based upon quasi-elastic laser light scattering. It measures the time dependence of light intensity fluctuations due to interference created by the scattering of incident coherent laser light by particles in motion (New, 1990). LUVs in aqueous suspension undergo a Brownian type motion, which is size dependent, small particles diffusing more rapidly than larger ones. Thus the translational diffusion coefficient can be measured, which can then be used to determine the mean hydrodynamic radius of the particles present, using the Stokes-Einstein equation. The experimental set-up consisted of a Malvern Instrument (Malvern Instruments, Malvern, U.K.) laser light source that was focused on a highly polished square glass cuvette housed within a thermostatically-controlled goniometer cell. (Accurate temperature control is essential in order to minimise random

convection currents, which would superimpose on the Brownian motion present, and lead to substantial errors in size measurements. Also fluid viscosity would vary, which affects calculations.) The spectrometer was mounted on an air table to minimise vibration and it was housed in a dark room to avoid problems produced by neighbouring strong light sources. The samples were filtered several times before use to remove any potential dust particles. Similarly, the cuvettes were soaked in strong acid to clean them and then washed in filtered, distilled water before use. Scattered light was detected by a photomultiplier assembly. This scattering was measured at three different angles for each sample, and the resultant recorded photomultiplier bursts were then 'correlated'. This was achieved by a computer programme, which multiplied the amplitudes of the signal and the time-delayed copies together at different times to give a correlation function. As the signals become more and more out of phase with one another, their respective randomness increases, which causes an exponential decay in the correlation function to a constant value. Mathematical equations link the value of the correlation function at any given time separation to the diffusion coefficient (D) of the particles present, and thence the particle radius can be calculated from the Stokes-Einstein equation :

$$D = \frac{kT}{6\pi\eta R} \qquad 7.2$$

where k=Boltzmann's constant, T=absolute temperature, η =solvent viscosity, and R= mean hydrodynamic radius. A standard sample, consisting of a uniform suspension of 90nm diameter beads, was used for calibration purposes. Thus the mean size of the population of LUVs that was present in each sample was determined.

7.3c Lipid Mixing Assay

Several attempts by myself to obtain positive proof of the fusogenic capacity of the FeLV fusion peptide were unsuccessful. The main reason for this was the insolubility of this peptide. I performed solubility tests on both the crude and the less

pure (<75%) peptide fractions that were obtained from Albachem, since the pure peptide was extremely expensive and also in very short supply. These peptide fractions did not dissolve well in DMSO, which agreed with the reports from the chemist who synthesised the FeLV peptide: she recorded that it would dissolve only in >30% TFA, >50% ACN and other very hydrophobic solvents. None of these are suitable for use in aqueous-based fusion assays. Surprisingly, the solubility of the >95% pure peptide was eventually found to be quite reasonable in DMSO. The other main problems were the lack of a reliable fluorimeter, and the numerous small practical difficulties encountered when attempting to set up an assay on the basis of reports in published papers. Many of these were overcome; for example the detection of osmotically-induced liposomal lysis when using the concentrations of experimental buffers for the internal and external liposomal solutions that were reported in a paper by Kendall and Macdonald (1982). Ultimately, some direct proof of fusogenic activity for the FeLV peptide was urgently required, in order to complement the DSC, NMR and X-ray diffraction work and allow its publication. Thus, as part of our collaboration, the successful fusion assays were performed by Dr. R.F. Epand, McMaster University, Hamilton, Canada.

Lipid mixing was measured, using the probe dilution method of Struck *et al* (1981). Thus the increase in NBD-PE fluorescence was measured as a function of time. A SLM Aminco Bowman Series 2 Luminescence Spectrometer (Urbana, IL, USA) with excitation and emission slits of 4nm was used. Peak absorbance of samples was kept at <0.1 to reduce inner filter effects. Crossed polarisers were used to reduce light scattering. Lowering the pH, and thus increasing the concentration of hydrogen ions (H^+) present, induces liposomal aggregation. Liposomes of PE can be thought of as existing in a state of metastable equilibrium, where small changes in pH, ionic strength or divalent cation concentration can lead to substantial changes in aggregation of the membranes (Allen *et al*, 1990). Aggregation is a prerequisite to fusion and, moreover, it represents the rate-limiting step in the overall process of fusion between two initially distinct membranes (e.g. Bentz *et al*, 1983; Bentz and Ellens, 1988; Ott and Wunderli-Allenspach, 1994; Ott *et al*, 1994). Thus the 'pH-jump' technique can be used to produce a potentially fusogenic liposomal population,

which is not affected by the kinetics of pre-aggregation. Similarly, an increase in the concentration of sodium ions (Na^+) present can induce liposomal aggregation. It is critical to measure a baseline value for any parameter studied using pure PE liposomes for the duration of the experiment in order to take any spontaneous liposomal fusion into account.

The LUVs were initially premixed, at a ratio of 1:9 labelled:unlabelled, in a fluorimeter cuvette containing Hepes buffer of pH 7.0 at 37°C. The residual fluorescence was measured and this was set at zero. The pH at which the fusion assay was performed was 7.0, as PE does not always aggregate well at pH 7.4 (e.g. Allen *et al*, 1990 studied egg PE, and found that inhibition of liposomal aggregation was seen in the pH range of 7.4- 8.0). The medium in the cuvettes was stirred continuously so that mixing of the peptide and vesicles was as rapid as possible. The temperature of the sample was monitored by a thermistor probe inserted into the cuvette. The LUVs comprised 1% of the total volume in the cuvette. The final lipid concentration was 300μM. There was no detectable change in pH upon addition of the LUVs, since the volumes of LUVs added were very small. The excitation wavelength used was 470nm, and the emission of NBD was recorded at 530nm.

The FeLV and SIV peptides were dissolved separately in DMSO at a concentration of 1mg/ml. The peptide must partition from the aqueous phase into the membrane to account for the possible effects of the bilayer interface on the adopted peptide conformation (Deber and Goto, 1996). Thus the peptide was added externally to the vesicles. The stock solutions of peptide were added to LUV preparations in the fluorimeter cuvettes, to give a final peptide concentration of 10μM. DMSO alone was also used as a control. 100% lipid mixing was obtained by addition of 10% Triton X-100 to the vesicle suspension to a final concentration of 0.1%. This eliminated RET by lysing the vesicles, and this signal represented NBD fluorescence obtained at infinite dilution. The effect of Triton X-100 on the quantum yield of NBD-PE was also measured, and the appropriate corrections for this and sample dilution were applied to obtain the final value for 100% lipid mixing.

7.5 Fusion Assay Results and Discussion

Figure 7.2 shows a typical cryo-transmission EM that was obtained for a sample of freeze-thaw extruded LUVs. The sample contained vesicles that were composed of 50 mol% DOPC/50 mol% DOPE. No multilamellar vesicles are present, and the two individual monolayers of the bilayer can be distinguished in some of the vesicles. A total of 15 cryo-EMs were obtained on 7 liposome samples that contained different types of phospholipids. No MLVs were observed in any of these micrographs, nor in any of the 12 negatively stained EMs, which were taken from 6 distinct liposome samples. A typical example of the micrographs that were obtained using the negative staining technique is shown in Figure 7.3. This was taken from a sample of 50 mol% DOPC/50 mol% DOPG LUVs. It is thus clear that this method reliably produces unilamellar vesicles.

The distribution of the size of vesicles in a sample of 50 mol% DOPC/50 mol% DOPS liposomes is shown in Figure 7.4. The percentage of vesicles whose diameter is within each range in nm is plotted. It can be seen that >70% have diameters between 52.6nm and 101.69nm, whilst the range of possible diameters for vesicles varies from 25nm to 1000nm.

In conclusion, the method of Hope *et al* (1985) results in a good homogeneous population of vesicles. Not surprisingly over the past few years this method has become the standard method of LUV preparation for fusion assays. No EM or PCS studies were performed on the MeDOPE vesicle preparations that were used in the fusion assays, due to geographical displacement from the required equipment. However, the extensive nature of the tests that I had performed previously in the U.K. on LUVs having a wide variety of different phospholipid compositions, had unfailingly yielded the same qualitative results. These, together with previously published studies, were regarded as sufficient proof of the nature of the vesicles used in the fusion assays.

Figure 7.5 shows the percentages of lipid mixing which took place between LUVs composed of MeDOPE in the presence of the SIV and FeLV fusion peptides. The SIV peptide promoted rapid lipid mixing, and thus membrane fusion, between the labelled and unlabelled LUV populations, as seen by the increase in NBD-PE

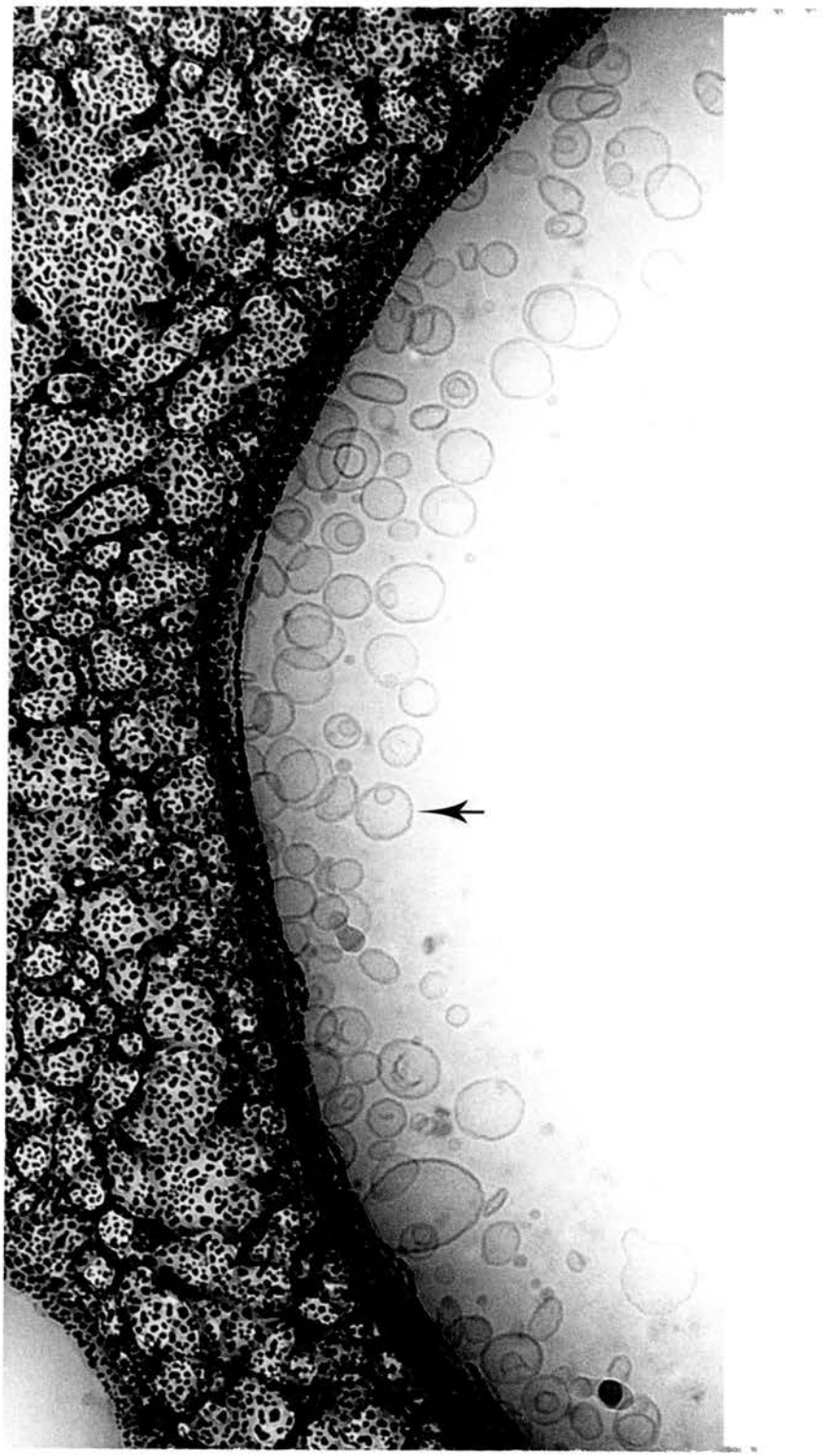

Figure 7.2. Cryo-transmission EM of freeze thaw extruded LUVs, composed of 50 mol% DOPC/50 mol% DOPE. Some individual bilayers are visible; for example, see arrow.

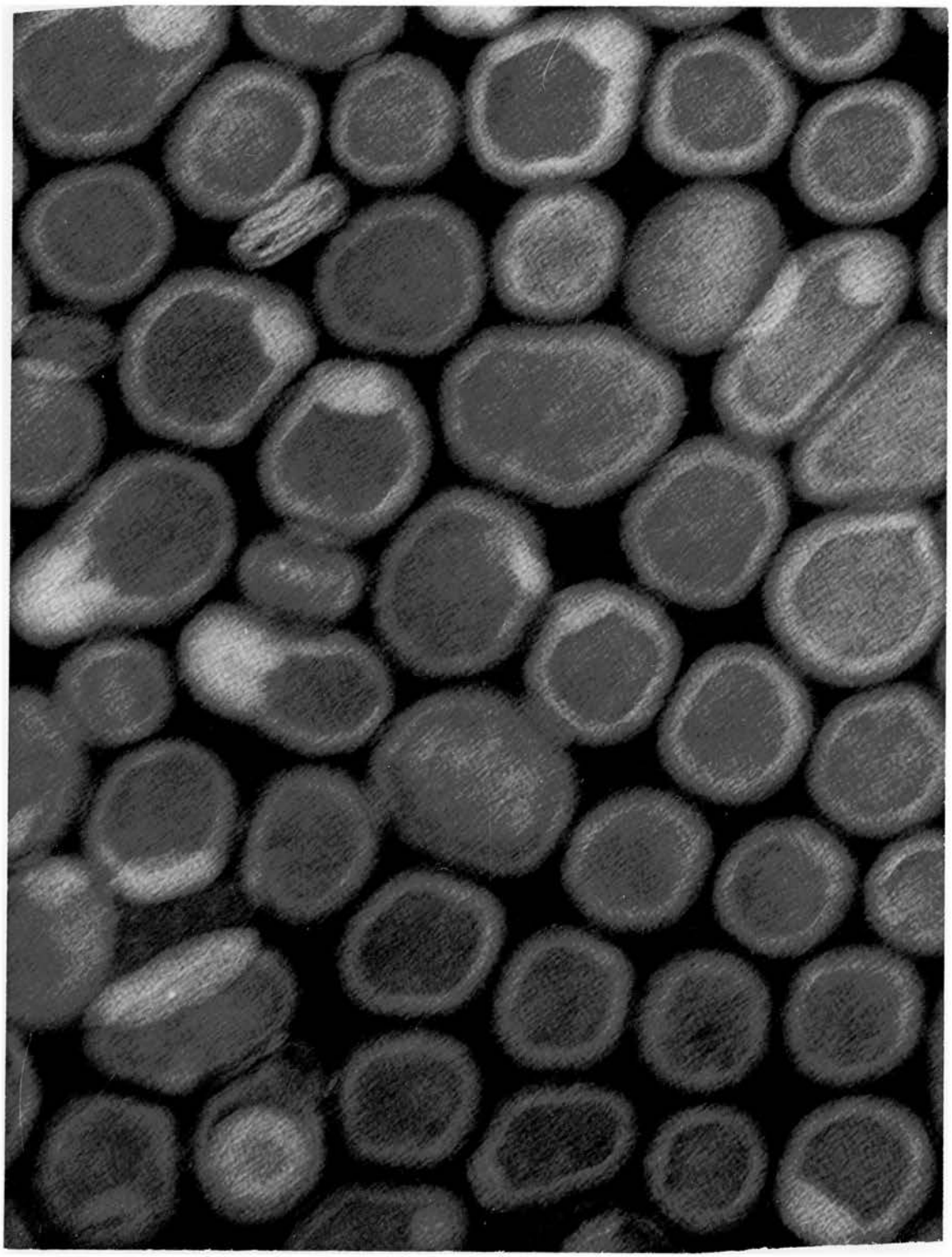

Figure 7.3. Negatively stained transmission EM of freeze thaw extruded LUVs, composed of 50 mol% DOPC/50 mol% DOPG.

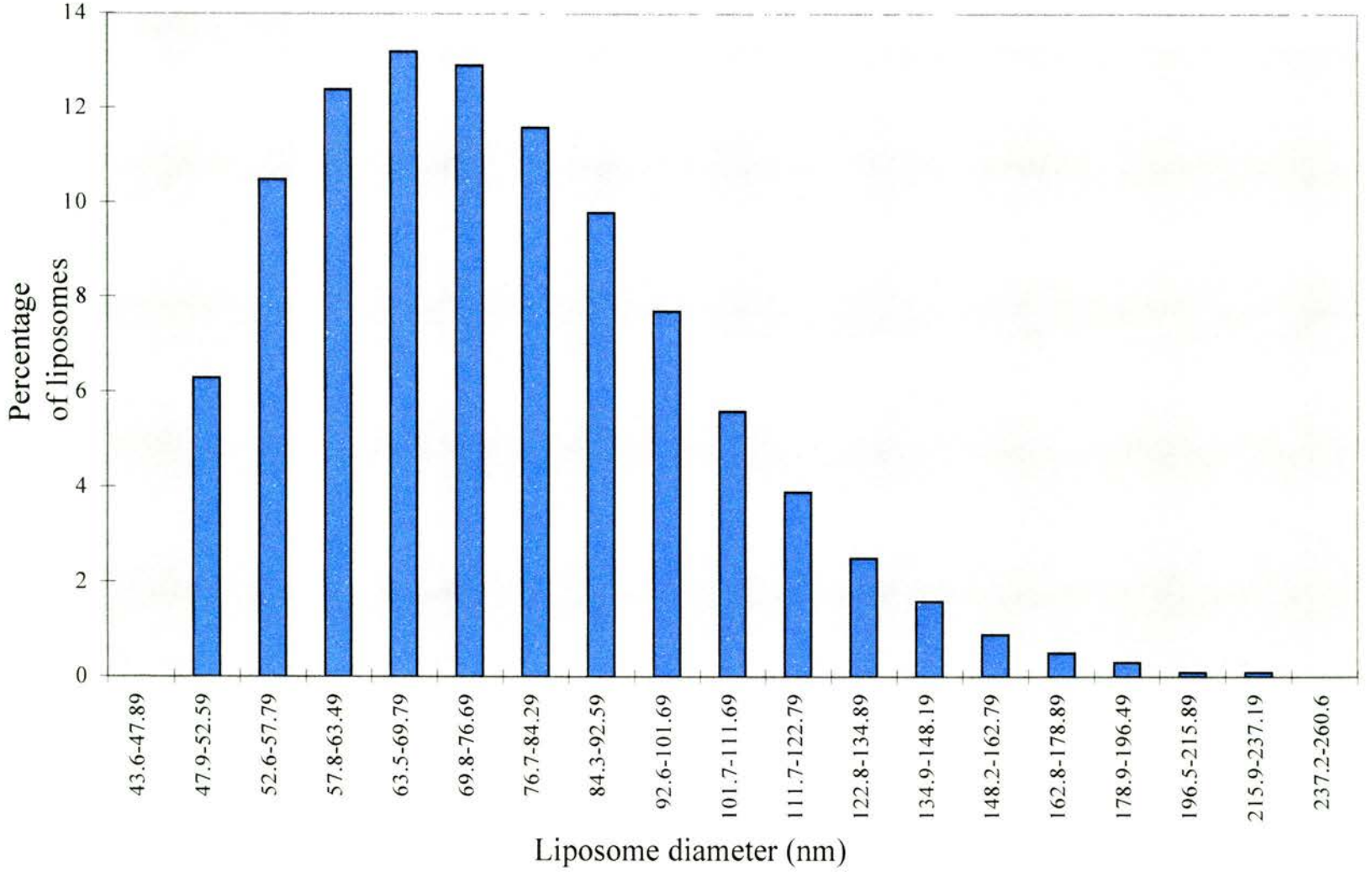

Figure 7.4. Graph of the size distribution of DOPC/DOPS liposomes, which were prepared by freeze-thawing and high pressure extrusion.

fluorescence upon probe dilution. These results agree very closely with previous experiments performed using this peptide (Martin *et al*, 1994). The FeLV peptide also produced membrane fusion, as shown by an increase in lipid mixing when compared with that seen for an aliquot of DMSO identical to that in which the peptide was added to the liposomal preparation (top DMSO curve).

Using this particular lipid system, the SIV peptide showed greater enhancement of fusion. This difference in potency may reflect the many differences between these two peptides, viz their lengths, overall electrical charges, solubility characteristics and probable miscibilities with different lipid species. Moreover, different viral fusion peptides have been shown to require different specific experimental conditions in order to promote maximum membrane fusion. The retroviral Ebola virus fusion peptide requires the presence of phosphatidylinositol (PI) in the target membrane for fusion to occur (Ruiz-Argüello *et al*, 1998). Calcium ions might also be involved in this process. Similarly, SFV requires the presence of ceramide (Nieva *et al*, 1994a; Corver *et al*, 1995; Wilschut *et al*, 1995). The presence of only 1-2 mol% of sphingolipid is sufficient to produce half-maximal fusion, and so sphingolipids have been suggested as being co-factors for SFV fusion, possibly by interacting directly with the fusion peptide and thus activating it (Wilschut *et al*, 1995). Cholesterol is also required for SFV fusion (e.g. White and Helenius, 1980), with the 3β-hydroxyl group being the crucial factor (Phalen and Kielian, 1991). The role of cholesterol appears to be in the binding of the peptide to the membrane, rather than the actual fusion events (Wilschut *et al*, 1995). VSV requires PS (Eidelman *et al*, 1984), which has been proposed as the cellular receptor for this virus (Schlegel *et al*, 1983). Düzgünes and Shavnin (1992) studied synthetic peptides corresponding to the fusion peptides of Influenza virus, VSV and Sendai virus. Whilst all three fusion peptides were found to induce membrane destabilisation of lipid vesicles, the occurrence and extent of destabilisation were dependent upon the phospholipid composition of the LUVs. Finally, Larsen and co-workers (1993) showed that the fusion activity of HIV-1 virus with model membranes was greatly enhanced by the presence of cardiolipin.

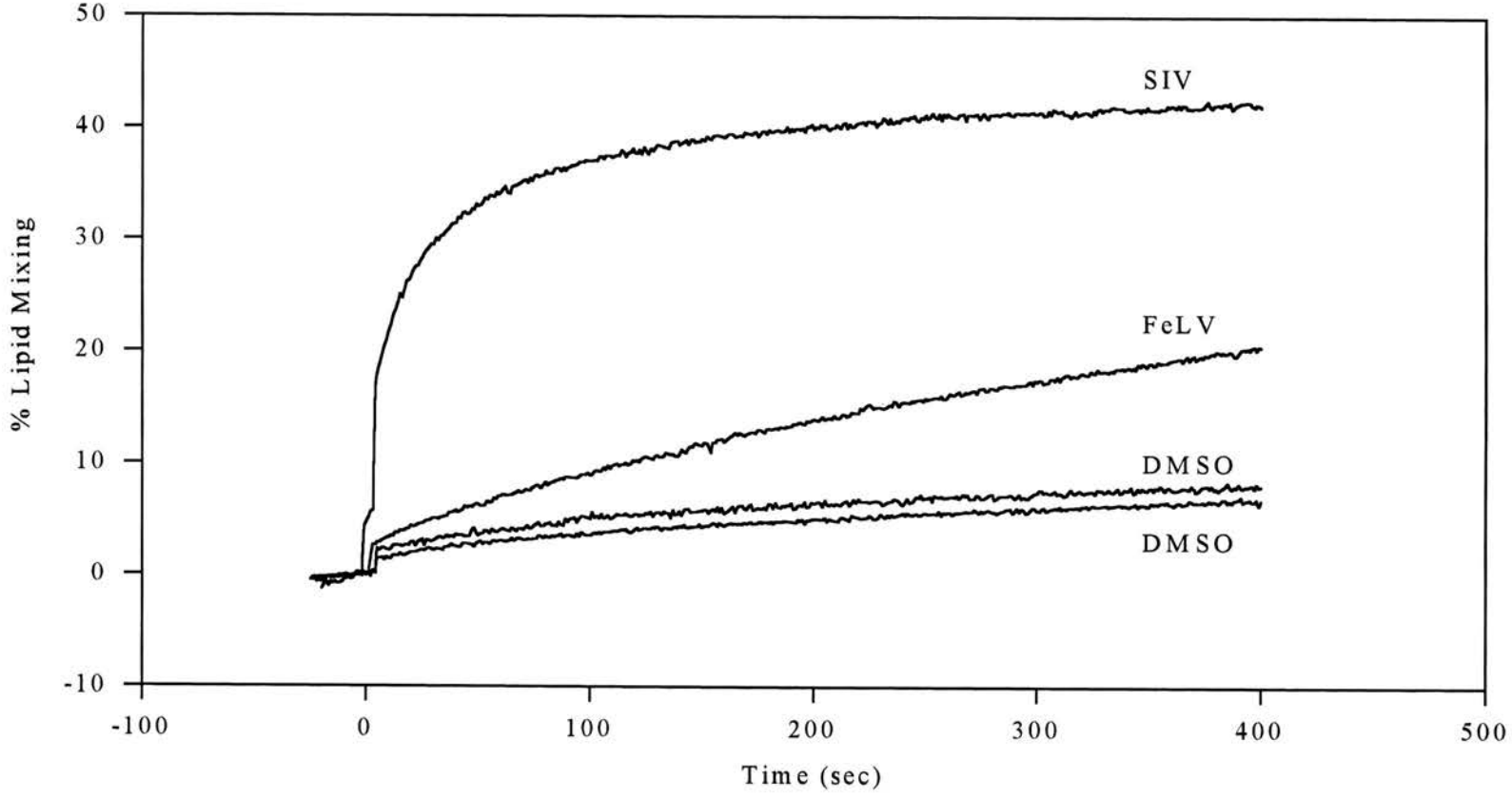

Figure 7.5. The percentages of lipid mixing between MeDOPE LUVs induced by the SIV and FeLV fusion peptides. The peptides, which were dissolved in DMSO, were added at time 0. Changes in fluorescence due to equivalent aliquots of the pure DMSO solvent are also shown. The top DMSO curve corresponds to 52µl of added solvent as used for the FeLV peptide and the bottom curve to 24µl as used for the SIV peptide. Measurements were performed at 37°C, and at pH 7.0.

It is certainly possible that interaction of peptides occurs with particular lipid species rather than with the membrane as a whole (Polozov *et al*, 1997). Thus the experimental conditions used here may not provide optimal fusogenic conditions for the FeLV fusion peptide. Future experiments using LUVs of different lipid compositions could determine the lipid requirements of this peptide in order to obtain maximal fusion. In particular, it would be interesting to use liposomes of lipid compositions that closely represented the target membranes of FeLV *in vivo*, for example the feline T cell and granulocyte plasma membranes. Pereira *et al* (1997) studied the induction of fusion by the HIV-1 fusion peptide between LUVs that were devoid of a net charge, using published information on the composition of the membrane environment into which this peptide should partition *in vivo* (Aloia *et al*, 1993). Similarly, Ruiz-Argüello and co-workers (1998) examined the fusogenic capacity of the Ebola virus fusion peptide using LUVs of a lipid composition which is close to that of the hepatocyte cell membrane, as the hepatocyte is one of the main target cells of this virus. These fusion experiments, and indeed all other fusion assays to characterise the FeLV fusion peptide, should be performed for a range of peptide concentrations, to determine whether the rate of fusion is dependent upon the amount of peptide present, and thus to demonstrate further that it is the fusion peptide that is the active catalyst in this process.

It is possible that the biological fusion domain of FeLV may be a different length from the 27 amino acid peptide that is quoted in the literature. A study of the N-terminal region of a B strain of Influenza virus showed that the peptide corresponding to the N-terminal 20 amino acids was more fusogenic than shorter, 16 or less amino acid peptide fragments (Lear and Degrado, 1987). Similarly, Defrise-Quertain and co-workers (1992) examined the fusion capacity of the N-terminal region of BLV, and found that the longest peptide fragment that was studied, which was 24 amino acids in length, promoted the greatest amount of fusion between vesicles. Conversely, Martin *et al* (1991) studied a variety of synthetic peptides which corresponded to different lengths of the putative fusion peptide of SIV. They found that the most fusogenic of the peptides was the shortest, 12 amino acid peptide.

Further fusion assays using FeLV fusion peptides of different lengths could determine the length of peptide which produces maximal fusion.

Mutagenesis studies of the FeLV fusion peptide could provide further evidence for the role of the precise amino acid sequence of this N-terminal region of p15E in fusion.

As mentioned earlier, it is advisable to perform assays of the mixing of liposomal contents as well as lipid mixing assays, since lipid mixing may not correlate purely with fusion. As an example of a potential error, Ellens *et al* (1989) found that MeDOPE liposomes showed greatly increased fusion rates in the temperature range at which isotropic ^{31}P NMR resonances were seen but true fusion, as measured by the mixing of liposomal contents, dramatically decreased as T_H was reached, due to collapse of liposomes and the concurrent leakage of liposomal contents. Lipid mixing, however, was observed to continue, since adjacent membranes were being transformed into H_{II} structures. Rapid leakage of vesicle contents is, however, often observed with isolated synthetic fusion peptides, which precludes the use of contents mixing assays. Thus, Martin and co-workers (1993) found that the addition of HIV-1 peptide to several different vesicle preparations induced such a rapid leakage that contents mixing could not be observed. It has been suggested that fusion proteins may serve to prevent the lysis of one or more of the membranes participating in fusion (Hughson, 1995), and hence this effect will be lost when studying the isolated fusion peptide. Shangguan and co-workers (1996), however, studied the fusion between whole Influenza virus and liposomes, and discovered this process too was very leaky. Attempts at assaying the mixing of vesicle contents would be worthwhile, since this step represents the completion of fusion, and the precise role(s) of these viral fusion peptides in the multi-step fusion process are still not known.

Work by Düzgünes and Shavnin (1992) (see above) found that none of the fusion peptides from the three viruses studied induced complete fusion of LUVs. They noted that previous studies, which had reported the production of complete fusion by viral fusion peptides (e.g. Lear and Degrado, 1987; Murata *et al*, 1987; Wharton *et al*, 1988) had used SUVs in the main. It has been suggested that other sections of viral fusion proteins may also be required for full fusion to occur (Wharton *et al*,

1988; Düzgünes and Shavnin, 1992). The ultimate function of the fusion peptide may therefore depend upon the remainder of the fusion protein, and LUV-synthetic peptide systems do not allow for any effects caused by additional functionally relevant domains in p15E or gp70.

With this in mind, Pécheur *et al* (1997) studied the fusion induced by a small 11 amino acid peptide, which was anchored to a lipid membrane. Their aim was to mimic more closely the normal membrane-anchored state of viral fusion peptides, since fusion peptides are always found in a polypeptide chain with a transmembrane anchoring segment. The peptide did not induce fusion when in the free monomeric form. Both lipid mixing and contents mixing were, however, readily observed using the membrane-anchored peptide. They suggested that the free peptide could fold along the vesicle surface, while the membrane-anchored peptide was restricted in this action and hence showed increasing hydrophobic interactions with the target membrane. Fusion studies of the FeLV fusion peptide in a membrane-anchored state would thus be beneficial, since it is normally bound to the remainder of p15E, the transmembrane protein segment of gp85.

Biological membranes are asymmetric in composition, and this asymmetry may be important in fusion (Eastman *et al*, 1992; Devaux *et al*, 1993). Creating asymmetry in model membranes is very difficult and such manipulations produce only crude changes at best (Eastman *et al*, 1992). Similarly, transmembrane electrochemical gradients could also affect the interaction of the FeLV fusion peptide with its target membrane under physiological conditions and these are absent from the model membrane systems described.

In Chapter 6 the apparent anomaly of the interaction of a negatively charged peptide with a hydrophobic lipid membrane was mentioned. The peptide that was studied by Pécheur and co-workers (1997) was negatively charged: it contained three Glu residues at positions 3, 7 and 10. These fusion experiments were carried out at neutral pH, and so neutralisation of the peptide's negative charge is not required for fusion to proceed. The FeLV peptide has a glutamate residue at its amino terminus, and this amino acid has been used in several previous mutagenesis studies of fusion peptides. Düzgünes and Gambale (1988) found that a mutant of the Influenza virus

fusion peptide, which had a glutamate residue inserted at the N-terminal position showed a reduced membrane-penetrating activity compared to the wild type fusion peptide. Rafalski *et al* (1991) found that this same mutant peptide bound less tightly to lipid vesicles, showed a lower degree of bilayer penetration and produced much less leakage from vesicles than the wild type fusion peptide. The work by Ruiz-Argüello *et al* (1988) on the putative fusion peptide of Ebola virus showed that the inclusion of the naturally-ocurring glutamate residue at the N-terminus severely impaired peptide-vesicle interaction: only~12% of peptide bound to LUV when the glutamate was present, whereas without it ~33% of the peptide bound. Masking this residue would, therefore, optimise the partitioning of this putative fusion peptide into the target membrane. It is worth remembering, however, that the experiments described here were all aimed at detecting maximal fusion. Possibly under physiological conditions, the slight impairment of fusion could be beneficial to viral replication; for example, by the avoidance of cell-cell fusion. Furthermore, FeLV is a relatively slow viral infection, which can take years to produce a state of disease, unlike the acute infections induced by agents such as Influenza virus.

It would be useful to have some method of determining the amount of FeLV fusion peptide that binds to vesicles under different experimental conditions. Previous studies (e.g. Lear and Degrado, 1987; Ruiz-Argüello *et al*, 1988) have used the change in fluorescence of a tryptophan residue present in the fusion peptide, and the decrease in the quenching of this tryptophan by the aqueous marker KI (Ruiz-Argüello *et al*, 1988) to confirm the interaction of the peptide with phospholipid bilayers. Tryptophan shows a blue shift on interaction with a lipid membrane (Dufourcq and Faucon, 1977), which is due to the indole group becoming partially immersed in the membrane (Lakowicz, 1983). Unfortunately, the wild type FeLV fusion peptide does not contain any tryptophan residues, nor is it quantitatively detectable by any of the usual methods of determination of protein/peptide concentration (e.g. Markwell *et al*, 1981). This problem has been encountered with other fusion peptides, for example that of SIV (R.M. Epand, personal communication). One possibility would be to synthesise a mutant peptide that contained a tryptophan residue, but this might alter the true nature and degree of the

fusogenic capacity of the peptide. Quantitative amino acid analysis of samples containing LUVs with bound peptide present could be performed after passage of the vesicles down a filtration column or following density flotation and centrifugation to remove any unbound peptide. This is, however, an extremely expensive technique to use on a routine basis.

In conclusion, the major problems associated with the development of a reliable, functional fusion assay to study the FeLV fusion peptide appear to have been overcome. Evidence for ability of this peptide to promote fusion between lipid membranes has been obtained, using a resonance energy transfer technique. A number of potential experiments, which have been discussed, could now be performed in order to determine more precisely the conditions required by this peptide to enable it to catalyse fusion.

Chapter 8: Conclusions

Conclusions

At the outset of this thesis, August 1994, there were no published experimental data on the putative fusion peptide of FeLV. The work described herein demonstrates membrane fusion activity for the FeLV peptide, in the form of lipid mixing between liposomes. It also provides evidence that this peptide has effects on lipid properties that are characteristic of viral fusion peptides. Thus, there are many indications that fusion peptides do not act merely as aggregation agents for neighbouring bilayers. The induction of membrane destabilisation by a fusion peptide demonstrates the capacity of the peptide to play an active role in the actual molecular changes that occur during the multistep fusion process. Structural studies of the effects of the FeLV fusion peptide on lipid polymorphism confirmed this ability. Using the technique of DSC, this fusion peptide was, indeed, shown to destabilise the L_α phase with respect to the H_{II} phase. Similarly, the X-ray diffraction results demonstrated its capacity to increase the negative monolayer curvature of both the L_α and H_{II} lipid phases, and also to promote the formation of a novel lipid phase, of increased negative monolayer curvature compared to that of the other two phases. It can be seen, therefore, that the FeLV fusion peptide promotes the destabilisation of the bilayer phase relative to lipid phases of higher negative curvature. Moreover, the NMR results showed that this peptide enhances the formation of highly curved, isotropic lipid structures, which are thought to be involved in the rate-limiting stages of the fusion pathway.

The molecular mechanism by which the FeLV fusion peptide promotes fusion may depend upon the nature of the target membrane and also upon what the rate-determining step is in that particular fusion pathway. The differences that were seen for the interaction of the FeLV fusion peptide with bilayers of distinct lipid composition (see Chapters 5 and 6) agree with the hypothesis that the interaction of viral fusion peptides with a cell membrane will depend, at least in part, upon the membrane environment into which the peptide partitions. The results of the DSC, NMR and X-ray diffraction chapters suggested that the FeLV fusion peptide may

accelerate both the rate of stalk formation, as well as the partitioning of the TMC intermediate towards the formation of a fusion pore.

Exposure of hydrophobic regions of viral fusion proteins, including the fusion peptides, in the space between apposed membranes may help apposing bilayers to bypass or overcome the strong repulsive hydration force that is present (Bentz *et al*, 1990). Perturbation of the target bilayer by the fusion peptide might have the same effect if some of the lipid tails in the hydrophobic interior of the membrane became exposed. Neutron diffraction studies revealed that the FeLV fusion peptide altered the packing of certain lipid bilayers in a manner that agreed with the concept of precession of a fusion peptide within a bilayer. Furthermore, the process of the insertion of a peptide into a bilayer is likely to produce a certain amount of exposure of the hydrophobic lipid region, since even the interfacial region contains methylene groups from the edges of the hydrocarbon core (Wiener and White, 1992).

The formation of fusion pores may be enhanced by fusion peptides. Thinning of a bilayer, which was suggested by the observed change in the distribution of 'heavy' water in the presence of the FeLV fusion peptide (see Chapter 5), could reduce the tension that is required to rupture that bilayer. Schoch and Blumenthal (1993) showed that the fusion peptide of Influenza virus played an important role in the widening of the fusion pore. It is possible that some of the fusion peptides stabilise fusion protein oligomeric assemblies by interacting with the transmembrane portion of the viral envelope protein or with neighbouring fusion peptides of adjacent monomers, whilst other fusion peptides simultaneously interact with the target membrane. Thus pore stabilisation and its widening may require specific peptide-peptide interactions. Certainly, the FeLV fusion peptide demonstrated an extreme tendency towards self-aggregation.

To my knowledge, this work provides the first published experimental evidence of both fusogenic activity and the effects on lipid polymorphism of the FeLV fusion peptide. It also demonstrates the phenomenon of structural plasticity for this fusion peptide, a property which may be characteristic of many viral fusion peptides.

Whilst the precise role of viral fusion peptides in the overall process of fusion is still uncertain, major advances are being made in our understanding of these

biological molecules. It is hoped that work with specific fusion proteins and peptides, such as the FeLV fusion peptide, will continue to shed light upon the basic molecular mechanisms which underlie this essential life process.

There are a number of further experiments that would be of interest to conduct, in the light of the findings described in this thesis. Fusion assays performed under a variety of experimental conditions could help to determine the factors required for the optimal fusogenic activity of the FeLV fusion peptide. In particular, the effects of the presence of physiological concentrations of calcium ions and also different lipid species could be determined. The rates of fusion should also be measured in the presence of several different peptide concentrations, in order to verify that the fusion peptide is indeed the active catalyst. CD studies of FeLV peptide-containing proteoliposomes after filtration to remove any unbound peptide would enable the determination of the secondary structure of purely membrane-bound peptide, and the use of FTIR as well would provide a more accurate estimation of the β sheet content of these samples. A repetition of the TRXRD study using a slower scan rate might enable definite identification of the novel, peptide-induced lipid phase described in Chapter 4. Moreover, a similar study using MeDOPE might provide further evidence of the ability of the FeLV fusion peptide to induce cubic phase formation. Since the DSC results were based upon one set of data, it would also be beneficial to repeat this study. Specific deuteration of the FeLV fusion peptide would enable measurement, using neutron diffraction, of the exact position of the deuterated amino acid residues with respect to the lipid bilayer, and thus the extent and depth to which this peptide penetrates membranes. Determination of the effects of non-conservative mutations in the sequence of the FeLV fusion peptide upon the ability of this peptide to destabilise lipid bilayers, to promote the formation of negatively curved non-bilayer structures and to promote fusion might identify amino acid residues that are crucial to the functional ability of this peptide. Similarly, the use of fragments of the fusion peptide sequence of differing length could determine the minimum length of peptide required to produce these various effects, and also the optimum peptide length. Concurrent CD and FTIR studies of the secondary structures of these various peptides would allow the discovery of possible links between structure and function.

Bibliography

Bibliography

Alford, D., Ellens, H. & Bentz, J. (1994) Fusion of Influenza virus with sialic acid-bearing target membranes. *Biochemistry*, **33**, 1977-1987.

Allen, T.M. & Cleland, L.G. (1980) Serum-induced leakage of liposome contents. *Biochim. Biophys. Acta*, **597**, 418-426.

Allen, T.M., Hong, K. & Papahadjopoulos, D. (1990) Membrane contact, fusion, and hexagonal (H_{II}) transitions in phosphatidylethanolamine liposomes. *Biochemistry*, **29**, 2976-2985.

Almers, W. & Tse, F.W. (1990) Transmitter release from synapses- does a preassembled fusion pore initiate exocytosis. *Neuron*, **4**, 813-818.

Aloia, R.C., Tian, H.R. & Jensen, F.C. (1993) Lipid composition and fluidity of the Human immunodeficiency virus envelope and host cell plasma membranes. *Proc. Natl. Acad. Sci. USA.*, **90**, 5181-5185.

Anderson, D.M., Gruner, S.M. & Leibler, S. (1988) Geometrical aspects of the frustration in the cubic phases of lyotropic liquid crystals. *Proc. Natl. Acad. Sci. USA.*, **85**, 5364-5368.

Asano, K. & Asano, A. (1988) Binding of cholesterol and inhibitory peptide derivatives with the fusogenic hydrophobic sequence of F-glycoprotein of HVJ (Sendai virus)- possible implications in the fusion reaction. *Biochemistry*, **27**, 1321-1329.

Bacon, G.E. (1975) Neutron diffraction (third edition). *Oxford University Press, London*, 48-50.

Bailey, A.L. & Cullis, P.R. (1997) Membrane fusion with cationic liposomes: effects of target membrane lipid composition. *Biochemistry*, **36**, 1628-1634.

Barker, R.W., Bell, J.D., Radda, G.K. & Richards, R.E. (1972) Phosphorus nuclear magnetic resonance in phospholipid dispersions. *Biochim. Biophys. Acta*, **260**, 161-163.

Basáñez, G., Nieva, J.L., Rivas, E., Alonso, A. & Goñi, F.M. (1996) Diacylglycerol and the promotion of lamellar-hexagonal and lamellar-isotropic phase transitions in lipids- implications for membrane fusion. *Biophys. J.*, **70**, 2299-2306.

Basáñez, G., Ruiz-Argüello, M.B., Alonso, A., Goñi, F.M., Karlsson, G. & Edwards, K. (1997) Morphological changes induced by phospholipase C and by sphingomyelinase on large unilamellar vesicles: a cryo-transmission electron microscopy study of liposome fusion. *Biophys. J.*, **72**, 2630-2637.

Bayley, P.M. (1973) The analysis of circular dichroism of biomolecules. *Progr. Biophys. Mol. Biol.*, **27**, 3-79.

Bentz, J., Nir, S. & Wilschut, J. (1983) Mass action kinetics of vesicle aggregation and fusion. *Colloids and Surfaces*, **6**, 333-363.

Bentz, J., Düzgünes, N. & Nir, S. (1985) Temperature dependence of divalent cation induced fusion of phosphatidylserine liposomes- evaluation of the kinetic rate constants. *Biochemistry*, **24**, 1064-1072.

Bentz, J., Ellens, H. & Szoka, F.C. (1987) Destabilization of phosphatidylethanolamine-containing liposomes- hexagonal phase and asymmetric membranes. *Biochemistry*, **26**, 2105-2116.

Bentz, J., Alford, D., Cohen, J. & Düzgünes, N. (1988) La^{3+}-induced fusion of phosphatidylserine liposomes- close approach, intermembrane intermediates, and the electrostatic surface potential. *Biophys. J.*, **53**, 593-607.

Bentz, J. & Ellens, H. (1988) Membrane fusion- kinetics and mechanisms. *Colloids and Surfaces.*, **30**, 65-112.

Bentz, J., Ellens, H. & Alford, D. (1990) An architecture for the fusion site of Influenza hemagglutinin. *FEBS Lett.*, **276**, 1-5.

Benveniste, R.E., Sherr, C.J. & Todaro, G.J. (1975) Evolution of type C viral genes: origin of Feline leukemia virus. *Science*, **190**, 886-888.

Bizebard, T., Gigant, B., Rigolet, P., Rasmussen, B., Diat, O., Bosecke, P., Wharton, S.A., Skehel, J.J. & Knossow, M. (1995) Structure of Influenza virus haemagglutinin complexed with a neutralising antibody. *Nature*, **376**, 92-94.

Blobel, C.P., Wolfsberg, T.G., Turck, C.W., Myles, D.G., Primakoff, P. & White, J.M. (1992) A potential fusion peptide and an integrin ligand domain in a protein active in sperm-egg fusion. *Nature*, **356**, 248-252.

Blumenthal, R., Pak, C.C., Raviv, Y., Krumbiegel, M., Bergelson, L.D., Morris, S.J. & Lowy, R.J. (1995) Transient domains induced by Influenza hemagglutinin during membrane fusion. *Mol. Membr. Biol.*, **12**, 135-142.

Bodian, D.L., Yamasaki, R.B., Buswell, R.L., Stearns, J.F., White, J.M. & Kuntz, I.D. (1993) Inhibition of the fusion-inducing conformational change of Influenza hemagglutinin by benzoquinones and hydroquinones. *Biochemistry*, **32**, 2967-2978.

Bolognesi, D.P., Montelaro, R.C., Frank, H. & Schäfer, W. (1978) Assembly of type C oncornaviruses: a model. *Science*, **199**, 183-186.

Boomer, S., Eiden, M., Burns, C.C. & Overbaugh, J. (1997) Three distinct envelope domains, variably present in subgroup B Feline leukemia virus recombinants, mediate Pit1 and Pit2 receptor recognition. *J. Virol.*, **71**, 8116-8123.

Bosch, M., Earl, P., Fargnoli, K., Picciafuoco, S., Giombini, F., Wong Staal, F. & Risser, R. (1989) Identification of the fusion peptide of primate immunodeficiency viruses. *Science*, **244**, 694-697.

Boulay, F., Doms, R.W., Webster, R.G. & Helenius, A. (1988) Posttranslational oligomerization and cooperative acid activation of mixed Influenza hemagglutinin trimers. *J. Cell. Biol.*, **106**, 629-639.

Bradshaw, J.P. (1997) Phosphatidylglycerol promotes bilayer insertion of salmon calcitonin. *Biophys. J.*, **72**, 2180-2186.

Bradshaw, J.P., Dempsey, C.E. & Watts, A. (1994) A combined X-ray and neutron diffraction study of selectively deuterated melittin in phospholipid bilayers: effect of pH. *Mol. Membr. Biol.*, **11**, 79-86.

Bragg, W.L. (1913) The diffraction of short electromagnetic waves by a crystal. *Proc.Cambridge Philos.Soc.* **17**, 43-57.

Brand, C.M. & Skehel, J.J. (1972) Crystalline antigen from the Influenza virus envelope. *Nature new Biol.*, **238**, 145-147.

Brasseur, R., Cornet, B., Burny, A., Vandenbranden, M. & Ruysschaert, J.M. (1988) Mode of insertion into a lipid membrane of the N-terminal HIV gp41 peptide segment. *AIDS Res. and Hum. Retr.*, **4**, 83-90.

Brasseur, R., Vandenbranden, M., Cornet, B., Burny, A. & Ruysschaert, J. (1990) Orientation into the lipid bilayer of an asymmetric amphipathic helical peptide located at the N-terminus of viral fusion proteins. *Biochim. Biophys. Acta.*, **1029**, 267-273.

Brasseur, R., Pillot, T., Lins, L., Vandekerckhove, J. & Rosseneu, M. (1997) Peptides in membranes: tipping the balance of membrane stability. *Trds. Biochem. Sci.*, **22**, 167-171.

Bross, I.D.J. & Gibson, R. (1970) Cats and childhood leukaemia. *J. Medicine*, **1**, 180.

Büldt, G., Gally, H.U., Seelig, A., Seelig, J. & Zaccai, G. (1978) Neutron diffraction studies on selectively deuterated phospholipid bilayers. *Nature*, **271**, 182-184.

Büldt, G., Gally, H.U., Seelig, J. & Zaccai, G. (1979) Neutron diffraction studies on phosphatidylcholine model membranes. *J. Mol. Biol.*, **134**, 673-691.

Bullough, P.A., Hughson, F.M., Skehel, J.J. & Wiley, D.C. (1994) Structure of Influenza haemagglutinin at the pH of membrane fusion. *Nature*, **371**, 37-43.

Caffrey, M. (1989) The study of lipid phase transition kinetics by time-resolved X-ray diffraction. *Annu. Rev. Biophys. Biophys. Chem.*, **18**, 159-186.

Callebaut, I., Tasso, A., Brasseur, R., Burny, A. & Mornon, J.P. (1994) Common prevalence of alanine and glycine in mobile reactive centre loops of serpins and viral fusion peptides: Do prions possess a fusion peptide? *J. Comput.-Aid. Mol. Des.*, **8**, 175-191.

Campbell, I.D. & Divek, R.A. (1984) Optical activity. *Biological Spectroscopy.* (ed. by I.D. Benjamin and R.A. Divek), 255-277.

Carr, C.M. & Kim, P.S. (1993) A spring-loaded mechanism for the conformational change of Influenza hemagglutinin. *Cell*, **73**, 823-832.

Chan, D.C., Fass, D., Berger, J.M. & Kim, P.S. (1997) Core structure of gp41 from the HIV envelope glycoprotein. *Cell*, **89**, 263-273.

Chandler, D.E. (1984) Comparison of quick-frozen and chemically fixed sea urchin eggs -structural evidence that cortical granule exocytosis is preceded by a local increase in membrane mobility. *J. Cell Sci*, **72**, 23-36.

Chang, C.T., Wu, C.S.C. & Yang, J.T. (1978) Circular dichroic analysis of protein conformation; inclusion of the beta-turns. *Anal. Biochem.*, **91**, 13-31.

Chang, D., Cheng, S. & Chein, W. (1997) The amino-terminal fusion domain peptide of Human immunodeficiency virus type 1 gp41 inserts into the sodium dodecyl sulfate micelle primarily as a helix with a conserved glycine at the micelle-water interface. *J. Virol.*, **71**, 6593-6602.

Chang, H. & Epand, R.M. (1983) The existence of a highly ordered phase in fully hydrated dilauroylphosphatidylethanolamine. *Biochim. Biophys. Acta*, **728**, 319-324.

Cheetham, J.J. & Epand, R.M. (1987) Comparison of the interaction of the antiviral chemotherapeutic agents amantadine and tromantadine with model phospholipid membranes. *Biosci. Rep.*, **7**, 225-230.

Cheetham, J.J., Epand, R.M., Andrews, M. & Flanagan, T.D. (1990) Cholesterol sulfate inhibits the fusion of Sendai virus to biological and model membranes. *J. Biol. Chem.*, **265**, 12404-12409.

Cheetham, J.J., Nir, S., Johnson, E., Flanagan, T.D. & Epand, R.M. (1994) The effects of membrane physical properties on the fusion of Sendai virus with human erythrocyte ghosts and liposomes. *J. Biol. Chem.*, **269**, 5467-5472.

Chen, S.S.L., Lee, C.N., Lee, W.R., Mcintosh, K. & Lee, T.H. (1993) Mutational analysis of the leucine zipper-like motif of the Human immunodeficiency virus type-1 envelope transmembrane glycoprotein. *J. Virol.*, **67**, 3615-3619.

Chen, Y.H., Yang, J.T. & Chau, K.H. (1974) Determination of the helix and beta forms of proteins in aqueous solution by circular dichroism. *Biochemistry*, **13**, 3350-3359.

Chernomordik, L.V., Kozlov, M.M., Melikyan, G.B., Abidor, I.G., Markin, V.S. & Chizmadzhev, Y.A. (1985) The shape of lipid molecules and monolayer membrane fusion. *Biochim. Biophys. Acta*, **812**, 643-655.

Chernomordik, L.V., Melikyan, G.B. & Chizmadzhev, Y.A. (1987) Biomembrane fusion- a new concept derived from model studies using two interacting planar lipid bilayers. *Biochim. Biophys. Acta*, **906**, 309-352.

Chernomordik, L.V., Vogel, S.S., Sokoloff, A., Onaran, H.O., Leikina, E.A. & Zimmerberg, J. (1993) Lysolipids reversibly inhibit Ca^{2+}-dependent, GTP-dependent and pH-dependent fusion of biological membranes. *FEBS Lett.*, **318**, 71-76.

Chernomordik, L., Chanturiya, A., Green, J. & Zimmerberg, J. (1995a) The hemifusion intermediate and its conversion to complete fusion: regulation by membrane composition. *Biophys. J.*, **69**, 922-929.

Chernomordik, L., Kozlov, M.M. & Zimmerberg, J. (1995b) Lipids in biological membrane fusion. *J. Membr. Biol.*, **146**, 1-14.

Chernomordik, L., Leikina, E., Cho, M.S. & Zimmerberg, J. (1995c) Control of baculovirus gp64-induced syncytium formation by membrane lipid composition. *J. Virol.*, **69**, 3049-3058.

Chernomordik, L.V. & Zimmerberg, J. (1995d) Bending membranes to the task: structural intermediates in bilayer fusion. *Curr. Opin. Struct. Biol.*, **5**, 541-547.

Chernomordik, L. (1996) Non-bilayer lipids and biological fusion intermediates. *Chem. Phys. Lipids*, **81**, 203-213.

Chou, P.Y. & Fasman, G.D. (1978) Empirical predictions of protein conformation. *Annu. Rev. Biochem.*, **47**, 251-257.

Clements, G.J., Pricejones, M.J., Stephens, P.E., Sutton, C., Schulz, T.F., Clapham, P.R., McKeating, J.A., McClure, M.O., Thomson, S., Marsh, M., Kay, J., Weiss, R.A. & Moore, J.P. (1991) The V3 loops of the HIV-1 and HIV-2 surface glycoproteins contain proteolytic cleavage sites- a possible function in viral fusion. *AIDS Res. Hum. Retr.*, **7**, 3-16.

Colotto, A., Martin, I., Ruysschaert, J.M., Sen, A., Hui, S.W. & Epand, R.M. (1996) Structural study of the interaction between the SIV fusion peptide and model membranes. *Biochemistry*, **35**, 980-989.

Colotto, A. & Epand, R.M. (1997) Structural study of the relationship between the rate of membrane fusion and the ability of the fusion peptide of Influenza virus to perturb bilayers. *Biochemistry*, **36**, 7644-7651.

Copeland, C.S., Doms, R.W., Bolzau, E.M., Webster, R.G. & Helenius, A. (1986) Assembly of Influenza hemagglutinin trimers and its role in intracellular transport. *J. Cell. Biol.*, **103**, 1179-1191.

Corver, J., Moesby, L., Erukula, R.K., Reddy, K.C., Bittman, R. & Wilschut, J. (1995) Sphingolipid-dependent fusion of Semliki forest virus with cholesterol-containing liposomes requires both the 3-hydroxyl group and the double bond of the sphingolipid backbone. *J. Virol.*, **69**, 3220-3223.

Cotter, S.M. & Essex, M.E. (1977) Animal model of human disease. Acute lymphoblastic leukemia, aplastic anemia. Animal model: feline acute lymphoblastic leukemia and aplastic anemia. *Am. J. Pathol.*, **87**, 265-267.

Creutz, C.E. (1981) Cis-unsaturated fatty-acids induce the fusion of chromaffin granules aggregated by synexin. *J. Cell. Biol.*, **91**, 247-256.

Cullis, P.R. & de Kruijff, B. (1978) Polymorphic phase behaviour of lipid mixtures as detected by ^{31}P NMR. Evidence that cholesterol may destabilise bilayer structure in membrane systems containing phosphatidylethanolamine. *Biochim. Biophys. Acta*, **507**, 207-218.

Cullis, P.R. & Hope, M.J. (1978) Effects of fusogenic agent on membrane structure of erythrocyte ghosts and the mechanism of membrane fusion. *Nature*, **271**, 672-674.

Cullis, P.R., Hope, M.J., de Kruijff, B., Verkleij, A.J. & Tilcock, C.P.S. (1985) Structural properties and functional roles of phospholipids in biological membranes. *Phospholipids and Cellular Regulations* (ed. by J.F. Kuo), CRC Press, Boca Raton, FL, 1-59.

Cullis, P.R., Tilcock, C.P.S. & Hope, M.J. (1991) Lipid polymorphism. *Membrane fusion* (ed. by J. Wilschut and D. Hoekstra), Marcel Dekker, New York, 35-64.

Curran, M.J., Cohen, F.S., Chandler, D.E., Munson, P.J. & Zimmerberg, J. (1993) Exocytotic fusion pores exhibit semi-stable states. *J.Membr. Biol.*, **133**, 61-75.

D'Souza, M.P. & Harden, V.A. (1997) Chemokines and HIV-1 second receptors. *Nature Med.*, **2**, 1293-1300.

Danieli, T., Pelletier, S.L., Henis, Y.I. & White, J.M. (1996) Membrane fusion mediated by the Influenza virus hemagglutinin requires the concerted action of at least 3 hemagglutinin trimers. *J. Cell. Biol.*, **133**, 559-569.

Daniels, R.S., Douglas, A.R., Skehel, J.J. & Wiley, D.C. (1983) Analyses of the antigenicity of Influenza hemagglutinin at the pH optimum for virus-mediated membrane fusion. *J. Gen. Virol.*, **64**, 1657-1662.

Daniels, R.S., Downie, J.C., Hay, A.J., Knossow, M., Skehel, J.J., Wang, M.L. & Wiley, D.C. (1985) Fusion mutants of the Influenza virus hemagglutinin glycoprotein. *Cell*, **40**, 431-439.

Daniels, R.S., Jeffries, S., Yates, P., Schild, G.C., Rogers, G.N., Paulson, J.C., Wharton, S.A., Douglas, A.R., Skehel, J.J. & Wiley, D.C. (1987) The receptor binding and membrane fusion properties of Influenza virus variants selected using anti-hemagglutinin monoclonal antibodies. *EMBO J.*, **6**, 1459-1465.

Dawson, R.M.C., Irvine, R.F., Bray, J. & Quinn, P.J. (1984) Long chain unsaturated diacylglycerols cause a perturbation in the structure of phospholipid bilayers rendering them susceptible to phospholipase attack. *Biochem. Biophys. Res. Comm.*, **125**, 836-842.

Deber, C.M., Khan, A.R., Li, Z., Joensson, C., Glibowicka, M. & Wang, J. (1993) Val-Ala mutations selectively alter helix-helix packing in the transmembrane segment of phage M13 coat protein. *Proc. Natl. Acad. Sci. USA.*, **90**, 11648-11652.

Deber, C.M. & Goto, N., K. (1996) Folding proteins into membranes. *Nature Struct. Biol.*, **3**, 815-818.

Defrise-Quertain, F., Martin, I., Zarkik, S., Vandenbranden, M., Saermark, T., Brasseur, R., Burny, A. & Ruysschaert, J.M. (1992) Fusogenic activity of BLV (Bovine leukemia virus) peptides located in the gp30 NH2 terminal domain. *FASEB J.*, **6**, A 499.

DeGrado, W.F. & Lear, J.D. (1990) Conformationally constrained α-helical peptide models for protein ion channels. *Biopolymers*, **29**, 205-213.

Delahunty, M.D., Rhee, I., Freed, E.O. & Bonifacino, J.S. (1996) Mutational analysis of the fusion peptide of the Human immunodeficiency virus type-1 - identification of critical glycine residues. *Virology*, **218**, 94-102.

Delwart, E.L., Mosialos, G. & Gilmore, T. (1990) Retroviral envelope glycoproteins contain a leucine zipper-like repeat. *AIDS Res. Hum. Retr.*, **6**, 703-706.

Devaux, P.F., Mathivet, L., Cribier, S. & Farge, E. (1993) How lipid asymmetry can make vesicles fusion competent by inhibition of the thermal undulations. *Biochem. Soc. Trans.*, **21**, 276-280.

Doms, R.W., Helenius, A. & White, J. (1985) Membrane fusion activity of the Influenza virus hemagglutinin- the low pH-induced conformational change. *J. Biol. Chem.*, **260**, 2973-2981.

Doms, R.W. & Helenius, A. (1988) Properties of a viral fusion protein. *Molecular Mechanisms of Membrane Fusion* (ed. by S. Ohki, D. Doyle, T.D. Flanagan, S.W. Hui and E. Mayhew), Plenum Press, New York, 385-398.

Doms, R.W., Lamb, R.A., Rose, J.K. & Helenius, A. (1993) Folding and assembly of viral membrane proteins. *Virology*, **193**, 545-562.

Dubay, J.W., Roberts, S.J., Brody, B. & Hunter, E. (1992) Mutations in the leucine zipper of the Human immunodeficiency virus type-1 transmembrane glycoprotein affect fusion and infectivity. *J. Virol.*, **66**, 4748-4756.

Dubay, J.W., Dubay, S.R., Shin, H.J. & Hunter, E. (1995) Analysis of the cleavage site of the Human immunodeficiency virus type-1 glycoprotein- requirement of precursor cleavage for glycoprotein incorporation. *J. Virol.*, **69**, 4675-4682.

Duff, K.C., Cudmore, A.J. & Bradshaw, J.P. (1993) The location of amantadine hydrochloride and free base within phospholipid multilayers: a neutron and X-ray diffraction study. *Biochim. Biophys. Acta*, **1145**, 149-156.

Duff, K.C., Gilchrist, P.J., Saxena, A.M. & Bradshaw, J.P. (1994) Neutron diffraction reveals the site of amantidine blockade in the Influenza A M2 ion channel. *Virology*, **202**, 287-293.

Dufourcq, J. & Fauçon, J.-F. (1977) Intrinsic fluorescence study of lipid-protein interactions in membrane models. Binding of melittin, an amphipathic peptide, to phospholipid vesicles. *Biochim. Biophys. Acta*, **467**, 1-11.

Dunne, S., Cornell, R.B., Johnson, J.E., Glover, N.R. & Tracey, A.S. (1996) Structure of the membrane binding domain of CTP: phosphocholine cytidylyltransferase. *Biochemistry*, **35**, 11975-11984.

Dupont, Y., Gabriel, A., Chabre, M., Gulik-Krzywicki, T. & Schechter, E. (1972) Use of a new detector for X-ray diffraction and kinetics of the ordering of the lipids in *E.coli* membranes and model systems. *Nature*, **238**, 331-333.

Durrer, P., Galli, C., Hoenke, S., Corti, C., Gluck, R., Vorherr, T. & Brunner, J. (1996) H^+-induced membrane insertion of Influenza virus hemagglutinin involves the HA2 amino-terminal fusion peptide but not the coiled-coil region. *J. Biol. Chem.*, **271**, 13417-13421.

Düzgünes, N. (1985) Membrane fusion. *Subcellular Biochemistry* (ed. by D.B. Roodyn), p.195. Plenum Press, London.

Düzgünes, N. & Gambale, F. (1988) Membrane action of synthetic N-terminal peptides of Influenza virus hemagglutinin and its mutants. *FEBS Lett.*, **227**, 110-114.

Düzgünes, N. & Shavnin, S.A. (1992) Membrane destabilisation by N-terminal peptides of viral envelope proteins. *J. Membr. Biol.*, **128**, 71-80.

Eastman, S.J., Hope, M.J., Wong, K.F. & Cullis, P.R. (1992) Influence of phospholipid asymmetry on fusion between large unilamellar vesicles. *Biochemistry*, **31**, 4262-4268.

Eidelman, O., Schlegel, R., Tralka, T.S. & Blumenthal, R. (1984) pH-dependent fusion induced by Vesicular stomatitis virus glycoprotein reconstituted into phospholipid vesicles. *J. Biol. Chem.*, **259**, 4622-4628.

Ellens, H., Bentz, J. & Szoka, F.C. (1984) pH-induced destabilization of phosphatidylethanolamine containing liposomes- role of bilayer contact. *Biochemistry*, **23**, 1532-1538.

Ellens, H., Bentz, J. & Szoka, F.C. (1986) Fusion of phosphatidylethanolamine-containing liposomes and mechanism of the L_{α}-H_{II} phase transition. *Biochemistry*, **25**, 4141-4147.

Ellens, H., Siegel, D.P., Alford, D., Yeagle, P.L., Boni, L., Lis, L.J., Quinn, P.J. & Bentz, J. (1989) Membrane fusion and inverted phases. *Biochemistry*, **28**, 3692-3703.

Epand, R.F., Martin, I., Ruysschaert, J.M. & Epand, R.M. (1994) Membrane orientation of the SIV fusion peptide determines its effect on bilayer stability and ability to promote membrane fusion. *Biochem. Biophys. Res. Comm.*, **205**, 1938-1943.

Epand, R.M. (1985) Diacylglycerols, lysolecithin, or hydrocarbons markedly alter the bilayer to hexagonal phase transition temperature of phosphatidylethanolamines. *Biochemistry*, **24**, 7092-7095.

Epand, R.M. (1986) Virus replication inhibitory peptide inhibits the conversion of phospholipid bilayers to the hexagonal phase. *Biosci. Rep.*, **6**, 647-653.

Epand, R.M., Epand, R.F. & McKenzie, R.C. (1987) Effects of viral chemotherapeutic agents on membrane properties- studies of Cyclosporin-A, Benzyloxycarbonyl-d-Phe-l-Phe-Gly and Amantadine. *J. Biol. Chem.*, **262**, 1526-1529.

Epand, R.M. (1990) Hydrogen bonding and the thermotropic transitions of phosphatidylethanolamines. *Chem. Phys. Lipids*, **52**, 227-230.

Epand, R.M., Epand, R.F., Ahmed, N. & Chen, R. (1991) Promotion of hexagonal phase formation and lipid mixing by fatty acids with varying degrees of unsaturation. *Chem. Phys. Lipids*, **57**, 75-80.

Epand, R.M., Cheetham, J.J., Epand, R.F., Yeagle, P.L., Richardson, C.D., Rockwell, A. & DeGrado, W.F. (1992) Peptide models for the membrane destabilising actions of viral fusion proteins. *Biopolymers*, **32**, 309-314.

Epand, R.M., Epand, R.F., Richardson, C.D. & Yeagle, P.L. (1993) Structural requirements for the inhibition of membrane fusion by carbobenzoxy-d-Phe-Phe-Gly. *Biochim. Biophys. Acta*, **1152**, 128-134.

Epand, R.M. & Epand, R.F. (1994) Relationship between the infectivity of Influenza virus and the ability of its fusion peptide to perturb bilayers. *Biochem. Biophys. Res. Comm.*, **202**, 1420-1425.

Epand, R.M., Shai, Y., Segrest, J.P. & Anantharamaiah, G.M. (1995) Mechanism for the modulation of membrane bilayer properties by amphipathic helical peptides. *Biopolymers*, **37**, 319-338.

Ewald, P.P. (1921) Das 'reziproca gitter' in der strukturtheorie. *Z. Kristollagr. Miner*, **56**, 129-156.

Fantini, J., Cook, D.G., Nathanson, N., Spitalnik, S.L. & Gonzalezscarano, f. (1993) Infection of colonic epithelial cell lines by type-1 Human immunodeficiency virus is associated with cell surface expression of galactosylceramide, a potential alternative gp120 receptor. *Proc. Natl. Acad. Sci. USA.*, **90**, 2700-2704.

Fass, D. & Kim, P.S. (1995) Dissection of a retrovirus envelope protein reveals structural similarity to Influenza hemagglutinin. *Curr. Biol.*, **5**, 1377-1383.

Feng, Y., Broder, C.C., Kennedy, P.E. & Berger, E.A. (1996) HIV-1 entry cofactor functional cDNA cloning of a 7 transmembrane, G-protein coupled receptor. *Science*, **272**, 872-877.

Fessenden, R.J. & Fessenden, J.S. (1990) Spectroscopy. *Fundamentals of Organic Chemistry* (ed. by G. Davies), Harper and Row, Inc. New York, 485-522.

Forster, V. T. (1949) Experimentelle und theoretische untersuchung des zwischenmolekularen übergangs von elektronenanregungsenergie. *Z. Naturforsch*, **A 4A**, 321-327.

Franks, N.P., Arunachalam, T. & Caspi, E. (1978) A direct method for determination of membrane electron density profiles on an absolute scale. *Nature (London)*, **276**, 530-532.

Franks, N.P. & Leib, W.R. (1979) The structure of lipid bilayers and the effects of general anaesthetics: an X-ray and neutron diffraction study. *J. Mol. Biol.*, **133**, 469-500.

Franks, N.P. & Lieb, W.R. (1981) X-ray and neutron diffraction studies of lipid bilayers. *Liposomes: from physical structure to theraputic applications* (ed. by Knight), Elsevier North Holland Biomedical press, 243-272.

Fraser, R.D.B. & Macrae, T.P. (1981) Unit cell and molecular connectivity in tendon collagen. *Int. J. Biol. Macromol.*, **3**, 193-200.

Freed, E.O., Myers, D.J. & Risser, R. (1990) Characterization of the fusion domain of the Human immunodeficiency virus type-1 envelope glycoprotein gp41. *Proc. Natl. Acad. Sci. USA.*, **87**, 4650-4654.

Frey, S., Marsh, M., Gunther, S., Pelchenmatthews, A., Stephens, P., Ortlepp, S. & Stegmann, T. (1995) Temperature dependence of cell-cell fusion induced by the envelope glycoprotein of Human immunodeficiency virus type-1. *J. Virol.*, **69**, 1462-1472.

Fuller, A.O. & Spear, P.G. (1987) Anti glycoprotein-D antibodies that permit adsorption but block infection by Herpes simplex virus-1 prevent virion cell fusion at the cell surface. *Proc. Natl. Acad. Sci. USA.*, **84**, 5454-5458.

Fung, B.K.-K. & Stryer, L. (1978) Surface density determination in membranes by fluorescence energy transfer. *Biochemistry*, **17**, 5241-5248.

Gagné, J., Stamatatos, L., Diacovo, T., Hui, S.W., Yeagle, P.L. & Silvius, J.R. (1985) Physical properties and surface interactions of bilayer membranes containing N-methylated phosphatidylethanolamines. *Biochemistry*, **24**, 4400-4408.

Gallaher, W.R., Segrest, J.P. & Hunter, E. (1992) Are fusion peptides really 'sided' insertional helices? *Cell*, **70**, 531-532.

Gething, M.J., White, J.M. & Waterfield, M.D. (1978) Purification of the fusion protein of Sendai virus: Analysis of the NH_2-terminal sequence generated during precursor activation. *Proc. Natl. Acad. Sci. USA.*, **75**, 2737-2740.

Gething, M.J. & Sambrook, J. (1981) Cell surface expression of Influenza hemagglutinin from a cloned DNA copy of the RNA gene. *Nature*, **293**, 620-625.

Gething, M.J., Doms, R.W., York, D. & White, J. (1986) Studies on the mechanism of membrane-fusion- site-specific mutagenesis of the hemagglutinin of Influenza virus. *J. Cell. Biol.*, **102**, 11-23.

Glaeser, R.M. & Jap, B.K. (1985) Absorption flattening in the circular dichroism spectra of small membrane fragments. *Biochemistry*, **24**, 6398-6401.

Glick, B.S. & Rothman, J.E. (1987) Possible role for fatty acyl-coenzymeA in intracellular protein transport. *Nature*, **326**, 309-312.

Gollins, S.W. & Porterfield, J.S. (1986) pH-dependent fusion between the flavivirus West Nile and liposomal model membranes. *J. Gen. Virol.*, **67**, 157-166.

Gray, C., Tatulian, S.A., Wharton, S.A. & Tamm, L.K. (1996) Effect of the N-terminal glycine on the secondary structure, orientation and interaction of the Influenza hemagglutinin fusion peptide with lipid bilayers. *Biophys. J.*, **70**, 2275-2286.

Gruner, S.M. (1985) Intrinsic curvature hypothesis for biomembrane lipid composition - a role for nonbilayer lipids. *Proc. Natl. Acad. Sci. USA.*, **82**, 3665-3669.

Gruner, S.M., Parsegian, V.A. & Rand, R.P. (1986) Directly measured deformation energy of phospholipid H_{II} hexagonal phases. *Faraday Discuss. Chem. Soc.*, **81**, 29-37.

Gruner, S.M., Tate, M.W., Kirk, G.L., So, P.T.C., Keane, D.T., Tilcock, C.P.S. & Cullis, P.R. (1988) X-ray diffraction study of the polymorphic behaviour of N-methylated dioleoylphosphatidylethanolamine. *Biochemistry*, **27**, 2853-2866.

Gruner, S.M. (1992) Nonlamellar lipid phases. *The Structure of Biological Membranes* (ed. by P.L. Yeagle), CRC Press, Boca Raton, 211-250.

Gulik, A., Luzzati, V., DeRosa, M. & Gambacorta, A. (1988) Tetraether lipid components from a thermoacidophilic archaebacterium. *J. Mol. Biol.*, **201**, 429-435.

Günther-Ausborn, S., Praetor, A. & Stegmann, T. (1995) Inhibition of Influenza-induced membrane fusion by lysophosphatidylcholine. *J. Biol. Chem.*, **270**, 29279-29285.

Gutensohn, N., Essex, M., Francis, D.P. & Hardy, W.D.J. (1980) Risk to humans from exposure to Feline leukaemia virus: epidemiological considerations. *Viruses in Naturally Occurring Cancers* (ed. by M. Essex, G.J. Todaro and H. zur Hausen), Cold Spring Harbor Laboratory, Cold Spring Harbor, New York, 699.

Hamilton, J.A., Bhamidipati, S.P., Kodali, D.R. & Small, D.H. (1991) The interfacial conformation and transbilayer movement of diacylglycerols in phospholipid bilayers. *J. Biol. Chem.*, **266**, 1177-1186.

Hamilton, J.A., Fujito, D.T. & Hammer, C.F. (1991) Solubilization and localization of weakly polar lipids in unsonicated egg phosphatidylcholine- a C-13 MAS NMR study. *Biochemistry*, **30**, 2894-2902.

Hardy, W.D.J., Hess, P.W., Essex, M. & Cotter, S. (1973) Horizontal transmission of Feline leukaemia virus. *Nature (London)*, **244**, 266-269.

Hart, T.K., Kirsh, R., Ellens, H., Sweet, R.W., Lambert, D.M., Petteway, S.R., Leary, J. & Bugelski, P.J. (1991) Binding of soluble CD4 proteins to Human immunodeficiency virus type-1 and infected cells induces release of envelope glycoprotein gp120. *Proc. Natl. Acad. Sci. USA.*, **88**, 2189-2193.

Harter, C., James, P., Bachi, T., Semenza, G. & Brunner, J. (1989) Hydrophobic binding of the ectodomain of Influenza hemagglutinin to membranes occurs through the fusion peptide. *J. Biol. Chem.*, **264**, 6459-6464.

He, K., Ludtke, S.J., Heller, W.T. & Huang, H.W. (1996) Mechanism of alamethicin insertion into lipid bilayers. *Biophys. J.*, **71**, 2669-2679.

He, K., Ludtke, S.J., Worcester, D.L. & Huang, H.W. (1995) Antimicrobial peptide pores in membranes detected by neutron in-plane scattering. *Biochemistry*, **34**, 15614-15618.

He, K., Ludtke, S.J., Worcester, D.L. & Huang, H.W. (1996) Neutron scattering in the plane of membrane: structure of alamethicin pores. *Biophys. J.*, **70**, 2659-2666.

Helfrich, W. (1973) Elastic properties of lipid bilayers: theory and possible experiments. *Z. Naturforsch*, **28c**, 693-703.

Heller, W.T., Ludtke, S.J., Harroun, T.A. & Huang, H.W. (1997) Effect of changing the size of lipid headgroup on peptide insertion into membranes. *Biophys. J.*, **73**, 239-244.

Helm, C.A., Israelachvili, J.N. & McGuiggan, P.M. (1989) Molecular mechanism and forces involved in the adhesion and fusion of amphiphilic bilayers. *Science*, **246**, 919-922.

Hernandez, L.D., Peters, R.J., Delos, S.E., Young, J.A.T., Agard, D.A. & White, J.M. (1997) Activation of a retroviral membrane fusion protein: soluble receptor-induced liposome binding of the ALSV envelope glycoprotein. *J. Cell. Biol.*, **139**, 1455-1464.

Hoekstra, D. & Kok, J.W. (1989) Entry mechanisms of enveloped viruses-implications for fusion of intracellular membranes. *Biosci. Rep.*, **9**, 273-305.

Hope, M.J., Bally, M.B., Webb, G. & Cullis, P.R. (1985) Production of large unilamellar vesicles by a rapid extrusion procedure. Characterisation of size distribution, trapped volume and ability to maintain a membrane potential. *Biochim. Biophys. Acta*, **812**, 55-65.

Hore, P.J. (1996) *Nuclear Magnetic Resonance*, Oxford University Press, Oxford, 1-90.

Horth, M., Lambrechts, B., Marinee, C., Bex, F., Thiriart, C., Ruysschaert, J., Burny, A. & Brasseur, R. (1991) Theoretical and functional analysis of the SIV fusion peptide. *EMBO J.*, **10**, 2747-2755.

Horwitz, A.F. & Klein, M.P. (1972) Magnetic resonance studies on membrane and model membrane systems: II. Phosphorus spectra and relaxation rates. *J. Supramol. Struct.*, **1**, 19-28.

Hoyt, D.W. & Gierasch, L.M. (1991) Hydrophobic content and lipid interactions of wild-type and mutant OmpA signal peptides correlate with their *in vivo* function. *Biochemistry*, **30**, 10155-10163.

Huang, C (1971) Carriers and specificity in membranes. IV. Model vesicles and membranes. Phosphatidylcholine vesicles: formation, physical characteristics and dye-lipid interaction. *Neurosci. Res. Prog. Bull.*, **9**, 380-381.

Huang, H.W. (1995) Elasticity of lipid bilayer interaction with amphiphilic helical peptides. *J. Phys. II France*, **5**, 1427-1431.

Hughson, F.M. (1995) Structural characterisation of viral fusion proteins. *Curr. Biol.*, **5**, 265-274.

Hui, S.W., Stewart, T.P. & Boni, L.T. (1983) The nature of lipidic particles and their roles in polymorphic transitions. *Chem. Phys. Lipids*, **33**, 113-126.

Hui, S.W., Stewart, T.P., Yeagle, P.L. & Albert, A.D. (1981) Bilayer to non-bilayer transition in mixtures of phosphatidylethanolamine and phosphatidylcholine-implications for membrane properties. *Arch. Biochem. Biophys.*, **207**, 227-240.

Hunter, E. & Swanstrom, R. (1990) Retrovirus envelope glycoproteins. *Curr. Top. Microbiol. Immunol.*, **157**, 187-253.

Hvoslef, J. (1958) A neutron diffraction study of pentaerythritol. *Acta Crystallogr.*, **11**, 383-388.

Ishiguro, R., Matsumoto, M. & Takahashi, S. (1996) Interaction of fusogenic synthetic peptide with phospholipid bilayers- orientation of the peptide alpha-helix and binding isotherm. *Biochemistry*, **35**, 4976-4983.

Israelachvili, J.N., Marcelja, S. & Horn, R.G. (1980) Physical principles of membrane organisation. *Q. Rev. Biophys.*, **13**, 121-200.

Jacobs, R.E. & White, S.H. (1989) The nature of the hydophobic binding of small peptides at the bilayer interface: implications for the insertion of transbilayer helices. *Biochemistry*, **28**, 3421-3437.

Jacrot, B. (1976) The study of biological structures by neutron scattering from solution. *Rep. Prog. Phys.*, **39**, 911-953.

Jarrett, O. (1971) Virology and host range of Feline leukaemia virus. *J. Am. Vet. Med. Assoc.*, **158**, 1032-1036.

Jarrett, O., Laird, H.M. & Hay, D. (1969) Growth of Feline leukaemia virus in human cells. *Nature (London)*, **224**, 1208-1209.

Jarrett, O. & Russell, P.H. (1978) Differential growth and transmission in cats of Feline leukaemia viruses of subgroups A and B. *Int. J. Cancer*, **21**, 466-472.

Jarrett, W., Jarrett, O., Mackey, L., Laird, H., Hardy, W.D.J. & Essex, M. (1973) Horizontal transmission of leukemia virus and leukemia in the cat. *J. Nat. Cancer Inst.*, **51**, 833-841.

Jarrett, W.F.H., Crawford, E.M., Martin, W.B. & Davie, F. (1964) A virus-like particle associated with leukemia (lymphosarcoma). *Nature (London)*, **202**, 567-568.

Jasanoff, A. & Fersht, A.R. (1994) Quantitative determination of helical propensities from trifluoroethanol titration curves. *Biochemistry*, **33**, 2129-2135.

Junankar, P.R. & Cherry, R.J. (1986) Temperature and pH dependence of the haemolytic activity of Influenza virus and of the rotational mobility of the spike glycoproteins. *Biochim. Biophys. Acta.*, **854**, 198-206.

Kanaseki, T., Kawasaki, K., Murata, M., Ikeuchi, Y. & Ohnishi, S. (1997) Structural features of membrane fusion between Influenza virus and liposome as revealed by quick-freezing electron microsocopy. *J. Cell. Biol.*, **137**, 1041-1056.

Kelsey, D.R., Flanagan, T.D., Young, J. & Yeagle, P.L. (1990) Peptide inhibitors of enveloped virus infection inhibit phospholipid vesicle fusion and Sendai virus fusion with phospholipid vesicles. *J. Biol. Chem.*, **265**, 12178-12183.

Kelsey, D.R., Flanagan, T.D., Young, J.E. & Yeagle, P.L. (1991) Inhibition of Sendai virus fusion with phospholipid vesicles and human erythrocyte membranes by hydrophobic peptides. *Virology*, **182**, 690-702.

Kemble, G.W., Bodian, D.L., Rose, J., Wilson, I.A. & White, J.M. (1992) Intermonomer disulfide bonds impair the fusion activity of Influenza virus hemagglutinin. *J. Virol.*, **66**, 4940-4950.

Kemble, G.W., Danielli, T. & White, J.M. (1994) Lipid-anchored Influenza haemagglutinin promotes hemifusion, not complete fusion. *Cell*, **76**, 383-391.

Kendall, D.A. & MacDonald, R.C. (1982) A fluorescence assay to monitor vesicle fusion and lysis. *J. Biol. Chem.*, **257**, 13892-13895.

Kielian, M., Jungerwirth, S., Sayad, K.U. & Decandido, S. (1990) Biosynthesis, maturation, and acid activation of the Semliki forest virus fusion protein. *J. Virol.*, **64**, 4614-4624.

Kim, C.H., Macosko, J.C., Yu, Y.G. & Shin, Y.K. (1996) On the dynamics and conformation of the HA2 domain of the Influenza virus hemagglutinin. *Biochemistry*, **35**, 5359-5365.

King, G.I. & White, S.H. (1986) Determining bilayer hydrocarbon thickness from neutron diffraction measurments using strip-function models. *Biophys. J.*, **49**, 1047-1054.

Kirk, G.L., Gruner, S.M. & Stein, D.L. (1984) A thermodynamic model of the lamellar to inverse hexagonal phase transition of lipid membrane water systems. *Biochemistry*, **23**, 1093-1102.

Klenk, H.D. (1973) Virus membranes. *Biological Membranes* (ed. by D. Chapman and D.F.H. Wallach), p.145-183. Academic Press, London.

Kohler, S.J. & Klein, M.P. (1977) Orientation and dynamics of phospholipid head groups in bilayers and membranes determined from ^{31}P nuclear magnetic resonance chemical shielding tensors. *Biochemistry*, **16**, 519

Kolber, M.A. & Haynes, D.H. (1979) Evidence for a role of phosphatidyl ethanolamine as a modulator of membrane-membrane contact. *J. Membr. Biol.*, **48**, 95-114.

Korte, T., Ludwig, K. & Herrmann, A. (1992) pH-dependent hydrophobicity profile of hemagglutinin of Influenza virus and its possible relevance in virus fusion. *Biosci. Rep.*, **12**, 397-406.

Korte, T. & Herrman, A. (1994) pH-dependent binding of the fluorophore bis-ANS to Influenza virus reflects the conformational change of haemagglutinin. *Eur. Biophys. J.*, **23**, 105-113.

Kowalski, M., Potz, J., Basiripour, L., Dorfman, T., Wei, C.G., Terwilliger, E., Dayton, A., Rosen, C., Haseltine, W. & Sodroski, J. (1987) Functional regions of the envelope glycoprotein of Human immunodeficiency virus type-1. *Science*, **237**, 1351-1355.

Kozlov, M.M. & Markin, V.S. (1983) Possible mechanism of membrane fusion. *Biofizika*, **28**, 242-247.

Kozlov, M.M., Leikin, S. & Rand, R.P. (1994) Bending, hydration and interstitial energies quantitatively account for the hexagonal-lamellar-hexagonal re-entrant phase transition in dioleoylphosphatidylethanolamine. *Biophys. J.*, **67**, 1603-1611.

LaBranche, C.C., Sauter, M.M., Haggarty, B.S., Vance, P.J., Romano, J., Hart, T.K., Bugelski, P.J. & Hoxie, J.A. (1994) Biological, molecular, and structural analysis of a cytopathic variant from a molecularly cloned Simian immunodeficiency virus. *J. Virol.*, **68**, 5509-5522.

Laird, H.M., Jarrett, O. & Whalley, J.M. (1973) Electron microscopy of early interactions between Feline leukaemia virus and cells in tissue culture. *Bibl. Haemat.*, **39**, 133-138.

Lakowicz, J.R. (1983) *Principles of Fluorescence Spectroscopy* Plenum Publishing Corp. New York, 345-347.

Landh, T. (1995) From entangled membranes to eclectic morphologies - cubic membranes as subcellular space organizers. *FEBS Lett.*, **369**, 13-17.

Langlais, J., Zollinger, M., Plante, L., Chapdelaine, A., Bleau, G. & Roberts, K.D. (1981) Localisation of cholesterol sulphate in human spermatozoa in support of a hypothesis for the mechanism of capacitation. *Proc. Natl. Acad. Sci. USA.*, **78**, 7266-7270.

Larsen, C.E., Alford, D.R., Young, L.J.T., McGraw, T.P. & Düzgünes, N. (1990) Fusion of Simian immunodeficiency virus with liposomes and erythrocyte ghost membranes- effects of lipid composition, pH and calcium. *J. Gen. Virol.*, **71**, 1947-1955.

Larsen, C.E., Nir, S., Alford, D.R., Jennings, M., Lee, K. &, Düzgünes N. (1993) Human immunodeficiency virus type 1 (HIV-1) fusion with model membranes: kinetic analysis and the role of lipid composition, pH and divalent cations. *Biochim. Biophys. Acta*, **1147**, 223-236.

Lear, J.D. & DeGrado, W.F. (1987) Membrane binding and conformational properties of peptides representing the NH2 terminus of Influenza HA-2. *J. Biol. Chem.*, **162**, 6500-6505.

Lear, J.D., Wasserman, Z.R. & DeGrado, W.F. (1988) Synthetic amphiphilic peptide models for protein ion channels. *Science*, **240**, 1177-1181.

Lee, J. & Lentz, B.R. (1997) Evolution of lipidic structures during model membrane fusion and the relation of this process to cell membrane fusion. *Biochemistry*, **21**, 6251-6259.

Leenhouts, J.M., van den Wijngaard, P.W.J., de Kroon, A.I.P.M. & de Kruijff, B. (1995) Anionic phospholipids can mediate membrane insertion of the anionic part of a bound peptide. *FEBS Lett.*, **370**, 189-192.

Lehtonen, J.Y.A., Holopainen, J.M. & Kinnunen, P.K.J. (1996) Evidence for the formation of microdomains in liquid crystalline large unilamellar vesicles caused by hydrophobic mismatch of the constituent phospholipids. *Biophys. J.*, **70**, 1753-1760.

Leikin, S.L., Kozlov, M.M., Chernomordik, L.V., Markin, V.S. & Chizmadzhev, Y.A. (1987) Membrane fusion- overcoming of the hydration barrier and local restructuring. *J. Theor. Biol.*, **129**, 411-425.

Li, S.C. & Deber, C.M. (1994) A measure of helical propensity for amino acids in membrane environments. *Nature Struct. Biol.*, **1**, 368-373.

Lifson, J.D., Feinberg, M.B., Reyes, G.R., Rabin, L., Banapour, B., Chakrabarti, S., Moss, B., Wongstaal, F., Steimer, K.S. & Engleman, E.G. (1986) Induction of CD4-dependent cell fusion by the HTLV-III/LAV envelope glycoprotein. *Nature*, **323**, 725-728.

Lis, L.J., McAllister, M., Fuller, N., Rand, R.P. & Parsegian, V.A. (1982) Interactions between neutral phospholipid bilayer membranes. *Biophys. J.*, **37**, 657-666.

Long, D., Berson, J.F., Cook, D.G. & Doms, R.W. (1994) Characterization of Human immunodeficiency virus type-1 gp120 binding to liposomes containing galactosylceramide. *J. Virol.*, **68**, 5890-5898.

Longo, M.L., Waring, A.J. & Hammer, D.A. (1997) Interaction of the Influenza fusion peptide with lipid bilayers: area expansion and permeation. *Biophys. J.*, **73**, 1430-1439.

Lu, M., Blacklow, S.C. & Kim, P.S. (1995) A trimeric structural domain of the HIV-1 transmembrane glycoprotein. *Nature Struct. Biol.*, **2**, 1075-1082.

Lu, Z.X., Fok, K.F., Ericson, B.W. & Hugli, T.E. (1984) Conformational analysis of COOH-terminal segments of human C3A- evidence of ordered conformation in an active 21-residue peptide. *J. Biol. Chem.*, **259**, 7367-7370.

Lucy, J.A. (1970) The fusion of biological membranes. *Nature*, **227**, 815-817.

Ludtke, S.J., He, K. & Huang, H.W. (1995) Membrane thinning caused by magainin 2. *Biochemistry*, **34**, 16764-16769.

Ludtke, S.J., He, K., Heller, W.T., Harroun, T.A., Yang, L. & Huang, H.W. (1996) Membrane pores induced by magainin. *Biochemistry*, **35**, 13723-13728.

Lüneberg, J., Martin, I., Nussler, R.F., Ruysschaert, J.M. & Herrmann, A. (1995) Structure and topology of the Influenza virus fusion peptide in lipid bilayers. *J. Biol. Chem.*, **270**, 27606-27614.

Luzzati, V. (1968) X-ray diffraction studies of lipid-water systems. *Biological membranes.* (ed. by D. Chapman), Academic Press, New York, 71-123.

Luzzati, V. & Husson, F. (1962) The structure of the liquid-crystalline phases of lipid-water systems. *J. Cell. Biol.*, **12**, 207-219.

Luzzati, V. & Reiss-Husson, F. (1966) Structure of the cubic phase of lipid-water systems. *Nature (London)*, **210**, 1351-1352.

Luzzati, V., Vargas, R., Mariani, P., Gulik, A. & Delacroix, H. (1993) Cubic phases of lipid-containing systems- elements of a theory and biological connotations. *J. Mol. Biol.*, **229**, 540-551.

Macosko, J.C., Kim, C.H. & Shin, Y.K. (1997) The membrane topology of the fusion peptide region of Influenza hemagluttinin determined by spin-labelling EPR. *J. Mol. Biol.*, **267**, 1139-1148.

Markin, V.S., Kozlov, M.M. & Borovjagin, V.L. (1984) On the theory of membrane fusion. The stalk mechanism. *Gen. Physiol. Biophys.*, **3**, 361-377.

Markwell, M.K., Haas, S.M., Tolbert, N.E. & Bieber, L.L. (1981) Protein determination in membrane and lipoprotein samples: manual and automated procedures. *Meth. Enzymol.*, **72**, 296-303.

Marsh, D. (1996) Intrinsic curvature in normal and inverted lipid structures and in membranes. *Biophys. J.*, **70**, 2248-2255.

Marsh, M. & Helenius, A. (1989) Virus entry into animal cells. *Adv. Virus Res.*, **36**, 107-151.

Martin, I., Defrisequertain, F., Mandieau, V., Nielsen, N.M., Saermark, T., Burny, A., Brasseur, R., Ruysschaert, J.M. & Vandenbranden, M. (1991) Fusogenic activity of SIV (Simian immunodeficiency virus) peptides located in the gp32 NH2-terminal domain. *Biochem. Biophys. Res. Comm.*, **175**, 872-879.

Martin, I., Defrisequertain, F., Decroly, E., Vandenbranden, M., Brasseur, R. & Ruysschaert, J.M. (1993) Orientation and structure of the NH2-terminal of the HIV-1 gp41 peptide in fused and aggregated liposomes. *Biochim. Biophys. Acta*, **1145**, 124-133.

Martin, I., Dubois, M.C., Defrisequertain, F., Saermark, T., Burny, A., Brasseur, R. & Ruysschaert, J.M. (1994) Correlation between fusogenicity of synthetic modified peptides corresponding to the NH2-terminal extremity of Simian immunodeficiency virus gp32 and their mode of insertion into the lipid bilayer - an infrared spectroscopy study. *J. Virol.*, **68**, 1139-1148.

Martin, I. & Ruysschaert, J.M. (1995) Lysophosphatidylcholine inhibits vesicles fusion induced by the NH2-terminal extremity of SIV/HIV fusogenic proteins. *Biochim. Biophys. Acta- Biomembranes*, **1240**, 95-100.

Martin, I., Schaal, H., Scheid, A. & Ruysschaert, J.M. (1996) Lipid membrane fusion induced by the Human immunodeficiency virus type-1 gp41 N-terminal extremity is determined by its orientation in the lipid bilayer. *J. Virol.*, **70**, 298-304.

Mayorga, L.S., Colombo, M.I., Lennartz, M., Brown, E.J., Rahman, K.H., Weiss, R., Lennon, P.J. & Stahl, P.D. (1993) Inhibition of endosome fusion by phospholipase-A(2) (PLA2) inhibitors points to a role for PLA2 in endocytosis. *Proc. Natl. Acad. Sci. USA.*, **90**, 10255-10259.

McClure, M.O., Marsh, M. & Weiss, R.A. (1988) Human immunodeficiency virus infection of CD4-bearing cells occurs by a pH-independent mechanism. *EMBO J.*, **7**, 513-518.

McCune, J.M., Rabin, L.B., Feinberg, M.B., Lieberman, M., Kosek, J.C., Reyes, G.R. & Weissman, I.L. (1988) Endoproteolytic cleavage of gp160 is required for the activation of Human immunodeficiency virus. *Cell*, **53**, 55-67.

Mcintosh, T.J., Magid, A.D. & Simon, S.A. (1989) Cholesterol modifies the short-range repulsive interactions between phosphatidylcholine membranes. *Biochemistry*, **28**, 17-25.

McKenzie, R.C., Epand, R.M. & Johnson, D.C. (1987) Cyclosporin A inhibits Herpes simplex virus-induced cell fusion but not virus penetration into cells. *Virology*, **159**, 1-9.

Melikyan, G.B., White, J.M. & Cohen, F.S. (1995) GPI-anchored Influenza hemagglutinin induces hemifusion to both red blood cell and planar bilayer membranes. *J. Cell. Biol.*, **131**, 679-691.

Miller, C.R., Bennett, D.E., Chang, D.Y. & OBrien, D.F. (1996) Effect of liposomal composition on photoactivated liposome fusion. *Biochemistry*, **35**, 11782-11790.

Moore, J.P., McKeating, J.A., Weiss, R.A. & Sattentau, Q.J. (1990) Dissociation of gp120 from HIV-1 virions induced by soluble CD4. *Science*, **250**, 1139-1142.

Muga, A., Neugebauer, W., Hirama, T. & Surewicz, W.K. (1994) Membrane interaction and conformational properties of the putative fusion peptide of PH-30, a protein active in sperm-egg fusion. *Biochemistry*, **33**, 4444-4448.

Mulligan, M.J., Yamshchikov, G.V., Ritter, G.D., Gao, F., Jin, M.J., Nail, C.D., Spies, C.P., Hahn, B.H. & Compans, R.W. (1992) Cytoplasmic domain truncation enhances fusion activity by the exterior glycoprotein complex of Human immunodeficiency virus type-2 in selected cell types. *J. Virol.*, **66**, 3971-3975.

Murata, M., Sugahara, Y., Takahashi, S. & Ohnishi, S. (1987) pH-dependent membrane fusion activity of a synthetic 20 amino acid peptide with the same sequence as that of the hydrophobic segment of Influenza virus hemagglutinin. *J. Biochem*, **102**, 957-962.

Murata, M., Takahashi, S., Shirai, Y., Kagiwada, S., Hishida, R. & Ohnishi, S. (1993) Specificity of amphiphilic anionic peptides for fusion of phospholipid vesicles. *Biophys. J.*, **64**, 724-734.

Mutz, M. & Helfrich, W. (1990) Bending rigidities of some biological model membranes as obtained from the Fourier analysis of contour sections. *J. Physique*, **51**, 991-1002.

Myers, G., Wain-Hobson, S., Henderson, L.E., Korber, B., Jeang, K.T. & Pavlakis, G.N. (1994) Human retroviruses and AIDS. *Theor. Biol. Biophys. Grp. 10,* Los Alamos, NM.

New, R.R.C. (1990) *Liposomes a practical approach.* IRL press, Oxford.

Nichols, J.W. & Pagano, R.E. (1981) Kinetics of soluble lipid monomer diffusion between vesicles. *Biochemistry*, **20**, 2783-2789.

Nieva, J.L., Bron, R., Corver, J. & Wilschut, J. (1994a) Membrane fusion of Semliki forest virus requires sphingolipids in the target membrane. *EMBO J.*, **13**, 2797-2804.

Nieva, J.L., Nir, S., Muga, A., Goñi, F.M. & Wilschut, J. (1994b) Interaction of the HIV-1 fusion peptide with phospholipid vesicles: different structural requirements for fusion and leakage. *Biochemistry*, **33**, 3201-3209.

Nieva, J.L., Alonso, A., Basáñez, G., Goñi, F.M., Gulik, A., Vargas, R. & Luzzati, V. (1995) Topological properties of two cubic phases of a phospholipid-cholesterol-diacylglycerol aqueous system and their possible implications in the phospholipase C-induced liposome fusion. *FEBS Lett.*, **368**, 143-147.

Nir, S., Bentz, J. & Wilschut, J. (1980) Mass action kinetics of phosphatidylserine vesicle fusion as monitored by coalescence of internal vesicle contents. *Biochemistry*, **19**, 6030-6036.

Nir, S., Klappe, K. & Hoekstra, D. (1986) Mass action analysis of kinetics and extent of fusion between Sendai virus and phospholipid vesicles. *Biochemistry*, **25**, 8261-8266.

Nordmeier, E., Zeilinger, C. & Lechner, M.D. (1992) Phospholipid liposomes: preparation, characterization and uses. *J. Applied Polymer Sci.*, **44**, 533-544.

Novick, S.L. & Hoekstra, D. (1988) Membrane penetration of Sendai virus glycoproteins during the early stages of fusion with liposomes as determined by hydrophobic photoaffinity labeling. *Proc. Natl. Acad. Sci. USA.*, **85**, 7433-7437.

Ohnishi, S. (1988) Fusion of viral envelopes with cellular membranes. *Curr. Top. Membr. Transp.*, **32**, 257-296.

Oravecz, T., Pall, M. & Norcross, M.A. (1996) Beta-chemokine inhibition of monocytotropic HIV-1 infection. Interference with a postbinding fusion step. *J. Immunol.*, **157**, 1329-1332.

Ott, S., Schurtenberger, P. & Wunderli-Allenspach, H. (1994) Liposomes and Influenza viruses as an in vitro model for membrane interactions II. Influence of vesicle size and preparation methods. *Eur. J. Pharmaceut. Sci.*, **1**, 333-341.

Ott, S. & Wunderli-Allenspach, H. (1994) Liposomes and Influenza viruses as an in vitro model for membrane interactions 1. Kinetics of membrane fusion and lipid transfer. *Eur. J. Pharmaceut. Sci.*, **1**, 323-332.

Owens, R.J., Burke, C. & Rose, J.K. (1994) Mutations in the membrane spanning domain of the Human immunodeficiency virus envelope glycoprotein that affect fusion activity. *J. Virol.*, **68**, 570-574.

Paiement, J., Lavoie, C., Gavino, G.R. & Gavino, V.C. (1994) Modulation of GTP-dependent fusion by linoleic and arachidonic acid in derivatives of rough endoplasmic reticulum from rat liver. *Biochim. Biophys. Acta- Biomembr.*, **1190**, 199-212.

Palade, G.E. (1975) Intracellular aspects of the process of protein synthesis. *Science (Wash DC)*, **189**, 347-358.

Papahadjopoulos, D. & Miller, N. (1967) Phospholipid model membranes I. Structural characteristics of hydrated lipid crystals. *Biochim. Biophys. Acta*, **135**, 624-638.

Papahadjopoulos, D., Vail, W.J., Newton, C., Nir, S., Jacobson, K., Poste, G. & Lazo, R. (1977) Studies on membrane fusion: III. The role of calcium-induced phase changes. *Biochim. Biophys. Acta*, **465**, 579-598.

Parente, R.A., Nir, S. & Szoka, J., F.C. (1998) pH-dependent fusion of phosphatidylcholine small vesicles. *J. Biol. Chem.*, **263**, 4724-4730.

Parsegian, V.A. & Ninham, B.W. (1971) Towards the correct calculation of van der Waals interactions between lyophobic colloids in an aqueous medium. *J. Colloid Interface. Sci.*, **37**, 332-341.

Parsegian, V.A., Fuller, N. & Rand, R.P. (1979) Measured work of deformation and repulsion of lecithin bilayers. *Proc. Natl. Acad. Sci. USA.*, **76**, 2750-2754.

Paterson, R.G., Hiebert, S.W. & Lamb, R.A. (1985) Expression at the cell surface of biologically active fusion and hemagglutinin neuraminidase proteins of the paramyxovirus Simian virus-5 from cloned cDNA. *Proc. Natl. Acad. Sci. USA.*, **82**, 7520-7524.

Pécheur, E., Hoekstra, D., Sainte-Marie, J., Maurin, L., Bienvenue, A. & Philippot, J.R. (1997) Membrane anchorage brings about fusogenic properties in a short synthetic peptide. *Biochemistry*, **36**, 3773-3781.

Pedroso de Lima, M.C., Nir, S., Flasher, D., Klappe, K., Hoekstra, D. & Düzgünes, N. (1991) Fusion of Sendai virus with human HL-60 and CEM cells: different kinetics of fusion for two isolates. *Biochim. Biophys. Acta*, **1070**, 446-454.

Penrose, M. (1970) Cat leukaemia. *Br. J. Med.*, **1**, 755.

Pereira, F.B., Goñi, F.M. & Nieva, J.L. (1995) Liposome destabilisation induced by the HIV-1 fusion peptide. Effect of a single amino acid substitution. *FEBS Lett.*, **362**, 243-246.

Pereira, F.B., Goñi, F.M., Muga, A. & Nieva, J.L. (1997) Permeabilization and fusion of uncharged lipid vesicles induced by the HIV-1 fusion peptide adopting an extended conformation: dose and sequence effects. *Biophys. J.*, **73**, 1977-1986.

Perutz, M.F. (1954) The structure of haemaglobin III. Direct determination of the molecular transform. *Proc. Roy. Soc. ser. A*, **225**, 264-286.

Phalen, T. & Kielian, M. (1991) Cholesterol is required for infection by Semliki forest virus. *J. Cell. Biol.*, **112**, 615-623.

Pinheiro, T.J.T., Elove, G.A., Watts, A. & Roder, H. (1997) Structural and kinetic description of cytochrome C unfolding induced by the interaction with lipid vesicles. *Biochemistry*, **36**, 13122-13132.

Pinter, A., Honnen, W.J., Tilley, S.A., Bona, C., Zaghouani, H., Gorny, M.K. & Zollapazner, S. (1989) Oligomeric structure of gp41, the transmembrane protein of Human immunodeficiency virus type-1. *J. Virol.*, **63**, 2674-2679.

Pinto da Silva, P. & Nogueira, M.L. (1977) Membrane fusion during secretion: a hypothesis based on electron microscope observation of *Phytophthore Palmivora* zoospores during encystment. *J. Cell. Biol.*, **73**, 161-181.

Plattner, H., Lumpert, C.J., Gras, U., Vilmart-Seuwen, J., Stecher, B., Hohne, B. & Momayezi, M. (1988) *Molecular mechanisms of membrane fusion* (ed. by S. Ohki, D. Doyle, T.D. Flanagan, S.W. Hui and E. Mayhew), Plenum Press, New York, 477-494.

Polozov, I.V., Polozova, A.I., Molotkovsky, J.G. & Epand, R.M. (1997) Amphipathic peptide affects the lateral domain organisation of lipid bilayers. *Biochim. Biophys. Acta*, **1328**, 125-139.

Poste, G. & Pasternak, C.A. (1978) Virus-induced cell fusion. *Cell Surf. Rev.*, **5**, 306-349.

Price, N.C. (1996) Circular dichroism in protein analysis. *Encyclopaedia of Molecular Biology and Molecular Medicine* (ed. by R.A. Meyers), VCH, Weinheim, 384-396.

Provencher, S.W. & Glöckner, J. (1981) Estimation of globular protein secondary structure from circular dichroism. *Biochemistry*, **20**, 33-37.

Pryor, C.L., Loew, L.M. & Bridge, M. (1983) Vesicle and non-vesicle pH-dependent behavior of phosphatidylethanolamine dispersions. *Biophys. J.*, **41**, 349a (Abstract)

Rafalski, M., Lear, J.D. & DeGrado, W.F. (1990) Phospholipid interactions of synthetic peptides representing the N-terminus of HIV gp41. *Biochemistry*, **29**, 7917-7922.

Rafalski, M., Ortiz, A., Rockwell, A., van Ginkel, L.C., Lear, J.D., DeGrado, W.F. & Wilschut, J. (1991) Membrane fusion activity of the Influenza virus hemagglutinin: interaction of HA2 N-terminal peptides with phospholipid vesicles. *Biochemistry*, **30**, 10211-10220.

Rance, M. & Byrd, R.A. (1983) Obtaining high-fidelity spin-1/2 powder spectra in anisotropic media: phase-cycled Hahn Echo spectroscopy. *J. Magn. Reson.*, **52**, 221-240.

Rand, R.P. (1981) Interacting phospholipid bilayers- measured forces and induced structural changes. *Annu. Rev. Biophys. Bioeng.*, **10**, 277-314.

Rand, R.P. & Parsegian, V.A. (1989) Hydration forces between phospholipid bilayers. *Biochim. Biophys. Acta*, **988**, 351-376.

Reddy, G.L. & Nagaraj, R. (1989) Circular dichroism studies on synthetic signal peptides indicate β-conformation as a common structural feature in highly hydrophobic environment. *J. Biol. Chem.*, **264**, 16591-16597.

Redmond, S., Peters, G. & Dickson, C. (1984) Mouse mammary tumor virus can mediate cell fusion at reduced pH. *Virology*, **133**, 393-402.

Rein, A., Mirro, J., Gordon Haynes, J., Ernst, S.M. & Nagashima, K. (1994) Function of the cytoplasmic domain of a retroviral transmembrane protein: p15E-p2E cleavage activates the membrane fusion capability of the Murine leukemia virus Env protein. *J. Virol.*, **68**, 1773-1781.

Richardson, C.D., Scheid, A. & Choppin, P.W. (1980) Specific inhibition of paramyxovirus and myxovirus replication by oligopeptides with amino acid sequences similar to those at the N-termini of the F_1 or HA_2 viral polypeptides. *Virology*, **105**, 205-222.

Richardson, J.S. & Richardson, D.C. (1989) Principles and patterns of protein conformation. *Prediction of Protein Structure and the Principles of Protein Conformation.* (ed. by G.D. Fasman), Plenum Press, New York, 1-98.

Rickard, C.G., Post, J.E., Noronha, F. & Barr, L.M. (1969) A transmissible virus-induced lymphocytic leukaemia of the cat. *J. Nat. Cancer Inst.*, **42**, 987-1014.

Roberts-Austen, W.C. (1899) Fifth report to the alloys research committee: steel. *Proc. Inst. Mech. Engrs.*, **1**, 35-68.

Rodríguez-Crespo, I., Gómezgutiérrez, J., Encinar, J.A., González-Ros, J.M., Albar, J.P., Peterson, D.L. & Gavilanes, F. (1996) Structural properties of the putative fusion peptide of Hepatitis-B virus upon interaction with phospholipids- circular dichroism and Fourier transform infrared spectroscopy studies. *Eur. J. Biochem.*, **242**, 243-248.

Rohn, J.L., Gwynn, S.R., Lauring, A.S., Linenberger, M.L. & Overbaugh, J. (1996) Viral genetic variation, AIDS, and the multistep nature of carcinogenesis: the Feline leukemia virus model. *Leukemia*, **10**, 1867-1869.

Rojko, J.L. & Hardy, W.D.J. (1994) Feline leukemia virus and other retroviruses. *The Cat- Diseases and Clinical Management* (ed. by R.G. Sherding), Churchill Livingstone Press, New York, 229-332.

Roseman, M. & Thompson, T.E. (1980) Mechanism of the spontaneous transfer of phospholipids between bilayers. *Biochemistry*, **19**, 439-444.

Rosenheck, K. & Doty, P. (1961) The far ultraviolet absorption spectra of polypeptides and protein solutions and their dependence on conformation. *Proc. Natl. Acad. Sci. USA.*, **47**, 1775-1785.

Rost, B. & Sander, C. (1993) Improved prediction of protein secondary structure by use of sequence profiles and neural networks. *Proc. Natl. Acad. Sci. USA.*, **90**, 7558-7562.

Ruigrok, R.W.H., Aitken, A., Calder, L.J., Martin, S.R., Skehel, J.J., Wharton, S.A., Weis, W. & Wiley, D.C. (1988) Studies on the structure of the Influenza virus hemagglutinin at the pH of membrane fusion. *J. Gen. Virol.*, **69**, 2785-2795.

Ruigrok, R.W.H., Hewat, E.A. & Wade, R.H. (1992) Low pH deforms the Influenza virus envelope. *J. Gen. Virol.*, **73**, 995-998.

Ruiz-Argüello, M.B., Goñi, F.M., Pereira, F.B. & Nieva, J.L. (1998) Phosphatidylinositol-dependent membrane fusion induced by a putative fusogenic sequence of Ebola virus. *J. Virol.*, **72**, 1775-1781.

Santini, M.T., Indovina, P.L., Cantafora, A. & Blotta, I. (1990) The cesium-induced delay in myoblast membrane fusion is accompanied by changes in isolated membrane lipids. *Biochim. Biophys. Acta*, **1023**, 298-304.

Santini, M.T., Indovina, P.L. & Cantafora, A. (1991) The cesium-induced delay in myoblast membrane fusion is accompanied by changes in cellular subfraction lipid composition. *Biochim. Biophys. Acta*, **1070**, 27-32.

Sarkar, D.P. & Blumenthal, R. (1987) The role of the target membrane structure in fusion with Sendai virus. *Membr. Biochem.*, **7**, 231-247.

Schaal, H., Klein, M., Gehrmann, P., Adams, O. & Scheid, A. (1995) Requirement for N-terminal amino acid residues of gp41 for Human immunodeficiency virus type-1 mediated cell fusion. *J. Virol.*, **69**, 3308-3314.

Schäfer, W. & Bolognesi, D.P. (1977) Mammalian C-type oncornaviruses: relationships between viral structural and cell-surface antigens and their possible significance in immunological defense mechanisms. *Contemp. Top. Immunobiol.*, **6**, 127-167.

Schawaller, M., Smith, G.E., Skehel, J.J. & Wiley, D.C. (1989) Studies with crosslinking reagents on the oligomeric structure of the Env glycoprotein of HIV. *Virology*, **172**, 367-369.

Schellman, J.A. & Nielsen, E.B. (1967) The spectra of amides. Theoretical considerations. *J. Phys. Chem.*, **71**, 3914-3921.

Schellman, J.A. & Oriel, P. (1962) Origin of the Cotton effect of helical polypeptides. *J. Chem. Phys.*, **37**, 2114-2124.

Schlegel, R., Tralka, T.S., Willingham, M.C. & Pastan, I. (1983) Inhibition of VSV binding and infectivity by phosphatidylserine: Is phosphatidylserine a VSV binding site? *Cell*, **32**, 639-646.

Schmid, F.X. (1989) Spectral methods of characterising protein conformation and conformational changes. *Protein structure: a practical approach* (Ed. by T.E. Creighton), IRL Press, Oxford, 251-285.

Schmidt, W., Patzak, A., Lingg, G., Winkler, H. & Plattner, H. (1983) Membrane events in adrenal chromaffin cells during exocytosis- a freeze-etching analysis after rapid cryofixation. *Eur. J. Cell. Biol.*, **32**, 31-37.

Schoch, C. & Blumenthal, R. (1993) Role of the fusion peptide sequence in initial stages of Influenza hemagglutinin-induced cell fusion. *J. Biol. Chem.*, **268**, 9267-9274.

Schudt, C. & Pette, D. (1976) Influence of monosaccharides, medium factors and enzymatic modification on fusion of myoblasts in vitro. *Cytobiologie*, **13**, 74-84.

Seddon, J.M. (1990) Structure of the inverted hexagonal (H_{II}) phase and non-lamellar phase transitions of lipids. *Biochim. Biophys. Acta*, **1031**, 1-69.

Seddon, J.M. (1992) Inverse cubic phases of membrane lipids, and their relevance to the static and dynamic structure of biomembranes. *Acta Pharm.*, **42**, 255-262.

Seddon, J.M., Harlos, K. & Marsh, D. (1983) Metastability and polymorphism in the gel and fluid bilayer phases of dilauroylphosphatidylethanolamine- two crystalline forms in excess water. *J. Biol. Chem.*, **258**, 3850-3854.

Seelig, J., Gally, H.U. & Wohlgemuth, R. (1977) Orientation and flexibility of the choline headgroup in phosphatidylcholine bilayers. *Biochim. Biophys. Acta*, **467**, 109-119.

Segawa, S.I., Fukuno, T., Fujiwara, K. & Noda, Y. (1991) Local structures in unfolded lysozyme and correlation with secondary structures in the native comformation- helix-forming or helix-breaking propensity of peptide segments. *Biopolymers*, **31**, 497-509.

Segrest, J.P., Jackson, R.L., Morrisett, J.D. & Gotto, A.M.J. (1974) A molecular theory for protein-lipid interactions in plasma lipoproteins. *FEBS Lett.*, **38**, 247-253.

Shangguan, T., Alford, D. & Bentz, J. (1996) Influenza virus-liposome lipid mixing is leaky and largely insensitive to the material properties of the target membrane. *Biochemistry*, **35**, 4956-4965.

Shangguan, T., Siegel, D.P., Lear, J.D., Axelsen, P.H., Alford, D. & Bentz, J. (1998) Morphological changes and fusogenic activity of Influenza virus hemagglutinin. *Biophys. J.*, **74**, 54-62.

Shoemaker, K.R., Kim, P.S., York, E.J., Stewart, J.M. & Baldwin, R.L. (1987) Tests of the helix dipole model for stabilisation of α-helices. *Nature*, **326**, 563-567.

Siegel, D.P. (1984) Inverted micellar structures in bilayer membranes- formation rates and half-lives. *Biophys. J.*, **45**, 399-420.

Siegel, D.P. (1986a) Inverted micellar intermediates and the transitions between lamellar, cubic and inverted hexagonal phases. I. Mechanism of the L_α-H_{II} phase transitions. *Biophys. J.*, **49**, 1155-1170.

Siegel, D.P. (1986b) Inverted micellar intermediates and the transitions between lamellar, cubic and inverted hexagonal phases II. Implications for membrane-membrane interactions and membrane fusion. *Biophys. J.*, **49**, 1171-1183.

Siegel, D.P. (1986c) Inverted micellar intermediates and the transitions between lamellar, cubic and inverted hexagonal amphophile phases. III. Isotropic and inverted cubic state formation via intermediates in transitions between L_α-H_{II} phases. *Chem Phys Lipids*, **42**, 279-301.

Siegel, D.P. (1993) Energetics of intermediates in membrane fusion- comparison of stalk and inverted micellar intermediate mechanisms. *Biophys. J.*, **65**, 2124-2140.

Siegel, D.P. (1994) A stalk-mediated mechanism for lamellar inverted cubic and lamellar inverted hexagonal phase-transitions. *Biophys. J.*, **66**, A 174

Siegel, D.P. & Banschbach, J. (1990) Lamellar/Inverted Cubic (L_α/Q_{II}) phase transition in N-methylated dioleoylphosphatidylethanolamine. *Biochemistry*, **29**, 5975-5981.

Siegel, D.P., Banschbach, J., Alford, D., Ellens, H., Lis, L.J., Quinn, P.J., Yeagle, P.L. & Bentz, J. (1989a) Physiological levels of diacylglycerols in phospholipid membranes induce membrane fusion and stabilize inverted phases. *Biochemistry*, **28**, 3703-3709.

Siegel, D.P., Banschbach, J. & Yeagle, P.L. (1989b) Stabilization of H_{II} phases by low levels of diglycerides and alkanes - an NMR, calorimetric, and X-ray diffraction study. *Biochemistry*, **28**, 5010-5019.

Siegel, D.P., Burns, J.L., Chestnut, M.H. & Talmon, Y. (1989c) Intermediates in membrane fusion and bilayer nonbilayer phase transitions imaged by time-resolved cryo-transmission electron microscopy. *Biophys. J.*, **56**, 161-169.

Siegel, D.P. & Epand, R.M. (1997) The mechanism of lamellar-to-inverted hexagonal phase transitions in phosphatidylethanolamine: implications for membrane fusion mechanisms. *Biophys. J.*, **73**, 3089-3111.

Simon, S.A., Mcintosh, T.J. & Latorre, R. (1982) Influence of cholesterol on water penetration into bilayers. *Science*, **216**, 65-67.

Singer, S.J. & Nicolson, G.L. (1972) The fluid mosaic model of the structure of cell membranes. *Science*, **175**, 720-731.

Sizer, P.J.H., Miller, A. & Watts, A. (1987) Functional reconstruction of the integral membrane proteins of Influenza virus into phospholipid liposomes. *Biochemistry*, **26**, 5106-5113.

Skehel, J.J., Bayley, P.M., Brown, E.B., Martin, S.R., Waterfield, M.D., White, J.M., Wilson, I.A. & Wiley, D.C. (1982) Changes in the conformation of Influenza virus hemagglutinin at the pH optimum of virus mediated membrane fusion. *Proc. Natl. Acad. Sci. USA.*, **79**, 968-972.

Slepushkin, V.A., Andreev, S.M., Sidorova, M.V., Melikyan, G.B., Grigoriev,V.B., Chumakov, V.M., Grinfeldt, A.E., Manukyan, R.A. & Karamov, E.V. (1992) Investigation of Human immunodeficiency virus fusion peptides. Analysis of interrelations between their structure and function. *Aids Res. Hum. Retrov.*, **8**, 9-18.

Spear, P., Wittels, M., Fuller, A., WuDunn, D. & Johnson, R. (1989) Herpes simplex virus: pathway of entry into cells. *Cell Biology of Virus Entry, Replication and Pathogenesis* (ed. by R. Compans, A. Helenius and M. Oldstone), Liss, New York, 163-175.

Spruce, A.E., Iwata, A., White, J.M. & Almers, W. (1989) Patch clamp studies of single cell fusion events mediated by a viral fusion protein. *Nature*, **342**, 555-558.

Spruce, A.E., Iwata, A. & Almers, W. (1991) The first milliseconds of the pore formed by a fusogenic viral envelope protein during membrane fusion. *Proc. Natl. Acad. Sci. USA.*, **88**, 3623-3627.

Spuhler, P., Anantharamaiah, G.M., Segrest, J.P. & Seelig, J. (1994) Binding of apolipoprotein-A-1 model peptides to lipid bilayers- measurement of binding isotherms and peptide-lipid headgroup interactions. *J. Biol. Chem.*, **269**, 23904-23910.

Stegmann, T. (1993) Influenza hemagglutinin mediated membrane fusion does not involve inverted phase lipid intermediates. *J. Biol. Chem.*, **268**, 1716-1722.

Stegmann, T., Hoekstra, D., Scherphof, G. & Wilschut, J. (1985) Kinetics of pH-dependent fusion between Influenza virus and liposomes. *Biochemistry*, **24**, 3107-3113.

Stegmann, T., Booy, F.P. & Wilschut, J. (1987) Effects of low pH on Influenza virus activation and inactivation of the membrane fusion capacity of the hemagglutinin. *J. Biol. Chem.*, **262**, 17744-17749.

Stegmann, T., Doms, R.W. & Helenius, A. (1989) Protein mediated membrane fusion. *Annu. Rev. Biophys. Biophys. Chem.*, **18**, 187-211.

Stegmann, T., White, J.M. & Helenius, A. (1990) Intermediates in Influenza induced membrane fusion. *EMBO J.*, **9**, 4231-4241.

Stegmann, T., Delfino, J.M., Richards, F.M. & Helenius, A. (1991) The HA2 subunit of Influenza hemagglutinin inserts into the target membrane prior to fusion. *J. Biol. Chem.*, **266**, 18404-18410.

Stein, B.S., Gowda, S.D., Lifson, J.D., Penhallow, R.C., Bensch, K.G. & Engleman, E.G. (1987) pH-independent HIV entry into CD4-positive T cells via virus envelope fusion to the plasma membrane. *Cell*, **49**, 659-668.

Stollery, J.G. & Vail, W.J. (1977) Interactions of divalent cations or basic proteins with phosphatidylethanolamine vesicles. *Biochim. Biophys. Acta*, **471**, 372-390.

Struck, D.K., Hoekstra, D. & Pagano, R.E. (1981) Use of resonance energy transfer to monitor membrane fusion. *Biochemistry*, **20**, 4093-4099.

Sturman, L.S., Ricard, C.S. & Holmes (1985) Proteolytic cleavage of the E2-glycoprotein of murine coronavirus- activation of cell fusing activity of virions by trypsin and separation of two different 90k-cleavage fragments. *J. Virol.*, **56**, 904-911.

Surewicz, W.K., Muga, A. & Mantsch, H.H. (1992) Determination of protein secondary structure by Fourier transform infrared spectroscopy: a critical assessment. *Structural and Dynamic Properties of Lipids and Membranes* (ed. by P.J. Quinn and R.J. Cherry), Portland Press, London, 153-164.

Takahashi, S. (1990) Conformation of membrane fusion active 20-residue peptides with or without lipid bilayers. Implication of α-helix formation for membrane fusion. *Biochemistry*, **29**, 6257-6261.

Tanford, C. & Reynolds, J.A. (1976) Characterisation of membrane proteins in detergent solutions. *Biochim. Biophys. Acta*, **457**, 133-170.

Tate, M.W. & Gruner, S.M. (1987) Lipid polymorphism of mixtures of dioleoylphosphatidylethanolamine and saturated and monounsaturated phosphatidylcholines of various chain lengths. *Biochemistry*, **26**, 231-236.

Tate, M.W., Eikenberry, E.F., Turner, D.C., Shyamsunder, E. & Gruner, S.M. (1991) Nonbilayer phases of membrane lipids. *Chem. Phys. Lipids*, **57**, 147-164.

Tate, M.W., Shyamsunder, E., Gruner, S.M. & Damico, K.L. (1992) Kinetics of the lamellar inverse hexagonal phase transition determined by time-resolved X-ray diffraction. *Biochemistry*, **31**, 1081-1092.

Tatulian, S.A., Hinterdorfer, P., Baber, G. & Tamm, L.K. (1995) Influenza hemagglutinin assumes a tilted conformation during membrane fusion as determined by attenuated total reflection FTIR spectroscopy. *EMBO J.*, **14**, 5514-5523.

Thomas, D.J., Wall, J.S., Hainfeld, J.F., Kaczorek, M., Booy, F.P., Trus, B.L., Eiserling, F.A. & Steven, A.C. (1991) gp160, the envelope glycoprotein of Human immunodeficiency virus type-1, is a dimer of 125-kilodalton subunits stabilized through interactions between their gp41 domains. *J. Virol.*, **65**, 3797-3803.

Tilcock, C.P.S., Bally, M.B., Farren, S.B. & Cullis, P.R. (1982) Influence of cholesterol on the structural preferences of dioleoylphosphatidylethanolamine dioleoylphosphatidylcholine systems -a ^{31}P and deuterium nuclear magnetic resonance study. *Biochemistry*, **21**, 4596-4601.

Tilcock, C.P.S., Cullis, P.R. & Gruner, S.M. (1986) On the validity of ^{31}P NMR determinations of phospholipid polymorphic phase behavior. *Chem. Phys. Lipids*, **40**, 47-56.

Tsui, F.C., Ojcius, D.M. & Hubbell, W.L. (1986) The intrinsic pKa values for phosphatidylserine and phosphatidylethanolamine in phosphatidylcholine host bilayers. *Biophys. J.*, **49**, 459-468.

Tsurudome, M., Gluck, R., Graf, R., Falchetto, R., Schaller, U. & Brunner, J. (1992) Lipid interactions of the hemagglutinin HA2 NH2-terminal segment during Influenza virus induced membrane fusion. *J. Biol. Chem.*, **267**, 20225-20232.

Turner, D.C. & Gruner, S.M. (1992) X-ray diffraction reconstruction of the inverted hexagonal (H_{II}) phase in lipid water systems. *Biochemistry*, **31**, 1340-1355.

Unwin, N. (1993) Nicotinic acetylcholine receptor at 9 Angstrom resolution. *J. Mol. Biol.*, **229**, 1101-1124.

van Gorkom, L.C.M., Nie, S.Q. & Epand, R.M. (1992) Hydrophobic lipid additives affect membrane stability and phase behavior of N-monomethyldioleoyl-phosphatidylethanolamine. *Biochemistry*, **31**, 671-677.

Van Meer, G., Davoust, J. & Simons, K. (1985) Parameters affecting low pH mediated fusion of liposomes with the plasma membrane of cells infected with Influenza virus. *Biochemistry*, **24**, 3593-3602.

Vanderwerf, P. & Ullman, E.F. (1980) Monitoring of phospholipid vesicle fusion by fluorescence energy transfer between membrane-bound dye labels. *Biochim. Biophys. Acta*, **596**, 302-314.

Vargas, R., Mariani, P., Gulik, A. & Luzzati, V. (1992) Cubic phases of lipid containing systems- the structure of phase- Q223 (space group Pm3n)- an X-ray scattering study. *J. Mol. Biol.*, **225**, 137-145.

Verkleij, A.J. (1984) Lipidic intramembranous particles. *Biochim. Biophys. Acta*, **779**, 43-63.

Verkleij, A.J., Mombers, C., Leunissen-Bijvelt, J. & de Kruijff, B. (1979) Lipidic intramembranous particles. *Nature (London)*, **279**, 162-163.

Vogel, H., Nilsson, L., Rigler, R., Vosges, K.P. & Jung, G. (1988) Structural fluctuations of a helical polypeptide traversing a lipid bilayer. *Proc. Natl. Acad. Sci. USA.*, **85**, 5067-71.

Vogel, S.S., Chernomordik, L.V. & Zimmerberg, J. (1992) Calcium-triggered fusion of exocytotic granules requires proteins in only one membrane. *J. Biol. Chem.*, **267**, 25640-25643.

Voyta, J.C., Leikina, E.A. & Chernomordik, L.V. (1978) Accessibility of lysolecithins in catecholamine secretory vesicles to acyl coA: lysolecithin acyl transferase. *Biochem. Biophys. Res. Comm.*, **80**, 413-417.

Walter, A. & Siegel, D.P. (1993) Divalent cation-induced lipid mixing between phosphatidylserine liposomes studied by stopped-flow fluorescence measurements- effects of temperature, comparison of barium and calcium, and perturbation by DPX. *Biochemistry*, **32**, 3271-3281.

Warren, R.C. (1987) *Physics and the Architecture of Cell Membranes.* Adam Hilger, Bristol.

Waterhous, D.V. & Johnson, W.C. (1994) Importance of environment in determining secondary structure in proteins. *Biochemistry*, **33**, 2121-2128.

Webb, M.S., Hui, S.W. & Steponkus, P.L. (1993) Dehydration-induced lamellar-to-hexagonal-II phase transitions in DOPE/DOPC mixtures. *Biochim. Biophys. Acta*, **1145**, 93-104.

Weber, T., Paesold, G., Galli, C., Mischler, R., Semenza, G. & Brunner, J. (1994) Evidence for H^+-induced insertion of Influenza hemagglutinin HA2 N-terminal segment into viral membrane. *J. Biol. Chem.*, **269**, 18353-18358.

Webster, R.G., Brown, L.E. & Jackson, D.C. (1983) Changes in the antigenicity of the hemagglutinin molecule of H3-labeled Influenza virus at acidic pH. *Virology*, **126**, 587-599.

Weis, W., Brown, J.H., Cusack, S., Paulson, J.C., Skehel, J.J. & Wiley, D.C. (1988) Structure of the Influenza-virus hemagglutinin complexed with its receptor, sialic acid. *Nature*, **333**, 426-431.

Weislander, A. & Karlsson, O.P. (1997) Regulation of lipid syntheses in Acholeplasma laidlawii. *Lipid polymorphism and membrane properties* (ed. by R.M. Epand), Academic Press, San Diego, 517-541.

Weiss, C.D., Levy, J.A. & White, J.M. (1990) Oligomeric organization of gp120 on infectious Human immunodeficiency virus type-1 particles. *J. Virol.*, **64**, 5674-5677.

Weiss, R. (1992) Cellular receptors and viral glycoproteins involved in retrovirus entry. *The Retroviruses* (ed. by J. Levy), Plenum Press, New York, 1-108.

Weissenhorn, W., Dessen, A., Harrison, S.C., Skehel, J.J. & Wiley, D.C. (1997) Atomic structure of the ectodomain from HIV-1 gp41. *Nature*, **387**, 426-430.

Weissman, D., Rabin, R.L., Arthos, J., Rubbert, A., Dybul, M., Swofford, R., Venkatesan, S. & et al (1997) Macrophage-tropic HIV and SIV envelope proteins induce a signal through the CCR5 chemokine receptor. *Nature*, **389**, 981-985.

Wharton, S.A., Calder, L.J., Ruigrok, R.W.H., Skehel, J.J., Steinhauer, D.A. & Wiley, D.C. (1995) Electron microscopy of antibody complexes of Influenza virus hemagglutinin in the fusion pH conformation. *EMBO J.*, **14**, 240-246.

Wharton, S.A., Martin, S., Ruigrok, R., Skehel, J. & Wiley, D. (1988) Membrane fusion by peptide analogues of Influenza virus hemagglutinnin. *J. Gen. Virol.*, **69**, 1847-1857.

Wharton, S.A., Ruigrok, R.W.H., Martin, S.R., Skehel, J.J., Bayley, P.M., Weis, W. & Wiley, D.C. (1988) Conformational aspects of the acid-induced fusion mechanism of Influenza virus hemagglutinin- circular dichroism and fluorescence studies. *J. Biol. Chem.*, **263**, 4474-4480.

Wharton, S.A., Skehel, J.J. & Wiley, D.C. (1986) Studies of Influenza hemagglutinin-mediated membrane fusion. *Virology*, **149**, 27-35.

White, J.M. (1990) Viral and cellular membrane fusion peptides. *Annu. Rev. Physiol.*, **52**, 675-697.

White, J.M. (1992) Membrane fusion. *Science*, **258**, 917-924.

White, J.M. (1995) Membrane Fusion: the Influenza paradigm. *Cold Spring Harbor Symp. Quant. Biol.*, **60**, 581-588.

White, J.M. & Helenius, A. (1980) pH-dependent fusion between the Semliki forest virus membrane and liposomes. *Proc. Natl. Acad. Sci. USA.*, **77**, 3273-3277.

White, J., Kartenbeck, J. & Helenius, A. (1982) Membrane fusion activity of Influena virus. *EMBO J.*, **1**, 217-222.

White, J., Kielian, M. & Helenius, A. (1983) Membrane fusion proteins of enveloped animal viruses. *Q. Rev. Biophys.*, **16**, 151-195.

White, J.M. & Wilson, I.A. (1987) Anti-peptide antibodies detect steps in a protein conformational change- low-pH activation of the Influenza virus hemagglutinin. *J. Cell. Biol.*, **105**, 2887-2896.

White, S.H., Wimley, W., C. & Selsted, M.E. (1995) Structure, function and membrane integration of defensins. *Curr. Opin. Struct. Biol.*, **5**, 521-527.

Wiener, M.C., King, G.I. & White, S.H. (1991) Structure of a fluid dioleoylphosphatdiylcholine bilayer determined by joint refinement of X-ray and neutron diffraction data. I. Scaling of neutron data and the distributions of double bonds and water. *Biophys. J.*, **60**, 568-576.

Wiener, M.C. & White, S.H. (1992) Structure of a fluid dioleoylphosphatidylcholine bilayer determined by joint refinement of X-ray and neutron diffraction data III. Complete structure. *Biophys. J.*, **61**, 434-447.

Wild, C.T., Shugars, D.C., Greenwell, T.K., McDanal, C.B. & Matthews, T.J. (1994) Peptides corresponding to a predictive alpha-helical domain of Human immunodeficiency virus type-1 gp41 are potent inhibitors of virus infection. *Proc. Natl. Acad. Sci. USA.*, **91**, 9770-9774.

Wiley, D.C. & Skehel, J.J. (1987) The structure and function of the hemagglutinin membrane glycoprotein of Influenza virus. *Annu. Rev. Biochem.*, **56**, 365-394.

Wilschut, J., Düzgünes, N. & Papahadjopoulos, D. (1981) Calcium/magnesium specificity in membrane fusion: kinetics of aggregation and fusion of phosphatidylserine vesicles and the role of bilayer curvature. *Biochemistry*, **20**, 3126-3133.

Wilschut, J., Corver, J., Nieva, J.L., Bron, R., Moesby, L., Kasireddy, C.R. & Bittman, R. (1995) Fusion of Semliki forest virus with cholesterol-containing liposomes at low pH: a specific requirement for sphingolipids. *Mol. Membr. Biol.*, **12**, 143-149.

Wilson, I.A., Skehel, J.J. & Wiley, D.C. (1981) Structure of the hemagglutinin membrane glycoprotein of Influenza virus at 3Å resolution. *Nature*, **289**, 366-373.

Wimley, W., C. & White, S., H. (1996) Experimentally determined hydrophobicity scale for proteins at membrane interfaces. *Nature Struct. Biol.*, **3**, 842-848.

Woody, R.W. & Tinoco, I., Jr. (1967) Optical rotation of oriented helices. III Calculation of the rotatory dispersion and circular dichroism of the alpha- and 3_{10}-helix. *J. Chem. Phys.*, **46**, 4927-4945.

Worcester, D.L. (1976) Neutron beam studies of biological membranes and membrane components. *Biological Membranes* (ed. by D. Chapman and D.F.H. Wallach), Academic Press, London, 1-46.

Worcester, D.L. & Franks, N.P. (1976) Structural analysis of hydrated egg lecithin and cholesterol bilayers. II Neutron Diffraction. *J. Mol. Biol.*, **100**, 359-378.

Wu, C.S.C. & Yang, J.T. (1978) Conformation of naturally-occurring peptides in surfactant solution: its relation to the structure forming potential of amino acid sequence. *Biochem. Biophys. Res. Comm.*, **82**, 85-91.

Wu, C.S.C., Hachimori, A. & Yang, J.T. (1982) Lipid-induced ordered conformation of some peptide hormones and bioactive oligopeptides- predominance of helix over β-form. *Biochemistry*, **21**, 4556-4562.

Wu, Y., He, K., Ludtke, S.J. & Huang, H.W. (1995) X-ray diffraction study of lipid bilayer membrane interacting with amphiphilic helical peptides: diphytanoyl phosphatidylcholine with alamethicin at low concentrations. *Biophys. J.*, **68**, 2361-2369.

Yeagle, P.L. (1994) Lipids and lipid-intermediate structures in the fusion of biological membranes. *Curr. top. membr.*, **40**, 197-214.

Yeagle, P.L., Epand, R.M., Richardson, C.D. & Flanagan, T.D. (1991) Effects of the "Fusion peptide" from Measles virus on the structure of N-methyl dioleoylphosphatidylethanolamine membranes and their fusion with Sendai virus. *Biochim. Biophys. Acta*, **1065**, 49-53.

Yeagle, P.L., Young, J., Hui, S., W. & Epand, R.M. (1992) On the mechanism of viral and vesicle membrane fusion by carbobenzoxy-d-phenylalanylglycine. *Biochemistry*, **31**, 3177-3183.

Yeagle, P.L., Smith, F.T., Young, J.E. & Flanagan, T.D. (1994) Inhibition of membrane fusion by lysophosphatidylcholine. *Biochemistry*, **33**, 1820-1827.

Yu, Y.G., King, D.S. & Shin, Y.K. (1994) Insertion of a coiled-coil peptide from Influenza virus hemagglutinin into membranes. *Science*, **266**, 274-276.

Zaccai, G., Blasie, J.K. & Schoenborn, B.P. (1975) Neutron diffraction studies on the location of water in lecithin bilayer model membranes. *Proc. Natl. Acad. Sci. USA.*, **72**, 376-380.

Zachowski, A., Henry, J.P. & Devaux, P.F. (1989) Control of transmembrane lipid asymmetry in chromaffin granules by an ATP-dependent protein. *Nature*, **340**, 75-76.

Zellmer, S., Cevc, G. & Risse, P. (1994) Temperature- and pH-controlled fusion between complex lipid membranes. Examples with the diacylphosphatidylcholine/fatty acid mixed liposomes. *Biochim. Biophys. Acta*, **1196**, 101-113.

Zhu, N., Cannon, P.M., Chen, D. & French Anderson, W. (1998) Mutational analysis of the fusion peptide of Moloney murine leukemia virus transmembrane protein p15E. *J. Virol.*, **72**, 1632-1639.

Zimmerberg, J., Blumenthal, R., Sarkar, D.P., Curran, M. & Morris, S.J. (1994) Restricted movement of lipid and aqueous dyes through pores formed by Influenza hemagglutinin during cell fusion. *J. Cell. Biol.*, **127**, 1885-1894.

Zimmerberg, J., Vogel, S.S., Whalley, T., Plonsky, I., Sokoloff, A., Chanturia, A. & Chernomordik, L.V. (1995) Intermediates in membrane fusion. *Cold Spring Harbor Symp. Quant. Biol.*, **60**, 589-599.

Zingler, K. & Littman, D.R. (1993) Truncation of the cytoplasmic domain of the Simian immunodeficiency virus envelope glycoprotein increases Env incorporation into particles and fusogenicity and infectivity. *J. Virol.*, **67**, 2824-2831.

Appendix: Publications and Communications arising from Research Conducted during the course of this PhD.

Appendix

Publications

Davies, S.M.A., Epand, R.F., Bradshaw, J.P. and Epand, R.M., (1998) 'Modulation of lipid polymorphism by the Feline leukaemia virus fusion peptide: implications for biological fusion?' *Biochemistry*, **37**, 5720-5729.

Davies, S.M.A., Kelly, S.M., Price, N.P. and Bradshaw, J.P., (1998) 'Structural plasticity of the Feline leukaemia virus fusion peptide, a circular dichroism study.' *FEBS Lett.*, **425**, 415-418.

Davies, S.M.A., Darkes, M.J.M. and Bradshaw, J.P., (1998) 'A neutron study of the Feline leukaemia virus fusion peptide: implications for biological fusion?' *Physica B*, in press.

Darkes, M.J.M., Davies, S.M.A. and Bradshaw, J.P., (1998) 'Interaction of tachykinins with phospholipid membranes: a neutron diffraction study'. *Physica B*, in press.

Bradshaw, J.P., Davies, S.M.A. and Hauss, T., 'Interaction of Substance P with phospholipid bilayers: a neutron diffraction study.' *Biophysical Journal*, in press.

Bradshaw, J.P., Darkes, M.J.M. and Davies, S.M.A., 'Improved accuracy and phasing of lamellar neutron diffraction data by real-time swelling series method.' *Physica B*, in press.

Bradshaw, J.P., Darkes, M.J.M., Davies, S.M.A., (1998) 'Neutron diffraction studies of the interaction of tachykinins with phospholipid bilayers.' *Biophysical Journal*, **74**, A122.

Communications

Oral presentation: 'Biophysical studies of the Feline leukaemia virus fusion peptide and its role in the fusion mechanism: pores for thought?'
Faculty Research Emphasis Day, University of Edinburgh, Edinburgh, April, 1997.

Poster: 'A neutron study of the Feline leukaemia virus fusion peptide: implications for biological fusion?'
International Conference of Neutron Scattering, Univeristy of Toronto, Toronto, Canada, August, 1997.

Modulation of Lipid Polymorphism by the Feline Leukemia Virus Fusion Peptide: Implications for the Fusion Mechanism

Sarah M. A. Davies, Raquel F. Epand, Jeremy P. Bradshaw, and Richard M. Epand

Department of Preclinical Veterinary Sciences, Royal (Dick) School of Veterinary Sciences, University of Edinburgh, Summerhall, Edinburgh EH9 1QH, Scotland, U.K., and Department of Biochemistry, McMaster University Health Sciences Centre, Hamilton, Ontario L8N 3Z5, Canada

Biochemistry®

Reprinted from
Volume 37, Number 16, Pages 5720–5729

Modulation of Lipid Polymorphism by the Feline Leukemia Virus Fusion Peptide: Implications for the Fusion Mechanism†

Sarah M. A. Davies,*,‡ Raquel F. Epand,§ Jeremy P. Bradshaw,‡ and Richard M. Epand§

Department of Preclinical Veterinary Sciences, Royal (Dick) School of Veterinary Sciences, University of Edinburgh, Summerhall, Edinburgh EH9 1QH, Scotland, U.K., and Department of Biochemistry, McMaster University Health Sciences Centre, Hamilton, Ontario L8N 3Z5, Canada

Received January 28, 1998

ABSTRACT: The structural effects of the fusion peptide of feline leukemia virus (FeLV) on lipid polymorphism were studied, using differential scanning calorimetry (DSC), ^{31}P nuclear magnetic resonance (NMR), and time-resolved X-ray diffraction. This peptide lowers the bilayer to inverted hexagonal phase transition temperature, T_H, of dipalmitoleoylphosphatidylethanolamine (DiPoPE) at peptide mole fractions of up to 1.5×10^{-3} at pH 5.0 and at pH 7.4. The temperature at which isotropic ^{31}P NMR signals for monomethyldioleoylphosphatidylethanolamine (MeDOPE) first occurred is lowered by the FeLV peptide. The amount of isotropic signal seen at 40 °C is directly correlated to the peptide:lipid molar ratio. In the peptide-containing samples, more lipid remains in the isotropic state over the whole recorded temperature range. Isotropic ^{31}P NMR signals were observed for DiPoPE in the presence of the FeLV peptide for the entire recorded temperature range of 35−50 °C, while pure DiPoPE showed no significant amount of isotropic signal. X-ray studies of DiPoPE show the formation of a new lipid phase with peptide, which is not seen in the pure lipid samples. Disordering of the L_α phase is evidenced by broadening of the diffraction peaks, and the hexagonal cell parameter is decreased with peptide present. Our results suggest that the FeLV peptide is increasing the negative curvature of the lipid system, which is thought to be crucial to the formation of highly bent, high-energy structural fusion intermediates, such as the "stalk" model. Fusion activity for this putative fusogenic peptide was also demonstrated, using a resonance energy transfer (RET) lipid mixing assay. To our knowledge, this work provides the first published experimental evidence of both fusogenic activity and effects on lipid polymorphism for the FeLV fusion peptide.

Membrane fusion plays a vital role in a large and diverse number of essential biological processes. Despite this fact, the precise molecular events which occur during fusion are still not known. Specific catalysts can promote fusion, and these differ between individual fusion processes. Fusion proteins from enveloped viruses, such as influenza virus hemagglutinin (*1*, *2*) and gp160 from human immunodeficiency virus (*3*) are among the most thoroughly studied fusion catalysts. It has been proposed that, although the initial triggers for the fusion pathway show great diversity, the actual lipid changes which occur in the fusing membranes may be very similar indeed for many fusion systems (*4*). Thus, studies of one particular fusion pathway may have wide-ranging implications for fusion in all eukaryotic cells as well as for infective mechanisms of all intracellular parasites.

In order for two initally distinct membranes to fuse, the lipid molecules comprising the two bilayers must rearrange temporarily into highly curved intermediates at the fusion site. It was first suggested that fusion intermediates were formed during lipid transitions from the planar lamellar to curved, nonbilayer phases (*5*). Studies by Ellens et al. (*6*) revealed increased liposome fusion rates in the same temperature range in which Gagne et al. (*7*) observed isotropic ^{31}P NMR[1] resonances of the same lipid. Isotropic resonances are due to lipid structures of high curvature in which lateral diffusion of phospholipids can motionally average the chemical shift anisotropy. They correlate with the presence of lipidic particles, seen by electron microscopy (*7*, *8*), and with amorphous and inverted cubic phases, measured by

† We thank the Wellcome Trust for support: S.M.A.D. holds a Wellcome Trust Veterinary Research Training Scholarship. S.M.A.D. traveled to Canada on a Birrel−Gray Scholarship. Support from the Medical Research Council of Canada (Grant MT-7654) and the British Council for Canada is also gratefully acknowledged.

* Author to whom correspondence should be addressed.
‡ University of Edinburgh.
§ McMaster University Health Services Centre.

[1] Abbreviations: FeLV, feline leukemia virus; DiPoPE, dipalmitoleoylphosphatidylethanolamine; MeDOPE, monomethyldioleoylphosphatidylethanolamine; RET, resonance energy transfer; SIV, simian immunodeficiency virus; L_α, liquid crystalline lamellar phase; H_{II}, inverted hexagonal phase; T_H, $L_\alpha-H_{II}$ phase transition temperature; DSC, differential scanning calorimetry; ^{31}P NMR, ^{31}phosphorus nuclear magnetic resonance; HPLC, high-performance liquid chromatography; I_s, lipid structures producing isotropic NMR signals; T_i, temperature at which isotropic signals are first detected; d_L, lamellar phase unit cell repeat distance (*d* spacing); d_H, inverted hexagonal phase unit cell repeat distance (*d* spacing); AA, amino acid; R_0, spontaneous radius of curvature of the lipid monolayer; DG, diacylglycerol; MLV, multilamellar vesicle; SUV, small unilamellar vesicle; TMC, transmonolayer contact intermediate; NBD-PE, L-α-*N*-(4-nitrobenzo-2-oxa-1,3-diazole)-PE from egg; Rh-PE, L-α-*N*-(lissamine-rhodamine B sulfonyl)PE from egg; ILA, interlamellar attachment; DMSO, dimethyl sulfoxide.

S0006-2960(98)00227-X CCC: $15.00
Published on Web 03/28/1998

X-ray diffraction (*9*). These highly curved isotropic lipid arrangements may be fusion intermediates. Diacylglycerols (DGs), which are fusion promoters, lowered the threshold temperature at which isotropic structures occurred (*10*). Isotropic structures were observed in the presence of DGs (*11*). The fusion peptide of simian immunodeficiency virus (SIV) promoted the formation of isotropic structures, while a nonfusogenic mutant of this peptide did not (*12*). Similar results were seen with the fusion peptide from influenza virus hemagglutinin (*13*); the wild-type peptide increased isotropic phase formation, but only at fusogenic pH, while the two mutant nonfusogenic peptides studied did not. These isotropic lipid mesophases occur on the pathway from the lamellar phase to the inverted hexagonal (H_{II}) or ordered cubic phases. Correlations have been found between the inhibition of membrane fusion by certain compounds and their ability to raise the lipid bilayer to inverted hexagonal phase transition temperature (T_H) as measured by high-sensitivity DSC (*14*). Similarly, fusion promoters have been shown to lower T_H (*15*, *12*, *13*). While kinetically stable lipid phases such as H_{II} and bicontinuous cubic phases may not be involved in biological fusion, the first steps in their transition pathways from the lamellar phase may be very important, in particular the bilayer destabilization thus produced.

A number of models have been proposed for the molecular arrangements of the lipid in fusion intermediates. These are based on a combination of experimental findings and theoretical calculations of the energetics involved. The most recent model (*16*) suggests the initial formation of a highly bent modified stalk structure, composed of the outer lipid monolayers of each bilayer, which then converts to a transmonolayer contact intermediate (TMC). This intermediate can then evolve into either a fusion pore/cubic phase fomation or into H_{II} phases (*17*). There is much theoretical (e.g., *18*, *19*) and experimental evidence (e.g., *17*, *20*−*22*) to support this model. Recently, Lee and Lentz (*23*) have identified distinct kinetic steps in the fusion pathway, which support the stalk−pore hypothesis. The highly bent stalk structure would be likely to give rise to isotropic NMR signals. Fusion catalysts are thought to affect the kinetics of the phase transitions, and not the thermodynamic stability of the individual lipid phases themselves. Thus, a favoring of the conversion of the lipid bilayer to nonlamellar phases should enhance the rate of formation of the fusion stalk, while an alternative mechanism would be a change of partitioning of the TMC intermediate toward the fusion pore/cubic phase pathway, as suggested for the influenza virus fusion peptide (*24*).

Modeling studies have suggested that fusion peptides insert obliquely into target lipid membranes and thus destabilize lipid molecular packing (*25*). Longitudinal precession of the obliquely oriented peptide would lead to greater disruption of the bilayer center than of its surface, thereby increasing the negative curvature pressure, and hence favoring the formation of inverted lipid phases (*26*, *13*). We have studied the effect of the fusion peptide from feline leukemia virus (FeLV) on lipid polymorphism. FeLV is a pathogenic exogenous retrovirus of cats (*27*) and the main cause of nontraumatic death in adult domestic cats worldwide. The proposed fusion peptide of FeLV is the hydrophobic amino terminus of p15E, the transmembrane-like region of the viral envelope glycoprotein spike gp85 (*25*). Its amino acid sequence shows similarity to that of the known fusion peptide of SIV (*28*), and also to those of other leukemia-producing Retroviridae (Swiss Protein Data Bank). Using a resonance energy transfer (RET) lipid mixing assay, we have also demonstrated fusion activity for this peptide. To our knowledge, this is the first published experimental work using this fusion peptide. The results are discussed in the light of current concepts of the fusion mechanism.

MATERIALS AND METHODS

Dipalmitoleoylphosphatidylethanolamine (DiPoPE) and monomethyldioleoylphosphatidylethanolamine (MeDOPE) were purchased from Avanti Polar Lipids (Alabaster, AL). Thin-layer chromatography showed a single spot for each. L-α-*N*-(4-nitrobenzo-2-oxa-1,3-diazole)PE from egg (NBD-PE) and L-α-*N*-(lissamine-rhodamine B sulfonyl)PE from egg (Rh-PE) were also purchased from Avanti. Dimethyl sulfoxide (DMSO) was obtained from BDH Chemicals (Toronto, ON).

The FeLV 28 amino acid and SIV 12 amino acid peptides were synthesized by Albachem Ltd. (26 Craigleith View, Edinburgh, EH4 3JZ, Scotland, U.K.) using solid-phase synthesis. Their purities were >95%, as determined by analytical HPLC, Maldi−Tof mass spectrometry, and amino acid analysis.

The FeLV peptide sequence, obtained from the Swiss Protein Data Bank, was EPISLTVALMLGGLTVGGIA-AGVGTGTK. The lysine was included on the carboxy terminus to increase solubility. It is the next naturally occurring residue on p15E. The SIV peptide sequence was GVFVLGFLGFLA, which has been shown previously to promote lipid mixing and thus membrane fusion (*29*).

Preparation of Lipid and Lipid/Peptide Films. Weighed amounts of the required lipid, or lipid plus peptide, were vortexed thoroughly in chloroform. The peptide-containing samples were then sonicated until the peptide dissolved. The chloroform was evaporated using nitrogen gas, and the samples were then placed under vacuum for 4 h, followed by lyophilization overnight to remove any trace residual solvent. The resulting films were then suspended in buffer and vortexed vigorously at room temperature for 10 min. The buffers used for the DSC, NMR, and X-ray diffraction studies were 20 mM PIPES, 1 mM EDTA, 150 mM NaCl, and 0.002% NaN_3 for pH 7.4 samples, or 10 mM citrate, 0.15 M NaCl for pH 5.0 samples, and for the RET assays, 10 mM glycine, 0.1 mM NaCl, 0.1 mM EDTA for the pH 9.5 buffer, and 10 mM Hepes, 0.15 M NaCl, 1 mM EDTA for the pH 7.0 buffer.

Differential Scanning Calorimetry. The samples were made to a final DiPoPE concentration of 10 mg/mL, including varying peptide concentrations as required, and they and the reference buffer were degassed under vacuum just prior to use. Thorough mixing was applied to ensure a uniform sample suspension for injection into the sample chamber. An MC-2 high-sensitivity scanning calorimeter (Microcal Co., Amherst, MA) was employed, at a scan rate of 45 K/h. The sample chamber held 1.4 mL. Continuous heating scans were run from 25 through to 60 °C. A single van't Hoff component was used to fit the recorded bilayer

to hexagonal phase transition, and the reported transition temperature is that for the fitted curve.

^{31}P NMR. A Bruker drx500 spectrometer, operating at a frequency of 202.45 MHz with broad band proton decoupling, was used to obtain the spectra. Three freeze−thaw cycles were carried out prior to measurement to ensure that all the lipid present was in the lamellar phase and also to ensure full hydration of the dry MeDOPE and DiPoPE. The suspensions were then vortexed vigorously to produce a lipid paste and loaded into 5 mm diameter thin-walled NMR tubes. The high lipid concentration of 50 mg/mL aids the formation of nonbilayer phases. The lipid/peptide molar ratios were 100:1 or 200:1 for the peptide-containing samples. Samples were heated in 5 or 10 °C steps. An equilibration time of around 15 min was used after raising the sample temperature, which was maintained to within ± 0.1 °C by a Bruker B-VT 1000 variable temperature unit. A relaxation delay of 3 s was used between scans. Prior to Fourier transformation, exponential line-broadening of 100 Hz was applied.

X-ray Diffraction. The X-ray diffraction experiments were performed at station 8.2 of the synchotron radiation source at the Daresbury Laboratory. The radiation wavelength was 1.54 Å. A Teflon-lined brass chamber with mica windows was used as sample holder, and an external circulating water bath was used to control the sample temperature, which was continuously monitored via a thermocouple. The temperature of the sample cell was linearly increased from 30 to 70 °C, at a heating rate of 90 °C/h. All samples were at pH 7.4. Each temperature scan consisted of 120 frames of diffraction data. The XOTOKO program was used to correct the raw data. Corrections for sample thickness and variation in detector response were applied, and background counts were subtracted. Detector response was determined by measuring a fixed source, ^{59}Fe, for several hours, at the start and the end of data collection. The detector was calibrated for small angle scattering using rat tail collagen, mounted in a cell and lightly stretched, as a standard. Under these conditions, collagen has a unit cell size of 676.08 Å (*30*). The corrected data were then plotted using this calibrated *x*-axis.

Liposome Preparation for Fusion Studies. Liposomes were made from lipid films prepared as above, using pure MeDOPE for the unlabeled LUVs, and with 2 mol % of both NBD-PE and Rh-PE present for the labeled LUVs. The dried lipid films were suspended initially in an iso-osmotic glycine buffer at pH 9.5, at a lipid concentration of 20 mg/mL. After vigorous vortexing, the lipid suspensions were subjected to five freeze−thaw cycles, by immersion in liquid nitrogen for 2 min, followed by plunging into a water bath, at a temperature of 40−60 °C, until the samples thawed. Next the samples were filtered 10 times through two stacked polycarbonate membranes, of pore size 0.1 μm, (Nucleopore Corp., Pleasanton, CA), using a high-pressure extruder (Lipex Biomembranes Inc., Vancouver, Canada) to yield LUVs.

Lipid Mixing Fusion Assay. Lipid mixing was measured using the method of monitoring the change in the intensity of fluorescence which results from fluorescence energy transfer between the two bilayer-inserted probes, NBD-PE and Rh-PE (*31*). A SLM Aminco Bowman Series 2 Luminescence Spectrometer with excitation and emission slits of 4 nm was used. The LUVs were added, at a ratio of 1:9 labeled:unlabeled, into a continuously stirred fluorimeter cuvette containing Hepes buffer of pH 7.0 at 37 °C. The LUVs comprised 1% of the total volume in the cuvette. The final lipid concentration was 300 μM. There was no detectable change in pH on addition of LUVs, since the volumes of LUVs added were very small. The excitation wavelength used was 470 nm, and the emission of NBD was recorded at 530 nm. A baseline fluorescence was measured for these suspensions. The FeLV and SIV peptides were dissolved separately in DMSO at a concentration of 1 mg/mL. These stock solutions of peptide were added to LUV preparations in the fluorimeter cuvettes to give a final peptide concentration of 10 μM. DMSO alone was also used as a control. One hundred percent lipid mixing was obtained by addition of 10% Triton X-100 to a final concentration of 0.1%.

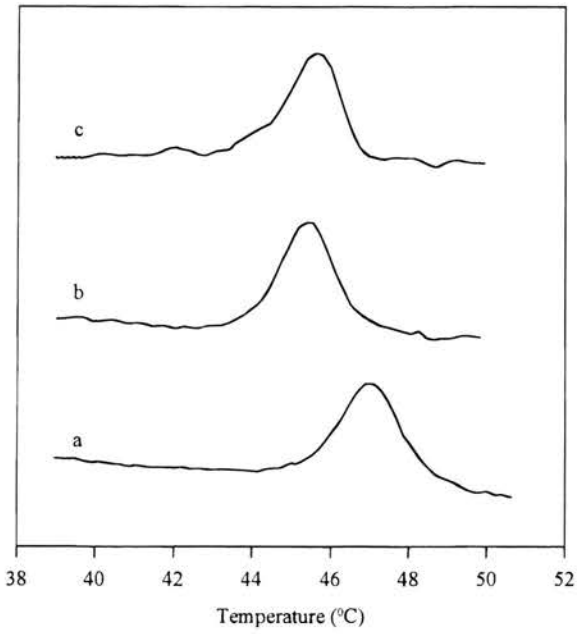

FIGURE 1: Some representative thermograms obtained at pH 7.4. Pure DiPoPE (a), DiPoPE with FeLV peptide present at a peptide mole fraction of 0.5×10^{-3} (b), and 0.65×10^{-3} (c). T_H is lowered in the presence of the FeLV fusion peptide. DSC heating scan rate was 45K/h.

RESULTS

Differential Scanning Calorimetry. Figure 1 shows three representative thermograms, at pH 7.4, from which values for T_H were obtained. It can be seen that T_H is lowered in the presence of both concentrations of FeLV fusion peptide shown. Plots of change in T_H with increasing peptide mole fraction, at pH 7.4 and pH 5.0, are shown in Figure 2, parts a and b, respectively. The resultant curves show an initial decrease in T_H, followed by an increase in T_H with consecutive rises in the peptide mole fraction. At peptide mole fractions of $>1.5 \times 10^{-3}$ a broadening of the enthalpy peaks was observed, indicating a decrease in cooperativity for this transition. The two pH curves are at least biphasic; obviously the possibility exists that these curves are described by more complex functions.

T_H is a measure of the relative stability of the L_α and H_{II} lipid phases. The reduction in T_H observed initially with increasing peptide concentration suggests that, at peptide mole fractions below 1.5×10^{-3}, this fusion peptide favors the formation of the H_{II} phase over the L_α phase at both pH

Table 1: Comparison of Effect of Viral Fusion Peptides on T_H of DiPoPE

viral fusion peptide	slope of line (°C/mole fraction peptide) at pH 5.0	slope of line (°C/mole fraction peptide) at pH 7.4
influenza HA2	-453 ± 112[a]	301 ± 49[a]
SIV	not studied	360 ± 100[b]
FeLV	-2128 ± 233	-1116 ± 444

[a] From Epand and Epand (*13*). [b] From Epand et al. (*12*).

5.0 and pH 7.4. The FeLV virus fuses with biological cells at pH 7.4 (*32*), so a decrease in T_H at both pH values is to be expected with this fusion peptide. Previous experiments which studied the effect of the influenza virus fusion peptide on T_H also found a difference with pH (13): the influenza virus fusion peptide lowered T_H at pH 5.0, but increased T_H at pH 7.4. These findings correlate with this peptide's pH-dependent fusogenic ability. In the same study of the influenza peptide, two nonfusogenic mutants were found to raise T_H, at both pH 5.0 and pH 7.4. DSC experiments performed using the SIV fusion peptide at pH 7.4 showed a decrease in T_H with the wild-type fusion peptide, and little change in T_H with a nonfusogenic mutant (*12*). This suggests that, at low peptide concentrations, a lowering of T_H is a fundamental property of viral fusion peptides. Table 1 shows the values of the slopes for the dependence of T_H on the mole fraction of fusion peptide for these three peptides: it should be noted that the range of peptide concentrations included here is not the same for FeLV as it is for the other two peptides studied, as we are only comparing the FeLV data which shows a reduction in T_H, i.e., the first half of the plotted results. This may explain in part why our gradients are so much steeper for the FeLV data. However, some of the quantitative differences between these values may be due to the difference in the structures of the fusion peptides. The FeLV peptide has an acidic residue on its amino terminus, the influenza peptide has several acidic residues along its length, and the SIV peptide has no polar residues. These factors will affect the depth and angle of peptide penetration into the lipid bilayer; alteration of the amino acid sequences of fusion peptides changes the membrane orientation of these peptides (*25*). Enhancement of H_{II} formation may be due to disruption of lipid packing and/or effects on lipid hydration, producing an increase in monolayer negative curvature strain (*33*). X-ray studies of the H_{II} phase lattice constant at constant temperature can determine whether alteration of the spontaneous radius of curvature of the lipid/water interface, R_0, occurs, and thus a change in monolayer negative curvature strain. This is seen for DiPoPE samples containing the FeLV peptide (see X-ray Diffraction Results).

T_H is seen to increase at FeLV peptide mole fractions above 1.5×10^{-3}, at both pH 5.0 and pH 7.4. We propose that this is due to increased self-aggregation of the extremely hydrophobic FeLV peptide molecules at these higher concentrations, thus preventing them, in part, from inserting into the lipid bilayers. Grossly, the peptide does appear to self-aggregate in these concentration ranges, as seen by the formation of gel-like masses in these samples by the end of the heating scans. A similar phenomenon has been observed with Amphotericin B, which is also extremely hydrophobic in nature (Epand, R. M., unpublished observation). T_H is

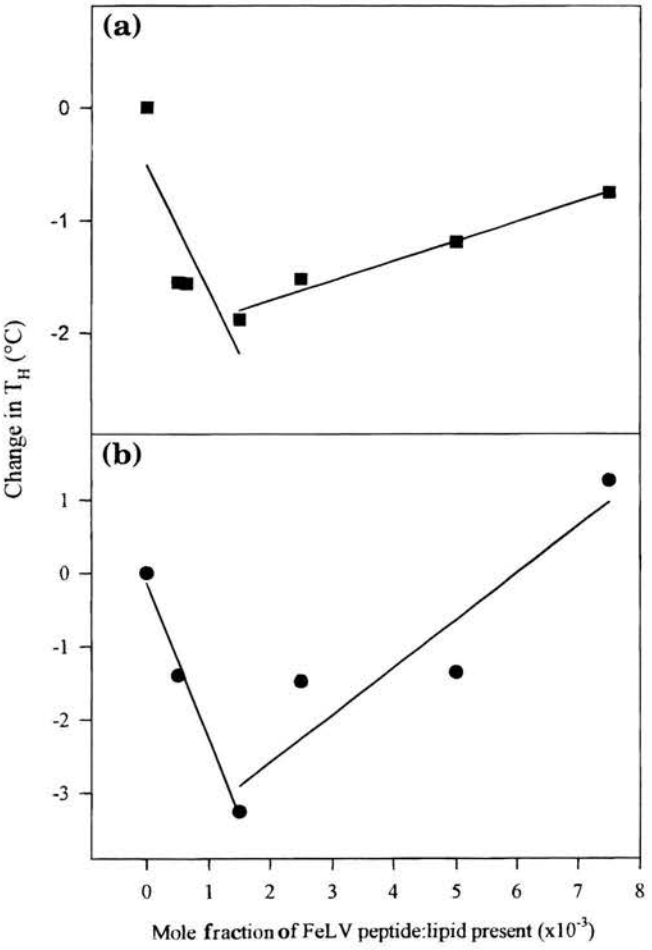

FIGURE 2: Change in lamellar to inverted hexagonal phase transition temperature of DiPoPE as a function of mole fraction of feline leukemia virus fusion peptide at (a) pH 7.4 (■) and (b) pH 5.0 (●).

seen to increase more in the presence of the FeLV peptide at pH 5.0 than at pH 7.4; presumably there is more self-aggregation of the peptide at this pH, possibly due to a decrease in negative charge of the glutamate residues at acidic pH. We suggest that the aggregated FeLV peptide fraction may lie along the bilayer surface, rather than insert into the membrane, and actually stabilize the L_α phase, possibly by reducing its negative curvature strain.

^{31}P NMR Spectroscopy. Figure 3 shows the ^{31}P NMR powder patterns obtained for pure MeDOPE and for MeDOPE plus FeLV fusion peptide as a function of temperature. The temperature at which isotropic resonances are first detected, T_i, drops with increasing peptide concentration. There is also a direct correlation between the mole fraction of peptide present and the amount of isotropic signal seen at 40 °C. Moreover, in the presence of the FeLV fusion peptide, a larger percentage of the lipid remains in this isotropic state over the full range of recorded temperatures. At 82 °C, a small amount of MeDOPE with FeLV peptide has converted to the H_{II} phase, whereas by 75 °C, the pure lipid already has a larger H_{II} signal. No significant differences were found between the pH 7.4 and the pH 5.0 samples. Figure 4 shows the ^{31}P NMR powder patterns obtained for pure DiPoPE and for DiPoPE plus FeLV fusion peptide as a function of temperature. The pure DiPoPE samples show no significant isotropic peak at any of the

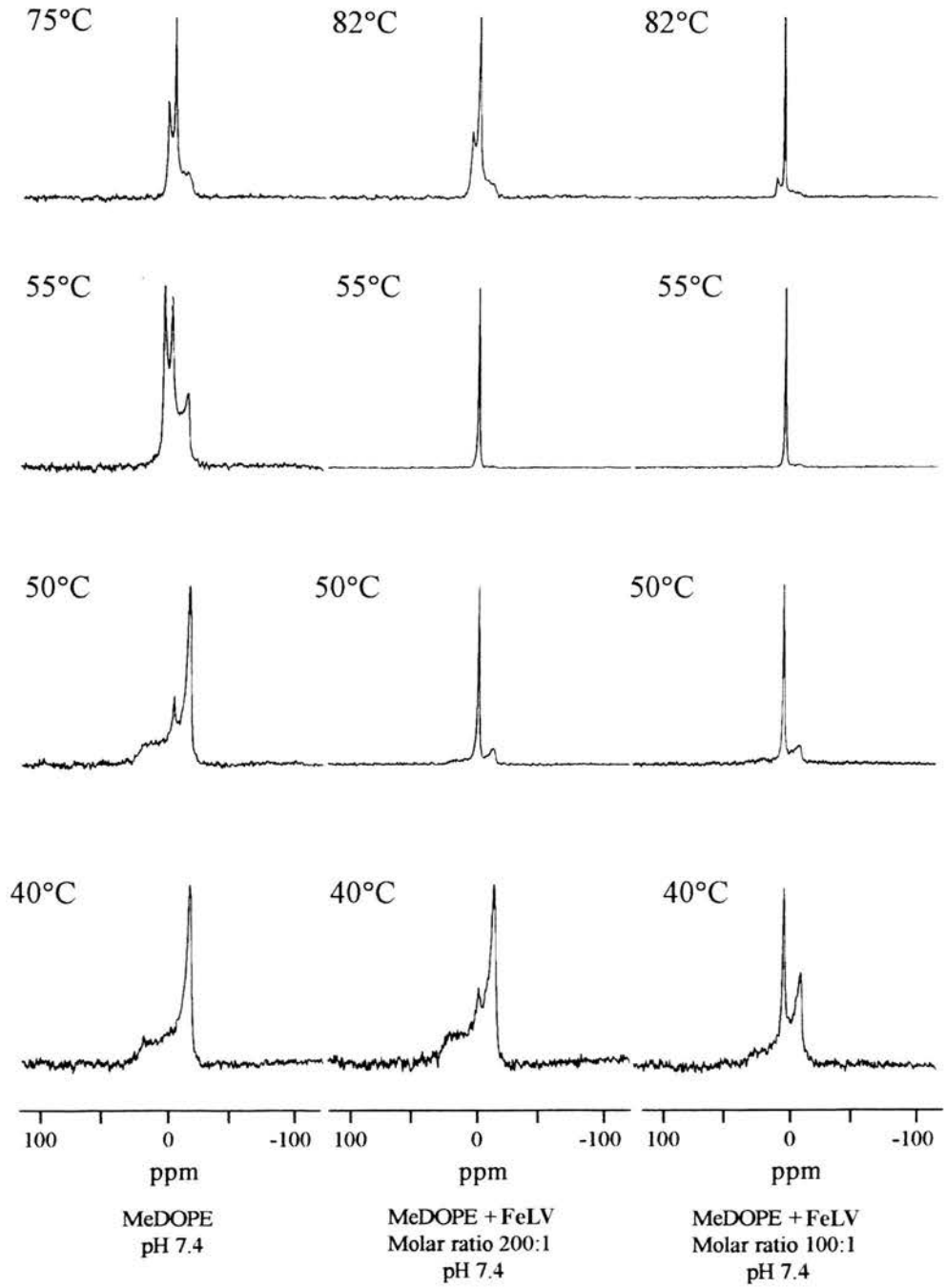

FIGURE 3: ^{31}P NMR spectra of pure MeDOPE, and samples containing different molar ratios of feline leukemia virus peptide, as a function of temperature. Lipid concentration in all samples is 50 mg/mL. Only pH 7.4 data are shown, but the pH 5.0 results were qualitatively similar.

recorded temperatures. However, in the presence of the FeLV peptide, a substantial isotropic component is seen throughout the entire recorded temperature range.

The shapes of ^{31}P powder patterns are determined by the extent of motional averaging, on the ^{31}P NMR time scale, of the chemical shift anisotropy of the ^{31}P atom present in the phospholipid headgroup. This, in turn, is directly influenced by the types of motion possible within the phospholipid dispersions. The amount of isotropic ^{31}P NMR resonance (I_s) present in the NMR spectrum has been directly correlated with the rate of membrane fusion between MeDOPE vesicles (*34*). Furthermore, the initial appearance of I_s has coincided with the start of membrane fusion (*35*). Similar findings have occurred with vesicles of different lipid compositions (*35*). Phospholipid molecules in inverted cubic phases generate isotropic ^{31}P NMR spectra (*36*). It is unlikely that ordered cubic phases are intermediates in fusion. Fusion intermediates are isolated structures, not phases. Furthermore, cubic phases have extreme kinetic stability (*37*). This view is supported by our NMR data, which show persistence of isotropic signals through a wide temperature range, over a period of hours. However, it has been suggested that fusion intermediates resemble intermediates formed on the pathway to cubic phase formation (*17*). Work with the fusion peptides from SIV (*12*) and influenza virus (*13*) showed enhancement of I_s in their presence. Our results presented here for the putative fusion peptide from FeLV suggest that it is indeed favoring the formation of lipid

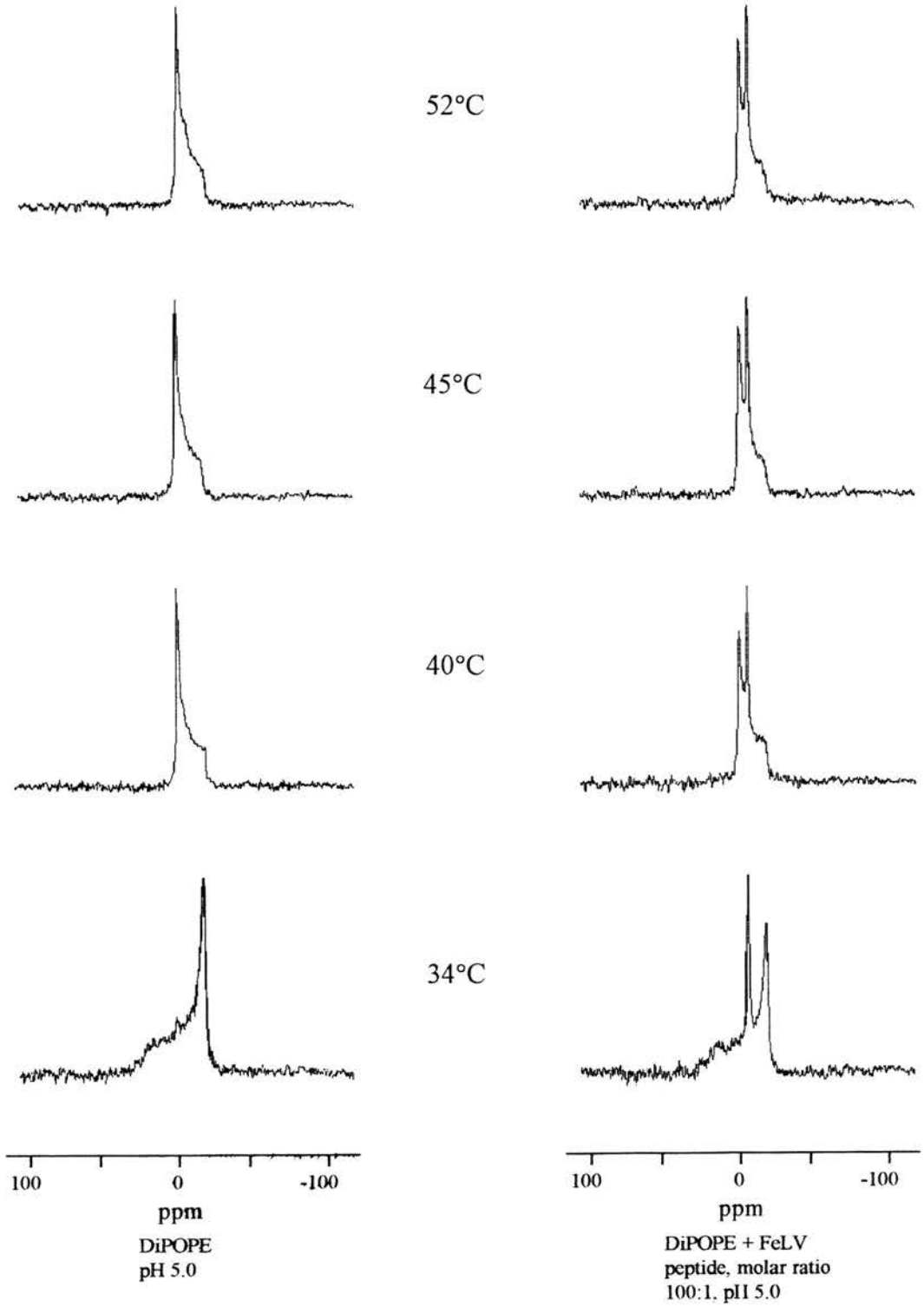

FIGURE 4: ^{31}P NMR spectra of DiPoPE alone and in the presence of a 100:1 molar ratio of lipid:FeLV peptide. Only pH 5.0 data are shown, but the pH 7.4 results were qualitatively similar. Lipid concentration in all samples is 50 mg/mL.

structures which are likely to be involved in the rate-limiting intermediate stages of the fusion pathway.

X-ray Diffraction Experiments. Time-resolved X-ray diffraction data were obtained to confirm the phase transitions measured by DSC and to determine any effects of the FeLV peptide on lipid structural parameters. The diffraction patterns verify that the transitions taking place in the DSC experiments are from L_α to H_{II}, no other phases being observed in the X-ray data. However, it is possible that very transient phases are not detected due to the high scan rate employed (disordered structures would not be seen either). Figure 5 shows a 3-dimensional plot of the series of diffraction patterns obtained for DiPoPE plus FeLV peptide present at a peptide mole fraction of 3.1×10^{-3} for the entire measured temperature range. Figure 6 shows a typical diffractogram for the T_H region of the scan; this was taken from the data for DiPoPE with FeLV peptide present at a peptide mole fraction of 1.6×10^{-3} and at 42 °C. Samples were assigned the H_{II} phase if a minimum of three diffraction peaks were observed which indicated spacings in the ratios

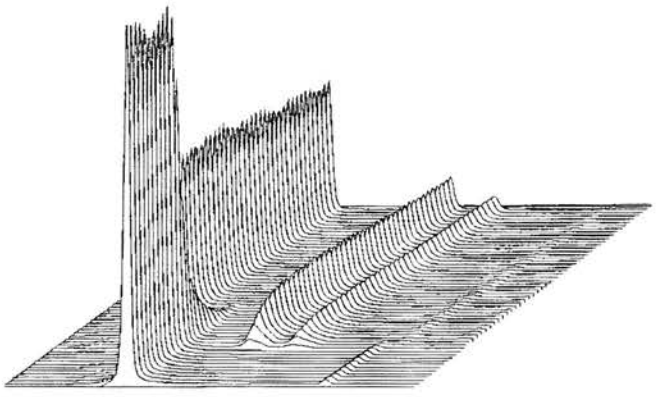

FIGURE 5: Three-dimensional plot of the series of consecutive diffraction patterns obtained on heating from 30 °C to 70 °C for DiPoPE plus FeLV fusion peptide, at a peptide mole fraction of 3×10^{-3}. The heating scan rate was 90 °C/h. The origin is on the left, and the right-hand limit represents channel 270 of the 512 recorded. The first two lamellar and first three hexagonal diffraction orders are visible as well-defined peaks. The transition from the lamellar to the hexagonal phase can be seen. The presence of a third, peptide-induced phase can be seen as a shoulder on the first and second hexagonal phase peaks.

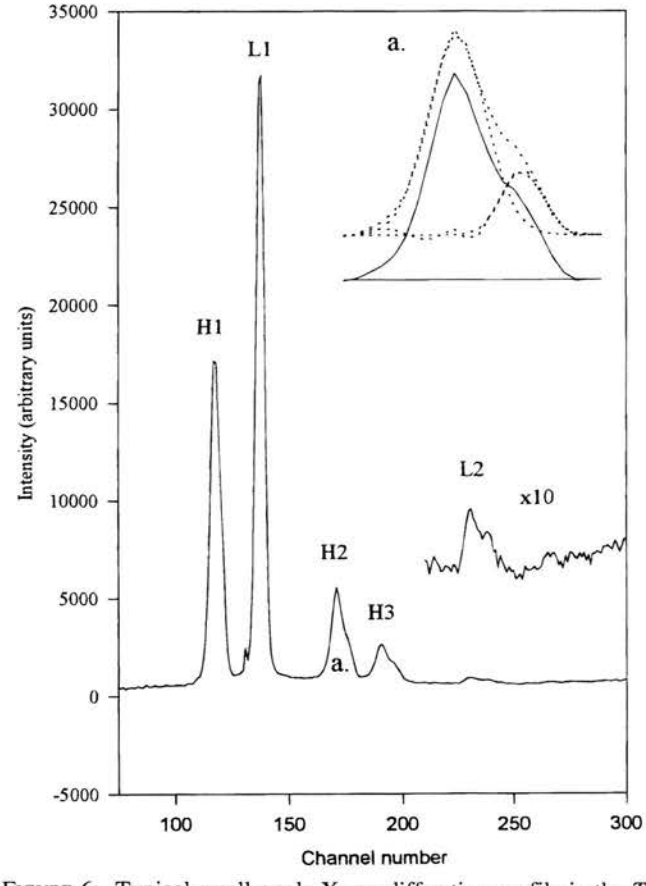

FIGURE 6: Typical small-angle X-ray diffraction profile in the T_H region of the scan series for DiPoPE plus FeLV fusion peptide at a peptide mole fraction of 1.6×10^{-3}, at 42 °C. Channel numbers 1−300 of the 512 recorded are shown. Part of the data has been amplified by a factor of 10 (×10) for the sake of clarity. The inset, (a), shows an enlargement of the Bragg peak for the second diffraction order of the H_{II} phase, and the presence of a smaller peak, of smaller d spacing than the main H_{II} peak (solid lines). Gaussian analysis of the two peaks is shown above (dotted lines).

$1:\sqrt{3}:\sqrt{4}:\sqrt{7}$. The d spacings for all samples were calculated from the distance of peaks from the origin. The d spacings for the L_α and H_{II} phases for pure DiPoPE and the

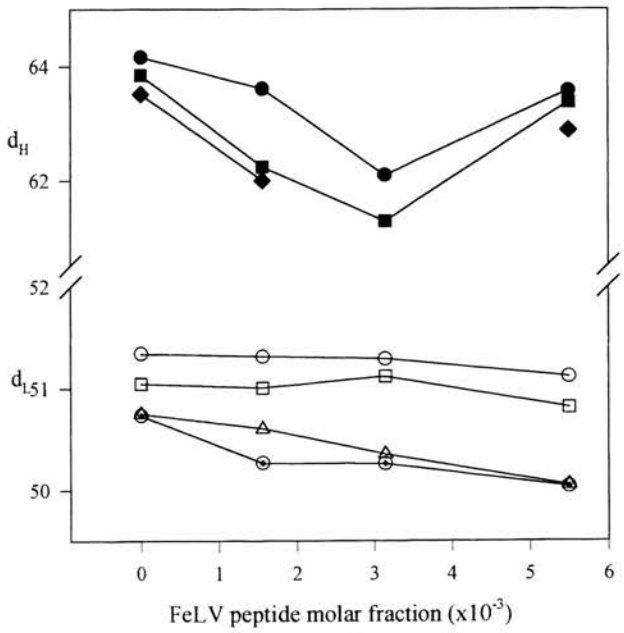

FIGURE 7: Variation in d spacings (Å) for the L_α and H_{II} phases of DiPoPE with increasing FeLV peptide concentration. d_H measured (●) at 49 °C, (■) at 50 °C, and (◆) at 52 °C. d_L measured (○) at 33 °C, (□) at 40 °C, (Δ) at 44 °C, and (⊕) at 45 °C.

peptide-containing samples are plotted in Figure 7. The d spacings found in the present work are in good agreement with those previously reported (*24*, *38*). It should be noted that in the values presented in the references the definition used for the repeat spacing was that adopted by Gruner and others (*39*) in which the d space corresponds to the distance from the center of one H_{II} cylinder to the next. This distance is related to the lattice spacing reported in the present work by multiplying the lattice spacing by $2/\sqrt{3}$. The small differences between the two sets of data may be the result of different heating protocols, different batches of DiPoPE, and different calibrations. The transition from the L_α to the H_{II} phase is ordered, i.e., both lamellar and hexagonal phase domains coexist in the transition temperature region. This was seen for the pure lipid and the peptide-containing samples. No cubic intermediates are seen. The slow rate of water penetration into the nascent H_{II} phase seen with multilamellar vesicle (MLV) samples may prolong the detection of coexistence of L_α and H_{II} domains. Figure 6a (inset) shows the Gaussian analysis of the Bragg peak of the second diffraction order of the hexagonal phase. It can be seen that, in the presence of the FeLV peptide, a second and different lattice was observed, of slightly narrower d spacing than that of the main H_{II} phase. As one cannot assign a lipid phase on less than three diffraction orders, it is not possible to state definitely what this novel, peptide-induced phase is; there are only two observable diffraction peaks for this phase, which represent the second and third diffraction orders. The diffraction amplitudes of higher orders are too small to detect, and the first orders of the two hexagonal phases probably overlap due to the decrease in spatial resolution seen at smaller diffraction angles. This may account for the observed slight increase in mosaic spread of the first order of diffraction of the hexagonal phase in the presence of peptide. However, the two observed novel peaks fit to a d spacing of $1:\sqrt{3}$, and they occur as a shoulder on the definitely identified main H_{II} phase. Thus, this may

represent a novel H_{II} phase, which was most noticeable in the 1.6×10^{-3} FeLV peptide mole fraction samples. A measure of the maximum percentage of DiPoPE present in this phase as a proportion of total amount of hexagonal phase lipid yielded the following data: 0% with no peptide present, 32%, 20%, and 21% at peptide mole fractions of 1.6×10^{-3}, 3.1×10^{-3}, and 5.5×10^{-3}, respectively. Evidence of the peptide-induced lattice disappeared completely as heating continued well above T_H, indicating that this phase is transient. No extra peaks were seen in the pure lipid samples, and thus it is clear that this novel phase is due to the presence of peptide. Not all of the peptide is incorporated into these domains, since the d spacing of the main H_{II} phase (d_H) is also decreased in the presence of the FeLV peptide (see Figure 7); this also suggests that the FeLV peptide is decreasing R_0 of the system in this peptide concentration range. A reduction in R_0 will destabilize bilayer structures relative to inverted nonbilayer phases. DGs have been found to decrease R_0, i.e., to increase the spontaneous negative curvature, of MeDOPE (*35*). Physiological levels of DGs are known to promote fusion (*40*) and have also been found to enhance a L_α to cubic phase transition (*11*), to bicontinuous Q^{224} (*41*). This cubic phase is related to the putative fusion intermediate, in the patch-the-puncture fusion model (*42*). An interesting observation in our experiments is that of marked broadening of the L_α diffraction peaks on heating in the presence of the FeLV peptide, and in a peptide concentration-dependent manner. (The width of the peaks was determined by fitting Gaussians and measuring the width at half-height). This represents disordering of the L_α phase and may be consistent with the start of a transition to an inverted cubic phase (*9*). X-ray studies of DiPoPE with an SIV mutant fusion peptide at pH 7.4 (*38*) and from influenza virus at pH 5.0 (*24*) have indeed detected the formation of a cubic phase. The heating scan rates used in these studies were considerably slower than that used here, which may explain why no ordered cubic phase was detected in our study. When rapid heating was used with the influenza fusion peptide, no cubic phase was observed (*24*). It has also been observed that, even with pure MeDOPE, the extent of cubic phase formation is very dependent on scan rate (*10*, *43*). The FeLV peptide also produced broadening of the H_{II} peaks. Part of the peak broadening may be due to vesiculation of the multilamellar vesicles (MLVs) present in the samples, as suggested for the SIV fusion peptide/MeDOPE system; the conversion of MLVs to smaller vesicles with fewer lamellae is thermodynamically favorable, but the fusion peptide may greatly accelerate this process (*38*). The effect of the FeLV peptide on d_H is seen to exhibit a biphasic trend with peptide concentration, reminiscent of that seen for T_H in our DSC measurements. The fusion peptide had little effect on d_L at temperatures well below T_H, (see Figure 8), but as T_H is approached, d_L decreases with increasing peptide concentration. It can be seen from Figure 8 that the temperature-dependence of d_H and d_L is very similar for both pure lipid and the peptide-containing samples.

Fusion Assay. Figure 9 shows the percentages of lipid mixing between MeDOPE LUVs obtained in the presence of the SIV and FeLV fusion peptides. MeDOPE was used, since DiPoPE does not form stable liposomes. The SIV peptide promotes rapid lipid mixing (and thus membrane fusion) between the labeled and unlabeled LUV populations,

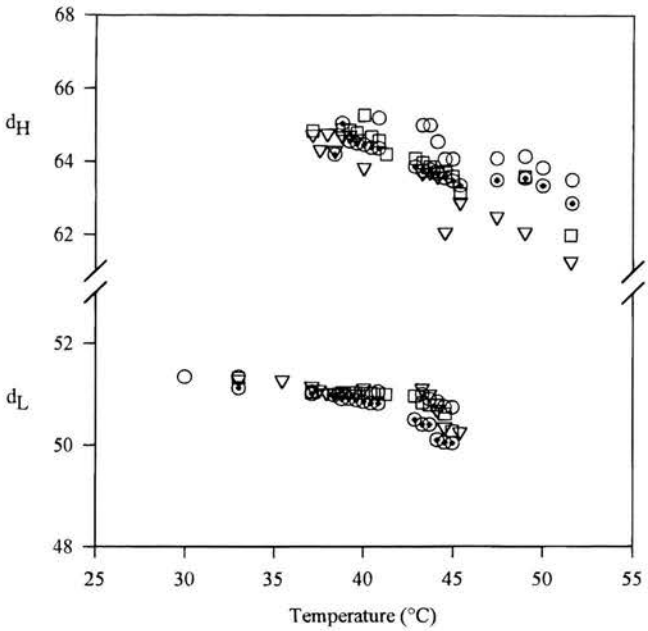

FIGURE 8: Change in d spacings (Å) of the L_α and H_{II} phases with temperature as calculated from the X-ray diffraction patterns. DiPoPE alone (○); DiPoPE plus FeLV peptide at a peptide mole fraction of 1.6×10^{-3} (□), 3.1×10^{-3} (▽), and 5.5×10^{-3} (⊕).

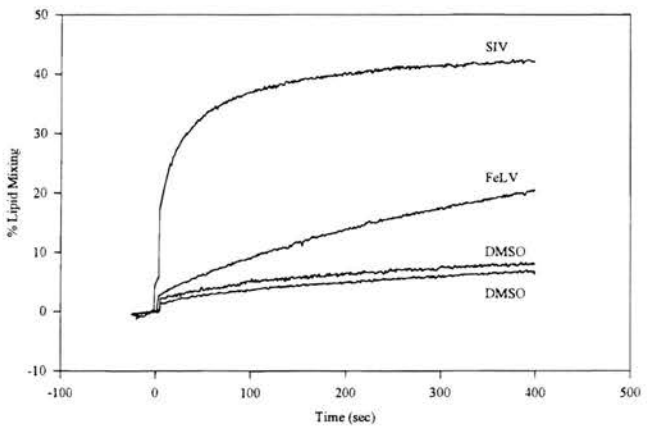

FIGURE 9: The percentages of lipid mixing between MeDOPE LUVs induced by the SIV and FeLV fusion peptides. The peptides, which were dissolved in DMSO, were added at time 0. Changes in fluorescence due to equivalent aliquots of the pure DMSO solvent are also shown. The top DMSO curve corresponds to 52 μL of added solvent as used for the FeLV peptide, and the bottom curve to 24 μL as used for the SIV peptide. Measurements were performed at 37 °C, and at pH 7.0.

as seen by the change in NBD fluorescence on probe dilution. Our results agree very closely with previous experiments performed using this peptide (*29*). The FeLV peptide also clearly produces membrane fusion, as shown by lipid mixing. The SIV peptide shows greater enhancement of fusion using this particular lipid system. This difference in potency may reflect the many differences between these two peptides, for example their lengths, overall electrical charges, solubility characteristics, and probable miscibilities with different lipid species. Moreover, different viral fusion peptides have been shown to require different specific experimental conditions in order to promote maximum membrane fusion (e.g., ref *44*–*46*). Thus, the experimental conditions used here may not provide optimal fusogenic conditions for the FeLV fusion peptide. The SIV fusion peptide was chosen as a control

since it is the most homologous retroviral fusion peptide for which there is definite experimental proof of fusogenic activity.

DISCUSSION

Two aspects of membrane fusion mechanisms can explain the relationship between a peptide-induced increase in membrane fusion rates and the effect of the peptide on lipid polymorphism. The first aspect is the formation of a stalk or interlamellar attachment (ILA) intermediate which has overall negative curvature (*16*). Thus the formation of this first intermediate would be accelerated by agents or conditions which favor the formation of inverted phases. The monolayers involved in the formation of this stalk intermediate are the trans or contacting monolayers (*22*). There are several examples of viral fusion peptides which lower T_H and therefore favor the formation of inverted phases, including both the SIV fusion peptide (*12*, *38*) and the influenza fusion peptide (*13*). In the present work we demonstrate, by DSC and X-ray diffraction, that the putative fusion peptide of FeLV can lower T_H of DiPoPE, at least at low peptide mole fractions. This peptide also causes d_H to decrease (Figure 7), indicating that the peptide promotes negative monolayer curvature.

Another mechanism by which peptides can promote the rate of fusion is by favoring the partitioning of the TMC intermediate toward the fusion pore/cubic phase pathway (*17*). This mechanism has been suggested for the influenza fusion peptide (*24*). The possibility of such a phenomenon occurring with the FeLV peptide is suggested by the fact that low concentrations of peptide promote the formation of isotropic resonances in ^{31}P NMR of MeDOPE and DiPoPE (Figures 3 and 4). Although no cubic phases were observed for DiPoPE by X-ray diffraction, this lipid forms cubic phases less readily. As a pure lipid, the cubic phase has never been observed with DiPoPE and in the presence of the influenza peptide the cubic phase is only found with DiPoPE mixed with other phases and with a low degree of order, presenting limited evidence for the formation of a cubic phase. The relationship between conditions leading to cubic phase formation and to increased rates of membrane fusion has also been noted with DAG-induced fusion (*11*, *47*).

The present work provides evidence that the N-terminus of the fusion protein of FeLV has effects on lipid properties which are characteristic of viral fusion peptides. It also demonstrates membrane fusion activity for the FeLV peptide, in the form of lipid mixing between liposomes. Furthermore, this peptide is an N-terminal segment, released by proteolytic activation of the fusion protein, which is also a feature shared with several other viral fusion peptides. The molecular mechanism by which it promotes fusion may depend on the nature of the target membrane and also on what the rate-determining step is in fusion. This peptide is suggested to accelerate both the rate of stalk formation as well as the partitioning of the TMC intermediate toward the formation of a fusion pore.

ACKNOWLEDGMENT

Grateful thanks to Mr. D. W. Hughes for technical assistance with NMR data collection, and to Dr. B. U. Komanschek for expert help with the running of station 8.2 at Daresbury.

REFERENCES

1. Bullough, P. A., Hughson, F. M., Skehel, J. J., and Wiley, D. C. (1994) *Nature 371*, 37.
2. White, J. M. (1995) *Cold Spring Harbor Symp. Quant. Biol. 60*, 581.
3. Freed, E. O., and Martin, M. A. (1995) *J. Biol. Chem. 270*, 23883.
4. Chernomordik, L. V., and Zimmerberg, J. (1995) *Curr. Opin. Struct. Biol. 5*, 541.
5. Papahadjopoulos, D., Vail, W. J., Newton, C., Nir, S., Jacobson, K., Poste, G., and Lazo, R. (1977) *Biochim. Biophys. Acta 465*, 579.
6. Ellens, H., Bentz, J., and Szoka, F. C. (1986) *Biochemistry 25*, 4141.
7. Gagné, J., Stamatatos, L., Diacovo, T., Hui, S. W., Yeagle, P. L., and Silvius, J. R. (1985) *Biochemistry 24*, 4400.
8. Hui, S. W., Stewart, T. P., and Boni, L. T. (1983) *Chem. Phys. Lipids 33*, 113.
9. Gruner, S. M., Tate, M. W., Kirk, G. L., So, P. T. C., Turner, D. C., Keane, D. T., Tilcock, C. P. S., and Cullis, P. R. (1988) *Biochemistry 27*, 2853.
10. van Gorkom, L. C. M., Nie, S.-Q., and Epand, R. M. (1992) *Biochemistry 31*, 671.
11. Basáñez, G., Nieva, J. L., Rivas, E., Alonso, A., and Goñi, F. M. (1996) *Biophys. J. 70*, 2299.
12. Epand, R. F., Martin, I., Ruysschaert, J. M., and Epand, R. M. (1994) *Biochem. Biophys. Res. Commun. 205*, 1938.
13. Epand, R. M., and Epand, R. F. (1994) *Biochem. Biophys. Res. Commun. 202*, 1420.
14. Epand, R. M. (1986) *Biosci. Rep. 6*, 647.
15. Siegel, D. P., Banschbach, J., and Yeagle, P. L. (1989) *Biochemistry 28*, 5010.
16. Siegel, D. P. (1993) *Biophys. J. 65*, 2124.
17. Siegel, D. P., and Epand, R. M. (1997) *Biophys. J. 73*, 3089.
18. Markin, V. S., Kozlov, M., M., and Borovjagin, V. L. (1984) *Gen. Physiol. Biophys. 3*, 361.
19. Kozlov, M. M., Leikin, S. L., Chernomordik, L. V., Markin, V. S., and Chizmadzhev, Y. A. (1989) *Eur. Biophys. J. 17*, 121.
20. Hui, S. W., Stewart, T. P., Boni, L., and Yeagle, P. L. (1981) *Science 212*, 921.
21. Melikyan, G. B., White, J. M., and Cohen, F. S. (1995) *J. Cell Biol. 131*, 679.
22. Chernomordik, L. (1996) *Chem. Phys. Lipids 81*, 203.
23. Lee, J. K., and Lentz, B. R. (1997) *Biochemistry 21*, 6251.
24. Colotto, A., and Epand, R. M. (1997) *Biochemistry 36*, 7644.
25. Brasseur, R., Vandenbranden, M., Cornet, B., Burny, A., and Ruysschaert, J.-M. (1990) *Biochim. Biophys. Acta 1029*, 267.
26. Epand, R. M., Cheetham, J. J., Epand, R. F., Yeagle, P. L., Richardson, C. D., Rockwell, A., and DeGrado, W. F. (1992) *Biopolymers 32*, 309.
27. Rojko, J. L., and Hardy, W. D. J. (1994) in *The Cat-Diseases and Clinical Management* (Sherding, R. G., Ed.) p 263, Churchill Livingstone Press, New York.
28. Bosch, M., Earl, P., Fargnoli, K., Picciafuoco, S., Giombini, F., Wong Staal, F., and Risser, R. (1989) *Science 244*, 694.
29. Martin, I., Dubois, M.-C., Defrise-Quertain, F., Saermark, T., Burny, A., Brasseur, R., and Ruysschaert, J.-M. (1994) *J. Virol. 68*, 1139.
30. Fraser, R. D. B., and MacRae, T. P. (1981) *Int. J. Biol. Macromol. 3*, 193.
31. Struck, D. K., Hoekstra, D., and Pagano, R. (1981) *Biochemistry 20*, 4093.
32. Laird, H. M., Jarrett, O., and Whalley, J. M. (1973) *Bibl. Haematol. 39*, 133.
33. Gruner, S. M. (1985) *Proc. Natl. Acad. Sci. U.S.A. 82*, 3665.
34. Yeagle, P. L., Young, J., Hui, S. W., and Epand, R. M. (1992) *Biochemistry 31*, 3177.

35. Ellens, H., Siegel, D. P., Alford, D., Yeagle, P. L., Boni, L., Lis, L. J., Quinn, P. J., and Bentz, J. (1989) *Biochemistry 28*, 3692.
36. Siegel, D. P., Banschbach, J., Ellens, H., Alford, D., and Bentz, J. (1989) *Biophys. J. 55*, 28A (Abstract).
37. Yeagle, P. L. (1994) *Curr. Top. Membr. 40*, 197.
38. Colotto, A., Martin, I., Ruysschaert, J.-M., Sen, A., Hui, S. W., and Epand, R. M. (1996) *Biochemistry 35*, 980.
39. Gruner, S. M. (1991) in *The Structure of Biological Membranes* (Yeagle, P., Ed.) p 211, CRC Press, Boca Raton, FL.
40. Siegel, D. P., Banschbach, J., Alford, D., Ellens, H., Lis, L. J., Quinn, P. J., Yeagle, P. L., and Bentz, J. (1989) *Biochemistry 28*, 3703.
41. Luzzati, V., Vargas, R., Mariani, P., Gulik, A., and Delacroix, H. (1993) *J. Mol. Biol. 229*, 540.
42. Nieva, J. L., Alonso, A., Basáñez, G., Goñi, F. M., Gulik, A., Vargas, R., and Luzzati, V. (1995) *FEBS Lett. 368*, 143.
43. Siegel, D. P., and Banschbach, J. (1990) *Biochemistry 29*, 5975.
44. White, J. M. (1990) *Annu. Rev. Physiol. 52*, 675.
45. Larsen, C. E., Nir, S., Alford, D. R., Jennings, M., Lee, K.-D., and Düzgünes, N. (1993) *Biochim. Biophys. Acta 1147*, 223.
46. Nieva, J. L., Nir, S., Muga, A., Goni, F. M., and Wilschut, J. (1994) *Biochemistry 33*, 3201.
47. Basáñez, G., Ruiz-Argüello, B., Alonso, A., Goñi, F. M., Karlsson, G., and Edwards, K. (1997) *Biophys. J. 72*, 2630.

BI980227V

Structural plasticity of the feline leukaemia virus fusion peptide: a circular dichroism study

Sarah M.A. Davies[a,*], Sharon M. Kelly[b], Nicholas C. Price[b], Jeremy P. Bradshaw[a]

[a] *Department of Preclinical Veterinary Sciences, Royal (Dick) School of Veterinary Studies, University of Edinburgh, Summerhall, Edinburgh EH9 1QH, UK*

[b] *Department of Biological and Molecular Sciences, University of Stirling, Stirling FK9 4LA, UK*

Received 20 November 1997; revised version received 23 January 1998

Abstract The secondary structure of the feline leukaemia virus (FeLV) fusion peptide was investigated using circular dichroism (CD). Our results show that this peptide can readily flip between random, α-helical and β-sheet conformations, depending upon its environment. The CD spectrum changes from one characteristic of random coil to predominantly β-sheet type, and finally to that showing the characteristics of α-helical structure on moving from an aqueous solvent, through several increasingly hydrophobic systems, to a highly hydrophobic solvent. Electron microscopy confirmed the presence of β structure. We propose that the structural plasticity demonstrated here is crucial to the ability of the fusion peptide to perturb lipid bilayers, and thus promote membrane fusion.

Key words: Spectrophotometry; Circular dichroism; Electron microscopy; Feline leukemia virus; Fusion peptide; Structural plasticity

1. Introduction

Membrane fusion, the merging of two distinct lipid bilayers to form one common bilayer, is essential to life, occurring many times daily within every animal cell [1]. Intercellular fusion is also important, for example between sperm and egg in the mammalian fertilisation process [2]. In addition, many intracellular parasites, including all enveloped animal viruses, utilise fusion to gain entry to their target cells, and thus cause disease [3]. However, despite the clear importance of fusion, the precise mechanisms involved in this process are still not known.

Enveloped viruses have specific envelope glycoprotein 'spikes', viral fusion proteins, which mediate fusion between the virus and its target cell [4]. Each fusion protein contains a fusion peptide, a span of relatively hydrophobic amino acids, which is thought to insert into the host cell target membrane and disrupt bilayer stability, so initiating the fusion process [5]. The active participation of fusion peptides in the fusion process, for example those of influenza virus and human immunodeficiency virus (HIV), has been shown by a variety of techniques including hydrophobic affinity labelling experiments [6] and site-directed mutagenesis studies [7,8]. Studies using synthetic peptides, which correspond to the sequences of viral fusion peptides, have helped to determine some of the molecular mechanisms involved in viral-mediated fusion. In particular, these synthetic peptides appear to be most useful for studies on the minimum and precise molecular and structural requirements for membrane destabilisation [9–11].

Translocation from an aqueous environment, such as extracellular fluid, to a lipid environment is likely to involve substantial structural alterations of a peptide. Many proteins and peptides insert into membranes, and concomitantly alter their own secondary structure, but they do not trigger huge changes in the arrangements of the lipid molecules in their target membranes.

There is much conflicting evidence on the active secondary structure of fusion peptides. A modelling study of several viral fusion peptides assumed that they completely formed α helices on membrane insertion [5]. However, Gallaher et al. have cautioned against the earlier assumption that all fusion peptides are 'sided' helices in their active form [12]. Indeed, the measles virus fusion peptide was found to adopt a conformation of 73% β sheet in one study [13], and, under different experimental conditions, fusion peptides from different HIV strains have been shown to be mainly α-helical [14] or conversely mainly β-sheet [15] in their active forms. Hepatitis B virus fusion peptide favours a β-sheet conformation in the presence of lipid vesicles [16], as does PH-30, a sperm fusion peptide involved in sperm-egg fusion [17]. However, none of these studies examines the same fusion peptide in a whole range of different solvent systems.

We wished to examine the secondary structure of the fusion peptide from the retrovirus feline leukemia virus (FeLV) in a variety of environments. The FeLV peptide contains significant numbers of amino acids that characteristically favour three different secondary structures, namely the α helix, the β sheet and a coiled conformation. The conclusion drawn from the various studies mentioned above is that fusion peptides change from one defined, inactive secondary structure to another different and equally well-defined active secondary structure. We speculated that this might lead to a large amount of dynamic structural flexibility for the FeLV fusion peptide. Indeed, computer modelling work has hinted that this might be an important factor for fusion peptides in general [18]. Since membrane fusion is a dynamic process, involving large changes in the component molecules, structural plasticity may be an essential property of these initiators of fusion.

2. Materials and methods

A 28-residue peptide (sequence EPISLTVALMLGGLTVGGIAAGVGTGTK), which corresponds to the common sequence of the amino-terminal fusion peptide of all documented strains of FeLV [19], was synthesised. A lysine (which is the next naturally occurring carboxy-terminal residue in the fusion protein) was included on the carboxy-terminus to increase peptide solubility. Peptide synthesis and purification were performed by Albachem Ltd, 26 Craigleith View,

*Corresponding author. Fax: (44) (131) 650-6576.
E-mail: sdavies@lab0.vet.ed.ac.uk

PII S0014-5793(98)00274-9

Edinburgh EH4 3JZ, UK. The peptide was synthesised on an Applied Biosystems 430A instrument, using Fmoc chemistry with the side chain protecting groups selected as tBu (Ser, Thr) and OtBu (Glu). The completed peptide was cleaved with a solution of TFA/H_2O (95:5) plus scavengers (ethanedithiol/thioanisole/triisopropanesilicane) and the solution was evaporated under vacuum. The crude peptide was dissolved in 50% TFA/H_2O and purified by reverse phase HPLC, using a RPC4 (10×100 mm) column, eluting with a linear gradient from 10% acetonitrile in water (0.1% TFA) to 60% acetonitrile in water (0.1% TFA) over 30 min. The peptide was characterised by mass spectra (MALDI, PerSeptive Biosystem laserTec), amino acid analysis (LKB 4150 alpha amino acid analyser) and analytical HPLC using PRC4 (4.6×100 mm), RPC8 (4.6×220 mm) and Vydac C8 (4.6×250 mm) columns, running a linear gradient of 10% acetonitrile in water (0.1% TFA) to 90% acetonitrile in water (0.1% TFA) over 30 min. The assembly of the peptide was reasonably efficient but the purification process was found to be very difficult. The peptide was found to be very insoluble; accordingly 50% TFA was added to take it into solution. However, a very broad peak without any resolution was obtained under normal eluting conditions, unless a very dilute solution was applied. Thus the purification could only be carried out batchwise on a small scale (0.5–1.0 mg per run).

The fusion peptide was added at a concentration of 1 mg/ml to (a) 2 M guanidine/50% ethanol, a solvent often used for peptide addition to fusion assays, (b) trifluoroethanol (TFE), and (c) hexafluoroisopropanol (HFIP). These samples were then diluted 1:1 with distilled water, giving a final peptide concentration of 0.5 mg/ml. Peptide was also added to sodium dodecylsulphate (SDS) at concentrations (c) 3 mM, (d) 6 mM in distilled water, to give a final peptide concentration of 0.5 mg/ml. The resulting suspensions were sonicated in a bath sonicator until the peptide dissolved. All chemicals were supplied by Sigma Chemical Co., UK.

CD spectra were recorded using a JASCO J-600 spectropolarimeter, over the wavelength range 195–260 nm, in a cell of path length of 0.02 cm, at 25°C. At least four spectra were averaged for each sample. Analysis of the spectra for secondary structure content utilised the CONTIN procedure of Provencher and Glöckner [20] to determine the amounts of α helix and β sheet present, and the method of Chang et al. [21] was used to verify the overall trend in α helix contents.

Negative staining transmission electron microscopy was used to examine the peptide samples for the presence of β structure. The peptide solutions were dried onto plastic-coated carbon grids, and then negatively stained using 4% sodium phosphotungstate at pH 7.2. A Philips 400 TEM was used, at 80 kV, and ×60 000 magnification. Negative controls were performed by staining an empty plastic-coated carbon grid, and also by staining the corresponding pure solvent.

3. Results

The far ultraviolet CD spectra of the FeLV fusion peptide in the various solvents are shown in Fig. 1. Satisfactory data could be obtained down to 195 nm; below this wavelength the noise levels prevented accurate determination of ellipticity. The CD spectra exhibit an increase in α-helical character on moving from 1 M guanidine/25% ethanol, through a selection of increasingly hydrophobic solvents, to 50% HFIP. In the guanidine/ethanol sample, the peptide shows a spectrum characteristic of random coil secondary structure, which is to be expected for a hydrophobic peptide in a polar solvent containing a chaotropic agent. The critical micellar concentration (CMC) of SDS is 8 mM at 20°C. In 3 mM SDS, the CD spectrum is typical of a β sheet, but as the concentration of SDS increases towards the CMC, the spectrum indicates that some α-helical structure is present. The CD spectrum in 50% TFE shows considerably more α-helical character and this is even more pronounced in 50% HFIP. Analysis of the spectra gives the percentages of α helix and β sheet in each sample listed in Table 1. The exact values of these estimates should be viewed with caution, since (a) ellipticity data could only be collected down to 195 nm instead of 190 nm, which is the preferred lower limit, and (b) it may be inappropriate to apply the methods of analysis which have been derived for proteins to oligopeptides. Moreover, the amounts of helix present may well be underestimated, as up to twofold reductions in ellipticity have been found in membrane-bound proteins [22]. However, an overall trend from random coil through predominantly β sheet to significant amounts of α helix can clearly be seen.

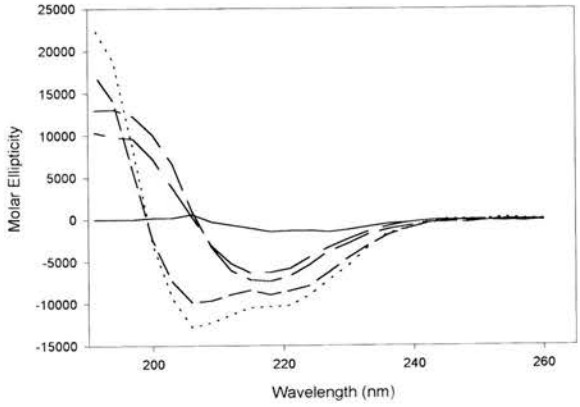

Fig. 1. CD spectra of the FeLV fusion peptide in a variety of solvents. Solid line: in 1 M guanidine/25% ethanol; short dash: in 50% TFE; dotted line: in 50% HFIP; long dash: in 3 mM SDS; medium dash: in 6 mM SDS.

Fig. 2 shows electron micrographs of FeLV peptide in 3 mM SDS, FeLV peptide in 50% HFIP and negative control: stained empty grid. Beta fibrils are visible in the 3 mM SDS sample, and were only seen when there was little evidence of α-helical content by CD spectroscopy (other data not shown).

Table 1
Percentages of FeLV peptide secondary structure, as calculated by the methods of Provencher and Glöckner [20] and Chang et al. [21]

Sample FeLV peptide (0.5 mg/ml) in:	% Secondary structure as calculated by the methods of:	
	Provencher and Glöckner [20] (helix, sheet)	Chang et al. [21] (helix)
1 M guanidine in 25% ethanol	0, nd[a]	0
50% TFE	20, 36	16
50% HFIP	30, 35	22
3 mM SDS	2, 57	11
6 mM SDS	12,47	14

[a]The value for the sheet content of this sample could not be determined using the method of Provencher and Glöckner [20] without an unacceptably large error.

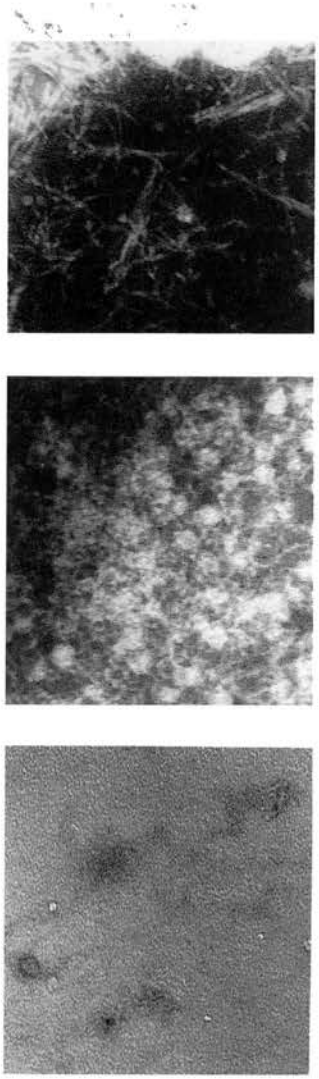

Fig. 2. Electron micrographs of (top) FeLV peptide in 3 mM SDS, (middle) FeLV peptide in 50% HFIP and (bottom) stained grid control.

These β fibrils appeared long and unbranched and were arranged in a meshwork.

4. Discussion

A limited amount of Fourier transform infrared spectroscopy has been performed on the fusion peptides of two retroviruses simian immunodeficiency virus (SIV) [23] and HIV [24]. These peptides were found to show a partial conversion from a β-sheet conformation in an aqueous solvent to an α helix in a lipid environment. Filtration to remove the non-lipid bound peptide yielded an increase in the amount of recorded α helix. Certainly the increase in the proportion of α helix which we observed for the FeLV peptide on increasing the solvent hydrophobicity agrees with these data. However, the assumption from the SIV and HIV studies was that the α-helical form is the single, fusion-active conformation. Work on other fusion peptides [15,16] and a different study on the HIV peptide [14] have all suggested that the β conformation may be the fusion-active state.

Fusion is an extremely rapid, multi-step process, and so structural measurements are obtained mainly on fusion end products. Thus only the final peptide conformations are observed, but none of the intermediate changes in conformation, which are adopted during the different stages of fusion, are seen. We propose that structural flexibility, rather than the rigid adoption of a particular secondary structure, may be a key property of fusion peptides. Membrane fusion is a dynamic process involving large structural changes in the participating molecules. We therefore suggest that it is possible that the critical feature of these catalytic peptides is their ability to 'flip' between different secondary structures extremely rapidly, rather than the adoption of any single, well-defined secondary structure. The energy barriers between these different secondary conformations must be low: the peptide must be able to adopt, at least transiently, these various structures, which presumably represent local energy minima. Clearly the secondary structures adopted under certain conditions may vary between individual fusion peptides, due to differences in their primary structures. However, previous computer modelling has hinted that structural flexibility may be a common property of fusion peptides [18]. Here we provide direct experimental proof of such flexibility for one fusion peptide. It is interesting to note that there is an analogy with the structural plasticity previously observed in a pathogenic prion peptide, PrP(106–126) [25], which has been implicated in prion-related diseases.

Acknowledgements: We wish to thank Mr S.R. Mitchell for expert technical assistance with the electron microscopy work, the Wellcome Trust for the award of a Prize Veterinary Research Training Scholarship to S.M.A.D., and the Biotechnology and Biological Sciences Research Council for provision of the CD facility.

References

[1] White, J.M. (1990) Annu. Rev. Physiol. 52, 675–697.
[2] Blobel, C.P., Wolfsberg, T.G., Turck, C.W., Myles, D.G., Primakoff, P. and White, J.M. (1992) Nature 356, 248–252.
[3] White, J.M. (1992) Science 258, 917–924.
[4] Hoekstra, D. (1990) J. Bioenerg. Biomembr. 22, 121–155.
[5] Brasseur, R., Vandenbranden, M., Cornet, B., Burny, A. and Ruysschaert, J. (1990) Biochim. Biophys. Acta 1029, 267–273.
[6] Harter, C., James, P., Bachi, T., Semenza, G. and Brunner, J. (1989) J. Biol. Chem. 264, 6459–6464.
[7] Gething, M.J., Doms, R.W., York, D. and White, J. (1986) J. Cell Biol. 102, 11–23.
[8] Bosch, M., Earl, P., Fargnoli, K., Picciafuoco, S., Giombini, F., Wong Staal, F. and Risser, R. (1990) Science 244, 694–697.
[9] Lear, J.D. and DeGrado, W.F. (1987) J. Biol. Chem. 162, 6500–6505.
[10] Düzgünes, N. and Shavnin, S.A. (1992) J. Membr. Biol. 128, 71–80.
[11] Gray, C., Tatulian, S.A., Wharton, S.A. and Tamm, L.K. (1996) Biophys. J. 70, 2275–2286.
[12] Gallaher, W.R., Segrest, J.P. and Hunter, E. (1992) Cell 70, 531–532.
[13] Epand, R.M., Cheetham, J.J., Epand, R.F., Yeagle, P.L., Richardson, C.D., Rockwell, A. and DeGrado, W.F. (1992) Biopolymers 32, 309–314.
[14] Rafalski, M., Lear, J.D. and DeGrado, W.F. (1990) Biochemistry 29, 7917–7922.
[15] Nieva, J.L., Nir, S., Muga, A., Goni, F.M. and Wilschut, J. (1994) Biochemistry 33, 3201–3209.
[16] Rodriguez Crespo, I., Gomez Gutierrez, J., Encinar, J.A., Gonzalez Ros, J.M., Albar, J.P., Peterson, D.L. and Gavilanes, F. (1996) Eur. J. Biochem. 242, 243–248.
[17] Muga, A., Neugebauer, W., Hirama, T. and Surewicz, W.K. (1994) Biochemistry 33, 4444–4448.
[18] Callebaut, I., Tasso, A., Brasseur, R., Burny, A. and Mornon, J.P. (1994) J. Computer-Aided Mol. Design 8, 175–191.

[19] Swiss Protein Data Bank (1996) Release number 34.0.
[20] Provencher, S.W. and Glöckner, J. (1981) Biochemistry 20, 33–37.
[21] Chang, C.T., Wu, C.S.C. and Yang, J.T. (1978) Anal. Biochem. 91, 13–31.
[22] Glaeser, R.M. and Jap, B.K. (1985) Biochemistry 24, 6398–6401.
[23] Martin, I., Dubois, M.C., Defrisequertain, F., Saermark, T., Burny, A., Brasseur, R. and Ruysschaert, J.M. (1994) J. Virol. 68, 1139–1148.
[24] Martin, I., Defrisequertain, F., Decroly, E., Vandenbranden, M., Brasseur, R. and Ruysschaert, J.M. (1993) Biochim. Biophys. Acta 1145, 124–133.
[25] Hope, J., Shearman, M.S., Baxter, H.C., Chong, A., Kelly, S.M. and Price, N.C. (1996) Neurodegeneration 5, 1–11.

ELSEVIER

Physica B 000 (1998) 000–000

PHYSICA B

A neutron study of the feline leukaemia virus fusion peptide: Implications for biological fusion?

Sarah M.A. Davies[a,*], Malcolm J.M. Darkes[b], Jeremy P. Bradshaw[a,b]

[a] *Department of Preclinical Veterinary Sciences, R(D)SVS, University of Edinburgh, Summerhall, Edinburgh EH9 1QH, UK*
[b] *Department of Biochemistry, School of Medicine, University of Edinburgh, George Square, Edinburgh EH8 9XD, UK*

Abstract

Neutron diffraction studies were performed on stacked phospholipid bilayers to determine the effects of the feline leukaemia virus (FeLV) fusion peptide on membrane structure. Bilayers were composed of dioleoylphosphatidylcholine with 50% (mol) dioleoylphosphatidylglycerol. Neutron scattering profiles with peptide present showed an increase in scattering density in the lipid-tails region, whilst scattering by the lipid headgroup region was decreased. This is interpreted as a lowering of the packing density of the lipid headgroups and an increase in the packing density of the lipid tails. Modelling studies and experimental evidence have suggested that fusion peptides catalyse fusion by increasing the negative curvature of the target membrane's outer monolayer. Our results presented here add support to this hypothesis for the fusion mechanism. The ^2H_2O scattering profile was also slightly perturbed in the lipid headgroup region with 1% (mol) FeLV fusion peptide present. The FeLV peptide had no significant effect on the organisation of bilayers containing only dioleoylphosphatidylcholine.

Keywords: Viral fusion peptide; Neutron diffraction; Negative curvature

1. Introduction

Membrane fusion is essential to life, occurring many times daily in every eukaryotic cell's homeostatic processes. It also plays a key role in the infective mechanisms of many intracellular pathogens. Despite its importance, the precise molecular structures and the energetics involved in fusion are still unknown. Fusion follows a multistep pathway, through several uncertain, highly bent lipid intermediate conformations, resulting in fusion pore-formation. Viral fusion peptides, the fusogenic domains of specific viral envelope glycoprotein spikes, operate as catalysts of fusion. The kinetics of fusion have been characterised extensively [1,2]; less is known about the structural changes involved. Several models have been devised for putative lipid intermediates involved in fusion [3,4]. It has been suggested that fusion peptides catalyse fusion by increasing the negative curvature of the target membrane's outer monolayer [5,6]. We wished to investigate the effects of the feline leukaemia virus (FeLV) fusion peptide on the structure of lipid bilayers, to determine any changes produced in molecular organisation.

* Corresponding author: Fax: +44 131 650 6142; e-mail: sdavies@lab0.vet.ed.ac.uk.

0921-4526/97/$17.00
PII S0921-4526(97)00812-0

2. Materials and methods

2.1. Materials

The FeLV peptide sequence, obtained from the Swiss Protein Data Bank, was EPISLTVAL-MLGGLTVGGIAAGVGTGTK. Lysine was included on the carboxy terminus to improve solubility. It is the next naturally occurring residue. The 28-amino acid peptide was synthesised by Albachem (University of Edinburgh, Scotland, UK) using solid-phase synthesis. Its purity was > 95%, as determined by analytical HPLC, mass spectrometry and amino-acid analysis. Dioleoylphosphatidylcholine

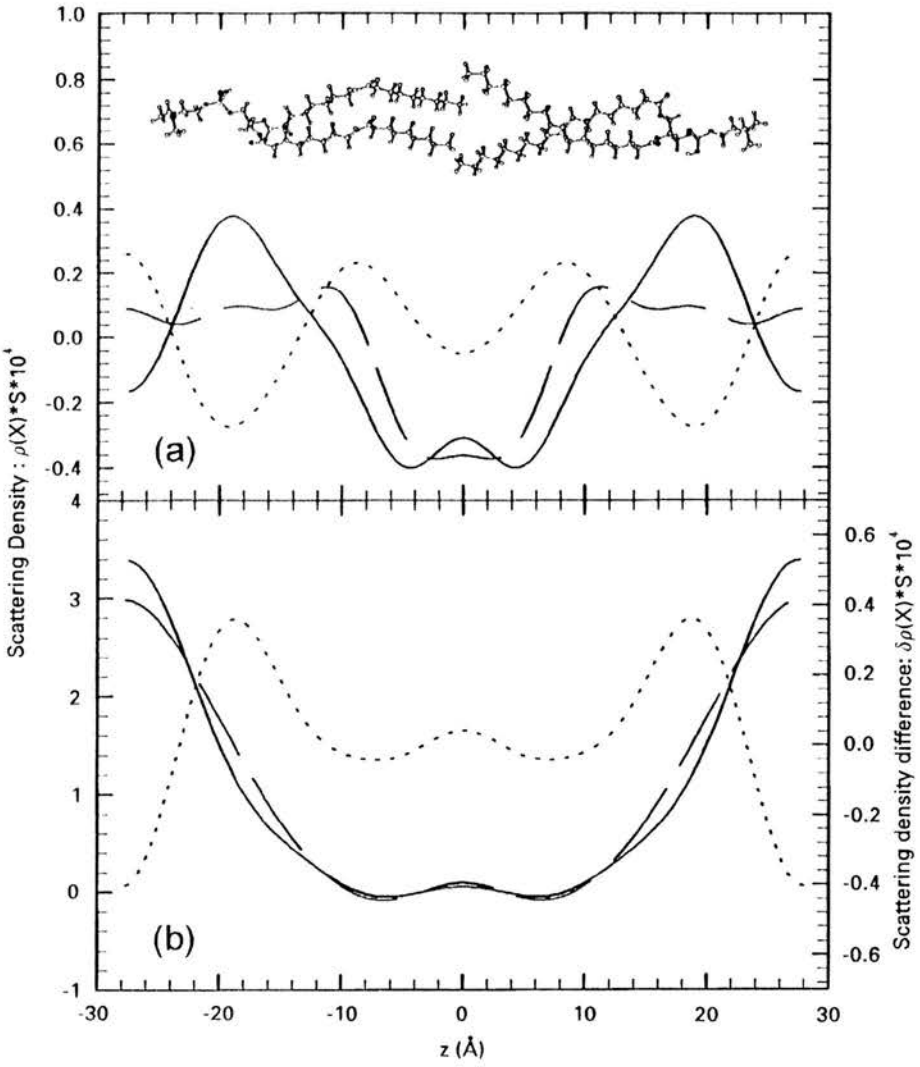

Fig. 1. (a) Neutron scattering density profiles of pure DOPC/DOPG bilayers (solid line) and of DOPC/DOPG with 1% (mol) FeLV peptide (broken line), and difference profile calculated by subtracting structure factors for DOPC/DOPG bilayers from structure factors for DOPC/DOPG with 1% (mol) FeLV peptide (dotted line). Phospholipid molecules are shown above the profiles to orientate the scattering densities. (b) ^2H_2O distribution within and between bilayers of DOPC/DOPG (solid line) and DOPC/DOPG with 1% (mol) FeLV peptide (broken line), and difference profile of ^2H_2O distribution due to the presence of FeLV peptide (dotted line).

(DOPC) and dioleoylphosphatidylglycerol (DOPG) were purchased from Avanti Polar Lipids (Alabaster, AL, USA).

2.2. Neutron diffraction

Neutron diffraction measurements were performed on the D16 instrument at the Institut Laue et Langevin (Grenoble, France). 20 mg of total lipid, or lipid plus 1% (mol) peptide, were vortexed thoroughly in chloroform. The peptide-containing samples were then sonicated until the peptide dissolved. Thereafter, sample preparation, method details and data processing were essentially as described previously [7]. Samples were applied to quartz slides using an airbrush spraying technique. A minimum of 12 h was allowed for sample drying time in vacuo, and also for rehydration with H_2O, 50% ^2H_2O or 100% ^2H_2O. All samples were run at 25°C. The data were phased using the information from $H_2O/^2H_2O$ exchange, and put on a 'relative absolute scale' using the method in Ref. [8]. ^{14}C-phospholipids and ^{3}H-water were used to determine the water content of each sample. Six orders of diffraction were recorded and analysed. The calculated *d*-repeats were 55.25 Å for DOPC/DOPG and 55.60 Å for DOPC/DOPG plus FeLV peptide.

3. Results

Fig. 1a shows the neutron scattering density profiles at 8.1% ^2H_2O of bilayers of 50% (mol) DOPC/DOPG alone and in the presence of 1% (mol) FeLV peptide, and also the difference profile, calculated by subtracting the scattering density due to lipid alone from the profile for lipid with peptide present. Phospholipid molecules are shown above the profile to orientate the relative densities seen. The profile produced with peptide present shows decreased scattering density in the lipid headgroup region, and an increase in scattering density in the lipid tail region. Fig. 1b shows the ^2H_2O distribution within and between bilayers of pure DOPC/DOPG and DOPC/DOPG plus peptide, and the difference profile for ^2H_2O distribution due to the presence of the FeLV peptide. Results obtained for samples of pure DOPC with and without FeLV peptide showed negligible effect for the fusion peptide on bilayer structure (data not shown).

4. Discussion

The difference profile for the bilayer neutron scattering density (dotted line, Fig. 1a) shows that the addition of FeLV peptide to the bilayers causes an increase in scattering density close to the bilayer centre, a reduction at the surface and an increase in the water region. The scale of these perturbations is much too high for them to represent simply the scattering density of the peptide: the amount of peptide present is tiny, only 1% (mol). They must therefore be caused by alterations in the phospholipid packing (changes in water distribution have been eliminated from the figure by showing the 8.1% ^2H_2O profiles). We interpret the difference profile, therefore, as an increase in the packing density of the phospholipid fatty acids, and a decrease in the packing density of their headgroups. This interpretation is totally consistent with the emerging model for the mode of action of a fusion peptide: this suggests that the peptide inserts obliquely into lipid bilayers and precesses, i.e. it traces out an inverted cone-shaped motion. Thus, it will increase the negative curvature of the target lipid monolayers. As our lipids are confined to a planar bilayer configuration, changes in elastic monolayer curvature forces will be expressed as effects on molecular packing. Fig. 2 shows a model of this concept. The profiles in Fig. 1b show that the

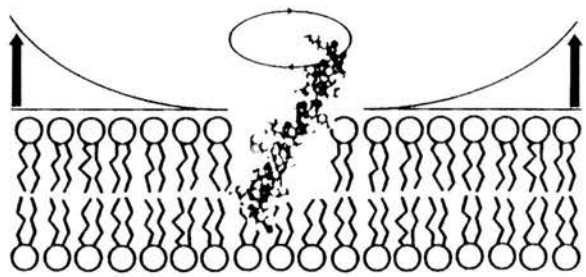

Fig. 2. Model of the FeLV peptide inserting into a lipid bilayer and precessing. This favours the bending of the lipid molecules into a negatively curved, non-bilayer conformation.

^2H_2O distribution also changes, possibly as a result of bilayer thinning. Our results add support to the hypothesis that fusion peptides act by increasing the negative curvature of the target cell's outer monolayer, thus causing this to bend towards the opposing bilayer, and allowing closer approach of the two initially distinct membranes.

Acknowledgements

SMAD holds a Wellcome Trust Veterinary Research Training Scholarship. The measurements were carried out at the Institut Laue et Langevin, with the assistance of Dr. V. Gordeliy.

References

[1] J.L. Nieva, S. Nir, A. Muga, F.M. Goni, J. Wilschut, Biochemistry 33 (1994) 3201.
[2] J.M. White, Annu. Rev. Physiol. 52 (1990) 675.
[3] D.P. Siegel, Biophys. J. 65 (1993) 2124.
[4] L.V. Chernomordik, J. Zimmerberg, Curr. Opinion Struct. Biol. 5 (1995) 541.
[5] R. Brasseur, M. Vandenbranden, B. Cornet, A. Burny, J. Ruysschaert, Biochim. Biophys. Acta 1029 (1990) 267.
[6] R.M. Epand, R.F. Epand, Biochem. Biophys. Res. Commun. 202 (1994) 1420.
[7] K.C. Duff, A.J. Cudmore, J.P. Bradshaw, Biochim. Biophys. Acta 1145 (1993) 149.
[8] M.C. Weiner, G.I. King, S.H. White, Biophys. J. 62 (1991) 2762.

Version date: July 7, 1997

Interaction of tachykinins with phospholipid membranes: a neutron diffraction study

Malcolm J. M. Darkes[a], Sarah M. A. Davies[b] & Jeremy P. Bradshaw[a,b].

[a]Department of Biochemistry, University of Edinburgh School of Medicine, George Square, Edinburgh, EH8 9XD, Scotland, UK.

[b]Department of Preclinical Veterinary Sciences, R. (D.) S. V. S., University of Edinburgh, Summerhall, Edinburgh, EH9 1QH, Scotland, UK.

Abstract

Tachykinins are a group of peptides which bind to G-protein coupled receptors. Receptor affinity appears to depend on different secondary structures of tachykinin which share the same hydrophobic carboxy-terminal sequence, FXGLM. Receptor activation is thought to be due to the carboxy-terminal submerging into the bilayer and the amino-terminal binding on the surface. Binding of tachykinins to phospholipid bilayers may take place both on the aqueous membrane surface and in the hydrophobic region. The two-state equilibrium appears to depend on the surface charge of the membrane. Deuterating substance P and neurokinin A at their carboxy-terminals, our results show two populations of label for each peptide. One is very close to the water-hydrocarbon interface, the other some 13Å deeper. We report that the bilayer location of the two tachykinins is remarkably similar, thereby inferring that receptor specificity must be controlled by finer levels of structure.

Keywords: Tachykinins, substance P, neurokinin A, neutron diffraction.

Corresponding author: M.J.M.Darkes, Department of Biochemistry, University of Edinburgh School of Medicine, George Square, Edinburgh, EH8 9XD, Scotland, UK. Fax: + 44 131 650 6576. Email Mdarkes@Lab0.Vet.Ed.Ac.UK

Introduction

Substance P (SP) and neurokinin A (NKA) belong to the tachykinin family, a group of six small amphipathic peptides which bind to G-protein coupled receptors. They are found in a wide range of tissues including the central and peripheral nervous systems and gastro-intestinal tract. Tachykinin receptor binding sites appear to involve both the extracellular loops and the transmembrane domains [1]. An address-message model [2] has been proposed where the flexible cationic N-terminal region, or "address domain", is responsible for receptor selectivity and the structurally extended and conserved hydrophobic C-terminal delivers the message.

The binding of tachykinins to phospholipid bilayers appears to take place both on the aqueous membrane surface and in the hydrophobic region. This two-state equilibrium may depend on the surface charge of the membrane [3]. NMR (nuclear magnetic resonance), CD (circular dichroism) and molecular modelling studies [4,5,6] have shown that SP has longer binding times and a more complex structure in negatively charged lipid-based systems than zwitterionic ones. In contrast, there is an argument against a membrane-mediated receptor mechanism, based on the observation that a SP analogue with a charged C-terminus, may not insert into the hydrophobic core of membranes, still shows SP agonist activity [4].

Our measurements test the hypothesis that different members of the tachykinin family position their C-terminal message at different depths within the membrane. Neutron diffraction was used to define the location of the specifically deuterated C-terminus of each peptide in synthetic phospholipid bilayers.

Materials and Methods

Neutron diffraction measurements were carried out on the V1 membrane diffractometer at the Berlin Neutron Scattering Centre, Germany. Dioleoylphosphatidylcholine (DOPC) and dioleoylphosphatidylglycerol (DOPG) were purchased from Avanti Polar Lipids (Alabama, USA) and used without further purification. Peptide synthesis was carried out by Albachem (Edinburgh, UK) to the following sequences: SP (RPKPQQFFGLM-NH_2); NKA (HKTDSFVGLM-NH_2). Both

peptides were synthesised in an undeuterated form and with leucine replaced by a deuterated analogue which contained a total of 10 deuterons. Sample preparation, neutron data collection and data analysis were as previously described [7]. The experimental temperature was 25 ° C. Each tachykinin was added singly at 10 mol% with respect to the lipid and the water baths contained pure water, at one of three isotopic compositions: 0%, 50% or 100% ^2H_2O to assist with phase assignment.

The data were placed on a 'relative absolute' scale [8] using the known neutron scattering densities of $^2H_{10}$-Leu and ^2H_2O as previously described [7]. This method requires knowledge of the molar percentage of water in the samples, which was determined as described in [9].

Results and Discussion

Figure 1 displays the neutron scattering density profiles across a DOPC:DOPG bilayer. The inter-bilayer water compartment is at the outer region of the graph. A pair of phospholipid molecules are also shown, to assist with interpretation of the profile.

Figure 2 shows difference profiles representing the distribution of deuterium label in bilayers containing SP (b), and in bilayers containing NKA (c). The profiles were calculated by the difference method. There are two distributions of label in each sample, one located close to the water-hydrocarbon interface and another located approximately 8Å from the bilayer centre. This is summarised in Table 1. These findings are consistant with the two-state model. Membrane insertion of SP and NKA allows water to penetrate deeper into the bilayer (data not shown).

Consistent with the monolayer area measurements of Seelig [3] these neutron data clearly demonstrate bilayer penetration of both tachykinins into anionic lipid bilayers. However, the depth of penetration of the two tachykinins studied is remarkably similar. Schwyzer [10] has proposed that receptor binding and specificity of the tachykinins is a property of the membrane-bound conformation of the peptides. Our evidence suggests that, in terms of membrane location, the membrane bound forms of these two peptides is rather similar, implying that receptor specificity is controlled by finer levels of structural detail.

Acknowledgements

The measurements were carried out at the Berlin Neutron Scattering Centre with the assistance of Thomas Hauß.

References

[1] Y. Yokota, C. Akazawa, H. Ohkubo and S. Nakanishi, EMBO J. 11 (1992) 3585.

[2] R. Schwyzer, EMBO J. 6 (1987) 2255.

[3] A. Seelig and P.M. MacDonald, Biochemistry 28 (1989) 2490.

[4] A. Seelig, T. Alt, S. Lotz and G. Holzemann, Biochemisty 35 (1996) 4365.

[5] D.A. Keire and T.G. Fletcher, Biophys. J. 70 (1996) 1716.

[6] J.K. Young, C. Anklin and R.P. Hicks, Biopolymers 34 (1994) 1449.

[7] K.C. Duff, A.J. Cudmore and J.P. Bradshaw, Biochem. Biophys. Acta. 1145 (1993) 149.

[8] M.C. Wiener, G.I. King and S.H. White, Biophys. J. 60 (1991) 568.

[9] J.P. Bradshaw, Biophys. J. 72 (1997) 2180.

[10] D.F. Sargent and R. Schwyzer, Proc. Natl. Acad. Sci. USA. 83 (1986) 5774.

Table 1: Location of deuterium label on ($^2H_{10}$-Leu 10)-substance P and ($^2H_{10}$-Leu 9)-neurokinin A. The centre , position and full width at half height (FWHH) of Gaussian distributions, fitted by least-squares refinement in reciprocal space, are given.

Population	**Parameter**	**Substance P**	**Distribution**	**Neurokinin A**	**Distribution**
1	Position (distance from centre of bilayer)	8.82 ± 0.22 Å	65.6 ± 5.5 %	7.48 ± 0.48 Å	69.5 ± 7.5 %
	Width (FWHH)	6.99 ± 0.33 Å		9.60 ± 0.97 Å	
2	Position (distance from centre of bilayer)	22.34 ± 0.83 Å	34.3 ± 5.5 %	22.17 ± 0.65 Å	30.5 ± 7.5 %
	Width (FWHH)	7.54 ± 0.66 Å		6.73 ± 1.13 Å	

Figure Legends

Figure 1: Neutron scattering density profiles of bilayers containing 50:50 (mol) DOPC and DOPG. 5 orders of diffraction were measured on the V1 instrument at the Berlin Neutron Scattering Center. The sample conditions were 25°C, 100% relative humidity and the hydrated solvent was 8.07% $^{2}H_{2}O$. At this concentration the solvent is effectively invisible to neutrons making the phospholipid the sole contributer to the profile shown. Also shown are two phospholipid molecules, to assist interpretation of the profile.

Figure 2: Difference neutron scattering density profiles calculated using 6 orders of diffraction for SP and 5 for NKA. The profiles show the distribution of $^{2}H_{10}$-leucine in 10% (mol) SP (b) or NKA (c) in bilayers containing DOPC:DOPG 50:50. The exact location, width and peak of each label was calculated by fitting Gaussians to the difference structure factor amplitudes in diffraction space, thereby avoiding the termination error observed in Fourier subtractions. The Fourier subtractions (solid line) fit well with the Gaussians (broken line), the poorer NKA fit is probably due to the lower resolution of diffraction data.

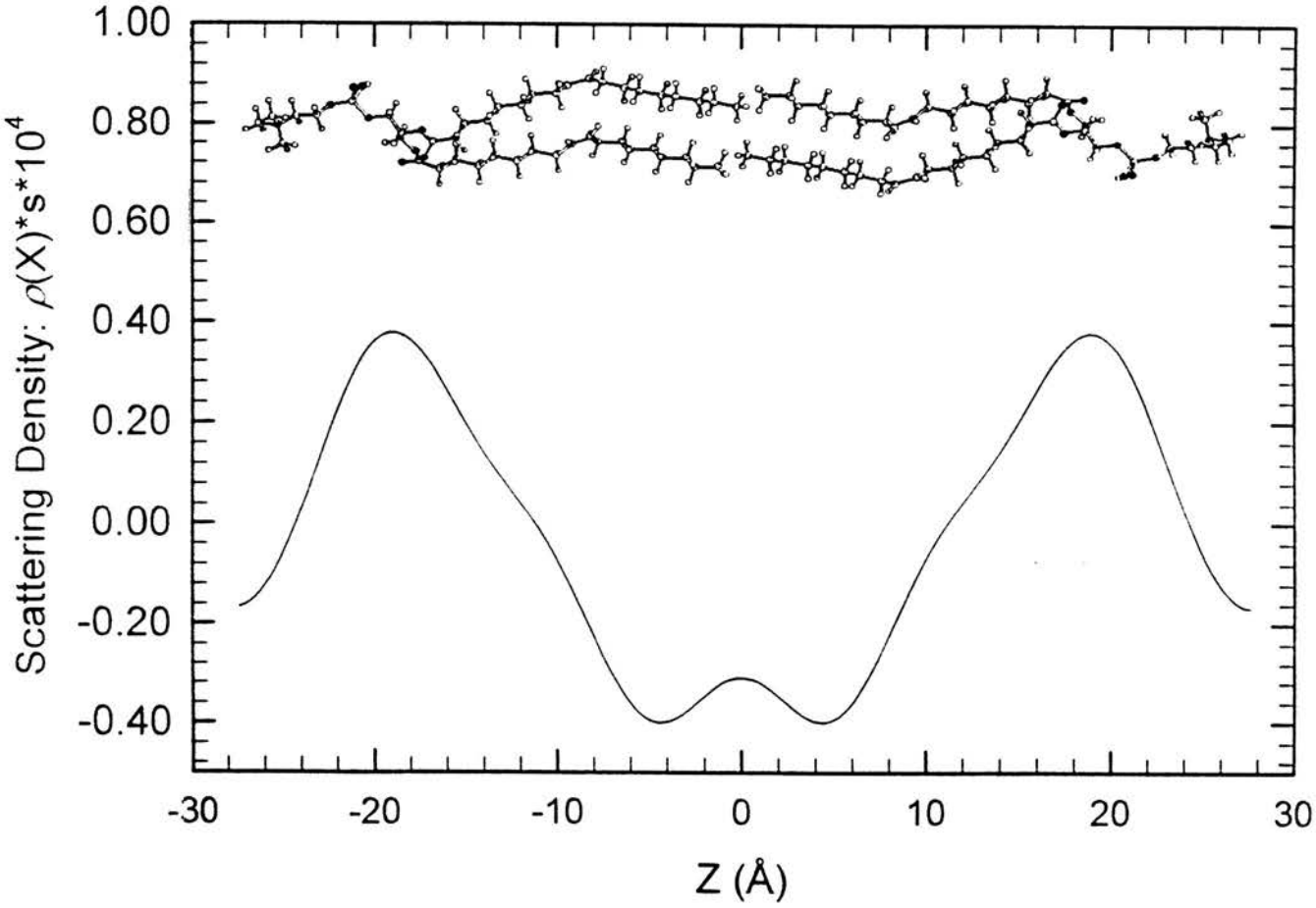
1.00
0.80
0.60
0.40
0.20
0.00
-0.20
-0.40
Scattering Density: ρ(X)*s*10^4
-30
-20
-10
0
10
20
30
Z (Å)

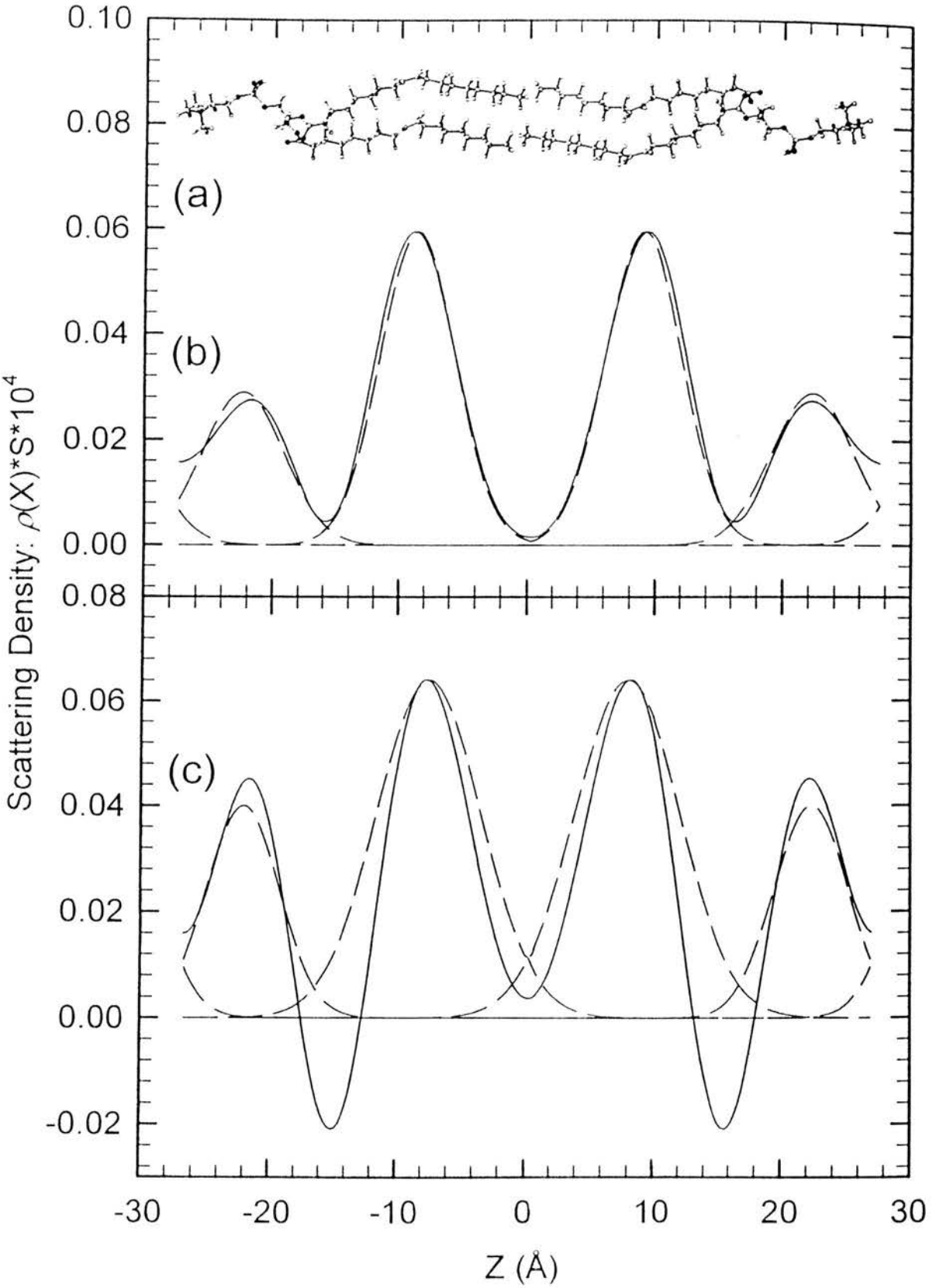
0.10
0.08
0.06
0.04
0.02
0.00
0.08
0.06
0.04
0.02
0.00
-0.02
(a)
(b)
(c)
Scattering Density: ρ(X)*S*10^4
-30
-20
-10
0
10
20
30
Z (Å)

(submitted to Biophysical Journal on 20th January 1998)

Interaction of Substance P with Phospholipid Bilayers, a Neutron Diffraction Study

Jeremy P. Bradshaw[1,2], Sarah M. A. Davies[1] & Thomas Hauβ[3]

1) Department of Preclinical Veterinary Sciences, R. (D.) S. V. S., University of Edinburgh, Summerhall, Edinburgh, EH9 1QH, Scotland, UK

2) Department of Biochemistry, University of Edinburgh School of Medicine, Hugh Robson Building, George Square, Edinburgh, EH8 9XD, Scotland, UK

3) Hahn-Meitner-Institut, Glienicker Straβe 100, D-14 109 Berlin, Germany

KEYWORDS: tachykinin, neurotransmitter, peptide, conformation, deuterium-labelling

RUNNING TITLE Bilayer interaction of substance P.

ABSTRACT: Neutron diffraction has been used to study the membrane-bound structure of substance P (SP), a member of the tachykinin family of neuropeptides. The depth of penetration of its C-terminus in zwitterionic and anionic phospholipid bilayers was probed by specific deuteration of leucine 10, the penultimate amino acid residue. The results show that the interaction of SP with bilayers, composed of either dioleoylphosphatidylcholine (DOPC), or a 50:50 mixture of DOPC and the anionic phospholipid dioleoyl-phosphatidylglycerol (DOPG), takes place at two locations. One requires insertion of the peptide into the hydrophobic region of the bilayer, the other is much more peripheral. The penetration of the peptide into the hydrophobic region of the bilayer is reflected in a marked difference in the water distribution profiles. SP is seen to insert into DOPC bilayers, but a larger proportion of the peptide is found at the surface when compared to the anionic bilayers. The positions of the two label populations show only minor differences between the two types of bilayer.

ACKNOWLEDGEMENTS

The experiments at BENSC in Berlin were supported by the European Commission through the TMR (Training and Mobility of Researchers) Programme, "Access to large-scale facilities" (Contract: ERB CHGE CT 920014). SMAD holds a Wellcome Trust Veterinary Research Scholarship.

INTRODUCTION

Substance P (SP) belongs to the tachykinin family, a group of six small amphipathic peptides that bind to G-protein coupled receptors. The receptors are found in a wide range of tissues including the central and peripheral nervous systems and the gastro-intestinal tract. The tachykinin family of peptides shares a common C-terminus, F*x*GLM-NH_2, where *x* is F or V in mammals.

The ligand-binding sites of tachykinin receptors appear to involve both the extracellular loops and the transmembrane domains (Y. Yokota *et al.,* 1992). An address-message model (Schwyzer, 1987) has been proposed where the flexible cationic N-terminal region of SP, or "address domain", is responsible for receptor selectivity, whilst the structurally extended and conserved hydrophobic C-terminal delivers the message. The proposed mechanism involves an interaction between tachykinin and phospholipids which results in insertion of the C-terminal amino acids into the lipid bilayer, followed by lateral diffusion of the peptide to reach the ligand-binding site of a membrane-bound receptor. Seelig *et al.* (1996) have presented an argument against the proposed membrane-mediated receptor mechanism, based on their observation that a SP analogue with a charged C-terminus, which they suggest would not insert into the hydrophobic core of membranes, still shows SP agonist activity. However, the central role of peptide-lipid interactions in the proposed scheme is supported by a number of observations that show that the conformation of SP is determined by the nature of its local chemical environment (e.g. Chuen-Shang *et al.*, 1982; Chassaing *et al.*, 1986; Woolley and Deber, 1987; Convert *et al.*, 1991).

There have been several biophysical studies comparing the structure of SP in zwitterionic and anionic lipid environments. Based on monolayer expansion measurements, Seelig and MacDonald (1989) concluded that SP does insert into monolayers containing negatively charged 1-palmitoyl-2-oleoyl-phosphatidylglycerol (POPG), but does not insert into zwitterionic monolayers composed of 1-palmitoyl-2-oleoyl-phosphatidylcholine (POPC).

Wu and Yang (1981) have proposed that polypeptides with a helix-forming potential can only assume a helical conformation in hydrophobic environments, such as the core of biological membranes, where the milieu enhances the intramolecular hydrogen bonding necessary for the stabilisation of these structures. This argument has been developed (Wu *et al.,* 1982) with the demonstration that such helical structures can only form by interaction with lipids when the peptide carries either no charge or charges which are opposite to those of the polar head group of the lipid. When this principle was applied to SP they showed that circular dichroism (CD) spectra revealed an unordered structure in water or phosphatidylcholine, but a partial helix in negatively-charged phosphatidylserine or sodium dodecylsulphate (SDS).

In contrast, Wooley and Deber (1987) have reported CD data from SP in the presence of SDS, lysophosphatidylcholine and lysophosphatidylglycerol micelles that show that the induced helical structure is independent of the lipid headgroup type. Keire and Fletcher (1996) also concluded from CD and ^{1}H-NMR studies that the conformation of SP is independent of lipid head group type. They calculated SP structures to 1-2 Å resolution from NMR measurements of SP in three different solution environments (SP/dodecylphosphocholine, SP/dodecylphosphocholine/NaCl

and SP/SDS/NaCl) and found them all to be similar. The structure they determined for SP is shown in Figure 1.

Against this background, the aim of the study described here was to test the hypothesis that SP interacts with biological phospholipids in such a way that the 'message' portion of the peptide is delivered at a specific depth, or 'address' within a bilayer. In order that the findings might also contribute to the debate on whether the membrane interaction of SP is phospholipid-dependent, two different bilayer compositions were used. In one system the bilayers were composed of the zwitterionic phospholipid dioleoylphosphatidylcholine (DOPC); the other system contained a 50:50 (mol) mixture of DOPC and the anionic phospholipid dioleoyl-phosphatidylglycerol (DOPG).

MATERIALS AND METHODS

Sample preparation:

DOPC and DOPG were purchased from Avanti Polar Lipids (Alabama, USA) and used without further purification. The 11 amino acid peptide (RPKPQQFFGLM-NH_2) was synthesised by Albachem Ltd. (26 Craigleith View, Edinburgh, EH4 3JZ, Scotland, UK). The synthesis was carried out on an Applied Biosystems 430A instrument, using Fmoc chemistry with the side chain protecting groups selected as tBu (Ser, Thr) and OtBu (Glu). The completed peptide was cleaved with a solution of TFA/H_2O (95:5) plus scavengers (ethanedithiol/thioanisole/triisopropanesilicane) and the solution was evaporated under vacuum. The peptide was purified by reverse phase HPLC and characterised by mass spectra (MALDI, PerSeptive Biosystem laserTec), amino acid analysis (LKB 4150 alpha amino acid analyser) and analytical HPLC. Two batches of peptide were produced, one undeuterated and one containing deuterated leucine (10 deuterons) at position 10. The purity of each peptide was above 95%, as determined by analytical HPLC, mass spectrometry and amino acid analysis. 20 mg samples of lipid, some of which contained 3% (mol) peptide, were deposited on quartz microscope slides (75 mm by 25 mm) using an artists' airbrush. The spraying solvent was methanol. The slides were placed in a vacuum dessicator for twelve hours to remove all traces of the solvent, before rehydration for 24 hours at 25°C in an atmosphere of 100% relative humidity.

Neutron data collection:

Neutron diffraction measurements were carried out on the V1 membrane diffractometer at the Berlin Neutron Scattering Centre, Germany. The sample environment was a standard aluminium can, in which temperature control is achieved by circulating water through an integral water jacket, and humidity control by changing the solution in two Teflon water baths at the base of the can. These water baths contained pure water, at one of three isotopic compositions: 0%, 50% or 100% ^2H_2O. Using the $^2H_2O/H_2O$ exchange technique, every sample was measured at all three ^2H_2O concentrations. At each change of solvent, the sample was first dried out under vacuum, then rehydrated in an atmosphere saturated with water at the new isotopic composition for at least 24 hours. All samples were run at 25°C. The

scanning protocol consisted of sequential θ scans around the predicted Bragg angle for each order. Each scan covered the angular range (θ_n - 0.5°) to (θ_n + 0.5°), where θ_n is the Bragg angle for the n^{th} order of lamellar diffraction.

Neutron data analysis:

The 2-dimensional array of detector counts for each frame of neutron diffraction data was corrected for variations in pixel response by division by a corresponding array of data recorded from water. The complete set of frames from each scan was then collapsed into a linear spectrum and combined to generate a pseudo θ - 2θ scan. Up to this stage of the analysis, all calculations were carried out using the V1 instrument software.

The background around each peak was fitted and subtracted using SigmaPlot v3.0 (Jandel Scientific Software GmbH), a commercial spreadsheet and graphs package. Gaussian curves were then fitted to the Bragg reflections and the angular position, width and area of each peak were recorded. Absorption and Lorentz corrections were applied and the intensities square-rooted to produce structure factor amplitudes. The relative scaling of the different data sets and the phases of each of their orders were determined by least-squares fitting to straight line functions, as shown in Figure 2.

The D-repeat of each sample was calculated by least-squares fitting of the observed values of 2θ to the Bragg equation: $n\lambda = 2D.\sin(\theta_{n+s})$ where s is the angular offset (misalignment) of the detector.

The data were placed on a 'relative absolute' scale (Wiener *et al.*, 1991; Wiener & White, 1991; Jacobs & White, 1989) using the known neutron scattering densities of ^2H and H to scale the [DOPC + ^2H_2O] – [DOPC + H_2O] differences and the [DOPC + ($^2H_{10}$-Leu)-SP] – [DOPC + SP] differences. This method requires knowledge of the molar percentage of water in the samples, which was determined as described below.

Gaussian distributions were fitted to the deuterated leucine sites by least-squares methods. The process was carried out in reciprocal space, whereby each Gaussian model is tested by comparing its calculated structure factors to the differences between observed structure factors for deuterated and undeuterated peptides.

Determination of water content:

The neutron diffraction sample preparation was repeated using ^{14}C-labelled DOPC and tritiated water so that scintillation counting could be used to determine the water:lipid molar ratio. Microscope coverslips (22 x 22 mm) were cut in half to provide a suitable substrate which would fit into a standard scintillation counter tube. In order to give the same sample thickness, approximately 5.0 mg of lipid was spread on each half-coverslip. After vacuum dehydration and rehydration for 24 hours, in small batches, at 25°C, the coverslips were quickly transferred to tubes of scintillant. ^{14}C and ^3H activity were measured using a Packard 1900CA Liquid Scintillation Counter. Control samples containing tritiated water (1.2µl) or ^{14}C-DOPC, equivalent

to 5.0 mg of the experimental phospholipid were used to calibrate the scintillation counter channel and cross-channel response. Clean coverslips served as controls for the experiment, to ensure that the amount of water condensing on the reverse side was negligible.

RESULTS

Table 1 shows the neutron structure factors of DOPC bilayers with 3% (mol) SP or ($^2H_{10}$-Leu)-SP and bilayers of DOPC with 50% (mol) DOPG and 3% (mol) SP or ($^2H_{10}$-Leu)-SP. Figure 2 shows an example of the structure factor data, scaled and phased so that straight lines pass though each order of the structure factors from each $^2H_2O/H_2O$ exchange series. Neutron scattering density profiles, calculated by Fourier transformation structure factors are shown in Figures 3 to 5.

The *D*-repeats of the various samples were 53.2 ± 0.4 Å, 55.4 ± 1.0 Å and 54.8 ± 1.0 Å for the pure DOPC, DOPC with 3% (mol) SP and 3% (mol) ($^2H_{10}$-Leu 10)-SP and 52.6 ± 0.9 Å, 55.0 ± 1.0 Å and 55.4 ± 1.0 Å for the corresponding DOPC/DOPG samples. These differences in *D*-repeat, though well within the generally accepted range (up to 1 Å), are a potential source of error when the structure factors, or profiles calculated from them, are subtracted from each other. This error is most marked in the 100% ^2H_2O structure factors, where even a small difference in the amount of water present can represent a considerable change in the scattering density of that region of the sample. The level of deuteration of the peptide in this study is relatively low when compared to the ^2H_2O-H_2O differences so, in order to reduce the effect of these errors, all profiles and subtractions were calculated at 8.07% ^2H_2O, at which isotopic composition water has a net scattering density of zero.

The mosaic spread of all samples used in the analysis was less than 0.5° (full width at half height). There was no significant variation between the different samples. The water content of the samples, measured by scintillation counting was DOPC, 26.08 waters per lipid; DOPC + DOPG, 30.49; DOPC + SP, 26.35; DOPC + DOPG + SP, 28.40. The maximum error in these measurements was estimated to be ± 1.0 waters per lipid.

Two different model-fitting approaches were taken in order to interpret the neutron data. The simpler of the two types of model was two Gaussian distributions (and their mirror images in the centrosymmetric unit cell). The Gaussian distributions were fitted to the observed differences between deuterated and undeuterated SP, the variables being height, width and position along the bilayer normal. The fitting process was carried out in reciprocal (diffraction) space by comparing the calculated structure factors of each model to the observed difference structure factors. The results of this approach are summarised in Table 2.

The second approach was used to determine the location of the whole peptide relative to the bilayer. It was essentially an elaboration of the Gaussian technique in which the neutron scattering profile of SP was calculated by combining the molecular co-ordinates of the peptide from a recent NMR structure determination (Keire & Fletcher 1996) with the coherent scattering length of its component atoms. A

Gaussian distribution, the integral of which was equal to the scattering length of that atom, represented each atom. In the case of the deuterium label distributions, the scattering length of all atoms other than the deuteriums was set to zero. The scattering length of the deuteriums was set at 1.041×10^{-12} cm, equivalent to the difference between the scattering lengths of ^{1}H and ^{2}H. The best fit to the label distribution in DOPC bilayers was found to be when the centre of the whole peptide was 12.0 Å and 24.4 Å from centre of bilayer. The axis of the peptide was parallel to the bilayer normal for the inserted peptide and perpendicular to the normal for the surface peptide. In this calculation a smearing factor of 5.3 Å was applied to each atom of the inserted peptide and 4.4 Å for the surface peptide. The corresponding figures for the DOPC/DOPG bilayers were 14.2 Å and 24.5 Å from centre of bilayer, with a 4.0 Å smearing factor for both populations of peptide. The results of both model-fitting approaches are summarised in Figures 4 and 5. It should be noted that the figures show a comparison of the calculated and observed scattering profiles in real space; the actual model fitting was carried out in reciprocal space. Also shown is the calculated scattering profile of SP, using the peptide locations and smearing factors determined by the deuterium peak model fitting.

DISCUSSION

DOPC with DOPG bilayers:

Figures 4 and 5 and Table 2 clearly show that the interaction of SP with the phospholipid membranes employed in this study takes place at two locations. One involves insertion of the peptide into the hydrophobic region of the bilayer, the other is much more peripheral. The penetration of the peptide into the hydrophobic region of the bilayer is reflected in a marked difference in the water distribution profiles (Figure 3) in the presence of peptide. These profiles which, more correctly, represent not just the water, but also deuterium-exchanged sites on the peptide, each show a large presence of deuterium right across the bilayer profile.

The difference profiles, showing the bilayer distribution of deuterated leucine on SP clearly demonstrate two populations of peptide. In order to interpret these findings in more detail, a model-fitting approach was employed, based on a recently published NMR structure of micelle-bound SP (Keire and Fletcher, 1996), in which the peptide:lipid ratio was similar to that used in the neutron work. The NMR structure was positioned on the bilayer normal, its exact location being determined by fitting the calculated neutron scattering from the deuterium label sites to the observed scattering in difference profiles. This approach is particularly appropriate for the deeper location, as it positions the peptide relative to the surrounding phospholipids in a very similar manner to that described in the NMR work. The conformation of SP in the peripheral location is much less certain, but for want of a better alternative, we have again used the Keire structure in our interpretation, but oriented with its long axis parallel to the bilayer. In support of this, it should be noted that the work by Keire and Fletcher only presents one structure for the peptide, whilst it is quite feasible that their samples also contained two populations of peptide.

An alternative explanation for the two deuterium peaks would be to suggest that the peptide aggregates in an anti-parallel manner. Three arguments refute this

suggestion. Firstly, the relative sizes of the two populations of label are not stoichiometric and differ between the two types of bilayer studied. Secondly, in order to insert in the alternative (antiparallel) direction, the peptide would need to introduce its N-terminus, together with its three positive charges, into the hydrophobic core of the bilayer. Finally, the Fourier-transform infrared study of Choo and co-workers (1994) reported that SP aggregates in the presence of charged lipids, but not in an anti-parallel manner.

Once the peptide structures had been located and oriented using the deuterium label information, it was a straightforward matter to calculate the contribution of scattering from all peptide atoms to the neutron scattering profiles. Figure 5(b) illustrates the comparison of such a profile to the corresponding profile derived from observed data, using the difference method. Reference to the figures shows that the calculated scattering profile is relatively low and featureless. Thus any of a number of surface peptide conformations could have been used in the calculation, without seriously affecting the results. A comparison of the profiles shows that the majority of the scattering difference comes from neither the peptide, nor the water, since the profile corresponds to a bilayer with 8.07% ^2H_2O, at which isotopic composition water has a net coherent neutron scattering density of zero. The differences between the profiles can only, therefore, represent rearrangements of the phospholipid. Wu and coworkers (1995) have reported membrane thinning as a direct result of peptide incorporation into phospholipid bilayers. It is quite possible that the insertion of SP may have a similar effect on phospholipids.

DOPC bilayers

In order to contribute to the discussion on whether SP inserts into zwitterionic membranes, neutron measurements were also performed on DOPC bilayers, some of which contained SP at 3.0% (mol). The results, summarised in Table 2, show that SP does indeed insert into DOPC bilayers, but it is interesting that more of the peptide is found at the surface when compared to the anionic bilayers.

In comparison to the DOPC results, the positions of the two label populations show only minor differences. Indeed, it is noticeable in Figure 3 that the water distribution between adjacent bilayers is wider in those bilayers containing only DOPC (a), indicating that the anionic bilayers are wider than the zwitterionic ones. For practical reasons, the location of the label sites in Table 2 is expressed in terms of distance from the centre of the bilayer. Were it possible to present the results as distance from the bilayer surface, it is likely that the difference between the two lipids would be even smaller.

Keire & Fletcher (1996) have reported that the conformation of SP, as determined by ^{1}H-NMR, does not differ significantly between anionic and zwitterionic micelles. In both systems they observed a similar conformation for association of the QQFFGLM residues with lipid micelles. The only variations in structure were observed in the N-terminal residues, RPKP. This was interpreted as indicating that the structure of SP at a micelle surface is determined largely by hydrophobic forces, whilst the electrostatic interactions determine the amount of SP

that is bound. This interpretation is in close agreement with the neutron results reported here.

However, the neutron data do not appear to agree with the monolayer expansion measurements of Seelig and MacDonald (1988), who concluded that SP does not insert into zwitterionic monolayers. It should be noted, however, that both the lipids used (DOPC instead of POPC) and their arrangement (bilayers instead of monolayers) differs between the two studies. It is arguable that monolayers do not present an accurate representation of bilayers, especially when considering the insertion of molecules into the bilayer centre, or beyond. Conversely, it is possible that the nature of the neutron samples, in which adjacent bilayers are separated by a narrow (15 - 20 Å) water channel, artificially increases the concentration of peptide close to the surface of the bilayers. This contrasts with the monolayer expansion system, in which the peptide was introduced into the aqueous layer. The binding of SP to the monolayer surface was reported to be dominated by electrostatic interaction. Therefore an anionic surface would be predicted to attract the positively charged peptide much more readily than would a zwitterionic surface.

The message-address model of Schwyzer (1987) requires that each tachykinin interacts in a tightly controlled manner with phospholipid membranes. In order for the message to be delivered at the correct address, the C-terminal portion of the peptide must be located at a specific depth within the bilayer, irrespective of its phospholipid composition. Whilst the neutron measurements reported here can neither support or refute such a model, they clearly demonstrate that SP is able to interact with both zwitterionic and anionic membranes in such a way that the C-terminus of the peptide is positioned at a tightly controlled depth below the membrane surface. Moreover, in agreement with other studies, the proportion of peptide that penetrates the membrane is shown to be dependent upon the phospholipid composition of the bilayer.

REFERENCES

Chassaing, G., O. Convert and S. Lavielle. 1986. Preferential conformation of substance P in solution. *Eur. J. Biochem.* 154:77-85

Chuen-Shang C. W., A. Hachimori and J.T. Yang. 1982. Lipid-induced ordered conformation of some peptide hormones and bioactive oligopeptides: predominance of helix over β form. *Biochemistry* 21:4556-4562

Choo, L.-P., M. Jackson and H. H. Mantsch. 1994. Conformation and self-assocoation of the peptide hormone substance P: Fourier-transform infrared spectroscopic study. *Biochemical Journal.* 301:667-670.

Convert, O., H. Duplaa, S. Lavielle and G. Chassaing. 1991. Influence of the replacement of amino-acid by its d-enantiomer in the sequence of substance-P. 2. Conformational-analysis by NMR and energy calculations. *Neuropeptides* 19:259-270

Jacobs, R. E. and S. H. White. 1989. The nature of the hydrophobic binding of small peptides at the bilayer interface: implications for the insertion of transbilayer helices. *Biochemistry.* 28:3421-3437.

Keire, D. A. and T. G. Fletcher. 1996. The conformation of substance P in lipid environments. *Biophysical Journal.* 70:1716-1727

Schwyzer, R. 1987. Membrane-assisted molecular mechanism of neurokinin receptor subtype selection. *EMBO J.* 6:2255-2259.

Seelig, A. and P. M. MacDonald. 1988. Binding of a neuropeptide, substance P, to neutral and negatively charged lipids. *Biochemistry.* 28:2490-2496

Seelig, A., Alt, T., Lotz, S. & Holzemann, G. 1996. Binding of substance P agonists to lipid membranes and to the neurokinin-1 receptor. *Biochemistry.* 35:4365-4374

Wiener M. C. and S. H. White. 1991. Fluid bilayer structure determination by the combined use of x-ray and neutron diffraction. *Biophysical Journal.* 59:162-185.

Wiener, M. C., G. I. King and S.H. White. 1991. Structure of fluid DOPC bilayer determined by joint refinement of x-ray and neutron data. *Biophysical Journal.* 62:2762-2772.

Woolley, G. A. and C. M. Deber. 1987. Peptides in membranes - lipid-induced secondary structure of substance-P. *Biopolymers* 26:S109-S121

Wu, C. C. and J. T. Yang, 1981. Sequence-dependent conformations of short polypeptides in a hydrophobic environment. Molecular and Cellular *Biochemistry* 40: 109-122

Wu, C. C., A. Hachimori, and J. T. Yang. 1982. Lipid-induced ordered conformation of some peptide hormones and bioactive oligopeptides: predominance of helix over β form. *Biochemistry.* 21: 4556-4562

Wu, Y. L, K. He, S. J. Ludtke and H. W. Huang. 1995. X-ray-diffraction study of lipid bilayer-membranes interacting with amphiphilic helical peptides - diphytanoyl phosphatidylcholine with alamethicin at low concentrations. *Biophys. J.* 68:2361-2369

Yokota, Y., C. Akazawa, H. Ohkubo and S. Nakanishi. 1992. Delineation of structural domains involved in the subtype specificity of tachykinin receptors through chimeric formation of substance-P substance-K receptors. *EMBO J.* 11:3585-3591.

Figure 1: The structure of substance P as determined by Keire and Fletcher (1996), as used in the analysis of neutron diffraction data as described here. Both space-filling (top) and wire-model (bottom) representations are shown. Leucine 10, the residue that was deuterated in some of the peptide used in this study is indicated in black.

Figure 2: An example of the structure factors and their phase assignment using $H_2O/^2H_2O$ exchange, in this instance DOPC with 50% (mol) DOPG and 3.0% (mol) substance P. Each order has been fitted (least squares) to a straight line with negative slope for odd numbered orders and positive slope for even numbered orders. This relationship breaks down at higher order numbers, indicating that, at higher resolution, the shape of the water distribution can no longer be described as a single Gaussian distribution. For clarity, the eight orders are split between two plots; a) shows the first four orders; b) shows orders 5 to 8 on an enlarged vertical scale. The phasing of orders 7 and 8 is uncertain. All subsequent calculations only used the first six orders.

Figure 3: The distribution of deuterium, introduced in the form of 50% ^2H_2O, within and between bilayers of: a) DOPC (solid line, left hand scale), DOPC with 3.0% (mol) substance P (dashed line, right hand scale), and DOPC with 3.0% (mol) ($^2H_{10}$-Leu 10)-substance P (dotted line, right hand scale); b) DOPC with 50% (mol) DOPG (solid line, left hand scale), DOPC with 50% (mol) DOPG and 3.0% (mol) substance P (dashed line, right hand scale), and DOPC with 50% (mol) DOPG and 3.0% (mol) ($^2H_{10}$-Leu 10)-substance P (dotted line, right hand scale).

Figure 4: Model-fitting (1). Difference neutron scattering density profiles, calculated from six orders of diffraction, showing the distribution of deuterium in 3% (mol) ($^2H_{10}$-Leu 10)-substance P in (a) DOPC bilayers and (b) DOPC/DOPG bilayers (50:50). The subtraction was carried out using structure factors representing 8.07% 2H2O, to reduce the effect of slight differences in hydration level between the samples. Each panel also shows (dashed line) the sum of two pairs of Gaussian distributions, fitted to the difference data in reciprocal space (6 orders of diffraction).

Figure 5: Model-fitting (2). a) The distribution of deuterium in 3% (mol) ($^2H_{10}$-Leu 10)-substance P in DOPC/DOPG bilayers (50:50), shown as difference neutron scattering density profiles calculated from six orders of diffraction. Also shown are the calculated neutron scattering density distributions for deuterium in 3% (mol) ($^2H_{10}$-Leu 10)-substance P, using the NMR structure for SP of Keire and Fletcher (1996). In Model 1 the peptide is arranged perpendicular to the bilayer and in Model 2 parallel to the bilayer, as indicated. b) Predicted neutron scattering profile of 3% (mol) substance P (solid line) calculated using the whole Keire and Fletcher structure, with the peptide arranged in two populations arranged as in (a). The dotted line is the observed neutron scattering density profile at 8.07% ^2H_2O, calculated by subtracting the DOPC/DOPG profile from the (SP + DOPC/DOPG) profile. The two profiles shown are very different, indicating that the dotted line includes scattering contributions from sources other than the peptide alone. Since the dotted profile represents a bilayer at 8.07% ^2H_2O, at which isotopic composition water is effectively invisible to neutrons, the difference between the predicted and observed profiles can only be caused by rearrangements of the phospholipids.

DOPC, 3% (mol) Substance P, 0% ^2H_2O								
(1)	-0.68 ±0.05	-3.64 ±0.11	1.46 ±0.11	2.09 ±0.11	-0.86 ±0.05	-0.65 ±0.05	±0.69 ±0.05	±0.64 ±0.05
DOPC, 3% (mol) Substance P, 100% ^2H_2O								
(2)	-13.27 ±0.25	3.02 ±0.10	0.75 ±0.05	0.20 ±0.05	1.03 ±0.08	0.58 ±0.05	±0.57 ±0.05	±0.78 ±0.05
DOPC, 3% (mol) ($^2H_{10}$-Leu 10)-Substance P, 0% ^2H_2O								
(3)	-0.52 ±0.11	-2.85 ±0.11	0.98 ±0.11	0.80 ±0.11	-0.72 ±0.11	-0.85 ±0.11	±0.93 ±0.11	±0.82 ±0.11
DOPC, 3% (mol) ($^2H_{10}$-Leu 10)-Substance P, 100% ^2H_2O								
(4)	-13.14 ±0.25	3.55 ±0.10	0.75 ±0.05	-0.30 ±0.05	1.22 ±0.08	0.38 ±0.05	±0.55 ±0.05	±0.75 ±0.05
DOPC+DOPG (50:50), 3% (mol) Substance P, 0% ^2H_2O								
(5)	-0.90 ±0.05	-3.45 ±0.10	1.28 ±0.08	0.38 ±0.05	-0.71 ±0.05	0.39 ±0.05	±0.06 ±0.05	±0.69 ±0.05
DOPC+DOPG (50:50), 3% (mol) Substance P, 100% ^2H_2O								
(6)	-12.51 ±0.25	2.64 ±0.10	1.15 ±0.08	0.45 ±0.05	-0.47 ±0.05	-0.38 ±0.05	±0.32 ±0.05	±0.05 ±0.05
DOPC+DOPG (50:50), 3% (mol) ($^2H_{10}$-Leu 10)-Substance P, 0% ^2H_2O								
(7)	-0.43 ±0.05	-4.19 ±0.15	-0.68 ±0.05	-0.93 ±0.05	0.00	0.68 ±0.05	±0.90 ±0.05	±0.79 ±0.05
DOPC+DOPG (50:50), 3% (mol) ($^2H_{10}$-Leu 10)-Substance P, 100% ^2H_2O								
(8)	-12.05 ±0.25	3.03 ±0.10	-0.81 ±0.05	-0.56 ±0.05	0.00	-0.14 ±0.05	±0.01 ±0.05	±0.16 ±0.05
DOPC, 0% ^2H_2O								
(9)	-8.14 ±0.20	-19.37 ±0.26	10.20 ±0.20	-3.63 ±0.15	-3.33 ±0.15	0.00	0.00	±0.75 ±0.05
DOPC, 100% ^2H_2O								
(10)	-161.48 ±1.00	28.29 ±0.30	5.58 ±0.15	8.51 ±0.20	-8.53 ±0.20	0.00	±5.30 ±0.15	±1.69 ±0.08
DOPC+DOPG (50:50), 0% ^2H_2O								
(11)	-14.67 ±0.25	-30.93 ±0.30	17.80 ±0.26	-2.45 ±0.10	2.95 ±0.10	-6.19 ±0.18	±4.57 ±0.15	±4.15 ±0.15
DOPC+DOPG (50:50), 100% ^2H_2O								
(12)	-166.76 ±1.00	41.02 ±0.35	-12.91 ±0.25	5.99 ±0.15	4.06 ±0.15	-5.30 ±0.15	±4.31 ±0.15	±0.83 ±0.06

Table 1: Experimentally determined, corrected and scaled neutron structure factors of stacked bilayers of DOPC, DOPC with 3% (mol) SP or ($^2H_{10}$-Leu)-SP, DOPC with 50% (mol) DOPG and DOPC with 50% (mol) DOPG and 3% (mol) SP or ($^2H_{10}$-Leu)-SP. The measurements were made at 25°C and 100% relative humidity. The phasing of orders 7 and 8 is uncertain. All subsequent calculations used only the first six

orders. The errors are related to the deviations of the observed points to straight lines fitted through structure factors at three ^2H_2O concentrations, as in Figure 2.

Site	Parameter	DOPC	Distribution	DOPC+DOPG	Distribution
1	Position*	6.61 ±0.22 Å	57.5 ±5.5 %	8.82 ±0.22 Å	65.6 ±5.5 %
	Width#	9.18 ±0.88 Å		6.99 ±0.33 Å	
2	Position*	22.04 ±0.22 Å	42.5 ±5.5 %	22.34 ±0.83 Å	34.3 ±5.5 %
	Width#	8.27 ±0.83 Å		7.54 ±0.66 Å	

Table 2: Gaussian models of deuterium label distribution of 3.0% (mol) ($^2H_{10}$-Leu 10)-Substance P in bilayers of DOPC or DOPC+DOPG (50:50). The position, width and size of Gaussian distributions were fitted, in reciprocal space, to difference neutron structure factors. Six orders of diffraction were used in the fitting procedure. * The position of each label site is expressed as distance from the centre of the bilayer. # The width is the full width at half height.

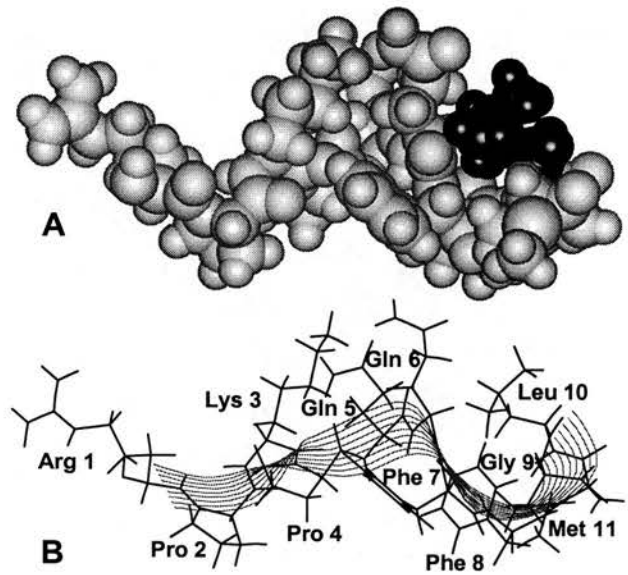
A
B
Arg 1
Lys 3
Gln 5
Gln 6
Leu 10
Gly 9
Phe 7
Met 11
Pro 2
Pro 4
Phe 8

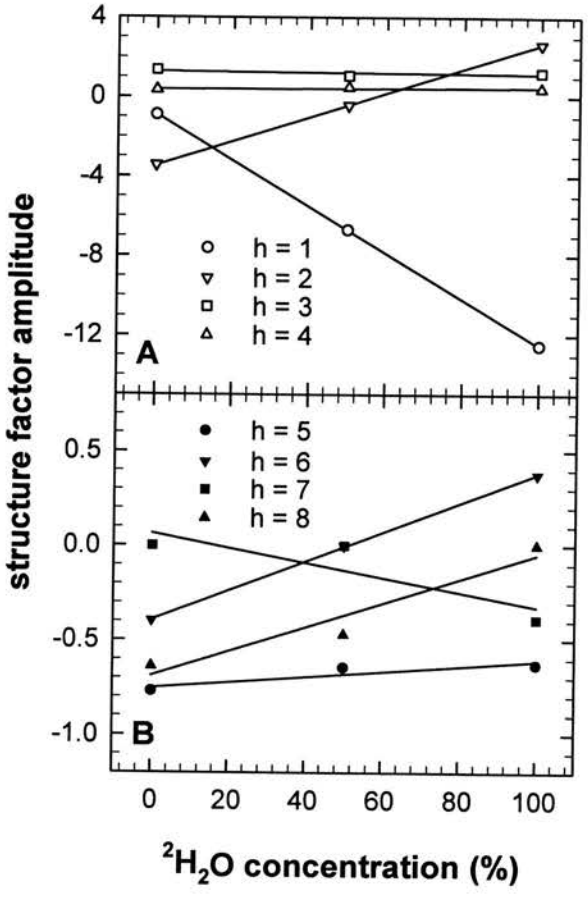
structure factor amplitude
4
0
-4
-8
-12
A
h = 1
h = 2
h = 3
h = 4
0.5
0.0
-0.5
-1.0
B
h = 5
h = 6
h = 7
h = 8
0
20
40
60
80
100
^2H_2O concentration (%)

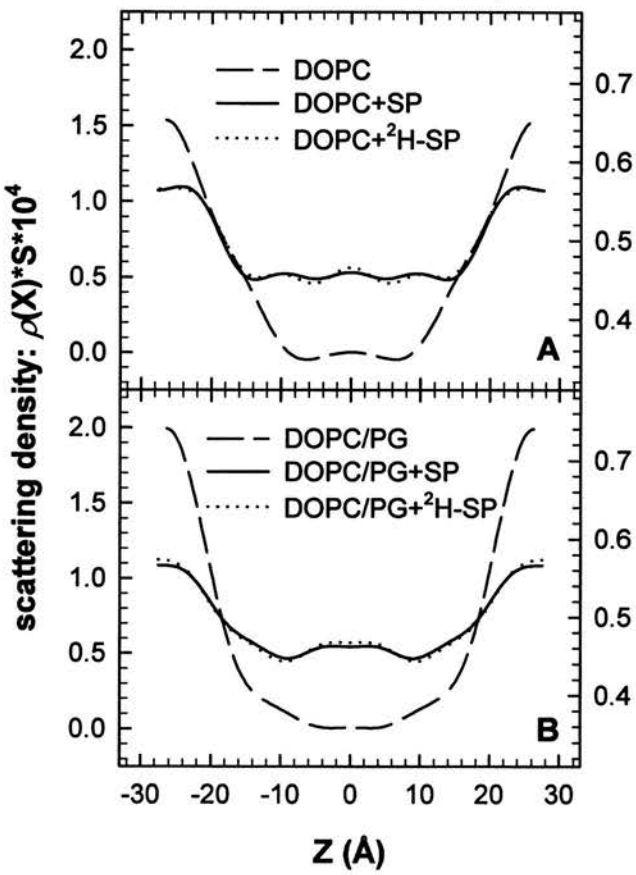
DOPC
DOPC+SP
DOPC+^{2}H-SP
A
DOPC/PG
DOPC/PG+SP
DOPC/PG+^{2}H-SP
B
scattering density: $\rho(X)*S*10^4$
Z (Å)
2.0
1.5
1.0
0.5
0.0
0.7
0.6
0.5
0.4
-30
-20
-10
0
10
20
30

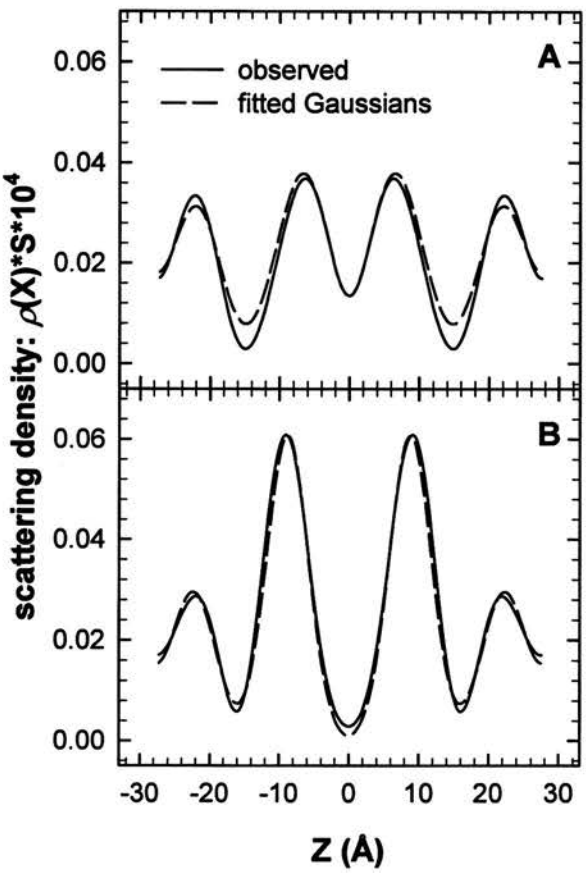
observed
fitted Gaussians
A
B
0.06
0.04
0.02
0.00
scattering density: ρ(X)*S*10⁴
-30
-20
-10
0
10
20
30
Z (Å)

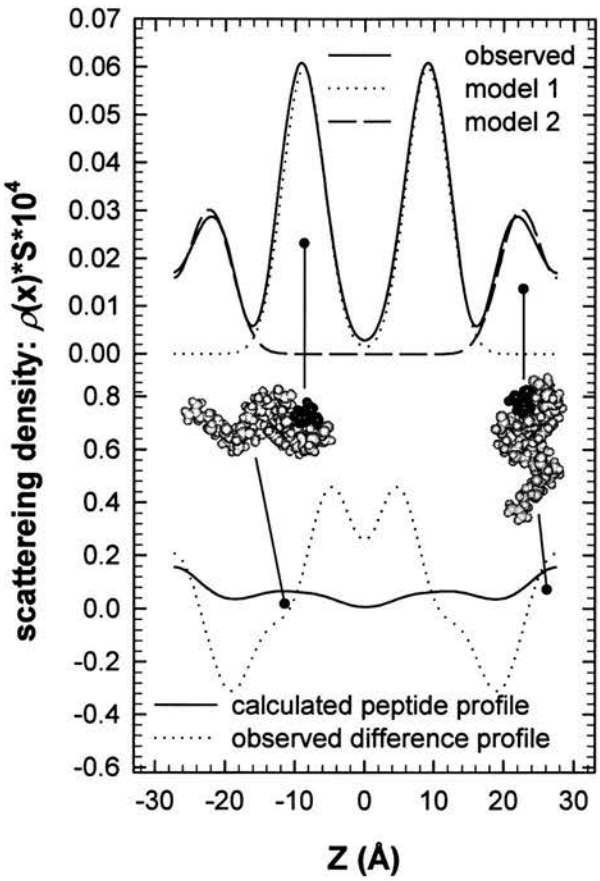
observed
model 1
model 2
calculated peptide profile
observed difference profile
scattereing density: ρ(x)*S*10^4
Z (Å)
0.07
0.06
0.05
0.04
0.03
0.02
0.01
0.00
0.8
0.6
0.4
0.2
0.0
-0.2
-0.4
-0.6
-30
-20
-10
0
10
20
30

PHYSB 2827

Bala PADMINI

TYPESET FROM AUTHOR'S DISK

ELSEVIER

Physica B 000 (1997) 000–000

PHYSICA B

Improved accuracy and phasing of lamellar neutron diffraction data by real-time swelling series method

Jeremy P. Bradshaw[a,b,*], Malcolm J.M. Darkes[a], Sarah M.A. Davies[b]

[a] *Department of Biochemistry, University of Edinburgh School of Medicine, George Square, Edinburgh EH8 9XD, Scotland, UK*
[b] *Department of Preclinical Veterinary Sciences, Royal (Dick) School of Veterinary Sciences, University of Edinburgh, Summerhall, Edinburgh EH9 1QH, Scotland, UK*

Abstract

The analytic continuation method has been widely used to phase Bragg reflections from lamellar samples of phospholipids. Here we describe its application to neutron diffraction data, collected from liquid-crystalline (L_α phase) samples of 1,2-dioleoyl-sn-glycero-phosphocholine (DOPC) under a state of shifting lamellar spacing. To provide a comparison with the more normal neutron approach of isotopic substitution using ^2H_2O, data were collected from similar samples, using the same experimental and optical conditions. We compare the two methods in terms of accuracy of structure factor determination, unambiguity of phase assignment and ease of use.

Keywords: Neutron diffraction; Phospholipid; Phase assignment

1. Introduction

When performing neutron diffraction experiments on lamellar phospholipid samples, it is necessary to ensure that each sample has reached equilibrium with the humid atmosphere of the sample can, before starting the data collection. It is normal practice, upon loading a new multi-bilayer lipid sample, to monitor the position of a strong lamellar diffraction peak. As the bilayers take up water from the atmosphere the lamellar distance (D-repeat) increases, a process which is reflected in a decreasing angle of diffraction. This is often preceded by a period of reducing lamellar spacing as the sample continues to dehydrate from its exposure to the, usually, dryer outside atmosphere. The whole process may take several hours, depending upon the size of the can, the surface area of the water baths and the previous state of the sample. Obviously, it helps if the disturbance to the sample's hydration state is kept to a minimum by transferring it as quickly as possible from its sealed container to the experimental vessel.

The movements of diffraction peaks during sample equilibration are accompanied by a rise or fall

* Corresponding author: Present address: Department of Preclinical Veterinary Sciences, Royal (Dick) School of Veterinary Sciences, University of Edinburgh, Summerhall, Edinburgh EH9 1QH, Scotland, UK. Fax: + 44 131 650 6576; e-mail: j.bradshaw@ed.ac.uk.

0921-4526/98/$19.00
PII S0921-4526(97)00807-7

in diffracted intensity as the Bragg angles sample different spatial frequencies on the molecular (bilayer) transform. This property has been used to determine the structure factor phases in X-ray experiments, when a pseudo-continuous transform is mapped out using a number of samples, each prepared to a different lamellar spacing by controlling the humidity of the atmosphere or the osmotic pressure of the solution [1]. Here we show that the oscillations of a Bragg peak in a sample seeking equilibrium may be used both as an aid to phasing the peak and to improve the accuracy of its measurement. The method is presented in a side-to-side comparison with the more widely used $^2H_2O/H_2O$ exchange approach to phasing, in which the isotopic substitution of hydrogen by deuterium is used in an adaptation of the crystallographic method of isomorphous derivatives.

2. Materials and methods

2.1. Sample preparation

1,2-dioleoyl-sn-glycero-phosphocholine (DOPC) was purchased from Avanti Polar Lipids (Birmingham, AL) and used without further purification. 20 mg of the sample was deposited on quartz microscope slides (75 mm × 25 mm) using an artist's airbrush. The spraying solvent was chloroform. The slides were placed in a vacuum dessicator for 12 h to remove all traces of the solvent.

2.2. Neutron data collection

Neutron diffraction measurements were carried out on the D16 membrane diffractometer at the Institut Laue et Langevin, Grenoble, France. The sample environment was a standard aluminium can, in which temperature control is achieved by circulating water through an integral water jacket, and humidity control by changing the solution in two Teflon water baths at the base of the can. All samples were run at 25°C. The water baths contained pure water, at one of three isotopic compositions: 0%, 50% or 100% ^2H_2O.

In the ^2H_2O H_2O exchange experiments, each sample was run at all three ^2H_2O concentrations. Each sample was rehydrated at 25°C in an atmosphere of 100% relative humidity for at least 24 h before being transferred to the D16 sample can. At each subsequent change of solvent, the sample was first dried out, then rehydrated in an atmosphere saturated with water at the new isotopic composition for at least 24 h. The scanning protocol consisted of sequential θ (sample angle) scans around the predicted Bragg angle for each order. Each scan covered the angle $-0.6°$ to $+0.6°$.

The mosaic spread of the second order of diffraction was determined for each sample, using standard procedures.

For the swelling series measurements, the dry DOPC sample, on its quartz slide, was quickly transferred straight from its vacuum desiccator into the D16 can together with two water troughs, containing water. A series of continuous $\theta - 2\theta$ scans was immediately initiated. Each scan (from $\theta = 1.5°$ to $15.0°$) took approximately 3 h to complete.

2.3. Data analysis (1) $^2H_2O/H_2O$ exchange

The two-dimensional array of detector counts for each frame of data was corrected for variations in pixel response by division by a corresponding array of data recorded from water (H_2O). The complete set of frames from each scan were then collapsed into a linear spectrum and combined to generate a pseudo-($\theta - 2\theta$) scan. Up to this stage, all of the analysis was carried out by the D16 instrument software.

The background around each peak was fitted and subtracted using SigmaPlot (Jandel Scientific Software GmbH), a commercial spreadsheet and graphing package. Gaussian curves were then fitted to the Bragg reflections and the angular position, width and area of each peak recorded. Absorption and Lorentz corrections were applied and the intensities square-rooted to produce structure factor amplitudes. The relative scaling of the different data sets and the phases of each of their orders were determined by least-squares fitting to straight line functions, as shown in

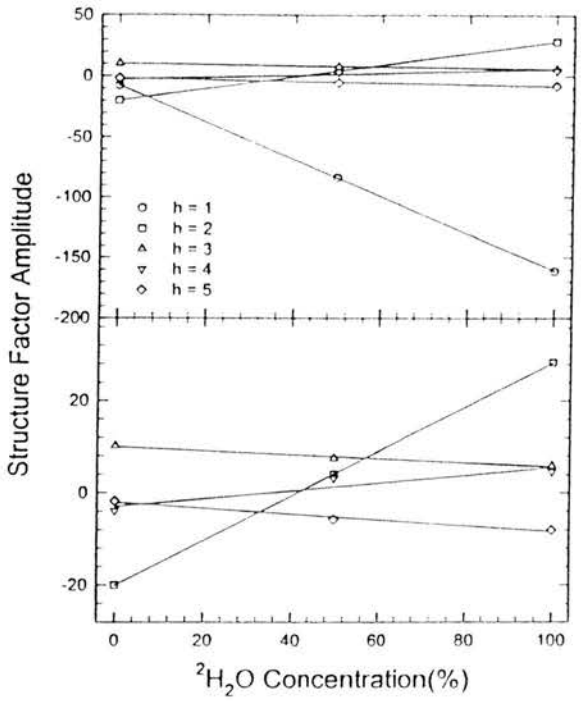

Fig. 1. Plot of structure factor amplitude versus ^2H_2O concentration for stacked bilayers of DOPC in a saturated atmosphere at 25°C. The measurements were made on the D16 instrument at the Institut Laue et Langevin. Least-squares fitting was used to scale the three data sets to each other and to phase the individual orders of each set. The bottom panel shows orders 2–5 on an expanded scale.

Fig. 1. The whole procedure has been described previously [2].

The *D*-repeat (lamellar repeat distance) was calculated by least-squares fitting of the observed angles of diffraction (2θ) to the Bragg equation: $h\lambda = 2D\sin(\theta_h + x)$ where λ is the wavelength of neutrons, h is the order of diffraction and x is the angular offset (misalignment) of the detector.

The data were placed on a 'relative absolute' [3–5] scale using the known neutron scattering densities of ^2H_2O and H_2O to scale the (DOPC + ^2H_2O) − (DOPC + H_2O) difference. This method requires knowledge of the molar percentage of water in the samples, which was determined as described below.

2.4 *Determination of water content*

The neutron diffraction sample preparation was repeated using ^{14}C-labelled DOPC and tritiated water so that scintillation counting could be used to determine the water : lipid molar ratio. Microscope coverslips (22 × 22 mm) were cut into half to provide a suitable substrate which would fit into a standard scintillation counter tube. In order to give the same sample thickness, approximately 5.0 mg of lipid was spread on each half-coverslip. After vacuum dehydration and rehydration for 24 h, in small batches, at 25°C, the coverslips were quickly transferred to tubes of scintillant. ^{14}C and ^3H activity were measured using a Packard 1900CA Liquid Scintillation Analyzer. Calibration samples containing tritiated water (1.0 μl) or ^{14}C-phospholipid equivalent to 5.0 mg of DOPC were used to calibrate the scintillation counter channel and cross-channel response. Clean coverslips served as controls for the experiment, to ensure that the amount of water condensing on the reverse side was negligible.

2.5. *Data analysis (2) swelling series*

Background subtraction and Gaussian-fitting were carried out as for the $^2H_2O/H_2O$ exchange data. After correction with absorption and Lorentz factors the structure factors were calculated from the intensities and plotted against their spatial frequencies, as shown in Fig. 2. Interpolation between the points produced sets of structure factors, which were then used to calculate [1] the continuous transforms, also shown in the figure.

3. Results and discussion

Figs. 1 and 2 show the structure factors determined by each method. Neutron scattering density profiles, calculated by Fourier transformation of the $^2H_2O/H_2O$ exchange data are shown in Fig. 3. Fig. 4 is a swelling series of bilayer profiles calculated from sets of structure factors determined by interpolation between the observed points, as shown in Fig. 2.

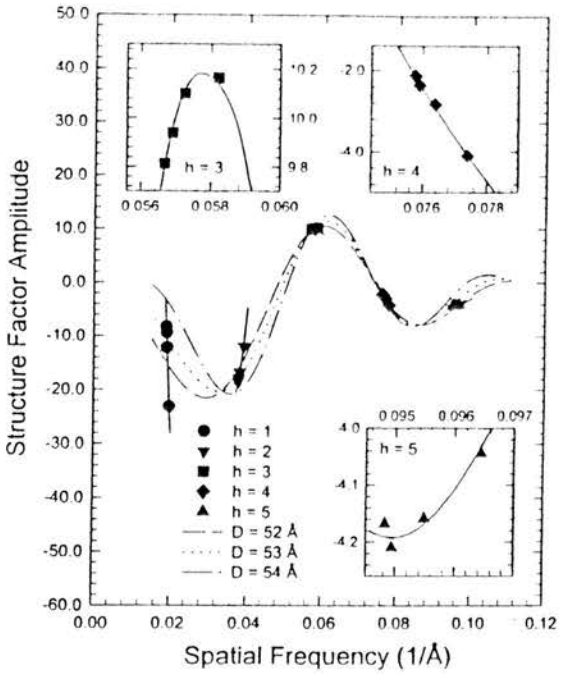

Fig. 2. Plot of structure factor amplitude versus spatial frequency of data points collected by real-time swelling series from stacked bilayers of DOPC at 25 C. The dry DOPC sample was placed in a D16 sample can along with water troughs containing 100% H_2O. Four consecutive $\theta - 2\theta$ scans were run over a total period of 12 h. The three inset graphs are enlargements of the regions corresponding to the third, fourth and fifth orders of diffraction. Also shown are continuous transforms calculated using the method of King and Worthington [1].

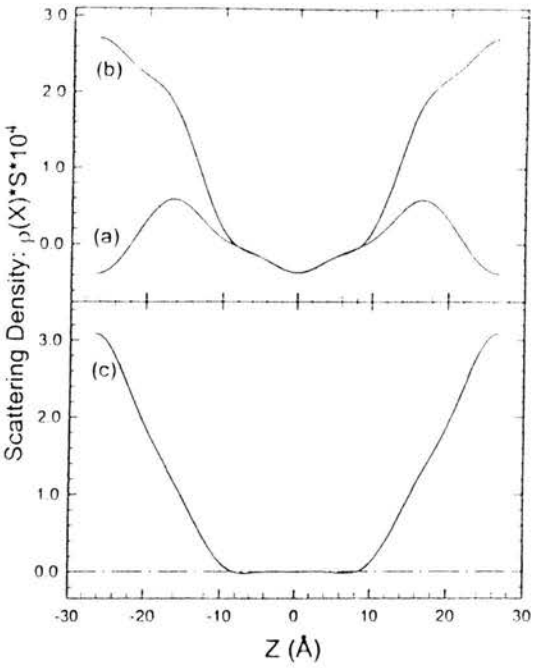

Fig. 3. Neutron scattering density profiles of pure DOPC at 25 C and 100% relative humidity (a) 100% H_2O, (b) 50% H_2O with 50% ^2HO. Profile (c) is a difference profile, showing the distribution of ^2H_2O, calculated by subtracting profile (a) from (b).

The D-repeats of the $^2H_2O/H_2O$ exchange samples were 53.5 ± 0.5, 53.1 ± 0.5 and 53.1 ± 0.5 Å for the 0%, 50% and 100% ^2H_2O samples, respectively. The D-repeat of the swelling series sample increased from 50.8 to 53.2 Å over the 12 h of data collection. The mosaic spreads (half-width at $1/e$ height) for the $^2H_2O/H_2O$ exchange samples were 0.38°. The mosaic spreads of the swelling series sample was 0.34°, 0.38°, 0.38° and 0.36° for the four scans. The water content of pure DOPC bilayers at 25°C was determined to be 26.8 ± 0.5 waters per lipid. The tritium signal from the control coverslips was less than 1/200th of that from the sample coverslips.

There was no noticeable increase or decrease in the sample disorder throughout the swelling series measurements, as determined by mosaic spread. The low mosaic spread is typical for measurements of (static) unsaturated phospholipids, such as DOPC, but is perhaps not expected in dynamic systems as reported here. We explain our findings in terms of the sample quickly achieving equilibrium with the atmosphere inside the sample can compared to the very much slower equilibration of the can atmosphere with the water at the base of the can. The design of the water baths was such that the surface area was relatively small (approximately 5 cm^2) and positioned some 1.5 cm below the rim.

Both of the methods used in this study give phase information. In the case of the $^2H_2O/H_2O$ exchange approach, the phases are determined as those which give the best fit to straight lines when the structure factors of each order are plotted against the percentage of ^2H_2O (see Fig. 1). Since

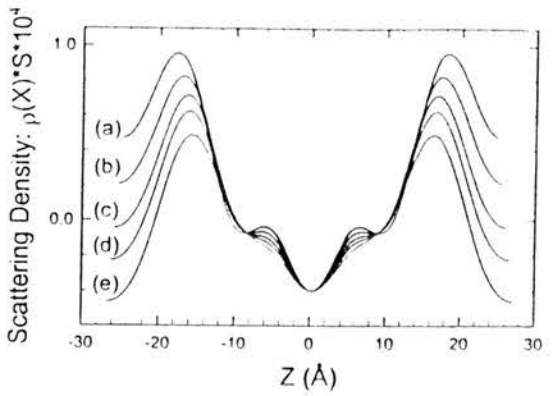

Fig. 4. A swelling series of neutron scattering density profiles calculated by Fourier transformation of structure factors determined by interpolation between the observed points, as shown in Fig. 2: (a) $D = 50$ Å; (b) $D = 51$ Å; (c) $D = 52$ Å; (d) $D = 53$ Å; (e) $D = 54$ Å.

the distribution of ^2H_2O approximates to a Gaussian peak centred at the origin, the phases are predicted to alternate, with odd-numbered orders negative and even ones positive. However, this Gaussian approximation breaks down as the order number increases because the width of the ^2H_2O peak is wide, and is actually better represented as a pair of Gaussian distributions [2,4]. In the case of the swelling series approach, all possible phase combinations are tried, the correct one being identified as that which gives best agreement between the observed points and the continuous transform calculated from them [1]. This is shown in Fig. 2. Reference to the figure shows that the neutron structure factors, determined at a range of spatial frequencies, do not lie on the same continuous transform. The explanation for this is discussed below. However, it is clear from the figure that each order traces out its own curve through the observed points. This is even true for the first order reflections, which show the largest change in spatial frequency. The point at a spatial frequency of 0.0197 $Å^{-1}$ was the first point measured, from an effectively dry sample; even though it lies well outside the continuous transforms shown, it still fits the curve plotted through the other first-order points. This curve may be interpolated to calculate sets of structure factors of any intermediate D-repeat (since the hydration of the sample increased steadily throughout the experiment, no two measured points index to the same D-repeat). Continuous transforms, calculated from these points, using the method of King and Worthington show a smooth variation in amplitude, reinforcing faith in the phase assignments.

Interpolation between the measured values of each structure factor allows determination of the bilayer structure at any D-repeat within the range covered by the measurements. This feature compliments the standard neutron procedure of difference calculation, which is most powerful when both data sets in a subtraction have exactly the same D-repeat. However, this is rarely the case; typically one has to be content with a difference up to 2% or so. Fig. 4 shows a series of bilayer scattering profiles, calculated from points on the lines interpolated between the swelling series points. The difference between profiles which differ by only 1.0 Å is apparent. Using the swelling series method, each set of structure factors in a difference subtraction can be calculated for the same D-repeat, thereby removing ambiguity from the subtraction result.

It is apparent from Fig. 2 that the observed points do not trace out a continuous transform. One possible explanation is that the bilayer structure changes during the hydraton process. This point has been raised by Worcester [6], who has suggested that the conformation of phosphate-containing head group of dimyristoylphosphatidylcholine in the L_α phase is dependent upon hydration level. It is possible that our data demonstrate the same phenomenon, though it is not certain that the current resolution ($h = 5$) would be sufficient to show this. However, unless any structural rearrangement occurred over a very small change in D-repeat (the smooth curves through each order in Fig. 2 do not show this to be the case) then calculating an intermediate set of structure factors between the observed points will simply result in an intermediate structure.

An alternative (or complementary) explanation is that increasing amounts of (negatively scattering) water modify the unit-cell structure in such a way that it is not valid to fit all of the swelling series to the same continuous transform. This suggestion is supported by Fig. 4 which compares the bilayer

structure at different points on the swelling series. It is clear that water penetration into the head group region reduces the height of the phosphate-ester peaks, and shifts their centre of mass into the bilayer.

Fig. 4 shows that the effect of increasing the water content is to reduce the neutron-scattering contrast of the system. The reason for this is that the region to which the negatively scattering water is introduced is immediately adjacent to and, indeed, totally overlaps (see Fig. 3), the region of highest scattering density, namely the phosphates and ester linkages. In order to avoid this effect, and more-accurately mimic the X-ray technique, it would be necessary to use 8.06% ^2H_2O; at this isotopic composition, water has a net neutron scattering density of zero.

Despite the fact that the individual observed points cannot be fitted to a single continuous transform, for the reasons explained above, it is our assertion that it is still quite legitimate to interpolate between the observed points in order to derive sets of structure factors.

Table 1 compares the structure factors obtained by the two methods. One distinct advantage of the swelling series method is the potential increase in the accuracy of intensity measurement. Any change in D-repeat, caused by temperature or humidity fluctuations, or incomplete equilibration, can result in large differences in intensity of any given order. This effect is seen at its most extreme in the first order, where a change in D-repeat of 2.5 Å (from 50.8 to 53.2 Å) causes a 280% change in amplitude (which is equivalent to nearly 800% change in intensity). These variations may occur within the duration of the scanning of one sample (typically 12 h or so), or the same sample may equilibrate to a slightly different D-repeat in any of the set of measurements in a $^2H_2O/H_2O$ exchange series. Instead of simply averaging out these differences, the swelling series method, proposed here, provides a much more systematic treatment of the data. Each reflection is indexed individually to its spatial frequency. Moreover, with more than one point for each order, it is possible to determine the precise structure factor amplitude at any intermediate point on the spatial frequency scale. When neutron beam time is limited, the advantage of not needing to wait for hours to be certain of complete equilibration of a new sample is considerable.

Another weakness in the $^2H_2O/H_2O$ exchange method which is overcome by the swelling series approach is the requirement to scale the different data sets to each other in the former. This requirement is alleviated in the latter, since the entire series of measurements is made on the same sample, without disturbing its alignment in the beam. No correction is therefore necessary.

In practice, we do not see the swelling method being used exactly in the way we have described here. DOPC is a well-understood phospholipid, so it was a reasonable choice for this study. However,

Table 1
Relative absolute neutron structure factors $F^*(h)$ for oriented bilayer stacks of DOPC at 25 C. The D-repeat of each set is 53.2 Å

	$F^*(1)$	$F^*(2)$	$F^*(3)$	$F^*(4)$	$F^*(5)$
DOPC ($^2H_2O/H_2O$ exchange method)[a]	− 7.68	− 20.10	9.96	− 3.00	− 2.09
	± 0.30[b]	± 0.50	± 0.34	± 1.72	± 0.57
DOPC (swelling series method)[c]	− 8.34	− 18.89	9.57	− 1.57	− 4.13

[a]These data were calculated by least-squares fitting to measured structure factors at 0%, 50% and 100% ^2H_2O.
[b]The errors quoted are the maximum deviation of each order from the least-squares fitted straight line (as shown in Fig. 1) and are, therefore, only an approximation. The two major contributions to the errors are likely to come from combining data from different D-repeats and inaccuracies inherent in the measuring process itself. It is not easy to calculate meaningful error estimates for the swelling series data, but they are expected to be no larger than those quoted for the $^2H_2O/H_2O$ exchange data. Indeed, they are likely to be much improved since the former of the two major contributors to the errors does not apply to these data.
[c]These data were calculated from curves fitted to structure factors measured from a sample as its D-repeat increased from 50.8 to 53.2 Å, over a period of 12 h.

when applied to less well-studied lipids, unexpected lyotropic phase transitions or phase separations may well manifest themselves which, though easy to identify in the neutron data, would detract from the value of the technique. How we do see the swelling method being applied is way of breaking down each data collection run into several consecutive scans. Each scan would be analysed independently. A comparison of the position and amplitude of each order from the consecutive scans would then allow a more accurate estimation of the amplitude, as well as reveal useful phase information.

Taking all these advantages together, the improved accuracy, reduced equilibration time and the ability to calculate structure factor sets at any selected *D*-repeat (within a given range), the swelling series method has much to recommend its adoption for neutron diffraction studies. We therefore recommend the swelling method, not as a replacement for the more usual neutron approach of isotopic substitution, but rather as a complimentary technique which can help to improve the accuracy of structure factor determination, whilst also providing an independent 'second opinion' for phase determination. Its added advantage of reducing the requirement for sample equilibration time at the start of an experiment will assist in the optimal utilisation of neutron beam time allocations. For maximum benefit, and closest parallel to the X-ray method from which it is derived, the samples should be run at 8.07% ^2H_2O, though it will yield increased information content at any ^2H_2O concentration.

Acknowledgements

We thank Dr. Valentin Gordelii of the Institut Laue et Langevin for expert assistance with the data collection. This work was supported by the Institut Laue et Langevin, Grenoble, France.

References

[1] G.I. King, C.R. Worthington, Phys. Lett. 35A (1971) 259.
[2] K.C. Duff, P.J. Gilchrist, A.M. Saxena, J.P. Bradshaw, Virology 202 (1994) 287.
[3] M.C. Wiener, G.I. King, S.H. White, Biophys. J. 62 (1991) 2762.
[4] M.C. Wiener, S.H. White, Biophys. J. 59 (1991) 162.
[5] R.E. Jacobs, S.H. White, Biochemistry 28 (1989) 3421.
[6] D.L. Worcester, in: D. Chapman, D.F.H. Wallach (Eds.), Biological Membranes, vol. 3, Academic Press, London, 1976.

Tu-AM-D4

Neutron diffraction studies of the interaction of tachykinins with phospholipid bilayers ((Jeremy P. Bradshaw Malcolm J. M. Darkes Sarah M. A. Davies.)) Department of Preclinical Veterinary Sciences. University of Edinburgh. R. (D.) S. V. S.. Summerhall. Edinburgh. EH9 1QH. Scotland. UK.

The tachykinins are a group of peptides which bind to G-protein coupled receptors. Receptor affinity appears to depend on different secondary structures of tachykinin which share the same hydrophobic carboxy-terminal sequence. FXGLM. Receptor activation is thought to be due to the carboxy-terminal submerging into the bilayer and the amino-terminal binding on the surface. We have used neutron diffraction measurements of specifically deuterated tachykinins to study the bilayer interaction of these peptides and determine the depth of bilayer penetration of their carboxy-termini. We report that the bilayer locations of two tachykinins. substance P and neurokinin A. are remarkably similar. thereby inferring that finer levels of structure must control receptor specificity. We present data relating the bilayer penetration to the phospholipid composition of the membrane and present structural models derived by using the location of deuterated peptides to position NMR structures of the peptides relative to the bilayer normal.